Design and optimization of flexible multi-generation systems

PhD Thesis

$$(EIv'')''=q-\rho A\ddot{v}$$

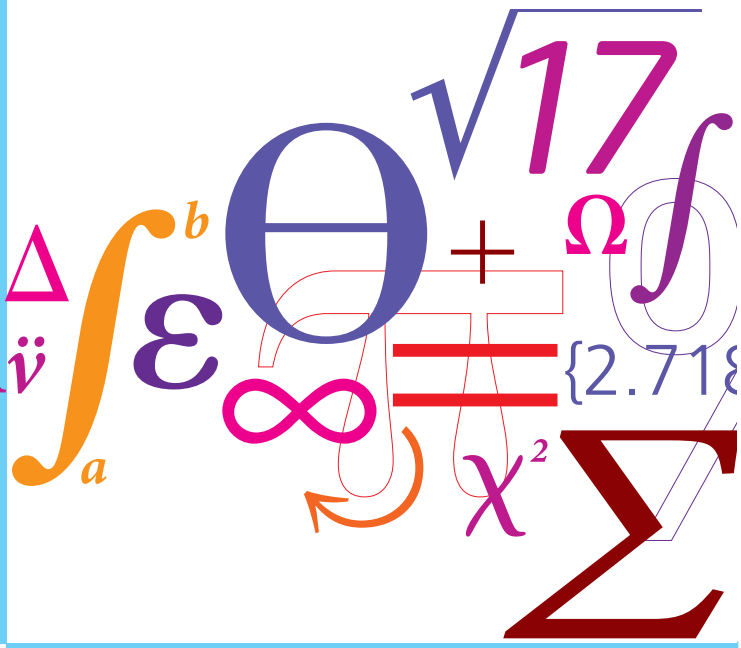

Christoffer Ernst Lythcke-Jørgensen
DCAMM Special Report No. S218
April 2016

DTU Mechanical Engineering
Department of Mechanical Engineering

TECHNICAL UNIVERSITY OF DENMARK

Ph.D. project:

Design and optimization of flexible multi-generation systems

Christoffer Ernst Lythcke-Jørgensen

April 2016

Department of Mechanical Engineering, Thermal Energy
Department of Management Engineering, System Analysis

Design and optimization of flexible multi-generation systems

PhD Thesis
DCAMM Special Report no. S218
ISBN: 978-87-7475-474-9
Printed by STEP

DTU Department of Mechanical Engineering
Thermal Energy

Nils Koppels Allé, Building 403
DK-2800 Kgs. Lyngby
Denmark

Phone: (+45) 45 25 41 31
Fax: (+45) 45 88 43 25
www.mek.dtu.dk

PREFACE

This thesis is submitted in partial fulfilment of the requirements for the degree of Doctor of Philosophy in Mechanical Engineering at the Technical University of Denmark (DTU).

The project was conducted at the Department of Mechanical Engineering, Thermal Energy, and at the Department of Management Engineering, System Analysis. In addition, a part of the research was carried out at, and in collaboration with, the Industrial Process and Energy Systems Engineering Group at École Polytechnique Fédérale de Lausanne (EPFL). The third case study treated in the project was developed and carried out in collaboration with the Danish Transmission System Operator (TSO) Energinet.dk.

The project represents a workload of 36 months and was carried out over the period from September 2012 to April 2016, including seven months of parental leave. It was supervised by Fredrik Haglind and Lasse Røngaard Clausen, DTU Mechanical Engineering, and Marie Münster, DTU Management Engineering. The research conducted at EPFL was supervised by Adriano Viana Ensinas, EPFL, Industrial Process and Energy Systems Engineering group (IPESE). The project was funded by DONG Energy and DTU, and included attending PhD level courses corresponding to six months workload (31.5 ECTS points), plus lecturing and teaching at master and bachelor courses, supervising master and bachelor theses, and developing and supervising special courses for engineering student.

This thesis represents a compilation of five ISI-indexed journal papers and three peer-reviewed conferences papers, and is written with the intention of synthesizing and linking the various outcomes of the research project in a single document. In addition to this, the sections of the thesis offer additional perspective on the contents and outcomes of previously published works. References to the original publications are made throughout the thesis where relevant.

ABSTRACT

This thesis focuses on the design of flexible multi-generation systems, which are dynamic and integrated energy conversion systems characterized by the ability to adjust operation in response to fluctuating operating conditions. It is the hypothesis that these systems may support the balancing of variable renewable energy sources in a cost-effective way by linking the different sectors in the energy system with local energy supply systems.

A key challenge faced in the development of flexible multi-generation system is the knowledge gap between process design practices, which simplify energy system variations and dynamics, and energy system analysis, which fails to consider process integration synergies in local systems. The primary objective of the thesis is to derive a methodology for linking process design practices with energy system analysis for enabling coherent and holistic design optimization of flexible multi-generation systems.

A methodology is presented for optimizing the design of flexible multi-generation systems which considers: Selection, dimensioning, location and integration of processes; operation optimization with respect to both hourly variations in operating conditions as well as long term energy system development; biomass supply chains and local resource availability; combined with global sensitivity and uncertainty analysis. The methodology includes a novel method for aggregating external operating condition datasets, named the CHOP method. In addition, three case studies focusing on integrating biomass processing and energy conversion technologies in existing combined heat and power plants in Denmark are conducted using the developed methods.

The outcomes of this thesis indicate that the developed design methodology is efficient in screening for promising designs of flexible multi-generation system. In addition, the case study results emphasize the importance of considering flexible operation, systematic process integration, and systematic assessment of uncertainties in the design optimization. It is recommended that future research focus on assessing system impacts from flexible multi-generation systems and performance improvements from storage options.

Keywords: Biomass conversion, design optimization, energy conversion, flexible multi-generation, operation optimization, polygeneration, process integration, smart energy.

DANSK RESUMÉ

Denne afhandling fokuserer på fleksible multigenerationssystemer, som er dynamiske og integrerede energikonverteringsanlæg kendetegnet ved deres evne til at indpasse driften i forhold til variationer i eksterne driftsforhold. Hypotesen er at disse anlæg kan bidrage til omkostningseffektiv balancering af fluktuerende produktion fra vedvarende energikilder ved at sammenkoble de forskellige energisektorer med lokale energidistributionssystemer.

En central udfordring i udviklingen af fleksible multigenerationssystemer er den manglende kobling mellem procesdesign, hvori variationer og dynamik i det overordnede energisystem simplificeres, og energisystemsanalyse, hvori procesintegrations-synergi ikke overvejes. Det overordnede formål med denne afhandling er at udvikle en metode der sammentænker procesdesign med energisystemsanalyse for derigennem at kunne udføre en sammenhængende og holistisk designoptimering af fleksible multigenerationssystemer.

I afhandlingen præsenteres en metode til designoptimering af fleksible multigenerations-systemer der forholder sig til: Valg, dimensionering, placering og integration af processer; driftsoptimering i forhold til både timevise variationer i eksterne driftsforhold samt i forhold til den langsigtede udvikling i energisystemet; biomasse-forsyningskæder og tilgængelighed af lokale ressourcer; kombineret med global følsomheds- og usikkerheds-analyse. Metoden inkluder en nyudviklet teknik til at aggregere data for eksterne driftsforhold, kaldet CHOP metoden. Derudover præsenteres tre cases der behandler integration af biomasseforarbejdning og anden energikonverteringsteknologi i eksisterende danske kraftvarmeværker ved brug af den udviklede metode.

Resultaterne indikerer at den udviklede designmetode er effektiv til at identificere lovende designs blandt mange muligheder. Derudover understreger case-resultaterne vigtigheden af at man i designoptimering forholder sig systematisk til variationer i eksterne driftsforhold, procesintegration samt usikkerhedsanalyse. Det foreslås at videre forskning undersøger mulige energisystemeffekter fra fleksible multigenerationssystemer, samt udvikling af designoptimeringsmetoden så den kan forholde sig til lagre.

Søgeord: Biomasseforarbejdning, designoptimering, driftsoptimering, energikonvertering, fleksible multigenerationssystemer, polygeneration, procesintegration, smart energi.

PUBLICATIONS

Publications developed during the project with the PhD candidate as first author are listed below. The papers are included in Appendix B-I.

Peer-reviewed journals

1. C.E. Lythcke-Jørgensen, F. Haglind, and L.R. Clausen. *Exergy analysis of a combined heat and power plant with integrated lignocellulosic ethanol production*. Energy Conversion and Management 85:817-827, 2014.

2. C.E. Lythcke-Jørgensen and F. Haglind. *Design optimization of a polygeneration plant producing power, heat, and lignocellulosic ethanol*. Energy Conversion and Management 91:353-366, 2015.

3. C.E. Lythcke-Jørgensen, M. Münster, A.V. Ensinas, and F. Haglind. *A method for aggregating external operating conditions in multi-generation system optimization models*. Applied Energy 166:59-75, 2016.

4. C.E. Lythcke-Jørgensen, A.V. Ensinas, M. Münster, and F. Haglind. *A methodology for designing flexible multi-generation systems*. Energy (in press).

5. C.E. Lythcke-Jørgensen, L.R. Clausen, L. Algren, A.B. Hansen, M. Münster, R.Ø. Gadsbøll, and F. Haglind. *Optimization of a flexible multi-generation system based on CHP, wood chip gasification, and methanol production*. (Submitted for Applied Energy, special issue on energy supply networks. Manuscript number: APEN-D-16-02936).

Peer-reviewed conference proceedings

1. C.E. Lythcke-Jørgensen, F. Haglind, and L.R. Clausen. *Thermodynamic and economic analysis of integrating lignocellulosic ethanol production in a Danish combined heat and power plant*. 21st European Biomass Conference & Exhibition (EUBCE). Copenhagen, Denmark, 2013.

2. C.E. Lythcke-Jørgensen, F. Haglind, and L.R. Clausen. *Exergy analysis of a combined heat and power plant with integrated lignocellulosic ethanol production*. 26th International Conference on Efficiency, Cost, Optimization, Simulation and Environmental Impact of Energy Systems (ECOS), Guilin, China, 2013.
3. C.E. Lythcke-Jørgensen, M. Münster, A.V. Ensinas, and F. Haglind. *Design optimization of flexible biomass-processing polygeneration plants using characteristic operation periods*. World Renewable Energy Congress XIII. London, UK, 2014.

ACKNOWLEDGEMENTS

First of all, I would like to thank my supervisors Fredrik Haglind, Lasse Røngaard Clausen, and my former supervisor Mogens Bech Laursen, for offering me the PhD position in the first place, and DONG Energy for supporting the project financially. I am grateful that you gave me this opportunity, and hope that my work and contributions have lived up to your expectations.

Fredrik, thank you for trusting me with the freedom to manage and steer the project on my own with very few restrictions, and for supporting me in the decisions I have made throughout the project. The trust you have shown in me and my ideas has made this project an invaluable experience, and your thorough feedback on manuscripts as well as general work always encouraged me to strive for further development and improvement.

Lasse, thank you for all the discussions and suggestions on the development of the project, for your feedback and inputs regarding the modelling of biomass processing technology, and last but not least for the close and fruitful collaboration on the development of *Case III* for this project. I really hope we will get a chance to work together again in the future.

Mogens, thank you for believing in me as the right candidate for the project, for providing firm and carrying guidance in the beginning of the project, and for offering your feedback and council even after you left DONG Energy. You have been, and are still, a great inspiration to me as a professional as well as a person, and I am appreciative of having had the opportunity to work with you.

Next, I want to say a warm and grateful thank you to my supervisor Marie Münster. I will never forget how you pulled over on your way home from work and took your time to discuss energy system theory, ongoing research and collaboration opportunities when a young Ph.D. student called a late afternoon with a frank invitation. You have been a source of motivation and energy for me ever since you got on board the project, and I really enjoyed our meetings and passionate talks about energy research, politics, social life, career as well as many other topics. I really appreciate that you prioritized to take part in my project, and I look forward to staying in touch with you in the future!

I want to express my gratitude towards Adriana Viana Ensinas, my research supervisor during my visit at EPFL in Lausanne. I am really happy that we were introduced during the ECOS conference in China in 2013, and I am grateful that you invited me to visit you and the IPESE group in Lausanne. You were an extraordinary mentor for me, patient and ever-available with answers and support during my stay. I hope our paths will cross again.

On a related note, I want to thank all my colleagues from the IPESE lab at EPFL: Mathias, Manuel, Priscilla, Hossein, Victor, Stefano, Stephane, Nils, Elfie, Alberto, Raman, Maziar, and all the rest!! The time I spent with you guys was the peak of my PhD project period and I will never forget it! Thank you!

I want to acknowledge Anders Bavnhøj Hansen and Loui Algren from Energinet.dk for fruitful collaboration on *Case III* in the project. I appreciate that you found interest and saw perspectives in my research, and it has been a pleasure working with you.

I also wish to say a warm thank you to Bodil Diemer for providing linguistic feedback and inputs for several of my paper manuscripts. I find you a true word-artist, and I am thankful for your help in improving the quality of my written works.

Furthermore, I want to thank Anish, Pelle, Ju and all the other office mates I have had at DTU through the years for deep academic discussions as well as cosy small talk on food, family life, culture etc. It has been a pleasure sharing the office with you. I also want to thank Tuong-Van for introducing me to Adriano and the IPESE group, for interesting talks on research, and for providing competent feedback for this thesis.

Last but not least I want to thank my family and friends for trying to find interest in my geeky project, for being patient with me when I haven't reached out to you or responded to messages or calls during busy periods, for helping looking after the twins so I could focus on my work, and especially for always being able to provide a bit of general perspective and reality check on my everyday life. I especially want to thank Claus Elberling for relevant and ever-interesting discussions on general science, the scientific method, and ethics in academia.

Finally, to my lovely Sofie, Alexander and Theodor: Though sometimes a man of many words, I don't have any for expressing what I wish to tell you on this page, but I trust you know what I'm trying to say anyways <3

TABLE OF CONTENTS

ABSTRACT ..... **vii**
LIST OF TABLES ..... **xvii**
LIST OF FIGURES ..... **xix**
NOMENCLATURE ..... **xxiii**

1 INTRODUCTION **1**
1.1 Context 1
1.2 Motivation 6
1.3 Research objectives 7
1.4 Thesis outline 8

2 STATE-OF-THE-ART ON THE DESIGN AND OPTIMIZATION OF MULTI-GENERATION SYSTEMS **9**
2.1 Relevant aspects of designing flexible multi-generation systems 9
2.2 Design methodologies in literature 10
2.3 Methodology comparison and discussion 12

3 METHODS **15**
3.1 The CHOP Method: A novel method for aggregating external operating conditions when designing multi-generation systems 15
3.2 A methodology for designing flexible multi-generation systems 32

4 CASE STUDIES **47**
4.1 Case studies: Background and overview 47
4.2 Case I: Multi-generation of electricity, heat, and cellulosic ethanol in a retrofitted extraction CHP unit 49
4.3 Case II: Multi-generation of cellulosic ethanol, biomethane, heat and electricity in a retrofitted combined cycle CHP unit 63
4.4 Case III: Multi-generation of methanol, electricity, heat, and industry energy utility in a local FMG symbiosis 70
4.5 Summary of findings 80

5 CONCLUSION 83
5.1 Summary of findings 83
5.2 Recommendations for further research 87

REFERENCES 91

OVERVIEW OF APPENDICES 105
APPENDIX A Project chronology 107
APPENDIX B Journal paper 1 109
APPENDIX C Journal paper 2 121
APPENDIX D Journal paper 3 137
APPENDIX E Journal paper 4 155
APPENDIX F Journal paper 5 (manuscript) 177
APPENDIX G Conference paper 1 215
APPENDIX H Conference paper 2 225
APPENDIX I Conference paper 3 239
APPENDIX J Report on uncertainty analysis methodology 251
APPENDIX K Modelling example: Case III 265

LIST OF TABLES

Table 2.1: Comparison of selected design aspects considered in multi-generation system design methodologies presented in literature. 14

Table 3.1: Optimization results obtained from solving the optimization model without thermal storage when applying each of the six different EOC datasets..... 26

Table 3.2: Optimization results obtained from solving the optimization model including thermal storage. 28

Table 4.1: Overview of design and operation aspects considered in the three cases. 48

Table 4.2: Operation characteristics and standard exergy efficiency of the investigated operating modes..... 55

Table 4.3: *Case II*, design and operation variables considered. 65

Table 4.4: *Case II*, input parameter uncertainty distributions..... 66

Table 4.5: *Case II*, characteristics of the selected designs..... 68

Table 4.6: *Case III*, design and operation variables considered. 74

Table 4.7: *Case III*, distributions of uncertain input parameter. 74

Table 4.8: *Case III*, design and performance characteristics of the four selected designs.. 76

LIST OF FIGURES

Figure 1.1: Predicted electricity generation by fuel and by plant type within the European Union [7]. 2

Figure 1.2: Energy flows and sector interactions in a scenario for the integrated Danish energy system in 2050, developed by the Danish transmission system operator (TSO) Energinet.dk [6]. 4

Figure 1.3: Conceptual sketch of a flexible multi-generation system. Dotted arrows indicate a range of technological pathways for linking the energy system sectors [19]. 6

Figure 3.1: Sketch of the data aggregation principle applied in the CHOP method. Operating points O_i are clustered and merged into CHOP groups G_j with aggregated weight factors. 18

Figure 3.2: Overall sequence of the CHOP method [36]. 19

Figure 3.3: Illustration of the suggested two-step approach for defining characteristic intervals based on the cumulative value curve for a relevant and varying EOC (left). Interval break points are set for a) important values, and b) even division. The characteristic intervals are indicated by arrows on the second axis in b) [36]. 20

Figure 3.4: Feasible heat and electricity generation range of the reference and linearized CHP plant models [36]. 24

Figure 3.5: Scatter diagram showing operating points of the initial dataset, annually averaged dataset, monthly averaged dataset, seasonal peak/off-peak averaged dataset, CHOP dataset, and revised CHOP datasets [36]. Note that some of the CHOP and revised CHOP operating points are overlapping and that a few of the reference operating points are outside the electricity price boundaries of the plot. 25

Figure 3.6: Thermal energy storage contents over the 5-year period in the solutions to the optimization model with thermal storage, obtained using the full EOC dataset and the revised CHOP dataset [36]. 29

Figure 3.7: Structure and sequence of the developed design methodology. Note that an MILP algorithm is used for optimizing process integration and operation within the genetic algorithm optimization [19]. 34

Figure 3.8: Example of a scatter plot of sigma-scaled elementary effects from various input parameters q on a model output h. The two lines forming the wedge represent the double standard error of the mean. Input parameters with sigma-scaled elementary effects inside the wedge are considered negligible with respect to variations in h, while parameters outside are considered to have significant impact on variations in h. 42

Figure 4.1: Simplified process layout of the system treated [20]. 51

Figure 4.2: Outlines of the two operation modes of the integrated system [20]. 51

Figure 4.3: Methodology applied on *Case I*, including publication milestones. 52

Figure 4.4: Sankey diagrams of specific heat flows in the ethanol facility per kg/s straw treated at zero (top) and maximum (bottom) district heating generation. Note that additional heat is required when district heating generation is included [20]. 54

Figure 4.5: Specific exergy flows in the ethanol facility per kg/s of straw treated when all heat exchange occurs at 10K. Exergy losses and destruction (L&D) are also indicated for the processes [20]. 55

Figure 4.6: Specific exergy flows in the ethanol production in operating mode IV (top) and V (bottom) [20]. 56

Figure 4.7: Specific ethanol cost and important cost components as function of ethanol facility dimension σ_{eth} given in kg/s straw processed [15]. 58

Figure 4.8: Duration of three characteristic operation modes over the year as a function of σeth [15]. 60

Figure 4.9: Specific energy costs as functions of σ_{eth}. Note that electricity costs include lost electricity sales [15]. 60

Figure 4.10: Average standard exergy efficiency of the ethanol production over the year as a function of σ_{eth} [15]. 61

Figure 4.11: Yearly average specific exergy flows in the ethanol production for the optimized design [15]. 61

Figure 4.12: Spider plot showing the impact on specific ethanol production cost from varying different cost parameter values [15]. 62

Figure 4.13: Superstructure of the FMG concept considered in *Case II*. The gas turbine and the Rankine cycle are grey as they represent the existing system that is considered for retrofitting [19]. 64

Figure 4.14: Scatter plot of optimized design solutions with respect to NPV and TCE, with performance variability indicated for three selected designs. NPV performance intervals represent 10^{th} to 90^{th} percentiles of predicted performance, while TCE intervals represent 0^{th} to 90^{th} percentiles of predicted performance [19]. 68

Figure 4.15: Performance of selected designs if systematic process integration had not been considered [19]. 69

Figure 4.16: Conceptual sketch of energy flows in the reference system [37]. 72

Figure 4.17: Retrofit superstructures for locating the biorefinery next to the CHP unit (top, referred to as Scenario A) or next to the slaughterhouse (bottom, referred to as Scenario B). DH is short for district heating [37]. 73

Figure 4.18: Scatter plot of optimized design solutions with respect to NPV and TCE, with 10^{th} to 90^{th} percentiles NPV performance intervals indicated for the four selected designs [37]. 76

Figure 4.19: Performances of the four selected designs under the various energy system scenarios. Results of the investment cost uncertainty analysis are indicated as well [37]. 77

Figure 5.1: Illustration of the connection between the FMG design methodology, energy system models and process models in the present version (left) and the suggested feedback mechanism between the FMG design methodology and an energy system model (right). 88

NOMENCLATURE

Abbreviations

CCHP	Combined cooling, heating and power
CHOP	Characteristic operating pattern
CHP	Combined heat and power
DESS	Distributed energy supply systems
EPFL	École Polytechnique Fédérale de Lausanne
EOC	External operating condition
FMG	Flexible multi-generation system
GWP100a	100-years global warming potential
IPESE	Industrial Process and Energy Systems Engineering group
L&D	(exergy) losses and destruction
MILP	Mixed integer-linear programming model
MINLP	Mixed integer-nonlinear programming model
NPV	Net present value
O&M	Operation and maintenance
RES	Renewable energy sources
SOEC	Solid oxide electrolysis cell
SPG	Static polygeneration system
TCE	Total CO_2 emission impact
TSO	Transmission system operator

Roman Latin letters

A_B	Cultivation area for distributed biomass B
B_{an}	Annual consumption of distributed biomass B (ton)
b	Number of value levels uncertain parameters can take in Morris screening
C_0	Net present value (€)
$c_{0,j}$	Total operating cost in period j (€)
c_B	Marginal cost of distributed biomass B (€)
c_{B0}	Marginal reference cost of distributed biomass B (€)

$c_{B,tr}$	Marginal transportation and logistics cost for distributed biomass B (€)
C_{HEN}	Estimated investment cost of heat exchanger network (€)
$C_{inv,S}$	Investment cost of process S (€)
$C_{inv,S0}$	Reference investment cost of process S (€)
$c_{op,S,j}$	Operating cost of process S in period j (€)
$\dot{CP}_{f,j}$	Heat flow capacity of thermal flow f in period j (kJ/kg-s)
D	Distribution
$\dot{e}_{f,S,j}$	Thermal energy flow f associated with process S in period j (MJ/s)
$EE_{q_n,h}$	Elementary effect of uncertain input parameter q_n on output h (-)
G_j	CHOP group j
$\Delta H_{u,j}$	Enthalpy change over temperature interval u in period j (J)
h	Optimization model output function
$i_{rv,j}$	Characteristic interval number of rv in CHOP group j
$\dot{m}_{f,S,j}$	Mass flow f associated with process S in period j (kg/s)
N_{CHOP}	Number of CHOP groups (-)
$N_{CHOP,pot}$	Number of potential CHOP groups (-)
N_q	Number of uncertain input parameters q (-)
n_{rv}	Number of characteristic intervals defined for rv (-)
O_i	Operating point
$\dot{P}$	Electricity generation (MW)
p	EOC parameter value
pf_S	Power factor for investment cost calculations for process S (-)
PV_j	Present value factor of CHOP group j (-)
$\dot{Q}$	Heat generation (MJ/s)
q	Uncertain input parameter
q_n^*	Significant uncertain input parameter for design n
r	Interest rate (-)
rv	Relevant and varying external operating condition
S	Surrogate process model
SD	Standard deviation
$SEE_{q_n,h}$	Sigma-scaled elementary effect of q_n on output h.
$T_{f,in}$	Inlet temperature of thermal energy flow f (K)
$T_{f,out}$	Outlet temperature of thermal energy flow f (K)
T_u	Maximum temperature in temperature interval u (K)
t	Duration (h)

u_{max}	Total number of heat intervals in the thermal energy flow layer (-)
w_{MC}	Number of samples used in Monte Carlo simulations (-)
w_{MS}	Number of samples used in Morris screening (-)
Y_i	Year of occurrence for operating point i (-)
y_S	Installation delay of process S (years)
Z_0	Overall global warming potential of the system (MTon)
$z_{0,j}$	Global warming potential result of operation over period j (MTon)
$Z_{inst,HEN}$	Global warming potential from production, installation, and scraping of the heat exchanger network (MTon)
$Z_{inst,S}$	Global warming potential from production, installation, and scraping of process S (MTon)

Greek letters

α	Back-pressure operation parameter (-)
β	Relative district heating generation in the ethanol facility (-)
Δ	Pertubation factor for input parameters in Morris screening (-)
η_{ex}	Standard exergy efficiency (-)
κ	Choice between integrated or separate operation (-)
$\lambda_{S,j}$	Load of process S in period j (-)
μ	Mean of a distribution (-)
$\nu_{S,j}$	Operation decision for process S in period j (-)
σ_S	Dimension of process S
σ_{S0}	Reference dimension of process S
ω_S	Installation decision and location of process S (-)

Subscripts

f	Flow function index
i	Operating point index
j	CHOP group index
k	Relevant and varying EOC index
l	Flow layer index
m	Generic count index
n	Optimized and selected FMG design index
rv	Relevant and varying EOC parameter
u	Temperature interval index

1 INTRODUCTION

This chapter introduces the context of the project and describes the project motivation and research objectives. The thesis outline is presented as well.

1.1 Context

1.1.1 Energy outlook

In order to mitigate climate changes, substantial and sustained reductions of greenhouse gas emissions are necessary [1]. In consequence, scenario simulations suggest that the global energy systems must undergo a large-scale transition towards low carbon emissions already by 2050 if temperature changes by the end of the century are to be kept below 2°C relative to pre-industrial levels [2][1]. Key strategies within this transition include efficiency enhancements in the conversion from energy resources to energy services, and decarbonisation of electricity generation through the utilization of renewable energy sources (RES) [2].

Within the European Union, it is expected that half of the electricity generation will be based on RES by 2050, including 35% electricity generation from variable resources such as wind and solar power as illustrated in Figure 1.1. This figure, however, conceals large regional differences. In Denmark, for instance, wind turbines already generated 42.1% of the consumed electricity in 2015 [3], and the current political target is to increase this number to 50% by 2020 [4]. Furthermore, scenario simulations estimate that the majority of electricity generation in Denmark must come from wind power by 2050 in order to meet the ambition of an energy system with low carbon emissions [4–6].

[1] The ambition of keeping the global temperature increase 'well below 2°C' was reaffirmed in the Paris Agreement from December 2015, adopted by 195 countries at the 21st session of the United Nations Framework Convention on Climate Change (UNFCCC), also referred to as COP21 [122].

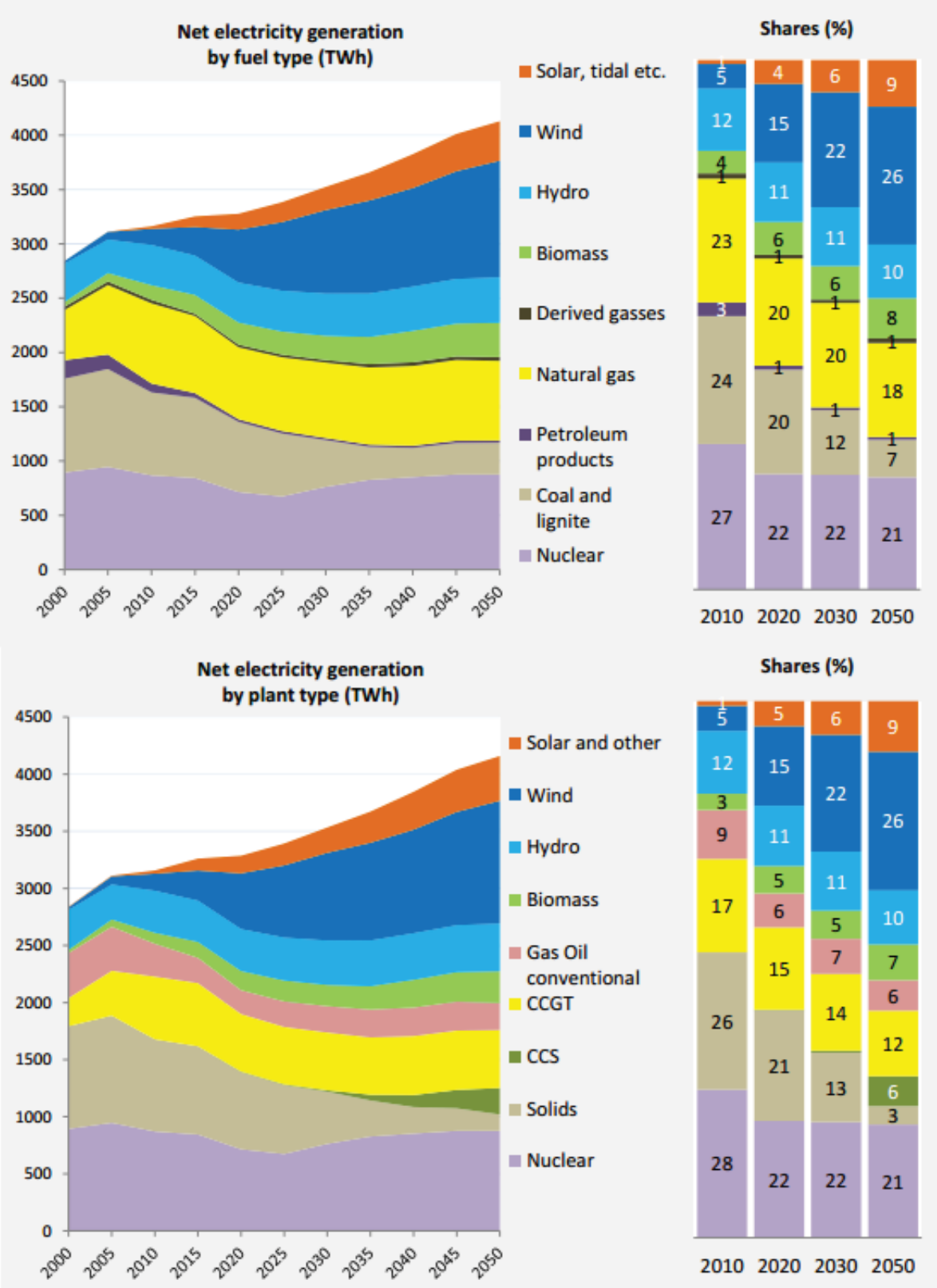

Figure 1.1: Predicted electricity generation by fuel and by plant type within the European Union [7].

Such large-scale integration of variable electricity generation challenges the electricity grid balancing as peak generation from variable RES and peak consumption may not be aligned. For example, already during 2015 the electricity generation from wind turbines in West Denmark exceeded the electricity consumption for a total of 1460 hours [3]. An increased share of variable RES in the electricity grid necessitates increased balancing capacity and operational flexibility. In addition to this, the integration of RES must not counteract the ambition of increasing the overall efficiency of the energy system.

1.1.2 Smart energy systems and process integration

Smart grid concepts have been suggested for solving the balancing issue of integrating variable electricity generation from renewables through the facilitation of flexible electricity consumption. Among others, smart grids consider the use of information technology, electricity storage, electric vehicles and vehicle-to-grid technology for shifting demand in response to price signals. However, it has lately been argued that a more holistic energy system approach should be taken in order to avoid sectoral optimization that may lead to suboptimal solutions with respect to the overall efficiency of the energy system [8,9]. In opposition to the smart grid concept and its sole focus on the electricity sector, Mathiesen et al. [10] introduced the concept of *smart energy systems* based on the hypothesis that synergies from integrating the different energy sectors, e.g. by converting electricity to heat or gas for which large-scale storage options already exists [11], may provide system balancing solutions which are cost- and energy effective when compared to solving the issues secluded within each sector. Consequently, smart energy systems include smart electricity grids, smart thermal grids, and smart gas grids, plus other fuel infrastructures and a number of interactions between these. An example of energy flows in an integrated and smart energy system, including interactions between different energy sectors, is presented in Figure 1.2.

While the smart energy system approach focuses on overall energy system impacts from merging the energy sectors through energy conversion technologies, it does not directly consider synergies from local integration of processes, technologies, and energy supply networks in flexible energy conversion systems. However, these synergies may be of great importance in the transition towards sustainable energy systems [12]. For biomass conversion in particular, it has been suggested that the integration with other energy conversion processes in multi-generation systems through the application of process systems engineering approaches may increase the energy- and cost-efficiency of the

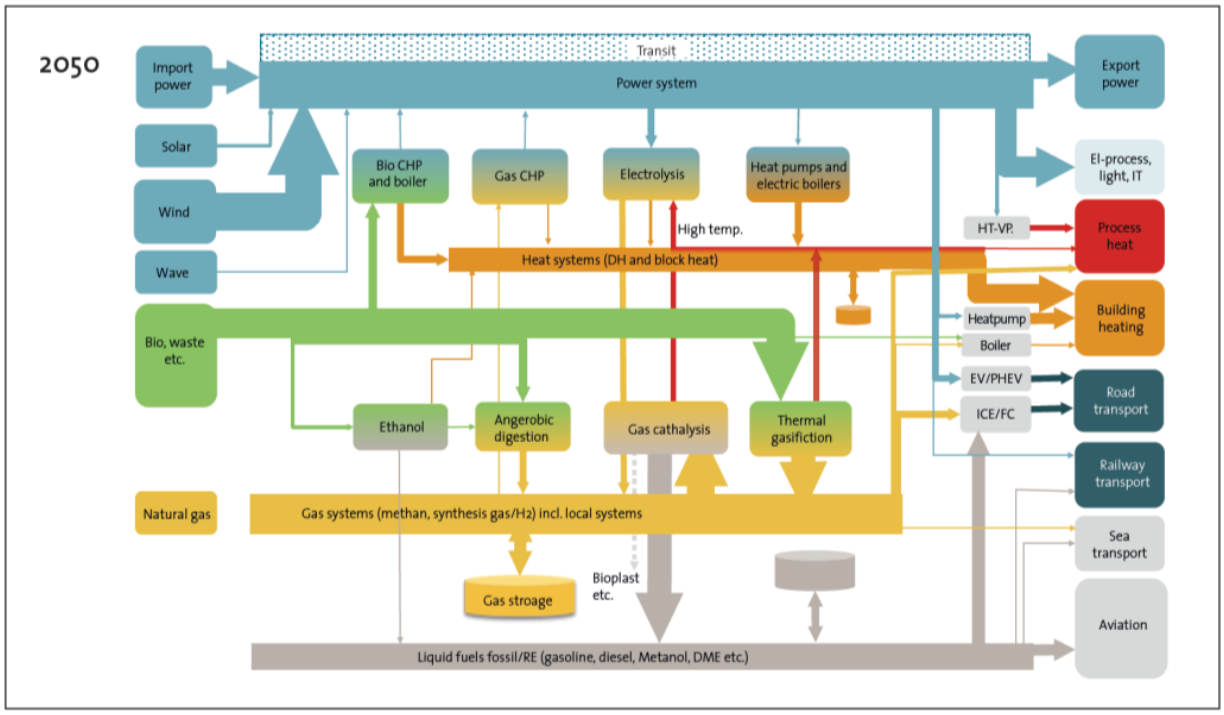

Figure 1.2: Energy flows and sector interactions in a scenario for the integrated Danish energy system in 2050, developed by the Danish transmission system operator (TSO) Energinet.dk [6].

overall system [13–16]. In fact, an engineering discipline named energy systems engineering[2] was recently introduced, with a focus on increasing energy conversion efficiency in society by systematically identifying and exploiting process integration synergies in the development, design, integration and operation of energy systems [8,17]. These process integration synergies ought to be considered when developing sustainable energy systems using the smart energy systems approach.

1.1.3 Flexible multi-generation systems[3]

Flexible multi-generation systems (FMGs) are integrated and agile systems that are capable of converting one or several energy sources into various energy services and other valuable products, e.g. heating, cooling, electricity, bio-fuels and bio-chemicals [18]. The following definition of FMGs was introduced by Lythcke-Jørgensen et al. [19]:

[2] 'Energy systems engineering' was introduced as a sub-discipline within the field of process systems engineering in 2007 by prof. Efstratios Pistikopoulos [123].

[3] This section is based on the introduction from the article 'A methodology for designing flexible multi-generation systems' [19].

- A flexible multi-generation system is a system of integrated facilities that provide multiple links between layers of the energy system, enabling adjustable operation in response to changes in prices and demands of the consumed and delivered services.[4]

According to this definition, FMGs may be either centralized facilities or distributed systems, as long as the various facilities are integrated. It should be emphasized that FMGs may include static processes, e.g. cellulosic ethanol production [20], as well as variable processes that are not fully dispatchable, e.g. wind turbines, as long as the combined system has a degree of operational flexibility.

The main advantages of FMGs are: The embedded possibility for optimizing operation in response to varying demand and price schemes by altering feedstock, process loads, products, and services [9,21–24]; the possibility of integrating and balancing generation from variable RES such as wind, solar, wave and tidal in a cost-effective way [25–27]; and the possibility of achieving high aggregated energy conversion efficiencies through process integration synergies [28–31]. The latter is of special relevance for biomass processing systems as the biomass resource is limited on a global level, and competition for biomass resources between the food, energy and material sectors represents a social, economic and environmental challenge [14,32,33].

FMGs may use a variety of different energy conversion technologies for integrating the various energy sectors, as conceptually illustrated in Figure 1.3. In case the economic incentive structures are aligned with the balancing requirements of the electricity system, FMGs may be operated as efficient 'energy system valves' that provide or extract electricity from the grid in response to imbalances induced by variable RES. In summary, FMGs combine the merging of energy sectors in the overarching energy system as proposed by the *smart energy systems* approach with efficiency enhancements through process integration and coupling with local and regional energy supply networks as proposed by the *energy systems engineering approach* [19]. FMGs may therefore play a central role in the development and operation of sustainable energy systems.

[4] The definition of an FMG may be overlapping with the terms 'polygeneration' and 'energy hubs'. In a recent review, Adams and Ghouse [124] defined 'polygeneration' as a thermochemical process which simultaneously generates electricity and produces at least one type of chemical or fuel without being a co- or tri-generation unit. 'Energy hubs' may refer to homes, large energy consumers, power plants or regions [125] as well as integrated facilities [21,126]. The FMG definition was introduced in Lythcke-Jørgensen et al. [19] in order to characterize integrated facilities that may actively contribute to the balancing of the overall energy system.

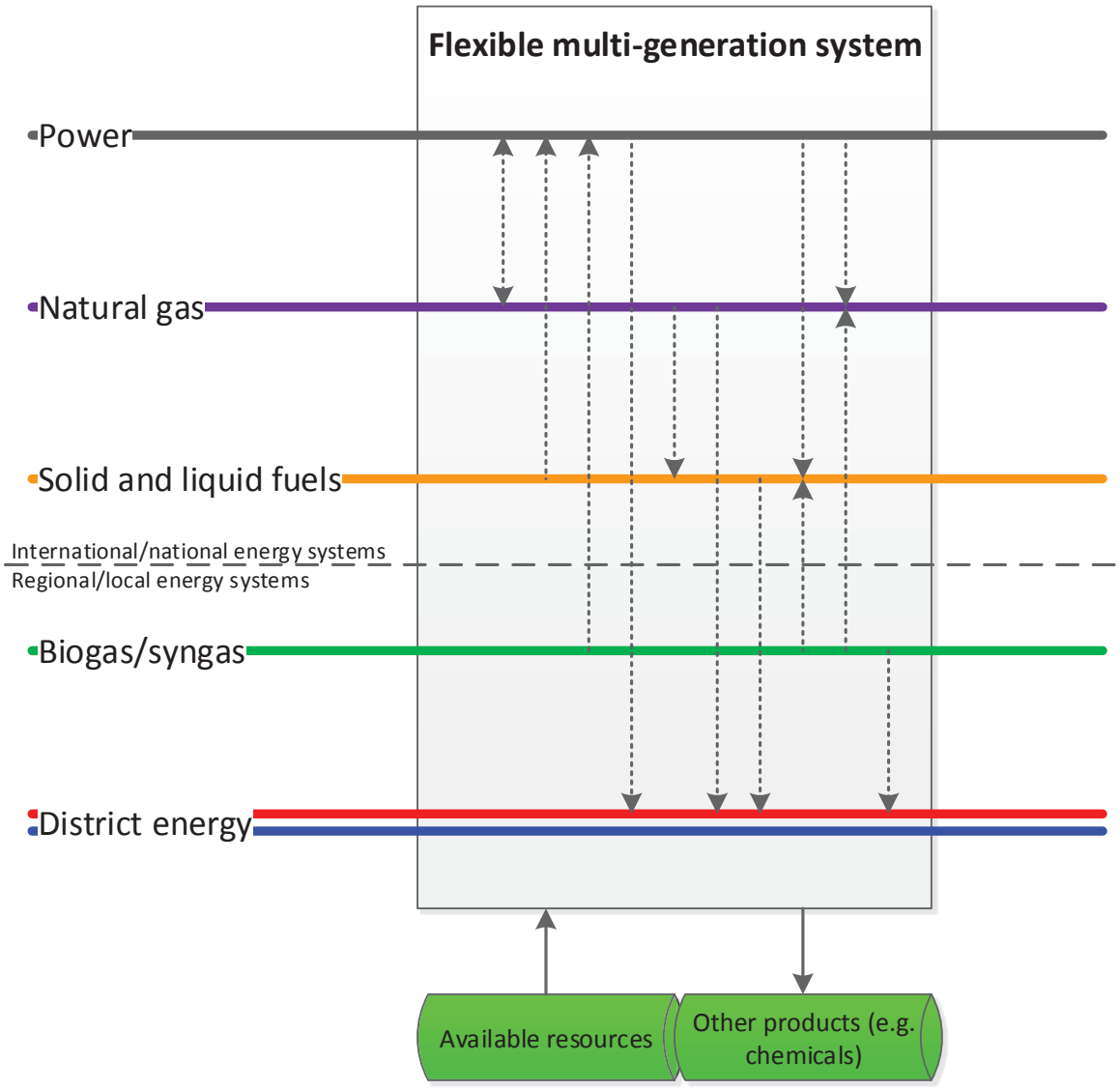

Figure 1.3: Conceptual sketch of a flexible multi-generation system. Dotted arrows indicate a range of technological pathways for linking the energy system sectors [19].

1.2 Motivation

Following the previously stated potentials of FMG concepts, this project was motivated by the hypothesis that FMGs, if carefully designed, may support the balancing of electricity generation from variable RES and provide options for linking the different energy sectors in a cost- and energy-effective way. The overall ambition was to test this hypothesis by systematically optimizing the design and performance of FMG concepts in energy systems with fluctuating operating conditions.

In order to optimize the performance of FMG concepts, both design and operation optimization aspects must be considered. Therefore, information on variations in energy system conditions must be combined with detailed process integration approaches. However, variations in operating conditions are on one hand often neglected or simplified in current design methodologies that involve process integration, even if process integration synergies in practice may be constrained by local energy demands and capacities of existing equipment. On the other hand, energy system models that capture the fluctuating nature of operating conditions induced by variable RES, e.g. EnergyPLAN [26], Balmorel [34] or the TIMES model [35], focus on pre-defined processes and thereby fail to consider synergies from integrating different energy conversion technologies [28]. This knowledge gap between detailed process design practices and energy system analysis is considered a primary obstacle for the development of efficient and competitive FMG concepts.

1.3 Research objectives

In response to the project motivation and the outlined knowledge gap, the following general research questions were used for setting the project frame:

- What are the current best-practices for developing FMGs?
- How can fluctuating energy system data efficiently be taken into account in design optimization models?
- What is the benefit of process integration synergies in FMGs when operated in energy systems with fluctuating operating conditions?
- How does process integration synergies relate to economy-of-scale benefits in FMGs?

Answering to the listed research questions, the main objectives of this project were to:

- Develop a methodology for designing FMGs that contributes to bridging the knowledge gap between process design practices and energy system analysis.
- Assess the performance of various FMG concepts in energy systems with large shares of variable RES through case studies.
- Analyse and quantify the importance of process integration synergies in FMGs.
- Contribute to the scientific knowledge pool on the topic by documenting the work in ISI-indexed journal papers.

In order to meet the research objectives, methods from operational research, applied thermodynamics, process systems engineering, and energy system analysis were applied.

1.4 Thesis outline

The present thesis is structured as follows:

Chapter 1 presents the context and motivation behind of the project, and describes the research objectives and outline of the thesis.

Chapter 2 presents a state-of-the-art review on the design and optimization of multi-generation systems. Existing design methodologies are introduced and discussed with respect to design aspects considered and methods applied. In the end, suggestions for relevant developments are outlined.

Chapter 3 presents the two methods developed in response to the suggestions from the literature review of the previous chapter: A method for aggregating non-cyclic operating condition datasets; and an overall methodology for designing FMGs. The data aggregation method is verified, and the potentials and drawbacks of the combined methodology are discussed.

Chapter 4 presents the background, methods applied, and results of the three case studies conducted as a part of the project. In addition, the case studies are used for verifying the developed design methodology. The chapter also features a summary and discussion on the case study findings.

Chapter 5 concludes the thesis by summarizing the project findings and providing recommendations for further research on the topic of FMG concepts.

2 STATE-OF-THE-ART ON THE DESIGN AND OPTIMIZATION OF MULTI-GENERATION SYSTEMS

This chapter contains a merging and extension of the literature studies featured in the manuscripts [19,36,37]*. First, a number of principal challenges to consider when designing FMGs are listed. Second, a review on the state-of-the-art approaches to optimize the design of various kinds of multi-generation systems is presented. Third, the design methodologies featured in the review are compared and benchmarked against the relevant design aspects.*

2.1 Relevant aspects of designing flexible multi-generation systems

Being complex systems by nature, it is evident that multiple design aspects need to be considered when developing FMG concepts. Relevant design aspects include, but are not necessarily limited to:

- Selection of processes and technologies from many alternatives
- Geographical location of facilities
- Process dimensioning
- Process integration
- Operation optimization with respect to hourly variations in prices and demands
- Performance analysis considering potential long-term energy system developments
- Assessment of local resource availability
- Investment planning
- Sensitivity and uncertainty analysis

All relevant design aspects must be treated in an integrated manner as they may be interdependent. To cope with this complexity, a systematic optimization approach is needed for the design optimization of FMG concepts [28].

2.2 Design methodologies in literature

Polygeneration and multi-generation systems are well-described concepts, and numerous approaches to the design optimization of such systems have been presented in literature [18,38]. A review on recent design methodologies for various kinds of multi-generation systems is presented here.

Liu et al. [39] presented a methodology for designing *static polygeneration systems*[5] (SPGs) based on a multi-period mixed integer-linear programming (MILP) model. The methodology considered long-term changes in operating conditions from developments in the energy system, and allowed for investment planning optimization. In three sequential works, the methodology was extended by converting the MILP model into a mixed integer-nonlinear programming (MINLP) model [40], allowing for multi-objective optimization [41], and finally converting the entire model into a stochastic optimization model to account for operational uncertainties [42]. However, thermal process integration and short-term variations in operating conditions were not considered in the methodology.

Gassner and Maréchal [43] presented a combined genetic algorithm/MILP methodology for designing SPGs. The methodology was based on the OSMOSE tool[6] [44] and involved the selection and dimensioning of processes, systematic process integration using pinch analysis [45], and assessment of multiple objectives in the design optimization. In a sequential work, the design methodology was extended to allow for systematic life cycle assessment when evaluating designs [46]. The methodology was later on applied in a case study of an SPG superstructure for generating electricity, heat, and liquid fuels from biomass [47,48]. Among other things, the results of the case study highlighted process integration as a key element for increasing energy conversion efficiency and economic performance of multi-generation systems. The presented design methodologies did not consider flexible operation, variations in operating conditions or uncertainty analysis.

Chen et al. [49] presented a deterministic methodology for optimizing the design and operation of a previously developed SPG superstructure. Running the design optimization

[5] Static polygeneration systems refer to polygeneration systems as defined by Adams and Ghouse [124] which are not designed for flexible short-term operation.

[6] OSMOSE is a computer aided process engineering tool, developed at EPFL in the Industrial Process & Energy System Engineering (IPESE) group, for designing and optimizing integrated energy systems. The tool provides an interface that combines pinch analysis [45] with economic analysis of process systems [89]. For more information, refer to [44] or the IPESE group homepage: http://ipese.epfl.ch/.

for a number of scenarios with different external operating conditions, it was found that the economic performance of optimized SPG designs would always outperform the corresponding economic performance of optimized single product plant designs. The methodology was later extended to allow for daily and seasonal operation flexibility, in effect allowing for designing of *flexible polygeneration systems*[7] [23]. Based on a number of case studies, it was concluded that increased operational flexibility led to higher net present values (NPVs) in polygeneration systems, at the cost of larger initial investment costs. In both methodologies, simple heat balances were applied for estimating process integration benefits which could lead to overestimated efficiency improvements, as also discussed in Chen [50]. Furthermore, uncertainty analysis was not included.

Maréchal et al. [51] presented a multi-period, multi-objective methodology for designing FMGs based on the OSMOSE tool[6]. It considered technology selection and dimensioning, process integration, facility location selection, operation optimization, and network layout. Later developments of the overall methodology comprise: A method for selecting typical cyclic operating periods [52]; a method for including daily thermal storages [53]; and a method for including distribution networks [54]. However, a shortcoming of the combined methodology is the fact that only variations in one external operating condition, namely outdoor temperature, was considered when developing the methods, meaning that flexible interactions with other parts of the energy system were not considered. In addition, uncertainties are not addressed in the combined methodology.

A particular branch of FMGs are *combined cooling, heating and power* (CCHP)[8] systems. Marnay et al. [55] presented the DER-CAM methodology for finding the optimal combination and dimensioning of various technologies with the aim of minimizing CCHP generation costs for commercial buildings by. Rubio-Maya et al. [56,57] presented a heuristic, two-level methodology for designing local FMGs for CCHP and fresh water generation. Technology selection and preliminary process dimensioning were handled on the first level based on monthly-averaged demands. Promising designs were selected and provided for the second level optimization, where the final component dimensioning was optimized based on monthly mean-day demands. Piacentino et al. [58] introduced an MILP-based methodology for maximizing NPV of CCHP systems for building clusters, which

[7] Flexible polygeneration systems refer to polygeneration systems according the definition by [124], which are designed for flexible short-term operation.
[8] CCHP systems are also referred to as trigeneration systems.

considered component selection and dimensioning, and operation optimization with respect to hourly energy demands, with the overall aim of maximizing the NPV of the system. However, none of the technologies considered process integration, long-term energy system development, and uncertainty analysis.

Distributed energy supply systems (DESS), which include distributed generation of energy services and integrated supply infrastructures, represent another type of FMGs treated in literature. Voll et al. [59] presented a methodology for designing DESS using an evolutionary algorithm, which considered the selection, location and operation of multiple processes for meeting local energy demands. Petruschke et al. [60] combined this methodology with a heuristic-based pre-selection of candidate technologies in a hybrid approach for designing DESS. Zhou et al. [61] presented a methodology for designing DESS based on a two-stage stochastic programming model, which accounted for selection, dimensioning, and operation optimization of combinations of equipment under uncertain operating conditions. Martínez Ceseña et al. [62] presented a DESS design methodology which considered initial design, flexible operation optimization, and investment planning in response to long-term uncertainty in external operating conditions. In addition, Leung Pah Hang et al. [63] presented an iterative methodology for designing local production systems based on a combined MILP/MINLP model and focusing solely on annual demands, with the aim of minimizing resource consumption by integrating food, water, and energy supply systems. However, a shortcoming of all listed DESS design methodologies with respect to designing FMGs is the fact that process integration is not considered.

2.3 Methodology comparison and discussion

Together, the design methodologies mentioned in the previous section represent current best-practices for designing various kinds of multi-generation systems. However, having different backgrounds and purposes, it is obvious that the individual design methodologies are concentrating on different design aspects.

Regarding FMGs as defined in the present work, the main hypotheses are that they may support the balancing of the electricity system through agile operation and integration with other energy sectors, whilst achieving high aggregated energy efficiency in the energy conversion through process integration. In order to design such FMGs, special attention must be given to the selection, dimensioning and integration of processes, as well as operational performance with respect to hourly variations and long-term trend

changes for multiple external operating conditions. Also, as FMGs are assumed to be capital intensive and owing to the fact that state-of-the-art technology may be considered in the designs, it is important to systematically assess performance variations in response to uncertainties in investment and operating cost and changes in operating conditions. Accordingly, five central design aspects have been identified for FMGs:

- Process selection and dimensioning
- Process integration
- Short-term operation (assessment of performance with respect to hourly, daily and seasonal changes in operating conditions)
- Long-term operation (assessment of performance with respect to long-term developments in the surrounding energy system)
- Uncertainty analysis (assessment of design robustness and resilience to changes in external operating conditions and estimated parameter values)

Table 2.1 offers an overview and comparison of how the listed design aspects have been included in the various design methodologies presented in Section 2.2. It can be seen that although all the listed methodologies involve many degrees of freedom, none of them incorporate all of the five listed design aspects coherently. The methodology presented by Maréchal et al. [51], including associated method developments [52–54], gets close by considering process selection, dimensioning and integration, and short-term operation optimization. However, the methodology was developed with focus on a single variable external operating condition, outdoor temperature, and systematic consideration of uncertainties was not included. The methodology presented by Martínez Ceseña et al. [62] was the only that considered both short-term variations for multiple external operating conditions as well as long-term energy system development. However, systematic process integration was not considered as focus was on delivering heat and electricity for domestic and commercial buildings, for which process integration synergies are somewhat limited.

In summary, the outcomes of the literature study indicate the relevance of developing a comprehensive methodology for designing FMGs that include systematic selection and dimensioning of processes, process integration, variations in multiple external operating conditions in both short-term and long-term perspective, and uncertainty analysis. Responding to this, a novel design methodology considering all these aspects coherently was developed in the project. The methodology is presented in Chapter 3.

Table 2.1: Comparison of selected design aspects considered in multi-generation system design methodologies presented in literature.

Methodology	Selection and dimensioning	Process integration	Short-term operation	Long-term operation	Uncertainty analysis
Chen et al. [49]	✓	(✓)[a]			
Chen et al. [23]	✓	(✓)[a]	✓		
Gassner and Maréchal [43]	✓	✓			
Gerber et al. [46]	✓	✓			
Leung Pah Hang et al. [63]	✓				
Liu et al. [39–41]	✓			✓	
Liu et al. [42]	✓			✓	✓[c]
Maréchal et al. [51–54]	✓	✓	✓	(✓)[b]	
Marnay et al. [55]	✓		✓		
Martínez Ceseña et al. [62]	✓		✓	✓	✓[c]
Petruschke et al. [60]	✓		✓		
Piacentino et al. [58]	✓		✓		
Rubio-Maya et al. [56,57]	✓		✓		
Voll et al. [59] [d]	✓				
Zhou et al. [61]	✓		✓		✓[c]

[a] Systematic thermal integration of processes was not considered.
[b] In theory, long-term developments in the energy system can be included using the method presented in [52]. However, only cyclic annual changes in outdoor temperature levels were considered in the case study used for verifying the method.
[c] Only uncertainties in operating conditions are considered.
[d] Static operating conditions were considered for each month of the year.

3 METHODS

This chapter introduces the theory behind the methods developed as a part of the project. First, a method for aggregating external operating conditions is introduced and verified. Second, the overall methodology for designing FMGs is presented. The design methodology is verified through two case studies presented in Chapter 4. For a practical example of how the design methodology was implemented, refer to Appendix K.

3.1 The CHOP Method: A novel method for aggregating external operating conditions when designing multi-generation systems[9]

3.1.1 Background and novelty

A fundamental issue in mathematical optimization models is the trade-off between the level of detail and ease of solving the model. In optimization models for designing multi-generation systems, it is especially relevant to reduce the number of periods used for describing variable external operating conditions (EOCs[10]) as the complexity of multi-period optimization models increases significantly with the number of periods considered [64]. In effect, several methods for reducing EOC data have been presented in literature.

Common methods for reducing EOC datasets in multi-generation design optimization models can be divided into three groups: *Chronological period approaches*, *representative period approaches*, and *characteristic period approaches*.

Chronological period approaches involve the clustering of EOC conditions in chronological and sequential time-periods. Advantages with these methods are that they may reduce the EOC datasets substantially while sustaining long-term time chronology between

[9] This section is based on the article 'A method for aggregating external operating conditions in multi-generation system optimization models' [36].
[10] EOCs may include any external condition that affects the operation of a given system, e.g. power price, wind profile, heating demands, etc.

periods. Drawbacks include the facts that information on short-term variations and correlations between EOC parameters are lost in the averaged datasets, and that peak values and extreme combinations of EOC parameter values may be hidden unless specifically accounted for. Examples of chronological period approaches are listed below:

- Yearly averaging [39,41,65]
- Monthly averaging [56,57,66,67]
- Sequential time-slice averaging[11] [68,69]

Representative period approaches focus on identifying a small number of time series that can be repeated a number of times in order to approximate the initial EOC dataset. These time series, called representative periods, are often selected from historical data using either heuristic approaches or clustering algorithms. Advantages of these methods are that short-term variations and correlations in EOCs plus time chronology are sustained within the representative periods, allowing for the inclusion of dynamic constraints and storages in the design optimization models. However, representative period approaches rely on the assumption that EOC conditions are cyclic and repetitive, an assumption that may prove inaccurate in energy systems with large shares of variable RES. In addition, information on peak values and extreme combinations of EOCs are not necessarily sustained in the representative periods, potentially leading to significant errors in peak operation performances as also reported by Fazlollahi et al. [52]. A promising optimization approach for selecting representative days which addresses the listed shortcomings is currently being developed by Poncelet et al. [70], but a drawback reported by the authors is the fact that the selection-optimization itself is computationally expensive. Examples of representative period approaches are listed below:

- Typical weeks [71]
- Typical days [52,72,73]

Characteristic period approaches focus on aggregating operating points in a number of pre-defined characteristic period clusters, which then replace the initial operating points in a design optimization model. For each characteristic period, the associated EOC parameter values are defined by the average values of the clustered operating points,

[11] In these methods, load profiles are sliced into sequential periods of variable lengths. Nemet et al. [68] use an MILP model for determining number and duration of time-slices in order to achieve a certain level of accuracy in the reduced dataset, while Bungener et al. [69] exploits an evolutionary algorithm for slicing up annual load profiles into *n* sequential time-slices.

while the weight of each characteristic period is the aggregated duration of the clustered operating points. Characteristic period approaches may reduce EOC datasets significantly while allowing for considering both common and rare combinations of EOCs. However, information on time chronology is lost in the reduced EOC datasets unless the operating conditions are cyclic. Examples of characteristic operation approaches are listed below:

- Seasonal peak/off-peak period averaging [23,74]
- Monthly mean-days [56,57,75]
- TimeSliceTool[12] [76]

As discussed in Chapter 2, it is important to consider daily, weekly and seasonal EOC variations as well as long-term trend changes in EOCs when designing FMGs. Keeping this in mind, chronological period approaches were not considered advantageous in an FMG design methodology as an excessive number of periods would need to be defined. Similarly, a representative period approach would expectedly result in an excessive number of periods in case long term energy system development and extreme combinations of operating conditions should be included. Regarding characteristic period approaches, the methods listed above either assumed cyclic operating conditions [23,56,57,74,75] or neglected variations and differences within non-critical operating conditions [76]. Together, these reflections motivated the development of a novel method for reducing EOC datasets which could sustain information on common as well as rare operating conditions, non-cyclic energy system characteristics, hourly variations, and long term trend changes in the reduced datasets.

The developed method is named the *characteristic operating pattern (CHOP) method*, and it is an original *characteristic period* data aggregation method for reducing EOC datasets. In the CHOP method, reference operating points are clustered based on values of, and correlations between, relevant EOC parameters rather than time chronology, meaning that information on parameter value correlations is sustained in the reduced dataset. In addition, the method allows for clustering of operating points throughout the entire operating period considered, allowing for significant reductions in dataset sizes in case correlations between parameter values are similar for multiple operating points. The combination of these two aspects represents the novelty of the CHOP method.

[12] The TimeSliceTool sorts annual operating points into groups for four critical combinations of EOC parameter values for work and non-work days in each of the four seasons. In total, this results in 32 characteristic periods per year.

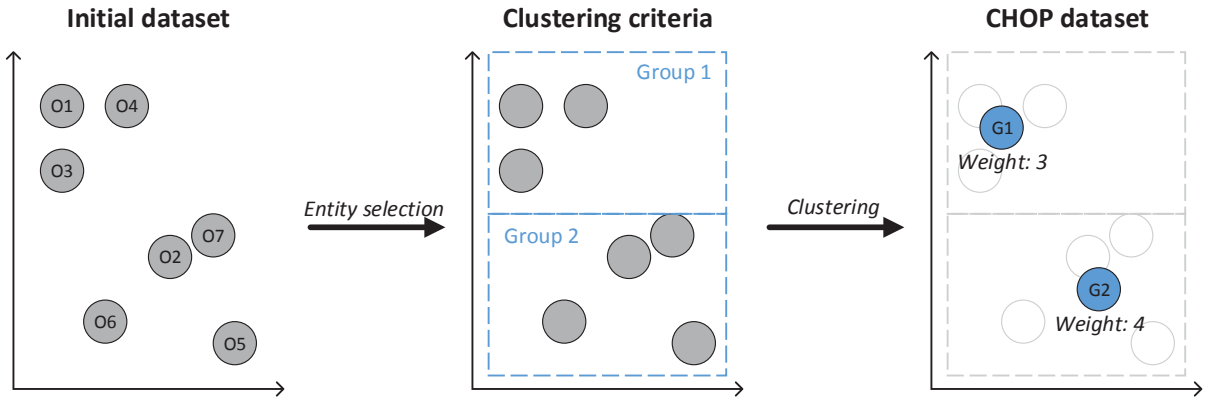

Figure 3.1: Sketch of the data aggregation principle applied in the CHOP method. Operating points $\boldsymbol{O_i}$ are clustered and merged into CHOP groups $\boldsymbol{G_j}$ with aggregated weight factors.

A preliminary version of the CHOP method was introduced in Lythcke-Jørgensen et al. [77], while the final method was presented in Lythcke-Jørgensen et al. [36]. The overarching data aggregation principle used in the CHOP method is illustrated in Figure 3.1.

3.1.2 Method overview

The CHOP method is applicable on EOC datasets in the form of operating points O_i. Each operating point is characterised by a year of occurrence within the period considered Y_i, a duration t_i[13] and a vector $\boldsymbol{p_i}$ which includes the values of all EOC parameters $\boldsymbol{p}$ in point O_i.

$$O_i = \{Y_i, t_i, \boldsymbol{p_i}\} \tag{3.1}$$

The ambition of the CHOP method is to convert the initial dataset of operating points into a reduced CHOP dataset, which consists of a number of CHOP groups G_j characterised by a duration t_j, a present value factor PV_j, and an EOC parameter value vector $\boldsymbol{p_j}$.

$$G_j = \{t_j, PV_j, \boldsymbol{p_j}\} \tag{3.2}$$

To make this conversion, the CHOP method involves a number of steps that are divided into two procedures: Data-aggregation, which is the core of the method, and error analysis. The overall method sequence is illustrated in Figure 3.2. For a step-by-step walk-through of the CHOP method plus an example of application, refer to Appendix D [36].

[13] Durations of 1h or less are generally recommended for reference operating points in order to properly include information on short-term variations and correlations of EOC parameters values.

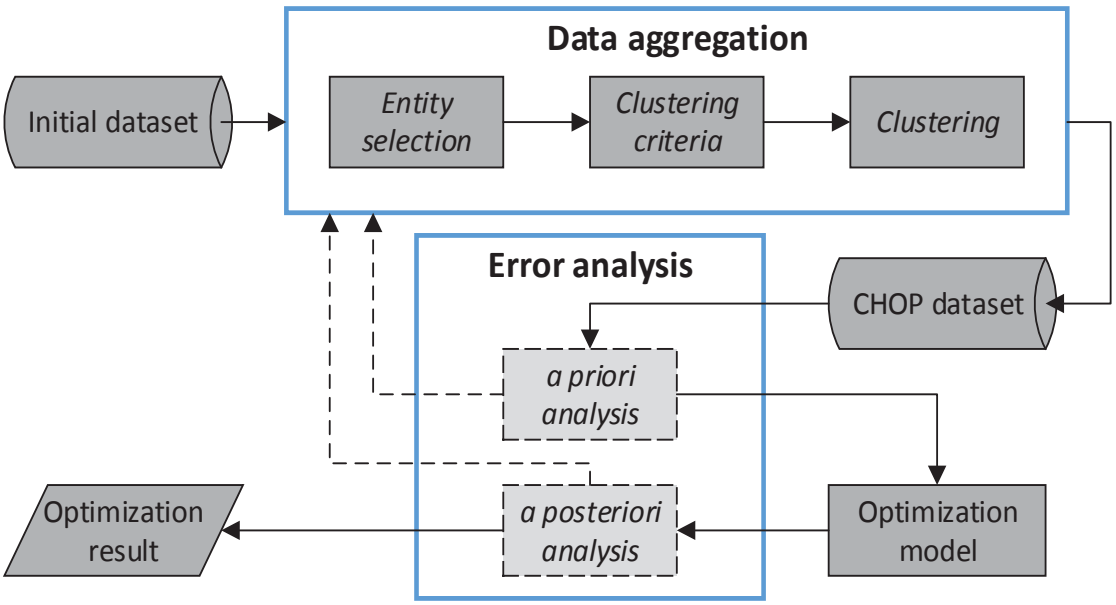

Figure 3.2: Overall sequence of the CHOP method [36].

Entity selection

The first step in the CHOP method is to select the relevant and varying EOCs which the clustering procedure is to be based upon. This implies (1) identifying relevant EOCs for the system of interest, and (2) assessing the parameter value variations of the identified EOCs.

(1) *Identification of relevant EOCs*: Within the CHOP method, a relevant EOC is defined as a boundary condition that may influence, but are hardly influenced by, operation decisions on plant level. For a small scale natural gas-based power plant, the electricity and natural gas prices would be relevant EOCs as these conditions affect, but are little affected by, the operation of the plant. Opposed to this, the wind profile could be an example of a non-relevant EOC.

(2) *Assessment of EOC variations*: Based on the reference dataset, the maximum, minimum and mean parameter values for the identified relevant EOCs are calculated. In order to reduce the size of the final CHOP dataset, it is recommended that only relevant EOCs with parameter value variations higher than $\pm 10\%$ of the period mean are considered in the clustering procedure.

The potential error made by not including relevant EOCs with variations below $\pm 10\%$ in the clustering procedure can be assessed as a part of the *posteriori* error analysis.

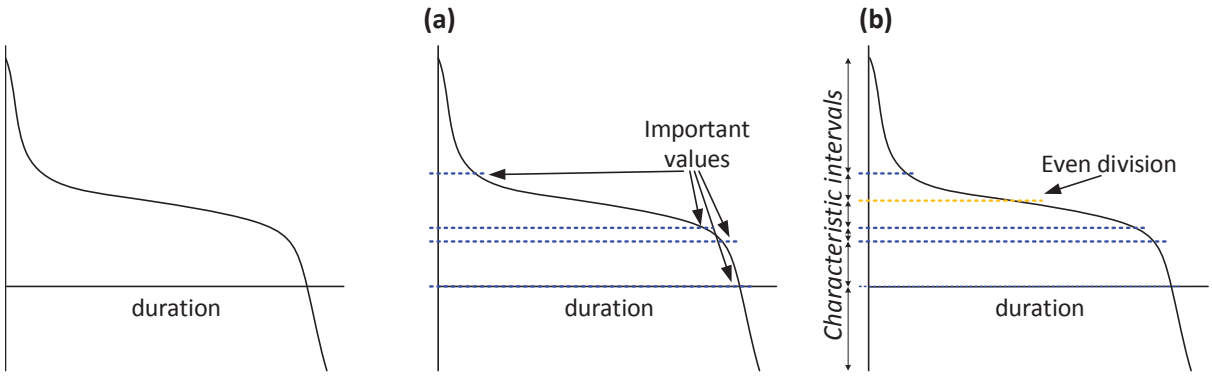

Figure 3.3: Illustration of the suggested two-step approach for defining characteristic intervals based on the cumulative value curve for a relevant and varying EOC (left). Interval break points are set for a) important values, and b) even division. The characteristic intervals are indicated by arrows on the second axis in b) [36].

Clustering criteria

Having identified the relevant and varying EOCs, the next step is to define the criteria for clustering operating points. This is done by splitting the parameter value range of the relevant and varying EOCs into a number of characteristic intervals. Being empirical in essence, the following two-step approach based on the cumulative EOC value curve is recommended for defining interval break points. The process is illustrated in Figure 3.3.

(1) *Important value breaks*: Certain parameter values may be of special interest, making it relevant to introduce interval breaks at these points. For the natural gas-based power plant, an important value for the electricity price could be the price at which electricity generation changes from being competitive to being uncompetitive under the set conditions.
(2) *Even division breaks*: If the already set break-points are far from each other in terms of both parameter value and duration, it is suggested that additional interval breaks are introduced to minimize the span. The break-points should be located so that the parameter value range is constant for each of the intervals.

The combined characteristic parameter intervals for an EOC must span all values included in the initial dataset. The number of intervals defined for each parameter may vary according to parameter value volatility, parameter significance, and available data. In the CHOP method, the quality of the defined characteristic intervals may be assessed as a part of the error analysis. Note that if only one characteristic interval is defined for a relevant and varying EOC, the EOC will be included as a constant in the final CHOP dataset and not be considered directly in the clustering procedure.

Clustering

The last step in the data aggregation procedure is the clustering, in which the aggregated CHOP groups are defined and the resulting CHOP dataset is obtained.

Any combination of characteristic parameter intervals for the relevant and varying EOCs is defined as a *potential CHOP group*. Denoting relevant and varying EOCs by rv and the number of characteristic parameter intervals defined for an rv by n_{rv},, then the number of potential CHOP groups in a dataset $N_{CHOP,pot}$ is given as

$$N_{CHOP,pot} = \prod_{k} n_{rv,k} \tag{3.3}$$

To maintain an overview, it is recommended that CHOP groups are indexed as

$$G_j = G\left(i_{1,j}, i_{2,j}, \dots, i_{N_{rv},j}\right) \tag{3.4}$$

In the equation, G_j is short for CHOP group, and $i_{k,j} \in \{1,2, \dots, n_{rv}\}$ is the characteristic interval number of rv associated with the specific CHOP group G_j. For example, if $N_{rv} = 2$, $n_1 = 4$ and $n_2 = 5$ in a CHOP dataset, then $G(2,5)$ refers to the CHOP group representing the combination of 'rv_1*, characteristic interval 2*' and 'rv_2*, characteristic interval 5*'.

Having defined the potential CHOP groups G_j, all operating points $O_i = \{Y_i, t_i, \boldsymbol{p_i}\}$ from the initial dataset are sorted into the groups:

$$O_i \in G_j \quad | \quad \boldsymbol{p_{rv,i}} \in \boldsymbol{i_{rv,j}} \tag{3.5}$$

Empty CHOP groups are excluded from the final CHOP dataset. The final number of CHOP groups N_{CHOP} may therefore be lower than the number of potential CHOP groups:

$$N_{CHOP} \leq N_{CHOP,pot} = \prod_{k} n_{rv,k} \tag{3.6}$$

Combining equation (3.5) and (3.6), it is evident that the final number of CHOP groups defined will never exceed the number of operating points in the initial dataset. In contrast, if the correlations between relevant and varying EOC parameter values are similar for multiple operating points, the CHOP dataset may be significantly smaller than the initial

dataset. In consequence, the optimization model to be solved will be less computationally expensive when the resulting CHOP groups replace the initial dataset of operating points.

For all non-empty CHOP groups G_j, the duration t_j and present value PV_j are calculated as the sum of durations t_i and present value factors PV_i of the clustered operating points O_i, while the parameter values $\boldsymbol{p_j}$ are calculated as the duration-weighted average of the parameter values in the clustered operating points.

$$G_j = \{t_j, PV_j, \boldsymbol{p_j}\}, \quad G_j \neq \emptyset \tag{3.7}$$

$$t_j = \sum_{O_i \in G_j} t_i \tag{3.8}$$

$$\boldsymbol{p_j} = \frac{\sum_{O_i \in G_j} \boldsymbol{p_i} \cdot t_i}{t_j} \tag{3.9}$$

$$PV_j = \sum_{O_i \in G_j} PV_i = \sum_{O_i \in G_j} t_i \frac{1}{(1+r)^{Y_i}} \tag{3.10}$$

In equation (3.10), r is the interest rate applied for calculating the present value of money. The fact that $\boldsymbol{p_{rv,i}} \in \boldsymbol{i_{rv,j}} \ \forall \ O_i \in G_j$ illustrates one of the main advantages of the CHOP method: Correlations between relevant and varying EOC parameter values, $\boldsymbol{p_{rv,i}}$, are sustained in the reduced CHOP dataset within a level of accuracy defined by the set characteristic intervals. The maximum error made by averaging over relevant and varying EOC parameter values in Equation (3.9) can be assessed as a part of the error analysis.

Error analysis

Error analysis is a central part of the CHOP method, as it is used to assess the quality of, and provide feedback to, the applied data aggregation procedure. Error analysis may be conducted both *a prior* as well as *a posteriori*, and it must be stressed that error analysis is necessary in order to verify any optimization results obtained using a CHOP dataset. However, as the choice of error analysis may be case specific, the CHOP method itself does not include a specific approach to error analysis. In Lythcke-Jørgensen et al. [36], the following three suggestions for relevant error analyses were presented and demonstrated in a case study:

- *A priori*: Standard deviation assessment of CHOP group parameters to assess the correlated spread of parameter values within each characteristic intervals.
- *A posteriori*: Sensitivity analysis of CHOP clustering criteria for assessing if additional interval breaks are required.
- *A posteriori*: Error analysis of neglecting a relevant EOC with parameter value variations below the arbitrarily set value of $\pm 10\%$ in the clustering procedure.

3.1.3 Method verification and constraints

The CHOP method was verified in Lythcke-Jørgensen et al. [36] through a case study, which treated the operation optimization of a fictive Danish extraction-based combined heat and power (CHP) unit for hourly time steps over a five-year period. The main sequence and case outcomes are presented and discussed in this section. For additional information on the process modelling, reference dataset, data aggregation approaches, and operation optimization models, refer to Appendix D [36].

Optimization models

A linear CHP unit operation model was developed based on a detailed thermodynamic model of the Danish extraction-based CHP unit Avedøreværket 1 [78], which was validated in [20,79]. The heat and electricity generation boundaries for the reference and linearized CHP unit models are illustrated in Figure 3.4. The CHP unit operation was constrained by the district heating demand, which had to be met by the unit at all times.

Two different operation optimization models were developed:

(1) Operation optimization without thermal storage.
(2) Operation optimization with thermal storage.

The optimization objective of both models was to minimize the total operating costs. In the first optimization model, the heat generation of the CHP unit had to equal the district heating demand at all times, while the inclusion of thermal storage in the second model allowed for shifting of heat generation. The thermal storage capacity was set to 8 GWh, equivalent to 24 hours of peak heat generation. The CHP unit was not allowed to shut down at any time, and no ramp constraints were considered in the optimization models.

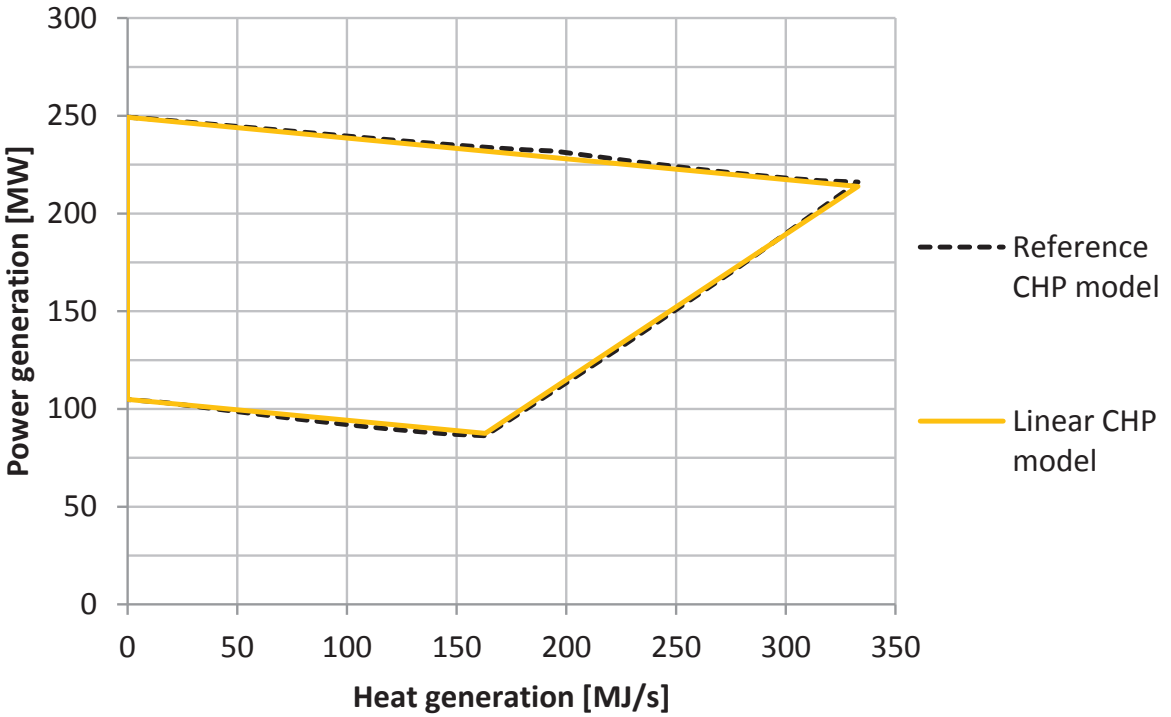

Figure 3.4: Feasible heat and electricity generation range of the reference and linearized CHP plant models [36].

External operating condition datasets

The operation optimization was conducted for hourly operating points over the period 2010-01-01 – 2014-12-31. Three relevant EOC parameters were identified for the CHP unit: Fuel price (coal price), electricity price, and district heating demand. The coal price was not included as a relevant and varying EOC parameter in the CHOP method as variations over the period were limited, i.e. within $\pm 10\%$.

Five different reduced EOC datasets were considered:

- Yearly averaged EOCs (*chronological period method*)
- Monthly averaged EOCs (*chronological period method*)
- Seasonal peak/off-peak averaged EOCs (*characteristic period method*)[14]
- CHOP dataset (no feedback from error analysis)
- Revised CHOP dataset (feedback from two different error analyses, one iteration)

[14] Method described by Chen et al. [23]: EOC parameter values are averaged over peak periods (7 a.m.-11 p.m.) and off-peak periods (11 p.m.-7 a.m.) in every season for all years considered.

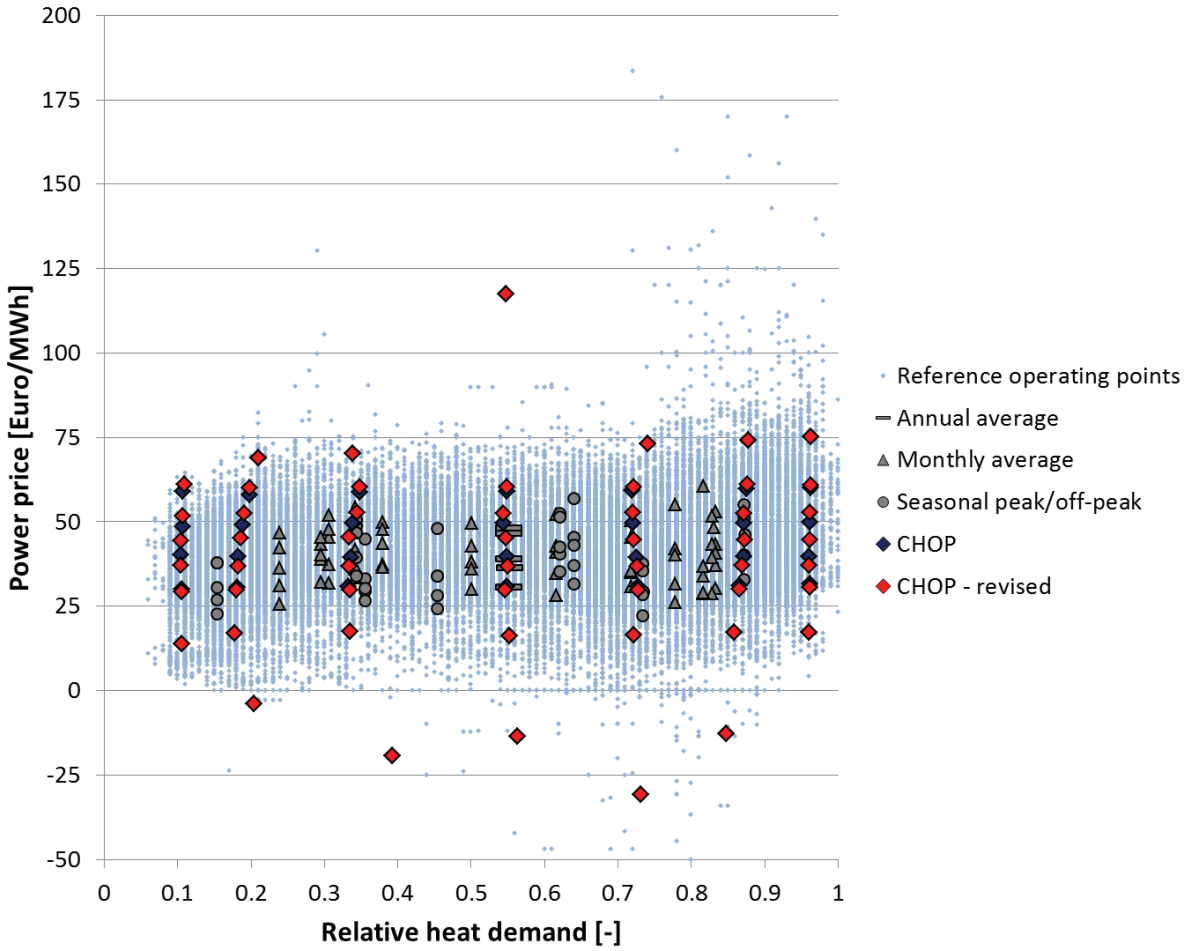

Figure 3.5: Scatter diagram showing operating points of the initial dataset, annually averaged dataset, monthly averaged dataset, seasonal peak/off-peak averaged dataset, CHOP dataset, and revised CHOP datasets [36]. Note that some of the CHOP and revised CHOP operating points are overlapping and that a few of the reference operating points are outside the electricity price boundaries of the plot.

The CHOP dataset was developed using only the two-step approach for defining clustering criteria as presented in Section 3.1.2. The revised CHOP dataset was developed by applying *posteriori* sensitivity analysis of the clustering criteria on the CHOP dataset and using outcomes for revising the clustering criteria. Documentation of the development of reduced EOC datasets can be found in Appendix D [36].

A scatter plot of reference and resulting operating points for all applied EOC datasets is shown in Figure 3.5. It was found that all resulting operating points of the yearly, monthly, and seasonal peak/off-peak averaged EOC datasets were well within the dense cloud of initial operating points. Opposed to this, the resulting operating points of the CHOP and the revised CHOP datasets are markedly more distributed, indicating that a larger degree of the parameter correlation diversity of the initial dataset is sustained.

Table 3.1: Optimization results obtained from solving the optimization model without thermal storage when applying each of the six different EOC datasets.

	Initial dataset	Yearly averaged	Monthly averaged	Seasonal peak/off-peak	Initial CHOP	Revised CHOP
Economic results						
Operating costs (M€)	0.38	8.53	8.02	5.96	0.76	0.37
Electricity sales (M€)	368.06	369.51	376.62	370.41	356.12	365.81
Fuel costs (M€)	368.44	377.81	384.64	376.38	356.88	366.18
Operation results						
Total heat generation (GWh)	8066	8066	8066	8066	8066	8066
Total electricity generation (GWh)	8664	8958	9161	8907	8309	8594
Total fuel consumption (GWh)	23,460	24,057	24,492	23,966	22,724	23,317
Optimization problem						
Number of periods	43,824	5	60	40	46	53
Variables per period	2	2	2	2	2	2
Constraints per period	4	4	4	4	4	4

Operation optimization without thermal storage

The results obtained from solving the optimization model with the initial dataset and each of the five reduced EOC datasets considered are presented in Table 3.1. The exact solution to the optimization model without thermal storage was obtained using the initial dataset, where the total CHP unit operating costs were found to be 0.38 M€.

Comparing the results obtained using the reduced datasets, it is seen that the total operating costs obtained when using the yearly averaged, monthly averaged, and seasonal peak/off-peak averaged EOC datasets deviated by 5.58M€-8.15M€ from the exact solution. In contrast to this, the operating cost result when using the initial CHOP dataset deviated by 0.38M€, while a deviation of 0.01M€ was obtained using the revised CHOP dataset.

For the yearly averaged, monthly averaged, and the seasonal peak/off-peak averaged EOC datasets, the deviations in economic results were found to be caused by increases in electricity generation of 2.8%-5.7% and in fuel consumption of 2.2%-4.4% when compared to the exact solution, while the increases in income from additional electricity sales, 0.4%-

2.3%, were exceeded by the increases in fuel costs of 2.2%-4.4%. This trend was caused by the fact that operating points with low electricity prices, for which electricity generation would be minimized in the reference case, were often included in clustered periods where the average electricity prices led to maximization of the electricity generation in the optimization. The opposite trend, where electricity generation was minimized for operating points where it would be maximized in the reference case, was also found to occur when using these reduced datasets, but to a minor extent than the electricity maximizing trend.

For the initial CHOP dataset, the electricity generation and fuel consumption were found to be reduced by 4.1% and 3.1% when compared to the reference solution, while the reductions in fuel costs, 3.2% and incomes from electricity sales, 3.1%, were almost identical in absolute terms. Combined, these outcomes led to a deviation in operating costs of 0.38M€ from the exact solution. The explanation is that in the CHOP method, the operating points merged in the CHOP groups had similar correlations and parameter values for the relevant and varying EOCs. Hence, the averaged electricity price for the resulting CHOP groups was close to the electricity prices of the clustered operating points. In consequence, if the electricity generation was minimized over an operating point where it would be maximized in the reference case, or vice versa, the economic difference would be small. Opposed to this, the deviations in electricity generation and fuel consumption were found to be significant and in magnitude comparable to the deviations obtained using the yearly averaged, monthly averaged, and seasonal peak/off-peak averaged EOC datasets. This suggested that the data aggregation could be optimized further.

For the revised CHOP dataset, total electricity generation and fuel consumption deviated by less than 1% when compared to the exact solution, while the operating cost result was practically identical to that of the exact solution. As mentioned, the revised dataset was developed using feedback from error analysis for revising the clustering criteria. The fact that the results obtained using the revised CHOP dataset have a markedly higher accuracy than the results obtained using the initial CHOP dataset illustrate the relevance of including error analysis when using the CHOP method for reducing EOC datasets.

Considering the optimization problem size, the revised CHOP dataset offered a reduction in number of periods by a factor 827, which was comparable to the reductions of a factor 730 when using monthly averaged dataset and a factor 1096 when using the peak/off-peak averaged dataset. The combination of increased accuracy and similar reductions in

dataset size illustrate the advantage of using the CHOP method over the yearly averaging, monthly averaging, and seasonal peak/off-peak averaging methods for reducing EOC datasets in energy systems with fluctuating operating conditions.

Operation optimization with thermal storage

The optimization model that included thermal storage was solved using the initial EOC dataset and the revised CHOP dataset in order to assess the drawback of losing information on time chronology. The physical dimension constraints of the storage could not be considered when solving the optimization model using the CHOP dataset as they required knowledge on time chronology to be included, and they were consequently slacked when solving the model. The optimization results are summarized in Table 3.2.

First of all, it was found that when solving the optimization problem using the initial dataset, the total operating costs became negative, illustrating the economic advantage of including short-term thermal storages in CHP units. This complies with outcomes reported in literature, e.g. [80,81]. It was found that that the electricity generation was slightly reduced while incomes from electricity sales were increased when comparing to the solution without heat storage, owing to the fact that the thermal storage allowed for a more flexible operating pattern.

Table 3.2: Optimization results obtained from solving the optimization model including thermal storage.

	Initial dataset	Revised CHOP[a]
Economic results		
Operating costs (M€)	-6.08	-8.06
Electricity sales (M€)	372.50	357.04
Fuel costs (M€)	366.42	348.97
Operation results		
Total heat generation (GWh)	8066	8066
Total electricity generation (GWh)	8602	8066
Total fuel consumption (GWh)	23,332	22,221
Optimization problem		
Number of periods	43,824	53
Variables per period	2	2
Constraints per period	6	4

[a] Note that the physical dimension constraints of the thermal storage were slacked when solving the optimization model using revised CHOP dataset.

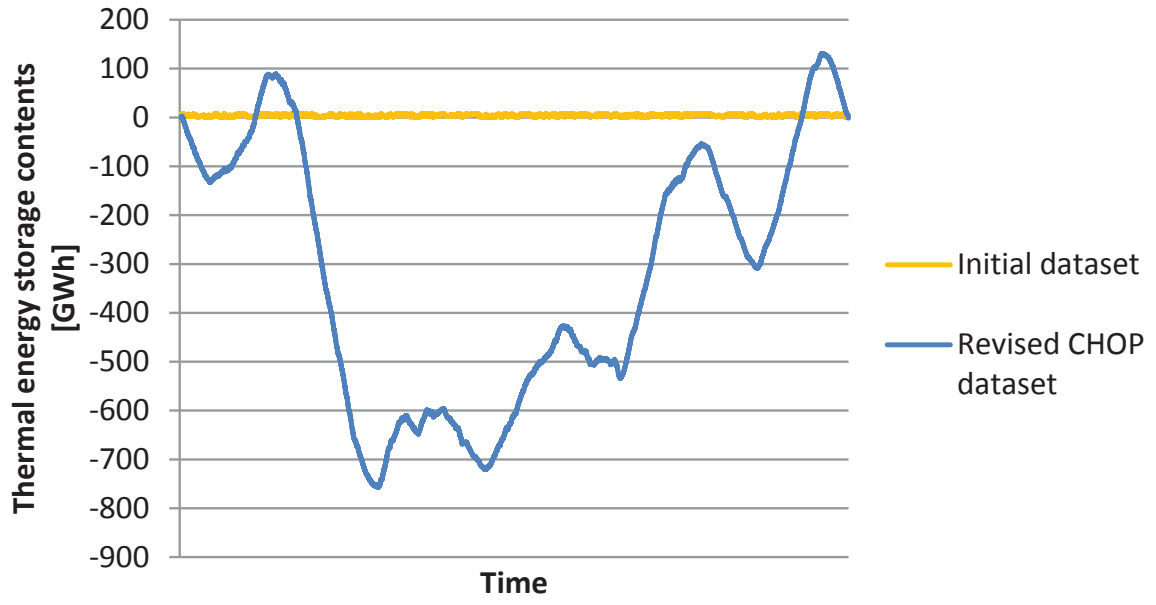

Figure 3.6: Thermal energy storage contents over the 5-year period in the solutions to the optimization model with thermal storage, obtained using the full EOC dataset and the revised CHOP dataset [36].

Secondly, it was found that the operating costs obtained when using the revised CHOP dataset were even lower than the exact solution obtained using the initial EOC dataset, suggesting that infeasible operating patterns where obtained. Applying the optimal operation pattern predicted by the CHOP solution on the initial EOC dataset, the resulting energy content in the thermal storage was calculated for each hour over the 5-year period. The results are presented in Figure 3.6, together with the results from the solution obtained using the initial dataset.

It was found that the CHOP solution significantly violates the physical capacity constraint of 8GWh of the thermal storage, and in addition resulted in negative storage contents for the majority of the period. This was caused by the fact that when the storage dimension constraints were slacked while the only constraint on heat generation was that it had to meet the aggregated consumption over the entire period. In effect, heat generation could be shifted freely over the entire period. Since electricity prices on average were higher in the first two years of the period, electricity generation was maximized at the cost of heat generation in 2010 and 2011, while excess heat was generated the following years. The graph also illustrate how additional heat was generated over the summer periods when the heat demand was low, and then stored for use in the winter when the heat demand was high. Though highly intuitive, this solution is infeasible in practice. This result illustrates the drawback of not considering dynamics in the CHOP reduced dataset.

Apart from this, the thermal storage results also illustrate the fluctuating nature of the initial EOC dataset. Had the dataset indeed been cyclic over days, months, peak/off-peak seasons or years, a cyclic storage content pattern would have been obtained using the CHOP dataset. This outcome illustrates how operating conditions can be non-cyclic and thereby supports the relevance of capturing non-cyclic trends in reduced EOC dataset.

3.1.4 Discussion

A main advantage of the CHOP method is the fact that it captures and sustains correlations between operating condition parameters in the reduced dataset. This is assumed to be of special relevance for flexible technologies operated in energy systems with large shares of variable renewable energy sources, where failing to account for the variability in operating conditions may lead to underestimations of the value of flexibility as also discussed by Poncelet et al. [70]. The advantage of sustaining information on short-term parameter correlations in the reduced dataset can be highlighted by the reduced datasets in the case: If the operation optimization instead of a CHP unit had treated an unspecified process with no dynamic constraints that would be competitive for electricity prices below 25.00 €/MWh, the process would not be operated at any point if annual or monthly averaged datasets were applied in the operation optimization. In case the peak/off-peak averaged dataset was applied, the process would be operated for 2192 hours over the five year period, while, it would be operated for 4550 hours, more than 10% of the period, if the CHOP dataset or the reference dataset were applied.

For the simple operation optimization example of a CHP unit without thermal storage, it was demonstrated how the optimization results obtained using the revised CHOP dataset were significantly more accurate than the results using any of the other reduced datasets, while reduction in optimization problem size was comparable for the CHOP, the monthly averaged, and the peak/off-peak averaged datasets. The combination of high accuracy and significant reduction in dataset size support the proposition that the CHOP method is relevant for reducing operating condition datasets in FMGs design optimization models.

In addition to this, another advantage of the CHOP method is the fact that larger initial datasets do not necessarily yield larger reduced datasets. In the case study, hourly heat demand and electricity price data were considered for a 5-year period. If the period considered was extended to a 30-year period, the number of data points would be multiplied by six for each of the three methods used for comparison, while it is likely that

the number of CHOP groups would not need to be changed. Instead, the weight given to each of the CHOP groups would increase as additional data points would be sorted into the groups. Note that it is likely that the increase in weight will not be the same for all CHOP groups due to non-cyclic trends and long term development of the energy system.

A curiosity of the CHOP method is the fact that in case a set of operating conditions indeed were cyclic over the monthly or yearly periods, such trends would be captured by the CHOP method in a dataset that in size would be smaller than or equal to the size of any dataset obtained using chronological period approaches. The same argument can be used for the seasonal peak/off-peak averaging method, suggesting that the CHOP method would be preferable over the averaging methods even for cyclic operating conditions[15]. The exception is if storages or dynamic constraints were to be considered, in which case it would be useful to use a representative period approach instead.

A significant shortcoming of the CHOP method is the fact that it does not allow for considering dynamic constraints and time chronology. This implies that ramp constraints and storages cannot be considered, potentially leading to infeasible or suboptimal operating patterns as discussed in the case study as well as in literature, e.g. [80–82]. One may say that while other methods for reducing EOC datasets may lead to underestimating operation variability, the CHOP dataset may lead to overestimating operation variability as operation shifting and smoothing through storages cannot be considered. Also, scheduling and investment planning cannot be considered. However, the latter can be solved by setting a time-span for investment planning, e.g. 5 years, and then derive a CHOP dataset for every 5-year period. However, this would increase the size of the resulting dataset.

Another potential drawback of the CHOP method is fact that the number of potential CHOP groups is combinatorial, meaning that the number will grow exponentially with the number of relevant and varying EOCs considered. How this affects the size of the resulting CHOP dataset depends on the correlation similarity between the initial operating points, but it is advised that the number of relevant and varying EOCs is minimized.

Finally, a drawback of the CHOP method as well as any other method for reducing EOC datasets is the fact that they are based on marginal analysis, and consequently assume that the surrounding energy system and related markets are infinite and unaffected by

[15] Datasets obtained would be smaller for cases where multiple chronological periods have comparable parameter correlations which would allow them to be merged in the same CHOP groups.

operation. In the CHOP method, this assumption is addressed by only allowing conditions that are assumed little affected by plant operation to be included in EOCs. This approach is assumed to yield robust results [83], but it also implies that system impact of FMG operation cannot be considered directly when using the CHOP method.

In summary, it is recommended that CHOP datasets are used in overall screening for promising FMG designs as they may offer significant reductions in EOC dataset size while sustaining parameter value correlations. Operation optimization that considers dynamics and time chronology can then be conducted for a number of promising design solutions in a sequential step. Also, it should be noted that the CHOP method was particularly developed for the use in combination with the OSMOSE tool[6]. However, it may as well be relevant for other models and tools, e.g. the TIMES model [35].

3.2 A methodology for designing flexible multi-generation systems[16]

3.2.1 Background and novelty

The state-of-the-art review presented in Chapter 2 indicated the relevance of developing a methodology for designing FMGs that coherently considers selection and dimensioning of processes, process integration, variations in multiple EOCs in both short-term and long-term perspective, and uncertainty analysis. Answering to this, a methodology for designing FMGs was developed in this project, which combines previously developed and verified methods and tools: The CHOP method [36]; the OSMOSE tool[6] [44]; and an uncertainty analysis methodology that combines extended Morris screening [84,85] and a Monte Carlo simulation procedure [85]. The design methodology is presented in this section. For full documentation of the methodology, refer to Appendix E [19].

3.2.2 Methodology overview

The purpose of the developed methodology is to conduct quick and reliable pre-feasibility analyses of FMG concepts, focusing on identifying advantageous designs for a given energy system context rather than estimating the optimal performance of a pre-designed FMG. The methodology coherently considers: Selection, location, and dimensioning of

[16] This section is based on 'A methodology for designing flexible multi-generation systems' [19].

processes from many alternatives; systematic heat and mass integration using pinch analysis; flexible operation optimization with respect to both short-term market fluctuations and long-term energy system development through the application of the CHOP method; investment planning; global sensitivity and uncertainty analysis; consideration of local resource availability, biomass supply chains, and market sizes; variable part-load performance; and multi-objective optimization considering net present value (NPV) and 100-years global warming potential (GWP100a) as objectives. In effect, the methodology incorporates all five relevant design aspects listed in Section 2.1, which is seen as the main advantage. This coherent design optimization considering variable EOCs as well as local conditions is a main novelty of the design methodology.

The developed design methodology is a tool for optimizing the design and operation of FMGs by coupling process models with energy system information. In addition, it may be used for comparing or benchmarking the performance of various energy conversion technologies in a given energy system context. A preliminary version of the design methodology was introduced in Lythcke-Jørgensen et al. [77], while the final methodology was presented in Lythcke-Jørgensen et al. [19]. The sequence of the design methodology is presented in Figure 3.7, which illustrates how the optimization problem has been decomposed into several parts. The contents of these parts are described below.

Input data

Four types of input data are required for running the design methodology: *Process and equipment models*, *energy system data*, *local resource data*, and *life cycle inventory data*.

Process and equipment models: Models of all considered processes must be provided. The models can be detailed thermodynamic and chemical models as well as simpler black box models, as long as they provide the information required for developing surrogate models.

Energy system data: This data corresponds to relevant EOCs for the processes considered, and must be provided in the form of operating points as discussed in Section 3.1.2.

Local resource data: This data is required to describe the availability, costs, and logistics of local resources considered for processing, e.g. biomass, manure, domestic, and industrial waste etc. This information may be important for the economic and environmental performance of FMGs when processing distributed biomasses due to diseconomy-of-scale for transportation costs, as also discussed by e.g. Jack [86].

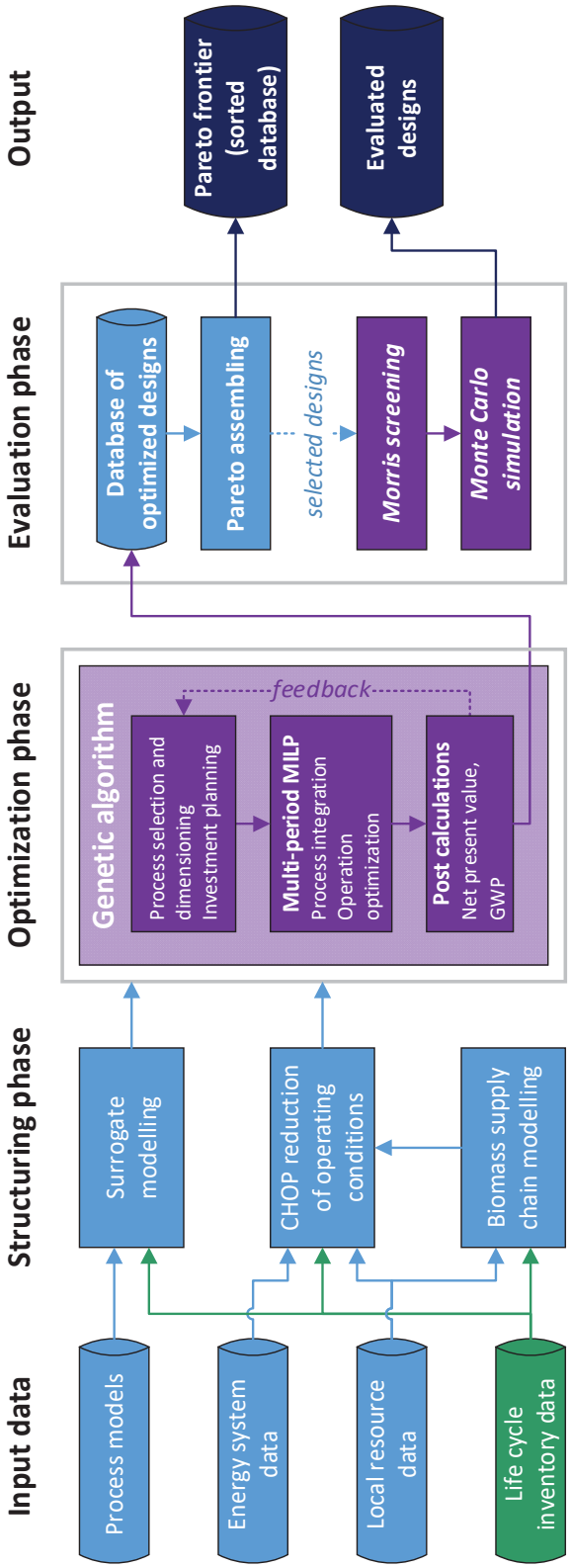

Figure 3.7: Structure and sequence of the developed design methodology. Note that an MILP algorithm is used for optimizing process integration and operation within the genetic algorithm optimization [19].

Life cycle inventory data: The 100-years global warming potential (GWP100a) was chosen as environmental impact parameter in the optimization due to its intuitive interpretation and straight-forward implementation. GWP100a indicates the global warming impact, in equivalent tons of CO_2 emissions, over a 100-year period from mining, production of equipment, installation, operation and maintenance, and decommissioning of a facility. GWP100a data must be provided for all considered resources, process equipment, displaced production, consumption, etc.

Structuring phase

In addition to the *CHOP reduction* of EOC datasets, the structuring phase involves two steps: S*urrogate modelling*, and *biomass supply chain modelling*, which are briefly explained below.

Surrogate modelling involves the conversion of reference process models into step-wise linearized surrogate models which are compatible with the OSMOSE tool[6]. The development of surrogate models is by default conducted by the user. However, the OSMOSE tool may apply thermodynamic and chemical process models developed directly from specific software [44].

In the optimization sequence, a surrogate model S is described by a dimension σ_S and the load at a time j, $\lambda_{S,j}$. The investment cost $C_{inv,S}(\sigma_S)$ for a surrogate process model S is calculated based on a reference investment cost $C_{inv,S0}$, a reference dimension σ_{S0}, and a power factor pf_S:

$$C_{inv,S}(\sigma_S) = C_{inv,S0}\left(\frac{\sigma_S}{\sigma_{S0}}\right)^{pfS} \tag{3.11}$$

The operation of S for a load $\lambda_{S,j}$ at time j is characterized by step-wise linear functions:

- Mass flows into and out of the process $\boldsymbol{\dot{m}_{S,j}}(\sigma_S, \lambda_{S,j})$
- Thermal flows[17] within, into and out of the process, $\boldsymbol{\dot{e}_{S,j}}(\sigma_S, \lambda_{S,j})$
- Operating cost $c_{op,S,j}(\sigma_S, \lambda_{S,j})$

[17] A thermal flow function $\dot{e}_f(\sigma_S, \lambda_{S,j})$ is characterized by an inlet temperature $T_{f,in}$, an outlet temperature $T_{f,out}$, and a heat flow capacity $\dot{CP}_{f,j}(\sigma_S, \lambda_{S,j})$, the latter being a linear function of $\lambda_{S,j}$.

Markets are defined as processes providing or consuming products or utilities with an operating cost corresponding to the market price for the products or utilities traded.

Biomass supply chain modelling allows for relating the marginal cost of locally distributed biomasses to the aggregated biomass feedstock consumption. A generic biomass supply chain model was integrated in the present design methodology inspired by a supply chain model for sugar beet developed in the BioChain project [87]. In the model, the marginal biomass unit cost $c_B(B_{an})$ is calculated as a function of the annual biomass quantity demanded B_{an} based on a fixed reference cost c_{B0} and a cost for transportation $c_{B,tr}(B_{an})$. The reference cost represents the price paid to local farmers for the biomass, while the transportation cost represents the variable costs of logistics for delivering biomass to the location of processing within the FMG.

$$c_B(B_{an}) = c_{B0} + c_{B,tr}(B_{an}) \tag{3.12}$$

It is assumed that $c_{B,tr}$ is fixed for spatial areas A_B around the FMG. The local resource dataset must contain information on $c_{B,tr,A}$ and corresponding annual biomass potential B_{an,A_B} for all areas A_B that are considered for providing biomass for the FMG. More details on the applied biomass supply chain model are offered in Appendix E [19].

Optimization phase

The optimization phase of the design methodology is based on the OSMOSE tool[6]. In short, the optimization phase consists of three steps: A *genetic algorithm* for selecting, locating, and dimensioning processes plus deciding upon the investment plan; a *multi-period MILP model* for optimizing process integration and operation of the given processes over the facility lifetime; and a *post calculation* step for calculating the overarching objective function values of each optimized design.

A *genetic algorithm* is a heuristic optimization algorithm that imitates the process of natural selection for solving an optimization problem. In OSMOSE, a genetic algorithm is preferred as the master optimization algorithm as it can be used for solving linear as well as non-linear models and is capable of conducting multi-objective optimization [66]. When running the genetic algorithm in OSMOSE, one defines the population size and number of generations, while the algorithm has pre-defined settings for selection, mutation, and crossover [44]. For general information on genetic algorithms, refer to e.g. [88].

In the design methodology, the objectives of the genetic algorithm are to maximize NPV, $C_0(\boldsymbol{\omega}, \boldsymbol{\sigma}, \boldsymbol{y})$, and minimize GWP100a, $Z_0(\boldsymbol{\omega}, \boldsymbol{\sigma}, \boldsymbol{y})$. Variables considered by the genetic algorithm are: ω_S, the decision of whether or not a process or piece of equipment S should be installed at a given location; σ_S, the dimension of S; and y_S, the installation delay of S in years. The optimization problem to be solved by the genetic algorithm in the design methodology can be written in condensed form as

$$\textit{Genetic algorithm}: \begin{cases} \min_{\boldsymbol{\omega},\boldsymbol{\sigma},\boldsymbol{y}} \begin{cases} -C_0(\boldsymbol{\omega}, \boldsymbol{\sigma}, \boldsymbol{y}) \\ Z_0(\boldsymbol{\omega}, \boldsymbol{\sigma}, \boldsymbol{y}) \end{cases} \\ \text{with variables} \\ \omega_S \in \{0,1\} \\ \sigma_S \in [\sigma_{S,min}, \sigma_{S,max}] \\ y_S \end{cases} \tag{3.13}$$

Given $(\boldsymbol{\omega}, \boldsymbol{\sigma}, \boldsymbol{y})$, a *multi-period MILP model* is used for optimizing process integration and operation for all defined CHOP groups G_j, which in total represents operation optimization over the lifetime of the FMG. The multi-period MILP model is advantageous as it reduces computation time compared to the genetic algorithm while guaranteeing global optimality.

In the MILP model, total FMG operating costs $c_{0,j}(\boldsymbol{\nu}_j, \boldsymbol{\lambda}_j)$ are minimized for each CHOP group G_j with variables: $\nu_{S,j}$, the decision on whether a process S is operated or shut down in period j; and $\lambda_{S,j}$, the load of the process S in period j if operated. The MILP model is constructed so that each type of mass flow in the system has its own layer l. Mass balance is applied as a constraint for each layer l in each period j.

$$\sum \dot{m}_{f,l,i} = 0 \tag{3.14}$$

Special layers are constructed for thermal energy flows, for which pinch analysis [45] is applied to optimize heat integration. Individual thermal energy layers must be defined for each area of the FMG for which heat integration is feasible. As mentioned, thermal energy flows $\dot{\boldsymbol{e}}(\boldsymbol{\sigma}, \boldsymbol{\lambda}_j)$ are assumed to have step-wise constant heat capacity flow rates $\dot{\boldsymbol{CP}}(\boldsymbol{\sigma}, \boldsymbol{\lambda}_j)$ over their temperature ranges. Enthalpy balances ΔH are calculated for each temperature interval u in each thermal layer.

$$\Delta H_{u,j} = (T_u - T_{u-1}) \sum_{f \in u} \dot{CP}_f(\boldsymbol{\sigma}, \boldsymbol{\lambda}_j) \tag{3.15}$$

The aggregated sum of enthalpy balances in each thermal energy layer must be zero to satisfy the first law of thermodynamics. Furthermore, the sum of enthalpy flows from the first temperature interval to any of the other temperature interval in each thermal energy layer must never be below zero to satisfy the second law of thermodynamics:

$$\sum \Delta H_{u,j} = 0 \tag{3.16}$$

$$\sum_{u=1}^{m} \Delta H_{u,j} \geq 0 \quad \forall\ m \in \{1,2,\dots,u_{max}\} \tag{3.17}$$

For each period, the total global warming impact of operation $z_{0,j}(\boldsymbol{\nu_j}, \boldsymbol{\lambda_j})$ is calculated, while the investment cost of the optimized heat exchanger network configuration is estimated within the OSMOSE tool based on a method from Turton et al. [89]. The OSMOSE default settings were used. For more information, refer to Bolliger [44].

The optimization problem to be solved by the multi-period MILP model in the design methodology can be written in condensed form as

$$\textit{Multi-period MILP model}: \begin{cases} \text{given } (\boldsymbol{\omega}, \boldsymbol{\sigma}, \boldsymbol{y}) \\ \min_{\boldsymbol{\lambda_j}, \boldsymbol{\nu_j}} c_{0,j}(\boldsymbol{\nu_j}, \boldsymbol{\lambda_j}) \\ \text{with variables} \\ \nu_{S,j} \in \{0,1\} \\ \lambda_{S,j} \in [\lambda_{S,min}, \lambda_{S,max}] \\ \text{and constraints} \\ eqs.\ (\mathbf{3.14}), (\mathbf{3.16}), (\mathbf{3.17}) \end{cases} \tag{3.18}$$

Having solved the multi-period MILP model, a *post calculation* step is used for evaluating the overall performance of the FMG design with respect to NPV and GWP100a. First, the heat exchanger network investment cost, C_{HEN}, is defined as the largest estimated heat exchanger investment cost for any period j:

$$C_{HEN} = \max_j C_{HEN,j} \tag{3.19}$$

The NPV of the design, C_0, and the GWP100a, Z_0, are calculated as

$$C_0 = -\left[C_{HEN} + \sum_S \frac{C_{inv,S}(\sigma_S)}{(1+r)^{y_S}}\right] - \sum_j c_{0,j}\left(\boldsymbol{\nu_j}, \boldsymbol{\lambda_j}\right) \cdot t_{PV,j} \tag{3.20}$$

$$Z_0 = Z_{inst,HEN} + \sum_S Z_{inst,S}(\sigma_S) + \sum_j z_{0,j}\left(\boldsymbol{\nu_j}, \boldsymbol{\lambda_j}\right) \cdot t_j \tag{3.21}$$

Here, $Z_{inst,HEN}$ is the global warming potential related to the production, installation, and scraping of the heat exchanger network, while $Z_{inst,S}(\sigma_S)$ is the global warming potential related to the production, installation, and scraping of a process S.

The calculated NPV and GWP100a are provided as feedback to the genetic algorithm. All data on optimized designs are stored in a database for later evaluation.

Evaluation phase

Once the genetic algorithm optimization has been conducted, a scatter plot of the found designs with respect to NPV and GWP100a is created in the *Pareto assembling*. In case a trade-off exist between the two objectives, the optimal trade-off can be identified from this scatter plot as the so-called Pareto curve.

Based on the scatter plot, a number of interesting designs n may be selected for further evaluation. For each selected design, the performance outputs $\boldsymbol{h}$ are given by

$$\boldsymbol{h}\left(\boldsymbol{\omega_n}, \boldsymbol{\sigma_n}, \boldsymbol{y_n}, \boldsymbol{\nu_{n,j}}, \boldsymbol{\lambda_{n,j}}, \boldsymbol{q}\right) = \begin{cases} -C_0\left(\boldsymbol{\omega_n}, \boldsymbol{\sigma_n}, \boldsymbol{y_n}, \boldsymbol{\nu_{n,j}}, \boldsymbol{\lambda_{n,j}}, \boldsymbol{q}\right) \\ Z_0\left(\boldsymbol{\omega_n}, \boldsymbol{\sigma_n}, \boldsymbol{y_n}, \boldsymbol{\nu_{n,j}}, \boldsymbol{\lambda_{n,j}}, \boldsymbol{q}\right) \end{cases} \tag{3.22}$$

All design and operation variables $\left(\boldsymbol{\omega_n}, \boldsymbol{\sigma_n}, \boldsymbol{y_n}, \boldsymbol{\nu_{n,j}}, \boldsymbol{\lambda_{n,j}}\right)$ were defined in the optimization phase, while an uncertainty distribution D_q is associated with each uncertain input parameter q. In consequence, $\boldsymbol{h}\left(\boldsymbol{\omega_n}, \boldsymbol{\sigma_n}, \boldsymbol{y_n}, \boldsymbol{\nu_{n,j}}, \boldsymbol{\lambda_{n,j}}, \boldsymbol{p}\right) = \boldsymbol{h}(\boldsymbol{q})$ in the evaluation phase.

In order to estimate output variability in response to input parameter uncertainties $\boldsymbol{D_q}$, a combined *sensitivity and uncertainty analysis* is applied which involves two steps:

(1) *Extended Morris screening* [84,85] is applied for each selected design to identify parameter uncertainties with significant impact on the overall performance variability.

(2) *Monte Carlo simulation* is applied for quantifying output uncertainties for each selected design.

Morris screening: As the design methodology is computationally intensive, it is desirable to reduce the number of parameter uncertainties D_q to sample from when quantifying output variations using Monte Carlo simulations. Therefore, the global sensitivity analysis method known as extended Morris screening [84,85] is applied in the first step to identify the parameters $\boldsymbol{q}_n^* \in \boldsymbol{q}$ that has a significant impact on variations in the outputs $\boldsymbol{h}_n$ of model n, and consequently must be accounted for in the uncertainty analysis. The main advantage of Morris screening is its low computational cost when compared to other global sensitivity analysis methods.

Extended Morris screening relies on estimating the elementary effect EE on each model output h from each uncertain input parameter q_n.

$$EE_{q_n,h} = \frac{h\left(q_1, q_2, \dots, q_n + \Delta, \dots, q_{N_q}\right)}{\Delta} \tag{3.23}$$

Here, Δ is a user-defined perturbation factor, and N_q is the total number of uncertain input parameters considered.

By definition, all $EE_{q_n,h}$ are local measures. In order to approximate the global distributions of all $EE_{q_n,h}$, Morris suggested that elementary effects are calculated for a number of points w_{MS} randomly sampled from the input space using the special Morris Sampling procedure [84]. In Morris Sampling, the uncertainty ranges of design parameters q are assumed uniform and discretized into b levels, and sampled parameters may only take the values of these levels. Morris suggests that the number of levels b is set as an even number and the perturbation factor Δ is defined as

$$\Delta = \frac{b}{2(b-1)} \tag{3.24}$$

which ensures that each possible $EE_{q_n,h}$ has an equal probability of selection [84]. The suggested perturbation factor definition is used de facto in the present methodology, leaving two degrees of freedom for the Morris screening: b, the number of value levels that an uncertain design parameter can take within its range; and w_{MS}, the number of samples from which the distributions of elementary effects are evaluated.

Once all $EE_{q_n,h}$ have been calculated for each random sample of uncertain input parameters, sigma-scaling [85] of all $EE_{q_n,h}$ is applied in order to compare impacts of different input parameters on the various outputs:

$$SEE_{q_n,h} = EE_{q_n,h}\frac{SD_{q_n}}{SD_h} \tag{3.25}$$

Here, SD_{q_n} is the standard deviation of the design parameter q_n, while SD_h is the standard deviation of the output h based on its distribution in the simulation results.

Next, the means μ and standard deviations SD of all $SEE_{p_n,h}$ are calculated and assembled in scatter plots. In each plot, two lines corresponding to the positive and negative double estimated standard error of the mean, μ, are drawn:

$$\mu = \pm 2 \cdot \frac{SD}{\sqrt{w_{MS}}} \tag{3.26}$$

As described by Sin et al. [85], these lines may be used for dividing uncertain parameters into significant or negligible with respect to model output variation. If the elementary effect of a parameter falls within the wedge formed by the two lines, its impact can be interpreted as negligible on the model output variation. An example of such scatter plot is presented in Figure 3.

Consequently, any uncertain input parameter q_n that is found to have significant impact on at least one of the model output variations is included in the reduced dataset $\boldsymbol{q}_n^*$.

Monte Carlo simulation: Following the Morris screening, Monte Carlo simulations using the procedure presented by Sin et al. [85] is applied for quantifying variations in NPV and GWP100a from uncertainties in input parameters $\boldsymbol{q}_n^*$. The Monte Carlo simulation was chosen for the design methodology as it can assess and quantify uncertainties in results without necessitating modifications in the original models, and because it facilitates identification of nonlinearities, thresholds, and discontinuities [90]. The procedure applied in this methodology involves three steps:

(1) *Specifying input uncertainty*: In general, the Monte Carlo simulations may consider uncertainty distributions D for all input data. However, in order to reduce parameter

distributions to sample from in the present methodology, only parameters $\boldsymbol{q}_n^*$ are considered as input uncertainty for the Monte Carlo method.

(2) *Sampling from input uncertainty*: In order to obtain dense stratification over the range of each sampled variable without having to manually define the stratification, the Latin Hypercube Sampling method [91] is applied for generating w_{MC} samples from uncertainties in input parameters $\boldsymbol{q}_n^*$.

(3) *Evaluating the model for sampled input uncertainty*: The performance variations of each design n are evaluated for all sampled datasets w_{MC}, providing a cumulative distribution function of output values as functions of input uncertainties.

It must be noted that uncertainties regarding topological parameters, such as equipment failure or forced outages, cannot be considered in the design methodology. In addition, uncertainties related to operating parameters should not be considered in the combined Morris Screening and Monte Carlo simulation as computation times would be prohibitive. To assess performance variations with respect to uncertainty in operating conditions, it is instead recommended to conduct the design optimization for a number of likely scenarios.

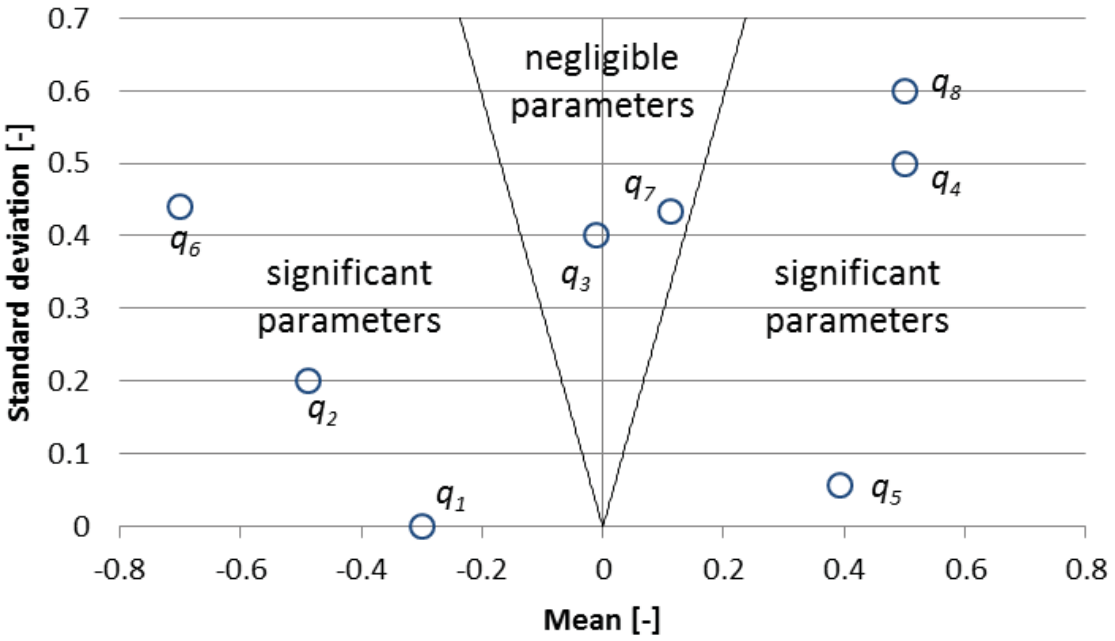

Figure 3.8: Example of a scatter plot of sigma-scaled elementary effects from various input parameters $\boldsymbol{q}$ on a model output $\boldsymbol{h}$. The two lines forming the wedge represent the double standard error of the mean. Input parameters with sigma-scaled elementary effects inside the wedge are considered negligible with respect to variations in $\boldsymbol{h}$, while parameters outside are considered to have significant impact on variations in $\boldsymbol{h}$.

Outputs

Two overall outputs are obtained when applying the developed design methodology:

- An assembled Pareto curve and a database of feasible designs that have been optimized with respect to NPV and GWP100a
- For selected designs: The sigma-scaled elementary effect of each uncertain input parameter on each of the two model outputs; and a quantification of model output variation as a function of input uncertainty.

3.2.3 Method verification

As mentioned in Section 3.2.1, it was the ambition to develop a coherent methodology for designing FMGs that systematically considered selection and dimensioning of processes, process integration, variations in multiple external operating conditions in both short-term and long-term perspective, and uncertainty analysis. These five parameters are addressed by the design methodology in the following way:

- *Selection and dimensioning*: Handled by the genetic algorithm. In addition, the genetic algorithm allows for selecting processes location in case multiple areas are considered, and for considering investment planning.
- *Process integration*: Handled by the *multi-period MILP model* using pinch analysis and mass balances. Process integration is optimized for each CHOP group G_j considered.
- *Short-term operation*: Included through the application of the *CHOP method* for reducing external operating conditions, as discussed in Section 3.1.
- *Long-term operation*: Included through the application of the *CHOP method* for reducing external operating conditions, as discussed in Section 3.1.
- *Uncertainty analysis*: Uncertainties in design parameters are handled using *extended Morris screening* and *Monte Carlo simulations*. Uncertainties in operating conditions can be considered by solving the design optimization for a number of likely scenarios to minimize computation time.

Apart from designing FMGs, the developed methodology may as well be used for comparing and benchmarking the performance of various energy conversion technologies, and developments of these, in a given energy system context.

The design methodology applies a number of methods. The validity of using these methods is discussed below:

First of all, the design methodology uses several features directly from the OSMOSE tool[6]: The genetic algorithm; the multi-period MILP operation optimization including pinch analysis [45]; and the estimation of heat exchanger network investment costs [89]. As described previously, the OSMOSE tool provides an interface that combines pinch analysis [45] with economic analysis of process systems [89], and the tool has been described, documented, verified, tested and applied in numerous studies on various kinds of integrated energy systems, e.g. [14,43,44,46–48,51–54,66,67]. In consequence, the features used from the OSMOSE tool are considered to be valid for the design methodology.

Secondly, the methodology uses extended Morris screening [84,85] for identifying input parameter uncertainties with significant impact on the overall performance variability, and Monte Carlo simulations [85] for quantifying output uncertainties for each selected design. Especially the Monte Carlo method is well described in literature and has been applied in a number of disciplines, e.g. molecular biology [92], medical physics [93], econometrics [94], engineering [95] etc. In the developed methodology, the tools for extended Morris screening and Monte Carlo simulations that were developed, documented and verified by Sin et al. [85] in an extensive study on sensitivity and uncertainty analysis methods are applied directly, as kindly allowed by the developer Gürkan Sin. As these tools have been implemented without any alternations, they are considered to be valid for the purpose as well.

Thirdly, the design methodology applies the CHOP method, which was introduced and verified in Lythcke-Jørgensen et al. [36]. It must be emphasized that the limitations that applies to the CHOP method, see the discussion in Section 3.1, also applies to the combined design methodology.

In summary, the design methodology consists of a number of methods which have been tested, either previously or as a part of this project, and are considered valid for the purposes of the methodology The combined methodology was tested and verified through two case studies, which are presented in Sections 4.3 and 4.4. The design methodology was proven effective in screening the solution space for efficient FMG designs, in assessing the importance of parameter uncertainties, and in estimating likely performance variability.

3.2.4 Discussion

In the design methodology, the genetic algorithm from the OSMOSE tool[6] is used as the master algorithm as it can digest all sorts of models. However, the genetic algorithm is heuristic by nature, meaning that optimality cannot be guaranteed. This is why the genetic algorithm is only applied for screening the design solution space, while the multi-period MILP is applied for operation optimization. Also, the present design methodology is not recommended for systems in which geographic network layout plays a central role nor for problems with significant focus on investment planning, as these combinatorial issues are not well handled by the genetic algorithm.

As discussed in Section 3.1, the CHOP method is considered advantageous for designing flexible systems in general as it is capable of reducing the size of an EOC dataset by a factor comparable to simpler averaging methods, while information on correlations between relevant EOCs is sustained in the reduced dataset. However, a main shortcoming is the fact that it prohibits the consideration of dynamics and storages. It is recommended that the designs selected as promising candidates are subjected to a sequential operation optimization step that involves storages and dynamic constraints.

Finally, a general challenge for the design methodology is the fact that it is based on marginal system analysis, implying that the energy system impact from FMG operation is neglected. However, as the central hypotheses for FMGs are related to benefits on system level, it is relevant to assess the aggregated impact of FMG operation from an energy system perspective. One way of doing this would be to apply the developed design methodology to identify a number of promising FMG designs, and then implement these designs in an energy system model [96] that would allow for operation optimization with respect to storages as well as assessment of system impact from FMG operation. The results from the energy system analysis could then be provided as feedback to the design methodology in an iterative loop for comprehensive design optimization of the designs.

In summary, the developed design methodology is regarded as a pre-feasibility tool useful in screening for promising FMG designs. However, the fact that dynamics and time chronology cannot be considered means that storages and dynamic constraints are neglected. In consequence, the optimized operating pattern calculated in the design methodology may overestimate the operation variability in the facilities. To overcome this challenge, it is suggested that the developed design methodology is used for screening for efficient FMG designs among a number of process combinations. From the outcomes,

interesting and promising design solutions may be selected for implementation in an energy system model [96] in order to assess:

(1) The impact of including storages and dynamic constraints in the operation optimization.
(2) The energy system impact from FMG operation.

The sequential implementation of promising FMG designs in energy system models is recommended as an area for future research.

4 CASE STUDIES

This chapter presents the outcomes of three case studies conducted as a part of the project. The background for case studies is first introduced, after which the outcomes of each study are presented. The final section offers a summary and perspective on the case findings.

4.1 Case studies: Background and overview

As outlined previously, a main idea behind the introduced definition of FMGs is that the optimal design of an FMG depends on the surrounding energy system. Consequently, FMG concepts must be 'tailored' to fit into the surroundings, and the choice of energy system context will affect the design optimization results.

In this project, three FMG case studies were conducted. All case studies focussed on the integration of biomass processing technology in existing CHP units in the Danish energy system, which was considered a relevant focus area for the following reasons:

- *Energy system aspect*: Generally speaking, FMGs are considered to be of special relevance in energy systems with large shares of variable RES where the value of operation flexibility may be high. Already in 2012, Lund et al. [9] categorized the Danish energy system at-the-time as having large-scale integration of variable RES, and the share of wind turbine generation is expected to grow markedly over the next decades as described in Chapter 1. The present and future Danish energy system was therefore considered a relevant context for the assessment of FMG concepts.
- *Biomass integration synergies*: Efficient utilization of the limited biomass resources is crucial in sustainable energy systems. Systematic integration of biomass processing technology with other energy conversion processes is a promising approach towards increasing the overall energy efficiency of biomass conversion [13,97,98].
- *The Danish CHP challenge*: Around 70% of the district heating generation in Denmark is based on CHP, but CHP units are challenged by low electricity prices and the current subsidy and tax schemes [99]. Integration of biomass processing offers a new business opportunity for CHPs that in addition to incomes from novel products may increase

operation flexibility of the CHP generation [98], thereby turning the CHPs into efficient biomass-processing FMGs that may be competitive in the present as well as future Danish energy system.

The FMG concepts treated in the three case studies are briefly outlined below:

- *Case I* treated the integration of cellulosic ethanol production based on Inbicon technology[18] in an extraction-based CHP unit.
- *Case II* treated the combined integration of: Cellulosic ethanol production based on the Inbicon technology[18]; anaerobic biogas production and methanation; a biomass burner; and compression heat pumps for district heating generation in a back-pressure CHP unit. The system was inspired by the Maabjerg Energy Concept[19].
- *Case III* treated the installation of a methanol-producing biorefinery based on the gasification of wood chips and solid oxide electrolysis cells (SOECs) in connection with either a waste incineration-based CHP unit or local industry. The biorefinery was inspired by concepts modelled by Clausen et al. [16,100]. Infrastructure investments and the use of hybrid absorption-compression water-ammonia heat pumps for generating industry utility heat were considered as well.

Case I was conducted using a case-specific design and operation optimization model, while *Case II* and *Case III* were conducted using the methodology presented in Chapter 3. Table 4.1 presents an overview of design and operation aspects considered in the different cases.

Table 4.1: Overview of design and operation aspects considered in the three cases.

	Case I	Case II	Case III
Technology selection		✓	✓
Dimensioning and integration	✓	✓	✓
Process location			✓
Short-term operation	✓	✓	✓
Long-term operation			✓
Input parameter uncertainties	✓	✓	✓
Scenario analysis			✓
Biomass supply chains		✓	

[18] Inbicon technology, is a patented technology for hydro-thermal pretreatment of cellulosic biomass owned by Inbicon A/S, a subsidiary to DONG Energy [121].

[19] The Maabjerg Energy Concept is a biorefinery concept that integrates CHP generation with the production of cellulosic ethanol and biomethane [120].

4.2 Case I: Multi-generation of electricity, heat, and cellulosic ethanol in a retrofitted extraction CHP unit

This case treated the integration of cellulosic ethanol production using Inbicon technology[18] in the Danish extraction CHP unit 'Avedøreværket 1'. The developed case was based on the master thesis 'Modelling and optimization of a steam co-generation plant with integrated lignocellulosic ethanol production' [79], and the case outcomes were presented in [15,20,101,102].

4.2.1 Introduction

Ethanol is presently the most widely used biofuel for transportation on a global basis and is consumed both as an individual fuel and in blends with gasoline [103]. Ethanol produced from cellulosic biomass is of special interest as it may support reduction of CO_2 emissions from transportation without linking fuel prices and food prices directly [14]. Furthermore, ethanol is a bulk-volume chemical used in industrial and consumer products, and cellulosic ethanol represents a green chemistry[20] alternative to the existing ethanol production from ethene hydration or through fermentation of sugars and starch [104]. However, the energy intensive nature of cellulosic ethanol production is a challenge with respect to production efficiency and economy.

Several studies have focused on potential synergies from integrating cellulosic ethanol production with CHP generation. Daianova et al. [105] and Ilic et al. [106] both reported better energy economy for integrated systems when compared to stand-alone production of the same energy products, assuming constant energy prices over the year. Bösch et al. [107] discussed how the energy economy of a system producing cellulosic ethanol, biogas and district heating might be increased by integrating electricity production. For a similar system, Modarresi et al. [108] conducted a pinch analysis and reported that heat integration can reduce the hot and cold utility demands by up to 40%, assuming operation in design point solely. Leduc et al. [109] conducted a sensitivity analysis of the important parameters for such systems in Sweden and found that incomes from heat and electricity sales were the most significant contributors towards reducing the specific ethanol

[20] Green chemistry consists of environmental friendly, sustainable chemicals and processes the use of which results in reduced waste, safer outputs, and reduced or eliminated pollution and environmental damage [127].

production costs. With regard to retrofitted systems, Palacios-Bereche et al. [110] studied the integration of cellulosic ethanol production in the conventional first-generation sugarcane ethanol process and reported higher exergy efficiency for the integrated scheme when considering only design point operation. In a study of conversion routes for winter wheat to ethanol, Bentsen et al. [111] suggested that energy savings could be achieved by integrating lignocellulosic ethanol production in existing CHP units. Starfelt et al. [112] investigated the integration of cellulosic ethanol production in an existing biomass-based CHP unit in Sweden and concluded that for the same production of heat, electricity and ethanol, the total biomass consumption would be lower for the integrated system than for a separate scenario. In a later study, Starfelt et al. [113] concluded that the integration of cellulosic ethanol production in Swedish CHP units with fixed heat-to-electricity ratios may be profitable if excess heat capacity is available in the CHP unit for a certain amount of time over the year. However, none of these studies assessed the overall impact on economic or thermodynamic performances of the ethanol production from hour-by-hour changes in CHP operation over the year in response to variations in heating demands, electricity prices, and shut-downs of the CHP unit.

This study assessed the market-dependent economic and thermodynamic performances of integrating cellulosic ethanol production using Inbicon technology[18] with flexible CHP generation in the Danish extraction CHP unit 'Avedøreværket 1'[21]. The Inbicon technology is considered beneficial as it, in opposition to competing concepts, applies steam rather than chemicals for pretreatment of the lignocellulosic straw. The integrated system was assumed advantageous when compared to separate systems for the following reasons:

- Energy cost for the ethanol production may be reduced.
- Exergy efficiency of the ethanol production may be increased.
- Integrated operation will make it possible to run the CHP unit with lower electricity generation, which may be advantageous in periods of mandatory district heating generation and low or negative electricity prices.

A simplified system layout is shown in Figure 4.1. The system can operate in integrated or separate mode as illustrated in Figure 4.2, with separate mode occurring when the CHP unit has no spare capacity for supplying steam for the ethanol production, e.g. due to high

[21] 'Avedøreværket 1' has a net electricity generation capacity of 250 MW in condensation mode and of 212 MW in full back pressure mode, with a full back-pressure heat generation capacity of 330 MJ/s (forward/return temperatures 100^0C/50^0C) [78].

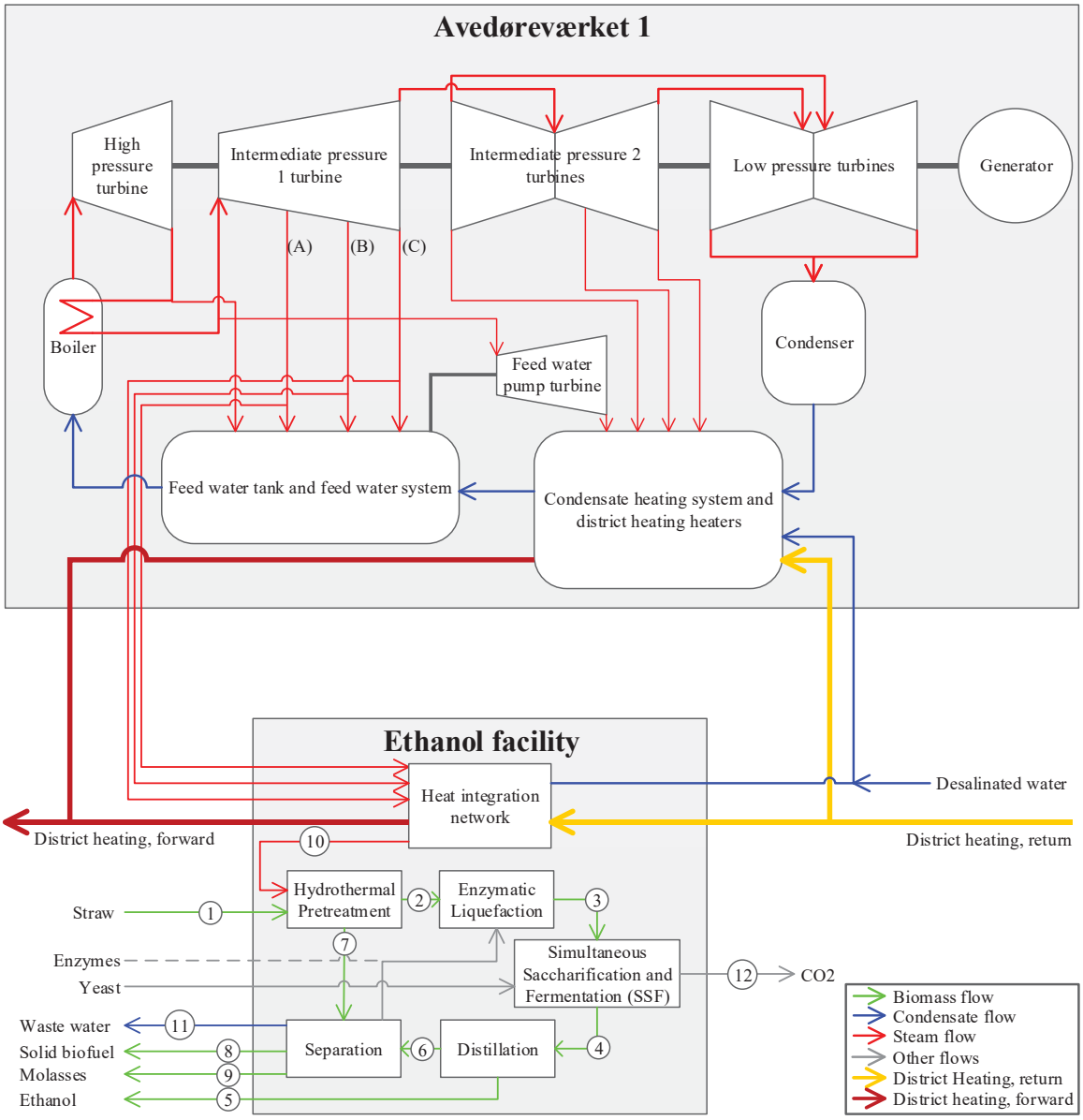

Figure 4.1: Simplified process layout of the system treated [20].

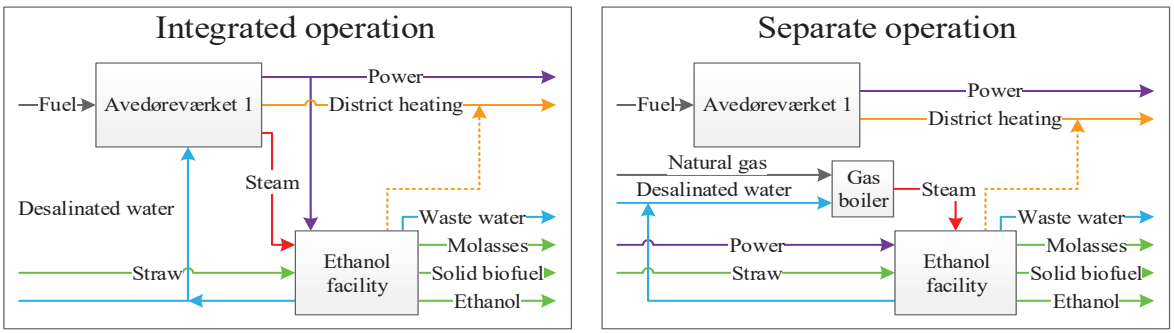

Figure 4.2: Outlines of the two operation modes of the integrated system [20].

loads or maintenance shut-downs. The main novelty of the work lies in the evaluation of average economic performance and exergy efficiency of coupling cellulosic ethanol production with flexible CHP generation by combining exergy analysis with design and operation optimization considering variable operating conditions and constraints on an hour by hour basis over the year.

4.2.2 Methodology

The system considered had previously been investigated in Lythcke-Jørgensen [79], where the heat integration scheme was optimized with respect to possible steam extraction for a fixed ethanol facility dimension. The main outcomes regarding economic performance and process integration were synthesised and analysed further in Lythcke-Jørgensen et al. [101]. At the same time, an exergy analysis was conducted for the heat integration solution in four extreme operating modes, and the results were presented in Lythcke-Jørgensen et al. [102]. The exergy analysis was later extended to consider the entire ethanol facility and two additional operating modes in Lythcke-Jørgensen et al. [20]. Based on the combined outcomes, a design optimization model was formulated in order to compare process integration synergies with economy-of-scale benefits in the ethanol production. The final outcomes of this study were presented in Lythcke-Jørgensen et al. [15]. The applied case methodology is illustrated in Figure 4.3.

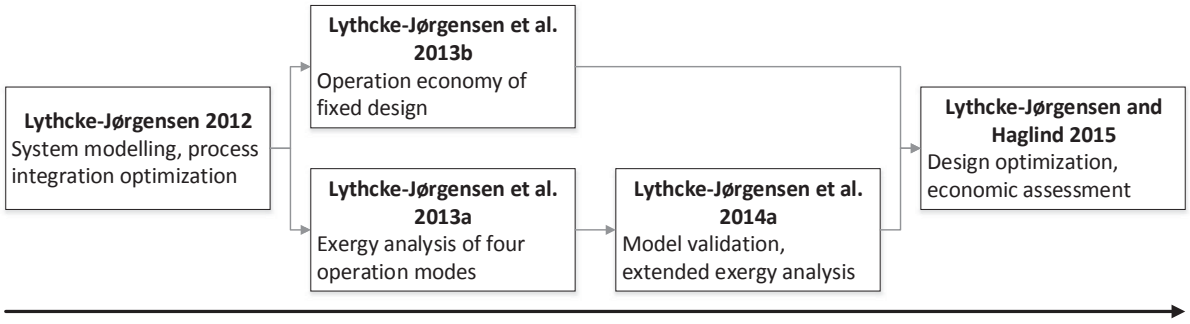

Figure 4.3: Methodology applied on *Case I*, including publication milestones.

The main outcomes regarding energy efficiency, exergy efficiency and design optimization of the FMG concept treated are presented in this section. Documentation and validation of the modelling, reference data, and exergy analysis approach can be found in Appendix B [20], while documentation of the design optimization model, the linearized CHP unit model and associated assumptions can be found in Appendix C [15].

4.2.3 Results and discussion

Energy efficiency assessment

The heat integration scheme was optimized for a set pinch point temperature difference of 10K. In addition, it was assessed how excess heat could be utilized for generating district heating. Specific heat flows within the ethanol facility for operation with zero and maximum district heating generation are illustrated in Sankey diagrams in Figure 4.4.

It was found that a significant amount of heat may be recovered for district heating purposes. However, the district heating forward temperature of $100℃$ combined with the set pinch point temperature difference of 10K necessitated the addition of heat above $110℃$ to raise the temperature sufficiently. For each unit of extra heat added for raising the temperature, 4.73 units of district heating were generated while the cold utility demand was markedly reduced at the same time. In total, 94.5% of the initial process heat demand of the ethanol facility could be recovered and utilized for district heating. This emphasizes how the inclusion of district heating generation may be used for increasing the overall first law efficiency of cellulosic ethanol production using Inbicon technology[18].

Exergy efficiency assessment

Based on the validated ethanol facility model, exergy analysis was applied to assess the exergy efficiency of the ethanol production in various operation modes. A Grassmann diagram of the specific exergy flows in the using Inbicon technology[18] based ethanol production under optimal heat exchange is presented in Figure 4.5. Under these conditions, a standard exergy efficiency of 0.91 was calculated for the ethanol facility.

In order to assess the exergy efficiency of the ethanol production under actual operation, six different operating modes were assessed which altered on three operating parameters: Separate mode or integrated mode operation as illustrated in Figure 4.2, $\kappa \in \{0\,,1\}$; minimum or maximum load in the CHP unit, $\lambda_{CHP} \in \{0.4\,,1\}$; and zero or maximum district heating generation in the ethanol facility as indicated in Figure 4.4, $\beta \in \{0.0\,,1.0\}$. For all six combinations of operating modes, the standard exergy efficiency of the ethanol production η_{ex} was calculated. The results are summarized in Table 4.2.

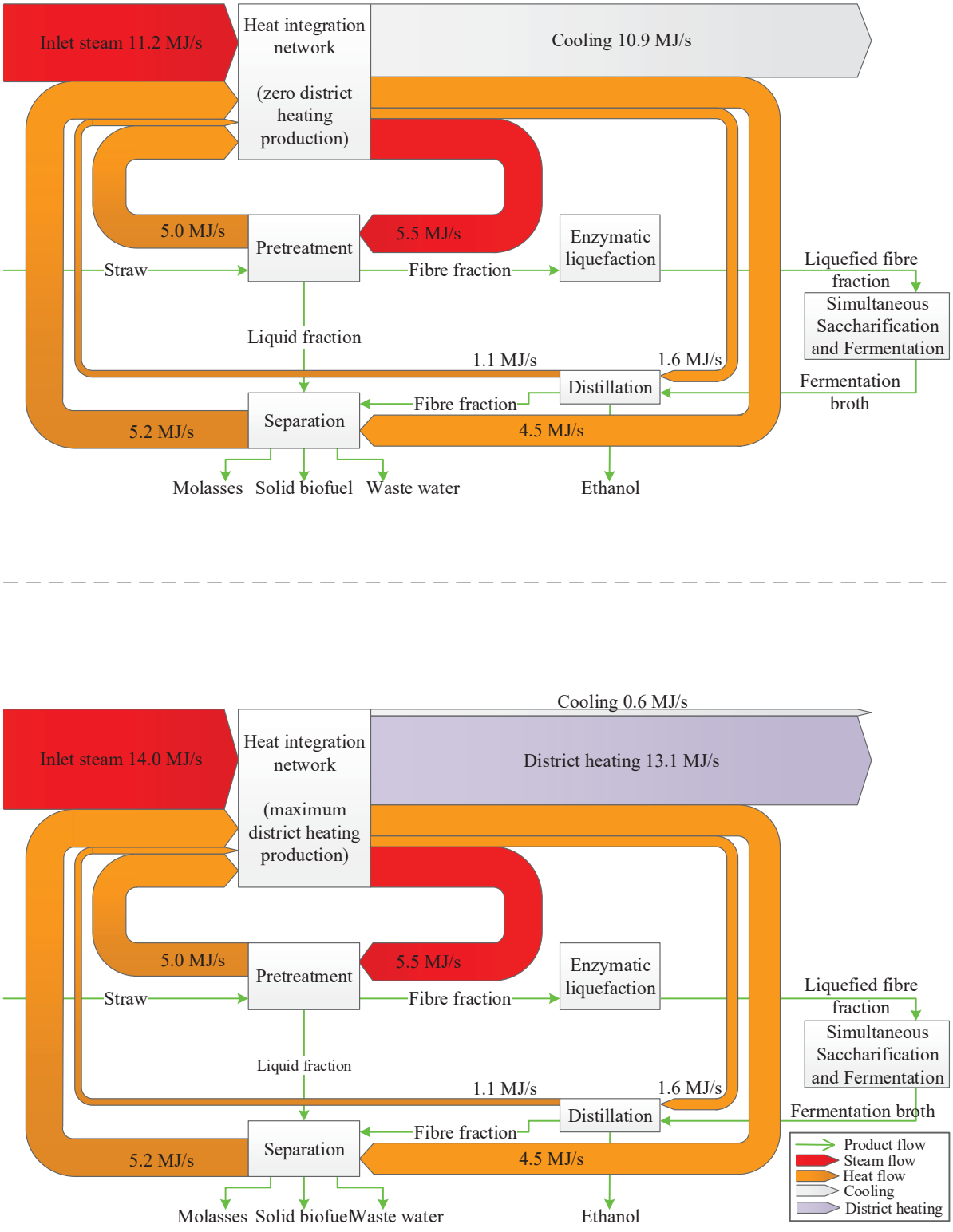

Figure 4.4: Sankey diagrams of specific heat flows in the ethanol facility per kg/s straw treated at zero (top) and maximum (bottom) district heating generation. Note that additional heat is required when district heating generation is included [20].

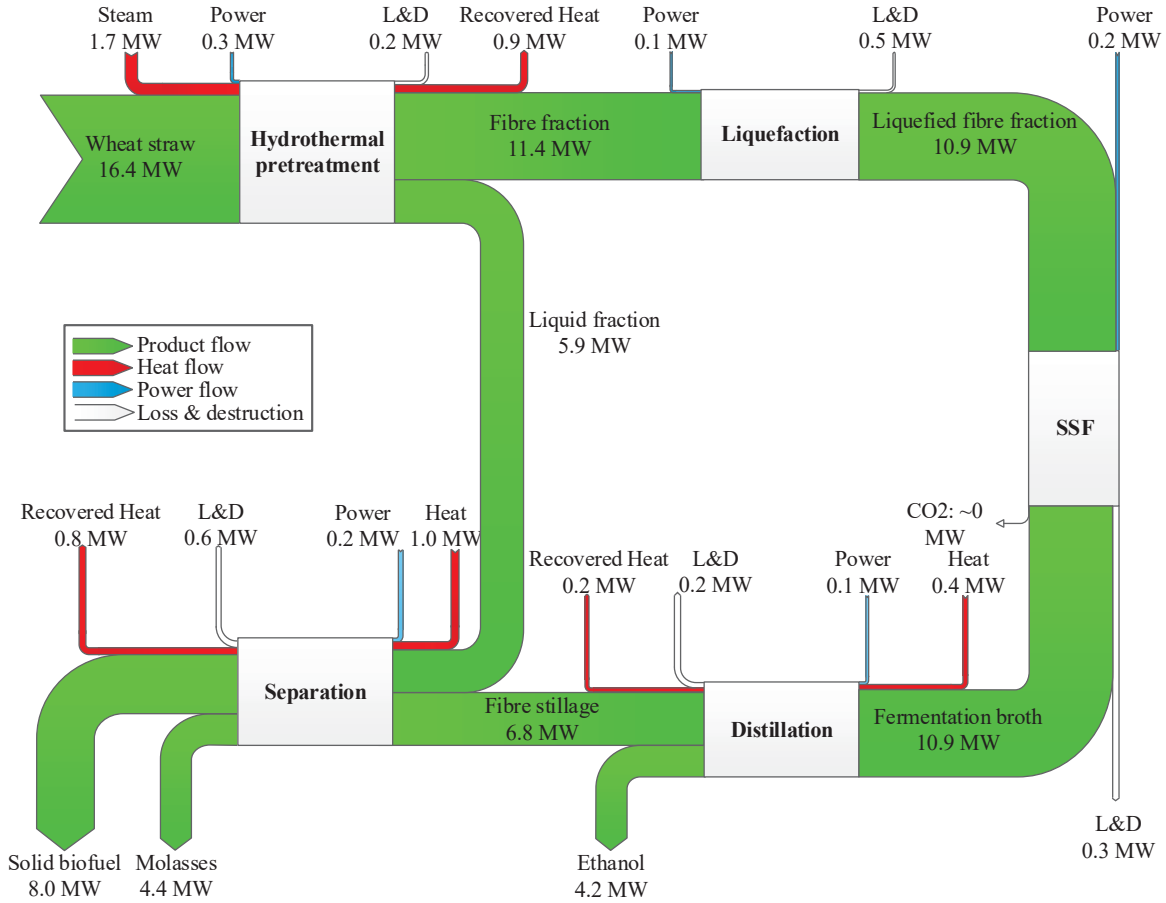

Figure 4.5: Specific exergy flows in the ethanol facility per kg/s of straw treated when all heat exchange occurs at 10K. Exergy losses and destruction (L&D) are also indicated for the processes [20].

Table 4.2: Operation characteristics and standard exergy efficiency of the investigated operating modes.

Operating mode	κ	λ_{CHP}	β	η_{ex}
I	1	1.0	0.0	0.787
II	1	1.0	1.0	0.843
III	1	0.4	0.0	0.795
IV	1	0.4	1.0	0.855
V	0	-	0.0	0.564
VI	0	-	1.0	0.589

For the six considered operating modes, the standard exergy efficiency of the ethanol production was found to vary between 0.564 in operating mode V and 0.855 in operating mode IV, see Table 4.2. The latter corresponded well with the exergy efficiency of 0.88 reported by Modarresi et al. [108] for a comparable system. However, comparing these

Figure 4.6: Specific exergy flows in the ethanol production in operating mode IV (top) and V (bottom) [20].

values to the standard exergy efficiency of 0.91 under optimal heat exchange, it is evident that heat exchange has a significant impact on the exergy efficiency of the ethanol production for the system treated. Grassmann diagrams illustrating exergy flows in operating mode IV and operating mode V are shown in Figure 4.6.

Among the operating parameters considered, the choice between integrated or separate operation was found to have the largest influence on the exergy efficiency. District heating

generation in the ethanol facility was also found to increase the exergy efficiency, while the exergy efficiency was increased slightly for lower CHP loads as the condition of the extracted steam here matched the temperature requirements of the ethanol production better. Combined, these outcomes illustrate that while major synergies can be achieved by integrating cellulosic ethanol production with CHP units, the overall efficiency benefit is highly dependent on operation. This emphasizes the importance of considering flexible operating patterns rather than design point operation for the integrated system when assessing the efficiency of such integration.

Design optimization

In order to quantify integration synergies and comparing these with economy-of-scale benefits during market-based operation, a design and operation optimization model was formulated for minimizing the specific ethanol production cost c_{eth} in the integrated system. Continuous variables in the model included: Ethanol facility dimension in kg/s straw treated, σ_{eth}; CHP unit load λ_{CHP}; back-pressure operation parameter in the CHP unit α_{CHP}; and district heating generation in the ethanol facility β_{eth}. The choice between integrated or separate operation κ was included as an integer variable.

The operation was optimized over the year of 2011 where the reference operating pattern of the CHP unit was known. As the system was set to replace Avedøreværket 1 in the Danish energy system, the operation was constrained by having to meet the reference heat generation $\dot{Q}_{i,ref}$ for all operating points O_i, while it was assumed that the electricity generation $\dot{P}_i$ could not exceed reference electricity generation $\dot{P}_{i,ref}$ at any time:

$$\dot{Q}_i(\sigma, \lambda_i, \alpha_i, \beta_i, \kappa_i) = \dot{Q}_{i,ref} \quad \forall\, O_i \tag{4.1}$$

$$\dot{P}_i(\sigma, \lambda_i, \alpha_i, \beta_i, \kappa_i) \leq \dot{P}_{i,ref} \quad \forall\, O_i \tag{4.2}$$

During integrated operation, district heating generation from the ethanol facility was prioritized over district heating generation in the CHP unit, while district heating generation in the ethanol facility was not considered during separate operation:

$$\beta_i = 0 \quad | \kappa_i = 0 \tag{4.3}$$

The design and operation optimization model developed can be formulated in condensed form as

$$\begin{cases} \min\limits_{\sigma_{eth},\lambda_{CHP},\alpha_{CHP},\beta_{eth},\kappa} [c_{eth}(\sigma_{eth},\lambda_{CHP},\alpha_{CHP},\beta_{eth},\kappa)] \\ \quad subject\ to\ constraints: \\ \text{eqs. (4.1), (4.2), (4.3)} \\ \quad with\ variables: \\ \sigma_{eth} \in [5,12]; \quad \alpha_{CHP},\beta_{eth} \in [0.0,1.0]; \\ \lambda_{CHP} \in [0.4,1.0]; \quad \kappa \in \{0,1\} \end{cases} \tag{4.4}$$

For full documentation and validation of the modelling and data used in the design optimization, refer to Appendix C [15].

Solving the design and operation optimization model (4.4) for the reference year of 2011, the minimized specific ethanol production cost as a function of σ_{eth} is plotted in Figure 4.7. The lowest average specific ethanol production cost, c_{eth} = 0.958 €/L was obtained for the design with the smallest ethanol facility dimension, $\sigma_{eth} = 5kg/s$. Comparing this value to the average ethanol price of 0.55 €/L on the European market in the period 2008-2010 [114], the results suggest that none of the feasible designs are competitive under the set conditions. For most designs, the specific ethanol production energy cost alone was found to exceed the historical ethanol market prices.

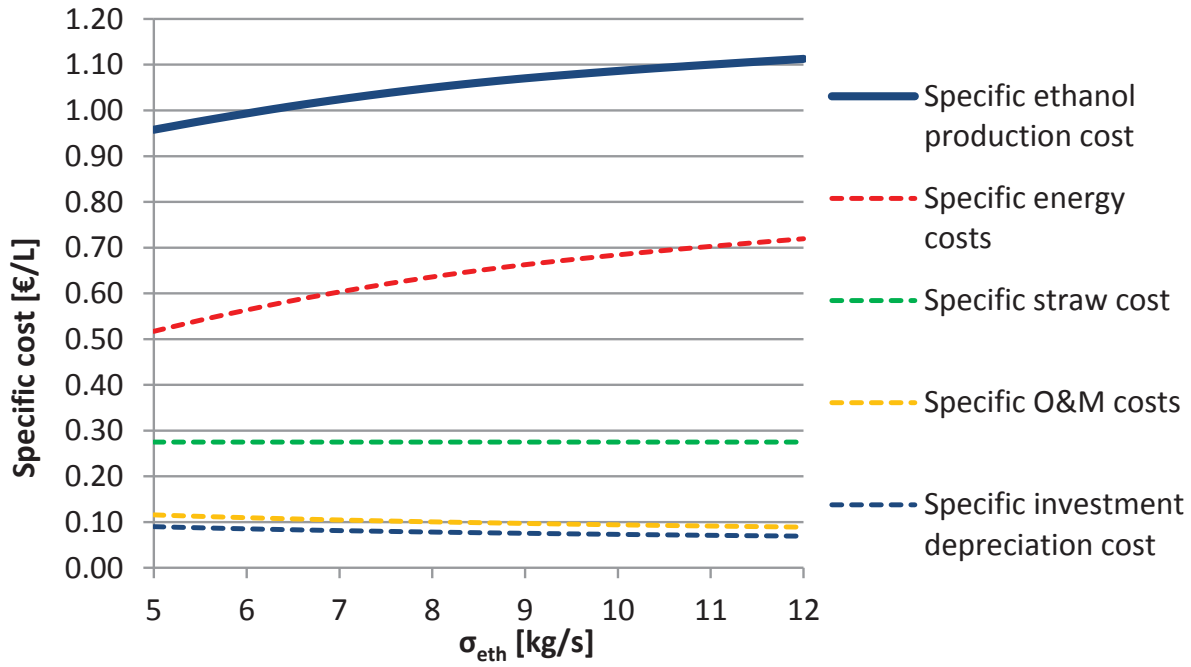

Figure 4.7: Specific ethanol cost and important cost components as function of ethanol facility dimension σ_{eth} given in kg/s straw processed [15].

For the optimized design, $\sigma_{eth} = 5kg/s$, the average specific energy costs of the ethanol production were found to be 0.213 €/L during integrated operation and 1.192 €/L during separate operation. This result underlines the economic inefficiency of separate operation.

An important outcome of the study is the diseconomies-of-scale trend that is found to apply for the ethanol production costs, which is in contrast to the commonly accepted economies-of-scale principle. In the present case, the diseconomy-of-scale trend was directly related to the energy costs of the production which increased with increasing σ_{eth}. The increase in energy costs was found to exceed the economy-of-scale benefits in specific investment costs and O&M (operation & maintenance) costs, as shown in Figure 4.7.

The increase in specific energy costs with σ_{eth} was found to be a consequence of changes in the operation pattern. To illustrate this, the duration of separate operation and integrated operation at maximum and minimum CHP load are plotted as a function of σ_{eth} in Figure 4.8. It was found that the duration of separate operation increased for increasing σ_{eth}. This effect was caused by the combination of high electricity prices and the reduced electricity generation potential during integrated operation for increasing σ_{eth}, causing the cost of lost electricity sales to exceed the cost of running the FMG in separate operation for an increasing amount of hours over the year. This observation is also evident from Figure 4.9, which illustrates how specific costs for electricity and gas are increased with increasing σ_{eth} due to longer duration of separate operation. Opposed to this, the specific coal cost is seen to decrease with increased σ_{eth} owing to the decrease in integrated operation duration and thereby CHP fuel consumption. In other words, the decrease in integration synergies was found to exceed the economy-of-scale benefits of larger ethanol production facilities for the system treated.

Another significant outcome with respect to operation is the low duration of integrated operation in minimum load. As described in Section 4.2.1, an assumed advantage of the integrated system was the potential of reducing electricity generation in periods with low or negative electricity prices. However, in the East Denmark electricity block anno 2011, the solution to the optimization problem (4.4) only exploited this advantage for 104h over the year, suggesting that this advantage has limited impact on system performance.

Regarding thermodynamic efficiency, Figure 4.10 shows the yearly averaged standard exergy efficiency of the ethanol production, η_{ex}, as a function of σ_{eth}. The efficiency was found to decrease for increasing σ_{eth}, mainly owing to the fact that the duration of separate operation increased for increasing σ_{eth}, during which natural gas, which has a

very high exergy-to-energy ratio, replaced steam from the CHP unit as hot utility. The average efficiency for the optimized design was $\eta_{ex} = 0.746$, which is still significantly lower than η_{ex} in the optimal operating mode. The average exergy flows in the ethanol production of the optimized design are shown in a Grassmann diagram in Figure 4.11.

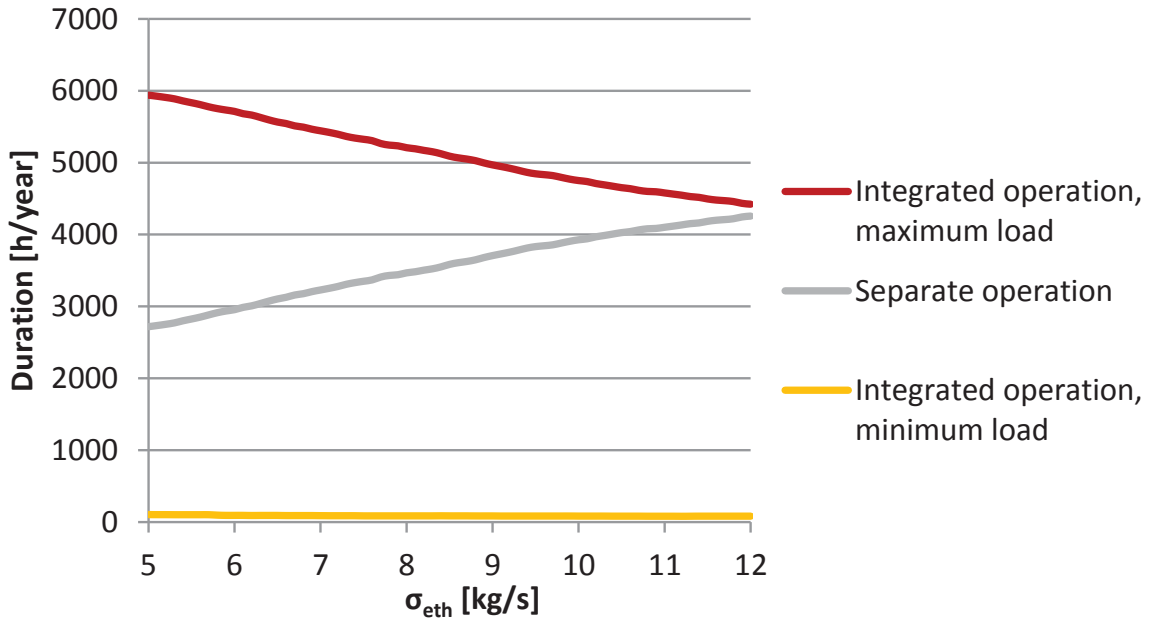

Figure 4.8: Duration of three characteristic operation modes over the year as a function of σ_{eth} [15].

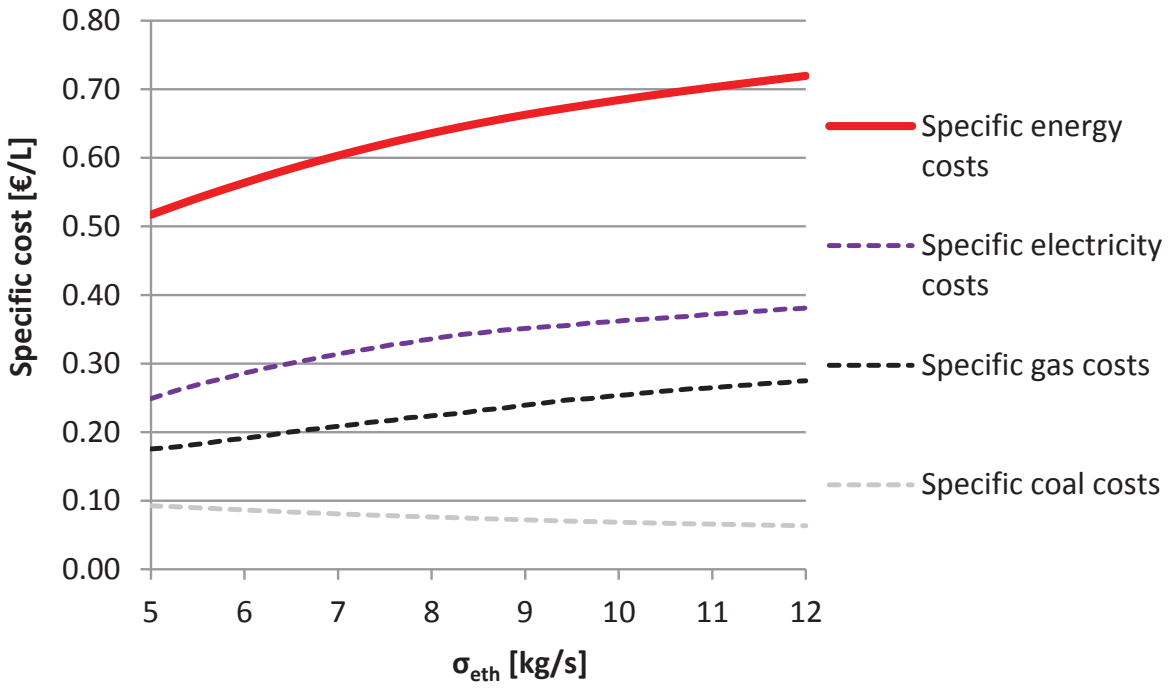

Figure 4.9: Specific energy costs as functions of σ_{eth}. Note that electricity costs include lost electricity sales [15].

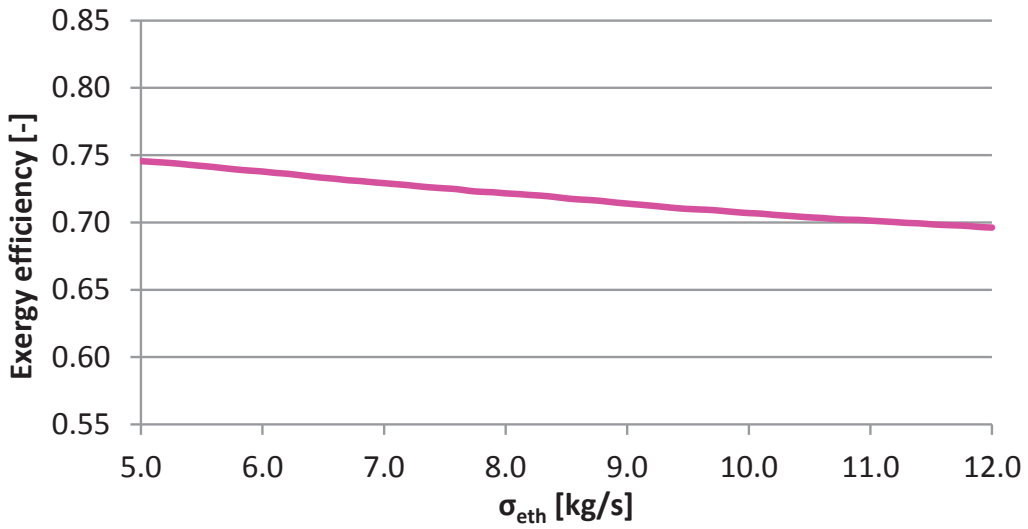

Figure 4.10: Average standard exergy efficiency of the ethanol production over the year as a function of σ_{eth} [15].

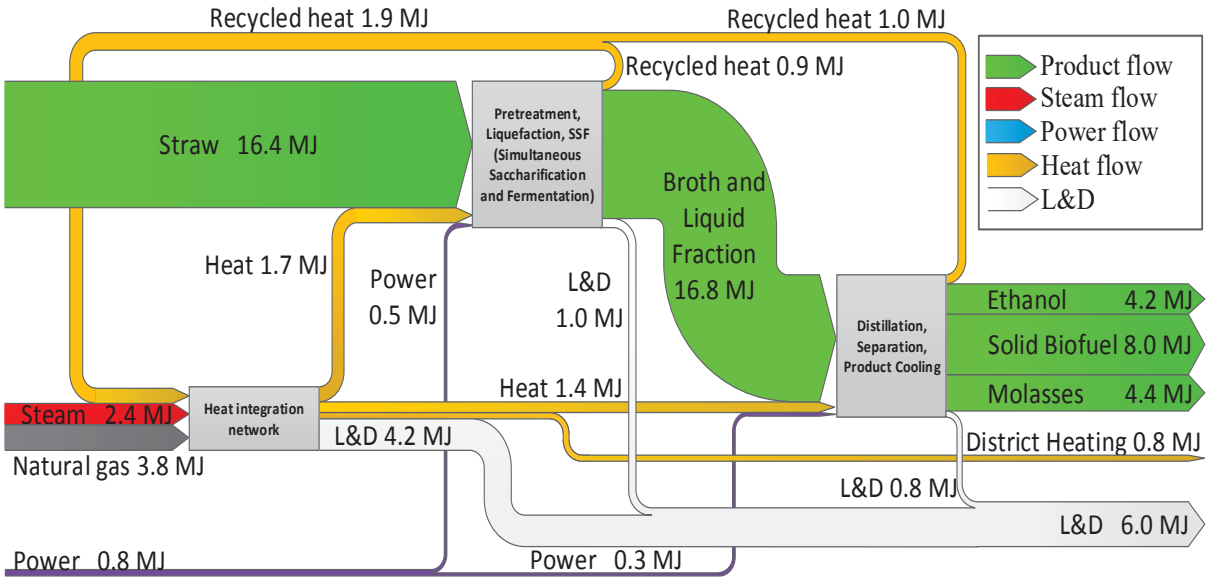

Figure 4.11: Yearly average specific exergy flows in the ethanol production for the optimized design [15].

Finally, local sensitivity analysis was applied for assessing variations in specific ethanol production cost for the optimized design in response to cost parameters variations. A spider plot of the results is presented in Figure 4.12. It was found that the straw price, natural gas price, and price of by-products would have the largest impact on the specific ethanol production cost. What is further of interest is the fact that increases in the power law scaling constant will reduce the specific ethanol production cost as the capacity of the optimal solution is smaller than the reference capacity. In effect, a higher capacity power factor will limit the increases in specific O&M and depreciation costs for smaller facilities.

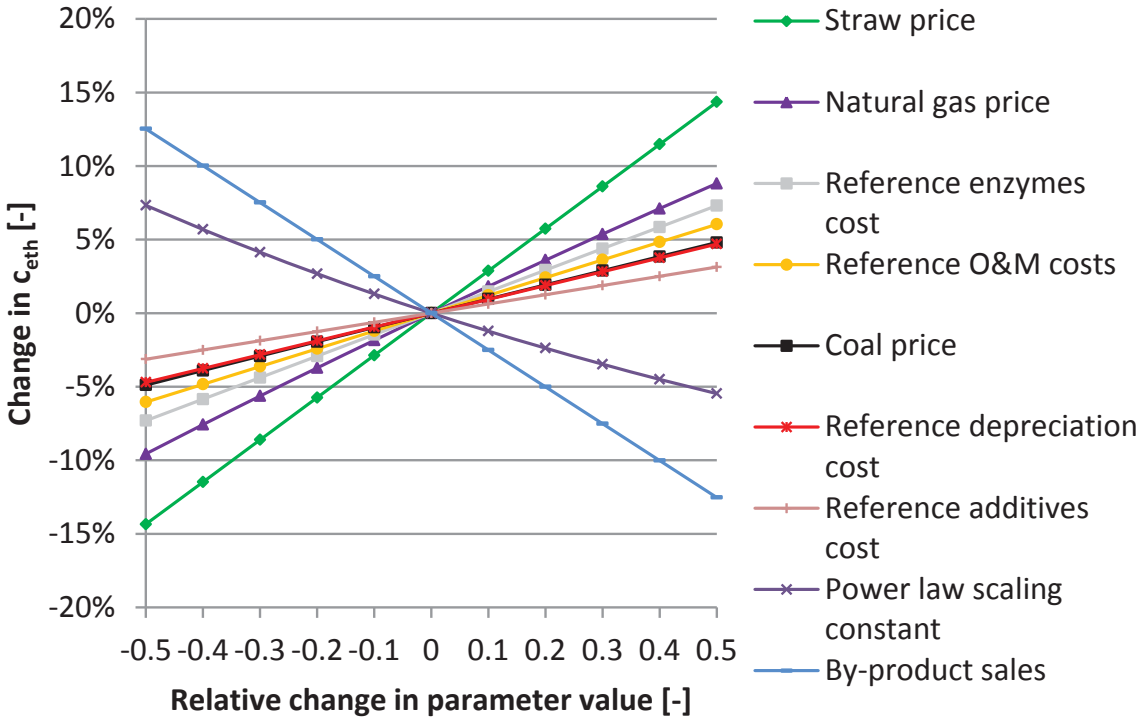

Figure 4.12: Spider plot showing the impact on specific ethanol production cost from varying different cost parameter values [15].

In addition to this, it was investigated how changes in coal and natural gas prices would affect the design optimization result. Varying the value of coal and natural gas prices from 0% to 1000% of the applied values, the design optimization result remained the same. This suggests that the diseconomy-of-scale trend prevails even for major changes in fuel costs.

4.2.4 Conclusions

The outcomes of the case study suggest that flexible operation ought to be considered when assessing the benefits of integrating biomass processing with CHP units. The integrated production of cellulosic ethanol with a CHP unit was found to increase energy efficiency, standard exergy efficiency and economic performance of the ethanol facility when compared to stand-alone production, complying with the outcomes of previous studies. However, these benefits necessitate integrated operation and a demand for district heating which cannot be expected all year round.

For the case treated, the static operation of the cellulosic ethanol production is found to induce inefficient separate operation over the year, which reduces the average standard exergy efficiency and leads to higher specific ethanol production costs when compared to

optimal design point operation. These results illustrate how system operation may have a significant impact on the overall thermodynamic and economic performances of FMGs.

In addition, the results indicate that there may be a trade-off between integration synergies and economy-of-scale benefits. For the system treated, a diseconomy-of-scale trend is found for the ethanol production, as reductions in integration synergies exceed economy-of-scale benefits for larger ethanol facilities.

The results further suggest that the integration of static facilities in flexible energy conversion systems may be troublesome, making it relevant to investigate means of inducing flexibility in otherwise static biomass processing facilities. Specifically for the case treated, it would be interesting to investigate if batch operation in the biomass pretreatment and product separation stages would be feasible, as these are found to be the most energy intensive parts of the ethanol production. If feasible, these energy intensive stages could be operated solely when excess steam capacity was available in the CHP unit, thereby reducing the demand for expensive and inefficient separate operation. The introduction of flexibility through batch processing and storages in otherwise static biomass processing is recommended as an area for future research.

4.3 Case II: Multi-generation of cellulosic ethanol, biomethane, heat and electricity in a retrofitted combined cycle CHP unit

This case treated a retrofit concept for the Danish combined cycle CHP unit 'Silkeborg Kraftvarmeværk'. The concept was inspired by the Maabjerg Energy Concept[19], and the case was used for verifying the developed design methodology and for assessing the benefit of process integration in FMGs. Pilot results were presented in Lythcke-Jørgensen et al. [77], while the final case was included in Lythcke-Jørgensen et al. [19].

4.3.1 Introduction

As described in Section 4.1, the integration of biomass processing may be seen as a business enhancement opportunity for Danish CHP units which are challenged in the present economic environment. This case treated the development of a biomass-processing FMG around the existing Danish combined cycle, back-pressure CHP unit

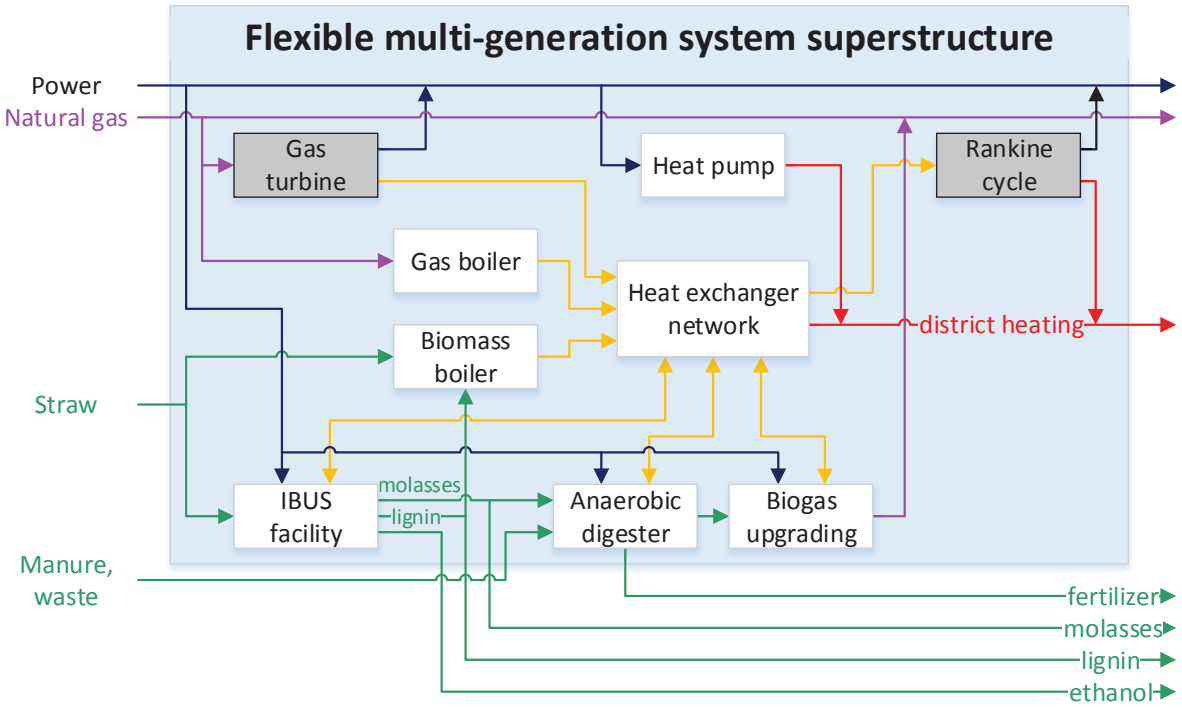

Figure 4.13: Superstructure of the FMG concept considered in *Case II*. The gas turbine and the Rankine cycle are grey as they represent the existing system that is considered for retrofitting [19].

'Silkeborg Kraftvarmeværk'[22]. The case was inspired by the Maabjerg Energy Concept[19], which is a combined FMG/biorefinery concept that integrates the conversion of local biomass resources into electricity, heat, biomethane, ethanol, and a solid lignin fraction that may be used as fuel in boilers or CHP units. In addition, the anaerobic digestion of manure reduces methane emissions from agriculture while biomass nutrients are extracted from the process and recycled as fertilizer.

Systems integrating the production of ethanol and biogas/biomethane with CHP generation have been investigated in several studies, e.g. [105–109]. Daianova et al. [105] and Ilic et al. [106] studied the grassroot design of such integrated systems and reported better energy economy for integrated production compared to stand-alone production of the same energy products, assuming constant energy prices over the year. Bösch et al. [107] studied the exergy efficiency in static design point operation for various integrated processes, among others the combined production of ethanol and biogas. Modarresi et al. [108] conducted a pinch analysis of the design point operation and reported that heat

[22] Silkeborg Kraftvarmeværk' has an electricity generation capacity of 108.3MW and heat generation capacity of 82.0MJ/s (forward/return temperatures 90^0C/40^0C) [128].

integration can reduce the hot and cold utility demands by up to 40%. Considering fixed operating conditions and no constraints on operating modes, Leduc et al. [109] conducted a parameter sensitivity analysis for such integrated systems in Sweden and found that incomes from heat and electricity sales were the most significant contributors towards reducing the specific ethanol production costs. However, none of these studies considered flexible operation or variable operating conditions.

The primary objective of this study was to evaluate if the integration synergies reported in literature could make the development of a Maabjerg Energy Concept system around an existing CHP unit a positive business case in the present Danish energy system when considering flexible operation. If the business case was found to be negative, an additional ambition was to analyse the trade-off between environmental impact and economy in the system. Apart from this, the case was used for verifying the developed design methodology. The main novelty lies in the design optimization of integrating ethanol and biomethane production in an existing CHP unit while coherently considering variable operating conditions and flexible operation as well as technology selection, process dimensioning and integration, and biomass supply chain costs. The retrofit options considered include: Ethanol production using Inbicon technology[18]; biomethane production based on the methanation of biogas from anaerobic digestion; biomass and natural gas burners; and ground-based compression heat pumps for generating district heating. A superstructure of the FMG concept is presented in Figure 4.13.

Table 4.3: *Case II*, design and operation variables considered.

Variable	Description	Lower bound	Upper bound
Design variables			
σ_{IB}	Ethanol facility dimension	5 kg straw/s	20 kg straw/s
ω_{AD}	Installation of a combined biogas facility	Integer decision $\{0,1\}$	
σ_{BB}	Biomass burner dimension, in MJ/s	0 MJ/s heat	100 MJ/s heat
σ_{HP}	District heating heat pump dimension	0 MJ/s heat	50 MJ/s heat
Operation variables			
ν_{GT}	Gas turbine operated	Integer decision $\{0,1\}$	
λ_{GT}	Gas turbine load	0.20	1.00
ν_{GT}	Steam Rankine cycle operated	Integer decision $\{0,1\}$	
λ_{SR}	Steam Rankine cycle load	0.40	1.00
λ_{GB}	Gas burner load	0.00	1.00
λ_{BB}	Biomass burner load	0.00	1.00
λ_{HP}	Heat pump load	0.00	1.00

Table 4.4: *Case II*, input parameter uncertainty distributions.

Parameter	Description	Distribution	Reference value	Lower bound	Upper bound
$C_{inv,IB0}$	Reference investment, ethanol facility	Uniform	256.0 M€	192.0 M€	320.0 M€
$C_{inv,AD0}$	Reference investment, biomethane facility,	Uniform	199.8 M€	149.9 M€	249.8 M€
$C_{inv,GB0}$	Reference investment, gas burner	Uniform	2.0 M€	1.5 M€	2.5 M€
$C_{inv,BB0}$	Reference investment, biomass burner	Uniform	40.0 M€	30.0 M€	50.0 M€
$C_{inv,HP0}$	Reference investment, heat pump	Uniform	6.8 M€	5.1 M€	8.5 M€
c_{eth}	Ethanol price	Uniform	5.70 €/GJ	4.28 €/GJ	7.13 €/GJ
z_{eth}	Ethanol, displaced CO_2 emission	Uniform	-69.2 kg/GJ	-41.5 kg/GJ	-69.2 kg/GJ
pf	General investment power factor	Uniform	0.75	0.6	0.9

4.3.2 Methodology

The case study was conducted using the FMG design methodology presented in Chapter 3. The system was set to meet local heating demands at all times, and no value was associated with district heating sales. Historical data from primo 2010 - ultimo 2014 was used for describing heat demands and electricity prices, and the data was aggregated using the CHOP method. The CHOP dataset weight was multiplied by six to represent a lifetime of 30 years. Taxes and subsidy schemes were not considered in the optimization.

Surrogate models were developed for all processes. The marginal cost of straw was calculated as a function of consumed straw quantity using the included biomass supply chain model and economic data from a report by the company EA Energianalyse [115].

Design and operation variables and associated constraints are presented in Table 4.3. For simplicity, the study only considered CO_2 emissions from facility production and avoided CO_2 emissions from displaced external production. In consequence, the environmental objective considered in the optimization was the total CO_2 emission impact (TCE) rather than GWP100a. The genetic algorithm was run for 5 generations with populations of 50.

Uncertainties in input parameters considered and their distributions are presented in Table 4.4. As no information was found on the quality or uncertainty distribution for any

of the parameters, uniform distributions were applied. The value range for investment costs and ethanol price were set to $\pm 25\%$, while it was set to $\pm 20\%$ for the investment scaling power factor. The displaced CO_2 emission from ethanol production was initially set to equal the emission of oil-based gasoline combustion. The uncertainty span for this parameter was given a value range of zero to -40%, representing the fact that the ethanol production may as well replace other biomass-based ethanol production. The extended Morris Screening was conducted using eight parameter value levels and 35 random samples of input parameters, $\{b, w_{MS}\} = \{8,35\}$. The Monte Carlo simulation was conducted using 250 random samples of input parameters, $w_{MC} = 250$, assuming no correlations between input parameter uncertainties.

Full documentation of the modelling and data applied is provided in Appendix D-E [19,36].

4.3.3 Results and discussion

Solving the optimization model, a database of feasible designs with optimized operation was obtained. Figure 4.14 shows a scatter plot of design solution performances.

It was found that NPV and TCE were reduced with increasing biomass processing facility dimensions, which illustrate the cost of avoided CO_2 emissions in the case study. It was further found that the cost of avoided CO_2 emission was higher for designs including both ethanol and biomethane production than for designs with only ethanol production. This trend was primarily caused by two effects: First, avoided CH_4 emissions from undigested manure were not considered in the calculations, which would expectedly reduce the TCE for designs with biomethane production further. Second, biogas upgrading occurred at all times, even when electricity price levels were high. In addition, operation with a district heating compression heat pump was found to be favourable for specific periods, but the investment costs made the overall economic performance of heat pumps unfavourable.

Three designs, *I*, *II*, and *III*, were selected for uncertainty analysis: *I*, the retrofit design with the highest NPV; *II*, the retrofit design with the lowest TCE; and *III*, the retrofit design with the highest NPV that included biomethane production. Characteristics of the designs are described in Table 4.5, together with the performance of the reference facility (Ref). The uncertainty analysis methodology was applied to assess performance variations of the selected designs. The resulting 10^{th} to 90^{th} percentile NPV performance interval and 0^{th} to 90^{th} percentile TCE performance interval are indicated in Figure 4.14 as well.

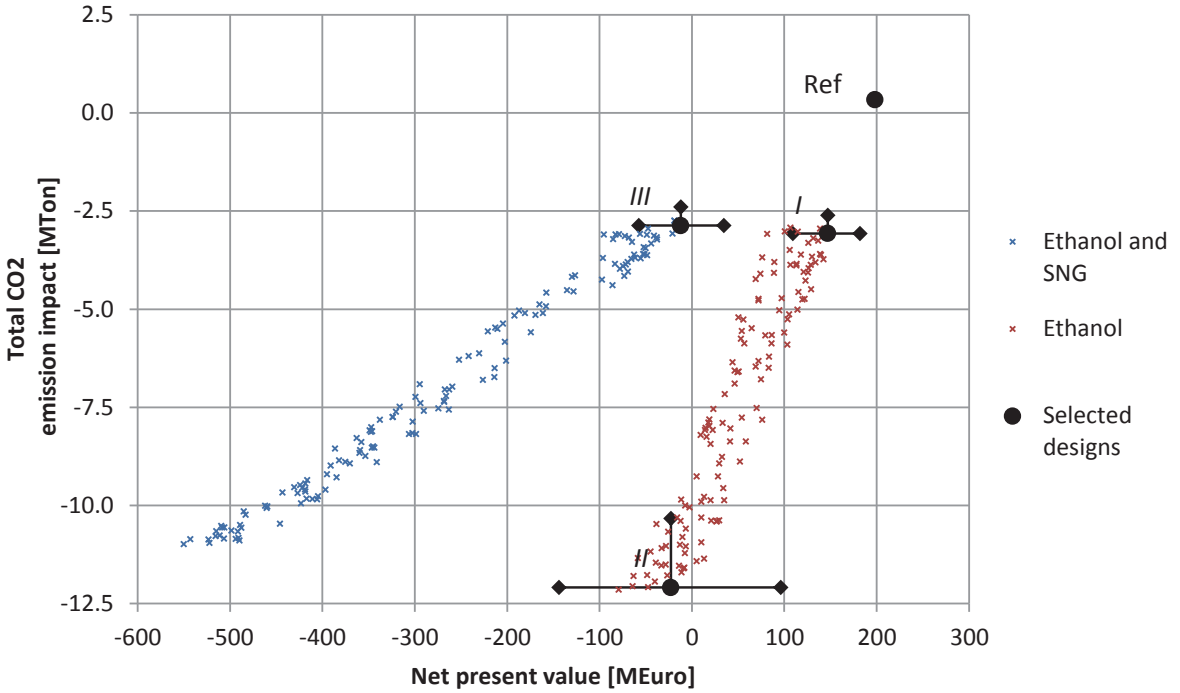

Figure 4.14: Scatter plot of optimized design solutions with respect to NPV and TCE, with performance variability indicated for three selected designs. NPV performance intervals represent 10th to 90th percentiles of predicted performance, while TCE intervals represent 0th to 90th percentiles of predicted performance [19].

Table 4.5: *Case II*, characteristics of the selected designs.

Design	NPV [M€]	TCE [MTon]	σ_{IB} [kg/s]	ν_{AD} [-]	σ_{GB} [MJ/s]	σ_{BB} [MJ/s]	σ_{HP} [MJ/s]	C_{HEN} [M€]
Ref	198.2	0.34	0.0	0	0.0	0.0	0.0	0
I	147.0	-3.07	5.2	0	80.1	1.1	0.3	4.83
II	-22.9	-12.09	19.6	0	143.8	11.1	19.8	7.51
III	-12.1	-2.87	5.3	1	70.0	1.3	9.0	4.98

The variations in NPV performance were found to be evenly distributed around the reference results as uncertainties in economic input parameters were defined as uniform and with even spans around the reference values. The absolute variations in performance were found to be larger for design *II* due to the fact that larger retrofit investments were included for this design, causing the relative uncertainties to have larger absolute impacts.

Regarding variations in TCE, it was found that the reference TCE was the lowest possible for all designs, and that the variability only pointed towards higher TCEs. This was expected, as the only uncertainty related to TCE considered, z_{eth}, was given an uncertainty span that only could lead to higher TCEs as discussed previously.

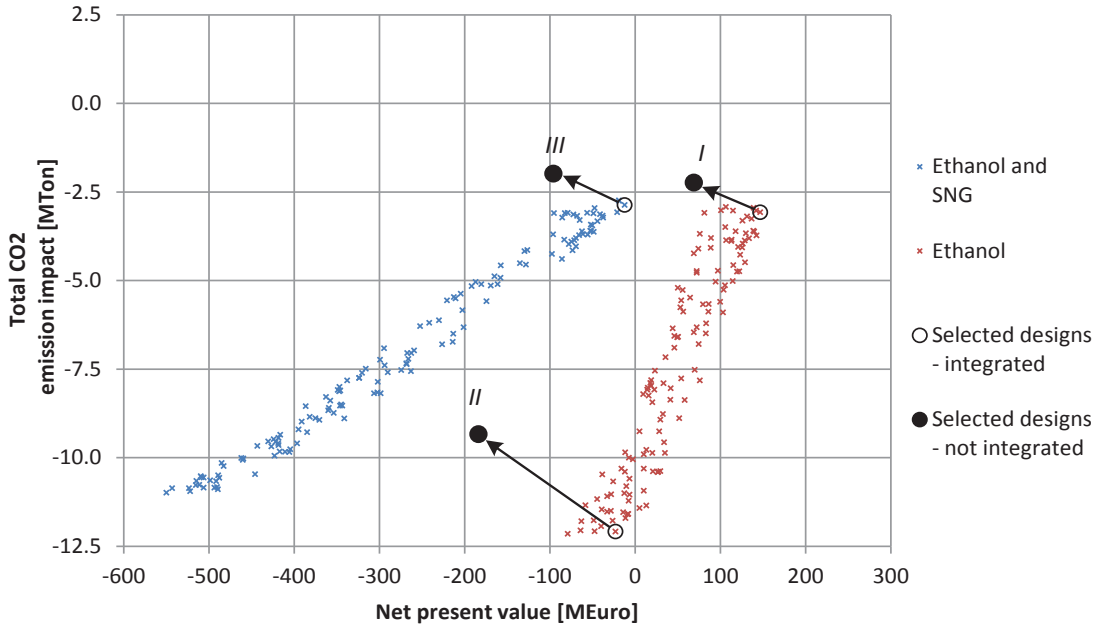

Figure 4.15: Performance of selected designs if systematic process integration had not been considered [19].

Finally, the performances of the three selected designs were evaluated if systematic process integration had not been considered. The changes in performances are shown in Figure 4.15. It was found that that without process integration, all three designs obtained performed markedly worse, with increases in TCEs of 27% to 30% and reductions in NPVs of 78M€ to 161M€. These findings emphasize the importance of considering process integration when designing FMGs in particular, but also when developing smart energy systems in general as process integration synergies offer a possibility for increasing the overall energy conversion efficiency and economy of the energy system.

Apart from the outcomes related to the specific system treated, the case was used for verifying the developed design methodology. The case work demonstrated that the design methodology is capable of optimizing the selection, dimensioning and integration of processes, of optimizing operation with respect to short-term variations, and in handling uncertainties. In effect, the case proved that the design methodology is effective in screening the solution space for efficient FMG designs, in assessing the importance of parameter uncertainties, and in estimating performance variabilities for promising designs in response to uncertainties in input parameters. However, the aspect of long-term variations due to energy system development was not treated in the present case, in which the reference data contained hourly operating conditions from a historical five-year period. The inclusion of long-term energy system development and scenario analysis is considered in *Case III*, which is presented in Section 4.4.

4.3.4 Conclusions

This case treats the development of an FMG around an existing Danish CHP unit which was inspired by the Maabjerg Energy Concept. It is found that the integration of biomass processing has a positive environmental impact but a negative economic impact on the system. The best trade-off between economy and environmental impact is obtained when integrating ethanol production but no biomethane production. In addition, the results of emphasize the importance of considering systematic process integration in the development of FMGs.

The present case is used for verifying parts of the developed design methodology. The work proves that the design methodology is effective in screening the solution space for efficient FMG designs, in assessing the importance of parameter uncertainties, and in estimating the likely performance variability for promising designs. However, the inclusion of long-term energy system development and scenario analysis is not considered.

4.4 Case III: Multi-generation of methanol, electricity, heat, and industry energy utility in a local FMG symbiosis

This case treated the development of an FMG symbiosis around the Danish CHP unit 'Horsens Kraftvarmeværk' and local industry through the installation of a methanol-producing biorefinery[23], industrial heat pumps, plus heat and gas infrastructures. The case was presented in Lythcke-Jørgensen et al. [37].

4.4.1 Introduction

Biorefineries combining gasification with the synthesis of fuels from the product gas offers a promising biomass-to-biofuel conversion route [116]. The biomass-to-biofuel conversion efficiency of such systems may be increased further by adding hydrogen to the product gas [16]. In this context, SOEC is an interesting technology for the efficient production of hydrogen from electricity. However, the integration of electricity-based hydrogen

[23] The following definition of a biorefinery was introduced by the International Energy Agency (IEA) Bioenergy Task 42: "Biorefinery is the sustainable processing of biomass into a spectrum of marketable products and energy" [129].

production is only relevant in case electricity prices in periods are lower than the biomass price or if biomass resources are limited. In addition, the high-temperature heat generated during SOEC operation should be utilized efficiently in order to obtain a high overall efficiency of the biofuel production. These observations call for a coherent approach towards the optimization of biorefinery concepts that allows for considering process integration optimization as well as energy system conditions.

This case treats the integration of a methanol-producing biorefinery[23] with the Danish waste-incineration based CHP unit 'Horsens Kraftvarmeværk'[24] and a local slaughterhouse in order to develop an efficient and competitive FMG symbiosis. The primary ambition is to assess the benefits of integrating the fuel-producing biorefinery concept with local energy supply networks for optimizing the economic and environmental performance of the combined system. The work addresses the knowledge gap between process design optimization and energy system optimization by taking system level variations into account when designing the local energy conversion system. The novelty of the study lies in the design optimization of an FMG symbiosis that coherently considers: Process selection and dimensioning; systematic process integration using pinch analysis; consideration of local demands for energy services and local infrastructures; performance assessment with respect to hourly variations in operating conditions as well as long-term energy system development; and uncertainty analysis considering uncertainties in important design parameters. In addition, the design optimization assesses performance variations with respect to various energy system scenarios. To the authors' best knowledge, no previous work has presented such comprehensive approach to the design optimization of an FMG symbiosis.

The design options considered in the case include: Biorefinery location and dimension; district heating connection between the areas; hybrid absorption-compression ammonia-water heat pumps for generating industrial process heat from district heating; and gas infrastructure for transporting unreacted product gas between the areas. The initial system layout is illustrated in Figure 4.16, while the retrofit superstructures are illustrated in Figure 4.17. The biorefinery was inspired by a concept modelled by Clausen et al. [100] and included a two-stage gasifier, a methanol synthesis reactor, and an SOEC for the production of oxygen for the gasification and hydrogen for boosting the product gas.

[24] 'Horsens Kraftvarmeværk' is a waste incineration based back-pressure CHP unit with a nominal capacity of 7.0 MWe and 25.0 MJ/s heat [130].

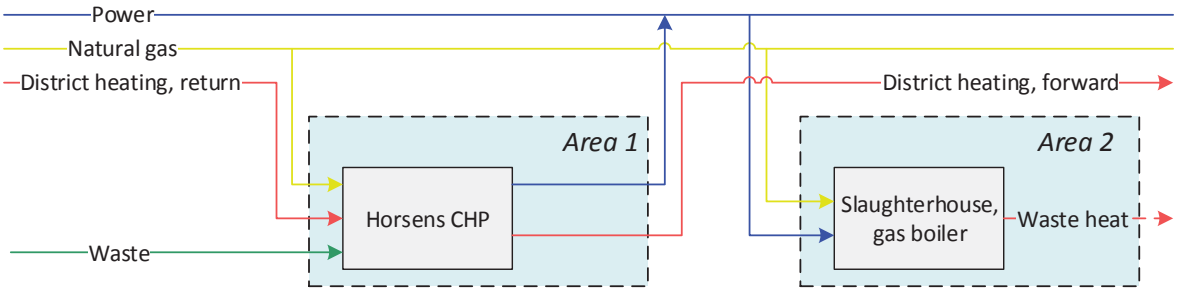

Figure 4.16: Conceptual sketch of energy flows in the reference system [37].

4.4.2 Methodology

The case study was conducted using the FMG design methodology presented in Chapter 3. The system was set to meet local heating demands at all times, no value was associated with district heating and slaughterhouse energy utility deliveries, and cooling was assumed freely available. The optimization considered operation over the period 2015-2035 using scenario data extracted from the energy system model SIFRE [117]. Data was extracted for the years 2015, 2025, and 2035. To represent the entire period, the data for 2015 and 2035 was repeated six times each while the data from 2025 was repeated eight times. The resulting dataset, which included electricity prices, heating demands, slaughterhouse energy utility demands, natural gas prices, wood chip prices, and methanol prices[25], was aggregated using the CHOP method.

Surrogate models were developed for all processes. Design and operation variables and associated constraints are presented in Table 4.6. For simplicity, TCE from facility production and avoided CO_2 emissions from displaced external production was applied as environmental objective in the optimization. The genetic algorithm was run for six generations with population sizes of 20.

Uncertainties in input parameters considered and their distributions are presented in Table 4.7. As the number of uncertain input parameters was limited, extended Morris Screening was not applied in the case study. The Monte Carlo simulation was conducted using 1000 random samples of input parameters, $w_{MC} = 1000$, assuming no correlations between input parameter uncertainties.

[25] In the study, the methanol price was defined as gasoline energy price plus CO_2 quota price of the emissions avoided by replacing gasoline with biomass-based methanol, which was set to have zero emissions in the case study.

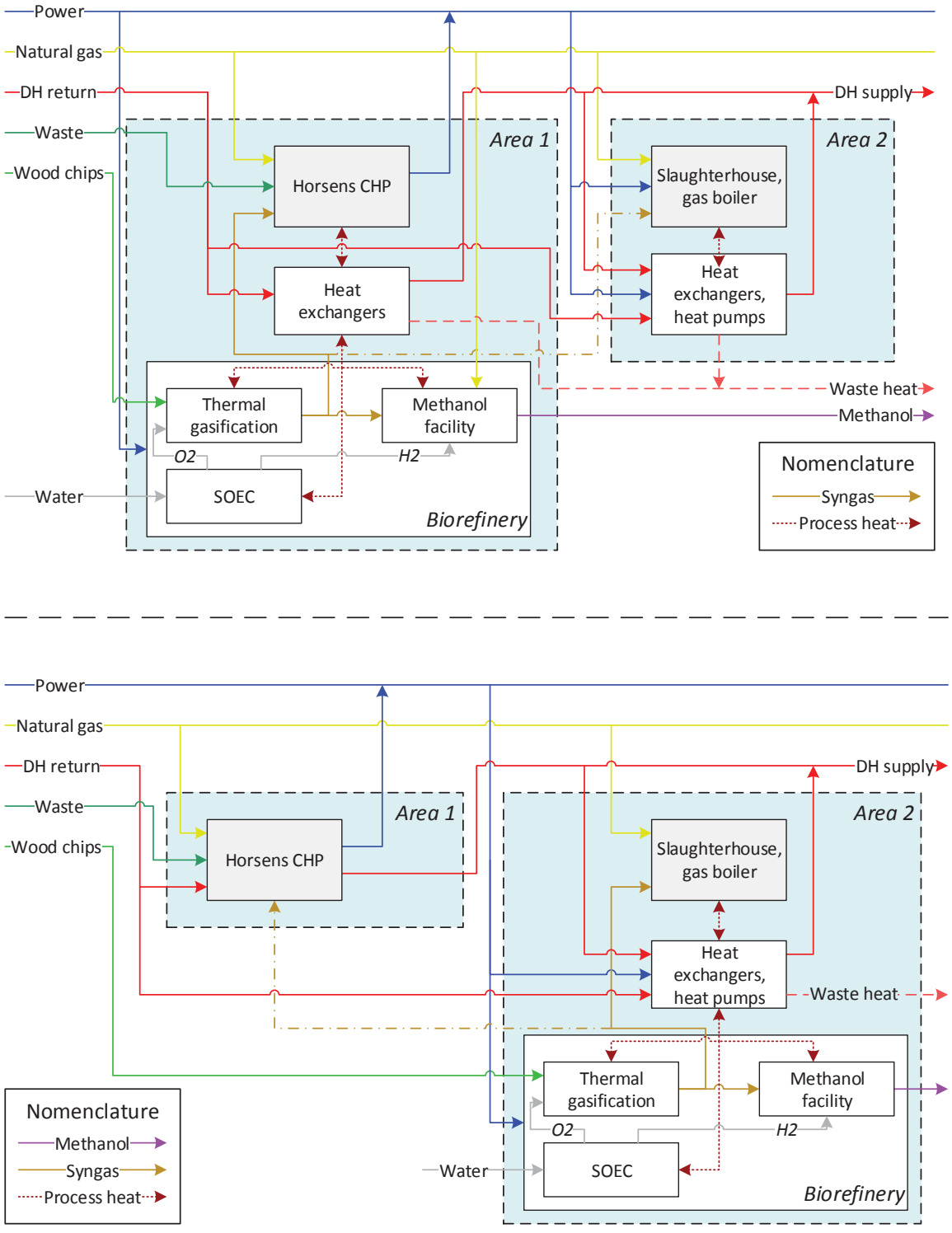

Figure 4.17: Retrofit superstructures for locating the biorefinery next to the CHP unit (top, referred to as Scenario A) or next to the slaughterhouse (bottom, referred to as Scenario B). DH is short for district heating [37].

Table 4.6: *Case III*, design and operation variables considered.

Variable	Description	Lower bound	Upper bound
Design variables			
σ_{bio}	Biorefinery dimension [MWth biomass]	5.0 MWth	200.0 MWth
ω_{bio}	Biorefinery location	Integer decision $\{0,1\}$	
ω_{gas}	Product gas connection between areas	Integer decision $\{0,1\}$	
ω_{DH}	District heating integration at slaughterhouse	Integer decision $\{0,1\}$	
Operation variables			
ν_{gt}	Gas turbine operated	Integer decision $\{0,1\}$	
λ_{gt}	Gas turbine load	0.40[a]	1.00
λ_{ran}	Waste incineration CHP load	0.75[b]	1.00
λ_{SOEC}	SOEC load	0.00	1.00
λ_{MeOH}	Methanol production load	0.00	1.00
$\lambda_{hp,ind}$	Heat pump load	0.00	1.00
$\lambda_{gb,ind}$	Industrial gas boiler load	0.00	1.00

[a] Minimum load constrained due to constraints on exhaust emissions [118].
[b] The unit was assumed operated at all times due to the demand for processing of local domestic waste.

Table 4.7: *Case III*, distributions of uncertain input parameter.

Parameter	Description	Distribution	Reference value	Lower bound	Upper bound
$C_{inv,bio0}$	Reference investment, biorefinery	Uniform	314.9 M€	236.18 M€	393.63 M€
$C_{inv,DH}$	Investment, district heating connection	Uniform	1.76 M€	1.31 M€	2.19 M€
$C_{inv,gas}$	Investment, gas infrastructure	Uniform	1.17 M€	0.88 M€	1.46 M€
$C_{inv,hp0}$	Reference investment, heat pump	Uniform	0.43 M€	0.32 M€	0.54 M€
p_f	Power factor	Uniform	0.75	0.6	0.9

To analyse the impact of variations in operating conditions, four additional scenarios were considered in the case study:

(1) A *low fuel price scenario*, where the methanol selling price was reduced by 25% compared to the reference scenario.
(2) A *high fuel price scenario*, where the methanol selling price was increased by 25% compared to the reference scenario.

(3) A scenario in which electricity prices for 2035 were taken from the *NonFlex scenario*[26] [119].
(4) A *low electricity price scenario* in which electricity prices in 2035 was reduced by a factor 7.5 compared to the NonFlex scenario.

Full documentation of the modelling and data applied can be found in Appendix F [37].

4.4.3 Results and discussion

Solving the optimization model, a database of feasible designs with optimized operation was obtained. Figure 4.18 shows a scatter plot of design solution performances. The integrated biorefinery concept was found to be competitive under the set conditions, and the larger the biorefinery dimension, σ_{bio} , the better the performance in NPV and TCE of the FMG symbiosis.

The increase in NPV as a function of σ_{bio} was found to be almost linear, suggesting that the economic result of operation, which was a linear function of σ_{bio}, had a more significant impact on the NPV than the investment cost, which was a non-linear function of σ_{bio}. In addition, it was found that the NPV and TCE were both marginally improved for designs where the biorefinery was located next to local industry due to process integration synergies and reduced infrastructure investments.

Four optimized designs, namely A1, A2, B1 and B2, were selected for uncertainty analysis: A1 was the retrofit design with the highest NPV where the biorefinery was located next to the CHP unit; A2 was an optimized retrofit design with a medium-sized biorefinery, $\sigma_{bio} \approx 80MWth$, located next to the CHP unit; and B1 and B2 were the corresponding designs where the biorefinery was located next to the slaughterhouse instead of next to the CHP. Design and performance characteristics of the four selected designs are summarized in Table 4.8.

Monte Carlo simulations were conducted for each of the four designs for the defined input parameter uncertainties, and the resulting 10th to 90th percentile NPV performance

[26] The NonFlex scenario is an energy system simulation scenario based on the assumption that smart grid technology will not break through in Denmark by 2035, meaning that the operation of electric vehicles, individual heat pumps and electrolysis plants is not optimized for the electricity price in the scenario simulations [119].

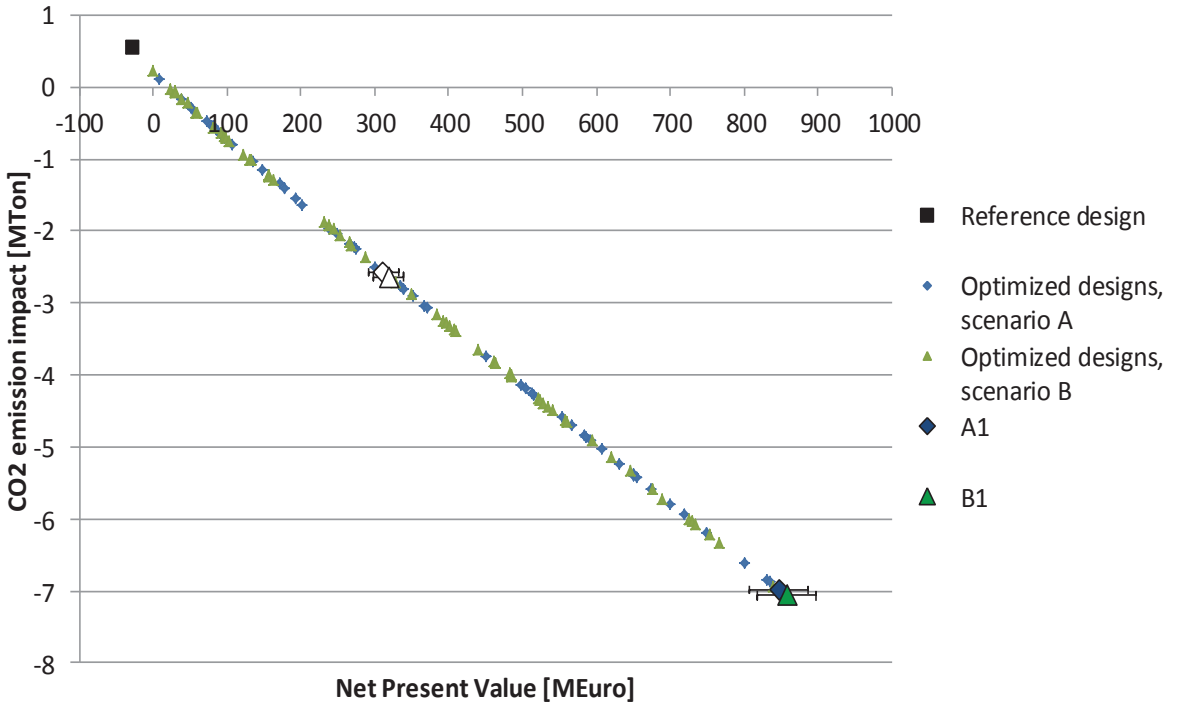

Figure 4.18: Scatter plot of optimized design solutions with respect to NPV and TCE, with 10th to 90th percentiles NPV performance intervals indicated for the four selected designs [37].

Table 4.8: *Case III*, design and performance characteristics of the four selected designs.

Design solution	NPV [M€]	CO_2 emission impact [MTon]	σ_{bio}	ω_{DH}	ω_{gas}
A1	847.3	-6.98	199.3	0	1
A2	312.0	-2.57	81.2	1	0
B1	857.6	-7.07	199.9	0	0
B2	319.0	-2.63	82.4	1	0

intervals are indicated on Figure 4.18. The performance variations of the designs were found to be minor when compared to the overall NPV result, supporting the claim that investment costs had less impact on the NPV than the operation result.

To assess the impact of variations in operating conditions, the performances of the four selected designs were optimized for each of the four additional energy system scenarios considered. The results are presented in a scatter plot in Figure 4.19.

From the figure, it is evident that the considered uncertainties in the methanol prices have a markedly higher impact on NPV for the designs than the uncertainties considered for investment costs. An increase of 25% in methanol price in the *high fuel price scenario* increased the NPVs of the four selected designs by 67%-75%, while a similar reduction in

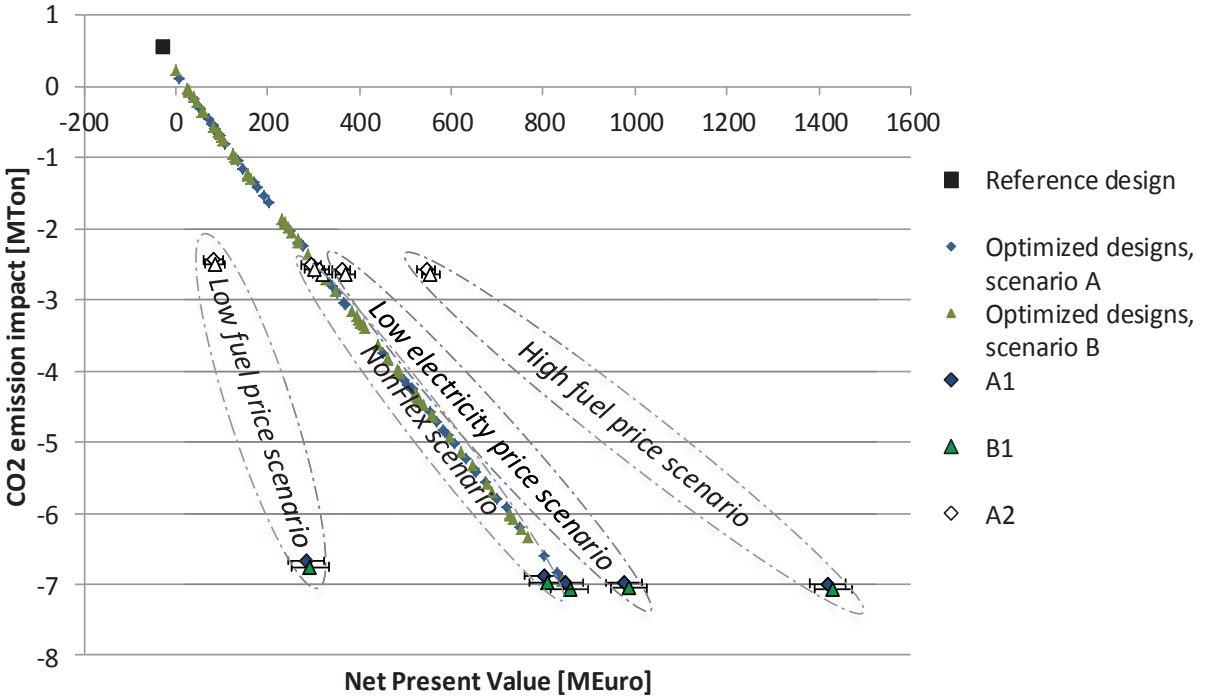

Figure 4.19: Performances of the four selected designs under the various energy system scenarios. Results of the investment cost uncertainty analysis are indicated as well [37].

methanol price of 25% in the *low fuel price scenario* resulted in NPV reductions of 66%-74%. Opposed to this, significant changes in electricity prices over the last six years of the period in the *low electricity price scenario* and *NonFlex scenario* were not found to have a similar significant impact on NPV performance for the FMG treated. The reason was that the considered changes in electricity prices had little effect on the operating pattern of the SOEC due to the high methanol prices. In general, it was found that the economic result from operating the SOEC was only marginal when compared to the economic result of converting wood chips to methanol in the gasifier alone.

In the case study, the SOEC included in the biorefinery concept was dimensioned after the maximum feasible hydrogen addition to the product gas. However, as the price on wood chips was cheaper than the electricity price at almost all times, it would be relevant to investigate how the performances of the designs would change if the SOEC installation decision and dimensioning had been included as design variables in the optimization.

Regarding environmental impact, the TCE was found to increase in the *low fuel price scenario* and *NonFlex scenario* for all designs. This was caused by the fact that the electricity-to-methanol price ratio was increased, making SOEC operation economically infeasible for increased durations over the period. As the CO_2 emissions associated with

electricity consumption on average were lower than the CO_2 emissions avoided by the produced methanol, the reduction in methanol production increased the TCE of the system in these scenarios.

Concerning TCE calculations in general, it must be emphasized that emissions associated with electricity generation and consumption may be regarded as conservative estimates as annually averaged electricity generation emissions were used. In practice, it is expected that the share of renewables in the electricity mix would be higher during periods of low electricity prices and lower during periods of high electricity prices. As the optimized FMG operation causes the system to increase electricity consumption and reduce generation in periods with low prices, and vice versa in periods with high prices, it is expected that the consumed electricity on average will have lower marginal CO_2 emissions while generated electricity is expected to replace production with higher marginal CO_2 emissions. In effect, this suggests that the overall TCE calculated for the optimized designs may be smaller than what is calculated. However, in order to verify these considerations, an assessment of the system impact from FMG operation must be conducted.

Regarding integration synergies, cooling was assumed available for free, meaning that benefits from increasing the overall energy conversion efficiency in the FMG are not directly evident from the economic performance. Adding to this, the limited operational flexibility of the CHP unit in the given case meant that the possibilities for utilizing excess process heat as district heating were limited. In consequence, the results indicate that the overall conversion efficiency decreases with increasing σ_{bio}, and the benefits from integration synergies were found to be marginal when compared to the impact of increasing the biorefinery dimension. It would be relevant to investigate how the optimal design would be affected by adding a value to the delivered energy services as well as constraining the availability of free cooling, as these impacts may change the design optimum for the given case.

In addition, only limited integration possibilities were considered in the modelled system. It would be relevant to assess the economic performance and energy conversion efficiency further for a system with a larger degree of freedom in the CHP unit, and to allow for a ‘tighter’ thermal integration between facilities, e.g. through the extraction of steam at various points in the Rankine cycle for running the biorefinery, to increase integration synergies and performances for the FMG symbiosis further.

On a more general note, the outcome regarding conversion efficiency points towards the dilemma of where to locate biorefineries and biomass-processing FMGs. On one hand, the utilization of excess heat for district heating purposes may increase the energy conversion efficiency of the systems significantly. However, the systems should also be located close to biomass resources in order to minimize transportation demands, and therefore not in densely populated areas where district heating is applicable. The trade-off between these two aspects is an interesting topic for further research.

Apart from the case-specific findings, this case further demonstrates that the design methodology is capable of considering long-term energy system development and scenario analysis. Combined with the findings of *Case II*, this shows that the developed design methodology is capable of considering all five design aspects that were listed as of special relevance in Chapter 2, thereby verifying the methodology.

4.4.4 Conclusions

In summary, the outcomes of this case illustrate how variations in operating conditions may have a significant impact on overall performances of FMGs. For the biorefinery concept treated, a reduction in methanol prices of 25% leads to decreases in NPV of 66%-74% for the selected designs, while changes in investment costs of $\pm 25\%$ result in NPV changes of up to $\pm 5\%$. These outcomes stress the importance of including uncertainty analysis in the design and optimization of FMG concepts.

On the contrary, the FMG performance is found to be robust with respect to significant changes in electricity prices during the last six years of the 20-year period. This is caused by the fact that the economic income from biorefinery operation is primarily driven by the high wood-chip-to-methanol price ratio. This finding suggests that investments in the SOEC are only beneficial in case investment resources are infinite, if biomass supply is limited, or if additional incentives are provided for converting electricity to fuels.

Another interesting outcome of the case study is the insignificant impact of integration synergies, caused by a combination of several factors. First of all, it is assumed that cooling utility is freely available, and zero income is associated with district heating and energy utility services for the slaughterhouse. In effect, energy efficiency is not accounted for directly in the NPV. Second, the energy demands of the slaughterhouse and district heating community are limited in comparison to the biorefinery dimensions considered,

and as the CHP operation has little operation flexibility, process integration synergies are found to be marginal when compared to the economic and environmental impact of the biorefinery. These outcomes illustrate how it may be challenging to retrofit existing systems when developing FMGs, and they stress how local system constraints must be considered in the design optimization of FMG concepts.

Finally, the case verifies that the developed design methodology is capable of considering long-term energy system development as well as handling scenario analysis.

4.5 Summary of findings

Three case studies on FMG concepts treating various technologies, design and operation aspects, and energy system settings have been conducted. The main outcomes of the studies are summarized here with respect to four overall aspects:

Process integration synergies

As illustrated by the findings of *Case I* and *Case II*, properly integrated FMGs may perform better with respect to both economy and environmental impact than stand-alone systems. However, the findings also illustrate how process integration synergies are constrained by the types and dimensions of the processes to be integrated and the expected operating patterns. In *Case III*, the combination of dimensional mismatch between the existing systems and the biorefinery concept considered and the lack of operation flexibility in the existing system caused benefits from process integration synergies to be marginal when compared to the overall economic and environmental performances of the FMG designs. This outcome demonstrates a challenge faced when retrofitting existing systems: Overall synergy potential depends on local conditions, dimensions of existing processes as well as type of technology considered. In effect, the case study findings recommend that process integration synergies are systematically assessed and quantified when optimizing FMG concepts, and that local conditions and constraints are considered in the assessment.

Variable operating conditions

As illustrated in *Case I*, flexible operating patterns ought to be considered when assessing and optimizing performances of FMG concepts. In the case, cellulosic ethanol production

is found to be competitive when operated in integration with a CHP unit, but as the integration is terminated for a significant part of the year due to CHP maintenance shut-downs and periods with high CHP unit loads, the overall ethanol production costs are found to be uncompetitive.

Uncertainty assessment

As illustrated by the findings of *Case III*, uncertainties ought to be assessed in order to estimate performance variations in response to uncertainties in input parameters and operating conditions. For the optimized design in the case, B1, the NPV is estimated to vary within the range 52.5 M€ to 1471.6 M€, or 6.1% to 171.6%, in response to value changes of $\pm 25\%$ in investment costs and methanol price. These results stress the importance of including systematic uncertainty assessment for evaluating performance robustness to input uncertainties when designing and optimizing FMG concepts.

Design methodology verification

In addition to these findings, *Case II* and *Case III* demonstrate how the developed design methodology is efficient in screening for promising FMG designs within the defined solution space, and that it can be used for considering process selection and dimensioning, process integration, short-term and long-term operation, and uncertainty analysis in a coherent manner. The two case studies thereby verify that the developed design methodology meets the expectations stated in Section 2.3, and they further suggest that the developed methodology may be useful, either directly applied or as a benchmark, for future research on FMG concepts.

Related to this, it must be stressed that the developed FMG design methodology is mainly seen as advantageous in the screening for relevant FMG designs when a large number of candidate technologies and long-term operation horizons are considered. In other words, the developed methodology may be regarded as a pre-feasibility tool, as also discussed in Chapter 3. The design methodology is not recommended for detailed short-term operation optimization of specific FMG designs.

5 CONCLUSION

This thesis is concluded with a summary of the findings regarding developed methods and case studies, along with suggestions for further research within the topic of FMGs.

5.1 Summary of findings

Methodology development

This project treated the design and optimization of flexible multi-generation plants (FMGs), which are defined as systems of integrated facilities that provide multiple links between layers of the energy system. The main hypothesis is that these systems can support the cost-efficient integration and balancing of variable renewable energy sources in the overall energy system by linking the different energy sectors and local energy supply systems. This implies that efficient FMG concepts must be designed to fit in with both the overarching energy system context as well as the local context.

Five design aspects have been identified as of special relevance when developing FMGs:

(1) *Process selection and dimensioning*
(2) *Process integration*
(3) *Short-term operation* (performance assessment with respect to hourly, daily and seasonal changes in operating conditions)
(4) *Long-term operation* (performance assessment with respect to long-term changes and developments in the surrounding energy system)
(5) *Uncertainty analysis* (assessment of performance variations in response to uncertainties in estimated parameter values and external operating conditions).

These aspects must be treated in an integrated manner as they may be interdependent. However, a literature study on methodologies for designing multi-generation systems illustrated how none of the previously presented design methodologies treated all five design aspects coherently.

Responding to this finding, a novel methodology for designing FMGs was developed. The methodology applies a number of methods, including pinch analysis, economic analysis of process systems, genetic algorithm and mixed integer-linear programming optimization, extended Morris screening, and Monte Carlo simulations. In addition, the methodology features a novel characteristic period method for aggregating external operating condition datasets, named the CHOP method, which is proven capable of sustaining information on parameter value correlations in the reduced dataset whilst achieving dataset reductions comparable to what is obtained using simple data averaging. Combined, the methodology allows for coherent design optimization of FMGS considering: Selection, dimensioning, location and integration of processes; operation optimization with respect to both hourly variations in operating conditions as well as long term energy system development; biomass supply chains and local resource availability; combined with uncertainty analysis. However, a main shortcoming of the methodology is the fact that storages cannot be considered.

Applied in two case studies, the design methodology was proved effective in screening the solution space for promising FMG designs, in assessing the importance of uncertainties in operating condition and parameter values, and in estimating the likely performance variability of promising designs. In effect, it coherently considers the five listed design aspects. The methodology is especially considered useful in the screening for promising FMG designs when a large number of candidate technologies and long-term operation horizons are considered, and may consequently be regarded as a pre-feasibility tool.

Case studies

Three FMG case studies were conducted, all focussing on developing FMGs by integrating biomass processing technology in existing Danish combined heat and power (CHP) units.

Case I treated the integration of cellulosic ethanol production in an extraction CHP unit. A design point thermodynamic analysis of the integrated system showed that up to 94.5% of the hot utility demand of the ethanol production could be recovered and utilized for district heating, while a standard exergy efficiency of 0.91 was calculated for the ethanol production if all heat exchange occurred at a temperature difference of 10K.

Optimizing the design of the integrated system considering ethanol facility dimension and hour-by-hour operation flexibility over the year, none of the feasible designs were found

to be competitive in producing ethanol when compared to an expected average ethanol market price of 0.55 €/L. The lowest specific ethanol production costs, 0.958 €/L, was obtained for the design with the smallest ethanol facility dimension. This diseconomy-of-scale result was caused by the combination of static ethanol production and variations in operation conditions and constraints on the CHP unit, which induced longer durations of separate operation over the year for larger ethanol facilities. The associated reductions in total process integration synergies for larger ethanol facilities were found to exceed the economy of scale benefits.

For the optimal design, average specific energy costs of the ethanol production were found to be 0.213 €/L during integrated operation and 1.192 €/L during separate operation. Combined, the results of *Case I* illustrate how integration with CHP units may provide substantial improvement to the efficiency and economic performance of biomass conversion technologies. However, the results also indicate that a trade-off may exist between integration synergies and economy-of-scale benefits for FMGs when retrofitting existing systems and they further stress the relevance of considering variable operating conditions when evaluating FMG performances.

Case II treated the development of an FMG concept inspired by the Maabjerg Energy Concept around an existing combined cycle CHP unit. Retrofit options included cellulosic ethanol production, biomethane production, biomass and gas burners, and ground based compression heat pumps for generating district heating. The developed design methodology was applied for solving the design optimization, which considered historical operating data. It was found that the biomass processing technologies considered were economically unfeasible under the set conditions, and a trade-off was identified between net present value (NPV) increases and CO_2 emissions reductions. The best trade-off was obtained when installing ethanol production and no biomethane production.

In a further assessment of three selected designs, it was found that all three designs performed markedly worse if systematic process integration had not been applied: The CO_2 emission impacts were increased by 27% to 30% while NPVs were reduced by 78M€ to 161M€ when process integration was not considered. These findings illustrate how process integration synergies may provide significant improvements for FMGs with respect to environmental and economic performance.

Case III treated the development of a local FMG symbiosis around an existing waste-incineration based CHP unit and a local slaughterhouse through the installation of a

methanol-producing biorefinery based on wood chip gasification and solid oxide electrolysis cells (SOECs). In addition, heating and gas infrastructure were considered for integrating the slaughterhouse and the CHP unit areas. The developed design methodology was applied for solving the optimization, which considered the period 2015-2035 using scenario data from an energy system simulation model.

Solving the design optimization, the biorefinery concept was found to be competitive under the set conditions. The optimized design involved the largest feasible biorefinery located next to the slaughterhouse and no infrastructure connections. The process integration synergies were found to be marginal for the case treated due to several causes: First of all, internal reuse of heat in the biorefinery meant that integration synergies were limited for this process. Secondly, steam extraction at intermediate stages in the CHP unit was not considered. Finally, the existing CHP unit was assumed to have limited operation flexibility, meaning that the possibility of utilizing excess heat from the biorefinery and slaughterhouse for district heating purposes was limited.

Assessing system uncertainties for four selected designs, it was found that variations in methanol prices would have significant impact on the economic performance of the designs: A methanol price increase of 25% would increase design NPVs by 67%-75%, while a similar reduction in methanol price of 25% resulted in NPV reductions of 66%-74%. Opposed to this, changes of $\pm 25\%$ in estimated investment costs only resulted in NPV changes of up to $\pm 5\%$, while very low electricity prices over the last 6 years of the period increased NPVs by 15%-16%. These outcomes illustrate how the economic performance of the methanol-producing biorefinery is highly dependent on fuel prices, and how operating condition uncertainties may have a significant impact on performance variations.

In summary, the outcomes of the case studies may be condensed into three general recommendations regarding the development of FMGs:

(1) *Process integration* may increase economic performance, reduce environmental impact, and increase the energy conversion efficiency of FMGs. However, the synergy potentials may be limited by local conditions, e.g. limited demands for district heating, as well as integration possibilities and constraints within the technologies considered. It is therefore recommended that integration synergy potentials are assessed when developing flexible energy conversion systems, and in case significant potentials are discovered, process integration ought to be included systematically in the design optimization of the FMG concept in question.

(2) *Variable operating conditions*, both in the overarching energy system and in local systems, may have a significant impact on the total performance of FMGs. The outcomes of the case studies indicate that assessment in design point operation is inadequate for estimating actual performances of FMG concepts. In effect, it is recommended that variable operating conditions are always considered in detail when assessing the performances of FMG concepts.
(3) *Uncertainty assessment* is important when evaluating the performance of FMGs. As indicated by the case results, minor variations in especially operating conditions may lead to significant variations in performances. In effect, it is recommended that systematic assessment of uncertainties is considered when evaluating FMG concepts in order to assess the robustness to changes of the identified designs.

5.2 Recommendations for further research

Design methodology development

In the developed design methodology, variable and fluctuating operating conditions were represented as fixed parameters in reduced datasets. This means that feedback mechanisms between FMG operation and the overarching energy system are not considered in the design optimization. One may say that the design methodology is founded at the process model level but tries to take energy system level details into account, as conceptually illustrated in Figure 5.1 (left). However, the CHOP method developed and applied for aggregating energy system data does not allow for the inclusion of dynamics and time chronology, meaning that dynamic constraints and storages cannot be considered when assessing the FMG performance. Though not unique when compared to other design methodologies presented, these facts are still considered as significant shortcomings of the design methodology.

In consequence, a logic sequential step to optimizations conducted using the design methodology would be to extract a number of promising designs from the results and include them as fixed designs in e.g. a national energy system model. Depending on the energy system model, this would allow for operation optimization considering both energy system feedback and storages for the extracted designs. Resulting performances could then be used as feedback for the design methodology, as conceptually illustrated in Figure 5.1 (right). In this way, the performance assessment of the designed FMGs would

be moved to the energy system level, while the drawbacks of not considering storages and dynamic constraints could be circumvented. In addition, outcomes of such iterations may provide valuable feedback for improving the FMG design methodology, and may ultimately be used for validating whether or not the design methodology is efficient at identifying promising design solutions when storages and dynamics are to be considered. Integrating the FMG design methodology with an energy system model is therefore recommended as an area for further research.

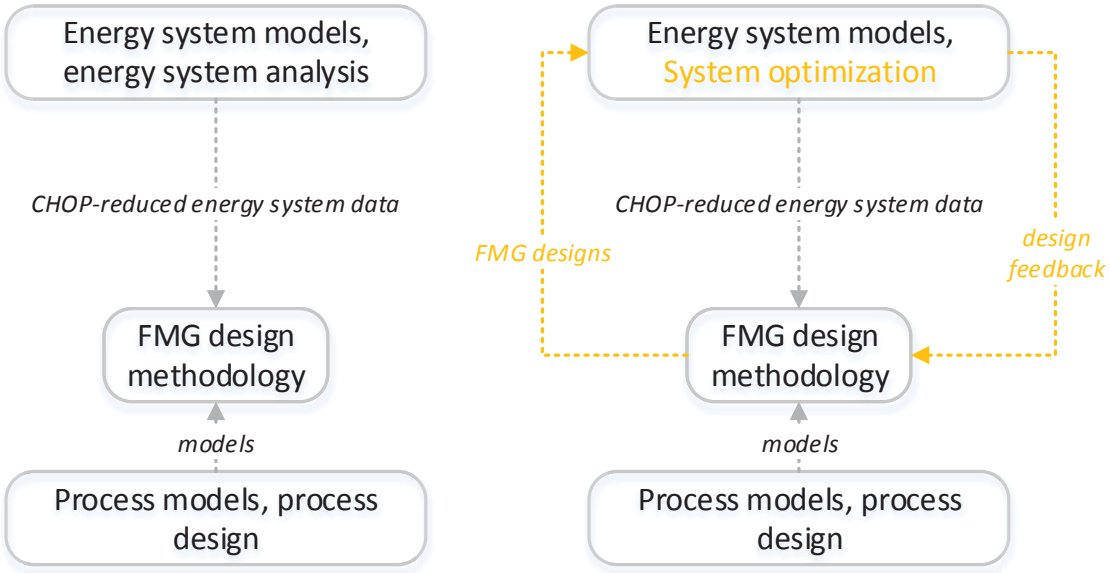

Figure 5.1: Illustration of the connection between the FMG design methodology, energy system models and process models in the present version (left) and the suggested feedback mechanism between the FMG design methodology and an energy system model (right).

Methodology application

Robust design optimization of FMGs

Another interesting topic for further research is to assess the robustness of optimized FMG designs under various energy system scenarios. This could be done by repeating the entire design optimization using the developed methodology for a number of likely energy system scenarios and assess how the optimal design, or the Pareto efficient designs, changes between the scenarios. The outcomes could then be used for estimating the frequency of each design configuration to be optimum, and thereby estimate the robustness of the designs with respect to variations in energy system development.

Benchmarking of biomass processing technology

The developed design methodology offers a framework for evaluating the performance of competing biomass processing technologies and biorefinery concepts with respect to a defined energy system context. The automated process integration further allows for assessing the integration synergy potentials of various technologies in FMG concepts. In addition, such assessment may reveal additional aspects that ought to be considered when designing FMGs, thereby allowing for iterative development of the design methodology. The assessment and comparison of competing biomass processing technology is suggested as an interesting area for further research.

Related research areas of interest

Adding flexibility to static biomass processing equipment

An outcome of this study is the finding that the integration and operation of static cellulosic ethanol production with flexible CHP generation may be challenging under variable operating conditions. In consequence, it is suggested that batch processing in the energy intensive stages of the ethanol production may be advantageous, as this would allow for shifting energy intensive operation to periods where energy prices are low. However, batch operation would necessitate larger processing equipment and the integration of storages, leading to additional investment costs. This trade-off between increased investments and improved operation flexibility cannot be considered within the developed methodology at its present state as it does not allow for inclusion of storages, but is recommended as an area for further research.

Practical obstacles towards the development of FMGs

Apart from the technical aspects of FMGs, there may be numerous non-technical obstacles towards the development of such 'energy symbioses' in practice. As revealed in the synthesis report from the seminar *Symbiose Strømme*[27], a major challenge perceived

[27] The 'Symbiose Strømme' was a working seminar organized in part by the Danish Symbiosis Center (http://www.symbiosecenter.dk/) and held in December 2014. Focus area was the development of industrial symbioses with respect to energy and material flows. More information can be found on the webpage: http://www.symbiosestroemme.org/

by industry towards the development of integrated systems and industrial symbioses is the implied dependency on other companies and bodies. So even if major technical, economic and environmental benefits may exist for FMGs and industrial symbioses, non-technical challenges may cause them to be impractical. As the outcomes of this study suggest that significant integration synergies may be obtained through the development of FMGs and industrial symbioses, it is recommended that future research address the non-technical challenges towards realising these potentials in practice.

REFERENCES

[1] IPCC. IPCC, 2013: Summary for Policymakers. Clim. Chang. 2013 Phys. Sci. Basis. Contrib. Work. Gr. I to Fifth Assess. Rep. Intergov. Panel Clim. Chang., 2013, p. 1–28. doi:10.1017/CBO9781107415324.

[2] IPCC. IPCC, 2014: Summary for Policymakers. 2014. doi:10.1007/s13398-014-0173-7.2.

[3] Energinet.dk. Dansk vindstrøm slår igen rekord – 42 procent (http://energinet.dk/DA/El/Nyheder/Sider/Dansk-vindstroem-slaar-igen-rekord-42-procent.aspx.) 2016.

[4] Energistyrelsen. Energiscenarier frem mod 2020, 2035 og 2050 2014.

[5] Energinet.dk. Strategisk energiplanlægning - Danmark 2025, 2035 og 2050 2014:1–12.

[6] Energinet.dk. Energy Concept 2030 – Summary (http://www.energinet.dk/DA/KLIMA-OG-MILJOE/Energianalyser/Analyser/Fremtidens-Energi/Sider/default.aspx). Energinet.dk 2015.

[7] European Commission. EU energy, transport and GHG emissions, trends to 2050. Reference scenario 2013. 2014. doi:10.2833/17897.

[8] Liu P, Pistikopoulos EN, Li Z. Energy systems engineering: Methodologies and applications. Front Energy Power Eng China 2010;4:131–42. doi:10.1007/s11708-010-0035-8.

[9] Lund H, Andersen AN, Østergaard PA, Mathiesen BV, Connolly D. From electricity smart grids to smart energy systems - A market operation based approach and understanding. Energy 2012;42:96–102. doi:10.1016/j.energy.2012.04.003.

[10] Mathiesen BV, Lund H, Connolly D, Wenzel H, Østergaard P a., Möller B, et al. Smart Energy Systems for coherent 100% renewable energy and transport solutions. Appl Energy 2015;145:139–54. doi:10.1016/j.apenergy.2015.01.075.

[11] Mathiesen BV, Lund H, Connolly D, Østergaard PA, Möller B. The design of Smart Energy Systems for 100% renewable energy and transport solutions. B. Abstr. 8th Conf. Sustain. Dev. Energy, Water Environ. Syst. — 2013, 2013, p. 1–19.

[12] DTU. DTU International Energy Report 2015 : Energy systems integration for the transition to non-fossil energy systems (http://www.natlab.dtu.dk/english/Energy_Reports/DIER-2015). 2015.

[13] Gassner M, Maréchal F. Thermo-economic optimisation of the polygeneration of synthetic natural gas (SNG), power and heat from lignocellulosic biomass by gasification and methanation. Energy Environ Sci 2012;5:5768. doi:10.1039/c1ee02867g.

[14] Gassner M, Marechal F. Increasing Efficiency of Fuel Ethanol Production from Lignocellulosic Biomass by Process Integration. Energy and Fuels 2013;27:2107–15.

[15] Lythcke-Jørgensen C, Haglind F. Design optimization of a polygeneration plant producing power , heat , and lignocellulosic ethanol. Energy Convers Manag 2015;91:353–66. doi:10.1016/j.enconman.2014.12.028.

[16] Clausen LR. Maximizing biofuel production in a thermochemical biorefinery by adding electrolytic hydrogen and by integrating torrefaction with entrained flow gasification. Energy 2015;85:94–104. doi:10.1016/j.energy.2015.03.089.

[17] Ogunnaike BA. Preface to the Special Issue on Process Engineering of Energy Systems. Ind Eng Chem Res 2013;52:3043–3043. doi:10.1021/ie400427a.

[18] Chicco G, Mancarella P. Distributed multi-generation: A comprehensive view. Renew Sustain Energy Rev 2009;13:535–51. doi:10.1016/j.rser.2007.11.014.

[19] Lythcke-Jørgensen C, Ensinas A V., Münster M, Haglind F. A methodology for designing flexible multi-generation systems (in press). Energy 2016:1–21.

[20] Lythcke-Jørgensen C, Haglind F, Clausen LR. Exergy analysis of a combined heat and power plant with integrated lignocellulosic ethanol production. Energy Convers Manag 2014;85:817–27. doi:10.1016/j.enconman.2014.01.018.

[21] Geidl M, Koeppel G, Favre-Perrod P, Klöckl B, Andersson G, Fröhlich K. Energy hubs for the future. IEEE Power Energy Mag 2007;5:24–30. doi:10.1109/MPAE.2007.264850.

[22] Song H, Starfelt F, Daianova L, Yan J. Influence of drying process on the biomass-based polygeneration system of bioethanol, power and heat. Appl Energy 2012;90:32–7. doi:10.1016/j.apenergy.2011.02.019.

[23] Chen Y, Adams TA, Barton PI. Optimal design and operation of flexible energy polygeneration systems. Ind Eng Chem Res 2011;50:4553–66. doi:10.1021/ie1021267.

[24] Capuder T, Mancarella P. Techno-economic and environmental modelling and optimization of flexible distributed multi-generation options. Energy 2014;71:516–33. doi:10.1016/j.energy.2014.04.097.

[25] Coronas A, Murthy SS, Carles Bruno J. Editorial for the special issue of applied thermal engineering on polygeneration. Appl Therm Eng 2013;50:1397–8. doi:10.1016/j.applthermaleng.2012.06.032.

[26] Lund H. Renewable Energy Systems: The Choice and Modeling of 100% Renewable Solutions. Academic Press publications; 2010.

[27] Capuder T. Flexible Multi-Generation Solutions for Future Low Carbon Energy Systems (http://www.britishscholarshiptrust.org/Tomislav_Capuder.pdf) 2013:1–3.

[28] Yuan Z, Chen B. Process synthesis for addressing the sustainable energy systems and environmental issues. AIChE J 2012;58:3370–89. doi:10.1002/aic.13914.

[29] Serra LM, Lozano M-A, Ramos J, Ensinas A V., Nebra SA. Polygeneration and efficient use of natural resources. Energy 2009;34:575–86. doi:10.1016/j.energy.2008.08.013.

[30] Zhou W, Yang H, Rissanen M, Nygren B, Yan J. Decrease of energy demand for bioethanol-based polygeneration system through case study. Appl Energy 2012;95:305–11. doi:10.1016/j.apenergy.2012.02.014.

[31] Ahmadi P, Dincer I, Rosen M a. Development and assessment of an integrated biomass-based multi-generation energy system. Energy 2013;56:155–66. doi:10.1016/j.energy.2013.04.024.

[32] Edenhofer O, Pichs Madruga R, Sokona Y. Renewable Energy Sources and Climate Change Mitigation (Special Report of the Intergovernmental Panel on Climate Change). Clim Policy 2012;6:1–1088. doi:10.5860/CHOICE.49-6309.

[33] Martín M, Grossmann IE. On the systematic synthesis of sustainable biorefineries. Ind Eng Chem Res 2013;52:3044–64. doi:10.1021/ie2030213.

[34] Risø National Laboratory Denmark, Elkraft System, AKF Institute of Local Government Studies, Stockholm Environment Institute, Institute of Physical Energetics, Lithuanian Energy Institute, et al. Balmorel: A Model for Analyses of the Electricity and CHP Markets in the Baltic Sea Region. 2001.

[35] Loulou R, Labriet M. ETSAP-TIAM: The TIMES integrated assessment model Part I: Model structure. Comput Manag Sci 2008;5:7–40. doi:10.1007/s10287-007-0046-z.

[36] Lythcke-Jørgensen C, Haglind F, Ensinas A V., Münster M. A method for aggregating external operating conditions in multi-generation plant optimization models. Appl Energy 2016;under revi:59–75. doi:10.1016/j.apenergy.2015.12.050.

[37] Lythcke-Jørgensen C, Clausen LR, Algren L, Hansen AB, Münster M, Gadsbøll RØ, et al. Optimization of a flexible multi-generation system based on wood chip gasification and methanol production. Submitt Appl Energy, Spec Issue Energy Supply Networks (Manuscript Number APEN-D-16-02936) 2016.

[38] Liu P, Pistikopoulos EN, Li Z. Polygeneration Systems Engineering. Process Syst. Eng., vol. 5, 2011, p. 1–38. doi:10.1002/9783527631292.ch1.

[39] Liu P, Gerogiorgis DI, Pistikopoulos EN. Modeling and optimization of polygeneration energy systems. Catal Today 2007;127:347–59. doi:10.1016/j.cattod.2007.05.024.

[40] Liu P, Pistikopoulos EN, Li Z. A mixed-integer optimization approach for polygeneration energy systems design. Comput Chem Eng 2009;33:759–68. doi:10.1016/j.compchemeng.2008.08.005.

[41] Liu P, Pistikopoulos EN. A Multi-Objective Optimization Approach to Polygeneration Energy Systems Design. AIChE J 2010;56:1218–34. doi:10.1002/aic.

[42] Liu P, Pistikopoulos EN, Li Z. Decomposition Based Stochastic Programming Approach for Polygeneration Energy Systems Design under Uncertainty. Ind Eng Chem Res 2010;49:3295–305. doi:10.1021/ie901490g.

[43] Gassner M, Maréchal F. Methodology for the optimal thermo-economic, multi-objective design of thermochemical fuel production from biomass. Comput Chem Eng 2009;33:769–81. doi:10.1016/j.compchemeng.2008.09.017.

[44] Bolliger R. Méthodologie de la synthèse des systèmes énergétiques industriels. 2010. doi:10.5075/epfl-thesis-4867.

[45] Kemp IC. Pinch Analysis and Process Integration. 2006. doi:10.1016/B978-075068260-2.50011-0.

[46] Gerber L, Gassner M, Maréchal F. Systematic integration of LCA in process systems design: Application to combined fuel and electricity production from lignocellulosic biomass. Comput Chem Eng 2011;35:1265–80. doi:10.1016/j.compchemeng.2010.11.012.

[47] Tock L, Gassner M, Maréchal F. Thermochemical production of liquid fuels from biomass: Thermo-economic modeling, process design and process integration analysis. Biomass and Bioenergy 2010;34:1838–54. doi:10.1016/j.biombioe.2010.07.018.

[48] Tock L, Maréchal F. Co-production of hydrogen and electricity from lignocellulosic biomass: Process design and thermo-economic optimization. Energy 2012;45:339–49. doi:10.1016/j.energy.2012.01.056.

[49] Chen Y, Adams TA, Barton PI. Optimal design and operation of static energy polygeneration systems. Ind Eng Chem Res 2011;50:5099–113. doi:10.1021/ie101568v.

[50] Chen Y. Optimal design and operation of energy polygeneration systems 2013. doi:http://dx.doi.org/10.1016/j.jprocont.2014.11.004.

[51] Maréchal F, Weber C, Favrat D. Multiobjective Design and Optimization of Urban Energy Systems. Process Syst. Eng., 2011, p. 39–83. doi:10.1002/9783527631292.ch1.

[52] Fazlollahi S, Becker G, Maréchal F. Multi-objectives, multi-period optimization of district energy systems: I. Selection of typical operating periods. Comput Chem Eng 2014;65:54–66. doi:10.1016/j.compchemeng.2014.02.018.

[53] Fazlollahi S, Becker G, Maréchal F. Multi-objectives, multi-period optimization of district energy systems: II-Daily thermal storage. Comput Chem Eng 2014;71:648–

62. doi:10.1016/j.compchemeng.2014.02.018.

[54] Fazlollahi S, Becker G, Maréchal F. Multi-objectives, multi-period optimization of district energy systems: III. Distribution networks. Comput Chem Eng 2014;66:82–97. doi:10.1016/j.compchemeng.2014.02.018.

[55] Marnay C, Venkataramanan G, Stadler M, Siddiqui AS, Firestone R, Chandran B. Optimal technology selection and operation of commercial-building microgrids. IEEE Trans Power Syst 2008;23:975–82. doi:10.1109/TPWRS.2008.922654.

[56] Rubio-Maya C, Uche-Marcuello J, Martínez-Gracia A, Bayod-Rújula A a. Design optimization of a polygeneration plant fuelled by natural gas and renewable energy sources. Appl Energy 2011;88:449–57. doi:10.1016/j.apenergy.2010.07.009.

[57] Rubio-Maya C, Uche-Marcuello J, Martínez-Gracia A. Sequential optimization of a polygeneration plant. Energy Convers Manag 2011;52:2861–9. doi:10.1016/j.enconman.2011.01.023.

[58] Piacentino A, Barbaro C, Cardona F, Gallea R, Cardona E. A comprehensive tool for efficient design and operation of polygeneration-based energy micro-grids serving a cluster of buildings. Part I: Description of the method. Appl Energy 2013;111:1204–21. doi:10.1016/j.apenergy.2012.11.079.

[59] Voll P, Klaffke C, Hennen M, Bardow A. Automated superstructure-based synthesis and optimization of distributed energy supply systems. Energy 2013;50:374–88. doi:10.1016/j.energy.2012.10.045.

[60] Petruschke P, Gasparovic G, Voll P, Krajačić G, Duić N, Bardow A. A hybrid approach for the efficient synthesis of renewable energy systems. Appl Energy 2014;135:625–33. doi:10.1016/j.apenergy.2014.03.051.

[61] Zhou Z, Zhang J, Liu P, Li Z, Georgiadis MC, Pistikopoulos EN. A two-stage stochastic programming model for the optimal design of distributed energy systems. Appl Energy 2013;103:135–44. doi:10.1016/j.apenergy.2012.09.019.

[62] Martínez Ceseña E, Capuder T, Mancarella P. Flexible Distributed Multienergy Generation System Expansion Planning Under Uncertainty. IEEE Trans Smart Grid 2015:1–10. doi:10.1109/TSG.2015.2411392.

[63] Leung Pah Hang M, Martinez-Hernandez E, Leach M, Yang A. Engineering Design of Localised Synergestic Production Systems. In: Huusom JK, Gernaey K V., Gani R,

editors. 25th Eur. Symp. Process Syst. Eng. 25th Symbposium Comput. Aided Process Eng., Copenhagen, Denmark: Elsevier; 2015.

[64] Iyer RR, Grossmann IE. Synthesis and operational planning of utility systems for multiperiod operation. Comput Chem Eng 1998;22:979–93. doi:10.1016/S0098-1354(97)00270-6.

[65] Pistikopoulos EN, Liu P, Li Z. Environmentally benign process design of polygeneration energy systems. FOCAPD 2009 (Foundations Comput Process Des 2009:585–92.

[66] Fazlollahi S, Mandel P, Becker G, Maréchal F. Methods for multi-objective investment and operating optimization of complex energy systems. Energy 2012;45:12–22. doi:10.1016/j.energy.2012.02.046.

[67] Fazlollahi S, Maréchal F. Multi-objective, multi-period optimization of biomass conversion technologies using evolutionary algorithms and mixed integer linear programming (MILP). Appl Therm Eng 2013;50:1504–13. doi:10.1016/j.applthermaleng.2011.11.035.

[68] Nemet A, Klemeš JJ, Varbanov PS, Kravanja Z. Methodology for maximising the use of renewables with variable availability. Energy 2012;44:29–37. doi:10.1016/j.energy.2011.12.036.

[69] Bungener S, Hackl R, Van Eetvelde G, Harvey S, Marechal F. Multi-period analysis of heat integration measures in industrial clusters. Energy 2015;93:220–34. doi:10.1016/j.energy.2015.09.023.

[70] Poncelet K, Höschle H, Viriag A, Delarue A, D'haeseleer W. Selection of Representative Days for Investment Planning Models TME Working Paper - An electronic version of the paper may be downloaded from the TME website: http://www.mech.kuleuven.be/tme/research/. 2015.

[71] Hedegaard K, Münster M. Influence of individual heat pumps on wind power integration - Energy system investments and operation. Energy Convers Manag 2013;75:673–84. doi:10.1016/j.enconman.2013.08.015.

[72] Domínguez-Muñoz F, Cejudo-López JM, Carrillo-Andrés A, Gallardo-Salazar M. Selection of typical demand days for CHP optimization. Energy Build 2011;43:3036–43. doi:10.1016/j.enbuild.2011.07.024.

[73] Ortiga J, Bruno JC, Coronas A. Selection of typical days for the characterisation of energy demand in cogeneration and trigeneration optimisation models for buildings. Energy Convers Manag 2011;52:1934–42. doi:10.1016/j.enconman.2010.11.022.

[74] Chen Y, Li X, Adams II TA, Barton PI. Decomposition Strategy for the Global Optimization of Flexible Energy Polygeneration Systems. AlChE 2012;58:3080–95. doi:10.1002/aic.13708.

[75] Mavrotas G, Diakoulaki D, Florios K, Georgiou P. A mathematical programming framework for energy planning in services' sector buildings under uncertainty in load demand: The case of a hospital in Athens. Energy Policy 2008;36:2415–29. doi:10.1016/j.enpol.2008.01.011.

[76] Karlsson K, Larsen H V., Petrovic S, Balyk O. TimeSliceTool (http://www.ens.dk/sites/ens.dk/files/info/facts-figures/) 2014.

[77] Lythcke-Jørgensen C, Münster M, Ensinas A V, Haglind F. Design optimization of flexible biomass-processing polygeneration plants using characteristic operation periods. World Renew. Energy Congr. XIII, London: 2014.

[78] Elmegaard B, Houbak N. Simulaton of the Avedøreværket Unit 1 Cogeneration Plant with DNA. Proc 16th Int Conf Effic Cost, Optim Simulation, Environ Impact Energy Syst (ECOS 2003) 2003:8 (1659–66).

[79] Lythcke-Jørgensen C. Modelling and Optimization of a Steam Co-generation Plant with Integrated Bio-ethanol Production. Technical University of Denmark, 2012.

[80] Rolfsman B. Combined heat-and-power plants and district heating in a deregulated electricity market. Appl Energy 2004;78:37–52. doi:10.1016/S0306-2619(03)00098-9.

[81] Martínez-Lera S, Ballester J, Martínez-Lera J. Analysis and sizing of thermal energy storage in combined heating, cooling and power plants for buildings. Appl Energy 2013;106:127–42. doi:10.1016/j.apenergy.2013.01.074.

[82] Rong A, Lahdelma R. An effective heuristic for combined heat-and-power production planning with power ramp constraints. Appl Energy 2007;84:307–25. doi:10.1016/j.apenergy.2006.07.005.

[83] Hindsberger M, Ravn HF. Multiresolution modeling of hydro-thermal systems.

PICA 2001 Innov Comput Power - Electr Energy Meets Mark 22nd IEEE Power Eng Soc Int Conf Power Ind Comput Appl (Cat No01CH37195) 2001. doi:10.1109/PICA.2001.932309.

[84] Morris MD. Factorial Sampling Plans for Preliminary Computational Experiments. Technometrics 1991;33:161–74. doi:10.2307/1269043.

[85] Sin G, Gernaey K V., Lantz AE. Good modeling practice for PAT applications: Propagation of input uncertainty and sensitivity analysis. Biotechnol. Prog., vol. 25, 2009, p. 1043–53. doi:10.1002/btpr.166.

[86] Jack MW. Scaling laws and technology development strategies for biorefineries and bioenergy plants. Bioresour Technol 2009;100:6324–30. doi:10.1016/j.biortech.2009.06.109.

[87] Boldrin A, Baral KR, Fitamo T, Vazifehkhoran AH, Jensen IG, Kjærgaard I, et al. A dynamic model for integrated optimization of Biogas Production – A case study on Sugar Beet Biomass. Energy (in Progress) n.d.

[88] Haupt RL, Haupt SE. Practical Genetic Algorithms. John Wiley & Sons, Inc.; 2006.

[89] Turton R, Bailie RC, Whiting WB, Shaeiwitz J a. Analysis, Synthesis, and Design of Chemical Processes. 1998.

[90] Helton JC, Davis FJ. Latin hypercube sampling and the propagation of uncertainty in analyses of complex systems. Reliab Eng Syst Saf 2003;81:23–69. doi:10.1016/S0951-8320(03)00058-9.

[91] McKay MD, Beckman RJ, Conover WJ. Comparison of three methods for selecting values of input variables in the analysis of output from a computer code. Technometrics 1979;21:239–45. doi:10.2307/1271432.

[92] Earl DJ, Deem MW. Monte Carlo simulations. Methods Mol Biol 2008;443:25–36. doi:10.1007/978-1-59745-177-2_2.

[93] Rogers DWO. Fifty years of Monte Carlo simulations for medical physics. Phys Med Biol 2006;51:R287–301. doi:10.1088/0031-9155/51/13/R17.

[94] Chib S, Greenberg E. Markov Chain Monte Carlo Simulation Methods in Econometrics. Econom Theory 1996;12:409–31. doi:10.2307/3532527.

[95] Amar JG. The Monte Carlo method in science and engineering. Comput Sci Eng

2006;8:9–19. doi:10.1109/MCSE.2006.34.

[96] Connolly D, Lund H, Mathiesen B V., Leahy M. A review of computer tools for analysing the integration of renewable energy into various energy systems. Appl Energy 2010;87:1059–82. doi:10.1016/j.apenergy.2009.09.026.

[97] Kohl T, Teles M, Melin K, Laukkanen T, Järvinen M, Park SW, et al. Exergoeconomic assessment of CHP-integrated biomass upgrading. Appl Energy 2015;156:290–305. doi:10.1016/j.apenergy.2015.06.047.

[98] Starfelt F. From combined heat and power to polygeneration (ISBN: 9789174852219). 2015.

[99] Energistyrelsen. Danmarks Energi- og klimafremskrivning 2014. 2014.

[100] Clausen LR, Elmegaard B, Ahrenfeldt J, Henriksen U. Thermodynamic analysis of small-scale dimethyl ether (DME) and methanol plants based on the efficient two-stage gasifier. Energy 2011;36:5805–14. doi:10.1016/j.energy.2011.08.047.

[101] Lythcke-Jørgensen C, Haglind F, Clausen LR. Thermodynamic and Economic Analysis of Integrating Lignocellulosic Bioethanol, Copenhagen, Denmark: European Biomass Conference and Exhibition; 2013, p. 1–8.

[102] Lythcke-Jørgensen C, Haglind F, Clausen LR. Exergy analysis of a combined heat and power plant with integrated lignocellulosic ethanol production, Guilin, China: 28th International Conference on Efficiency, Cost, Optimization, Simulation and Environmental Impact of Energy Systems; 2013, p. 1–12.

[103] Balat M. Production of bioethanol from lignocellulosic materials via the biochemical pathway: A review. Energy Convers Manag 2011;52:858–75. doi:10.1016/j.enconman.2010.08.013.

[104] Lee S, Shah YT. Biofuels and Bioenergy: processes and technologies. Green Chemestry Chem Eng 2013:93–139. doi:10.1016/S1351-4180(13)70475-6.

[105] Daianova L, Dotzauer E, Thorin E, Yan J. Evaluation of a regional bioenergy system with local production of biofuel for transportation, integrated with a CHP plant. Appl Energy 2012;92:739–49. doi:10.1016/j.apenergy.2011.08.016.

[106] Ilic DD, Dotzauer E, Trygg L. District heating and ethanol production through polygeneration in Stockholm. Appl Energy 2012;91:214–21.

doi:10.1016/j.apenergy.2011.09.030.

[107] Bösch P, Modarresi A, Friedl A. Comparison of combined ethanol and biogas polygeneration facilities using exergy analysis. Environ Eng Manag J 2013;12:1575–82. doi:10.1016/j.applthermaleng.2011.12.048.

[108] Modarresi A, Kravanja P, Friedl A. Pinch and exergy analysis of lignocellulosic ethanol, biomethane, heat and power production from straw. Appl Therm Eng 2012;43:20–8. doi:10.1016/j.applthermaleng.2012.01.026.

[109] Leduc S, Starfelt F, Dotzauer E, Kindermann G, McCallum I, Obersteiner M, et al. Optimal location of lignocellulosic ethanol refineries with polygeneration in Sweden. Energy 2010;35:2709–16. doi:10.1016/j.energy.2009.07.018.

[110] Palacios-Bereche R, Mosqueira-Salazar KJ, Modesto M, Ensinas A V., Nebra S a., Serra LM, et al. Exergetic analysis of the integrated first- and second-generation ethanol production from sugarcane. Energy 2013;62:46–61. doi:10.1016/j.energy.2013.05.010.

[111] Bentsen NS, Thorsen BJ, Felby C. Energy, feed and land-use balances of refining winter wheat to ethanol. Biofuels, Bioprod Biorefining 2009;3:521–33. doi:10.1002/bbb.170.

[112] Starfelt F, Thorin E, Dotzauer E, Yan J. Performance evaluation of adding ethanol production into an existing combined heat and power plant. Bioresour Technol 2010;101:613–8. doi:10.1016/j.biortech.2009.07.087.

[113] Starfelt F, Daianova L, Yan J, Thorin E, Dotzauer E. The impact of lignocellulosic ethanol yields in polygeneration with district heating - A case study. Appl Energy 2012;92:791–9. doi:10.1016/j.apenergy.2011.08.031.

[114] Statens Energimyndighet. Energiläget 2011. Eskilstuna, Sweden: 2011.

[115] EA Energianalyse. Opdatering af samfundsøkonomiske brændselspriser - BIOMASSE 2011.

[116] Ahrenfeldt J, Thomsen TP, Henriksen U, Clausen LR. Biomass gasification cogeneration - A review of state of the art technology and near future perspectives. Appl Therm Eng 2013;50:1407–17. doi:10.1016/j.applthermaleng.2011.12.040.

[117] Energinet.dk. SIFRE: Simulation of Flexible and Renewable Energy sources (http://energinet.dk/SiteCollectionDocuments/Danske%20dokumenter/El/sifre_fall2015.pdf). 2015.

[118] Energistyrelsen, Energinet.dk. Technology Data for Energy Plants - Generation of Electricity and District Heating, Energy Storage and Energy Carrier Generation and Conversion 2015:1–220. doi:ISBN: 978-87-7844-940-5.

[119] Energinet.dk, Dansk Energi. Smart Energy - hovedrapport (http://energinet.dk/DA/KLIMA-OG-MILJOE/Energianalyser/Analyser/Sider/Smart-Energy.aspx) 2015.

[120] Maabjerg BioEnergy Center. Maabjerg BioEnergy Center concept 2016. http://www.maabjergenergycenter.dk/.

[121] Larsen J, Haven MØ, Thirup L. Inbicon makes lignocellulosic ethanol a commercial reality. Biomass and Bioenergy 2012;46:36–45. doi:10.1016/j.biombioe.2012.03.033.

[122] European Commission. European Commission, Climate Action 2016. http://ec.europa.eu/clima/policies/international/negotiations/paris/index_en.htm (accessed March 26, 2016).

[123] Liu P, Georgiadis MC, Pistikopoulos EN. Advances in Energy Systems Engineering. Ind Eng Chem Res 2011;50:4915–26. doi:10.1021/ie101383h.

[124] Adams TA, Ghouse JH. Polygeneration of fuels and chemicals. Curr Opin Chem Eng 2015;10:87–93. doi:10.1016/j.coche.2015.09.006.

[125] Souleimanov E, Kraus J. Turkey: An Important East-West Energy Hub. Middle East Policy 2012;19:157–68. doi:10.1111/j.1475-4967.2012.00542.x.

[126] Hemmes K, Zachariah-Wolf JL, Geidl M, Andersson G. Towards multi-source multi-product energy systems. Int J Hydrogen Energy 2007;32:1332–8. doi:10.1016/j.ijhydene.2006.10.013.

[127] Anastas P, Eghbali N. Green chemistry: principles and practice. Chem Soc Rev 2010;39:301–12. doi:10.1039/b918763b.

[128] Silkeborg Forsyning. Silkeborg Forsyning 2015. http://www.silkeborgforsyning.dk/ (accessed September 13, 2015).

[129] Jong E De, Jungmeier G. Biorefinery Concepts in Comparison to Petrochemical Refineries. 2015. doi:10.1016/B978-0-444-63453-5.00001-X.

[130] Thiessen K. Fjernvarme Horsens (personal contact) 2015. fjho.dk.

OVERVIEW OF APPENDICES

Eleven appendices are attached to this thesis. A short overview of the appendix contents is given here:

Appendix A contains a description of the chronology of the project work, which may provide the reader with an insight into the considerations and decisions made thoughout the project.

Appendices B-E contains the four published journal papers included in this thesis.

Appendix F contains the manuscript 'Optimization of a flexible multi-generation system based on wood chip gasification and methanol production' which has been submitted for 'Applied Energy, special issue on energy supply systems'.

Appendiced G-I contains the three peer-reviewed conference papers included in this thesis.

Appendix J contains a report from the Ph.D. course '28 923 Uncertainty and Sensitivity Analysis of Numerical Models', in which the uncertainty analysis methodology developed for the FMG design methodology is described in detail.

Appendix K contains an example of the practical implementation of the developed design methodology. The example is taken from *Case III*. The coding only includes the parts actively developed as a part of the project, hence general codes with the OSMOSE tool as well as the sensitivity and uncertainty methods are not included.

APPENDIX A Project chronology

The chronology of the project work is explained in this section with the ambition of providing an insight into the considerations and decisions made. An overview of the project chronology is illustrated in Figure A1, with publication milestones indicated. The chronology is described below in detail.

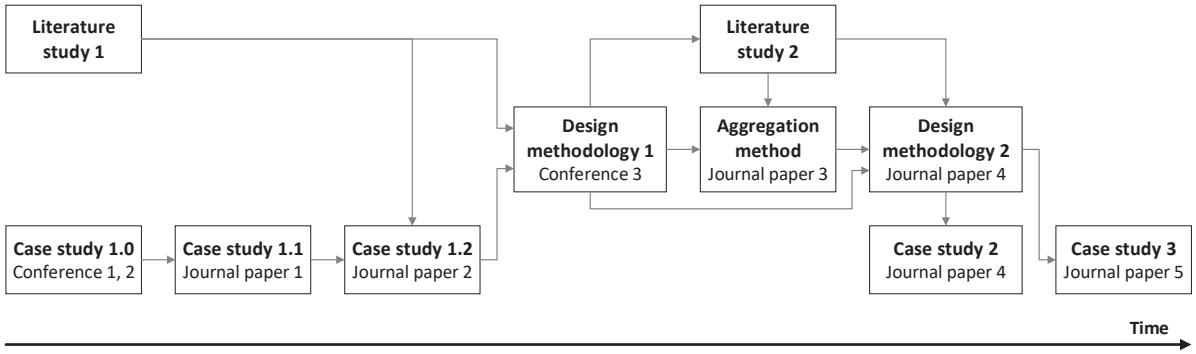

Figure A1: Overview of the chronological methodology of the project. Notice that the figure dimensions do not correspond to task duration.

In order to identify FMG design challenges, the project was initiated by a literature study on state-of-the-art approaches within the design and optimization of polygeneration and multi-generation systems. Parallel to this, work on Case Study 1[28] was commenced to investigate the impact of variable operating conditions on the economic and thermodynamic performance of an integrated system comprising a Rankine cycle-based combined heat and power (CHP) unit and a cellulosic ethanol production facility. Based on the outcomes (Lythcke-Jørgensen et al. 2013a; Lythcke-Jørgensen et al. 2013b), a detailed exergy analysis was conducted focussing on various operation modes of the system in question (Lythcke-Jørgensen et al. 2014a).

[28] The integrated system treated in Case Study 1 was inspired by the Inbicon system [121] and had previously been analysed in [79]. The study suggested that process integration is a useful tool for optimizing the performance of the integrated system, but questioned the overall economic and thermodynamic performance of the system under variable operating conditions and constraints.

Combining the outcomes of the literature study and the exergy analysis, a case-specific method for optimizing the design and operation of the previously treated FMG concept was developed [15]. The outcomes pointed towards the importance of developing a generic and systematic design methodology capable of taking variable operating conditions, process integration, and economy-of-scale into account.

In consequence, a collaboration was established with the Industrial Process and Energy Systems Engineering group (IPESE) at École Polytechnique Fédérale de Lausanne (EPFL) with the ambition of developing a generic methodology for designing FMGs using parts of their process integration and optimization tool OSMOSE[6] [44]. A first version of the design methodology was presented in (Lythcke-Jørgensen et al. 2014b).

In response to the outcomes of, and feedback to, the first version of the design methodology, it was deemed relevant to extract and enhance the data aggregation part in a separate data aggregation method (Lythcke-Jørgensen et al. 2016a). At the same time, an extended literature study focusing on design methodologies of multi-generation systems was conducted. Using the findings, the design methodology was extended by including a biomass supply chain model and systematic assessment of uncertainties. For verification, the design methodology was applied in Case Study 2 on an FMG concept inspired by the Maabjerg Energy Concept [120]. The design methodology and the case study were both presented in (Lythcke-Jørgensen et al. 2016b).

Finally, collaboration with the Danish transmission system operator (TSO), Energinet.dk, was initiated for developing Case Study 3. The case study treated the integration of a waste-incineration-based CHP plant, biomass gasification, methanol production, and high efficiency electrolysis using solid oxide electrolysis cells (SOEC) in an FMG that also supplied district heating and energy utility services for a local slaughterhouse. The ambitions were to investigate different approaches to linking the energy sectors through local FMGs, and to verify the developed design methodology. The outcomes of the case study were presented in (Lythcke-Jørgensen et al. 2016c).

APPENDIX B Journal paper 1

ISI Journal Paper

C.E. Lythcke-Jørgensen, F. Haglind, and L.R. Clausen. *Exergy analysis of a combined heat and power plant with integrated lignocellulosic ethanol production*. Energy Conversion and Management 85:817-827, 2014.

This paper is an extension of 'Conference paper 1'[102], and it presents the exergy analysis conducted as a part of *Case I* in this project.

Energy Conversion and Management 85 (2014) 817–827

Contents lists available at ScienceDirect

Energy Conversion and Management

journal homepage: www.elsevier.com/locate/enconman

Exergy analysis of a combined heat and power plant with integrated lignocellulosic ethanol production

Christoffer Lythcke-Jørgensen *, Fredrik Haglind, Lasse R. Clausen

Technical University of Denmark, Department of Mechanical Engineering, Nils Koppels Allé 403, DK-2800 Kgs. Lyngby, Denmark

ARTICLE INFO

Article history:
Available online 13 February 2014

Keywords:
Biofuel production
Exergy analysis
Lignocellulosic ethanol
Polygeneration
System operation

ABSTRACT

Lignocellulosic ethanol production is often assumed integrated in polygeneration systems because of its energy intensive nature. The objective of this study is to investigate potential irreversibilities from such integration, and what impact it has on the efficiency of the integrated ethanol production. An exergy analysis is carried out for a modelled polygeneration system in which lignocellulosic ethanol production based on hydrothermal pretreatment is integrated in an existing combined heat and power (CHP) plant. The ethanol facility is driven by steam extracted from the CHP unit when feasible, and a gas boiler is used as back-up when integration is not possible. The system was evaluated according to six operation points that alternate on the following three different operation parameters: Load in the CHP unit, integrated versus separate operation, and inclusion of district heating production in the ethanol facility. The calculated standard exergy efficiency of the ethanol facility varied from 0.564 to 0.855, of which the highest was obtained for integrated operation at reduced CHP load and full district heating production in the ethanol facility, and the lowest for separate operation with zero district heating production in the ethanol facility. The results suggest that the efficiency of integrating lignocellulosic ethanol production in CHP plants is highly dependent on operation, and it is therefore suggested that the expected operation pattern of such polygeneration system is taken into account when evaluating the potential of the ethanol production.

1. Introduction

The integrated production of biofuels in thermal power plants has received increasing attention in the recent years due to the potential synergies from thermal integration. One example is the gasification-based coproduction of heat, electricity, Fischer–Tropsch fuels, dimethyl ether (DME), and hydrogen from biomass feedstocks [1], like switchgrass [2] and black-liquor [3]. Another important example is the integrated production of bioethanol and synthetic natural gas (SNG) with combined heat and power (CHP) production [4]. Among biofuels, bioethanol is the most widely used for transportation on a global basis and is consumed both as an individual fuel and in blends with gasoline [5]. Bioethanol can be produced from sugars, starch, and lignocellulosic biomass, of which the latter often is considered the most sustainable option as it offers the possibility of reducing CO_2 emissions from transportation without linking fuel prices and food prices directly [4]. This study treats the integrated production of lignocellulosic ethanol in an existing CHP plant.

Several studies have focused on thermal integration synergies in systems with integrated production of power, heat, lignocellulosic ethanol, and SNG [6–10]. Daianova et al. [6] and Ilic et al. [7] both report better energy economy for the integrated system compared to stand-alone systems, while Bösch et al. [8] reports a potential increase in both first law energy efficiency and exergy efficiency when integrating the processes. Modarresi et al. [9] applied pinch analysis to improve the heat integration of the system, which yielded an integrated exergy efficiency of 88% for the ethanol process. Gassner and Maréchal [10] have investigated process integration in such polygeneration systems and conclude that both first and second law energy efficiencies are increased significantly by integrating lignocellulosic ethanol and SNG production in a CHP plant. Furthermore, a case study by Starfelt et al. [11] reports higher first-law energy efficiency for integrating lignocellulosic ethanol production in an existing CHP plant compared to a scenario with separate production. These results explain the industrial interest in retrofitting existing CHP units to obtain the mentioned polygeneration system benefits.

A previous study by the authors [12] evaluated the energy economy of integrating lignocellulosic ethanol production based on the hydrothermal pretreatment technology IBUS[1] [13] in the existing

* Corresponding author. Tel.: +45 30 42 72 00.
E-mail addresses: celjo@mek.dtu.dk (C. Lythcke-Jørgensen), frh@mek.dtu.dk (F. Haglind), lrc@mek.dtu.dk (L.R. Clausen).

[1] IBUS (Integrated Biomass Utilization System) is a patented lignocellulosic biomass pretreatment technology. The patent is owned by the Danish company Inbicon A/S, a subsidiary to DONG Energy.

http://dx.doi.org/10.1016/j.enconman.2014.01.018
0196-8904/

Danish CHP unit Avedøreværket 1 (AVV1). During integration, the hot utility demand of the ethanol facility was met by steam extracted from the turbines of AVV1, and when integration was not feasible due to high CHP loads or periods of CHP shut-down, a natural gas boiler was used to deliver the necessary heat while the power demand was met by power bought from the power market. The study suggested an ethanol production energy cost of 0.14 Euro/L on average during integrated operation, and 1.22 Euro/L on average during separate operation, underlining the potential benefits of integrating the production. Based on existing production patterns for AVV1, the study further suggested that the duration of separate operation over a year would be significant, reducing the overall benefit from the integration and questioning the average yearly efficiency of the ethanol production.

The overall objective of this study is to determine the irreversibilities related to the integration of lignocellulosic ethanol production in CHP units at various operation modes. This objective is targeted through a case study of a polygeneration system in which lignocellulosic ethanol production based on IBUS technology is integrated in the Danish CHP unit AVV1. Exergy analysis [14] is applied to a model of the ethanol production facility previously developed in Lythcke-Jørgensen et al. [12] to identify exergy flows in the ethanol production facility and its heat integration network. Exergy efficiencies are calculated for the individual process steps, and the exergy efficiency of the overall ethanol production is evaluated in six different operation points, covering both integrated and separate operation, zero and full district heating production in the ethanol facility, and various loads in the CHP unit. Based on the outcomes, the impact of polygeneration system operation on the average exergy efficiency of the ethanol production is discussed. The novelty of this paper lies in the evaluation of the average system exergy efficiency by combining exergy analysis with the performance analysis in the boundary points of the feasible operation range.

In this paper, the polygeneration system design, modelling and operation are presented in Section 2 together with the exergy analysis approach. Results of the analysis are presented in Section 3 and discussed in Section 4. Finally, a conclusion on the study is given in Section 5.

2. Methodology

2.1. Polygeneration system model

A numerical model of a polygeneration system that integrates lignocellulosic ethanol production based on IBUS technology in the Danish CHP unit AVV1 was previously developed and presented by the authors [12], and the same model is used in the present study. This section presents the system design and the modelling approach, system operation, and obtained data that are used in the exergy analysis. A simplified process layout of the modelled polygeneration system is presented in Fig. 1.

2.1.1. Modelling of AVV1

A numerical model of AVV1, developed by Elmegaard and Houbak [15] in the energy system simulator Dynamic Network Analysis (DNA) [16], was used for simulating flows and operation of AVV1. The model accuracy was evaluated at various loads by comparing electrical efficiencies, η_{el}, and first law energy efficiency, η_I, obtained in the model with efficiencies reported by the plant operator [17]. The two efficiencies are defined by the following equations:

$$\eta_{el} = \frac{P}{\dot{Q}_{fuel}} \tag{1}$$

$$\eta_I = \frac{P + \dot{Q}_{DH}}{\dot{Q}_{fuel}} \tag{2}$$

In the equations, P is the power production, $\dot{Q}_{DH}$ is the district heating production, and $\dot{Q}_{fuel}$ is the fuel input. The comparison was limited to condensation mode and full back-pressure mode operation as they represent the extreme cases of plant operation. Calculated and reported efficiencies are summarized in Tables 1 and 2.

It was found that the model assumed slightly larger fuel consumption in condensation mode than what was reported by the plant owner, resulting in electrical efficiencies that were between 2% and 8% lower for the model. For back pressure operation, the first law energy efficiency accuracy was found to be within a range of 2%, while the electrical efficiency deviated by up to 6%. The inaccuracy of the model was found to be related to the prediction of fuel consumption mainly, and the model was therefore considered adequate for use in the present study.

2.1.2. Modelling and dimensioning of the ethanol facility

In the ethanol facility, the lignocellulosic structure of the straw is broken down through treatment with pressurized steam in the hydrothermal pretreatment stage, whereupon the straw-steam mixture is split into a fibre fraction and a liquid fraction. The fibre fraction is liquefied by glucose-forming enzymes before fermentation is initiated in Simultaneous Saccharification and Fermentation (SSF) tanks. Ethanol is distilled from the resulting fermentation broth, leaving a fibre stillage which is treated in various separation stages alongside the pretreatment liquid fraction, generating a solid biofuel fraction, a molasses fraction, and a waste water fraction. The molasses fraction can be used in anaerobic fermentation to produce biogas [9] or as animal feed [18], while the solid biofuel can be used for combustion or gasification.

A model of the ethanol facility based on heat and mass balances over the system process steps was developed in a previous study by the authors [12] using the software Engineering Equation Solver (EES) [19]. The model was based on the layout reported by Larsen et al. [18] and Østergaard et al. [20]. Mass balances were calculated over each process step as

$$\sum \dot{m}_{in} = \sum \dot{m}_{out} \tag{3}$$

In flows with multiple compounds, the mass fraction of a compound i is termed x_i. The fraction of compound i recovered in a given output flow, $\varepsilon_{(flow),i}$, was defined as

$$\varepsilon_{(flow),i} = \frac{\dot{m}_{(flow)} x_{(flow),i}}{\sum_{n=inlet\ flows} \dot{m}_n x_{n,i}} \tag{4}$$

In process steps with compound conversion or degradation, the relation of output to input mass flow of a compound i, $\eta_{(flow),i}$, was defined as

$$\eta_{(flow),i} = \frac{\sum_{k=outlet\ flows} \dot{m}_k x_{k,i}}{\sum_{n=inlet\ flows} \dot{m}_n x_{n,i}} \tag{5}$$

The steam mass flow $\dot{m}_{steam}$ into the hydrothermal pretreatment process was modelled as a constant, K_{steam}, times the input biomass mass flow, $\dot{m}_{biomass}$, as suggested by Bentsen et al. [21].

$$\dot{m}_{steam} = K_{steam} \dot{m}_{biomass} \tag{6}$$

To determine resulting heating or cooling demand $\dot{Q}_j$ for a process j, the energy balance over the process step was calculated as

$$\dot{Q}_j = \sum_{n=inlet\ flows} \dot{m}_n h_n - \sum_{k=outlet\ flows} \dot{m}_k h_k \tag{7}$$

Here, h_i is the specific enthalpy of the flow i. The only exception to this was the distillation process, for which the hot and cold utility

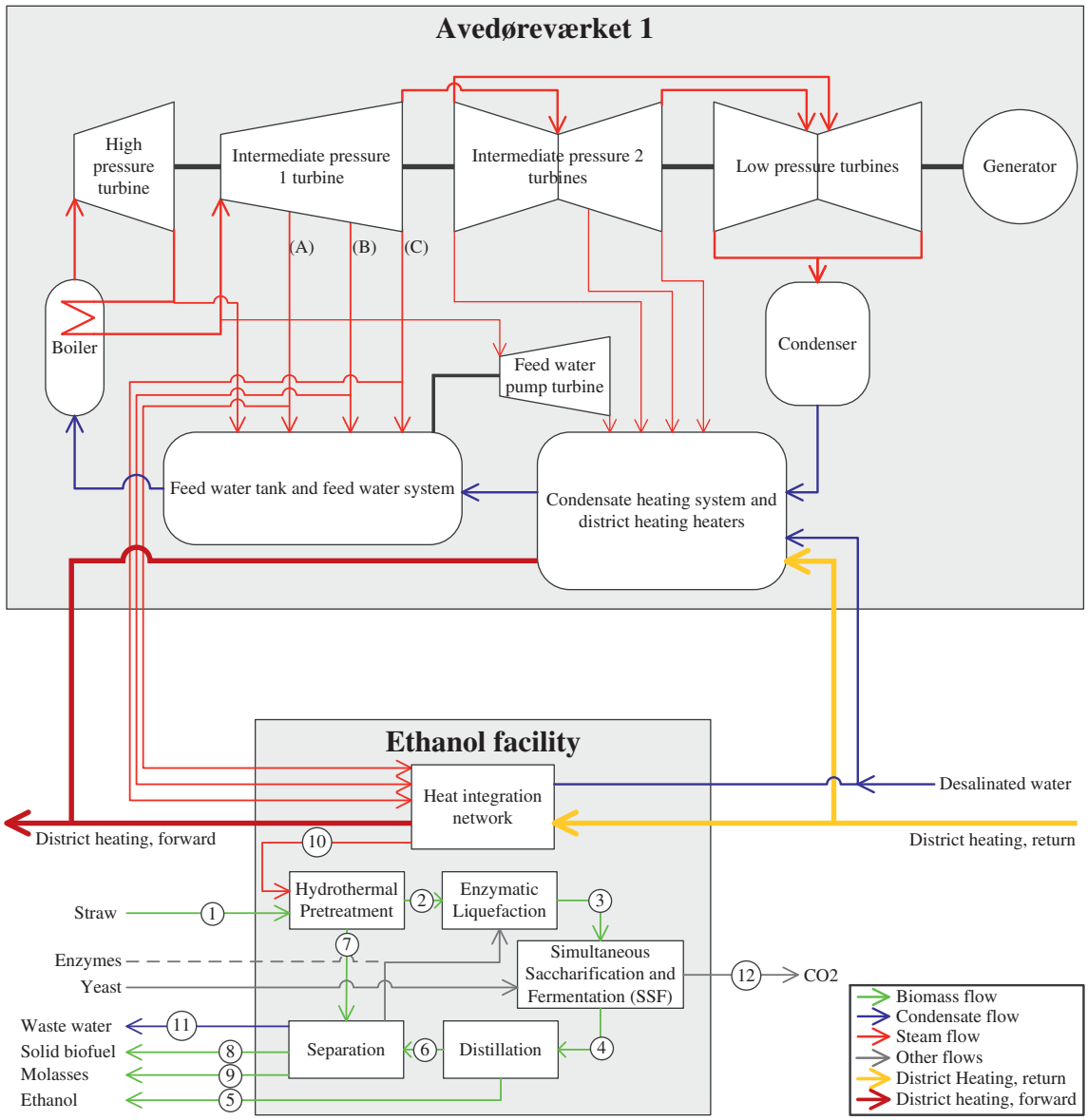

Fig. 1. Simplified process layout of the polygeneration system. Numbered streams are described in detail in Table 5.

Table 1
Comparison of model and reported plant efficiencies in AVV1 at condensation operation.

Condensation mode operation			
Load	η_{el}, model	η_{el}, reported [17]	η_{el}, deviation (%)
1.0	0.41	0.42	−2
0.8	0.40	0.42	−5
0.6	0.39	0.42	−7
0.4	0.37	0.40	−8

demands were calculated using the Aspen Plus [22] distillation column model.

The hydrolysis of cellulose to glucose, occurring during enzymatic liquefaction and simultaneous saccharification and fermentation (SSF), follows the reaction

$$C_6H_{10}O_5 + H_2O \rightarrow C_6H_{12}O_6 \quad (8)$$

The fermentation of glucose to ethanol during SSF follows the reaction

$$C_6H_{12}O_6 \rightarrow 2C_2H_5OH + 2CO_2 \quad (9)$$

For both reactions, molar weight ratios were used to relate the weight fraction increase of the reaction products to the weight fraction decrease of the reactants. The parameters used in the model to describe the system are summarized in Table 3, together with parameter values reported in literature.

In the model, degradation of hemicelluloses was assumed to occur solely during pretreatment, and no degradation or dissolving of lignin was considered in the processes. Hydrolysis was assumed to be the only means of cellulose conversion. The addition of yeast and enzymes was neglected in mass balance calculations. Cellulose, hemicellulose, lignin, and glucose were assumed to have constant heat capacities in the relevant temperature ranges, and mixtures of water and ethanol with ethanol mass fractions at or below 0.1 have been treated as if the water and ethanol were separated.

The accuracy of the ethanol facility model was evaluated by comparing model yields with yields reported for IBUS-based systems by literatures [13,18,21,23], see Table 4.

Table 2
Comparison of model and reported plant efficiencies in AVV1 at full back pressure operation.

Full back pressure mode operation						
Load	η_{el}, model	η_{el}, reported [17]	η_{el}, deviation (%)	η_{l}, model	η_{l}, reported [17]	η_{l}, deviation (%)
1.0	0.36	0.34	6	0.91	0.92	−1
0.8	0.35	0.34	3	0.91	0.92	−1
0.6	0.33	0.33	0	0.90	0.91	−1
0.4	0.30	0.30	0	0.88	0.90	−2

Table 3
Parameters and parameter values used in the model of the IBUS facility.

Parameter	Literature values	Used value
Biomass composition		
Cellulose mass fraction	0.327 [18]	0.327
Hemicellulose mass fraction	0.358 [18]	0.358
Lignin mass fraction	0.155 [18]	0.155
Water mass fraction	0.04 [18]	0.04
'Others' mass fraction	0.12 [18]	0.12
Pretreatment		
Steam to biomass ratio	1.93 [21][a] 2.0–2.7 [23][b]	2.0
Cellulose recovered in fibre fraction	0.955 [18] 0.969 [21]	0.96
Hemicelluloses recovered in the fibres	0.313 [18]	0.313
Lignin recovered in the fibres	–	1.00
Total hemicellulose recovery	0.68 [18]	0.68
Water mass fraction in fibre fraction	0.7–0.75 [18] 0.6–0.75 [23]	0.35
Liquefaction		
Unreacted input cellulose	0.6–0.7 [18]	0.65
Liquefaction residence time	6 h [18]	6 h
Simultaneous saccharification and fermentation		
Unreacted input cellulose	0.3–0.6[c] [18] 0.23–0.31 [21]	0.3
SSF residence time	170 h [18] 140 h [23]	140 h
Distillation		
Ethanol in distillation product	0.93–0.95 [18]	0.95
Ethanol in distillation stillage	0.0008 [18]	0.0008
Separation		
Wet-fuel water content	0.6 [18] 0.65–0.7 [23][d]	0.4[e]
Dry-fuel water content	0.05–0.2 [18] 0.09 [21] 0.1 [23]	0.1
Molasses water content	0.35 [23]	0.65
Hemicelluloses in wet-fuel	–	0.78

[a] Equals 3.8 GJ steam/ton of straw treated.
[b] Equalling operation at dry-matter contents of 30–40% in the pretreatment stage.
[c] Gives an ethanol concentration of the broth in the range 0.06–0.085.
[d] When using decanter technology.
[e] Is assumed achievable when using a filter press instead of decanters for wet-fuel extraction.

Table 4
Comparison of model yields and yields reported in the literature. All numbers are given in kg/ton of biomass treated.

	Model yield	[13]	[18]	[21]	[23]
Bioethanol	150.0	144	143	153.3	143.3
Solid biofuel	406.8	435	353	–	433.3
Molasses	371.0	371	420	–	370.0

It is seen that the yields reported by literature vary significantly. Compared to the yields reported the most recently [13], the model deviated by up to 6%. Due to the high uncertainties in facility yields reported in literature, the found accuracy was considered adequate for the present study.

The cost for biomass transportation is central when scaling facilities and developing business cases in the biorefinery sector [24]. To reflect this, a maximum wheat straw transportation distance of 50 km was considered for the modelled system as suggested by the IBUS technology owner [17]. A total of 196,000 tons of winter wheat straw is cultivated within this distance from the plant [25]. The ethanol facility was dimensioned to process all locally available winter wheat, resulting in a facility processing capacity of 22.4 tons of straw per hour, or 6.22 kg/s, all year round. A linear relation between biomass processing capacity and energy consumption was used for determining the energy demand of the ethanol facility. The power consumption was set to 220 kW h/ton of biomass treated as reported by Bentsen et al. [21]. Description, thermodynamic properties, and absolute mass flows of all numbered flows in the ethanol facility are given in Table 5.

2.1.3. Integration design

Based on temperature and pressure requirements for the steam to be delivered to the ethanol facility, a combined pinch analysis [26] and exergy analysis [14] was carried out to identify the best possible integration design, and the resulting steam, hot, and cold utility demands. District heating production with a forward temperature of 100 °C and a return temperature of 50 °C [15] was included in the pinch analysis to reduce the cooling load in the ethanol facility production. A 10 K pinch temperature difference was used, as suggested by Modarresi et al. [9] for a similar facility. The exergy analysis was applied to identify the integration solution having the lowest overall exergy destruction. The results of this analysis were previously presented in Lythcke-Jørgensen et al. [12].

The optimal integration solution involved steam extraction from three steam extraction points, marked (A), (B) and (C) in Fig. 1. The thermodynamic states of steam in the three points are summarized in Table 6. Steam for hydrothermal pretreatment was extracted from node (B) in AVV1 at CHP loads above 0.6, and from node (A) at CHP loads below 0.6. The steam for hydrothermal pretreatment was conditioned in the heat integration network to meet the exact temperature and pressure requirements of the hydrothermal pretreatment component, being 195 °C and 13 bar [17]. Heat released from steam conditioning was used internally in the ethanol facility. The remaining hot utility demand of the ethanol facility was covered by steam extracted from node (C). Heat from the extracted steam is released in the heat integration network from where it is distributed to the facility process steps. The condensate is recycled to the condenser of AVV1 where additional desalinated water is added to compensate for the loss of steam to the hydrothermal pretreatment. Cooling in the heat integration network is provided by sea water and by district heating water when district heating production is active in the ethanol facility.

Table 5
Descriptions and characteristics of flows in the ethanol facility. Note that the pretreatment liquid fraction (stream 7) has a lower temperature than the pretreatment fibre fraction (stream 2) as it is used to preheat the inlet straw in the pretreatment stage.

Flow no.	Description	Mass flow (kg/s)	Temperature (°C)	Pressure (bar)
(1)	Inlet straw	6.22	25	1
(2)	Pretreatment fibre fraction	9.77	100	1
(3)	Liquefied fibre fraction	9.77	50	1
(4)	Fermentation broth	8.89	33	1
(5)	Ethanol	0.93	25	1
(6)	Fibre stillage	7.96	100	1
(7)	Pretreatment liquid fraction	8.89	80	1
(8)	Solid biofuel	2.53	25	1
(9)	C5-rich molasses	2.31	25	1
(10)	Steam for pretreatment	12.44	195	13
(11)	Waste water fraction	12.01	25	1
(12)	CO2 from fermentation	0.88	33	1

Table 6
Thermodynamic state ranges in the steam extraction points of AVV1.

Point	Temperature range (°C)	Saturation temperature range (°C)	Pressure range
(A)	431–467	199.8–241.2	15.5–34.2
(B)	359–392	176.7–213.6	9.3–20.5
(C)	257–289	145.4–176.1	4.2–9.2

2.2. System operation

Because of load transition times of more than 180 h in the ethanol production facility [12], the ethanol production is assumed operated at full load all year round. As the same is not the case for AVV1, the ethanol production in the polygeneration system can be run in two ways: Integrated mode or separate mode. In integrated mode, steam extracted from turbines of the CHP unit is used for covering the hot utility demand of the ethanol facility, and the power demand is met by power from the CHP unit. In separate mode, a natural gas boiler with a first law energy efficiency of 0.96 is used for generating the steam required by the ethanol facility, and the power requirement is met by power bought from the grid. Separate operation occurs during periods of high CHP unit loads where no surplus capacity for steam extraction exists, and during periods of CHP unit shut-down due to maintenance or lack of demands for heat and power production in the energy system. The two polygeneration system operation modes are outlined in Fig. 2.

Pinch analysis [26] was applied to determine the hot utility demand, the internal reuse of heat, and the cooling load of the ethanol production facility. The results are presented in Lythcke-Jørgensen et al. [12]. The cooling load allowed for the production of district heating to the existing network, which is operated with a forward temperature of 100 °C and a return temperature of 50 °C [15]. The pinch point for the facility was found to be 91 °C, meaning that heat is readily available in the system to heat the return water from the district heating grid to this temperature at highest. As the forward temperature of the district heating grid is 100 °C, additional heat is required to raise the temperature of the district heating water to the required 100 °C, meaning that the hot utility demand of the ethanol facility was increased when district heating production was included. It was found that for each unit of extra heat added, 4.73 units of district heating are produced and the cold utility demand is significantly reduced. Sankey diagrams, illustrating the internal heat flows in the ethanol facility at zero and maximum district heating production, are presented in Fig. 3.

This study investigates the exergy efficiency of the ethanol facility in six polygeneration system operation points with varying operation modes, CHP unit loads, and district heating production in the ethanol facility. Characteristics of the six points are given in Table 7.

2.3. Exergy analysis

Exergy analysis [14] was applied to the ethanol facility to identify irreversibilities at the different operation points. The reference point for all exergy calculations was set to $T_0 = 298.15$ K and $p_0 = 1$ bar.

2.3.1. Exergy calculations

The specific exergy of a material stream, *ex*, was calculated as

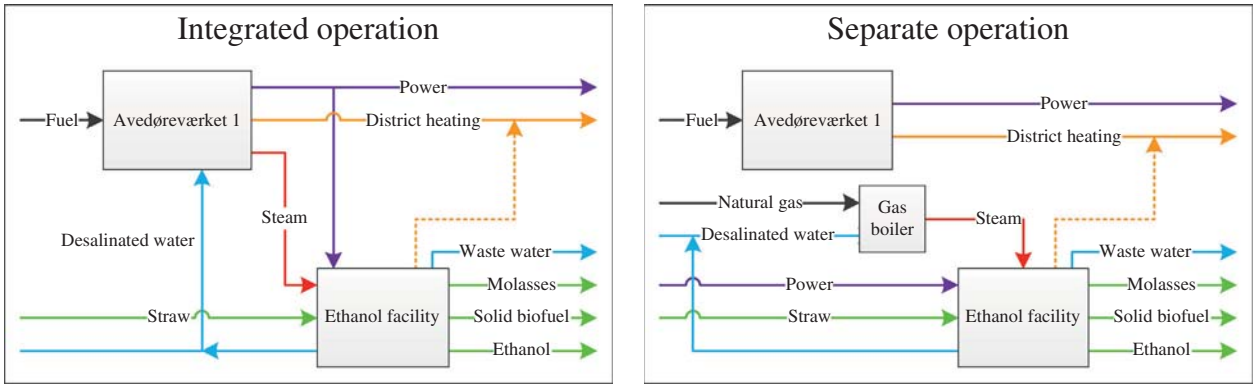

Fig. 2. Outlines of the two operation modes in the polygeneration system.

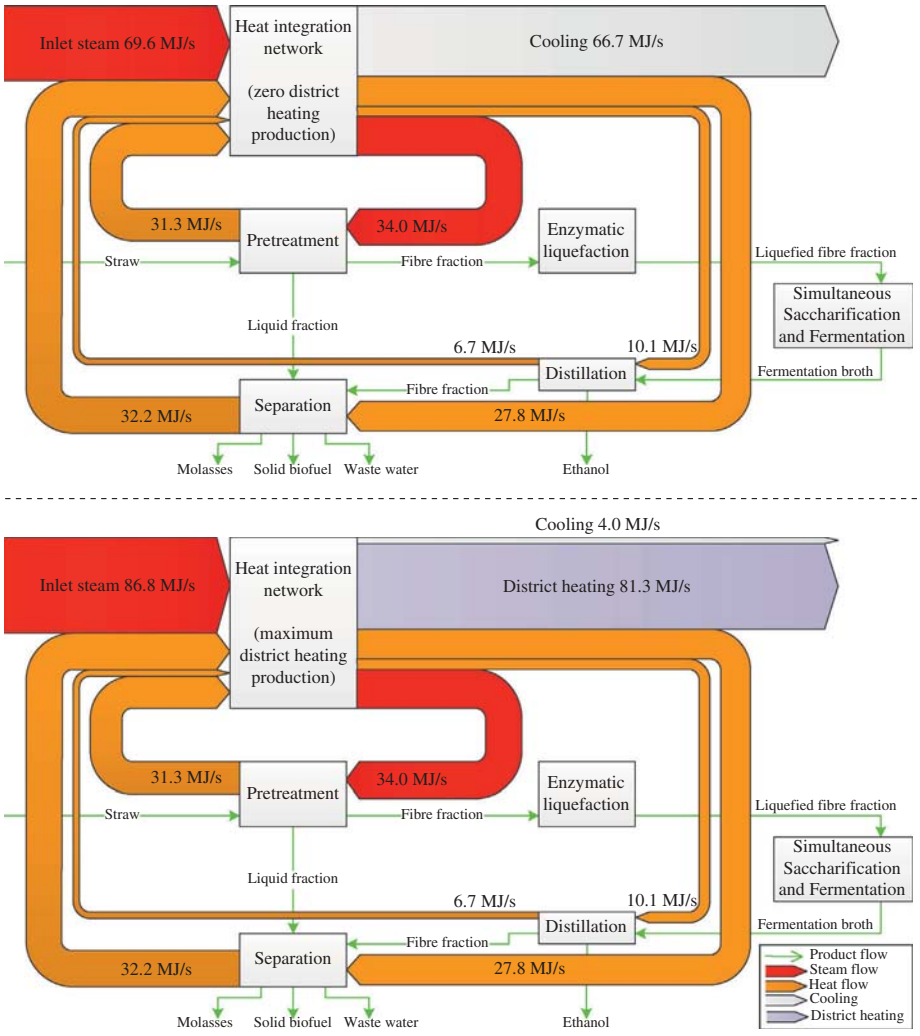

Fig. 3. Sankey diagrams of heat flows in the ethanol facility at zero (top) and maximum (bottom) district heating production.

Table 7
Characteristics of the six polygeneration system operation points investigated in the study.

Operation point no.	Integrated mode operation	Load in AVV1 (–)	District heating load (–)
I	Yes	1.0	0.0
II	Yes	1.0	1.0
III	Yes	0.4	0.0
IV	Yes	0.4	1.0
V	No	–	0.0
VI	No	–	1.0

$$ex = ex_{phys} + ex_{kin} + ex_{pot} + ex_{chem} \tag{10}$$

Here, ex_{phys} is the specific physical exergy, ex_{kin} is the specific kinetic exergy, ex_{pot} is the specific potential exergy, and ex_{chem} is the specific chemical exergy. ex_{kin} and ex_{pot} were not considered in the analysis as they are negligible in magnitude for the given material streams [8].

Exergy flows related to mass flows in the system, $\dot{E}X$, were calculated as the total specific exergy of the material stream, ex, times the mass flow of the stream, $\dot{m}$.

$$\dot{E}X = ex \cdot \dot{m} \tag{11}$$

Considering all useful material streams out of a process as valuable, the standard exergy efficiency η_{ex} of a process step was calculated as the exergy content in product flows, $\sum \dot{E}X_{products}$, divided by the exergy content in inlet flows, $\sum \dot{E}X_{in}$.

$$\eta_{ex} = \frac{\sum \dot{E}X_{products}}{\sum \dot{E}X_{in}} \tag{12}$$

In this study, the difference between the exergy content in inlet mass flows and in product mass flows from a process was caused partly by exergy destruction, partly by exergy content in unused heat or material flows from the process. For simplicity, these fractions were merged in a term called exergy losses and destruction (L&D), $\dot{E}X_{L\&D}$, which was calculated as

$$\dot{E}X_{L\&D} = \sum \dot{E}X_{in} - \sum \dot{E}X_{products} \tag{13}$$

As the main products of the ethanol facility are lignocellulosic ethanol and solid biofuel for combustion, the fuel exergy efficiency, $\eta_{ex,fuel}$, was evaluated for the ethanol facility as well.

$$\eta_{ex,fuel} = \frac{\dot{E}X_{ethanol} + \dot{E}X_{solid\,fuel}}{\sum \dot{E}X_{in,system}} \tag{14}$$

2.3.2. Chemical exergy

The chemical exergy of multi-component material streams, ex_{chem}, was calculated as the sum of the chemical exergy content

of the individual process steps $ex_{chem,i}$ multiplied by their weight fraction x_i:

$$ex_{chem} = \sum_i ex_{chem,i} x_i \quad (15)$$

The chemical exergy of materials that are found in the ethanol facility is summarized in Table 8. As suggested by Rian and Ertesvåg [27], the chemical exergy of natural gas was set to 43,497 kJ/kg and the lower heating value to 41,426 kJ/kg.

2.3.3. Physical exergy

As material flows in the system occur at reference pressure, the mechanical part of the physical exergy is zero. As suggested by Bösch et al. [8], heat capacities of biomass material streams were assumed constant over the relevant temperature ranges. The physical exergy of multi-component biomass materials was calculated according to the specific heat capacity of the material, c_p, and the temperature of the material, T, using the following equation [14].

$$ex_{phys,biomass} = c_p\left(T - T_0 - \ln\left(\frac{T}{T_0}\right)\right) \quad (16)$$

The heat capacity of multi-component materials was calculated as the sum of heat capacities of the individual process steps, $c_{p,i}$, multiplied by their weight fraction x_i. The values used are presented in Table 8.

$$c_p = \sum_i c_{p,i} x_i \quad (17)$$

2.3.4. Exergy in heat flows

The exergy content of heat flows in the system is associated with the exergy content in the applied heat exchange media. In the ethanol facility, water was assumed used as heat exchange media. As mentioned, heat is provided in the form of steam from the CHP unit or a gas boiler, and cooling is provided by district heating water and sea water at the given location.

In this study, best-case heat transfer is defined as heat transfer where the temperature difference between the hot and cold streams is equal to the minimum value throughout the heat exchanger. The minimum value was set to 10 K as suggested for a similar system by Modarresi et al. [9]. All losses associated with non-best-case heat exchange in the system are merged in the heat integration network in the analysis.

The reference pressure of the heat exchange media was set to 1 bar, but for phase change heat exchange, the pressure is changed to maintain the 10 K temperature difference over the entire phase change of the hot and cold flows. The heat flow transferred, $\dot{Q}$, the temperature interval, the necessary mass flow, $\dot{m}$, and heat exchange media pressure, p, of all heat exchange processes in the system are presented in Table 9. Pumping in the heat integration network was not considered. Further details about heat flows and pinch analysis of the integrated system are given in Lythcke-Jørgensen et al. [12].

Table 8
Chemical properties of material components in the ethanol facility. Heat capacities for water and ethanol are taken from the software EES [19], chemical exergy of natural gas is taken from a study by Rian and Ertesvåg [27], and all other values are from a study by Bösch et al. [8].

Material component	c_p (kJ/kg K)	ex_{chem} (kJ/kg)
Cellulose	1.28	18,808
Hemicellulose	1.28	18,808
Lignin	1.29	25,648
Monomers	1.15	16,687
Proteins	1.30	24,488
Ash	0.70	1006
Glucose	1.15	16,687
Ethanol	2.53	29,532
Water	4.18	51
Natural gas	–	43,497

3. Exergy analysis results

3.1. Ethanol production

Using the method described previously, exergy flows in the ethanol facility were calculated. The results are presented in a Grassmann diagram in Fig. 4. The diagram shows how the exergy content of the inlet wheat straw passes through the various processes in the facility until it ends up in the final energy products: ethanol, solid fuel and molasses. The exergy flows of heat transferred into the system, and of the heat recovered from the different process steps, all represent best-case heat exchange, as described in Section 2.3.4. The heat recovered is sent back into the heat integration network where it is reused internally, used for district heating production, or is cooled off. Exergy losses and destruction (L&D), which cover exergy destruction in process steps and exergy content of discarded material streams and heat losses, are illustrated as well. Exergy destruction in the ethanol facility is in general related to heat transfer over a temperature difference, frictional exergy destruction, heat losses, and material degradation.

The largest exergy L&D in the ethanol production was found to occur in the simultaneous saccharification and fermentation (SSF) process where the exothermal fermentation process takes place. Heat released from the fermentation is used to maintain an elevated temperature in the process, and the heat released is not recovered. L&D in this process step are associated with heat losses and product degradation from the fermentation process. The exergy L&D during the separation stage are also significant, mainly caused by large amounts of heat transfer and mechanical separation of flows. Standard exergy efficiencies of the individual process steps and the ethanol production as a whole are presented in Table 10.

The SSF is seen to be the least efficient ethanol facility process step in terms of exergy efficiency, while the ethanol production as a whole reaches a best-case exergy efficiency of 0.91.

3.2. Heat integration network and system efficiencies

Exergy flows in the heat integration network were studied for the six operation points described in Table 7. The exergy flows into and out of the heat integration network and the exergy L&D in the various operation points are summarized in Table 11. Exergy L&D in the heat integration network are related to exergy destruction from heat transfer over a temperature difference, and heat losses. Pumping work and frictional losses were not considered.

The main outcome of the results presented in Table 11 is the demonstration that exergy efficiency of the heat integration network is heavily influenced by the operation of the polygeneration system. Thus, district heating production and the choice between integrated and separate mode operation are seen to have significant impact on the exergy efficiency. Exergy efficiency is increased with district heating production as the production converts otherwise discarded heat flows, and their exergy contents, to the useful energy commodity district heating. However, this increase comes at the cost of slightly higher exergy flows into the heat integration network. Separate operation is found to decrease the exergy efficiency markedly when compared to integrated operation due to the fact that the heating source is switched from steam with low exergy-to-energy ratios to natural gas with very high exergy-to-energy ratio. The results further indicate that the exergy efficiency

Table 9
Best-case hot and cold streams in the ethanol facility during production.

Component	Flow type	$\dot{Q}$ (MJ/s)	T_{in} (C)	T_{out} (C)	p (bar)	$\dot{m}$ (kg/s)
Pretreatment	Hot	34.0	195	–	13	12.44
	Cold	2.1	90	180	0.7018	11.88
	Cold	26.7	90	91	0.7018	11.69
	Cold	0.6	70	90	1	6.78
	Cold	1.5	40	90	1	10.95
	Cold	0.4	25	40	1	5.97
Distillation	Hot	10.1	111	110	1.431	4.54
	Hot	0.1	47	43	1	7.84
	Cold	6.5	68	69	0.286	2.80
	Cold	0.2	25	90	1	0.62
Separation	Hot	27.2	111	110	1.431	12.19
	Hot	0.6	110	90	1.431	7.34
	Cold	27.2	90	91	0.7018	11.88
	Cold	5.0	25	90	1	18.47
District heating[a]	Cold	0.0–81.3	50	100	20	0.0–388.1

[a] District heating production in the ethanol facility can be varied.

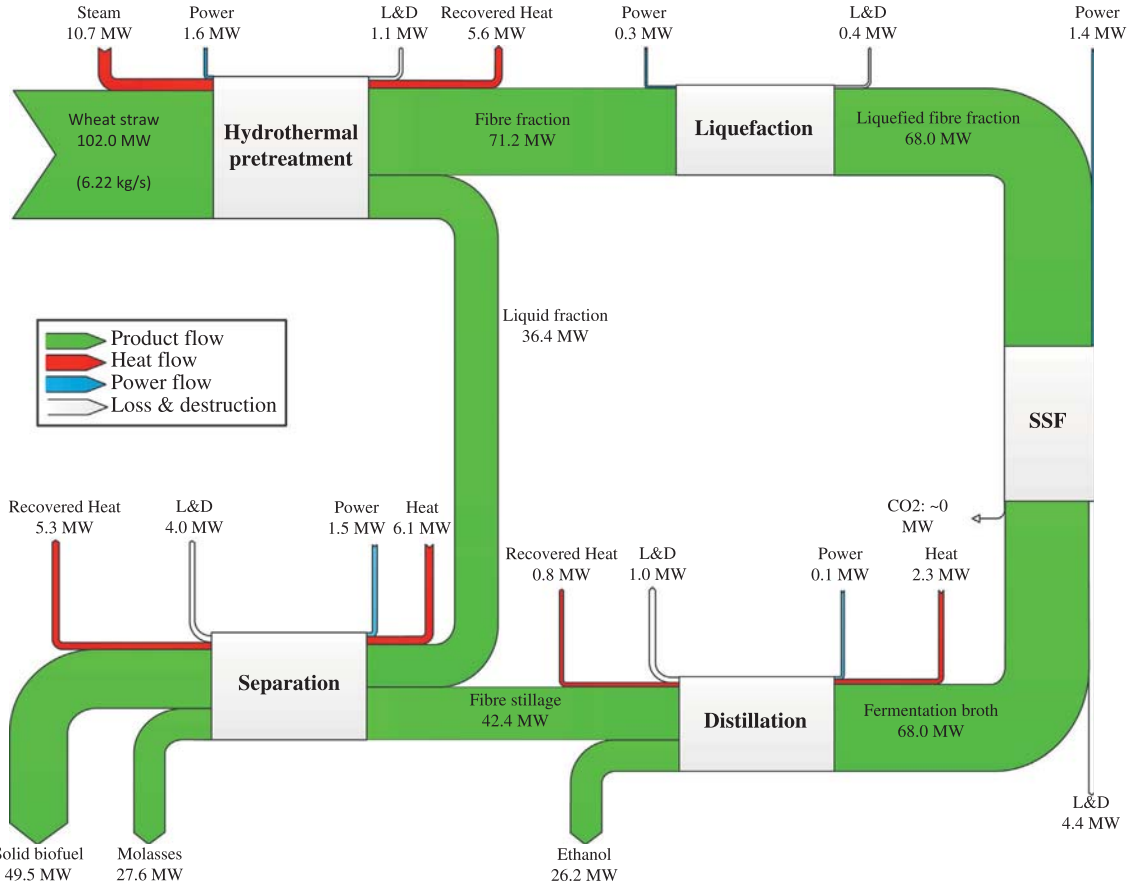

Fig. 4. Grassmann diagram illustrating exergy flows in the ethanol facility. Exergy losses and destruction (L&D) for the individual processes are also indicated.

Table 10
Standard exergy efficiency of the ethanol facility components and the overall ethanol production.

Process	Standard exergy efficiency, η_{ex}
Pretreatment	0.99
Liquefaction	0.99
SSF	0.94
Distillation	0.99
Separation	0.95
Ethanol facility, total	0.91

of the heat integration network depends only slightly on the load in the CHP unit.

For each of the six operation points of interest, the standard exergy efficiency, as defined in Eq. (12), and the fuel exergy efficiency, as defined in Eq. (14), were calculated for the entire ethanol facility. The results are presented in Table 12.

With regards to standard exergy efficiency, the ethanol facility was found to have an efficiency pattern equal to that of the heat integration network. The highest standard exergy efficiency of 0.855 was obtained in operation point IV where the production was carried out in integrated mode, the CHP unit was operated

Table 11
Exergy flows into and out of the heat integration network, and its standard exergy efficiency.

	I	II	III	IV	V	VI
Exergy in steam from AVV1 extraction point A (MW)	–	–	14.2	14.2	–	–
Exergy in steam from AVV1 extraction point B (MW)	13.9	13.9	–	–	–	–
Exergy in steam from AVV1 extraction point C (MW)	10.5	15.5	8.9	13.3	–	–
Exergy in natural gas supply (MW)	–	–	–	–	76.1	91.7
Exergy supplied to district heating (MW)	–	11.6	–	11.6	–	11.6
Exergy L&D (MW)	16.9	10.4	16.0	8.8	68.8	72.8
Standard exergy efficiency of the heat integration network (–)	0.53	0.75	0.55	0.78	0.22	0.30

Table 12
Standard exergy efficiency and fuel exergy efficiency for the integrated ethanol facility in the six investigated operation points.

Operation point	Standard exergy efficiency, η_{ex} (–)	Fuel exergy efficiency, $\eta_{ex,fuels}$ (–)
I	0.787	0.787
II	0.843	0.758
III	0.795	0.795
IV	0.855	0.769
V	0.564	0.564
VI	0.589	0.520

at a load of 0.4, and the district heating production in the ethanol facility was at full load. This number is quite similar to an exergy efficiency of 0.88 reported by Modarresi et al. [9] for a similar production. The lowest standard exergy efficiency of 0.564 occurred in operation point V where the ethanol facility is operated separately and no district heating production is included. Integrated operation at 0.4 partial load was found to yield higher exergy efficiencies than integrated operation at full load due to the fact that the exergy-to-energy ratio in the extracted steam was lower for the part-load operation. Grassmann diagrams of the polygeneration system in these two points are presented in Fig. 5.

At variance with these results, the fuel exergy efficiency was found to be inversely proportional to the district heating production. This is due to the fact that district heating production leads to a higher heating load on the system without yielding more fuel products. The highest fuel exergy efficiency obtained was 0.795 and occurred in operation point III, while the lowest obtained was 0.520 and occurred in operation point VI.

In general, the main message obtained from the results of this study is the fact that operation can have a major impact on the efficiency of lignocellulosic ethanol production when integrated in a CHP unit. For the six operation points evaluated, the standard exergy efficiency was found to vary from 0.564 to 0.855, and operation should therefore be taken into account when estimating the actual potentials of integrating lignocellulosic ethanol with combined

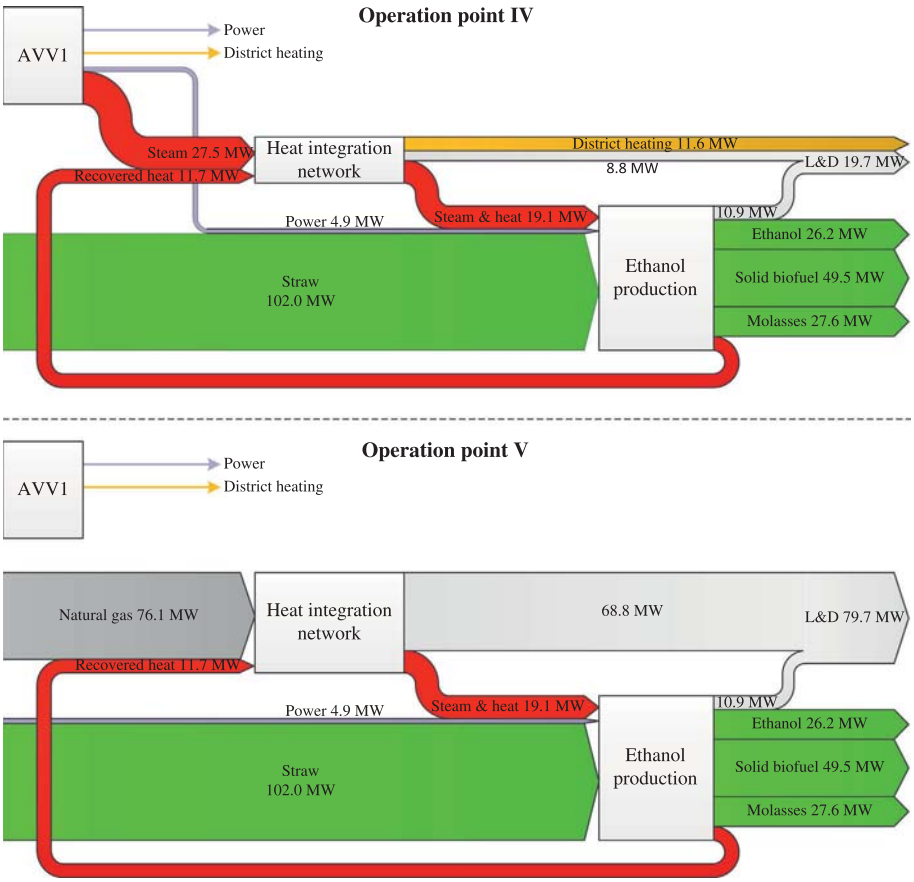

Fig. 5. Grassmann diagrams of the integrated process in operation points IV (top) and V (bottom).

heat and power production. A suggestion for further work would be to determine the average exergy efficiency of the treated ethanol facility through simulations of the yearly production for the entire polygeneration system.

4. Discussion

The results of this study suggest that operation can affect the efficiency of producing ethanol in integration with CHP plants. Three operation parameters were investigated in this study: CHP unit load, integrated versus separate operation and district heating production in the ethanol facility.

It was indicated that the CHP unit load only had a minor impact on the standard exergy efficiency of the ethanol production. The exergy content of the steam extracted was slightly lower for a load of 0.4 than for a load of 1.0 due to variations in the thermodynamic state of the steam extracted from the CHP unit at the various loads. However, this parameter was found to be the least significant of the three that were investigated.

Of the investigated parameters, separate operation was found to have the most significant negative impact on the standard exergy efficiency of the ethanol facility. Separate operation can be caused by high power loads on the CHP unit, or by periods of CHP unit shut-down. Another study of the investigated polygeneration system suggested that the separate operation would occur for almost 39% of the year in the present Danish energy system [12], and with further integration of wind power in the Danish grid it is likely that the periods of CHP shut-down will be extended in the future [28]. This might cause the average standard exergy efficiency of the ethanol production to be well below the levels calculated for integrated operation.

District heating production was found to increase the standard exergy efficiency of the ethanol facility. However, district heating is associated with both daily, weekly, and seasonally demand fluctuations. It is therefore unlikely that the benefits of district heating production can be obtained all year round.

Regarding exergy L&D in the ethanol facility, it was found that L&D in the heat integration network accounted for 45% of the total exergy losses in the best-case operation point, IV, while they accounted for 86% of the losses in the worst-case operation point, V. This suggests that the main focus point for increasing the efficiency of the system lies in the heat integration network. During integrated operation, the efficiency of the heat integration network could be increased by extracting steam with a lower exergy content that still satisfies the requirements of the ethanol production. However, a previous study [12] showed that no existing steam extraction points in the treated CHP unit could achieve this. During separate operation, the most straight forward improvement would be to replace the natural gas with another fuel or heat source that has a lower exergy-to-energy ratio. This could significantly improve the standard exergy efficiency of the ethanol facility during separate operation. Finally, the exergy efficiency of the heat integration network could be increased by technological developments of the ethanol production that will allow for a larger amount of internal reuse of heat, reducing both the hot and cold utility demands for the ethanol facility and thereby reducing the exergy losses and destruction in the heat integration network. Whether or not this is feasible is beyond the scope of this paper.

Several other research groups have investigated energy and exergy flows in systems producing lignocellulosic ethanol, heat, and power. As mentioned, Modarresi et al. [9] reported a lignocellulosic ethanol production exergy efficiency of 0.88 for a similar system, which is comparable to the 0.855 found in this study. Furthermore, the group reported a practical heat load reduction of 0.41 and a cooling load reduction of 0.40 through the application of pinch analysis, while it was only possible to reduce the heat and cooling load by 0.09 for the system investigated in this study when district heating was not included [12]. The main reason for this is the rigid choice of processing technology, and it is likely that technological changes can improve the heat integration potential significantly. This would be relevant to investigate in a future study. It should be highlighted that the inclusion of district heating production in the ethanol production was found to reduce the cooling load by up to 0.92 [12]. Furthermore, integration synergies could be expanded by using the lignin fuel from the ethanol production in the CHP unit directly as pointed out by Starfelt et al. [11]. This was not considered in the present study.

For a comparable polygeneration system, Bösch et al. [8] reported an exergy efficiency for the ethanol production of 0.74. In the system studied, the C5-molasses from the lignocellulosic ethanol production were used for biogas production through anaerobic fermentation. The produced biogas was fed to a combustion engine for the production of electricity and a part of the heat required by the ethanol production, while the rest of the heat demand was met by a gas combustion chamber. The conversion of C5-molasses and the combustion of the produced gas seems to be the reason for the lower exergy efficiency of this system.

Due to the potential operation impact on the system efficiency, it is relevant to investigate the expected operation patterns of such polygeneration system. A previous study by the authors [12] evaluated the operation of the system by applying a historical operation pattern for the CHP unit. With this operation pattern, separate operation would occur for 3375 h of the year, of which 2060 h were caused by shut-down of the CHP unit and the remaining 1685 h were caused by high heat and power loads on the CHP unit which prevented integrated operation. However, the study also suggested that the ethanol production economy is much better during integrated operation. It is therefore likely that the operation pattern of the polygeneration system would be changed to favour this production, which could be done by extending the operation time of the CHP unit over the year, and by reducing the power production of the CHP unit during peak load periods. Whether this would be done depends on a payoff between lost incomes from power sales and decreased costs for the ethanol production.

5. Conclusion

This study contained an exergy analysis of a polygeneration system in which hydrothermal pretreatment-based lignocellulosic ethanol production is integrated in the Danish combined heat and power unit Avedøreværket 1. The analysis was conducted for six different operation points that alters on three different operation parameters: Load in the CHP unit, integrated versus separate operation, and the inclusion of district heating production in the ethanol facility. The analysis suggested that the load in the CHP unit only had a minor impact on the standard exergy efficiency of the ethanol facility during integrated operation. Opposed to this, separate operation was found to yield significantly lower standard exergy efficiencies for the ethanol facility than integrated operation did. The inclusion of district heating production in the ethanol facility was found to increase the standard exergy efficiency slightly. The calculated standard exergy efficiency of the ethanol facility varied from 0.564 to 0.855, of which the highest was obtained for integrated operation at minimum CHP load and full district heating production in the ethanol facility, and the lowest for separate operation with zero district heating production in the ethanol facility. The results suggest that the efficiency of integrating lignocellulosic ethanol production in CHP plants is highly dependent on operation, and it is therefore suggested that the expected

operation pattern of such polygeneration system is taken into account when evaluating the potential performance of the polygeneration system.

Acknowledgements

The authors would like to thank Brian Elmegaard for allowing the use of his numerical model of the Danish combined heat and power unit Avedøreværket 1 in the study, and for his feedback on the method used for analysing exergy flows in the system.

References

[1] Ahrenfeldt J, Thomsen T, Henriksen U, Clausen LR. Biomass gasification cogeneration – a review of state of the art technology and near future perspectives. Appl Therm Eng 2013;50:1407–17.
[2] Larson ED, Jin H, Celik FE. Large-scale gasification-based coproduction of fuels and electricity from switchgrass. Biofuels Bioprod Biorefin 2009;3:174–94.
[3] Naqvi M, Yan J, Dahlquist E. Black liquor gasification integrated in pulp and paper mills: a critical review. Bioresour Technol 2010;101:8001–15.
[4] Gassner M, Maréchal F. Increasing efficiency of fuel ethanol production from lignocellulosic biomass by process integration. Energy Fuels 2013;27:2107–15.
[5] Balat M. Production of bioethanol from materials via the biochemical pathway: a review. Energy Convers Manage 2010;52:858–75.
[6] Daianova L, Dotzauer E, Thorin E, Yan J. Evaluation of a regional bioenergy system with local production of biofuel for transportation, integrated with a CHP plant. Appl Energy 2011;92:739–49.
[7] Ilic DD, Dotzauer E, Trygg L. District heating and ethanol production through polygeneration in Stockholm. Appl Energy 2011;91:214–21.
[8] Bösch P, Modarresi A, Friedl A. Comparison of combined ethanol and biogas polygeneration facilities using exergy analysis. Appl Therm Eng 2012;37:19–29.
[9] Modarresi A, Kravanja P, Friedl A. Pinch and exergy analysis of lignocellulosic ethanol, biomethane, heat and power production from straw. Appl Therm Eng 2012;43:20–8.
[10] Gassner M, Maréchal F. Increasing conversion efficiency in fuel ethanol production from lignocellulosic biomass by polygeneration – and a paradoxon between energy and exergy in process integration. In: ECOS 2010; 2010.
[11] Starfelt F, Thorin E, Dotzauer E, Yan J. Performance evaluation of adding ethanol production into an existing combined heat and power plant. Bioresour Technol 2009;101:613–8.
[12] Lythcke-Jørgensen C, Haglind F, Clausen LR. Thermodynamic and economic analysis of integrating lignocellulosic bioethanol production in a Danish combined heat and power plant. In: 21st European biomass conference & exhibition, Copenhagen; June 2013.
[13] Larsen J, Østergaard Haven M, Thirup L. Inbicon makes lignocellulosic ethanol a commercial reality. Biomass Bioenergy 2012;46:36–45.
[14] Bejan A, Tsatsaronis G, Moran M. Thermal design & optimization. John Wiley & Sons Inc.; 1996.
[15] Elmegaard B, Houbak N. Simulation of the Avedøreværket Unit 1 cogeneration plant with DNA. In: ECOS 2003, Copenhagen; 2003.
[16] Elmegaard B, Houbak N. DNA – a general energy system simulation tool. In: SIMS; 2005.
[17] Lythcke-Jørgensen C. Modelling and optimization of a steam co-generation plant with integrated bio-ethanol production, Technical University of Denmark, Kgs. Lyngby; 2012. <http://orbit.dtu.dk/en/projects/modelling-and-optimisation-of-novel-polygeneration-plants(3c273dec-db89-4628-839b-078cb414c573).html>.
[18] Larsen J, Petersen MØ, Thirup L, Li HW, Iversen FK. The IBUS process – lignocellulosic bioethanol close to a commercial reality. Chem Eng Technol 2008;5:765–72.
[19] F-Chart Software. <http://www.fchart.com/ees/> [accessed 25.02.13].
[20] Østergaard Petersen M, Larsen J, Hedegaard Thomsen M. Optimization of hydrothermal pretreatment of wheat straw for production of bioethanol at low water consumption without addition of chemicals. Biomass Bioenergy 2009;33:834–40.
[21] Bentsen NS, Felby C, Ipsen KH. Energy balance of 2nd generation bioethanol production in Denmark, Elsam A/S; 2006.
[22] AspenTech. <http://www.aspentech.com/products/aspen-plus.aspx> [accessed 16.08.13].
[23] Inbicon A/S. Making ethanol work for the world, Fredericia, Denmark; 2010. <http://www.inbicon.com/sitecollectiondocuments/pdf/kacelle/kacelle_brochure.pdf>.
[24] Jack MW. Scaling laws and technology development strategies for biorefineries and bioenergy plants. Bioresour Technol 2009;100:6324–30.
[25] Danmarks Statistik. Statistikbanken; 2012. <www.statistikbanken.dk> [accessed 17.05.12].
[26] Kemp IC. Pinch analysis and process integration. 2nd ed. Oxford (UK): Butterworth-Heinemann; 2006.
[27] Rian AB, Ertesvåg IS. Exergy evaluation of the arctic Snøhvit liquefied natural gas processing plant in northern Norway – significance of ambient temperature. Energy Fuels 2012;26:1259–67.
[28] Lund H, Mathiesen BV, Christensen P, Schmidt JH. Energy system analysis of marginal electricity supply in consequential LCA. Int J Life Cycle Assess 2010;15:260–71.

APPENDIX C Journal paper 2

ISI Journal Paper

C.E. Lythcke-Jørgensen and F. Haglind. *Design optimization of a polygeneration plant producing power, heat, and lignocellulosic ethanol*. Energy Conversion and Management 91:353-366, 2015.

This paper presents the contents and outcomes of the design optimization conducted for *Case I* in this project.

Energy Conversion and Management 91 (2015) 353–366

Contents lists available at ScienceDirect

Energy Conversion and Management

journal homepage: www.elsevier.com/locate/enconman

Design optimization of a polygeneration plant producing power, heat, and lignocellulosic ethanol

Christoffer Lythcke-Jørgensen *, Fredrik Haglind

Technical University of Denmark, Department of Mechanical Engineering, Nils Koppels Allé 403, DK-2800 Kgs. Lyngby, Denmark

ARTICLE INFO

Article history:
Received 3 October 2014
Accepted 10 December 2014

Keywords:
Combined heat and power
Design optimization
Exergy efficiency
Lignocellulosic ethanol
Operation optimization
Polygeneration

ABSTRACT

A promising way to increase the energy efficiency and reduce costs of biofuel production is to integrate it with heat and power production in polygeneration plants. This study treats the retrofitting of a Danish combined heat and power plant by integrating lignocellulosic ethanol production based on wheat straw with the aim of minimizing specific ethanol production cost. Previously developed and validated models of the facilities are applied in the attempt to solve the design optimization problem. Straw processing capacities in the range of 5–12 kg/s are considered, while plant operation is optimized over the year with respect to maximal income and with the limitations that the reference hourly district heating production has to be met while reference hourly power export cannot be exceeded.

The results suggest that the specific ethanol production cost increased continuously from 0.958 Euro/L at a straw processing capacity of 5 kg/s to 1.113 Euro/L at a capacity of 12 kg/s, indicating that diseconomies-of-scale applies for the suggested ethanol production scheme. A thermodynamic evaluation further discloses that the average yearly exergy efficiency decreases continuously with increasing ethanol production capacity, ranging from 0.746 for 5 kg/s to 0.696 for 12 kg/s. This trend results from operating constraints that induce expensive operation patterns in periods of high district heating loads or shut-down periods for the combined heat and power plant. A sensitivity analysis indicates that the found optimum is indifferent to major variations in fossil fuel prices. The results question the efficiency of the suggested retrofitting scheme in the present energy system, and they further point toward the importance of taking operating conditions into consideration when developing flexible polygeneration plant concepts as differences between design-point operation and actual operation may have a significant impact on overall plant performance.

1. Introduction

Biomass, being the only renewable resource of highly concentrated carbon, is often considered a cornerstone in renewable energy systems because of its storability and potential conversability to biofuels with high energy densities [1]. The biomass resource, however, is limited [2], and competition between food and energy production pose a sustainability challenge [3]. Efficient use and conversion of sustainably available biomass are therefore of crucial importance in renewable energy systems [4].

Among biofuels, ethanol is presently the most widely used for transportation on a global basis and it is consumed both as an individual fuel and in blends with gasoline [5]. Ethanol produced from lignocellulosic biomass is of special interest here because it may yield reduced CO_2 emissions from transportation without linking fuel prices and food prices directly [4]. Furthermore, ethanol is a bulk-volume chemical used in industrial and consumer products and lignocellulosic ethanol presents a green chemistry [6][1] alternative to the existing ethanol production from ethene hydration or through fermentation of sugars and starch [7]. However, the energy intensive nature of lignocellulosic ethanol production is a challenge with respect to production efficiency and economy.

In an extensive work on the integrated production of biogas, heat and power based on biomass gasification, Gassner and Maréchal [8] concluded that biofuel plants may increase energy- and cost-efficiency simultaneously by applying process systems engineering approaches and by considering integration with other processes in polygeneration plants (PGPs). Similarly, a promising

* Corresponding author. Tel.: +45 30 42 72 00.
E-mail addresses: celjo@mek.dtu.dk (C. Lythcke-Jørgensen), frh@mek.dtu.dk (F. Haglind).

[1] Green chemistry consists of environmental friendly, sustainable chemicals and processes the use of which results in reduced waste, safer outputs, and reduced or eliminated pollution and environmental damage [6].

http://dx.doi.org/10.1016/j.enconman.2014.12.028
0196-8904/

Nomenclature

Latin letters

C	cost (Euro)
c	specific cost (Euro/GJ)
D	dimension (–)
$\dot{E}X$	exergy flow (MJ/h)
ex	specific exergy flow (MJ/kg)
I	investment (Euro)
M	mass (kg)
M_f	capacity power factor (–)
$\dot{P}$	power production (MW)
Q	heat (MJ)
$\dot{Q}$	heat flow (MJ/s)
$\dot{Q}_{fuel}$	fuel input (MJ/s)
V_{eth}	volume ethanol production (L/h)

Greek letters

α	back-pressure operation parameter (–)
β	relative district heating production in the ethanol facility (–)
η_{eth}	mass efficiency of lignocellulosic-biomass-to-ethanol conversion (–)
η_{ex}	standard exergy efficiency (–)
κ	choice between integrated or separate operation (–)
λ	combined heat and power unit load (–)
ρ	density (kg/L)
σ	straw processing capacity of the ethanol production (kg/s)

Subscripts

add	additives
enz	enzymes
eth	ethanol
i	hour of the year
I	investment depreciation
O&M	operation and maintenance
ref	reference production
0	reference value

Abbreviations

AVV1	Avedøreværket 1
CHP	combined heat and power
DH	district heating
L&D	(exergy) losses and destruction
O&M	operation and maintenance
SSF	simultaneous saccharification and fermentation

way to increase energy- and cost-efficiency of lignocellulosic ethanol production is to integrate it with heat and power production [4]. Plants integrating the production of power, heat, bio-methane, and lignocellulosic ethanol have been investigated by several groups, both as grassroot design problems and retrofit design problems. Regarding grassroot design problems, Daianova et al. [9] and Ilic et al. [10] both reported better energy economy for integrated PGPs compared to stand-alone production of the same energy products, assuming constant energy prices over the year. Bösch et al. [11] discussed how the energy economy of a system producing lignocellulosic ethanol, biogas and district heating (DH) might be increased by integrating power production. For a similar system, Modarresi et al. [12] conducted a pinch analysis and reported that heat integration can reduce the hot and cold utility demands by up to 40%, assuming operation in design point solely. Leduc et al. [13] conducted a sensitivity analysis of the important parameters for such systems in Sweden and found that incomes from heat and power sales were the most significant contributors toward reducing the specific ethanol production costs. With regard to retrofitted systems, Palacios-Bereche et al. [14] studied the integration of lignocellulosic ethanol production in the conventional first-generation sugarcane ethanol process and reported higher exergy efficiency for the integrated scheme when considering only design point operation. Lythcke-Jørgensen et al. [15] investigated the introduction of lignocellulosic ethanol production in an existing combined heat and power (CHP) and also reported higher exergy efficiencies for integrated operation. In a study of conversion routes for winter wheat to ethanol, Bentsen et al. [16] suggested that energy savings could be achieved by integrating lignocellulosic ethanol production in existing CHP units. Starfelt et al. [17] investigated the integration of lignocellulosic ethanol production in an existing biomass-based CHP unit in Sweden and concluded that for the same production of heat, power, and ethanol, the total biomass consumption would be lower for the integrated system than for a separate scenario. And in a later study, Starfelt et al. [18] concluded that the integration of lignocellulosic ethanol production in Swedish CHP units with fixed heat-to-power ratios may be profitable if excess heat capacity is available in the CHP unit for a certain amount of time over the year.

In principle, the development and optimization of PGPs can be considered at three levels, similar to the optimization of energy systems [19] and distributed energy supply systems [20]: Synthesis level, design level, and operation level. At the synthesis level, the configuration of the PGP is optimized by either retrofitting an existing plant (retrofit design) or by developing a new plant concept (grassroot design),[2] which entails the selection of the desired products and processes. At the design level, one considers process dimensioning, process integration, required components, and technical specifications of the equipment. Finally, at the operation level, the operation mode of the given plant is optimized in the surrounding energy system; this is done by taking expected demands for, and costs of, energy services and utilities into account as well as interactions with other energy producers in the system. The operation level is especially important for flexible operating PGPs, e.g. those set to balance production from intermittent renewable energy sources [21] whenever economically advantageous [22]. Optimization on operation level has been investigated in literature for polygeneration plants producing power, heating, cold and fresh water, e.g. in a sequential optimization methodology presented by Uche et al. [23]. Grisi et al. [24] further illustrated how commodity market prices may affect operation decisions in a sugarcane biorefinery producing power, sugar, sugar- and bagasse-based ethanol, and biogas. However, to the authors' best knowledge the impact of flexible plant operation on economic performance has not been treated comprehensively in previous studies of the integrated production of power, heat, and lignocellulosic ethanol.

This study assesses the impact on economic and thermodynamic performance of integrating lignocellulosic ethanol production with flexible heat and power production. The study treats a retrofit design problem where lignocellulosic ethanol production

[2] A grassroot design is *a priori* always a solution to a retrofit design optimization problem [20].

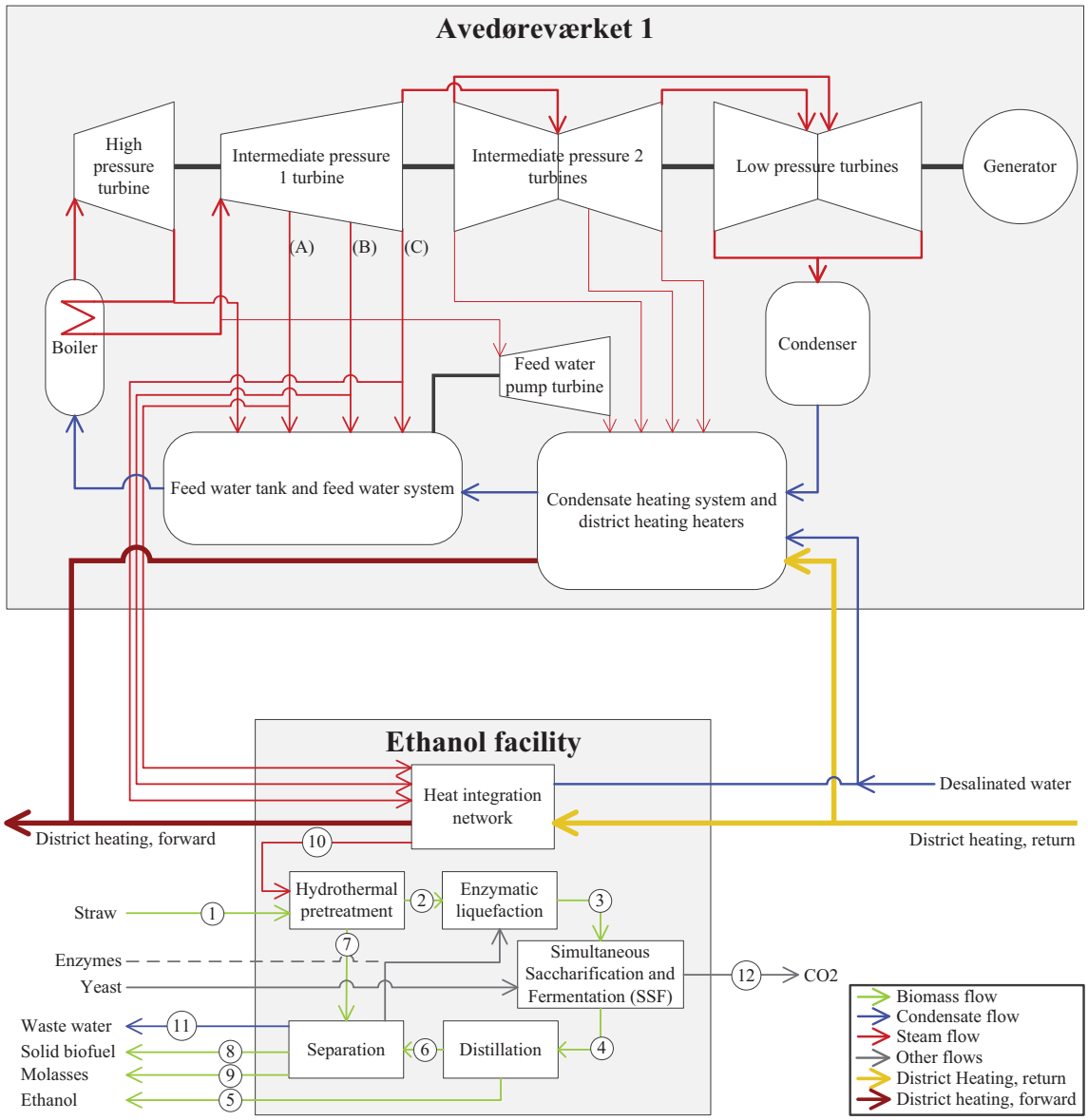

Fig. 1. Simplified process layout of the polygeneration plant in question. From Lythcke-Jørgensen et al. [15].

using the hydrothermal pretreatment technology IBUS [25][3] is sought integrated into the Danish CHP unit Avedøreværket 1 (AVV1). The system has previously been studied by the authors and the outcomes suggested that operating conditions may have a significant impact on both economy [26] and overall exergy efficiency [27,15] of the ethanol production. This work builds upon the previous study by optimizing the PGP at design and operation levels simultaneously with the aim of minimizing the break-even specific ethanol production costs. For each solution to the design problem, the thermodynamic performance of the ethanol production is further evaluated by applying exergy analysis [28] and calculating the average exergy efficiency of the ethanol production over the year.

In this paper, the modeling approach and outcomes of previous studies are given in Section 2. The design optimization scheme and the thermodynamic performance evaluation method are presented in Section 3. The outcomes are presented in Section 4 and discussed in Section 5. Finally, Section 6 contains a conclusion of the findings.

2. System description and previous work

2.1. System description

The design optimization problem treated in this study concerns the integration of lignocellulosic ethanol production based on IBUS technology in the existing Danish combined heat and power unit Avedøreværket 1. A simplified layout of the PGP is presented in Fig. 1. A thorough description of the plant synthesis and modeling, including choice of performance parameters and modeling validation, is presented in Lythcke-Jørgensen et al. [15].

Avedøreværket 1 (AVV1), which was commissioned in 1990, has a net electric power generation in condensation mode of 250 MW, and of 212 MW in full back pressure mode with a district heating (DH) production of 330 MJ/s (drive temperature/return temperature 100 °C/50 °C) [29]. Part-load operation in the CHP unit

[3] IBUS (Integrated Biomass Utilization System) is a patented cellulosic biomass pretreatment technology. The patent is owned by the Danish company Inbicon A/S, a subsidiary to DONG Energy.

Table 1
Mass conversion efficiencies of the products in the modeled ethanol facility.

Mass conversion efficiency	Nomenclature	Value (–)
Ethanol	η_{eth}	0.150
Molasses	η_{mol}	0.371
Solid biofuel	$\eta_{biofuel}$	0.407

is governed by sliding-pressure control [30]. A numerical model of AVV1, developed by Elmegaard and Houbak [29] in the energy system simulator Dynamic Network Analysis [31], was used for simulating flows and operation of the CHP unit.

An ethanol production facility based on IBUS technology produces lignocellulosic ethanol, solid biofuel, and molasses from wheat straw. In the facility, the lignocellulosic structure of the straw is broken down through treatment with pressurized steam in the hydrothermal pretreatment stage, whereupon the straw–steam mixture is split into a fiber fraction and a liquid fraction. The fiber fraction is liquefied by glucose-forming enzymes before fermentation is initiated in simultaneous fermentation and saccharification (SSF) tanks. Ethanol is distilled from the resulting fermentation broth, leaving a fiber stillage which is treated in various separation stages alongside the pretreatment liquid fraction, yielding a solid biofuel fraction, a molasses fraction, and a waste water fraction. The molasses fraction can be used in anaerobic fermentation to produce biogas [12] or as animal feed [32], while the solid biofuel can be used for combustion or gasification. A model of the ethanol facility based on heat and mass balances over each of the system processes was developed in the software Engineering Equation Solver (EES) [33] using the layout reported by Larsen et al. [32] and Østergaard Petersen et al. [34]. The flows of yeast and enzymes were neglected in mass balance calculations as they were found to be insignificant. The mass conversion efficiencies for the ethanol facility products are presented in Table 1.

2.2. Outcomes of previous work

In the previous studies of the polygeneration plant, a fixed design was applied to the system in which the ethanol facility was dimensioned to process all locally available winter wheat straw within a distance of 50 km from the plant, yielding a straw processing capacity of 6.22 kg/s all year round. Because of load transition times of more than 180 h in the ethanol production facility [34], load changes and stop-and-go operation were not considered feasible and full-load operation was therefore assumed for the whole year. As the CHP unit was operated according to flexible power and heat demands, the ethanol production in the PGP could be run in two ways: Integrated mode or separate mode. In integrated mode, steam extracted from turbines of the CHP unit was used for covering the hot utility demand of the ethanol facility. During integrated operation, DH production from the IBUS facility was prioritized over DH production from the CHP unit. In separate mode, a natural gas boiler with a first law energy efficiency of η_{boiler} = 0.96 [35] was used for generating the steam required by the ethanol facility, and DH production in the ethanol facility was not considered. The principles of the two PGP operation modes are outlined in Fig. 2.

In Lythcke-Jørgensen et al. [26], a combined pinch analysis [36] and exergy analysis [28] was carried out to identify the minimum hot and cold utility demands in the ethanol facility as well as the steam extraction pattern with the lowest exergy destruction during integrated mode operation. A 10 K pinch temperature difference was used, as suggested by Modarresi et al. [12] for a similar facility. The resulting specific hot and cold utility demands and power consumption of the ethanol production per kilogram of biomass treated are presented in Table 2.

As regards existing steam extraction points in AVV1 only, the optimal integration solution involved steam extraction from the points marked (A), (B), and (C) in Fig. 1. The thermodynamic states of steam in the three points are summarized in Table 3. Steam for hydrothermal pretreatment was extracted from node (B) in AVV1 at CHP loads above 0.6, and from node (A) at CHP loads below 0.6. The steam for hydrothermal pretreatment was conditioned in the heat integration network to meet the exact temperature and pressure requirements of the hydrothermal pretreatment component, 195 °C and 13 bar [37]. Heat released from steam conditioning was used internally in the ethanol facility. The remaining hot utility demand of the ethanol facility was covered by steam extracted from node (C). Condensate from the heat integration network is recycled to the condenser of AVV1 where additional desalinated water is added to compensate for the loss of steam to the hydrothermal pretreatment. Cooling in the heat integration network is provided by sea water and by DH water when DH production is activated in the ethanol facility.

The energy economy of the PGP was evaluated in Lythcke-Jørgensen et al. [26]. Considering the PGP as a substitute to AVV1 in the existing Danish energy system and assuming hour-wise quasi-static operation, the plant was set to produce the same

Table 2
Specific energy utility requirements of the ethanol production for operation with zero and full DH production in the ethanol facility.

Utility	Nomenclature	Energy (MJ/kg) – zero DH	Energy (MJ/kg) – full DH	Temperature (°C)	Pressure (bar)
Steam	q_{steam}	5.5	5.5	195	13
Heating	q_{heat}	5.7	8.0	>100	–
Cooling	q_{cool}	11.5	1.0	<20	–
Power	p	0.792[a]	0.792[a]	–	–

[a] A constant power consumption of 220 kW h/ton of straw treated was used as suggested by Bentsen et al. [37].

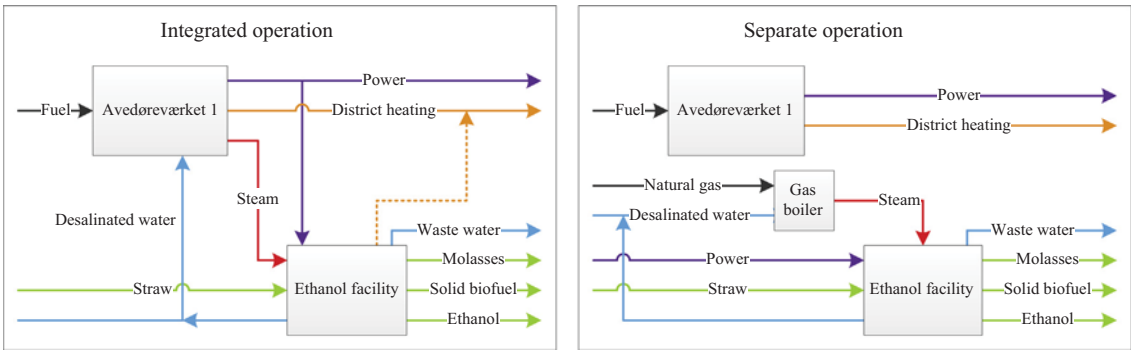

Fig. 2. Outlines of the two operation modes in the polygeneration plant. From Lythcke-Jørgensen et al. [15].

Table 3
Temperature (T), pressure (P), and specific exergy content (ex) of steam in the extraction points (A), (B), and (C) at various loads.

CHP load	(A)			(B)			(C)		
	T (C)	P (bar)	ex (kJ/kg)	T (C)	P (bar)	ex (kJ/kg)	T (C)	P (bar)	ex (kJ/kg)
1.0	467	34.2	1274	393	20.5	1121	289	9.2	911
0.9	449	31.1	1240	376	18.6	1090	275	8.3	885
0.8	431	27.9	1204	359	16.7	1058	261	7.5	858
0.7	431	25.1	1192	360	15.0	1046	262	6.7	846
0.6	432	22.1	1179	361	13.2	1032	263	6.0	832
0.5	432	18.9	1161	361	11.3	1014	264	5.1	814
0.4	433	15.5	1138	362	9.3	991	266	4.2	791

Table 4
Energy commodity costs used in the calculations.

Energy commodity	Nomenclature	Specific cost
Coal (CHP fuel)	C_{coal}	4.36 Euro/GJ [39]
Natural gas	C_{NG}	9.26 Euro/GJ [39]

hourly amounts of heat and power as the CHP unit delivered in 2011, the chosen reference year. Separate operation occurred in periods with high power demands where steam extraction for driving the ethanol production was not available and in periods where the CHP unit was shut down. The results suggested that on an average the specific energy cost for the ethanol production could be more than eight times higher during separate operation than during integrated operation, and that it might be economically advantageous to optimize the operation pattern of the PGP toward a longer duration of integrated operation. A scatter distribution of the hour-wise quasi-static operation points for the reference operation is presented in Fig. 3. It should be noted that separate operation occurred for 2060 h of the year due to CHP shut-down.

Two other studies by Lythcke-Jørgensen et al. [27,15] investigated six different operation points for the reference PGP and found that within these, the exergy efficiency of the ethanol production varied from 0.564 to 0.855. The highest exergy efficiency was obtained for integrated operation with full DH production in the ethanol facility and lowest possible load in the CHP unit, while the lowest exergy efficiency was obtained for separate operation. The reason for the large differences in exergy efficiency was primarily the fact that in integrated operation, low-quality steam was used as the heat source, while natural gas with a much higher exergy-to-energy ratio was used in separate operation. These results suggest that integrated operation might be desirable from a thermodynamic efficiency point-of-view as well.

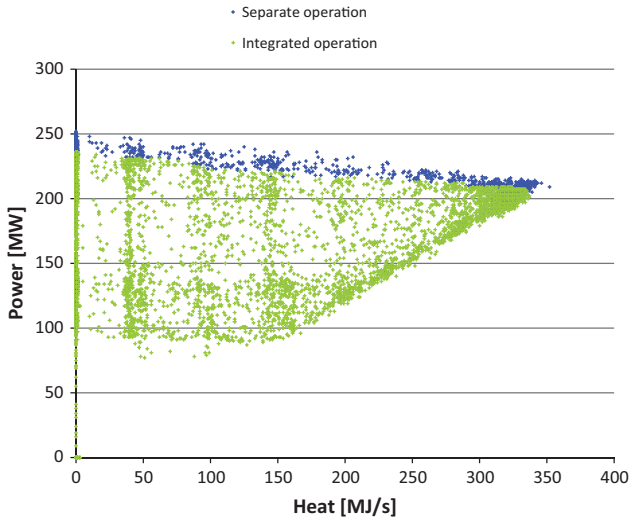

Fig. 3. Scatter distribution of the hour-wise quasi-static operating points of the reference polygeneration plant.

In summary, the previous work on the polygeneration plant suggested that integrated operation was advantageous compared to separate operation for the following reasons:

- Energy cost of the ethanol production might be significantly reduced during integrated operation [26].
- The exergy efficiency of the straw-to-ethanol conversion was markedly higher for integrated operation [27,15].
- Integrated operation made it possible to run the CHP with lower power production ratios, which could be advantageous in periods of forced DH production and low or negative power prices [26].

The present study seeks to quantify the impact of the suggested benefits by optimizing the design and operation of the suggested PGP concept.

3. Design optimization methodology

The pre-synthesized PGP is optimized simultaneously at the design and operation levels with the objective of minimizing the break-even specific ethanol production cost. Furthermore, the yearly average exergy efficiency of the ethanol production is calculated for each solution to the optimization problem in order to evaluate the efficiency of the ethanol production.

3.1. Economic data

Average costs of the energy commodities coal and gas over the reference year 2011, including overhead costs, are summarized in Table 4. Information on the market power price in the Denmark East block for each hour of 2011 was taken from the Nord Pool Spot database [38]. A scatter distribution showing the maximum, minimum, and average daily power prices is shown in Fig. 4. The average daily power price ranges from 0.153 Euro/kW h to 0.812 Euro/kW h, while the hourly power price ranges from −0.368 Euro/kW h to 1.902 Euro/kW h. The average yearly power price was 0.494 Euro/kW h.

Costs associated with the production of lignocellulosic ethanol in a full scale facility using IBUS technology, which means a straw processing capacity rate of 1000 tons/day or 11.57 kg/s, were estimated in a feasibility study by Larsen et al. [32]. The values from the feasibility study were used as reference values in the present study and are summarized in Table 5.

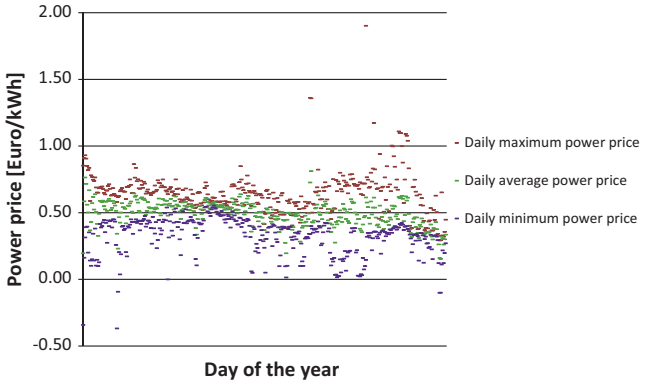

Fig. 4. Scatter distribution of the daily maximum, minimum, and average electricity prices in the block 'Denmark East' in 2011.

Table 5
Production costs per liter of lignocellulosic ethanol produced in a full scale ethanol facility based on IBUS technology. Values from Larsen et al. [32].

Cost parameter	Nomenclature	Specific cost (Euro/L)
Enzymes cost	$C_{enz,0}$	0.14
Additives cost	$C_{add,0}$	0.06
Operation and maintenance cost	$C_{0\&M,0}$	0.09
Depreciation cost	$C_{I,0}$	0.07
By-product sales (molasses and solid biofuel)	$C_{sales,0}$	0.24

3.2. Optimization model description

As far as board decisions and substantial investments are concerned, the main parameter for evaluating a lignocellulosic ethanol production facility is the break-even production cost per liter of ethanol, c_{eth} [32]. The objective of the optimization problem is to minimize c_{eth} as perceived by the plant owner by varying the design and operation of the plant. The specific ethanol production cost is made up of seven cost components: Specific cost for straw c_{straw}; specific investment depreciation cost c_I; specific operation and maintenance (O&M) costs $c_{O\&M}$; specific cost for enzymes c_{enz}; specific cost for additives c_{add}; specific energy costs c_{energy}; and specific incomes from sales of molasses and solid biofuel c_{sales}.

$$c_{eth} = c_{straw} + c_I + c_{O\&M} + c_{enz} + c_{add} + c_{energy} - c_{sales} \quad (1)$$

3.2.1. Decision variables

At *design level*, the previously found optimal integration design [26] with respect to steam extraction pattern is kept, while the straw processing capacity of the ethanol production σ is varied. The straw processing capacities investigated were set to range from 5 kg/s, being slightly smaller than the capacity of the ethanol production in the reference system, to 12 kg/s, which is about the size of a full scale IBUS ethanol production facility, as reported by Larsen et al. [32]:

$$\sigma \in [5, 12] \quad (2)$$

At *operation level*, four decision variables are considered for each operation hour i: The load of the CHP unit λ_i, which can be 0.0 or within the range [0.4; 1.0] [29]; the back-pressure operation parameter α_i, which can be varied within the range 0–1, with 0 representing condensation mode operation and 1 representing full back-pressure operation; the relative production of DH in the ethanol facility β_i, which can be varied from 0 to 1; and, finally, a dummy parameter describing the choice between integrated and separate operation κ_i, taking the value 1 for integrated operation and 0 for separate operation.

$$0.40 \leqslant \lambda_i \leqslant 1.00 \quad (3)$$

$$0.00 \leqslant \alpha_i \leqslant 1.00 \quad (4)$$

$$0.00 \leqslant \beta_i \leqslant 1.00 \quad (5)$$

$$\kappa_i \in \{0, 1\} \quad (6)$$

No DH production from the ethanol process is considered during separate operation, hence:

$$\beta_i = 0 | \kappa_i = 0. \quad (7)$$

3.2.2. Constraints

As in the previous studies, the plant is seen as a substitute to AVV1 in the present Danish energy system. As a consequence, two operation constraints were set. Regarding DH production, which is subject to strict legislation, the PGP was set to deliver the same hour-wise amount of heat Q_i over the year as the CHP unit produced in the reference operation, $Q_{i,ref}$:

$$Q_i(\sigma, \lambda_i, \alpha_i, \beta_i, \kappa_i) = Q_{i,ref} \ \forall i \quad (8)$$

With regard to power exports P_i, the plant is allowed to reduce its export in a given hour compared to the reference power export $P_{i,ref}$ as back-up capacity is assumed available in the grid. However, the plant is not allowed to exceed its reference power export in any hour as it is uncertain whether or not there would be buyers for the extra power in the grid at the given price.

$$P_i(\sigma, \lambda_i, \alpha_i, \beta_i, \kappa_i) \leqslant P_{i,ref} \ \forall i \quad (9)$$

Full hour-wise operation flexibility is assumed for the plant, which means that the choice of parameters in an hour $i + 1$ is independent of the choice of parameters in the preceding hour i.

3.2.3. Model equations

The cost for straw c_{straw} depends on several factors, such as cultivation soil type, crop type, irrigation, farm size, transportation distance, and production type (organic or non-organic) [39]. Especially transportation costs are relevant if one considers a plant processing locally distributed biomass. However, as the plant in question is located next to the sea on one side and the city of Copenhagen on the other, straw would most likely have to be imported from other regions, and transportation costs are therefore assumed to be independent of the processing capacity of the ethanol production. A study by the Danish Energy Agency, Ea Energianalyse, and Wazee [39] estimated that the total cost of straw C_{straw} for energy purposes in Denmark in 2011 was in the range of 48.6–52.5 Euro/ton. To represent the expected higher transportation costs from importing straw from the countryside, the highest straw price of C_{straw} = 52.5 Euro/ton was used in this study. The specific cost of straw per produced liter of ethanol c_{straw} was calculated according to the following equation:

$$c_{straw} = \frac{\eta_{eth}}{\rho_{eth}} C_{straw} \quad (10)$$

In this equation, η_{eth} is the mass-based conversion efficiency of straw to ethanol in the PGP, as presented in Table 1, while ρ_{eth} = 785.5 m^3/ton is the ethanol density taken from the software Engineering Equation Solver (EES) [33] for a temperature of 15 °C and a pressure of 1 bar.

The specific depreciation cost for the ethanol production, c_I, is assumed to be derived from a fixed annual depreciation rate, which is directly proportional to the investment cost of the equipment. It

is common to apply power laws [40] to calculate the investment cost $I(D)$ of equipment as a function of the equipment dimension D:

$$I(D) = I_0\left(\frac{D}{D_0}\right)^{M_f} \tag{11}$$

In the equation, I_0 is the investment in a piece of equipment with the base dimension D_0, and M_f is a scaling constant that depends on the type of equipment. Assuming that a capacity power law exists for the entire ethanol facility with a scaling constant M_f, the specific depreciation cost for a facility of capacity σ, $c_I(\sigma)$, is calculated using the following relation:

$$c_I(\sigma) = \left(\frac{\sigma_0}{\sigma}\right)c_{I,0}\left(\frac{\sigma}{\sigma_0}\right)^{M_f} \tag{12}$$

Here, $c_{I,0}$ is the reference depreciation cost presented in Table 5, and $\sigma_0 = 11.57$ kg/s is the reference straw processing capacity. In this study, a scaling constant of $M_f = 0.7$ is used, as suggested by Ilic et al. [10] for a similar facility.

Similar to the calculation of the investment, a capacity power law relationship with the same scaling constant M_f is assumed to apply when calculating the specific O&M cost, $c_{O\&M}$:

$$c_{O\&M}(\sigma) = \left(\frac{\sigma_0}{\sigma}\right)c_{O\&M,0}\left(\frac{\sigma}{\sigma_0}\right)^{M_f} \tag{13}$$

In the equation, $c_{O\&M,0}$ is the reference O&M cost associated with a facility of the size σ_0.

The specific energy cost of the ethanol production c_{energy} represents the extra energy costs from operating the PGP compared to the CHP over the reference year, divided by the PGP ethanol production. It consists of three components: Specific cost of extra CHP fuel (coal) c_{fuel}, specific cost of natural gas c_{gas}, and specific cost of power c_{power}:

$$c_{energy} = c_{fuel} + c_{gas} + c_{power} \tag{14}$$

Incomes from DH sales are not associated with the ethanol production as the PGP is set to deliver the same amounts of heat on an hourly basis as the CHP unit in the reference year. Furthermore, costs for external cooling are negligible because of the ready availability of sea water.

The CHP fuel cost for an hour i, $c_{fuel,i}$, is calculated as the difference in fuel cost between the chosen operation and the fuel cost for the reference operation:

$$c_{fuel,i}(\lambda_i) = \frac{\left(Q_{fuel,i}(\lambda_i) - Q_{fuel,i,ref}(\lambda_{i,ref})\right)\cdot c_{coal}}{V_{eth}} \tag{15}$$

Here, $\lambda_{i,ref}$ is the reference CHP unit load, $Q_{fuel,i}(\lambda_i)$ is the actual fuel consumption of the CHP unit, $Q_{fuel,i,ref}(\lambda_{i,ref})$ is the reference fuel consumption of the CHP unit, c_{coal} is the specific coal cost as given in Table 4, and V_{eth} is the hourly ethanol production volume calculated as

$$V_{eth} = \sigma\cdot\frac{\eta_{eth}}{\rho_{eth}}\cdot 3600\ \text{s/h} \tag{16}$$

Natural gas is consumed only during separate operation. The cost of natural gas in an hour i is a function of the straw processing capacity σ_j and the choice of integrated or separate operation κ_i.

$$c_{NG,i}(\sigma,\kappa_i) = (1-\kappa_i)\cdot\left[\sigma\left(\frac{q_{steam}+q_{heat}}{\eta_{boiler}}\right)\cdot c_{NG}\right] \tag{17}$$

Here, $q_{steam} + q_{heat}$ is the total specific heating demand of the ethanol facility, $\eta_{boiler} = 0.96$ is the thermal efficiency of the natural gas boiler and c_{NG} is the specific cost of natural gas, as given in Table 4.

The specific cost of power, c_{power}, represents both the cost of buying power for running the ethanol production during separate operation and the costs of lost power sales in integrated operation when the power exports of the PGP are lower than the reference power exports of the CHP unit. The specific cost of power in an hour i, c_{power}, is calculated as

$$c_{power,i}(\sigma,\lambda_i,\alpha_i,\beta_i,\kappa_i) = \frac{\left[(P_{i,ref} - P_i(\sigma,\lambda_i,\alpha_i,\beta_i,\kappa_i)) + \kappa_i\cdot P_{eth}(\sigma)\right]\cdot c_{el,i}}{V_{eth}} \tag{18}$$

In the equation, $P_{i,ref}$ is reference power production of the CHP unit, P_i is the power production of the PGP, $P_{eth}(\sigma)$ is the power consumption of the ethanol production, and $c_{el,i}$ is the power price in a given hour.

Using Eq. (14), the specific energy cost in a given hour i, $c_{energy,i}$, is then calculated according to the following equation:

$$\begin{aligned} c_{energy,i}(\sigma,\lambda_i,\alpha_i,\beta_i,\kappa_i) = {} & \frac{\left(\lambda_i - \lambda_{i,ref}\right)\cdot Q_{nom}\cdot c_{coal}}{V_{eth}} + (1-\kappa_i) \\ & \cdot\left[\sigma\left(\frac{q_{steam}+q_{heat}}{\eta_{boiler}}\right)\cdot c_{NG}\right] \\ & + \frac{\left[P_{i,ref} - P_i(\sigma,\lambda_i,\alpha_i,\beta_i,\kappa_i)\right]\cdot c_{el,i}}{V_{eth}} \end{aligned} \tag{19}$$

The yearly average specific energy cost c_{energy} is calculated as

$$c_{energy}(\sigma,\lambda,\alpha,\beta,\kappa) = \frac{\sum_{i=1}^{8760} c_{energy,i}(\sigma,\lambda_i,\alpha_i,\beta_i,\kappa_i)}{8760} \tag{20}$$

For the specific ethanol production costs, it is assumed that the specific cost for enzymes c_{enz}, additives c_{add}, and the specific incomes from by-product sales c_{sales} are independent of the ethanol facility capacity and operation of the CHP unit. The reference values presented in Table 5 are used for these parameters.

3.2.4. Objective function minimization

Given Eqs. (1)–(20) for costs and variable constraints, the objective function, which is the break-even specific ethanol production cost, is defined as

$$\begin{aligned} c_{eth}(\sigma,\lambda,\alpha,\beta,\kappa) = {} & \frac{\eta_{eth}}{\rho_{eth}}C_{straw} + c_{I,0}\left(\frac{\sigma}{\sigma_0}\right)^{M_f} + c_{O\&M,0}\left(\frac{\sigma}{\sigma_0}\right)^{M_f} \\ & + c_{enz} + c_{add} - c_{sales} + c_{energy}(\sigma,\lambda,\alpha,\beta,\kappa) \end{aligned} \tag{21}$$

The optimization problem can then be formulated as

$$\begin{cases} \min\limits_{\sigma,\lambda,\alpha,\beta,\kappa}\left[c_{eth}(\sigma,\lambda,\alpha,\beta,\kappa)\right] \\ \quad \text{subject to constraints :} \\ \text{Eqs. (7), (8)} \\ \quad \text{with variables :} \\ \sigma_j \in [5,12]; \quad \alpha,\beta \in [0.0,1.0]; \quad \lambda \in [0.4,1.0] \\ \qquad\qquad \kappa \in \{0,1\} \end{cases} \tag{22}$$

Solving the optimization problem (22) will result in the lowest possible break-even specific ethanol production cost for the treated PGP under the set conditions.

3.2.5. Linearization

As the PGP unit model is non-linear, the optimization problem (22) becomes non-linear. To simplify the calculations, a piece-wise linearization of the model for the integrated PGP operation was introduced. The non-linear operational range of the reference PGP, with a straw processing capacity of $\sigma_{ref} = 6.22$ as described in Section 2, is presented in Fig. 5, and six key operational points are indicated. The operational characteristics of the six key operation points are described in Table 6.

The difference in power exports between points (1) and (a) is a direct consequence of the extraction of steam and the consumption

of produced power to run the ethanol facility in integrated mode. As the steam extraction and power consumption are both linear functions of the ethanol facility capacity σ, the difference in power yield is assumed to be a linear function of σ as well:

$$\dot{P}_1(\sigma) = \dot{P}_a + \sigma \frac{(\dot{P}_{1,PGP,ref} - \dot{P}_a)}{\sigma_{ref}} = 249.3 - 3.54 \cdot \sigma \text{ (MW)} \quad (23)$$

Point (2) relates to point (a) in the sense that the CHP unit is operated in the same way, but with the difference that full ethanol DH production is activated. The maximum DH production from the ethanol facility is a linear function of the straw processing capacity σ, and the reduced power production potential is assumed to be a linear function of σ as well:

$$\dot{Q}_2(\sigma) = \sigma \frac{\dot{Q}_{2,PGP,ref}}{\sigma_{ref}} = 13.07 \cdot \sigma \text{ (MJ/s)} \quad (24)$$

$$\dot{P}_2(\sigma) = \dot{P}_a + \sigma \frac{(\dot{P}_{2,PGP,ref} - \dot{P}_a)}{\sigma_{ref}} = 249.3 - 3.99 \cdot \sigma \text{ (MW)} \quad (25)$$

Point (4) relates to point (c) in a similar way as (2) to (a), while (3) relates to (b) and (6) relates to (d). Using the same approach for these points, the following relations were obtained for heat and power yields in each of the points as a function of σ:

$$\dot{Q}_3(\sigma) = \dot{Q}_b + \sigma \frac{(\dot{Q}_{3,PGP,ref} - \dot{Q}_b)}{\sigma_{ref}} = 332.9 + 1.00 \cdot \sigma \text{ (MJ/s)} \quad (26)$$

$$\dot{P}_3(\sigma) = \dot{P}_b + \sigma \frac{(\dot{P}_{3,PGP,ref} - \dot{P}_b)}{\sigma_{ref}} = 216.0 - 3.06 \cdot \sigma \text{ (MW)} \quad (27)$$

$$\dot{Q}_4(\sigma) = \dot{Q}_c + \sigma \frac{(\dot{Q}_{4,PGP,ref} - \dot{Q}_c)}{\sigma_{ref}} = 163.1 + 2.30 \cdot \sigma \text{ (MJ/s)} \quad (28)$$

$$\dot{P}_4(\sigma) = \dot{P}_c + \sigma \frac{(\dot{P}_{4,PGP,ref} - \dot{P}_c)}{\sigma_{ref}} = 86.3 - 1.86 \cdot \sigma \text{ (MW)} \quad (29)$$

$$\dot{Q}_5(\sigma) = \dot{Q}_c + \sigma \frac{(\dot{Q}_{5,PGP,ref} - \dot{Q}_c)}{\sigma_{ref}} = 163.1 - 8.92 \cdot \sigma \text{ (MJ/s)} \quad (30)$$

$$\dot{P}_5(\sigma) = \dot{P}_c + \sigma \frac{(\dot{P}_{5,PGP,ref} - \dot{P}_c)}{\sigma_{ref}} = 86.3 - 1.68 \cdot \sigma \text{ (MW)} \quad (31)$$

$$\dot{P}_6(\sigma) = \dot{P}_d + \sigma \frac{(\dot{P}_{6,PGP,ref} - \dot{P}_d)}{\sigma_{ref}} = 104.9 - 2.40 \cdot \sigma \text{ (MW)} \quad (32)$$

It is furthermore assumed that for a PGP with straw processing capacity σ, the maximum and minimum potential power productions in integrated operation, $\dot{P}_{max}$ and $\dot{P}_{min}$, are piece-wise linear functions of the heat production $\dot{Q}$ between the key operation points according to the following relations:

$$\dot{P}_{max}(\dot{Q},\sigma) = \begin{cases} \dot{P}_1(\sigma) + \dot{Q}\left(\frac{\dot{P}_2(\sigma)-\dot{P}_1(\sigma)}{\dot{Q}_2(\sigma)-\dot{Q}_1(\sigma)}\right) & |\dot{Q} \in [\dot{Q}_1(\sigma), \dot{Q}_2(\sigma)] \\ \dot{P}_2(\sigma) + (\dot{Q} - \dot{Q}_2(\sigma))\left(\frac{\dot{P}_3(\sigma)-\dot{P}_2(\sigma)}{\dot{Q}_3(\sigma)-\dot{Q}_2(\sigma)}\right) & |\dot{Q} \in]\dot{Q}_2(\sigma), \dot{Q}_3(\sigma)] \end{cases} \quad (33)$$

$$\dot{P}_{min}(\dot{Q},\sigma) = \begin{cases} \dot{P}_6(\sigma) + \dot{Q}\left(\frac{\dot{P}_5(\sigma)-\dot{P}_6(\sigma)}{\dot{Q}_5(\sigma)-\dot{Q}_6(\sigma)}\right) & |\dot{Q} \in [\dot{Q}_6(\sigma), \dot{Q}_5(\sigma)] \\ \dot{P}_5(\sigma) + \left(\dot{Q} - \dot{Q}_5(\sigma)\right)\left(\frac{\dot{P}_4(\sigma)-\dot{P}_5(\sigma)}{\dot{Q}_4(\sigma)-\dot{Q}_5(\sigma)}\right) & |\dot{Q} \in]\dot{Q}_5(\sigma), \dot{Q}_4(\sigma)] \\ \dot{P}_4(\sigma) + \left(\dot{Q} - \dot{Q}_4(\sigma)\right)\left(\frac{\dot{P}_3(\sigma)-\dot{P}_4(\sigma)}{\dot{Q}_3(\sigma)-\dot{Q}_4(\sigma)}\right) & |\dot{Q} \in]\dot{Q}_4(\sigma), \dot{Q}_3(\sigma)] \end{cases} \quad (34)$$

Evaluating the piece-wise linearized model (23)–(34) for the PGP with the reference straw processing capacity, the deviation of the power values between the key operation points was found to be in the range of −0.69% to +0.77% when compared to the non-linear thermodynamic model.The load λ of the CHP unit on the line between the points (3) and (4) in Fig. 5 is seen as a linear function of the heat production $\dot{Q}$ as well:

$$\lambda(\dot{Q}) = \lambda_3 + (\dot{Q} - \dot{Q}_3(\sigma))\frac{(\lambda_4 - \lambda_3)}{(\dot{Q}_4(\sigma) - \dot{Q}_3(\sigma))}$$
$$= 1 - 0.6\frac{(\dot{Q} - \dot{Q}_3(\sigma))}{(\dot{Q}_4(\sigma) - \dot{Q}_3(\sigma))} \quad |\dot{Q} \in [\dot{Q}_4(\sigma), \dot{Q}_3(\sigma)] \quad (35)$$

The linearization (35) was found to have an accuracy of −0.00% to 3.0% as compared to the non-linear thermodynamic model.

Finally, the fuel consumption of the CHP unit as a function of the load λ, $Q_{fuel}(\lambda)$, was linearized using the linear trendline-function in Microsoft Excel:

$$Q_{fuel,i}(\lambda_i) = 1798.7 \cdot \lambda_i + 367.8 \text{ (GJ/h)} \quad (36)$$

The coefficient of determination for the approximated Eq. (36) was found to be 0.9998 when compared to the fuel consumption predicted in the thermodynamic model of the CHP unit.

Applying (23)–(36) and taking the optimization constraints into account, the optimal operation solution space is reduced *a priori* to the following four operation points for each hour.

(1) Integrated operation with maximum power delivery.
(2) Integrated operation with minimum power delivery.

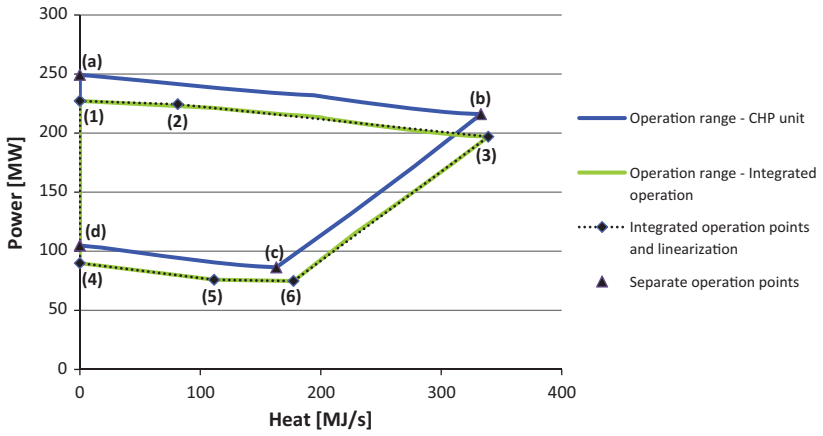

Fig. 5. Operational ranges for the reference PGP in integrated and separate operation. Characteristics of the six key operation points are described in Table 6.

Table 6
Operation characteristics and reference production values for the key operation points shown in Fig. 5.

Point	CHP unit load, λ (–)	Back-pressure operation parameter, α (–)	Ethanol facility heat production, β (–)	Reference PGP power production, $\dot{P}_{ref}$ (MW)	Reference PGP DH production, $\dot{Q}_{ref}$ (MJ/s)
(1)	1.0	0.0	0.0	227.2	0.0
(2)	1.0	0.0	1.0	224.5	81.3
(3)	1.0	1.0	1.0	197.0	339.1
(4)	0.4	1.0	1.0	74.8	177.4
(5)	0.4	1.0	0.0	75.9	111.5
(6)	0.4	0.0	0.0	89.9	0.0
(a)	1.0	0.0	–	249.3	0.0
(b)	1.0	1.0	–	216.0	332.9
(c)	0.4	1.0	–	86.3	163.1
(d)	0.4	0.0	–	104.9	0.0

(3) Separate operation with maximum power delivery.
(4) Separate operation with zero CHP load.

The reasoning is that under the given assumptions, separate operation is advantageous only when the cost of lost power sales is higher than the cost of natural gas for running the ethanol production. However, for the 2060 h during which the CHP unit was shut down in the reference scenario, the PGP is forced to operate in separate mode as well. When integrated operation is advantageous, it is either optimal to maximize or minimize power production, depending on whether income from power sales is higher or lower than the associated operating costs.

Table 7
Exergy content of biomass flows in the ethanol production per kg of straw treated. Values from Lythcke-Jørgensen et al. [15].

Flow description	Exergy content (MJ) – integrated operation	Exergy content (MJ) – separate operation
Straw	16.4	16.4
Natural gas	0.0	12.2
Steam	3.7–4.7[a]	0
Fermentation broth	10.9	10.9
Liquid fraction from pretreatment	5.9	5.9
Ethanol	4.2	4.2
Molasses	4.4	4.4
Solid biofuel	8.0	8.0

[a] The energy consumption for the ethanol production increases with increased DH production, while the specific exergy content of extracted steam depends on operation mode of the CHP unit.

3.3. Thermodynamic performance evaluation

The thermodynamic performance of any design solution is evaluated by calculating the average yearly exergy efficiency η_{ex} of the ethanol production:

$$\eta_{ex} = \frac{\sum_{i=1}^{8760} \eta_{ex,i}}{8760} \tag{37}$$

In Eq. (37), $\eta_{ex,i}$ is the hour-wise exergy efficiency of the ethanol production. Using the exergy analysis method described in Lythcke-Jørgensen et al. [15] for calculating exergy contents of the flows in the ethanol production, the hourly exergy efficiency is calculated as

$$\eta_{ex,i} = \frac{\sum \dot{E}X_{products,i}}{\sum \dot{E}X_{in,i}} \tag{38}$$

Here $\sum \dot{E}X_{in,i}$ is the sum of exergy contents in the power and natural gas or steam into the system over the hour i. $\sum \dot{E}X_{products,i}$ is the sum of exergy contents in the products delivered over the hour i, be it ethanol, molasses, solid biofuel, or, potentially, district heating. The calculated exergy contents of biomass flows per kg of biomass treated and the exergy content of the natural gas flow during integrated and separate operation are presented in Table 7.

The exergy content of the steam extracted from the CHP unit during integrated operation depends on the chosen operation mode according to the decision variables $\{\lambda_i, \alpha_i, \beta_i, \kappa_i\}$. The exergy content of the extracted steam in a given hour $\dot{E}X_{steam,i}$ was calculated directly in the PGP model, and the corresponding specific exergy content per kg of straw treated $ex_{steam,i}$ was calculated using the following equation:

$$ex_{steam,i}(\lambda_i, \alpha_i, \beta_i, \kappa_i) = \frac{\dot{E}X_{steam,i}(\lambda_i, \alpha_i, \beta_i, \kappa_i)}{\sigma} \tag{39}$$

4. Results

4.1. Cost minimization

When solving the optimization problem (22), the specific ethanol production cost obtained is plotted as a function of σ in Fig. 6 together with four of the key specific cost components: Specific energy costs, specific straw cost, specific O&M costs, and specific investment depreciation cost. The lowest specific ethanol production cost, c_{eth} = 0.958 Euro/L, was obtained for σ = 5 kg/s. The specific energy cost, on an average 0.517 Euro/L over the year for this solution, was found to be the largest single post in the total

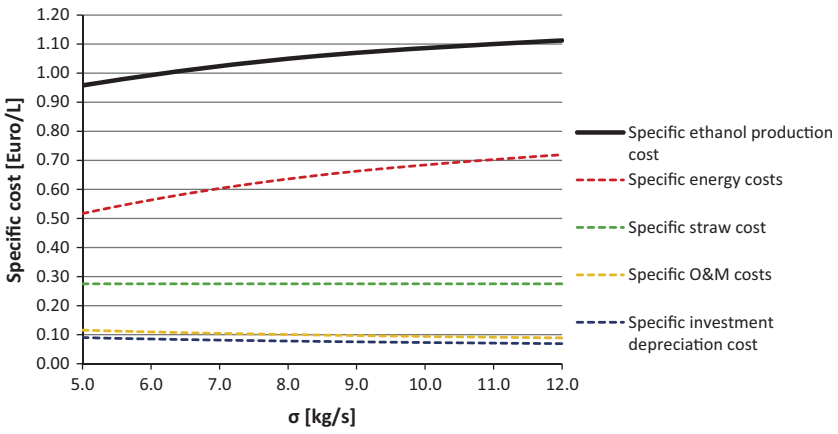

Fig. 6. Specific ethanol production cost and important cost components as functions of σ.

specific ethanol production cost. Average specific energy costs were found to be 0.213 Euro/L during integrated operation and 1.192 Euro/L during separate operation for the optimal solution, underlining the economic inefficiency of the separate operation. Comparing these costs to an average ethanol price of 0.55 Euro/L on the European market in the period 2008–2010 [41], the results suggest that even the optimal design is uncompetitive, mainly due to the duration of separate operation.

An important outcome of the study is the diseconomies-of-scale trend that is found to apply for the ethanol production costs, which is in contrast to the commonly accepted economies-of-scale principle. In the present case, the diseconomy-of-scale is directly related to the energy costs of the production whose increase with increased capacity σ exceeds the capacity-dependent decrease in specific investment costs and O&M costs, as shown in Fig. 6.

The increase in specific energy costs with σ was found to be a consequence of changes in the operation pattern. Fig. 7 shows the optimal operation characteristics of the solutions as a function of σ, and it is seen that the duration of separate operation increases with increased σ. This effect was caused by high power prices and the reduced power production potential during integrated operation with increasing σ, causing the cost of lost power sales to exceed the cost of running the PGP in separate operation for an increasing amount of hours over the year.

In Fig. 8, this effect is further highlighted by plotting the components of the specific energy cost as a function of σ. It is seen that the specific costs for power and gas increased with increasing σ because of the longer duration of separate operation, causing the overall specific energy costs to increase. The specific coal cost is seen to decrease with increased σ owing to the decreased duration of integrated operation.

Another significant outcome with respect to operation is the low duration of integrated operation in minimum load. As described in Section 2.2, one of the three assumed advantages of the integrated system was the potential of reducing power production in periods with low or negative power prices. However, in the East Denmark power block anno 2011, the solution to the optimization problem (22) found it optimal to use this advantage for only 104 h over the year. For the rest of the integrated operation points, the economical optimization maximized the power production within the set operational constraint (9). This is further evident from the scatter distribution of the optimal quasi-static hourly operation points for the solution with σ = 5 kg/s shown in Fig. 9, where only a few of the optimal operation points are found on the lower boarder of the feasible operation range. The main reason for the short use of this advantage is the low coal price and the resultant low break-even electricity production cost in the CHP unit, making it economically unattractive to minimize power production unless power prices are very low. What is further worth noticing in Fig. 9 is the gap between the upper boarder of the feasible operation range for integrated operation and the separate operation points. For the reference operation points located in this

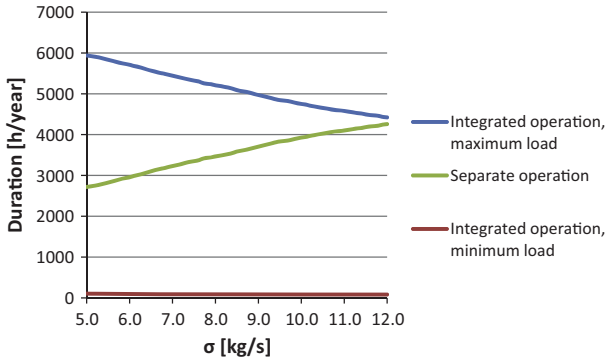

Fig. 7. Duration of integrated and separate operation of the optimized polygeneration plant as a function of σ.

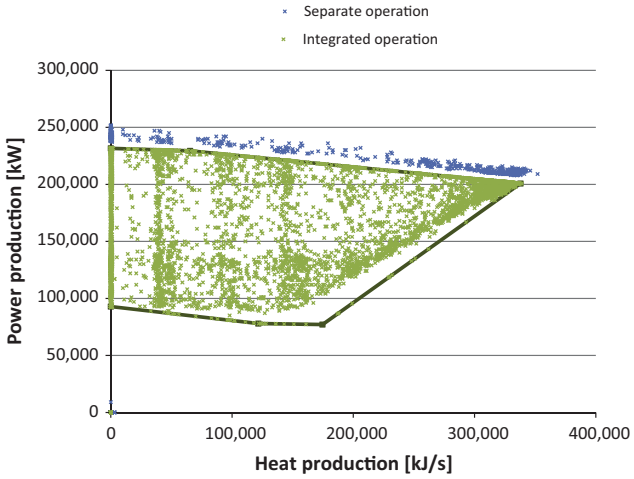

Fig. 9. Scatter distribution of hour-wise quasi-static operating points for the optimal solution.

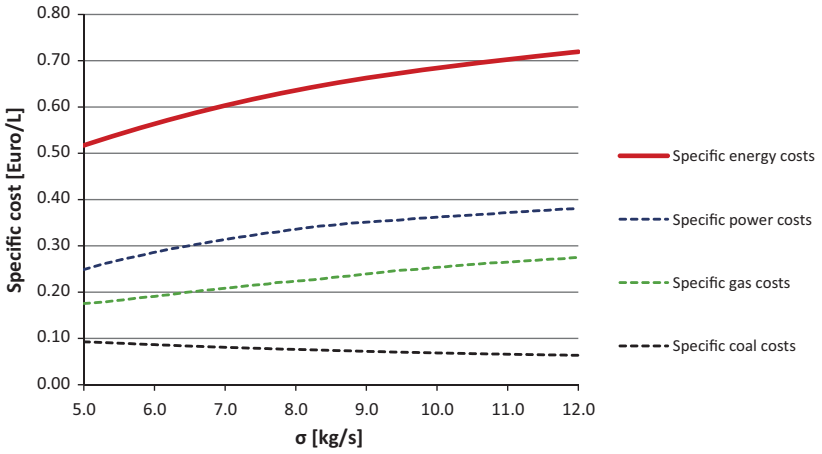

Fig. 8. Components of the specific energy cost as functions of σ.

Table 8
Exergy efficiency of the ethanol production in various operating points.

CHP load, λ_i	Exergy efficiency, η_{11}	
	$\alpha_i = 0,\ \beta_i = 0$	$\alpha_i = 1,\ \beta_i = 1$
1.0	0.786	0.842
0.9	0.789	0.845
0.8	0.791	0.849
0.7	0.793	0.851
0.6	0.796	0.854
0.5	0.791	0.850
0.4	0.795	0.855
Separate operation	0.564	

gap, the optimization found that the costs for sustaining integrated operation in terms of lost power sales were lower than the corresponding energy costs for running separate operation, hence integrated operation was preferred.

4.2. Thermodynamic performance

The exergy efficiency for the ethanol production in each of the operation points over the year was calculated. Results for selected operation points are presented in Table 8.

It is seen that the exergy efficiency of the ethanol production is significantly higher for integrated operation than for separate operation, mainly owing to the fact that steam from the CHP unit is replaced by natural gas, with a very high exergy-to-energy ratio, as the hot utility source during separate operation. Furthermore, the results suggest that the exergy efficiency is higher when full district heating production is activated in the ethanol facility because the exergy content of the waste heat from the processes, which would otherwise be lost to external cooling, is contained in the product 'district heating'. Finally, the exergy efficiency was found to increase with reduced load λ_i in the intervals 0.4–0.6 and 0.6–1.0. The reason for the increased efficiencies with reduced λ_i is the fact that the exergy content of the extracted steam decreases with decreased λ_i, as indicated by the values in Table 3. At loads below 0.6, the steam is extracted in a different pattern than for loads of 0.6 or higher in the CHP unit, as explained in Section 2, causing the break in the exergy efficiency trend at this point.

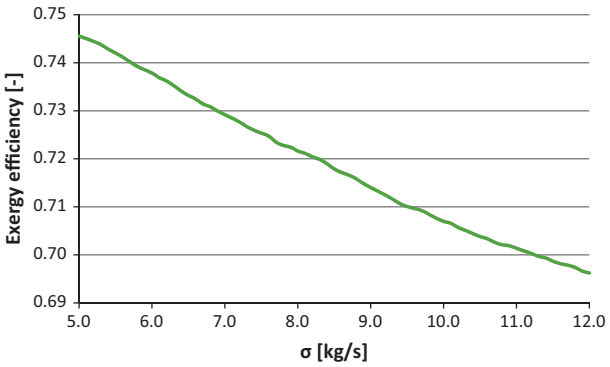

Fig. 10. Yearly average exergy efficiency of the ethanol production at optimized operation pattern for various σ.

The yearly average exergy efficiency of the ethanol production for the optimal operation pattern as a function of σ is plotted in Fig. 10. The average exergy efficiency is found to decrease with increased σ, mainly owing to the increased duration of separate operation. The highest yearly average exergy efficiency of $\eta_{II} = 0.746$ was obtained for the optimal operation pattern for $\sigma = 5$ kg/s.

A Grassmann diagram illustrating the yearly average exergy flows in the ethanol production for the optimal solution, $\sigma = 5$ kg/s is presented in Fig. 11. It is seen that the main part of exergy losses and destruction (L&D) occurs in the heat integration network, which is mainly caused by two factors: The use of high-quality natural gas as heat source in separate operation and the fact that waste heat is not always used for DH production.

Evaluating the simulation results for the optimized solutions, another interesting outcome was found with respect to thermodynamic performance of the PGP: The increase in CHP coal consumption in MJ/s during integrated operation was lower than the energy in the extracted steam in MJ/s to run the ethanol production when DH production was activated in the ethanol facility. The cause of this phenomenon was the DH production from waste heat in the ethanol facility: It allowed the CHP unit to reduce the steam extraction from turbines for DH production without compromising the total DH production, thereby allowing higher levels of power production in the CHP unit. A similar phenomenon was described for an analog system by Starfelt et al. [17]. This suggests that not just the exergy efficiency, but also the overall energy efficiency is higher for the integrated production of lignocellulosic ethanol.

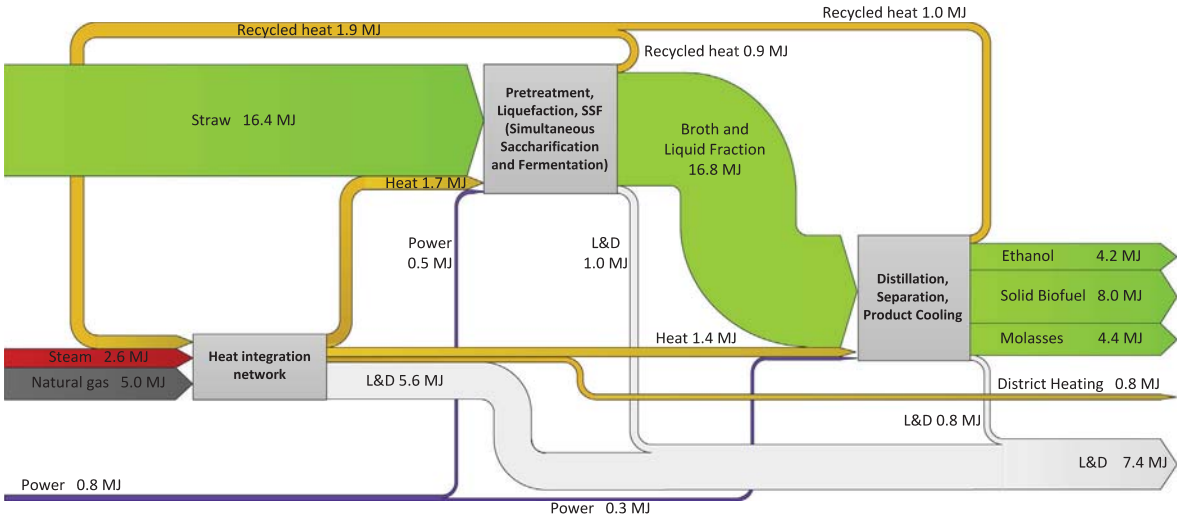

Fig. 11. Grassmann diagram illustrating yearly average exergy flows in the ethanol production for the optimal solution.

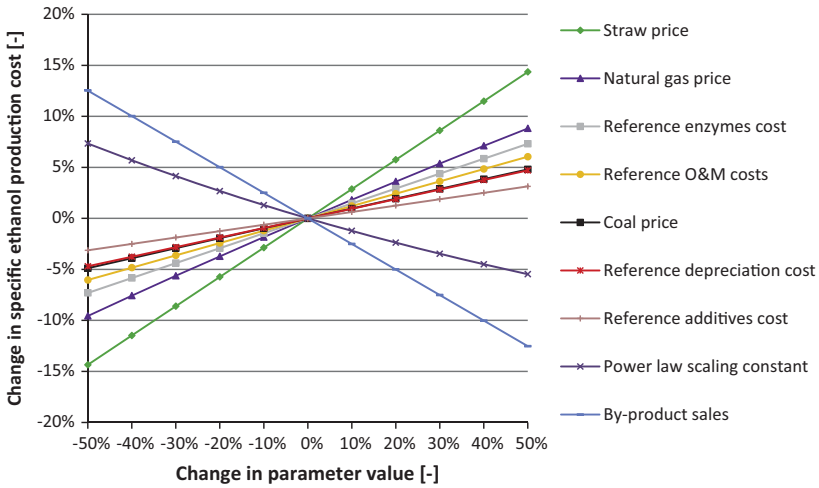

Fig. 12. Spider plot showing the impact on specific ethanol production cost from varying important parameters.

4.3. Sensitivity analysis

As several of the cost values are based on assumptions or approximations, a sensitivity analysis was carried out for nine parameters in the optimal solution in order to investigate the impact on the production cost of the break-even specific ethanol production cost. The results are presented in a spider plot in Fig. 12.

It is seen that variations in straw price, natural gas price, and the value of the sold by-products will have the highest impact on the specific ethanol production price. On the other hand, it is also seen that the break-even specific ethanol production cost is hardly affected by variations in coal price. What is further of interest is the fact that an increase in the power law scaling constant will reduce the specific ethanol production cost because the capacity of the optimal solution is smaller than the reference capacity; a higher capacity power factor will therefore limit the increases in specific costs for O&M and depreciation for the smaller facility.

Although having the highest impact on specific ethanol production costs, the straw price does not affect the optimal dimension of the ethanol facility as it is kept constant. Furthermore, as seen in Fig. 6, O&M, investment and depreciation costs were less significant than specific energy costs when determining the optimal dimension. As historical data were used for power price and heat demand, it was investigated if changes in the assumed coal and natural gas prices would affect the optimal dimension. However, varying the value of each of the parameters from 0% to 1000% of the assumed value, the optimal design remained unchanged. This suggests that the diseconomy-of-scale trend identified prevails even in case of major changes in fuel costs occurred.

5. Discussion

For the PGP treated in this study, integrated operation was found to be advantageous when compared to separate operation as it achieved a lower specific energy cost, a higher first law energy efficiency for the entire PGP when district heating production was activated in the ethanol facility, and a higher ethanol production exergy efficiency. These outcomes all comply with results reported by other studies on integrating lignocellulosic ethanol in CHP units. As a consequence, the expected long duration of separate operation over the year even for the optimal solution poses a major challenge for the ambition of reducing the costs of lignocellulosic ethanol production by integrating it with the CHP plant. The duration of separate operation over the year was found to increase with increased straw processing capacity σ of the ethanol facility, resulting in a diseconomy-of-scale trend for the suggested integration scheme. This trend was caused by the reduced power production potential with increased σ for integrated PGP operation, often making the cost of lost power sales exceed the costs of the inefficient separate operation.

For the optimal solution, separate operation occurred for 2718 h over the year, of which the 2060 h were caused by CHP unit down-time. The simplest way to increase the duration of integrated operation would be to reduce the duration of CHP unit down-time. Whether this is feasible for the given CHP unit is uncertain, but in general it underlines the importance of considering integration availability when integrating biomass-conversion processes in CHP units, a topic also discussed by Kohl et al. [42]. It should be mentioned here that the choice of reference year has a significant impact on the outcomes, as abnormalities in the chosen reference year affect the overall evaluation results. Whether or not 2011 is suitable as a reference year for the suggested polygeneration scheme should be investigated further before any final conclusion can be drawn with respect to the competitiveness of the suggested scheme. For instance, Starfelt et al. [18] considered a down-time of only 326 h for a CHP unit in their study, which however was the sole producer of heat in a local district heating network. Opposed to this, AVV1 competes with other heat producers in the greater Copenhagen district heating network, so the prolonged down-time could be a result of economic decisions. If so, the decisions may have been altered if ethanol production had been integrated in the CHP unit, which would have provided different options for optimizing operation economy in otherwise unfavourable market conditions, e.g. by minimizing power production while sustaining integrated mode operation.

When conducting the optimization on design and operation levels, it was assumed that the ethanol production was to be sustained at full load all year round. However, it might be possible to reduce the duration of separate operation if the load could be varied in the ethanol production, or if the straw pretreatment could be performed in batches. This would allow integrated operation during periods of lower power demands and no pretreatment during periods of high power demands, thereby significantly increasing the power production potential in integrated operation. Furthermore, the energy demands of the separation stage could possibly be reduced by applying state-of-the-art mechanical separation technologies. It is, however, beyond the scope of the present paper to evaluate whether or not these suggestions are technologically feasible.

Another assumption during the optimization was the constraint that the PGP had to meet the heat production of the reference CHP

unit for each hour of the year. If sufficient heat storage capacity was available, it might be possible to relax this constraint by assuming that the total production over a period of 24 h had to be met instead of the hour-wise production. This would allow operation flexibility within the 24 h periods and, potentially, longer durations of integrated operation over the year as well.

A simplification of the calculations entailed the assumption of constant biomass price independently of the processing capacity of the ethanol production. However, this assumption may not be valid for at least two reasons: Firstly, transportation costs will most likely increase with increased biomass consumption due to the distributed nature of straw, the biomass processed in this system [43]. And secondly, large-scale consumption of straw would induce competition with other straw-consumers causing straw prices to increase further. Such developments in the straw price might increase the diseconomies-of-scale trend for the costs of the integrated ethanol production. A more robust straw cost calculation model, taking into account the straw supply chain and competing uses, is a topic of future research for the authors.

One of the benefits of the suggested PGP is its ability to reduce the power production without compromising heat production during periods of low or negative power prices. For the optimal solution, this advantage was exploited for 104 h over the year of 2011. In the future, this advantage may become more pronounced as an increased production from intermittent renewable energy sources is integrated in the energy system, increasing the demand for balancing means in the heat-and-power sectors [1] and potentially providing another *raison d'être* for the PGP. However, in order to predict the development of the energy system, advanced energy system analysis methods [44] should preferably be applied. Integration of energy system analysis with the synthesis, design, and operation optimization of PGPs is another topic for future research for the authors.

Concludingly, the results of the study point toward two overall outcomes: Firstly, they question the efficiency of integrating lignocellulosic ethanol production in the Danish CHP unit AVV1 in the present energy system. Secondly, they illustrate how operating conditions may have a significant impact on plant performance; for the PGP in question, design point operation predicted a specific energy cost of 0.213 Euro/L ethanol produced and an exergy efficiency in the range 0.842–0.855, while a performance optimization with respect to expected operating conditions yielded a best-case average specific energy cost of 0.517 Euro/L ethanol and a yearly average exergy efficiency of 0.746.

6. Conclusion

This study treats the simultaneous optimization of design and operation levels for a polygeneration plant in which hydrothermal pretreatment-based lignocellulosic ethanol production is assumed integrated in the Danish combined heat and power unit Avedøreværket 1. The objective of the optimization is to minimize the specific ethanol production costs, as perceived by the plant owner. The optimization considers straw processing capacities in the ethanol production ranging from 5 kg/s to 12 kg/s, and quasi-static hour-wise operation over a year. The polygeneration plant operation is constrained by a fixed hourly heat production and an upper limit for the hourly power exports. Capacity power laws are used for predicting specific costs of investment depreciation and operation and maintenance (O&M), while the energy cost is calculated as a function of the operation over the year.

The results suggest that diseconomies of scale applies to ethanol production costs in the integrated polygeneration plant, with the lowest feasible specific ethanol production cost of 0.958 Euro/L being obtained for the design with the smallest ethanol facility capacity considered. The cause of the diseconomies-of-scale phenomenon is the high reference power production of the CHP unit, causing the costs from lost power sales and separate operation to exceed the economies-of-scale benefits from investment depreciation and O&M when increasing ethanol production capacity. A thermodynamic performance evaluation further indicates that the design with the smallest ethanol production capacity is optimal in terms of average yearly exergy efficiency of the ethanol production as well, as it obtains the shortest duration of exergy-wise less efficient separate operation over the year. A sensitivity analysis indicates that variations in straw price and by-products value would have the most significant impact on the specific ethanol production costs, whereas the optimum is indifferent to major variations in fossil fuel prices.

In summary, the outcomes of this study question the economic viability and thermodynamic efficiency of integrating lignocellulosic ethanol production in a combined heat and power unit under the given conditions. Furthermore, the outcomes point toward the importance of considering operating conditions when developing flexible polygeneration plant concepts.

Acknowledgements

The authors would like to acknowledge DONG Energy for their financial support of the research, and Brian Elmegaard for allowing the use of his numerical model of the Danish combined heat and power unit Avedøreværket 1 in the study.

References

[1] Lund H. Renewable energy systems: the choice and modelling of 100% renewable solutions. Burlington (USA): Elsevier; 2010.
[2] Edenhofer O, Pichs-Madruga R, Sokona Y. Renewable energy sources and climate change mitigation. New York (USA): Intergovernmental Panel on Climate Change and Cambridge University Press; 2012.
[3] Scharlemann JPW, Laruance WF. How green are biofuels? Environ Sci 2008;319:43–4.
[4] Gassner M, Maréchal F. Increasing efficiency of fuel ethanol production from lignocellulosic biomass by process integration. Energy Fuels 2013;27:2107–15.
[5] Balat M. Production of bioethanol from materials via the biochemical pathway: a review. Energy Convers Manage 2010;52:858–75.
[6] US Environmental Protection Agency. Green chemistry programme. Basic information; 8 August 2012 <http://www.epa.gov/greenchemistry/pubs/basic_info.html> [Accessed 05.08.13].
[7] Lee S, Shah YT. Ethanol from lignocellulose. In: Biofuels and bioenergy: processes and technologies, Boca Raton, Florida, USA: Taylor & Francis Group; 2013. p. 93–146.
[8] Gassner M, Maréchal F. Thermo-economic optimisation of the polygeneration of synthetic natural gas (SNG), power and heat from lignocellulosic biomass by gasification and methanation. Energy Environ Sci 2012;5:5768–89.
[9] Daianova L, Dotzauer E, Thorin E, Yan J. Evaluation of a regional bioenergy system with local production of biofuel for transportation, integrated with a CHP plant. Appl Energy 2011;92:739–49.
[10] Ilic DD, Dotzauer E, Trygg L. District heating and ethanol production through polygeneration in Stockholm. Appl Energy 2011;91:214–21.
[11] Bösch P, Modarresi A, Friedl A. Comparison of combined ethanol and biogas polygeneration facilities using exergy analysis. Appl Therm Eng 2012;37:19–29.
[12] Modarresi A, Kravanja P, Friedl A. Pinch and exergy analysis of lignocellulosic ethanol, biomethane, heat and power production from straw. Appl Therm Eng 2012;43:20–8.
[13] Leduc S, Starfelt F, Dotzauer E, Kindermann G, McCallum I, Obersteiner M, et al. Optimal location of lignocellulosic ethanol refineries with polygeneration in Sweden. Energy 2010;35:2709–16.
[14] Palacios-Bereche R, Mosqueira-Salazar KJ, Modesto M, Ensinas AV, Nebra SA, Serra LM, et al. Exergetic analysis of the integrated first- and second-generation ethanol production from sugarcane. Energy 2013;62:46–61.
[15] Lythcke-Jørgensen C, Haglind F, Clausen LR. Exergy analysis of a combined heat and power plant with integrated lignocellulosic ethanol production. Energy Convers Manage 2014;85:817–27.
[16] Bentsen NS, Thorsen BJ, Felby C. Energy: feed and land-use balances of refining winter wheat to ethanol. Biofuels Bioprod Biorefining 2009;3:521–33.
[17] Starfelt F, Thorin E, Dotzauer E, Yan J. Performance evaluation of adding ethanol production into an existing combined heat and power plant. Bioresour Technol 2009;101:613–8.
[18] Starfelt F, Daianova L, Yan J, Thorin E, Dotzauer E. The impact of lignocellulosic ethanol yields in polygeneration with district heating – a case study. Appl Energy 2012;92:791–9.

[19] Frangopoulos CA, von Spakovsky MR, Scubba E. A brief review of methods for the design and synthesis optimization of energy systems. Int J Appl Thermody 2002;4:151–60.
[20] Voll P, Lampe M, Wrobel G, Bardow A. Superstructure-free synthesis and optimization of distributed industrial energy supply systems. Energy 2012;45:424–35.
[21] Lund H, Andersen AN, Østergaard PA, Mathiesen BV, Connolly D. From electricity smart grids to smart energy systems – a market operation based approach and understanding. Energy 2012;42:96–102.
[22] Chen Y, Adams II TA, Barton PI. Optimal design and operation of flexible energy polygeneration systems. Ind Eng Chem Res 2011;50:4553–66.
[23] Rubio-Maya C, Uche J, Martínez A. Sequential optimization of a polygeneration plant. Energy Convers Manage 2011;52:2861–9.
[24] Grisi EF, Yusta JM, Khodr HM. A short-term scheduling for the optimal operation of biorefineries. Energy Convers Manage 2011;52:447–56.
[25] Larsen J, Østergaard Haven M, Thirup L. Inbicon makes lignocellulosic ethanol a commercial reality. Biomass Bioenergy 2012;46:36–45.
[26] Lythcke-Jørgensen C, Haglind F, Clausen LR. Thermodynamic and economic analysis of integrating lignocellulosic bioethanol production in a Danish combined heat and power plant. In: 21st European biomass conference & exhibition, Copenhagen, Denmark, June 3–7, 2013.
[27] Lythcke-Jørgensen C, Haglind F, Clausen LR. Exergy analysis of a combined heat and power plant with integrated lignocellulosic ethanol production. In: International conference on efficiency, cost, optimization, simulation, and environmental impact of energy systems, Guilin, China, July 16–19, 2013.
[28] Bejan A, Tsatsaronis G, Moran M. Thermal design & optimization. John Wiley & Sons Inc; 1996.
[29] Elmegaard B, Houbak N. Simulation of the Avedøreværket Unit 1 cogeneration plant with DNA. In: 16th international conference on efficiency, cost, optimization, simulation and environmental impact of energy systems, Kgs. Lyngby, Denmark, June 30–July 2, 2003.
[30] Spliethoff H. Power generation from solid fuels, München, Germany. Berlin Heidelberg: Springer-Verlag; 2010.
[31] Elmegaard B, Houbak N. DNA – a general energy system simulation tool. In: SIMS 2005: 46th conference on simulation and modeling, Trondheim, Norway, October 13–14, 2005. p. 43–52.
[32] Larsen J, Petersen MØ, Thirup L, Li HW, Iversen FK. The IBUS process – lignocellulosic bioethanol close to a commercial reality. Chem Eng Technol 2008;5:765–72.
[33] F-Chart Software <http://www.fchart.com/ees/> [accessed 25.02.13].
[34] Østergaard Petersen M, Larsen J, Hedegaard Thomsen M. Optimization of hydrothermal pretreatment of wheat straw for production of bioethanol at low water consumption without addition of chemicals. Biomass Bioenergy 2009;33:834–40.
[35] Energistyrelsen. Technology data for energy plants. Danish Energy Agency; 2010.
[36] Kemp IC. Pinch analysis and process integration. 2nd ed. Oxford (UK): Butterworth-Heinemann; 2006.
[37] Bentsen NS, Felby C, Ipsen KH. Energy balance of 2nd generation bioethanol production in Denmark. Elsam A/S; 2006.
[38] NordPoolSpot. Nord Pool Spot; 2011 http://www.nordpoolspot.com/ [accessed 22.06.12].
[39] Ea Energianalyse, Energistyrelsen, Wazee. Opdatering af samfundsøkonomiske brændselspriser. Ea Energianalyse, Copenhagen, Denmark; 2011.
[40] Smith R. Chemical process design and integration. West Sussex (England): John Wiley & Sons Ltd; 2005.
[41] Statens Energimyndighet. "Energiläget 2011". Statens Energimyndighet, Eskilstuna, Sweden; 2011.
[42] Kohl T, Laukkanen T, Järvinen M, Fogelholm C-J. Energetic and environmental performance of three biomass upgrading processes integrated with a CHP plant. Appl Energy 2013;107:124–34.
[43] Jack MW. Scaling laws and technology development strategies for biorefineries and bioenergy plants. Bioresour Technol 2009;100:6324–30.
[44] Connolly D, Lund H, Mathiesen B, Leahy M. A review of computer tools for analysing the integration of renewable energy in various energy systems. Appl Energy 2010;87:1059–82.

APPENDIX D Journal paper 3

ISI Journal Paper

C.E. Lythcke-Jørgensen, M. Münster, A.V. Ensinas, and F. Haglind. *A method for aggregating external operating conditions in multi-generation system optimization models*. Applied Energy 166:59-75, 2016.

This paper presents and verifies the developed CHOP method for aggregating external operating condition datasets.

Applied Energy 166 (2016) 59–75

Contents lists available at ScienceDirect

Applied Energy

journal homepage: www.elsevier.com/locate/apenergy

A method for aggregating external operating conditions in multi-generation system optimization models

Christoffer Ernst Lythcke-Jørgensen [a,*], Marie Münster [b], Adriano Viana Ensinas [c], Fredrik Haglind [a]

[a] Technical University of Denmark, Mechanical Engineering, Nils Koppels Allé 403, DK-2800 Kgs. Lyngby, Denmark
[b] Technical University of Denmark, Management Engineering, Produktionstorvet 424, DK-2800 Kgs. Lyngby, Denmark
[c] École Polytechnique Fédérale de Lausanne, Industrial Process and Energy Systems Engineering, Rue de l'Industrie 17, Case Postale 440, CH-1951 Sion, Switzerland

HIGHLIGHTS

- The CHOP method for aggregating energy system data is presented.
- The CHOP method is applied in a case study.
- The CHOP method is compared to three commonly used data aggregation methods.
- The comparison suggests that the CHOP method offers more accurate reduced datasets.

ARTICLE INFO

Article history:
Received 7 August 2015
Received in revised form 10 December 2015
Accepted 13 December 2015

Keywords:
Data aggregation
Flexibility
Multi-generation
Operation optimization
Polygeneration

ABSTRACT

This paper presents a novel, simple method for reducing external operating condition datasets to be used in multi-generation system optimization models. The method, called the Characteristic Operating Pattern (CHOP) method, is a visually-based aggregation method that clusters reference data based on parameter values rather than time of occurrence, thereby preserving important information on short-term relations between the relevant operating parameters. This is opposed to commonly used methods where data are averaged over chronological periods (months or years), and extreme conditions are hidden in the averaged values.

The CHOP method is tested in a case study where the operation of a fictive Danish combined heat and power plant is optimized over a historical 5-year period. The optimization model is solved using the full external operating condition dataset, a reduced dataset obtained using the CHOP method, a monthly-averaged dataset, a yearly-averaged dataset, and a seasonal peak/off-peak averaged dataset. The economic result obtained using the CHOP-reduced dataset is significantly more accurate than that obtained using any of the other reduced datasets, while the calculation time is similar to those obtained using the monthly averaged and seasonal peak/off-peak averaged datasets. The outcomes of the study suggest that the CHOP method is advantageous compared to chronology-averaging methods in reducing external operating condition datasets to be used in the design optimization models of flexible multi-generation systems.

1. Introduction

Large-scale integration of intermittent renewable energy sources (solar, wind, tidal and wave) in the energy system imposes a demand for generation–consumption balancing [1]. Flexible multi-generation systems (FMGs), here defined as flexibly operating facilities integrating the generation of two or more energy services (power, heating, cooling, fuels, etc.), may provide such balancing operation [2]. Furthermore, FMGs based on biomass may achieve high aggregated biomass conversion efficiencies through process integration [3], which is of crucial importance in sustainable energy systems as the biomass resource is limited on a global level [4,5]. Such process integration advantages may further be used for providing sustainable fuel and energy services in FMGs at competitive prices [6–8], thereby integrating various layers of the energy system. The development of efficient biomass-processing FMGs may therefore be seen as an integral part of the transition towards a smart energy system based on renewable energy sources [9].

* Corresponding author. Tel.: +45 30 42 72 00.
E-mail address: celjo@mek.dtu.dk (C.E. Lythcke-Jørgensen).

http://dx.doi.org/10.1016/j.apenergy.2015.12.050
0306-2619/

Nomenclature

Latin letters

C	cost (Euro)
C_v	ratio between lost power generation and increased district heating generation (–)
c	specific cost (Euro/MWh)
D	dataset
F	fuel consumption (MWh)
N	number of groups
n	number of characteristic parameter intervals
O	operating point
P	power (MWh)
p	operating condition parameter
Q	heat (MWh)
T	time of occurrence
t	duration (h)

Greek letters

α	back-pressure ratio (–)
λ	load (–)
σ	standard deviation (–)

Subscripts

aa	annually averaged
i	characteristic parameter interval index
j	data point index
k	EOC parameter index
l	CHOP group index
ma	monthly averaged
pot	potential
sp	seasonal peak/off-peak averaged

Superscripts

$*$	linearized

Abbreviations

CHOP	Characteristic Operating Pattern
CHP	combined heat and power
EOC	external operating condition
FMG	flexible multi-generation system

The design optimization of FMG concepts includes such challenges as synthesising processes from multiple technological alternatives, facility and process dimensioning, process integration, feedstock market-impacts, operation optimization, etc. In addition to this, a principal challenge is to optimize design and operational performance with respect to hourly fluctuations as well as long-term changes in demands and prices of various energy products. In principle, these data could be obtained by implementing a detailed energy system model [10] in the design optimization model, but the required data sampling, modelling, and computational effort can be prohibitive. It is therefore common to include external operating conditions (EOCs) that are hardly influenced by system operation, such as fuel price and heating demand, as fixed parameters in multi-period design optimization models. In a case study of a thermal energy system, Hindsberger and Ravn [11] demonstrated that robust results can be obtained by using fixed EOC datasets when external conditions are little affected by system operation.

A fundamental issue in mathematical optimization models is the trade-off between level of detail and ease of solving the model. As the complexity of multi-period optimization problems increases significantly with the number of periods defined [12], it is desirable to reduce the number of period datasets without plummeting result accuracy. One approach to reducing the number of periods is to average EOC parameter values over chronological time-periods. Among averaging methods, the simplest is to average the EOCs over the lifetime of a system (e.g. Ahmadi et al. [13], Gassner and Maréchal [14], and Chen et al. [15]). A related method is to assume annually static operating conditions, but defining each year as a period to allow for year-to-year variations caused by general energy system developments (e.g. Gerogiorgos et al. [16] and Liu et al. [17,18]). Another method is to consider monthly average values for one key operating parameter and static conditions for all other (e.g. Fazlollahi et al. [19,20]). A more detailed approach is to consider monthly averaged EOC parameter values in a first-step optimization model, and then conduct detailed hour-wise operation optimization in a sequential step for the most promising system designs (e.g. Rubio-Maya et al. [21] and Uche et al. [22]). However, neither monthly- nor annually-averaged operating parameter values provide information on short-term relations and variations between various operating conditions. While it may be acceptable to neglect this information for static operating facilities, it can be critical to the economy and thermodynamic performance of flexible facilities such as combined heat and power (CHP) plants [23] and FMGs [24,25]. Failing to consider short-term relations between relevant operating parameters may lead to sub-optimal solutions in the design optimization of FMGs [26].

One approach to reduce energy system data while maintaining details on hourly parameter relations is to represent each year by a small number of typical time-periods. Another approach is to define a number of characteristic periods, like peak-demand and off-peak-demand periods in each of the four seasons (e.g. Chen et al. [2,27]) or typical demand days for each month based on monthly average parameter values (e.g. Mavrotas et al. [28]). These approaches rely on the assumption that operating conditions and energy demands are linked and cyclic over the seasons, an assumption that may prove inaccurate in energy systems in transition and with large shares of intermittent renewable energy generation [1]. To overcome the assumption of cyclic behavior, several studies propose application of cluster analysis to identify typical periods that can be repeated in order to approximate the annual cumulative curves. Ortiga et al. [29] proposed a graphical method for selecting a few typical days that can be used for representing the annual cumulative heating and cooling demand curves. Domínguez-Muñoz et al. [30] and Fazlollahi et al. [31] used a partitional clustering analysis method, the *k*-Mediods method, to create k typical periods. However, such approaches may hide information on peak and extreme operating conditions and lead to significant errors on peak operation performance, as also reported by Fazlollahi et al. [31] in two illustrative examples. In order to overcome these drawbacks, the duration of the typical periods may be extended to several consecutive days or even weeks (e.g. Hedegaard and Münster [32]). However, this approach increases the computational effort significantly, thereby counteracting the initial ambition of reducing the number of period datasets. Instead, Bungener et al. [33] proposed a method that applied an evolutionary multi-objective optimization algorithm for identifying n sequential periods representing typical operations for an industrial cluster with the aim of minimizing standard deviation and, at the same time, maintain information on extreme operating conditions. Nemet et al. [34] presented a similar method for aggregating continuous thermal energy generation and demand into

sequential periods. They presented an MILP model for determining the number and duration of the periods required to obtain a certain level of accuracy over the aggregation. Karlsson et al. [35] proposed a simple method, called the TimeSlicesTool, which sorts annual operating points into three groups for critical combinations of operating characteristics and one group for all other operating points. This was done for work and non-work days in each of the four seasons, resulting in 32 groups. A drawback of this method is the fact that only information on extreme conditions is sustained, while detailed information on frequently occurring operating patterns is lost.

The present paper proposes a novel and simple aggregation-based method for reducing EOC datasets in optimization models. The method, named Characteristic Operating Pattern (CHOP) method, is tailored for reducing EOC datasets with non-cyclic behavior for FMG optimization models, but it may be used for reducing similar datasets for any system operating in multiple energy markets. In the CHOP method, EOC data points are clustered in a number of CHOP groups based on operating condition characteristics rather than on time chronology. The method thereby yields a reduction in calculation times similar to those of averaging methods [13–22] while maintaining information on short-term relations and variations between relevant operating parameters, leading to more accurate solutions. Another advantage of the CHOP method is the fact that all initial EOC data are included in the reduced dataset, as opposed to typical time-period approaches [27–32] where EOC datasets are sought represented by a limited number of periods. Furthermore, the CHOP method provides a possibility for including data on long-term energy system development without *de facto* increasing the number of periods, as opposed to several of the previously described methods [16–22,27,28,33–35]. The work builds upon a preliminary study presented by Lythcke-Jørgensen et al. [26].

In this paper, the structure and contents of the CHOP method are described in detail in Section 2, where an example is given to demonstrate the use of the method. In Section 3, a simple operation optimization model of a CHP plant is developed, and the model is solved using various reduced EOC datasets to compare the performance of the CHOP method to other common methods. Furthermore, *a posteriori* error analysis is applied to assess the quality of the results obtained. In Section 4 advantages and drawbacks of the CHOP method are discussed and a conclusion of the study is given in Section 5. Various reduced EOC datasets used in the case study are provided in Appendix A.

2. The Characteristic Operating Pattern method

The Characteristic Operating Pattern (CHOP) method is an original graphic-based data aggregation method for reducing external operating condition (EOC) datasets. The method assumes quasi-static operation and is applicable on datasets in the form of operating points O_j, with each point being characterised by a time of occurrence T_j, a duration t_j[1], and a number of operating condition parameters $\overline{p_j}$.

$$O_j = \{T_j, t_j, \overline{p_j}\} \quad (1)$$

In the CHOP method, EOC data points are clustered in groups based on data characteristics rather than the time of occurrence, as opposed to time-chronological averaging methods [13–22]. The clustered groups, called CHOP groups, are introduced as weighted periods in multi-period optimization models. A principal sketch of the data aggregation principle applied in the CHOP method is presented in Fig. 1. Dynamics cannot be considered in operation optimization models applying CHOP-reduced datasets as information on time chronology is lost.

Two overall procedures are associated with the CHOP method: The CHOP data aggregation method, and error analysis. The CHOP data aggregation method, which is the core of the method, consists of three principal steps:

1. *Entity selection*: Identification of relevant EOC parameters.
2. *Clustering criteria*: Definition of characteristic parameter intervals.
3. *Cluster procedure*: Establishment of CHOP groups.

As it is desirable to estimate the quality of the results obtained using the reduced dataset, error analysis is an integral part of the CHOP method. Within the framework presented here, one *a priori* and two *a posteriori* analyses are suggested, but others may relevant as well.

1. *A priori*: Evaluate the standard deviation of parameters in CHOP groups.
2. *A posteriori*: Evaluate the quality of the applied datapoint clustering. Analyse the errors made by neglecting dynamic constraints.

Both *a priori* and *a posteriori* error analyses may yield results necessitating reconfiguration of the data aggregation analysis. The overall CHOP method procedure is illustrated in Fig. 2.

Next, the contents of the CHOP data aggregation analysis and suggestions for error analyses are presented. The method is illustrated by an *example*, in which a historical 5-year EOC dataset for a fictive local extraction-based combined heat and power (CHP) plant located in West Denmark is reduced using the method. A principal sketch of the CHP plant is shown in Fig. 3.

2.1. CHOP data aggregation method

2.1.1. Entity selection

The first step in the CHOP data aggregation analysis is to select data entities for clustering. This implies (1) identification of EOC parameters p_k for the system of interest, and (2) assessment of parameter variation:

1) **Identification of relevant EOC parameters**: Within the CHOP method framework, EOCs are defined as boundary conditions that may influence, but are hardly influenced by, operation decisions within the system of interest, and are therefore regarded as fixed parameters. Any parameter fitting these criteria must be included as an EOC parameter.
2) **Parameter variation assessment**: For all identified EOC parameters, the maximum, minimum and mean parameter values over the selected period must be identified based on the reference datasets. As it is desirable to reduce the number of EOC parameters to define clustering from in order to keep computational effort low, it is recommended that clustering criteria are only defined for EOC parameters with variations higher than ±10% of the period mean value. The potential error from neglecting variations in specific EOC parameters must be assessed as a part of the *posteriori* error analysis, see Section 2.2.2.

Example: As illustrated in Fig. 3, the CHP plant of interest imports fuel, air, and cooling water, while it produces district heating, power, exhaust gases and heated cooling water.

[1] $t_{0_j} = 1h$ is commonly used when working with power markets [36], but other values of t_j may be used as well.

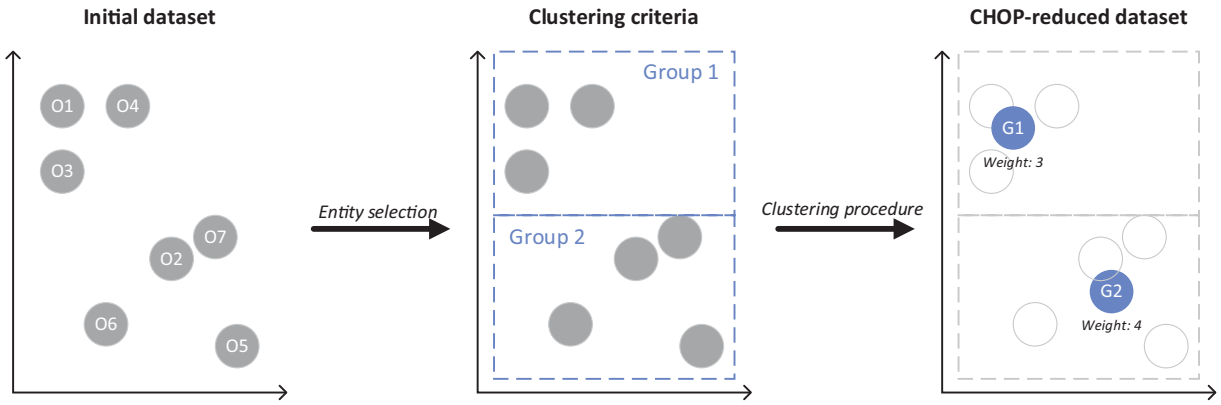

Fig. 1. Principal sketch of the data aggregation principle applied in the CHOP method. Operating points O_j are clustered and merged into CHOP groups G_j with aggregated weight factors.

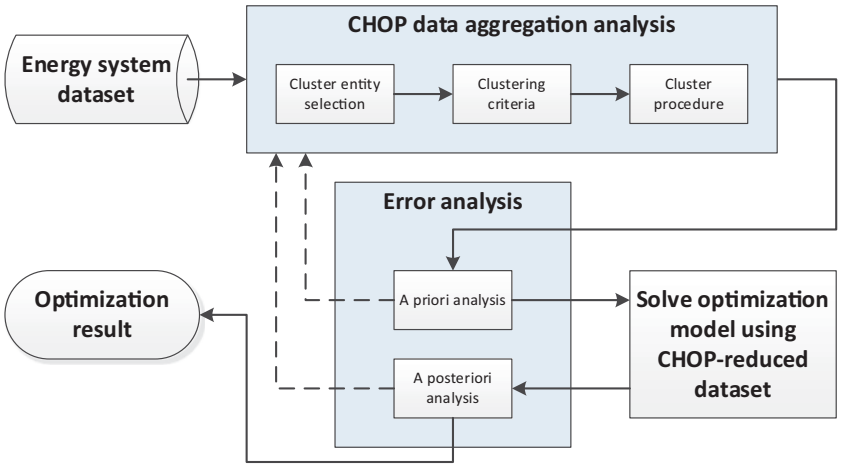

Fig. 2. The CHOP method procedure.

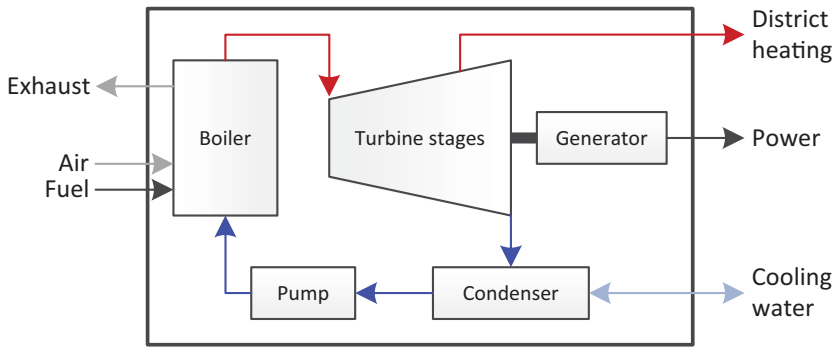

Fig. 3. Principal sketch of a Danish extraction-based CHP plant.

(1) Identification of the relevant EOC parameters

The assumed objective of the CHP plant owner is to obtain the most profitable operation. Being the sole heat producer in the district heating system, the operation of a CHP plant is constrained by the heating demand. Assuming that cooling is freely available from a cold reservoir, air is freely available from the surroundings, and neglecting taxes on emissions, three relevant EOC parameters exist: Fuel price (coal), heating demand, and power price. Being a single plant located in the well-integrated West Denmark power grid, the power and coal prices can be considered unaffected by the operation of the CHP plant. Assuming no demand flexibility on the consumer side, the heat demand is also unaffected by operation decisions. Hence, these three external parameters can be considered as EOC parameters in the CHOP method. This would not have been the case had the CHP plant been the main power producer in an isolated power grid, or if the CHP plant was fuelled by a local distributed biomass like straw [37], in which case the power and/or fuel prices would have been significantly influenced by plant operation decisions.

(2) **Assessment of parameter variation**

Historical parameter datasets over the period 2010-01-01–2014-12-31 are considered for the three EOC parameters.

According to data on coal prices from Key World Energy Statistics 2014 provided by the International Energy Agency [38], the yearly average coal price in Denmark's neighbouring country Poland was 80.75 USD/ton over the years 2010–2013, with a maximum price of 84 USD/ton and a minimum price of 78 USD/ton. Assuming that the coal price fluctuations in Poland are analogue to those in Denmark, the resulting variation range is −3.4% to +4% which is well below the recommended clustering threshold of ±10%. Therefore, the coal price is not considered as a varying EOC parameter for clustering in the case treated. The error of this assumption will be assessed as a part of the *posteriori* error analysis in Section 3.4. In the given case, the coal price is set to 15.70 Euro/MWh, which is the perceived coal price for 2012 reported by the Danish CHP owner DONG Energy [39].

Data on hourly power prices in West Denmark over the entire period has been extracted from the webpage of the Danish transmission system operator Energinet.dk. [40]. The average hourly power price was 40.08 Euro/MWh, with a maximum price of 2000.00 Euro/MWh and a minimum price of −200.00 Euro/MWh. As this variation is well above the recommended threshold of ±10% of the mean, power price is included as a varying EOC parameter for clustering.

Data on hourly relative heat demand in a Danish district heating system over a year has been extracted from the energy system model STREAM [41]. It is assumed that the annual relative heat demand pattern is repeated for each of the 5 years investigated. The average hourly relative heat demand over the period was 0.55, with a maximum of 1.00 and a minimum of 0.06. As this gives in a variation of −89% to +82% which is well above the recommended threshold of ±10% of the mean, relative heat demand is included as a varying EOC parameter for clustering.

2.1.2. Clustering criteria

Having identified the varying EOC parameters p_k, the second step of the CHOP data aggregation analysis is to define the clustering criteria for aggregating operating points. This is done by splitting the value range of each p_k into a number of characteristic intervals, n_{p_k}. Being empirical in essence, the following graphic-based two-step approach is suggested for breaking up a parameter value range into characteristic intervals based on the cumulative parameter curve. The process is illustrated in Fig. 4 with power price as the relevant EOC parameter.

(a) **Important values**: Some parameter values may be of special interest, making it relevant to introduce a break at these points. For the power price example, it may be relevant to introduce a break at a power price of 0.00 Euro/MWh to make sure that negative prices are grouped together. Also, if an operating decision, e.g. turning on a piece of equipment, is dependent on a given power price, an interval break should be introduced at this price as well. It is also suggested that if significant trend changes occur in the cumulative curve, the parameter values of points separating various trends should be included as important values.

(b) **Even division**: If the already set break-points are far from each other in terms of both parameter value and duration, it is suggested that additional interval breaks are introduced to minimize the span. The break-points should be located so that the parameter value range is constant for each of the intervals.

It is essential that all feasible parameter values are covered within the characteristic parameter intervals. It may be necessary to define the first and last of the characteristic intervals as open. The necessary number of intervals for each parameter depends on the parameter value volatility, the significance of the parameter and the data available. In Fig. 4, six intervals were defined in the visual power price example, while it may be sufficient to define just two or three intervals for less volatile parameters. In contrast, more intervals may be defined for the power price in case it has significant impact on the optimization model. It should be noticed that if only one characteristic interval is defined for a parameter, it will be included as a constant in the final CHOP-reduced dataset.

Example: The cumulative curve for power prices, also known as the power price duration curve, is obtained by sorting the data points according to the value of the power price value. The cumulative curve illustrates the aggregated duration of power prices over the period, and is shown in Fig. 5.

Using the suggested two-step approach for breaking up the cumulative curve for power prices, the following break points are obtained:

(a)	Important values:	0.00, 25.00, 65.00 (Euro/MWh)
(b)	Even division:	35.00, 45.00, 55.00 (Euro/MWh)

This leads to seven characteristic intervals for the power price, which are summarized in Table 1.

The cumulative curve for the relative heat demand, which illustrates the aggregated duration of relative heat loads over the period, is shown in Fig. 6.

Using the suggested two-step approach for breaking up the cumulative curve for relative heat demand, the following break points are obtained:

(a)	Important values:	0.25, 0.65, 0.95[b] (–)
(b)	Even division:	0.125, 0.45, 0.80 (–)

[b] *It is relevant to group peak heat-demand operating points together for heat generation dimensioning purposes.*

This leads to seven characteristic intervals for the relative heat demand, which are summarized in Table 2.

2.1.3. Cluster procedure

The final part of the data aggregation analysis is the cluster procedure, which involves the definition of CHOP groups and clustering and aggregation of data points in the CHOP groups.

By definition, any combination of characteristic parameter intervals is a potential CHOP group. Hence, the number of potential CHOP groups in a dataset, $N_{CHOP,pot}$, is determined by the number of characteristic parameter intervals n_{p_k} defined for each of the varying EOC parameters p_k:

$$N_{CHOP,pot} = \prod_{p_k} n_{p_k} \tag{2}$$

To maintain an overview, it is suggested that the potential CHOP groups are indexed using the following key:

$$G_l = G(i_{p_1}, i_{p_2}, \ldots, i_{p_k}) \tag{3}$$

Here, G is short for group, and $i_{p_n} \in \{1, \ldots, n_{p_k}\}$ is the interval number i of the varying EOC parameter p_k. For example, if two varying EOC parameters are defined in a CHOP-reduced dataset, the CHOP group $G(2, 5)$ represents the combination of 'p_1 interval 2' and 'p_2 interval 5'. EOC parameters considered as constants are not included in the indexing key.

All data points O_j of the initial dataset are sorted into the potential CHOP groups G_l based on their EOC parameter values. Each

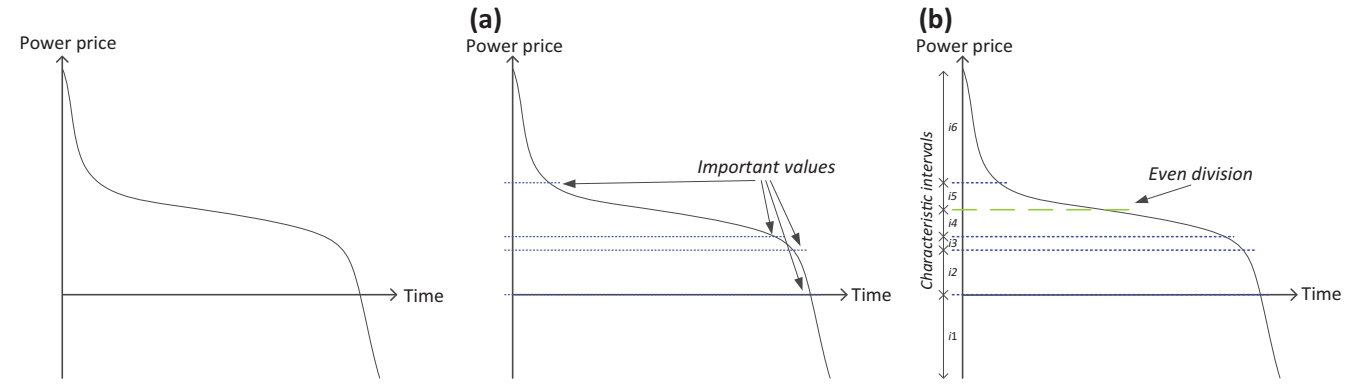

Fig. 4. Illustrative example of the suggested two-step approach for defining characteristic intervals based on the cumulative curve (left). Interval break points are set for (a) important values, and (b) even division. The characteristic intervals are indicated on the second axis in (b).

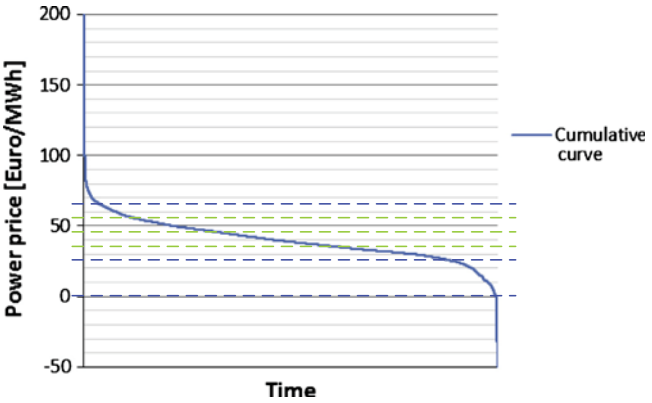

Fig. 5. Cumulative curve for the power price in West Denmark over the period 2010-01-01–2014-12-31, with interval break lines.

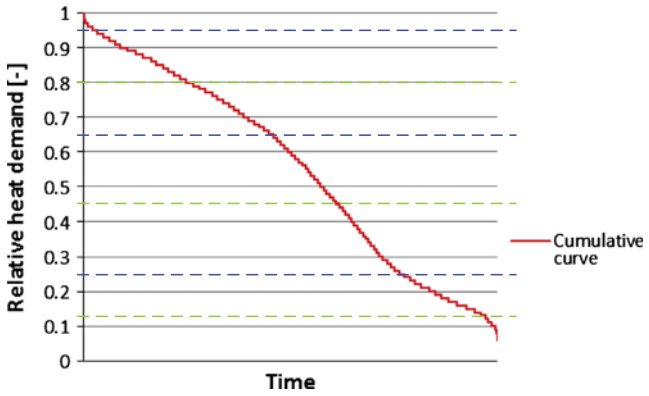

Fig. 6. Cumulative curve for the relative heat demand in Denmark over the period 2010-01-01–2014-12-31, with interval break lines.

Table 1
Characteristic power price intervals.

Power price interval number i	Smallest value (Euro/MWh)	Largest value (Euro/MWh)
1	$-\infty$[a]	−0.01
2	0.00	24.99
3	25.00	34.99
4	35.00	44.99
5	45.00	54.99
6	55.00	64.99
7	65.00	∞[a]

[a] Notice that the intervals are defined as open towards the infinite to cover all feasible power prices.

Table 2
Characteristic heat demand intervals.

Heat demand interval number i	Smallest value (–)	Largest value (–)
1	0.000	0.124
2	0.125	0.249
3	0.250	0.449
4	0.450	0.649
5	0.650	0.799
6	0.800	0.949
7	0.950	1.000

CHOP group G_l becomes an operating point in the final dataset characterised by a duration t_l (the sum of durations of the aggregated data points), and a number of operating condition parameters $\overline{p_l}$ (the weighted average parameter values of the aggregated data points).

$$G(i_{p_1}, i_{p_2}, \ldots, i_{p_k}) = G_l = \{t_l, \overline{p_l}\} \tag{4}$$

$$t_l = \sum_{O_j \in G_l} t_j \tag{5}$$

$$\overline{p_l} = \frac{\sum_{O_j \in G_l} \overline{p_j} \cdot t_j}{t_l} \tag{6}$$

It should be noted that the vector $\overline{p_l}$ includes all EOC parameters, but it may also include other external parameters that are considered unaffected by the plant operation. It is evident that the duration t_j represents the weight given to the operating point O_j in the CHOP dataset. In case the time-value of money is considered in the optimization model, t_j can be represented in the form of present value factor $t_{PV,j}$ as well.

If no data points belong to a potential CHOP group, the group is excluded from the final CHOP dataset. Hence, the final number of CHOP groups is lower than or equal to the number of potential CHOP groups:

$$N_{CHOP} \leqslant N_{CHOP,pot} = \prod_{p_k} n_{p_k} \tag{7}$$

The defined CHOP groups G_l replace the initial dataset of operating points in an optimization model, thereby reducing the number of periods to be considered.

Example: Three EOC parameters are considered: Relative heat demand p_1, power price p_2, and coal price p_3. The number of characteristic parameter intervals are $n_{p_1} = 7$, $n_{p_2} = 7$, and $n_{p_3} = 1$. Hence, the number of potential CHOP groups $N_{CHOP,pot}$ is

$$N_{CHOP,pot} = \prod_{p_k} n_{p_k} = 49 \quad (8)$$

Based on the reference dataset, a simple algorithm written in Excel was applied for sorting reference data points into CHOP groups. Using Eqs. (4)–(6), the algorithm further calculated durations and parameter values for the identified CHOP groups. The processing of the entire dataset took approximately 30 s using a laptop with an Intel® Core™ i7-3720QM CPU with 2.60 GHz and 8 GB RAM. The calculated values are summarized in Table 3.

The number of CHOP groups is found to be

$$N_{CHOP} = 46 < N_{CHOP,pot} \quad (9)$$

as no data points belongs to the potential CHOP groups $G(1, 1)$, $G(1, 7)$ and $G(7, 1)$. An illustration of the sorting of data points into CHOP groups and the resulting CHOP groups is presented in Fig. 7.

2.2. Error analysis

2.2.1. A priori

Having conducted the data aggregation analysis, it is possible *a priori* to calculate the standard deviation $\sigma_{p_{k,l}}$ for each parameter p_k in a CHOP group G_l.

$$\sigma_{p_{k,l}} = \sqrt{\frac{1}{t_l}\sum_j \left(t_j (p_{k,j} - p_{k,l})^2\right)} \quad (10)$$

with t_j being the duration of an operating point $O_j \in G_l$ and t_l being the summarized duration of G_l. The standard deviation may give an impression of the scatter of the merged operating points within each CHOP group and thereby estimate the accuracy error of aggregating numbers in the defined CHOP groups. If the standard deviation of a parameter is significantly larger in one CHOP group than in the others, the cause of the deviation should be investigated. Significant standard deviations may indicate that additional characteristic intervals have to be defined in the CHOP data aggregation analysis.

Example: The standard deviation is calculated for the relative heat demand and power price of the CHOP groups defined in Table 3. The results are presented in Tables 4 and 5.

Concerning the standard deviation of the relative heat demand, it is seen that the largest deviations occur for the heat intervals 3 and 4, owing to the fact that these two intervals are the ones with the largest value span. The standard deviations are not found to vary significantly, and it is therefore not considered necessary to change the characteristic intervals for the relative heat demand.

Regarding the standard deviation of the power price, significant differences are obtained for power price intervals 1 and 7. The reason is that the intervals contain extreme parameter values as they are open towards the infinite. Especially groups $G(5, 1)$ and $G(4, 7)$ show large standard deviations, which is also evident from Fig. 7. For $G(5, 1)$, the major deviation is caused by 8 h on the December 25th 2012 when the average power price was −174.87 Euro/MWh. For $G(4, 7)$, the main cause of the large deviation is 5 h on June 7th 2013 when the average power price was 1940.82 Euro/MWh. Based on these findings, it is not deemed relevant to change the characteristic intervals *a priori*.

2.2.2. A posteriori error analysis

Having solved an optimization model using CHOP-reduced datasets, two suggestions for *a posteriori* analyses are presented here: A sensitivity analysis for verifying the quality of the CHOP-groups and selection of varying EOC parameters, and an error analysis for estimating errors from neglecting time chronology-dependent constraints, such as operation ramp rates or thermal storages.

Table 3
Characteristics of the defined CHOP groups.

CHOP group characteristics							
	Power interval						
Heat interval	1	2	3	4	5	6	7
Duration (h)							
1	0	321	427	390	136	16	0
2	11	1178	2812	2327	1838	379	55
3	9	615	1808	1826	1739	640	178
4	22	717	1847	1828	1672	741	198
5	72	947	2380	2436	1649	803	273
6	30	582	2608	2932	1871	1158	903
7	0	46	262	442	272	217	211
Relative heat demand (–)							
1	–	0.105	0.106	0.104	0.107	0.108	–
2	0.204	0.178	0.181	0.183	0.189	0.199	0.210
3	0.392	0.334	0.333	0.336	0.338	0.348	0.339
4	0.563	0.553	0.548	0.549	0.544	0.549	0.547
5	0.731	0.721	0.727	0.726	0.720	0.719	0.740
6	0.848	0.858	0.866	0.871	0.872	0.875	0.878
7	–	0.961	0.961	0.960	0.961	0.963	0.963
Power price (Euro/MWh)							
1	–	13.91	30.06	40.14	48.52	59.09	–
2	−3.92	16.86	30.65	39.70	49.04	58.00	69.02
3	−19.24	17.43	30.77	39.43	49.58	58.53	70.32
4	−13.46	16.22	30.78	39.78	49.48	58.99	117.54
5	−30.81	16.58	30.73	39.54	49.58	59.13	72.97
6	−12.90	17.36	31.01	39.58	49.60	59.90	74.10
7	–	17.20	31.54	39.56	49.74	60.00	75.08

To verify the quality of the CHOP-group clustering criteria, new CHOP datasets can be defined from the initial EOC dataset but with additional characteristic intervals for each parameter. New operation optimization runs can then be made for selected designs using the new CHOP group datasets. If results of the various runs differ significantly, it may suggest that the characteristic intervals have been defined too loosely and that a more detailed CHOP data aggregation should be conducted for the dataset.

Example: An example of how to evaluate the CHOP group clustering criteria using sensitivity analysis, and to assess the expected error of including an EOC parameter as a constant, is given in Section 3.4.

Some optimization models may include constraints that require knowledge on time chronology, for instance ramp-rate or thermal storage constraints. However, this information is not sustained in CHOP-reduced datasets. If an optimization model with time chronology-dependent constraints is run using CHOP-reduced EOC datasets, the error of neglecting these constraints must be assessed *a posteriori*. This can be done by first solving the optimization model using the CHOP-reduced EOC dataset. The found optimal operation pattern can then be applied on the initial EOC dataset, and the resulting error of neglecting the constraint can be calculated.

Example: An example of how to assess the error of including a thermal storage in an optimization model using a CHOP-reduced EOC dataset is presented in Section 3.5.

3. Illustrative case: Operation optimization of a Danish extraction-based combined heat and power plant

In this section, the advantage of applying the CHOP method is illustrated by extending the CHP-example of Section 2. Here, the operation of the fictive Danish extraction-based CHP is optimized over the 5-year period 2010-01-01–2014-12-31. The optimization is carried out using the entire EOC dataset, the CHOP-reduced dataset, a yearly averaged dataset, a monthly averaged dataset, and a seasonal peak/off-peak averaged dataset. The results obtained are compared with respect to problem size and accuracy.

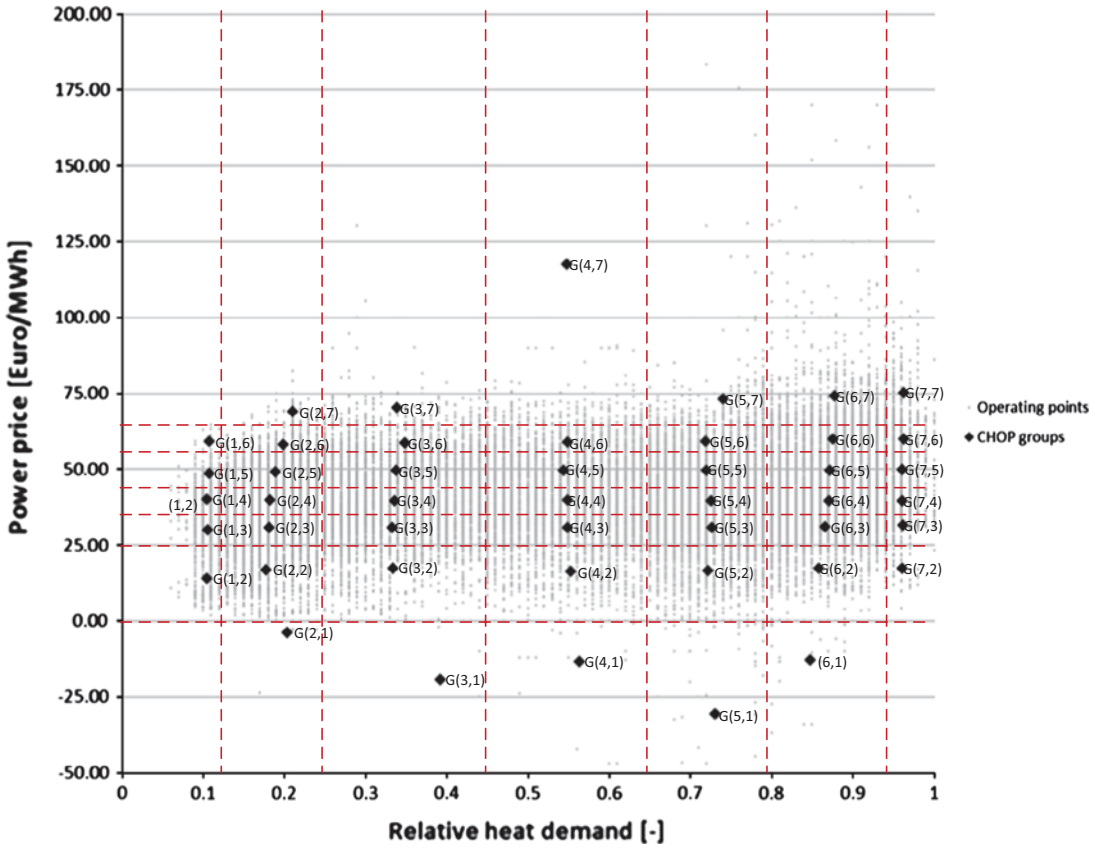

Fig. 7. Scatter diagram showing the reference operating points, characteristic interval breaks, and final CHOP groups. Notice that a small number of the reference operating points lies outside the power price boundaries of the diagram.

Table 4
CHOP group relative heat demand standard deviation, $\sigma_{\lambda_{heat}}$.

CHOP group $\sigma_{\lambda_{heat}}$ (–) Heat interval\power interval	1	2	3	4	5	6	7
1	–	0.011	0.012	0.012	0.012	0.011	–
2	0.026	0.032	0.032	0.033	0.031	0.029	0.020
3	0.065	0.058	0.059	0.060	0.061	0.058	0.059
4	0.055	0.058	0.058	0.058	0.059	0.060	0.061
5	0.040	0.041	0.044	0.044	0.043	0.045	0.044
6	0.038	0.042	0.042	0.042	0.042	0.042	0.042
7	-	0.011	0.013	0.012	0.013	0.014	0.013

Table 5
CHOP group power price standard deviation, $\sigma_{c_{power}}$.

CHOP group $\sigma_{c_{power}}$ (Euro/MWh) Heat interval\power interval	1	2	3	4	5	6	7
1	–	6.57	2.70	2.80	2.37	3.14	–
2	6.35	6.45	2.63	2.90	2.76	2.67	3.61
3	21.67	6.64	2.66	2.89	2.82	2.82	7.49
4	16.79	6.91	2.70	2.87	2.78	2.82	293.62
5	55.98	7.23	2.64	2.87	2.91	2.75	14.17
6	16.10	6.42	2.54	2.78	2.86	3.07	13.46
7	–	4.61	2.31	2.83	2.96	2.87	11.07

3.1. Optimization model

A linearized model of the existing Danish extraction-based CHP plant Avedøreværket 1 (AVV1) is developed to represent the fictive Danish CHP plant treated in the example. AVV1 was commissioned in 1990 and has a net power generation of 250 MW in condensation mode and 212 MW in full back pressure mode with a district heating generation of 330 MJ/s (drive temperature/return temperature 100 °C/50 °C) [42]. Part-load operation in the CHP unit is governed by sliding-pressure control [43]. The minimum load λ_{min} considered of AVV1 is $\lambda_{min} = 0.4$.

A thermodynamic model of AVV1 was previously developed by Elmegaard and Houbak [42] using the energy system simulator Dynamic Network Analysis [44]. The model was validated by Lythcke-Jørgensen et al. [24], who found that the model-predicted electrical efficiency in condensation mode was 2–8% lower than that reported by the plant owner, but that the model in general was accurate with respect to electrical and first-law energy efficiency. The linearized model developed here is based on the model by Elmegaard and Houbak [42].

The linearized model is based on two assumptions: The ratio between lost power generation and increased district heating generation C_v is constant, and the fuel-consumption is a linear function of the load. Four central operating points in the reference model {*A*, *B*, *C*, *D*} are used for developing the linearized model: *A* is operation in full-load condensation-mode, *B* is operation in minimum-load condensation-mode, *C* is operation in full-load back-pressure-mode, and *D* is operation in minimum-load back-pressure-mode.

In the linear model, the linearized operating points A^* and C^* are set equal to the reference points *A* and *C*, while heat generation in the linearized points B^* and D^* is set equal to the heat generation of reference points *B* and *D*.

$$A^* = A, \quad C^* = C, \quad Q_B^* = Q_B, \quad Q_D^* = Q_D \tag{11}$$

The linearized C_v^* is defined as the average of the overall ratio between lost power generation and increased district heating generation at maximum load, $C_{v,\lambda_{max}}$, and at minimum load $C_{v,\lambda_{min}}$:

$$C_{v,\lambda_{max}} = \frac{P_A - P_B}{Q_B} \tag{12}$$

$$C_{v,\lambda_{min}} = \frac{P_C - P_D}{Q_D} \tag{13}$$

$$C_v^* = \frac{C_{v,\lambda_{max}} + C_{v,\lambda_{min}}}{2} = 0.1063 \tag{14}$$

The power generation in the linearized points B^* and D^* are found using Eqs. (11) and (14). Data on the four reference points {A, B, C, D} and the corresponding linearized points {A^*, B^*, C^*, D^*} are presented in Table 6.

For any heat generation Q, the maximum power generation in the linearized model P^*_{max}, which corresponds to a power generation at a load $\lambda = 1.0$, is

$$P^*_{max} = P^*_A - C^*_v Q \tag{15}$$

Two constraints exist on the minimum power generation in the linearized model, P^*_{min1} and P^*_{min2}. P^*_{min1} is the minimum feasible power generation as a consequence of the minimum load constraint $\lambda_{min} = 0.4$, while P^*_{min2} is the minimum feasible power generation as a consequence of the back-pressure operation-mode constraint $\alpha_{max} = 1.0$. Both of these constraints must be satisfied.

$$P^*_{min1} = P^*_C - C^*_v Q \tag{16}$$

$$P_{min2} = P^*_D + (Q - Q^*_D)\frac{P^*_B - P^*_D}{Q^*_B - Q^*_D} \tag{17}$$

The feasible power-heat operation area of the linearized model is defined by the constraints (15)–(17). The power-heat operation area of the reference model, the linearized model, and the four reference operating points {A, B, C, D} are shown in Fig. 8.

Evaluating the accuracy of the linear approximated Eqs. (15)–(17), it is found that the accuracy on the power constraints is within −1.45% to 2.69%. The largest negative deviation occurs for the maximum power generation at $Q = 194.5$ MJ/s, and the largest positive deviation occurs for the minimum power generation at $Q = 118.6$ MJ/s.

In the linearized model, the load can be calculated as a function of the heat and power generation:

$$\lambda(P,Q) = \lambda_{min} + (1 - \lambda_{min})\frac{\left(P + \frac{Q}{C^*_v}\right) - P^*_C}{P^*_A - P^*_C} \tag{18}$$

The linearized fuel consumption $F^*(\lambda)$ in MJ/s as a function of the load is found using the first-order trendline function in Microsoft Excel on data for fuel consumption at various loads in the AVV1 model.

$$F^*(\lambda) = F^*(P,Q) = 499.64 \cdot \lambda(P,Q) + 102.179 \tag{19}$$

A coefficient of determination of $R^2 = 0.9998$ was obtained for this trendline function.

The operation of the fictive Danish CHP plant is to be optimized with the aim of minimizing the costs of generating heat to the district heating network over the period 2010-01-01–2014-12-31. The variables of the optimization model are the power generation P_j and heat generation Q_j in each period j. As discussed in Section 2.1, the CHP operation is constrained by the heating demand which has to be met at all times. *To simplify matters, thermal energy storage is neglected*, hence Q_j is constrained by

$$Q_j = Q_{j,ref} \quad \forall j \tag{20}$$

The power generation P_j is constrained by Eqs. (15)–(17). *Full hour-wise operation flexibility is assumed for the plant*, and, consequently, the choice of (P_{j+1}, Q_{j+1}) is independent of (P_j, Q_j).

Assuming that operation and maintenance costs are constant and therefore indifferent to the choice of (Q_j, P_j), that air is free and cooling is freely available from a cold reservoir, and neglecting taxes on emissions, the objective function to be minimized can be defined as

$$C_{heat}(Q_j, P_j) = \sum_j \left[F^*(P_j, Q_j) \cdot c_{fuel,j} - P_j \cdot c_{p,j}\right] \tag{21}$$

Here, $C_{heat}(Q_j, P_j)$ is the variable cost of the heat generation, $c_{fuel,j}$ is the cost of fuel, and $c_{p,j}$ is the power price in each operating point j.

Given Eqs. (15)–(21), the optimization problem can be written in condensed form as

$$\begin{cases} \min_{Q,P}[C_{heat}(Q_j, P_j)] \\ \quad \textit{subject to constraints}: \\ \text{equations } (15), (16), (17), (20) \\ \quad \textit{with variables}: \\ P_j, Q_j \in \mathbb{R}^+ \end{cases} \tag{22}$$

Table 6
Data on four central reference points {A, B, C, D} in the reference model of AVV1 [42], and their corresponding points {A^*, B^*, C^*, D^*} in the linearized model of AVV1.

Point, j	Load, λ	Back-pressure ratio, α	Power generation, P_j (MW)	Heat generation, Q_j (MJ/s)
A	1.0	0.0	249.3	0.0
A^*	1.0	0.0	249.3	0.0
B	1.0	1.0	216.0	332.9
B^*	1.0	1.0	213.9	332.9
C	0.4	0.0	104.9	0.0
C^*	0.4	0.0	104.9	0.0
D	0.4	1.0	86.3	163.1
D^*	0.4	1.0	87.5	163.1

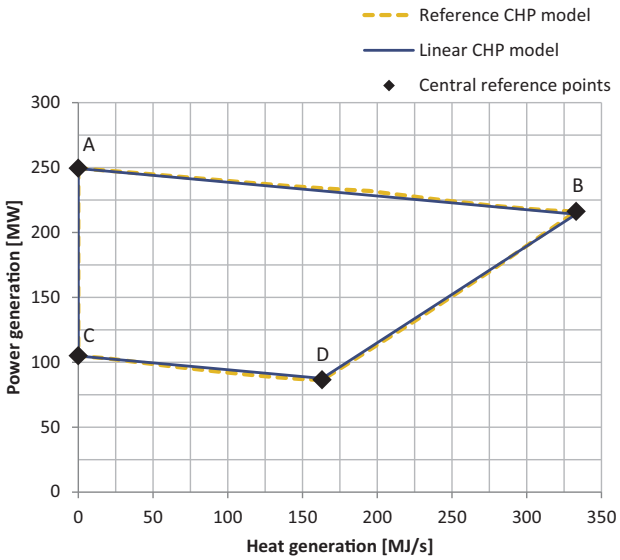

Fig. 8. Heat and power generation range of the reference CHP plant model [42] and the developed linearized model. The outlined areas represent the feasible generation points of the models. Four central operating points {A, B, C, D} are highlighted. Data for these operating points are presented in Table 6.

3.2. External operating conditions datasets

Five different EOC datasets are used for solving optimization problem (22): The full EOC dataset, which is obtained by combining data on hourly power prices in the West Denmark power grid [40] with data on hourly relative heat demand for Denmark [41], as discussed in Section 2.1.2; the CHOP-reduced EOC dataset D_{CHOP},

which is presented in Table 3; the annually averaged EOC dataset D_{AA}, in which the EOC parameter values are averaged over each of the five years; the monthly averaged EOC dataset D_{MA}, in which the EOC parameter values are averaged over each of the 60 months in the period; and, finally, the seasonal peak/off-peak averaged EOC dataset D_{SP}, which is inspired by the approach taken by Chen et al. [2] for representing EOC parameters. Here, EOC parameter values are averaged over the peak period, 7 a.m.–11 p.m., and off-peak period, 11 p.m.–7 a.m., for each of the four seasons each year. Datasets D_{AA}, D_{MA}, and D_{SP} are presented in Appendix A. A scatter diagram illustrating the reference EOC dataset and the reduced datasets is presented in Fig. 9.

Fig. 9 illustrates how the parameter value diversity of the reference dataset is sustained in the various reduced datasets. It is seen that the annual average EOC dataset yields five points, all located in the center of Fig. 9, that are almost identical with respect to relative heat demand and power price. The monthly averaged and seasonal peak/off-peak averaged EOC datasets are seen to be more distributed, but the resulting operating points are still far from the boarders of the dense cloud of reference operating points. Opposed to this, both the CHOP and the CHOP-revised EOC datasets are seen to be significantly more distributed in the figure, suggesting that a larger degree of the diversity in the reference dataset is sustained in these reduced datasets.

3.3. Results and comparison

The optimization problem (21) is solved using the open-source mixed-integer program solver CBC (COIN Branch and Cut) [45] in OpenSolver 2.6.1 [46] for Microsoft Excel. The optimization results obtained using each of the five EOC datasets are summarized in Table 7.

Firstly, it is evident that by optimizing the operation of the CHP unit using the full dataset it is possible to reduce the total variable heat generation cost to C_{heat} = 0.38 MEuro. This value is the exact solution to the optimization problem (21) under the given conditions and assumptions, and the results obtained using the full dataset are used as reference values for further comparison.

Among the reduced EOC datasets, the result obtained using D_{CHOP} gets closest to the reference value with a deviation of 0.38 MEuro in total variable heat generation cost. Compared to this, the deviation is 8.15 MEuro when using D_{AA}, 7.64 MEuro using D_{MA}, and 5.58 MEuro using D_{SP}. In terms of computation time, the number of calculations to be performed is 5 when using D_{AA}, 60 when using D_{MA}, 40 when using D_{SP}, and 46 when using D_{CHOP}. Hence, D_{CHOP} obtains the most accurate economic result of the reduced datasets for the case, while the relative reduction in computation time from using D_{CHOP} is comparable to those of using D_{MA} and D_{SP}. This demonstrates the relevance of the CHOP method for reducing datasets on external operating conditions.

For the results obtained using D_{AA}, D_{MA} and D_{SP}, it is seen that the total power generation and fuel consumption are larger than the reference values. This is caused by the fact that the operation optimization only considers the average power prices of the periods. Hence, if the average power price over a given period is economically attractive for power generation at the plant, power generation is maximized over the entire period even though the power price may not be attractive in all hours. This phenomenon results in an increased power generation, but also in increased fuel costs that exceed the increased income from power sales and yielding a higher C_{heat} for the three solutions compared to the reference solution. The opposite trend, where power generation is minimized for entire periods containing data points with advantageous power prices, also occurs when using D_{AA}, D_{MA} and D_{SP}, but the first trend is found to be dominant in the present case.

In contrast, the result obtained using the D_{CHOP} dataset underestimates the power generation in the case investigated, and also shows reduced income from power sales. At the same time an almost equal reduction in fuel costs occurs, resulting in the relatively low deviation in the heat price compared to the reference

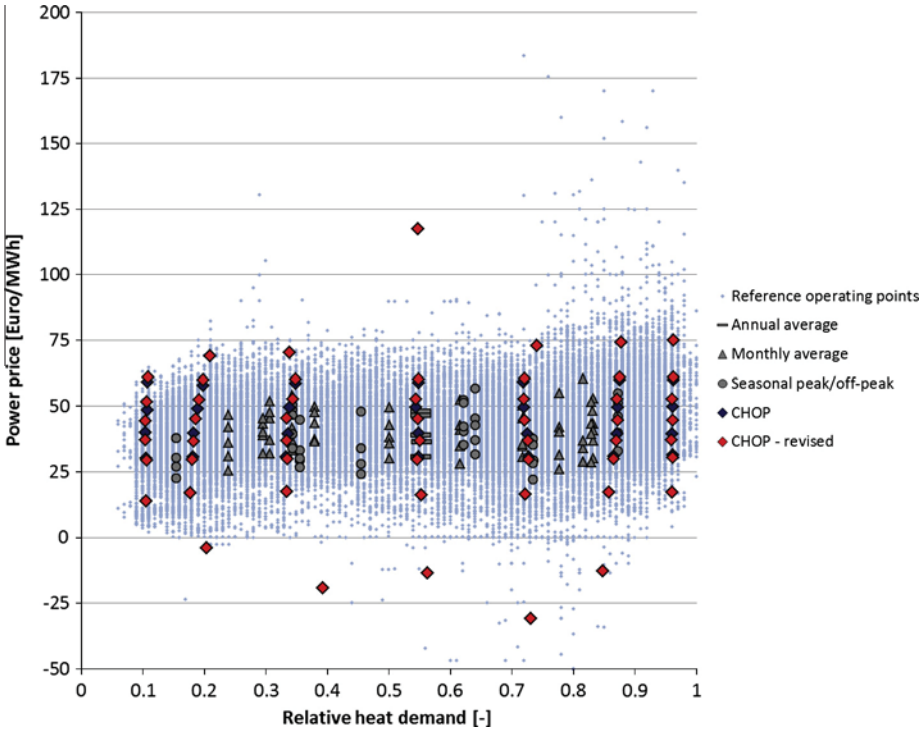

Fig. 9. Scatter diagram showing reference, annually averaged, monthly averaged, seasonal peak/off-peak, CHOP, and revised-CHOP operating points over the period 2010-01-01–2014-12-31. Notice that some of the CHOP and revised-CHOP operating points are overlapping.

Table 7
Optimization results obtained using the five different EOC datasets.

	Full dataset	Annually averaged	Monthly averaged	Seasonal peak/off-peak	CHOP-reduced
Results					
Total variable heat generation cost, C_{heat} (MEuro)	0.38	8.53	8.02	5.96	0.76
Total power sales (MEuro)	368.06	369.51	376.62	370.41	356.12
Total fuel costs (MEuro)	368.44	377.81	384.64	376.38	356.88
Operation data					
Total heat generation (GW h)	8066	8066	8066	8066	8066
Total power generation (GW h)	8664	8958	9161	8907	8309
Total fuel consumption (GW h)	23,460	24,057	24,492	23,966	22,724
Optimization problem					
Number of periods	43,824	5	60	40	46
Variables per period	2	2	2	2	2
Constraints per period	4	4	4	4	4

result. The explanation is that in the CHOP method, the data points merged in CHOP groups have similar parameter values. Hence, averaged parameter values are close to the parameter values of the data points. If the power generation is minimized over a data point where it would be maximized in the reference case, or vice versa, the economic difference is small. Thus, when using the D_{CHOP} dataset, the economic result is very close to that of the reference optimization.

Comparing the accuracy of results, it is seen that the estimated fuel consumption and power generation are overestimated by 2.5% and 3.4% using D_{AA}, by 4.4% and 5.7% using D_{MA}, by 2.2% and 2.8% using D_{SP}, while they are underestimated by 3.1% and 4.1% using D_{CHOP}. This indicates that the optimal operation pattern predicted using D_{CHOP} is different from the reference optimum for a significant amount of operating points for the given case, suggesting that the CHOP clustering criteria could be improved. This had not been obvious if the reference solution had not been known, or if only the economic objective had been considered. Therefore, it is suggested that sensitivity analysis is applied *a posteriori* for evaluating the quality of the applied clustering criteria, and thereby assessing the accuracy of the results.

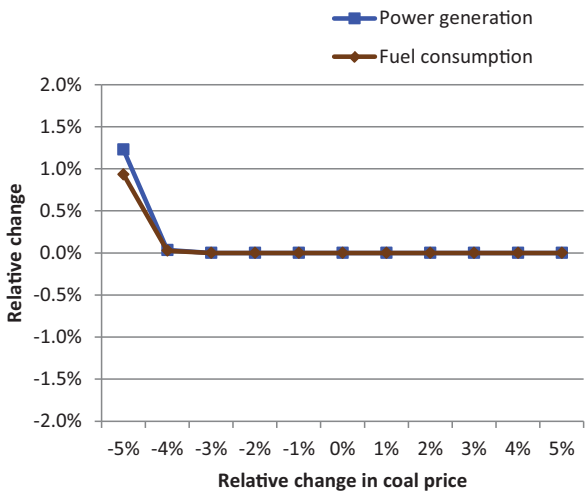

Fig. 10. Relative changes in optimized power generation and fuel consumption as a function of relative changes in the coal price. Notice that heat generation is unaffected by the coal price as it is constrained in the optimization model.

3.4. Sensitivity analysis

A posteriori, sensitivity analyses are conducted to evaluate the quality of the entity selection and the applied clustering criteria.

First, the impact of not including coal price as a varying EOC parameter in the CHOP analysis is assessed. As described in Section 2.1.1, the data suggested that the coal price varied within the range −3.4% to +4% of the average price over the period. It is here assessed how such variations would affect the optimized operating pattern when using the CHOP dataset.

In the optimization model, the heat generation is constrained and therefore unaffected by the coal price. However, power generation is flexible and depends on power prices and coal prices. The impact on power generation and fuel consumption from varying the coal price within the range ±5% over the entire period is shown in Fig. 10. It is seen that if the coal price is reduced by 5%, the power generation is increased by 1.2% and the fuel consumption by 0.9%. Apart from this, the power generation and fuel consumption are hardly affected by variations in the coal price over the set range. It is therefore considered acceptable to use the average coal price value in the CHOP dataset.

Next, the applied clustering criteria are assessed. Here, the number of characteristic intervals defined for the relative heat demand and power price is varied and new CHOP datasets are obtained. The optimization model is then run using each of the new CHOP datasets to evaluate the impact on the results of changing the clustering criteria.

Three sensitivity analyses are considered: Heat interval sensitivity, where the number of intervals defined for the relative heat demand is changed; power interval sensitivity, where the number of intervals defined for the power price is changed; and combined heat and power interval sensitivity, where the number of intervals defined for both the relative heat demand and the power price are changed simultaneously. The interval break points defined for the sensitivity analyses are given in Table 8.

The results obtained by running the optimization model with the modified CHOP datasets are compared with respect to income result, fuel cost, power generation and power sales. The outcomes are presented in Figs. 11–14.

Fig. 11 shows the variations in total variable heat cost from the different sensitivity analyses. It is seen that *reducing the number of power intervals with the suggested break-points significantly increases the total variable heat cost*, while increasing the number of intervals leads to slightly better results. A stable level is reached when increasing the number of power price intervals to 8–10 with the set break points. This suggests that the number of characteristic intervals for the power price should be increased in order to obtain a robust solution. Opposed to this, *the result is almost unaffected by the number of relative heat demand intervals defined*, suggesting that the initial resolution of 7 characteristic heat demand intervals is

Table 8
Interval break points as a function of the number of intervals defined.

No. of intervals	4	5	6	7	8	9	10
Relative heat demand interval breaks (–)	0.25	0.25	0.25	0.125	0.125	0.125	0.125
	0.65	0.45	0.45	0.25	0.25	0.25	0.25
	0.95	0.65	0.65	0.45	0.38	0.38	0.35
		0.95	0.80	0.65	0.52	0.52	0.45
			0.95	0.80	0.65	0.65	0.55
				0.95	0.80	0.75	0.65
					0.95	0.85	0.75
						0.95	0.85
							0.95
Power price interval breaks (Euro/MWh)	0.00	0.00	0.00	0.00	0.00	0.00	0.00
	25.00	25.00	25.00	25.00	25.00	12.50	8.00
	65.00	45.00	38.00	35.00	33.00	25.00	17.00
		65.00	52.00	45.00	41.00	33.00	25.00
			65.00	55.00	49.00	41.00	33.00
				65.00	57.00	49.00	41.00
					65.00	57.00	49.00
						65.00	57.00
							65.00

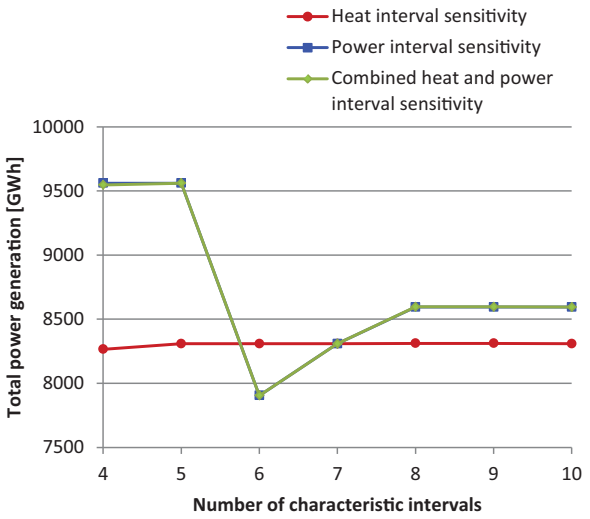

Fig. 13. Total power generation sensitivity analysis.

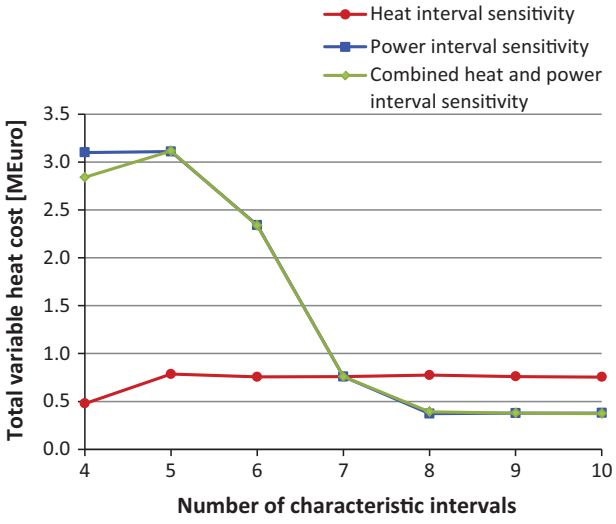

Fig. 11. Total variable heat cost sensitivity analysis.

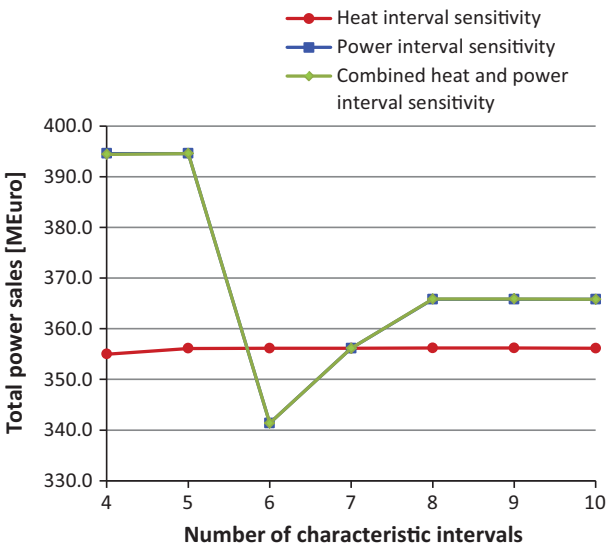

Fig. 14. Total power sales sensitivity analysis.

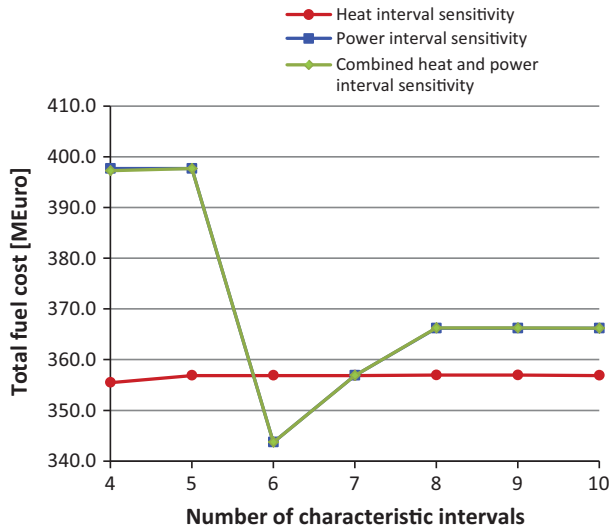

Fig. 12. Total fuel cost sensitivity analysis.

sufficient. Both findings are supported by the combined heat and power intervals sensitivity analysis, the trend of which is almost identical to that of the power interval sensitivity.

Furthermore, the findings above are supported by the analogue results obtained when comparing the sensitivity analysis results with respect to fuel costs (Fig. 12), power generation (Fig. 13), and power sales (Fig. 14). Again, it is found that the results are somewhat unaffected by minor changes in the number of relative heat demand characteristic intervals, while the results obtained become stable when the number of power price intervals is increased to 8 or more using the suggested interval break-points.

The sensitivity analysis suggests that the CHOP dataset should be reconfigured by changing the number of characteristic power price intervals to 8 using the interval break-points presented in Table 8. The revised CHOP dataset is presented in Table 9, while results obtained using the revised CHOP dataset are presented in Table 10. The results show that the C_{heat} obtained is practically identical to that found using the reference data when applying

Table 9
Characteristics of the revised CHOP groups.

CHOP group characteristics								
	Power interval							
Heat interval	1	2	3	4	5	6	7	8
Duration (h)								
1	0	321	356	306	242	55	10	0
2	11	1178	2198	2111	1872	980	195	55
3	9	615	1383	1673	1400	1150	407	178
4	22	717	1402	1600	1483	1085	518	198
5	72	947	1824	2163	1565	1139	577	273
6	30	582	1953	2641	1776	1301	898	903
7	0	46	189	365	267	195	177	211
Relative heat demand (–)								
1	–	0.105	0.106	0.105	0.105	0.107	0.109	–
2	0.204	0.178	0.180	0.182	0.186	0.191	0.199	0.210
3	0.392	0.334	0.335	0.334	0.334	0.344	0.348	0.339
4	0.563	0.553	0.546	0.550	0.547	0.544	0.549	0.547
5	0.731	0.721	0.727	0.726	0.721	0.720	0.721	0.740
6	0.848	0.858	0.866	0.870	0.872	0.871	0.876	0.878
7	–	0.961	0.961	0.960	0.962	0.961	0.963	0.963
Power price (Euro/MWh)								
1	–	13.91	29.32	37.20	44.49	51.62	61.11	–
2	−3.92	16.86	29.73	36.73	45.20	52.51	60.05	69.02
3	−19.24	17.43	29.80	36.80	45.40	52.64	60.23	70.32
4	−13.46	16.22	29.77	36.83	45.20	52.59	60.34	117.54
5	−30.81	16.58	29.75	36.82	44.74	52.63	60.39	72.97
6	−12.90	17.36	30.03	36.98	44.76	52.59	61.08	74.10
7	–	17.20	30.56	37.11	44.58	52.75	60.95	75.08

Table 10
Optimization results obtained using the CHOP and the revised CHOP EOC datasets.

	Full dataset	CHOP	CHOP-revised
Results			
Total variable heat generation cost, C_{heat} (MEuro)	0.38	0.76	0.37
Total power sales (MEuro)	368.06	356.12	365.81
Total fuel costs (MEuro)	368.44	356.88	366.18
Operation data			
Total heat generation (GW h)	8066	8066	8066
Total power generation (GW h)	8664	8309	8594
Total fuel consumption (GW h)	23,460	22,724	23,317
Optimization problem			
Number of periods	43,824	46	53
Variables per period	2	2	2
Constraints per period	4	4	4

the revised CHOP dataset, while the power generation and fuel consumption are underestimated by less than 1%, suggesting that the revised clustering criteria is more accurate than the initial one. In terms of reduction in relative computation time, the revised CHOP dataset requires 53 calculations, a number which is comparable to the number of calculations required when using D_{MA} and D_{SP} as well.

3.5. Optimization with thermal energy storage

As discussed by Rolfsman [47], the income from power sales in CHP plants may be increased by installing thermal energy storages that allows for operation shifting in periods with high power prices. Similar results were reported by Martinéz-Lear et al. [48] for combined heating, cooling and power plants for buildings. Hence, optimization models of multi-generation plants dealing with heating or cooling generation should preferably include an option for thermal storage. In this section, the optimization model (22) is rewritten to include short-term heat storage, and the error made from solving the problem using the revised CHOP dataset (Table 9) is assessed.

In the case of the fictive Danish CHP plant, it is assumed that a thermal energy storage capable of storing 24 h of peak heat generation is available on site.

$$Q_{storage,max} = 24 \cdot 332.91\ \text{MWh} = 7990\ \text{MWh} \tag{23}$$

Heat losses are neglected in the thermal energy storage model. The thermal energy storage content $Q_{storage,j}$ is calculated as

$$Q_{storage,j} = Q_{storage,j-1} + (Q_j - Q_{j,ref}), Q_{storage,0} = 0 \tag{24}$$

In the rewritten optimization problem, the constraint (19) is slacked and replaced by a new constraint stating that the total heat generation over the entire period must equal the total heat consumption

$$\sum_j Q_j = \sum_j Q_{j,ref} \tag{25}$$

Furthermore, two constraints are introduced representing the physical constraints of the thermal energy storage:

$$Q_{storage,j} \leqslant Q_{storage,max} \tag{26}$$
$$Q_{storage,j} \geqslant 0 \tag{27}$$

Given Eqs. (15)–(19) and (23)–(27), the optimization problem with thermal energy storage can be written in condensed form as

$$\begin{cases} \min\limits_{Q,P}[C_{heat}(Q_j, P_j)] \\ \quad \textit{subject to constraints}: \\ \text{equations } (15), (16), (17), (25), (26), (27) \\ \quad \textit{with variables}: \\ P_j, Q_j \in \mathbb{R}^+ \end{cases} \tag{28}$$

As constraints (26) and (27) require knowledge of the time chronology of the data points, the optimization problem (28) cannot be solved using the CHOP-reduced dataset. Therefore,

Table 11
Optimization results obtained from solving optimization problem (28) using the full EOC dataset and the revised CHOP dataset.

	Full dataset problem (22)	Full dataset problem (28)	CHOP-revised problem (28)[a]
Results			
Total variable heat generation cost, C_{heat} (MEuro)	0.38	−6.08	−8.06
Total power sales (MEuro)	368.06	372.50	357.04
Total fuel costs (MEuro)	368.44	366.42	348.97
Operation data			
Total heat generation (GW h)	8,066	8,066	8,066
Total power generation (GW h)	8,664	8,602	8,066
Total fuel consumption (GW h)	23,460	23,332	22,221
Optimization problem			
Number of periods	43,824	43,824	53
Variables per period	2	2	2
Constraints per period	4	6	4

[a] Constraints (26) and (27) were slacked when solving optimization problem (28) using the CHOP-revised dataset.

constraints (26) and (27) were slacked, and the resulting error was evaluated *a posteriori*. Results obtained from solving the problem (28) using the full EOC dataset and the revised CHOP dataset are presented in Table 11.

When solving problem (28) using the full EOC dataset, a total variable heat generation cost of -6.08 MEuro was obtained, as opposed to the solution where no heat storage was considered and a total variable heat generation cost of 0.38 MEuro was obtained. The negative costs means that power sales exceed the total fuel costs in optimal operation for the CHP plant. The result suggests that short-term thermal energy storage is an economic advantage in CHP operation, supporting the outcomes presented by Rolfsman [47] and Martinéz-Lear et al. [48]. It is further seen that the power generation is slightly reduced while incomes from power sales are increased when comparing to the situation without heat storage. This is owing to the fact that heat storage allows for a more flexible operation.

Solving problem (28) with the revised CHOP dataset gives a total variable heat cost of −8.06 MEuro. It is seen that the power generation, power sales, and fuel consumption are all reduced when compared to the solution obtained using the full EOC dataset. The economic result is slightly improved when compared to the result obtained using the full EOC dataset. However, the results cannot be directly compared without assessing the error that slacking of constraints (26) and (27) imposes on the CHOP solution.

By applying the optimal operation pattern predicted by the CHOP solution on the chronological EOC dataset, it is possible to evaluate the contents of the thermal energy storage over the 5-year period investigated. A plot of the thermal energy storage contents over the 5-year period for the optimal solutions to problem (28) obtained using the full EOC dataset and the revised CHOP dataset is presented in Fig. 15.

It is seen that the CHOP solution significantly violates the physical constraints of the thermal energy storage in the model over the 5-year period. The explanation is quite simple: When slacking constraints (26) and (27), the only constraint on the heat generation is that heat generation and consumption must be balanced over the entire period. As the power prices on average were higher in the first two years of the period (consult Table 12 in Appendix A), power generation is maximized at the cost of heat generation in 2010 and 2011, while excess heat is generation the following years

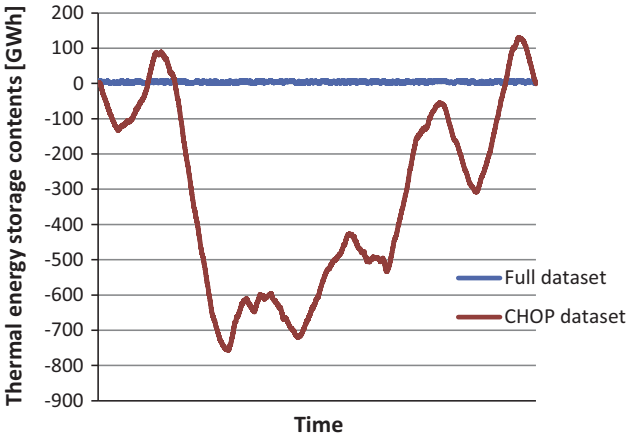

Fig. 15. Thermal energy storage contents over the 5-year period for the optimal solutions to problem (27) obtained using the full EOC dataset and the revised CHOP dataset.

Table 12
Annually averaged EOC dataset, D_{AA}.

Year	Duration (h)	Power price, $c_{p,j}$ (Euro/MWh)	Relative heat demand, q_j (–)
2010	8760	46.48	0.553
2011	8760	47.96	0.553
2012	8784	36.33	0.554
2013	8760	38.98	0.553
2014	8760	30.67	0.553

when power prices are lower. It can also be deducted from the graph that additional heat is generated in the summer periods when demand is low, and then stored for use in the winter when heat demand is high. Though highly intuitive, this solution is infeasible in reality due to thermal energy storage constraints. The result illustrates that the CHOP method may not be suitable for data reduction in models where short-term thermal energy storage is considered.

4. Discussion and perspective

As the optimization of FMG concepts is complex and involves such challenges as synthesising and dimensioning of processes, process integration, and operation optimization, it is desirable to reduce external operating condition (EOC) datasets to be used in multi-period optimization models in order to make the models solvable. The CHOP method presented in this paper is a simple method for reducing EOC datasets by clustering data points in groups. The main advantages of the CHOP method include the significant reduction in the size of input data to multi-period optimization problems and the consequent reduction in computation costs, the simple and straight-forward use, and the fact that short-term relations and variations between various operating conditions are sustained in CHOP-reduced dataset.

For the simple case study presented in this paper, which treated the operation optimization of a fictive Danish CHP plant, it was found that the solution obtained using the revised CHOP-reduced EOC dataset had a much higher accuracy in terms of economic result and estimations of power generation and fuel consumption than the solutions obtained using chronology-

averaged EOC datasets. Furthermore, it was found that the revised CHOP dataset reduced the relative amount of computations by approximately a factor 827, which is comparable to the reductions of approximately a factor 730 when using monthly averaged dataset and approximately a factor 1096 when using the peak/off-peak averaged dataset. For the simple case, the advantage of the reduction in computation costs was not evident as the linear optimization problem could be solved within a minute using the full dataset. However, if more advanced optimization models needed be evaluated, e.g. non-linear operation optimization models, and if these further needed be solved for a large number of different designs for each operating point as in the design optimization of complex FMGs, reductions in computation costs is needed. Hence, the combination of high accuracy and significant reduction in computation time support the proposition that the CHOP method is relevant for reducing EOC datasets to be used in optimization models of FMGs, and that the method is to be preferred over any of the three averaging methods mentioned in this paper.

The advantage of sustaining information on short-term parameter relations will assumedly be even more significant in more complex optimization models that consider multiple processes. For instance, if a process was considered for integration in the case study CHP plant which would only be economic advantageous to run when power prices are below 25.00 Euro/MWh, it would never be operated if annual or monthly averaged datasets were applied in the optimization model, while it would be run for 2192 h over the five year period if the peak/off-peak averaged dataset was used, and for 4550 h, or more than 10% of the time, if the CHOP-reduced dataset or the reference dataset were applied. Sustained data diversity in CHOP-reduced datasets thus allows for more accurate solutions. The fact that a large part of the initial dataset parameter diversity is sustained in the CHOP-reduced dataset is also evident from Fig. 9, which illustrates how the parameter diversity in defined CHOP groups is significantly larger than for any of the three averaged datasets. Furthermore, for equipment with performance that is a non-linear function of an EOC parameter, e.g. the power generation of a wind turbine as a function of the wind speed, the use of CHOP-reduced datasets rather than chronological-averaged datasets will assumedly yield more accurate results.

Another advantage of the CHOP method is the fact that larger datasets do not necessarily yield larger reduced datasets. In the case study, hourly heat demand and power price data were considered for a 5-year period. The initial 43,824 data points were reduced to 60 data points using the monthly averaging method, 40 data points using the seasonal peak/off-peak averaging method, and 53 using the CHOP method. If the period considered was extended to a 30-year period, the number of data points would be multiplied by six for each of the chronological-averaged methods, while it is likely that the number of CHOP-groups would not need to be changed. Instead, the weight given to each of the CHOP groups defined would increase as the additional data points are sorted into the groups. However, it is likely that the increase in weight will not be the same for all CHOP groups due to the development of the energy system. If the time-value of money needs to be considered, the time weight given to each sorted data point can be replaced by a present value weight factor, as discussed in Section 2.1.3, allowing for net present value calculations in design optimization models.

Error analysis is central in the CHOP method as it provides the feedback required to optimize the data aggregation strategy. In the present work, a number of approaches for conducting the error analysis were suggested. However, it must be emphasized that other methods may be applied as long as they do not counteract the initial ambition of reducing overall computation time. One example of a method that may be useful for error analysis in the CHOP method is the global sensitivity analysis Morris Screening [49], which could be applied *a posteriori* for assessing the quality of the defined characteristic interval breaks by estimating the aggregated impact of varying EOC parameters within the defined intervals, or to evaluate if a non-clustering EOC parameter ought to be included in the clustering analysis.

Two significant draw-backs exist for the CHOP method. Firstly, the number of CHOP groups defined is combinatorial as a function of the relevant EOC parameters defined for a given problem. In the case study, three EOC parameters were considered, of which one was excluded from the clustering analysis, and seven and eight characteristic intervals were defined for the other two, resulting in 56 potential CHOP groups according to Eq. (2). However, if two additional EOC parameters were considered for clustering with four characteristic intervals each, the number of potential CHOP groups would increase to 896. Even though the final number of CHOP groups may be lower according to Eq. (7), the combinatorial issue represents a significant challenge when applying the CHOP method on datasets with multiple EOC parameters. This also explains why it is relevant to seek to exclude less volatile parameters from the CHOP data aggregation in the entity selection. One way of circumventing the combinatorial issue is to set up relations for deriving various parameters from a few EOC parameters. For example, it may be possible to derive formulas for heating and cooling demands as a function of the outdoor temperature [50] or the cost of various fuels as a function of the expected oil price [2]. If such relations are introduced, the uncertainty of the applied relations should be included in the sensitivity and error analyses conducted for results obtained.

Secondly, the CHOP method does not permit consideration of dynamics and time chronology directly, which is also the case for yearly- and monthly-averaged datasets. This implies that ramp constraints on operation cannot be considered, potentially resulting in infeasible operation patterns as discussed by Rong and Lahdelma [51], and that thermal energy storages cannot be directly included, as discussed in Section 3.5. Also, scheduling of maintenance shut-downs cannot be considered when using CHOP-reduced datasets, and neither can investment planning if the entire reference dataset is reduced to a single CHOP-reduced dataset. The latter can be solved by setting a time-span for investment planning, e.g. 5 years, and then derive a CHOP-reduced dataset for every 5-year period. However, this would increase the size of the dataset significantly, counteracting one of the initial advantages of the CHOP-method.

To overcome the challenges of including thermal energy storage and ramp constraints, it is suggested that CHOP-reduced datasets, rather than yearly or monthly reduced datasets, are applied in a first-step design optimization run, and that a detailed operation optimization is carried out in a sequential step for the most promising designs, similar to the method presented by Rubio-Maya et al. [21] and Uche et al. [22].

5. Conclusion

This study presents a novel and simple method, the Characteristic Operating Pattern (CHOP) method, for reducing external operating condition (EOC) datasets in optimization models. The method has been tailored for optimization models of flexible multi-generation systems (FMGs), but may be suitable for any optimization model that involves a flexible system or facility operating on multiple markets.

In a case study, an operation optimization model of a Danish extraction-based combined heat and power plant is solved using the full EOC dataset, a CHOP-reduced EOC dataset, a yearly-averaged EOC dataset, a monthly-averaged EOC dataset, and a seasonal peak/off-peak EOC dataset. The results indicate that the CHOP-reduced dataset yields by far the most accurate solution among all the reduced EOC datasets, while achieving a reduction in the problem size similar to those achieved of using monthly-averaged and seasonal peak/off-peak-averaged datasets. It is found that CHOP-reduced datasets are not suited for models that consider short-term thermal energy storage as time chronology is not considered.

The outcomes of the paper suggest that the CHOP method is better suited for reducing EOC datasets in optimization models of FMGs than any of the three chronology-averaged methods used for comparison in this paper. If short-term thermal energy storage or ramp constraints are considered, it is suggested that the CHOP method is applied in a first-step design optimization method, and that detailed operation optimization, including dynamic constraints, is carried out in a sequential step for the most promising designs.

Acknowledgement

The authors would like to acknowledge DONG Energy for their financial support of the research.

Appendix A

This appendix presents the reduced external operating condition (EOC) datasets D_{AA} (Table 12), D_{MA} (Tables 13–15), and D_{SP} (Tables 16–18) as explained in Section 3.2.

Table 13
Monthly averaged EOC dataset, D_{MA}, period duration.

Duration (h)	2010	2011	2012	2013	2014
January	744	744	744	744	744
February	672	672	696	672	672
March	744	744	744	744	744
April	720	720	720	720	720
May	744	744	744	744	744
June	720	720	720	720	720
July	744	744	744	744	744
August	744	744	744	744	744
September	720	720	720	720	720
October	744	744	744	744	744
November	720	720	720	720	720
December	744	744	744	744	744

Table 14
Monthly averaged EOC dataset, D_{MA}, period power price.

Power price (Euro/MWh)	2010	2011	2012	2013	2014
January	43.29	52.89	37.01	40.77	30.26
February	43.45	51.75	48.35	39.40	28.74
March	42.09	55.14	31.51	40.33	26.05
April	41.11	52.33	34.76	42.82	28.13
May	41.73	54.35	36.06	36.82	33.34
June	45.49	51.99	37.21	47.74	31.88
July	46.81	42.20	25.55	36.24	31.02
August	43.28	45.42	39.01	40.17	32.11
September	49.86	47.79	37.40	43.67	36.58
October	49.48	42.76	38.11	35.90	30.13
November	50.45	45.45	34.91	35.60	30.78
December	60.50	33.97	36.86	28.80	28.99

Table 15
Monthly averaged EOC dataset, D_{MA}, period relative heat demand.

Relative heat demand (–)	2010	2011	2012	2013	2014
January	0.83	0.83	0.83	0.83	0.83
February	0.83	0.83	0.83	0.83	0.83
March	0.78	0.78	0.78	0.78	0.78
April	0.62	0.62	0.62	0.62	0.62
May	0.34	0.34	0.34	0.34	0.34
June	0.31	0.31	0.31	0.31	0.31
July	0.24	0.24	0.24	0.24	0.24
August	0.30	0.30	0.30	0.30	0.30
September	0.38	0.38	0.38	0.38	0.38
October	0.50	0.50	0.50	0.50	0.50
November	0.72	0.72	0.72	0.72	0.72
December	0.82	0.82	0.82	0.82	0.82

Table 16
Seasonal averaged peak/off-peak averaged EOC dataset, D_{SP}, period duration.

Duration (h)	2010	2011	2012	2013	2014
Winter, peak	1440	1440	1456	1440	1440
Winter, off-peak	720	720	728	720	720
Spring, peak	1470	1470	1470	1470	1470
Spring, off-peak	736	736	736	736	736
Summer, peak	1472	1472	1472	1472	1472
Summer, off-peak	736	736	736	736	736
Autumn, peak	1456	1456	1456	1456	1456
Autumn, off-peak	728	728	728	728	728

Table 17
Seasonal averaged peak/off-peak averaged EOC dataset, D_{SP}, period power price.

Power price (Euro/MWh)	2010	2011	2012	2013	2014
Winter, peak	55.11	51.29	46.21	40.09	32.95
Winter, off-peak	37.58	35.48	29.29	28.49	22.15
Spring, peak	45.49	56.95	37.08	42.97	31.62
Spring, off-peak	33.96	47.97	28.15	33.94	24.33
Summer, peak	48.85	50.75	39.44	46.76	34.01
Summer, off-peak	37.87	37.91	22.78	30.43	26.98
Autumn, peak	52.45	51.37	40.53	42.45	35.35
Autumn, off-peak	44.88	33.19	29.42	30.19	26.71

Table 18
Seasonal averaged peak/off-peak averaged EOC dataset, D_{SP}, period relative heat demand.

Relative heat demand (–)	2010	2011	2012	2013	2014
Winter, peak	0.87	0.87	0.87	0.87	0.87
Winter, off-peak	0.73	0.73	0.73	0.73	0.73
Spring, peak	0.64	0.64	0.64	0.64	0.64
Spring, off-peak	0.45	0.45	0.45	0.45	0.45
Summer, peak	0.34	0.34	0.34	0.34	0.34
Summer, off-peak	0.15	0.15	0.15	0.15	0.15
Autumn, peak	0.62	0.62	0.62	0.62	0.62
Autumn, off-peak	0.36	0.36	0.36	0.36	0.36

References

[1] Lund H. Renewable energy systems: the choice and modelling of 100% renewable solutions. Burlington (USA): Elsevier; 2010.
[2] Chen Y, Adams II TA, Barton PI. Optimal design and operation of flexible energy polygeneration systems. Ind Eng Chem Res 2011;50:4553–66.
[3] Coronas A, Murthy SS, Bruno JC. Editorial for the special issue of applied thermal engineering on polygeneration. Appl Therm Energy 2013;50:1397–8.
[4] Gassner M, Maréchal F. Increasing efficiency of fuel ethanol production from lignocellulosic biomass by process integration. Energy Fuels 2013;27:2107–15.
[5] Edenhofer O, Pichs-Madruga R, Sokona Y. Renewable energy sources and climate change mitigation. New York (USA): Intergovernmental Panel on Climate Change and Cambridge University Press; 2012.

[6] Daianova L, Dotzauer E, Thorin E, Yan J. Evaluation of a regional bioenergy system with local production of biofuel for transportation, integrated with a CHP plant. Appl Energy 2011;92:739–49.
[7] Ilic DD, Dotzauer E, Trygg L. District heating and ethanol production through polygeneration in Stockholm. Appl Energy 2011;91:214–21.
[8] Kohl T, Teles M, Melin K, Laukkanen T, Järvinen M, Park SW, et al. Exergoeconomic assessment of CHP-integrated biomass upgrading. Appl Energy 2015;156:290–305.
[9] Mathiesen B, Lund H, Connolly D, Wenzel H, Østergaard P, Möller B, et al. Smart energy systems for coherent 100% renewable energy and transport solutions. Appl Energy 2015;145:139–54.
[10] Connolly D, Lund H, Mathiesen B, Leahy M. A review of computer tools for analysing the integration of renewable energy in various energy systems. Appl Energy 2010;87:1059–82.
[11] Hindsberger M, Ravn HF. Multiresolution modeling of hydro-thermal systems. In: PICA: 22nd IEEE power engineering society international conference on power industry computer applications, Sydney, Australia; 2001.
[12] Iyer RR, Grossmann IE. Synthesis and operational planning of utility systems for multiperiod operation. Comput Chem Eng 1998;22:979–93.
[13] Ahmadi P, Rosen MA, Dincer I. Multi-objective exergy-based optimization of a polygeneration energy system using an evolutionary algorithm. Energy 2012;46:21–31.
[14] Gassner M, Maréchal F. Thermo-economic optimisation of the polygeneration of synthetic natural gas (SNG), power and heat from lignocellulosic biomass by gasification and methanation. Energy Environ Sci 2012;5:5768–89.
[15] Chen Y, Adams II TA, Barton PI. Optimal design and operation of static energy polygeneration systems. Ind Eng Chem Res 2010;50:5099–113.
[16] Liu P, Gerogiorgis DI, Pistikopoulus EN. Modeling and optimization of polygeneration energy systems. Catal Today 2007;127:347–59.
[17] Liu P, Pistikopoulus EN, Li Z. A multi-objective optimization approach to polygeneration energy systems design. Process Syst Eng 2010;56:1218–34.
[18] Liu P, Pistikopoulus EN, Li Z. Environmentally benign process design of polygeneration energy systems. In: Design for energy and the environment. Taylor and Francis Group, LLC; 2010. p. 585–92.
[19] Fazlollahi S, Mandel P, Becker G, Maréchal F. Methods for multi-objective investment and operating optimization of complex energy systems. Energy 2012;45:12–22.
[20] Fazlollahi S, Maréchal F. Multi-objective, multi-period optimization of biomass conversion technologies using evolutionary algorithms and mixed integer linear programming (MILP). Appl Therm Eng 2013;50:1504–13.
[21] Rubio-Maya C, Uche-Marcuello J, Martinéz-Garcia A, Bayod-Rújula AA. Design optimization of a polygeneration plant fuelled by natural gas and renewable energy sources. Appl Energy 2011;88:449–57.
[22] Rubio-Maya C, Uche J, Martínez A. Sequential optimization of a polygeneration plant. Energy Convers Manage 2011;52:2861–9.
[23] Christidis A, Koch C, Pottel L, Tsatsaronis G. The contribution of heat storage to the profitable operation of combined heat and power plants in liberalized electricity markets. Energy 2011;41:75–82.
[24] Lythcke-Jørgensen C, Haglind F, Clausen LR. Exergy analysis of a combined heat and power plant with integrated lignocellulosic ethanol production. Energy Convers Manage 2014;85:817–27.
[25] Lythcke-Jørgensen C, Haglind F. Design optimization of a polygeneration plant producing power, heat, and lignocellulosic ethanol. Energy Convers Manage 2015;91:353–66.
[26] Lythcke-Jørgensen C, Münster M, Ensinas AV, Haglind F. Design optimization of flexible biomass-processing polygeneration plants using characteristic operation periods. World renewable energy congress XIII, Kingston-upon-Thames, London; 2014.
[27] Chen Y, Adams II TA, Barton PI. Decomposition strategy for the global optimization of flexible energy polygeneration systems. Am Inst Chem Eng 2012;58:3080–95.
[28] Mavrotas G, Diakoulaki D, Florios K, Georgiou P. A mathematical programming framework for energy planning in services' sector buildings under uncertainty in load demand: the case of a hospital in Athens. Energy Policy 2008;36:2415–29.
[29] Ortiga J, Bruno J, Coronas A. Selection of typical days for the characterisation of energy demand in cogeneration and trigeneration optimisation models for buildings. Energy Convers Manage 2011;52:1934–42.
[30] Domínguez-Moñoz F, Cejudo-López JM, Carrilo-Andrés A, Gallardo-Salazar M. Selection of typical demand days for CHP optimization. Energy Build 2011;43:3036–43.
[31] Fazlollahi S, Bungener SL, Mandel P, Becker G, Maréchal F. Multi-objectives, multi-period optimization of district energy systems: I. Selection of typical operating periods. Comput Chem Eng 2014;65:54–66.
[32] Hedegaard K, Münster M. Influence of individual heat pumps on wind power integration – energy system investments and operation. Energy Convers Manage 2013;75:673–84.
[33] Bungener S, Hackl R, Eetvelde GV, Harvey S, Marechal F. Multi-period analysis of heat integration measures in industrial clusters. Energy 2015;93:220–34.
[34] Nemet A, Klemes JJ, Varbanov PS, Kravanja Z. Methodology for maximising the use of renewables with variable availability. Energy 2012;44:29–37.
[35] DTU management engineering; Danish energy agency; 1 December 2013. [Online]. Available: http://www.ens.dk/sites/ens.dk/files/info/facts-figures/scenarios-analyses-models/models/IntERACT/wp03_-_interact_times-dk_phase_1.pdf [accessed 7 July 2015].
[36] Nord pool spot. "Nord pool spot." [Online]. Available: http://www.nordpoolspot.com/#/nordic/table [accessed 4 November 2014].
[37] Jack MW. Scaling laws and technology development strategies for biorefineries and bioenergy plants. Bioresour Technol 2009;100:6324–30.
[38] International Energy Agency. Key world energy STATISTICS 2014. Paris: International Energy Agency; 2014.
[39] Lythcke-Jørgensen C. Modelling and optimization of a steam co-generation plant with integrated bio-ethanol production. Kgs. Lyngby: Technical University of Denmark; 2012.
[40] Energinet.dk. "Market data". Nord pool spot. [Online]. Available: energinet.dk. [accessed 28 January 2015].
[41] http://www.streammodel.org/. "The STREAM modelling tool." Ea Energy Anal [accessed 3 April 2014].
[42] Elmegaard B, Houbak N. Simulation of the Avedøreværket unit 1 cogeneration plant with DNA. In: 16th International conference on efficiency, cost, optimization, simulation and environmental impact of energy systems, DK-2800 Kgs. Lyngby; 2003.
[43] Spliethoff H. Power generation from solid fuels. München (Germany): Springer-Verlag Berlin Heidelberg; 2010.
[44] Elmegaard B, Houbak N. DNA – a general energy system simulation tool. SIMS; 2005.
[45] Forrest J, Lougee-Heimer R. CBC user guide; 2015. [Online]. Available: http://www.coin-or.org/Cbc/.
[46] OpenSolver. OpenSolver; 2015. [Online]. Available: opensolver.org.
[47] Rolfsman B. Combined heat-and-power plants and district heating in a deregulated electricity market. Appl Energy 2004;78:37–52.
[48] Martinéz-Lera S, Ballester J, Martinéz-Lera J. Analysis and sizing of thermal energy storage in combined heating, cooling and power plants for buildings. Appl Energy 2013;106:127–42.
[49] Morris MD. Factorial sampling plans for preliminary computational experiments. Technometrics 1991;33(2):161–74.
[50] Frederiksen S, Werner S. Heat and cold loads. In: District heating and cooling. Lund (Sweden): Studentlitteratur AB; 2013. p. 67–112.
[51] Rong A, Lahdelma R. An effective heuristic for combined heat-and-power production planning with power ramp constraints. Appl Energy 2007;84:307–25.

APPENDIX E Journal paper 4

ISI Journal Paper

C.E. Lythcke-Jørgensen, A.V. Ensinas, M. Münster, and F. Haglind. *A methodology for designing flexible multi-generation systems*. Energy (in press):1-21, 2016.

This paper presents the developed design methodology, plus the contents and outcomes of *Case II*.

Energy xxx (2016) 1–21

Contents lists available at ScienceDirect

Energy

journal homepage: www.elsevier.com/locate/energy

A methodology for designing flexible multi-generation systems

Christoffer Lythcke-Jørgensen [a, *], Adriano Viana Ensinas [b], Marie Münster [c], Fredrik Haglind [a]

[a] Technical University of Denmark, Mechanical Engineering, Denmark
[b] École Polytechnique Fédérale de Lausanne, Industrial Process and Energy Systems Engineering, Switzerland
[c] Technical University of Denmark, Management Engineering, Denmark

ARTICLE INFO

Article history:
Received 1 October 2015
Received in revised form
26 January 2016
Accepted 27 January 2016
Available online xxx

Keywords:
Design optimization
Energy efficiency
Flexible operation
Multi-generation
Polygeneration
Smart energy systems

ABSTRACT

An FMG (flexible multi-generation system) consists of integrated and flexibly operated facilities that provide multiple links between the various layers of the energy system. FMGs may facilitate integration and balancing of fluctuating renewable energy sources in the energy system in a cost- and energy-efficient way, thereby playing an important part in smart energy systems.

The development of efficient FMGs requires systematic optimization approaches. This study presents a novel, generic methodology for designing FMGs that facilitates quick and reliable pre-feasibility analyses. The methodology is based on consideration of the following points: Selection, location and dimensioning of processes; systematic heat and mass integration; flexible operation optimization with respect to both short-term market fluctuations and long-term energy system development; global sensitivity and uncertainty analysis; biomass supply chains; variable part-load performance; and multi-objective optimization considering economic and environmental performance.

Tested in a case study, the methodology is proved effective in screening the solution space for efficient FMG designs, in assessing the importance of parameter uncertainties and in estimating the likely performance variability for promising designs. The results of the case study emphasize the importance of considering systematic process integration when developing smart energy systems.

1. Introduction

FMGs (flexible multi-generation systems) are integrated, dynamic facilities that convert one or several energy resources into multiple energy services and other valuable products, e.g. electricity, heating, cooling, bio-fuels, and bio-chemicals [1]. FMGs are characterised by their ability to adjust operation in response to fluctuating demand patterns and varying price schemes. In the present work, the following definition of an FMG is introduced:

- A flexible multi-generation system (FMG) is a system of integrated facilities that provide multiple links between layers of the energy system, enabling adjustable operation in response to changes in prices and demands of the consumed and delivered services.[1]

The main advantages of FMGs are: The embedded possibility for optimizing operation by altering feedstock, products and services depending on demand and market price [2–4]; the possibility of integrating and balancing generation from intermittent renewable energy resources such as wind, solar, wave and tidal in a cost-efficient way [5,7], and the possibility of achieving high aggregated conversion efficiencies through process integration [8–11]. Through the conversion, conditioning and storing of multiple energy vectors, FMGs integrate the various layers of the energy

[1] In specific cases, the definition of an FMG may be overlapping with the terms 'polygeneration' and 'energy hubs'. In a recent review, Adams and Ghouse [75] have defined 'polygeneration' as a thermochemical process which simultaneously generates electricity and produces at least one type of chemical or fuel without being a co- or tri-generation unit. 'Energy hubs' may refer to homes, large energy consumers, power plants or regions [76] as well as integrated facilities [4,77]. The FMG definition is introduced in order to characterize integrated facilities that may actively contribute to the balancing of the energy system.

* Corresponding author. Nils Koppels Allé 403, 2800 Kgs. Lyngby, Denmark. Tel.: +45 30 42 72 00.
E-mail address: celjo@mek.dtu.dk (C. Lythcke-Jørgensen).

http://dx.doi.org/10.1016/j.energy.2016.01.084
0360-5442/

Nomenclature

Latin letters

A_a	Area size [km^2]
b	Number of parameter value levels in Morris screening [−]
C_{HEN}	Heat exchanger network investment cost [Euro]
$C_{inv,k}$	Process investment cost [Euro]
$C_{inv,k0}$	Process reference investment cost [Euro]
c_b	Marginal biomass cost [Euro]
c_{b0}	Reference biomass cost [Euro]
$c_{b,tr}$	Marginal biomass logistics cost [Euro]
c_{op}	Operating cost [Euro]
D_p	Uncertainty distribution of parameter p [−]
$d_{tr,a}$	Mean transportation distance from area a [km]
$\dot{e}_f$	Thermal energy flow [kW]
EE	Elementary effect [-]
f	Model output function
G_i	CHOP group
$\Delta H_{s,i}$	Sum of enthalpy flows in temperature interval s [kW]
i	Annual discount rate [−]
M	Number of uncertain model parameters [−]
M_f	Investment scaling constant [−]
$\dot{m}_f$	Mass flow [kg/s]
$mean_i$	Estimated standard error of the mean [−]
$N_{CHOP,max}$	Maximum number of CHOP groups [−]
n_p	Number of characteristic parameter intervals [−]
O_j	Operating point
p	Parameter
q_a	Annual biomass cultivation in area a [ton]
$q_{b,an}$	Annual biomass demand [ton]
R	Product or service market
R_{th}	Thermal energy market
R_b	Local biomass market
r_a	Maximum transportation distance, area a [km]
SEE	Sigma-scaled elementary effect [−]
s_{max}	Number of temperature intervals [−]
T	Temperature [°C]
t_i	CHOP group, duration [h]
t_j	Operating point, duration [h]
$t_{PV,i}$	CHOP group, present value factor [h]
w	Number of repetitions in Morris screening [−]
Y_j	Operating point, year of occurrence [−]
y_k	Installation delay of process k [years]
y_{lt}	Facility lifetime [years]
Z_0	Global warming potential [tCO$_2$]
z_{inv}	Global warming potential of investments [tCO$_2$]
z_{op}	Global warming potential of operation [tCO$_2$]

Greek letters

Δ	Perturbation factor in Morris screening [−]
$\lambda_{k,i}$	Process load of process k in period i [−]
$\nu_{k,i}$	Operation of process k in period i [−]
σ_k	Dimension of process k [−]
σ_{k0}	Process k reference dimension [−]
σ_{ut}	Utility process dimension [−]
ω_k	Installation decision for process k [−]

Subscripts

a	Biomass cultivation area index
b	Biomass flow index
f	Thermal and mass flow index
i	Period index
j	Operating point index
k	Process index
l	Layer index, used in the Mixed Integer-Linear Programming model
n	Characteristic parameter interval index
p	Parameter index
r	Market index
s	Temperature interval index
0	Reference

Abbreviations

AD	Combined anaerobic digester and biogas upgrading facility
BB	Biomass boiler
CCHP	Combined cooling, heating and power
CHOP	Characteristic operating pattern
CHP	Combined heat and power
DESS	Distributed energy supply system
FMG	Flexible multi-generation system
GB	Gas boiler
GT	Gas turbine
GWP100a	100-years global warming potential
HP	Ground-based district heating heat pump
LCA	Life cycle assessment
MILP	Mixed integer-linear programming
MINLP	Mixed integer-nonlinear programming
NPV	Net present value
SMG	Static multi-generation plant
SR	Steam Rankine cycle

system and are capable of providing supply-demand flexibility that can counteract energy system imbalances induced by e.g. intermittent renewable energy sources. In principle, FMGs can therefore be seen as efficient energy system valves that may play an important part in the development and operation of smart energy systems [12,13]. The generic FMG concept is illustrated in Fig. 1.

By definition, FMGs may be either centralized facilities or distributed systems, as long as the various facilities are integrated. The present manuscript differentiates between a *plant*, in which all considered facilities are co-located, and a *system*, in which facilities are distributed on several locations. It should be emphasized that FMGs may include static processes, e.g. cellulosic ethanol production [14] as well as intermittent processes that are not fully dispatchable, e.g. wind turbines and solar heating, as long as the combined system has a degree of operational flexibility.

The issues to be considered when designing FMGs comprise: The selection of processes and technologies from many alternatives; geographical location, dimensioning, and integration of processes with respect to thermal and mass flows; operation optimization with respect to hourly demand and price fluctuations and long-term energy system development; determination of local resource availability; investment planning; systematic evaluation of design uncertainties; and consideration of both economic and environmental objectives. All of these issues must be considered simultaneously as they affect one another. To cope with this complexity, a systematic optimization approach is needed for the design of FMGs [8].

Please cite this article in press as: Lythcke-Jørgensen C, et al., A methodology for designing flexible multi-generation systems, Energy (2016), http://dx.doi.org/10.1016/j.energy.2016.01.084

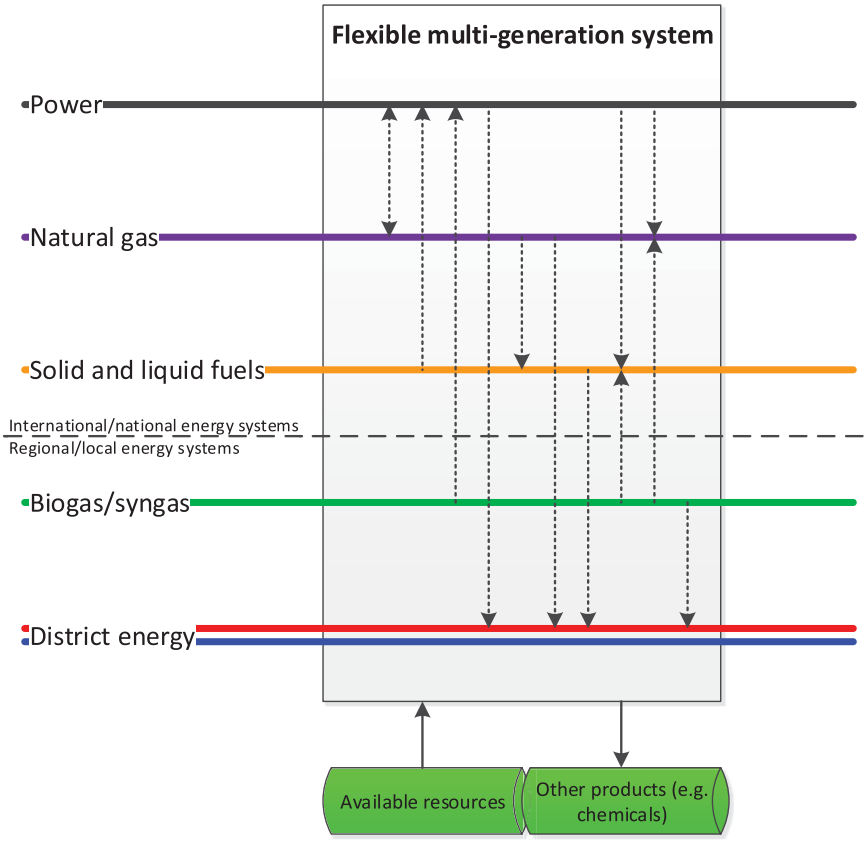

Fig. 1. Conceptual sketch of a flexible multi-generation system. Dotted arrows indicate a range of technological pathways for linking the energy system layers.

One branch of multi-generation plants treated in the literature combines the generation of power and production of chemicals. Gassner and Maréchal [15] presented a combined MINLP (mixed integer-nonlinear programming)/MILP (mixed integer-linear programming) methodology for the synthesis of facilities producing fuel from biomass through thermochemical conversion. The methodology considered the selection and dimensioning of processes, systematic process integration using pinch analysis, and assessment of multiple objectives including thermo-economic performance. In a second work the methodology was enhanced to allow for the systematic inclusion of LCA (life cycle assessment) in the design evaluation [16]. The methodology was later applied in a case study of a SMG (static multi-generation plant) generating fuel and electricity from biomass [17]. The developed methodology did not consider flexible operation and input parameter uncertainties.

Liu et al. studied SMGs generating power and methanol. In five related works, the group first presented a multi-period MILP model for the design and investment planning optimization of such SMGs whilst considering static operating conditions over periods of 5 years [18]. The model was later upgraded to an MINLP model [19] and extended to allow for multi-objective optimization [20] and stochastic programming using a decomposition strategy [21]. The group further presented one methodology for general investment planning and one for detailed design configuration of SMGs [22]. However, neither of the presented methodologies considered short-term operation flexibility.

Chen et al. also studied the multi-generation of power and chemicals. In three consecutive works, the group first presented a deterministic superstructure-based optimization model for designing static SMGs coproducing power, naphtha, diesel, and methanol from coal and biomass [23]. The model was later enhanced to allow for flexible operation optimization with respect to price variations over seasonal peak- and off-peak periods, and, based on a case study, the group concluded that FMGs may achieve higher NPVs (net present values) than static ones because of the operation flexibility, however at the cost of larger investments [24]. In a third study, the group implemented a modified decomposition algorithm based on the generalized Benders decomposition in their optimization model to reduce computational time [25], and demonstrated in two case studies that the modified methodology achieved faster calculation times than the BARON solver [26]. The group applied simple energy balances rather than detailed process integration methodologies to simulate process integration possibilities, which may have led to overestimated efficiency improvements, as also discussed by the authors [27]. Furthermore, uncertainties were not considered.

Another branch of multi-generation plants are facilities based on the CCHP (combined generation of cooling, heating, and power), also known as trigeneration. Marnay et al. [28] presented a methodology for minimizing the overall costs of CCHPs in commercial buildings by selecting and dimensioning technologies and optimizing operation based on diurnal load profiles. Rubio-Maya et al. [29,30] presented a heuristic, two-level approach for designing local FMGs generating power, heat, cooling and fresh water. Selection of technologies and a preliminary process dimensioning were handled in a first step based on monthly-averaged requirements, while a second step dealt with the final dimensioning of components, including thermal energy storage, based on monthly mean-day demands. Piacentino et al. [31] presented a deterministic MILP-based tool for optimizing trigeneration-based micro-grids with thermal storages with respect to NPV. Capuder

Please cite this article in press as: Lythcke-Jørgensen C, et al., A methodology for designing flexible multi-generation systems, Energy (2016), http://dx.doi.org/10.1016/j.energy.2016.01.084

and Mancarella [32,33] presented a framework for the techno-economic and environmental comparison of seven distributed FMG options for co-generating heat and power. The framework considered half-hour time steps on typical seasonal days, thermal energy storage, and ramp rate constraints between successive time periods. The group found that increased operation flexibility resulted in significant savings in investment and operating costs as well as in a reduced environmental impact when compared to the reference case of a district heating boiler. Recently, Capuder et al. [34] extended their work to consider the economic value of operational flexibility and investment flexibility under long-term operational uncertainty and found that consideration of investment flexibility both reduced expected costs and economic risks associated with investments in distributed FMGs co-generating heat and power.

With regard to DESS (distributed energy supply systems), Voll et al. [35] developed an approach for the superstructure-free synthesis and optimization of DESS using an evolutionary algorithm and applied the method on a numerical example of a DESS with time-varying heating and cooling loads. Following this, Voll et al. [36] presented a framework for automated superstructure generation and optimization of DESS using an MILP model. The group further developed a method for reducing non-linear DESS optimization problems into MILP models using a multivariate piecewise-affine surrogate modelling approach [37], and a method for exploring the near-optimal solution space when optimizing DESS [38]. In a recent study, the group presented a hybrid approach for optimizing the synthesis of renewable electricity systems by combining heuristic-based pre-selection of candidate technologies with the previously developed automated superstructure generation and optimization of DESS [39]. Zhou et al. [40] presented a two-stage stochastic programming model for designing DESS which further allowed for the consideration of uncertainties in the optimization. Finally, Leung Pah Han et al. [41] presented an iterative method combining MILP/MINLP for designing local production systems that integrate food, water, and energy systems based on annual demands, with the aim of minimizing the cumulative exergy destruction.

Concerning urban multi-generation plants, Lythcke-Jørgensen and Haglind [42] studied the design and operation optimization of an FMG generating power and heat and producing cellulosic ethanol. The study found that short-term operating patterns may be critical for the overall economy and efficiency of FMGs. Maréchal et al. [43] presented a multi-period, multi-objective MINLP/MILP approach for deterministic design optimization that comprised technology selection and dimensioning, process integration, facility location selection, and network layout. By considering monthly static operating patterns, Fazlollahi and Maréchal [44] used parts of this methodology for designing FMGs that provide energy services for district energy systems. In three parallel works, the group extended their work by incorporating the following methodology: A method for approximating energy system conditions by a number of typical periods with hourly and aggregated multi-hour time steps [45]; a model of daily thermal storages [46]; and a model of distribution networks [47]. Shortcomings of the combined methodology are the facts that only cyclic short-term operating patterns may be considered using the typical periods approach, and that input parameter uncertainties are not considered.

This study presents a novel, systematic methodology for designing FMGs. It applies node-based superstructure representation and is based on a genetic algorithm and multi-period MILP approach [48]. The purpose of the methodology is to conduct quick and reliable pre-feasibility analyses of FMGs for assessing which of the facility designs that would be efficient in a given energy system context, rather than estimating the optimal performance of pre-defined facility designs. The novelty of the methodology lies in the fact that it simultaneously considers the following: Selection, location, and dimensioning of processes from many alternatives; systematic heat and mass integration using pinch analysis; flexible operation optimization with respect to both short-term market fluctuations and long-term energy system development through the application of the CHOP (Characteristic Operating Pattern) method [49]; investment planning; global sensitivity and uncertainty analysis; consideration of local resource availability, biomass supply chains, and market sizes; variable part-load performance; and multi-objective optimization considering NPV and 100-years global warming potential (GWP100a). To the author's best knowledge, no previous methodology has considered all of these aspects in an integrated, systematic manner.

The paper is structured as follows: After the introduction, which also features a short literature review on methodologies for designing multi-generation systems, the developed design methodology is presented in Section 2. In Section 3, the methodology is applied in a case study of a conceptual FMG co-generating power and heat and producing cellulosic ethanol, synthetic natural gas, and fertilizer from natural gas, domestic and industrial waste, straw, and manure. Section 4 contains a discussion on advantages, drawbacks, and development possibilities for the design methodology. A conclusion on the study is given in Section 5.

2. Design methodology

The design methodology developed in the present study is a tool for optimizing the design and operation of FMGs by coupling process models with energy system information, as illustrated in Fig. 2. The structure of the design methodology is presented in Fig. 3, which illustrates how the optimization problem has been decomposed into several parts. The design methodology is introduced in this section, which is structured according to the five overarching steps of the methodology.

2.1. Input data

In general, four types of input data are required for running the design methodology: Process and equipment models, energy system data, local resource data, and life cycle inventory data. If sensitivity and uncertainty analyses are to be performed on selected designs, uncertainty distributions for input data D_p must be defined for all the considered uncertain input parameters p.

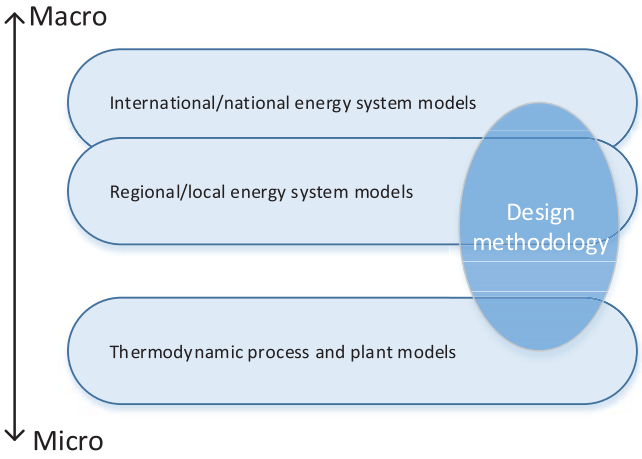

Fig. 2. Visualization of how the design methodology interacts with models at various levels.

Please cite this article in press as: Lythcke-Jørgensen C, et al., A methodology for designing flexible multi-generation systems, Energy (2016), http://dx.doi.org/10.1016/j.energy.2016.01.084

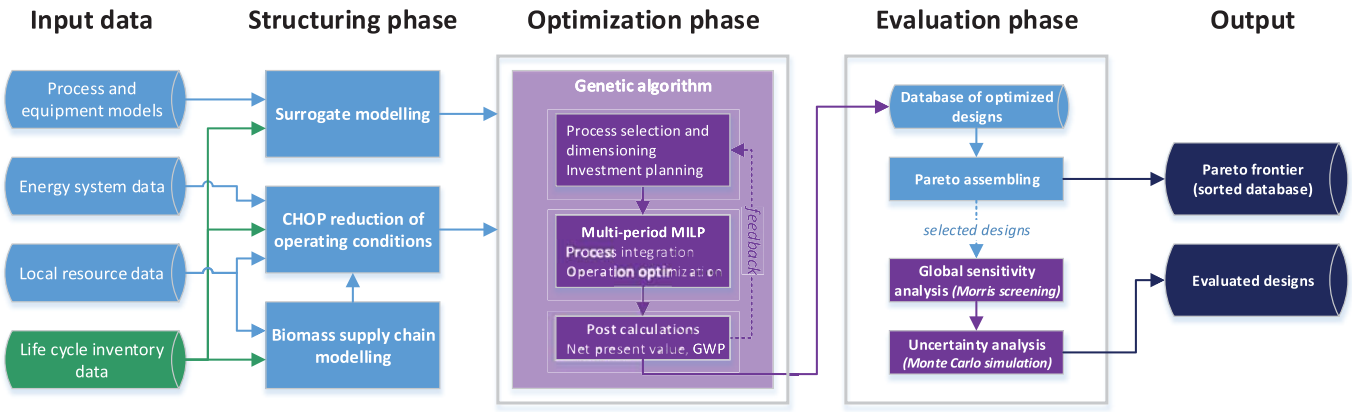

Fig. 3. Design methodology structure.

2.1.1. Process and equipment models

The first input to the design methodology is models of the processes and equipment to be considered for the FMG. The models can be detailed thermodynamic and chemical models as well as simpler black box models, as long as they provide the information required for developing surrogate models, as discussed in Section 2.2.

2.1.2. Energy system data

The second input to the design methodology is data on the surrounding energy system that the FMG is to operate within. Depending on the processes considered, energy system data may include parameters such as power price, demands for district energy, fossil fuel prices, subsidy schemes etc. All information must be provided for short time intervals, a few hours or less, in order to include details on short-term fluctuations in prices and demands that the FMG may respond to. The data must be provided for the entire lifetime of the FMG.

2.1.3. Local resource data

Local resource data describe the availability, costs, and logistics of local resources considered for processing in the FMG, e.g. biomass, manure, domestic and industrial waste, etc. This information may be essential for the economic viability of FMGs, as transportation and storage costs for processing locally distributed resources may induce a diseconomy-of-scale trend that can exceed the economy-of-scale benefits for larger processing equipment, as also discussed by Jack [50].

2.1.4. Life cycle inventory data

The environmental impact parameter considered in the design methodology is the 100-years global warming potential (GWP100a). GWP100a is an indicator of the global warming impact over a 100-year period from materials mining, production of equipment, installation, operation and maintenance, and decommissioning of a facility, measured in equivalent tons of CO_2 emissions. In order to consider the minimization of GWP100a when designing FMGs, life cycle inventory data must be provided on all considered process equipment, consumed resources, displaced production and consumption etc.

2.2. Structuring phase

2.2.1. CHOP-reduction of external operating conditions

In order to reduce computation time, external operating conditions are reduced using the Characteristic Operating Pattern (CHOP) method introduced by Lythcke-Jørgensen et al. [49]. The CHOP method is a visually-based aggregation method for clustering data on external operating conditions. Aggregation is conducted based on important parameter values rather than time of occurrence, thereby preserving important information on short-term relations between the relevant operating parameters. The CHOP method is briefly introduced below. Details on contents, validation, and application of the CHOP method have been given previously [49].

The CHOP method assumes quasi-static operation and is applicable on datasets in the form of operating points O_j, with each point being characterised by a year of occurrence after operation initiation Y_j, a duration t_j, and a number of operating condition parameters $\boldsymbol{p_j}$.

$$O_j = \left\{ Y_j, t_j, \boldsymbol{p_j} \right\} \tag{1}$$

A principal sketch of the data aggregation principle applied in the CHOP method is presented in Fig. 4.

The CHOP method consists of the three principal steps, which are described below:

2.2.1.1. Entity selection. In the first step of the CHOP method, the user has to identify the relevant volatile operating parameters $\boldsymbol{p}$ for the FMG of interest. The parameters selected are to be seen as boundary conditions for the operation of the FMG, and parameter values are therefore assumed to be unaffected by FMG operation. This assumption needs to be validated, perhaps à posteriori, when applying the design methodology. Relevant operating parameters could be power price, fossil fuel prices, and CO_2 tax schemes, depending on the processes considered for the FMG and the energy system of interest. If price functions can be established for some boundary conditions as a function of FMG operation, the function constants can be captured in the vector $\boldsymbol{p_i}$ as well.

2.2.1.2. Clustering criteria. Having identified the relevant parameters $\boldsymbol{p}$, the second step is to define the criteria for clustering operating points. This is done by splitting the value range of each relevant parameter p into a number of characteristic intervals, n_p, using a graphic-based two-step approach based on the cumulative parameter curve. The process is illustrated in Fig. 5 with power price chosen as parameter.

a) **Important values**: Some parameter values may be of special interest, making it relevant to introduce a break at these points. For instance, for the power price example it may be relevant to

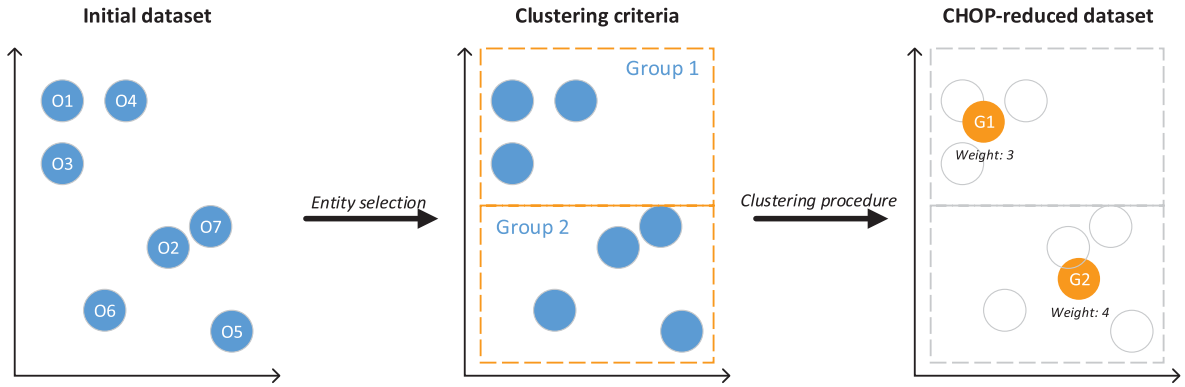

Fig. 4. Principal sketch of the data aggregation principle applied in the CHOP method. Operating points O_j are clustered and merged into CHOP groups G_i with aggregated weight factors. Figure from Ref. [49].

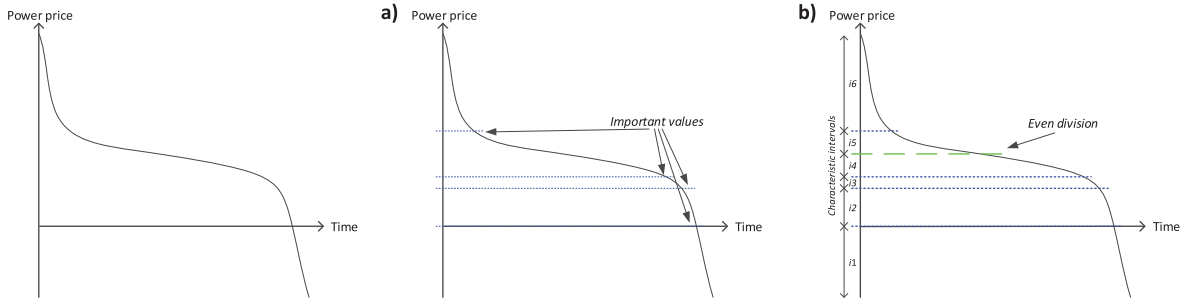

Fig. 5. Illustrative example of the suggested two-step approach for defining characteristic intervals based on the cumulative parameter curve (left). Interval break points are set for a) Important values, and b) Even division. The characteristic intervals are indicated on the second axis in b). Figure from Ref. [49].

introduce a break at a power price of 0.00 Euro/MWh to make sure that negative prices are grouped together. Also, if an operating decision, e.g. turning on a piece of equipment, is dependent on a given power price, an interval break should be introduced at this price as well.

b) **Even division**: If the already set break-points are far from each other in terms of both parameter value and duration, it is suggested that additional interval breaks are introduced to minimize the span. The break-points should be located such that the parameter value range is constant for each of the intervals.

2.2.1.3. Cluster procedure. Having defined the clustering criteria, the final step is to cluster the data in order to establish the final CHOP-groups G_i to replace the initial dataset of operating points O_j. Each G_i is characterised by a unique combination of characteristic parameter intervals, causing the maximum number of CHOP-groups to be:

$$N_{CHOP,max} = \prod_{p} n_p \tag{2}$$

All initial operating points O_j are sorted into the CHOP groups G_i based on parameter values. Any G_i with no O_j belonging to it is discarded. Each included G_i becomes an operating point in the final CHOP-reduced dataset characterised by a duration t_i (the sum of durations of the aggregated data points), a present value factor $t_{PV,i}$, and a number of operating condition parameters $\boldsymbol{p_i}$, which are the weighted average parameter values of the aggregated data points.

$$G_i = \{t_i, t_{PV,i}, \boldsymbol{p_i}\} \tag{3}$$

$$t_i = \sum_{O_j \in G_i} t_j \tag{4}$$

$$t_{PV,i} = \sum_{O_j \in G_i} \frac{t_j}{(1+i)^{Y_j}} \tag{5}$$

$$\boldsymbol{p_i} = \frac{\sum_{O_j \in G_i} \boldsymbol{p_j} \cdot t_j}{t_i} \tag{6}$$

with i being the annual discount rate.

If investment planning is not taken into account, a single CHOP-reduced dataset can be used for representing operating conditions over the lifetime of the FMG to be designed. In case investment planning is to be considered, one has to define a number intervals at the end of which novel investments are allowed, e.g. every 5th year, as suggested by Liu et al. [18]. If so, individual CHOP dataset must be developed for each investment interval, increasing the overall number of periods significantly in the final optimization model.

2.2.2. Surrogate modelling

In the design methodology, process and market models are reduced to step-wise linearized surrogate models in order to fit them into the optimization model developed. A generic illustration of a surrogate process model $K(\sigma_k, \lambda_{k,i})$, defined by a dimension σ_k and load $\lambda_{k,i}$, is presented in Fig. 6.

Please cite this article in press as: Lythcke-Jørgensen C, et al., A methodology for designing flexible multi-generation systems, Energy (2016), http://dx.doi.org/10.1016/j.energy.2016.01.084

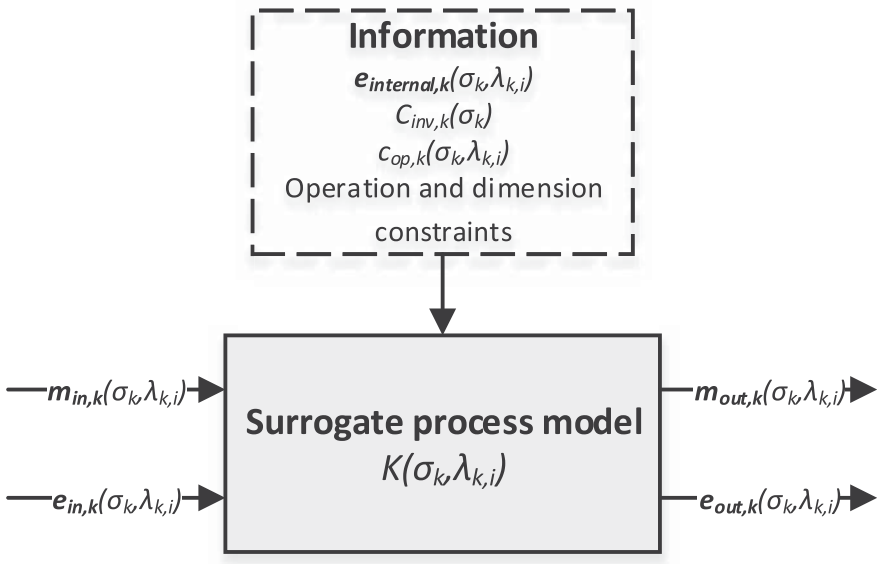

Fig. 6. Generic illustration of a surrogate process model.

Each surrogate process model $K(\sigma_k, \lambda_{k,i})$ is characterized by: A number of mass flows into the process $\dot{\boldsymbol{m}}_{\boldsymbol{in,k}}(\sigma_k, \lambda_{k,i})$, and mass flows out of the process $\dot{\boldsymbol{m}}_{\boldsymbol{out,k}}(\sigma_k, \lambda_{k,i})$; a number of internal thermal energy flows $\dot{\boldsymbol{e}}_{\boldsymbol{internal,k}}(\sigma_k, \lambda_{k,i})$, thermal energy flows into the process $\dot{\boldsymbol{e}}_{\boldsymbol{in,k}}(\sigma_k, \lambda_{k,i})$, and thermal energy flows out of the process $\dot{\boldsymbol{e}}_{\boldsymbol{out,k}}(\sigma_k, \lambda_{k,i})$; plus investment costs $C_{inv,k}(\sigma)$ and operating costs $c_{op,k}(\sigma, \lambda)$. Furthermore, dimensional and operational constraints may be associated with each $K(\sigma_k, \lambda_{k,i})$. Each mass flow function $\dot{m}_{f,i}(\sigma_k, \lambda_{k,i})$ and operating cost function $c_{op,k}(\sigma_k, \lambda_{k,i})$ must be a linear or step-wise linear function of the load $\lambda_{k,i}$ as defined in equations (7) and (8). Each thermal energy flow function $\dot{e}_{f,i}(\sigma_k, \lambda_{k,i})$ is characterized by an inlet temperature $T_{in,f}$, an outlet temperature $T_{out,f}$, and a heat flow capacity $\dot{CP}_{f,i}(\sigma_k, \lambda_{k,i})$ as defined in equation (9), with the latter being a linear or step-wise linear function of the load $\lambda_{k,i}$ as defined in equation (10).

$$\dot{m}_{f,i}(\sigma_k, \lambda_{k,i}) = \boldsymbol{f}_{\boldsymbol{linear}}(\sigma_k, \lambda_{k,i}) = \begin{cases} \sigma_k(a_1\lambda_{k,i} + b_1), \lambda_{k,i}\varepsilon I_1 \\ \sigma_k(a_2\lambda_{k,i} + b_2), \lambda_{k,i}\varepsilon I_2 \\ \dots \end{cases} \quad (7)$$

$$c_{op,k}(\sigma_k, \lambda_{k,i}) = \boldsymbol{f}_{\boldsymbol{linear}}(\sigma_k, \lambda_{k,i}) = \begin{cases} \sigma_k(c_1\lambda_{k,i} + d_1), \lambda_{k,i}\varepsilon I_1 \\ \sigma_k(c_2\lambda_{k,i} + d_2), \lambda_{k,i}\varepsilon I_2 \\ \dots \end{cases} \quad (8)$$

$$\dot{e}_{f,i}(\sigma_k, \lambda_{k,i}) = \left\{\dot{CP}_f(\sigma_k, \lambda_{k,i}), T_{in,f}, T_{out,f}\right\} \quad (9)$$

$$\dot{CP}_{f,i}(\sigma_k, \lambda_{k,i}) = \boldsymbol{f}_{\boldsymbol{linear}}(\sigma_k, \lambda_{k,i}) = \begin{cases} \sigma_k(g_1\lambda_{k,i} + h_1), \lambda_{k,i}\varepsilon I_1 \\ \sigma_k(g_2\lambda_{k,i} + h_2), \lambda_{k,i}\varepsilon I_2 \\ \dots \end{cases} \quad (10)$$

In the equations, $I_1, I_2, \dots$ are the load intervals for which the step-wise linear functions apply, while $\{a, b, c, d, g, h\}$ represent linear function constants. Note that power flows are modelled as mass flows as they do not require quality differentiation in process integration methods.

To represent possible economy of scale effects, power laws [51] are used to calculate investment costs $C_{inv,k}(\sigma_k)$ of the surrogate process models as a function of the dimension σ_k and a scaling constant $M_{f,k}$:

$$C_{inv,k}(\sigma_k) = C_{inv,k0}\left(\frac{\sigma_k}{\sigma_{k0}}\right)^{\mathrm{M_{f,k}}} \quad (11)$$

with $C_{inv,k0}$ being the reference investment cost and σ_{k0} the reference dimension of the process K.

Multiple process models may be merged into combined surrogate models if they are synchronized, i.e. their dimensions are aligned and they share the same load pattern at all times. Processes with non-synchronised dimensions and load patterns must be assigned individual surrogate models.

A generic illustration of surrogate models for product or service markets, $R(\boldsymbol{\lambda_i})$, thermal energy markets $R_{th}(\boldsymbol{\lambda_i})$, and local biomass markets $R_b(q_{b,an})$, which are functions of the FMG load vectors $\boldsymbol{\lambda_i}$, are presented in Fig. 7.

Each surrogate product market model R is characterized by: Mass flows of bought and sold products $\dot{m}_{bought}(\lambda)$, $\dot{m}_{sold}(\lambda)$; product price as a function of FMG operation $c(\lambda)$; and production and demand constraints. Each surrogate thermal energy market model R_{th} is characterised by: Forward and return thermal energy flows $\dot{e}_{forward}(\lambda)$, $\dot{e}_{return}(\lambda)$; thermal energy service price as a function of FMG operation $c_{th}(\lambda)$; temperatures of the thermal flows $T_{forward}$, T_{return}; and generation and demand constraints. Each surrogate local biomass market model is characterized by a mass flow of biomass $\dot{m}_b(q_{b,an})$ and a vector of marginal biomass costs $\boldsymbol{c_b}(q_{b,an})$ as functions of the annual biomass demand $q_{b,an}$, as described in more detail in Section 2.2.3.

2.2.3. Biomass supply chain modelling

If local biomass resources are to be consumed, a biomass supply chain model must be established to relate the marginal biomass unit cost to the biomass feedstock consumption. As discussed by e.g. Jack [50], transportation costs may be central for the economic analysis when using local biomass resources. In the present methodology, a generic biomass supply chain model inspired by a model for sugar beet from the Biochain Project has been integrated [52].

In the model, the biomass unit cost $c_b(q_{b,an})$ as a function of the annual biomass quantity demanded $q_{b,an}$ is assumed to consist of two components, namely a reference cost c_{b0} and a cost for transportation, $c_{b,tr}(q_{b,an})$. The reference cost is a fixed cost representing

Please cite this article in press as: Lythcke-Jørgensen C, et al., A methodology for designing flexible multi-generation systems, Energy (2016), http://dx.doi.org/10.1016/j.energy.2016.01.084

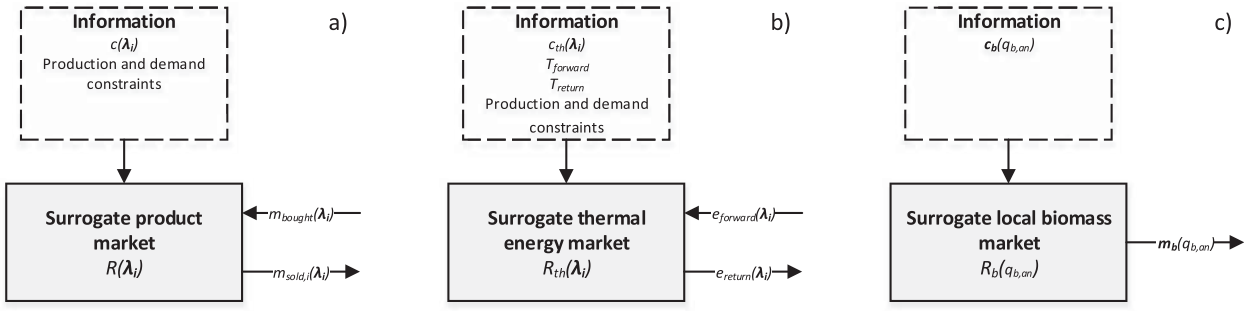

Fig. 7. Generic illustration of a) a surrogate product or service market, b) a surrogate thermal energy market, and c) a surrogate local biomass market.

the price paid to the local farmers for the biomass, while the transportation cost represents the variable costs of logistics for delivering biomass to the FMG.

$$c_b\left(q_{b,an}\right) = c_{b0} + c_{b,tr}\left(q_{b,an}\right) \tag{12}$$

In order to calculate $c_{b,tr}(q_{b,an})$, the land around the FMG is assumed divided as illustrated in Fig. 8.

It is assumed that the transportation cost for all biomass cultivated in an area A_h is constant and equal to the cost of transporting the biomass the mean transportation distance $d_{tr,h}$, which is calculated as

$$d_{tr,a} = r_{a-1} + \left(\frac{r_a - r_{a-1}}{\sqrt{2}}\right) \tag{13}$$

The marginal biomass unit cost $c_b(q_{an})$ is then calculated as

$$\boldsymbol{c_b}\left(q_{b,an}\right) = c_{b,ref} + \begin{cases} c_{trans,1}\left(d_{tr,1}\right) \middle| q_{b,an} \in [0; q_1] \\ c_{trans,2}\left(d_{tr,2}\right) \middle| q_{b,an} \in [q_1; q_1 + q_2] \\ \cdots \\ c_{trans,a}\left(d_{tr,a}\right) \middle| q_{b,an} \in \left[\sum_{a-1} q_a; \sum_i q_a\right] \end{cases} \tag{14}$$

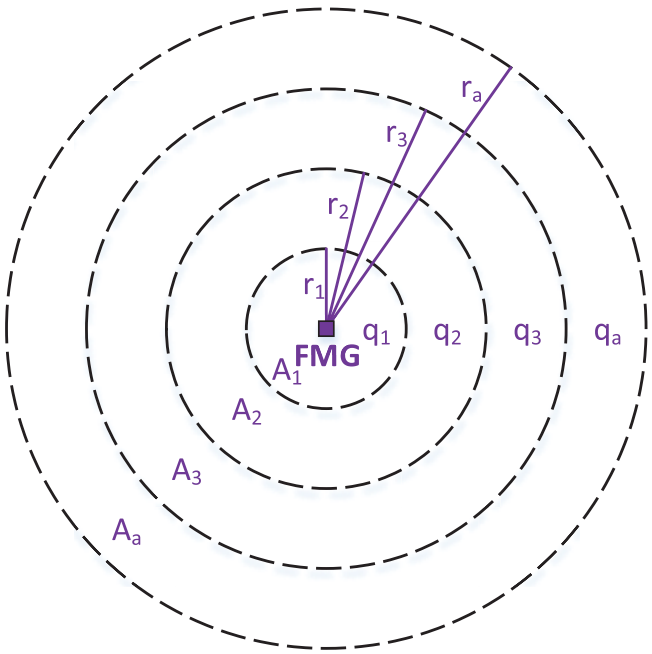

Fig. 8. Applied land division around the FMG, with each circular area $\boldsymbol{A_a}$ being represented by an annual biomass production quantity $\boldsymbol{q_a}$, a minimum transportation distance $\boldsymbol{r_{a-1}}$ and a maximum transportation distance $\boldsymbol{r_a}$. The number of circular areas $\boldsymbol{A_a}$ is defined by the user.

The annual biomass cultivation q_a in each area A_a is calculated from the input data on local resources.

The identified marginal biomass costs are included in the CHOP-reduced dataset for external operating conditions. This implies that any variation in the marginal biomass costs over the seasons or years can be taken into account in the optimization model. If several local biomass feedstocks are considered for processing, multiple BCM models can be defined in the design methodology.

2.3. Optimization phase

The optimization phase of the design methodology is based on a genetic algorithm and a multi-period mixed integer-linear programming (MILP) model from the OSMOSE software [48], which is developed at École Polytechnique Fédérale de Lausanne, Industrial Process and Energy Systems Engineering lab. In short, the optimization phase consists of three steps: 1. A genetic algorithm, used for selecting, locating, and dimensioning processes to be included in an FMG, and deciding upon possible investment plans; 2. a multi-period MILP model for optimizing process integration and operation of the given processes over the lifetime of the facility, and 3. a post calculation step for calculating the overarching objective function values of each optimized design. The calculated objective function values are provided as feedback to the genetic algorithm. The three steps are described in detail below.

2.3.1. Genetic algorithm

A genetic algorithm developed at EPFL [48] is used for selecting, locating and dimensioning processes to be included in the FMG, and for determining the strategy if investment planning is considered. The genetic algorithm is preferred as the master optimization algorithm as it can be used for solving linear as well as non-linear models and is capable of conducting multi-objective optimization [53].

In short, a genetic algorithm is a heuristic optimization algorithm that imitates the process of natural selection for solving an optimization problem. The variables of the optimization problem are seen as 'genes', while the objective function or functions describe the 'Darwinian fitness' of a solution. To start with, a population of a defined number of solutions with randomly assigned genes is generated, and the fitness of each solution is assessed. Next, a second population is 'bred' from a *selected* number of well-performing 'parent' solutions from the first population. The new solutions inherit genes from the parent solutions as defined by the genetic operator *crossover*, while some of the inherited genes may be altered by the genetic operator called *mutation*. The genetic algorithm then iterates over a defined number of generations in search for optimal combinations of genes.

When running the genetic algorithm in OSMOSE, one defines the population size and number of generations, while the algorithm

Please cite this article in press as: Lythcke-Jørgensen C, et al., A methodology for designing flexible multi-generation systems, Energy (2016), http://dx.doi.org/10.1016/j.energy.2016.01.084

has pre-defined settings for selection, mutation, and crossover [48]. For general information on genetic algorithms, consult e.g. Ref. [54].

The objectives of the genetic algorithm are to minimize the negative net present value $NPV(\boldsymbol{\omega}, \boldsymbol{\sigma}, \boldsymbol{y})$ and the global warming potential $GWP100a(\boldsymbol{\omega}, \boldsymbol{\sigma}, \boldsymbol{y})$. Variables considered are ω_k, the decision of whether or not a process or piece of equipment k should be installed at a given location; σ_k, the dimension of k; and y_k, the installation delay of k in years. The optimization problem to be solved by the genetic algorithm in the design methodology can be written in condensed form as

$$\begin{cases} \min_{\omega,\sigma,\boldsymbol{IP}} \begin{cases} -NPV(\boldsymbol{\omega}, \boldsymbol{\sigma}, \boldsymbol{y}) \\ GWP100a(\boldsymbol{\omega}, \boldsymbol{\sigma}, \boldsymbol{y}) \end{cases} \\ \textit{with variables} \\ \omega_k \in \{0, 1\} \\ \sigma_k \in [\sigma_{k,min}, \sigma_{k,max}] \\ y_k \end{cases} \tag{15}$$

Infrastructure for connecting facility locations is dimensioned by the genetic algorithm as well. The methodology is therefore not advantageous for systems with a large number of location options. Back-up utility processes are not dimensioned by the genetic algorithm, but by the MILP model based on required maximum capacities in the expected operating pattern.

2.3.2. Mixed integer-linear programming model

Given the selection and location $\boldsymbol{\omega}$, the dimension $\boldsymbol{\sigma}$, and the time of instalment $\boldsymbol{y}$ for all processes k, process integration and operation optimization over the lifetime of the FMG can be conducted. In order to reduce computation time and to guarantee that global optimality is reached for the operation optimization, a multi-period mixed integer-linear programming (MILP) model [48] is established to minimize operation costs $c_{op,i}(\boldsymbol{\nu_i}, \boldsymbol{\lambda_i})$ of the given FMG layout in each CHOP group i, which in total represents operation optimization over the lifetime of the facility. The variables are: $\nu_{k,i}$, the decision on whether a process k is running or shut down in period i; and $\lambda_{k,i}$, the load of the process if it is running.

The MILP model is constructed so that each type of mass flow in the system has its own layer l. Mass balance applies for each layer over each period i and is included as a constraint in the MILP model.

$$\sum \dot{m}_{f,l,i} = 0 \tag{16}$$

Special layers are constructed for thermal energy flows, for which pinch analysis [55] is applied to optimize heat integration. As heat integration over geographical distances may not be feasible, a thermal energy layer must be defined for each area within which heat integration is feasible. If all facilities considered in an FMG are co-located, it may be sufficient to define a single thermal energy layer.

As mentioned previously, hot and cold thermal energy flows $\dot{\boldsymbol{e}}(\boldsymbol{\sigma}, \boldsymbol{\lambda_i})$ from processes and markets are assumed to have step-wise constant heat capacity flow rates $\dot{\boldsymbol{CP}}(\boldsymbol{\sigma}, \boldsymbol{\lambda_i})$ over their temperature ranges. Assuming a pinch temperature difference of 10 K, the temperatures of hot streams are shifted 5 K up and the temperatures of cold streams are shifted 5 K down. For each thermal layer in the FMG model, enthalpy balances ΔH are calculated for each temperature interval s:

$$\Delta H_{s,i} = (T_s - T_{s-1}) \sum_s \dot{CP}_s(\boldsymbol{\sigma}, \boldsymbol{\lambda_i}) \tag{17}$$

To satisfy the first law of thermodynamics, the sum of all temperature interval enthalpy flows in each thermal energy layer must be zero. Furthermore, the sum of enthalpy flows from the first temperature interval to any of the other temperature interval in each thermal energy layer must never be below zero to make sure that the 2nd law of thermodynamics is satisfied:

$$\sum \Delta H_{s,i} = 0 \tag{18}$$

$$\sum_{s=1}^{m} \Delta H_{s,i} \geq 0 \quad \forall m \in \{1, 2, \ldots, s_{max}\} \tag{19}$$

The optimization problem to be solved by the MILP model in the design methodology can be written in condensed form as

$$\begin{cases} \textit{given}(\boldsymbol{\omega}, \boldsymbol{\sigma}, \boldsymbol{y}) \\ \min_{\lambda_i, \nu_i} c_{op,i}(\boldsymbol{\nu_i}, \boldsymbol{\lambda_i}) \\ \textit{with variables} \\ \nu_{k,i} \in \{0, 1\} \\ \lambda_{k,i} \in [\lambda_{k,min}, \lambda_{k,max}] \\ \textit{and constraints} \\ (16), (18), (19) \\ \textit{load and demand constraints} \end{cases} \tag{20}$$

Once the MILP model has been solved, the global warming impact of the optimized operation $z_{op,i}(\boldsymbol{\nu_i}, \boldsymbol{\lambda_i})$ is calculated for each period i.

In OSMOSE [48], the required investment in heat exchangers $C_{HEN,i}$ is estimated as a part of the pinch analysis for each operating mode i using a method from Ref. [56]. For more information, consult Bolliger [48].

In the MILP model, no constraint is put on the dimensions of utility services $\boldsymbol{\sigma_{ut}}$ in order to make sure that constraints (17) and (18) are satisfied at all operating points. Once the MILP model has been solved, $\boldsymbol{\sigma_{ut}}$ is identified as the largest required utility service demand experienced over the lifetime of the system, and the investment cost is calculated using the power law function given in equation (11).

2.3.3. Post computation

Once the MILP operation optimization has been conducted, a post-calculation step is used for evaluating the overall performance of the optimized FMG with respect to NPV and GWP100a.

First, the heat exchanger network investment cost, C_{HEN}, is defined as the largest estimated heat exchanger investment cost as identified by OSMOSE [48]:

$$C_{HEN} = \max_i C_{HEN,i} \tag{21}$$

The NPV, C_0, of the design is calculated as

$$C_0 = -\left[C_{HEN} + \sum_k \frac{C_{inv,k}(\sigma_k)}{(1+i)^{y_k}} \right] - \sum_i c_{op,i} \cdot t_{PV,i} \tag{22}$$

with y_{lt} being the facility lifetime and i the annual discount rate.

The global warming potential Z_0 of the design is calculated as

$$Z_0 = z_{inv,HEN} + \sum_k z_{inv,k}(\sigma_k) + \sum_i z_{op,i}(\boldsymbol{\nu_i}, \boldsymbol{\lambda_i}) \cdot t_i \tag{23}$$

Here, $z_{inv,HEN}$ is the global warming potential related to the production, installation, and scraping of the heat exchanger network, $z_{inv,k}(\sigma_k)$ is the global warming potential related to the production, installation, and scraping of the process $K(\sigma_k)$, and $z_{op,i}(\boldsymbol{\nu_i}, \boldsymbol{\lambda_i}) \cdot t_i$ is the overall global warming potential of the FMG operation in period i.

The calculated NPV and GWP100a are provided as feedback to the genetic algorithm. All data on optimized designs are stored in a database for later evaluation.

Please cite this article in press as: Lythcke-Jørgensen C, et al., A methodology for designing flexible multi-generation systems, Energy (2016), http://dx.doi.org/10.1016/j.energy.2016.01.084

2.4. Evaluation phase

2.4.1. Pareto assembly

Following the optimization phase, a Pareto frontier is assembled for optimized design solutions with respect to the two objectives, NPV and GWP100a. The Pareto frontier illustrates the border between the feasible solution space and the infeasible solution space of the optimization problem. Designs placed on the Pareto frontier are called efficient designs, as they represent the optimal pay-off between the two objectives of the optimization problem. An example of a Pareto frontier is developed as a part of the case study in Section 3 and can be seen in Fig. 11.

2.4.2. Sensitivity analysis and uncertainty analysis

Design optimization of FMGs involves many sources of uncertainty, e.g. technology learning curves, energy system development, policy schemes, estimated investment, operating costs etc. It is therefore important to assess variations in the performance of optimized designs as functions of input data uncertainty. In the present design methodology, uncertainties with respect to external operating conditions (energy systems) are considered by solving the developed optimization problem for various scenarios, while uncertainties of economic and environmental parameters are considered for a number of selected designs in each scenario using the following three-step procedure for assessing output uncertainty:

1. Selection of a number of interesting designs.
2. Morris screening [57] is applied on each selected design for assessing the relative impact on performance variability from input parameter uncertainty.
3. Monte Carlo simulation is applied for quantifying performance variability of each selected design.

Uncertainties regarding topological parameters, such as equipment failure or forced outages, are not considered in the design methodology.

2.4.2.1. Morris screening. Extended Morris screening [57,58] is a global sensitivity analysis method that is applied for assessing how the various input data uncertainties affect variations in model outputs. The method relies on estimation of elementary effect *EE* on each model output from each input parameter *p*. The main advantage of Morris screening is its low computational cost when compared to other global sensitivity analysis methods. The method uses a special sampling technique, Morris sampling, and it has two degrees of freedom to be specified by the user: *b*, the number of value levels that an uncertain input parameter can take within its range; and *w*, the number of elementary effects to be calculated for each input in order to identify the elementary effect distributions $\boldsymbol{D}_{\boldsymbol{EE},p_y}$ for each parameter p_y on each output function f.

The elementary effect vector $\boldsymbol{EE}_{p_y}$ for a parameter p_y is calculated as:

$$\boldsymbol{EE}_{p_y} = \frac{\boldsymbol{f}\left(p_1, p_2, \ldots, p_y + \Delta, \ldots, p_M\right)}{\Delta} \tag{24}$$

Here, $\boldsymbol{f}(p)$ are model output functions, and M is the total number of uncertain model parameters considered. Δ, a perturbation factor for the input parameters, is optimal when calculated as:

$$\Delta = \frac{p}{2(p-1)} \tag{25}$$

Once all EE_{ij} have been calculated for w random samples of input parameters, sigma-scaling [58] of EE_{p_y} is applied so that the impacts of input parameters on various outputs can be compared:

$$SEE_{p_y,f} = EE_{ij}\frac{(standard\ deviation)_{p_y}}{(standard\ deviation)_f} \tag{26}$$

Here, $(standarddeviation)_{p_y}$ is the standard deviation of the input parameter p_y, while $(standarddeviation)_f$ is the standard deviation of the output f from simulation results.

Based on the simulation results, the means and standard deviations of all sigma-scaled elementary effects $\boldsymbol{SEE}_{p_y}$ are calculated and assembled in scatter plots. In each plot, two lines corresponding to the positive and negative double estimated standard error of the mean, $mean_i$, are drawn:

$$mean_i = \pm 2 \cdot \frac{standard\ deviation_i}{\sqrt{w}} \tag{27}$$

As described by Sin et al. [58], these lines may be used for dividing uncertain input parameters into significant or negligible with respect to model output variation. If the elementary effect of a parameter falls within the two lines, its impact can be interpreted as negligible on the model output variation.

An example of the application of Morris screening and interpretation of its results is given in the case study in Section 3.

2.4.2.2. Monte Carlo simulation. Following the Morris screening, the Monte Carlo simulation procedure presented by Sin et al. [58] is applied for quantifying the overall model output variation with respect to each of the two performance objectives. The Monte Carlo simulation is a technique for investigating output variability through uncertainty sampling and probability statistics. It has been chosen for the design methodology as it may provide uncertainty results without necessitating modifications or manipulations of the original models and because it facilitates identification of nonlinearities, thresholds, and discontinuities [59]. The procedure applied in the design methodology involves three steps:

1. *Specifying input uncertainty*: In general, the Monte Carlo simulations may consider uncertainty distributions *D* for all input data. However, in order to reduce the number of parameter distributions to sample from, the parameters identified to have insignificant impact on model output variability in the Morris screening are not considered in the input uncertainty for the Monte Carlo simulations.
2. *Sampling from input uncertainty*: In order to obtain dense stratification over the range of each sampled variable without having to define the stratification manually, the Latin Hypercube Sampling method [60] is applied for sampling from input uncertainty.
3. *Evaluating the model for sampled input uncertainty*: The optimization model is run for all sampled datasets. The Monte Carlo results provide a cumulative distribution function of the output functions which may be evaluated using basic statistics.

2.5. Outputs

The design methodology yields two overall outputs:

1. An assembled Pareto curve and a database of feasible designs that have been optimized with respect to NPV and GWP100a.
2. For selected designs:
   a. The sigma-scaled elementary effect of each input parameter *p* on each model output.

Please cite this article in press as: Lythcke-Jørgensen C, et al., A methodology for designing flexible multi-generation systems, Energy (2016), http://dx.doi.org/10.1016/j.energy.2016.01.084

b. A quantification of model output variation as a function of input uncertainty.

To demonstrate the use of the design methodology, it is applied in a case study in Section 3.

3. Case study: conceptual FMG

In this section, the developed design methodology is applied in a simple case study which treats the retrofit of an existing combined cycle CHP (combined heat and power) plant. With the aim of strengthening the integration between layers of the energy system, a number of routes for converting local biomass into power, heating, fuels, and other products are considered for integration in the CHP plant, and the impact of such integration on the overall economic and environmental performance of the plant is then assessed. The retrofit options considered include the possible installation of: A straw-based cellulosic ethanol production facility based on IBUS technology [61]; a biomethane facility, which includes an anaerobic digester producing biogas from manure, industrial waste, and ethanol production molasses, with an integrated biogas upgrading facility; a biomass boiler and a natural gas boiler for utility heat; and a ground-based compression heat pump for district heating generation. A superstructure of possible retrofit options is presented in Fig. 9. All processes are assumed to be co-located, while investment planning is neglected. A preliminary version of the case study was presented in Ref. [62].

3.1. Input data and structuring

3.1.1. Surrogate process models

A surrogate model of a gas turbine (GT) and a bottoming steam Rankine cycle (SR) were developed based on data from the Danish back-pressure combined cycle CHP plant 'Silkeborg Kraftvarmeværk' [63]. In the surrogate models, temperature levels were assumed to be load-independent, while gas consumption, GT power generation, and off-gasses heat flow capacity were assumed to be directly proportional to the GT load λ_{GT}. The heat and power generation of the SR were assumed directly proportional to the SR load λ_{SR}. Both the GT and the SR were assumed to operate adiabatically. Data used for developing the GT and SR surrogate models are presented in Table 1.

A surrogate model of an IBUS ethanol facility (IB) was developed based on a validated IBUS facility model by Lythcke-Jørgensen et al. [14,64], with the modification that thermal separation stages were replaced by mechanical separation stages. A surrogate model of a biomethane facility (AD), consisting of a thermophilic anaerobic digestion reactor operating at 55 °C and a biogas upgrading facility, was developed based on models presented by Evald et al. [65]. The IB and the AD were assumed to have zero load flexibility.

Surrogate models of a gas boiler (GB), a biomass boiler (BB), and a district heating heat pump (HP) were developed based on data presented by the Danish Energy Agency [66].

Economic data on the surrogate models are presented in Table 2. In the calculations, a plant lifetime of $y_{lt} = 30$ *years* and an annual discount rate of $i = 0.06$ were assumed. For power law investment calculations as defined in equation (11), an investment scaling constant of $M_f = 0.75$ was used.

Thermal energy flows as functions of process variables are presented in Table 3. It was assumed that a cold water reservoir with a temperature of 15 °C was available for balancing heat flows in the system. As all processes were considered to be co-located, a single thermal energy layer was defined in the model.

Mass flows in the various layers as functions of process variables are presented in Tables 4–8. Note that power flows were modelled as mass flows in a separate layer. Market surrogate models were introduced into each layer to ensure mass balances.

3.1.2. Energy system, market, and environmental impact data

For the case study, the power price c_{el} and the relative district heating demand λ_{DH} were identified as relevant external operating parameters. A CHOP-reduced dataset of c_{el} and $\lambda_{DH,ref}$ based on

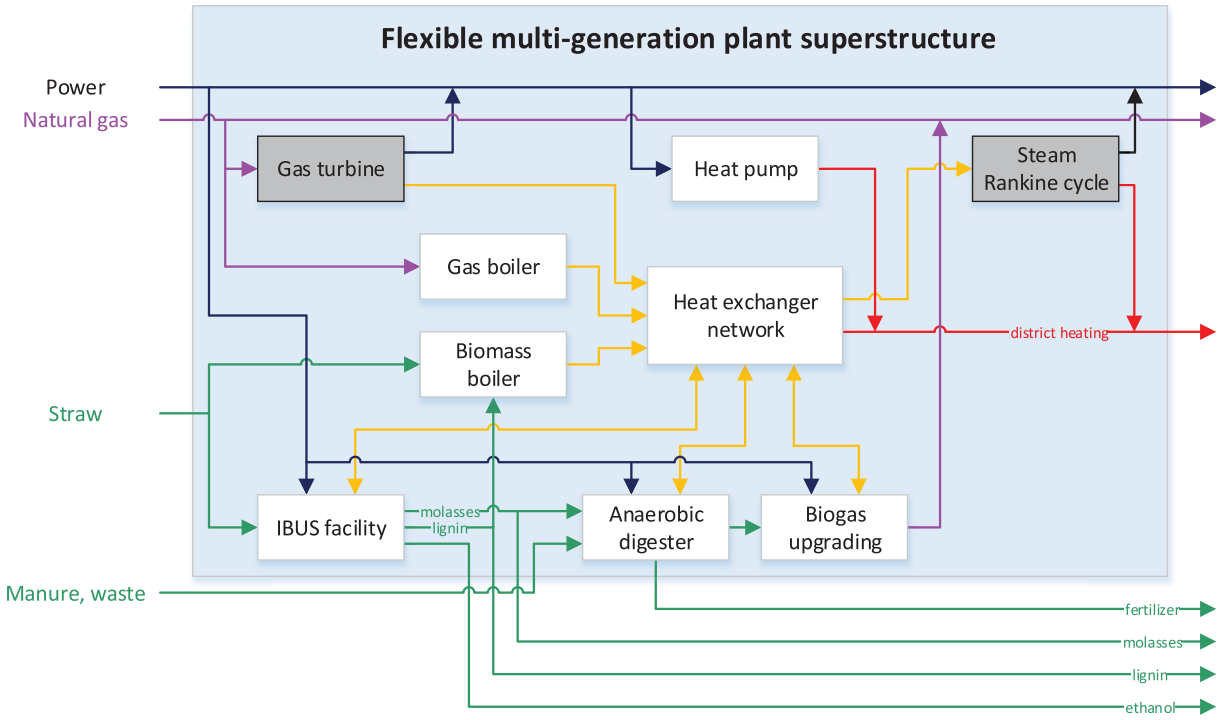

Fig. 9. Superstructure of considered retrofit options for the existing combined cycle CHP. The gas turbine and steam Rankine cycle are grey as they are already installed.

Please cite this article in press as: Lythcke-Jørgensen C, et al., A methodology for designing flexible multi-generation systems, Energy (2016), http://dx.doi.org/10.1016/j.energy.2016.01.084

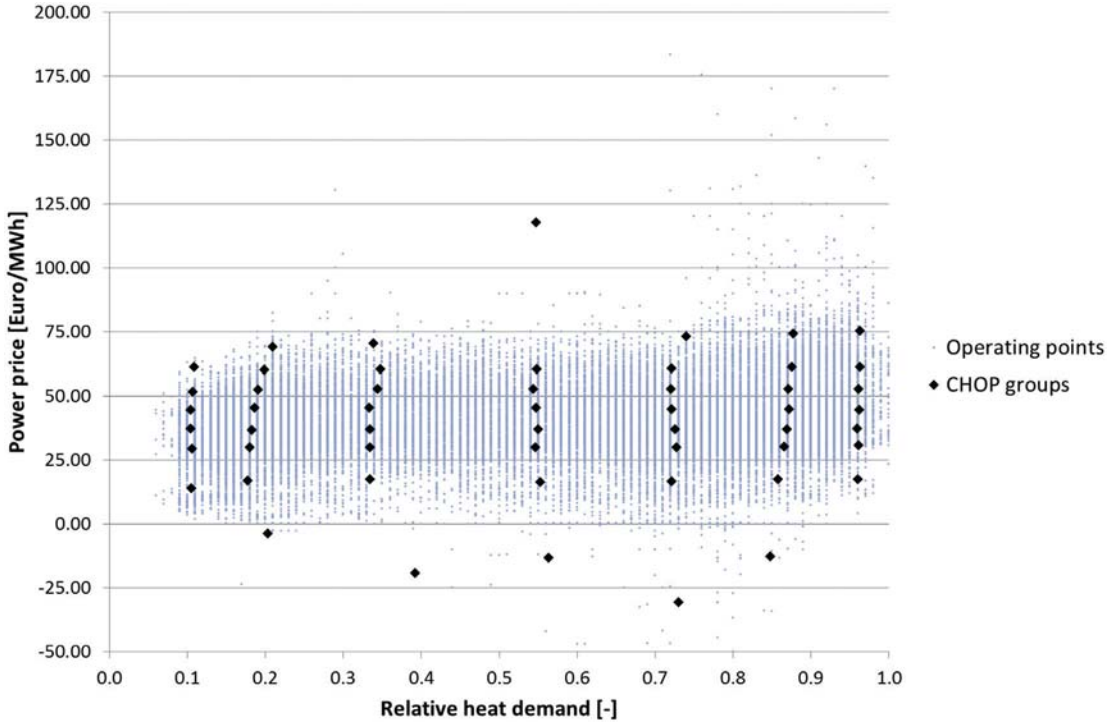

Fig. 10. Scatter plot of reference operating points and CHOP groups with respect to power price and relative heat demand.

historical data for western Denmark over the period primo 2010-ultimo 2014 has been presented by Lythcke-Jørgensen et al. [49]. This dataset was applied in the present case study as representative for operating conditions over the lifetime of the studied FMG. The CHOP-reduced dataset is presented in Tables 9–12. A scatter plot of original and reduced operating condition data points is presented in Fig. 10.

For simplicity, the environmental objective of the study only considered CO_2-emissions from facility production and avoided CO_2-emissions from displaced external production. Average emission values were in general applied for the displaced production. Marginal values may, however, be utilised, e.g. in combination with energy system analysis [67]. Economic and environmental data on consumed and sold products are presented in Table 13. Biomass was assumed to be CO_2 neutral. Manure was assumed to be delivered free of charge by local farmers in exchange for free, digested fertilizer. Manure emission impacts were not considered, although anaerobic digestion of manure may reduce greenhouse gas emissions significantly as compared to conventional use of undigested manure as fertilizer.

3.1.3. *Biomass supply chain model*

Apart from the straw cost paid to the producers as indicated in Table 13, an additional cost was placed on straw import to

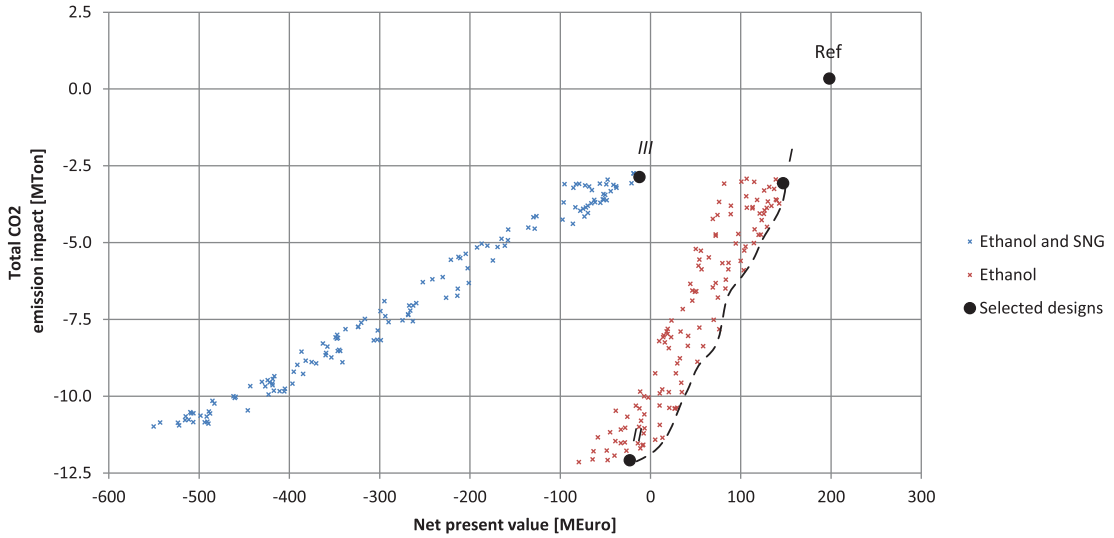

Fig. 11. Scatter plot of optimized design solutions with respect to NPV and CO_2 emission impact. The designs are clustered according to type of biomass treatment installed. The dotted line crudely illustrates the identified Pareto curve. The designs marked 'I', 'II' and 'III' are selected for further investigation. 'Ref' is the evaluated performance of the reference combined cycle CHP.

Please cite this article in press as: Lythcke-Jørgensen C, et al., A methodology for designing flexible multi-generation systems, Energy (2016), http://dx.doi.org/10.1016/j.energy.2016.01.084

Table 1
Data used for developing gas turbine and bottoming steam Rankine cycle surrogate models.

Facility	Variable	Description	Value	Reference
Gas turbine (GT)	P_{GT100}	Nominal power capacity	85 MW	[63]
	$\dot{m}_{GT,gas100}$	Nominal gas consumption	216.25 MW	[63][a]
	$\dot{e}_{GT,off100}$	Nominal off-gas heat flow	105.3 MJ/s	[63][a]
	$T_{off,in}$	Off-gas temperature, before heat exchange	465 °C	[63]
	$T_{off,out}$	Off-gas temperature after heat exchange	68 °C	[63]
Rankine cycle (SR)	P_{SR100}	Nominal power capacity	23.3 MW	[63][a]
	Q_{SR100}	Nominal district heating generation	82.0 MJ/s	[63][a]
	$p_{SR,turbine,in}$	Turbine inlet pressure	15.5 bar	Assumption
	$T_{SR,turbine,in}$	Turbine inlet temperature	450 °C	Assumption

[a] Calculated based on operation data from Ref. [63].

Table 2
Economic data on surrogate models.

Model	Reference investment cost $\boldsymbol{C_{inv,k0}}$	Reference operation and maintenance costs $\boldsymbol{c_{O\&M,k0}}$	Reference dimension $\boldsymbol{\sigma_{k0}}$
Gas turbine (GT)	–	2.50 Euro/MWh power [66]	–
Steam Rankine cycle (SR)	–	2.50 Euro/MWh power [66]	–
Ethanol facility (IB)	256.0 MEuro [65]	35.9 MEuro/year [65]	13.9 kg/s straw [65]
Biomethane facility (AD)	179.8 MEuro [65]	44.2 MEuro/year [65]	13.9 kg/s straw[a] [65]
Gas boiler (GB)	2.0 MEuro [66]	0.41 Euro/MWh heat [66]	20 MJ/s [66]
Biomass boiler (BB)	40 MEuro [66]	4.0 Euro/MWh heat [66]	50 MJ/s [66]
District heating heat pump (HP)	6.8 MEuro [66]	0.50 Euro/MWh heat [66]	10 MJ/s [66]

[a] The biogas upgrading facility is dimensioned to process all C5-molasses from the reference ethanol facility if installed.

Table 3
Thermal energy flow functions.

Process	Flow-description	Notation	Type	Function [MJ/s]	$\boldsymbol{T_{in}/T_{out}}$
Gas turbine (GT)	Off-gas heat flow	$\dot{e}_{GT,off}$	Hot	$1.053\cdot\lambda_{GT}$	465 °C/68 °C
Steam Rankine cycle (SR)	Water heating	$\dot{e}_{SR,c1}$	Cold	$0.200\cdot\lambda_{SR}$	120 °C/200 °C
	Water evaporation	$\dot{e}_{SR,c2}$	Cold	$0.653\cdot\lambda_{SR}$	200 °C/200 °C
	Steam superheating	$\dot{e}_{SR,c3}$	Cold	$0.200\cdot\lambda_{SR}$	200 °C/450 °C
	Condensation	$\dot{e}_{SR,h}$	Hot	$0.820\cdot\lambda_{SR}$	120 °C/120 °C
Ethanol facility (IB)	Steam generator, water heating	$\dot{e}_{IB,sg1}$	Cold	$1.501\cdot\sigma_{IB}$	15 °C/192 °C
	Steam generator, evaporation	$\dot{e}_{IB,sg2}$	Cold	$3.945\cdot\sigma_{IB}$	192 °C/192 °C
	Steam generator, superheating	$\dot{e}_{IB,sg3}$	Cold	$0.019\cdot\sigma_{IB}$	192 °C/195 °C
	Pretreatment, cooling 1	$\dot{e}_{IB,pr1}$	Hot	$0.341\cdot\sigma_{IB}$	190 °C/100 °C
	Pretreatment, cooling 2	$\dot{e}_{IB,pr2}$	Hot	$4.287\cdot\sigma_{IB}$	100 °C/100 °C
	Pretreatment, cooling 3	$\dot{e}_{IB,pr3}$	Hot	$0.092\cdot\sigma_{IB}$	100 °C/80 °C
	Pretreatment, cooling 4	$\dot{e}_{IB,pr4}$	Hot	$0.247\cdot\sigma_{IB}$	100 °C/50 °C
	Liquefaction cooling	$\dot{e}_{IB,lq}$	Hot	$0.060\cdot\sigma_{IB}$	50 °C/33 °C
	Distillation, heating 1	$\dot{e}_{IB,dsh1}$	Cold	$1.631\cdot\sigma_{IB}$	100 °C/100 °C
	Distillation, heating 2	$\dot{e}_{IB,dsh2}$	Cold	$0.021\cdot\sigma_{IB}$	33 °C/37 °C
	Distillation, cooling 1	$\dot{e}_{IB,dsc1}$	Cold	$1.044\cdot\sigma_{IB}$	68 °C/68 °C
	Distillation, cooling 2	$\dot{e}_{IB,dsc2}$	Cold	$0.807\cdot\sigma_{IB}$	100 °C/30 °C
Biomethane facility (AD)	Anaerobic digester, heating	$\dot{e}_{AD,h}$	Cold	$0.249\cdot\omega_{AD}\sigma_{IB}$	55 °C/55 °C
	Gas upgrading heat loss	$\dot{e}_{AD,l}$	Hot	$0.767\cdot\omega_{AD}\sigma_{IB}$	100 °C/30 °C
Gas boiler (GB)	Gas boiler off-gas	$\dot{e}_{GB}$	Hot	$\lambda_{GB}\sigma_{GB}$	465 °C/68 °C
Biomass boiler (BB)	Biomass boiler off-gas	$\dot{e}_{GB}$	Hot	$\lambda_{BB}\sigma_{BB}$	465 °C/68 °C
District heating heat pump (HP)	Heat pump heat delivery	$\dot{e}_{HP}$	Hot	$\lambda_{HP}\sigma_{HP}$	90 °C/90 °C
District heating demand (DH)	Heating of return flow	$\dot{e}_{DH}$	Cold	λ_{DH}	40 °C/80 °C

Table 4
Power flow functions.

Process	Flow-description	Notation	Function [MW]
Gas turbine (GT)	GT power generation	$\dot{m}_{GT,el}$	$0.85\cdot\lambda_{GT}$
Steam Rankine cycle (SR)	SR power generation	$\dot{m}_{SR,el}$	$0.233\cdot\lambda_{SR}$
Ethanol facility (IB)	IB power consumption	$\dot{m}_{IB,el}$	$-0.583\cdot\sigma_{IB}$
Combined biogas facility (AD)	AD power consumption	$\dot{m}_{AD,el}$	$-2.048\cdot\omega_{AD}\sigma_{IB}$
District heating heat pump (HP)	HP power consumption	$\dot{m}_{HP,el}$	$-0.357\cdot\sigma_{HP}$
Power market	Power market exchange	$\dot{m}_{R,el}$	

Please cite this article in press as: Lythcke-Jørgensen C, et al., A methodology for designing flexible multi-generation systems, Energy (2016), http://dx.doi.org/10.1016/j.energy.2016.01.084

Table 5
Straw flow functions.

Process	Flow-description	Notation	Function [MJ/s]
Ethanol facility (IB)	Ethanol straw consumption	$\dot{m}_{IB,straw}$	$-15.1\cdot\sigma_{IB}$
Biomass boiler (BB)	Biomass boiler straw consumption	$\dot{m}_{BB,straw}$	$-1.031\cdot\sigma_{IB}$
Straw market	Straw import	$\dot{m}_{R,el}$	

Table 6
Solid biofuel flow functions.

Process	Flow-description	Notation	Function [MJ/s]
Ethanol facility (IB)	Ethanol solid biofuel production	$\dot{m}_{IB,biofuel}$	$7.1\cdot\sigma_{IB}$
Biomass boiler (BB)	Biomass boiler biofuel consumption	$\dot{m}_{BB,biofuel}$	$-1.031\cdot\sigma_{BB}\lambda_{BB,biofuel}$
Solid biofuel market	Solid biofuel export	$\dot{m}_{R,biofuel}$	

represent costs for transport and logistics. The company EA Energy Analysis [73] has reported a fixed cost of 1.07 Euro/GJ for straw logistics in Denmark, including transportation for up to 10 km, while an additional cost of 0.009 Euro/(GJ/km) is charged for every additional kilometre. Assuming a mean winter wheat straw yield of 4183 kg/ha, as suggested by Bentsen et al. [74], and that 20% of the area around the facility has winter wheat cultivation, a surrogate biomass supply chain model was developed. The model is presented in Table 14. It was not assumed feasible to import biomass from outside the 50 km radius area around the facility.

3.1.4. Optimization constraints

Design variables and constraints in the case study are summarized in Table 15. As previously mentioned, investment planning was not considered in the present case.

Operation variables and constraints are summarized in Table 16 and equation (28). As the GB was considered a back-up utility, it was dimensioned in the operation optimization step based on maximum required load. Note that the ethanol facility and the combined biogas facility were assumed to be inflexible, implying that load variations are not considered in the operation optimization. The facility was considered to be the sole provider of heating for the district heating grid, and, consequently, the district heating generation must meet the demand at all times.

$$\lambda_{DH} \equiv \lambda_{DH,ref} \tag{28}$$

In the optimization phase, the genetic algorithm was run for a population size of 50 over 5 generations.

3.1.5. Sensitivity and uncertainty analysis

The uncertain input parameters considered in the case study and their distributions are given in Table 17.

The reference investment costs and the ethanol price were given a relative uncertainty of ±25% with a uniform distribution to represent cost and market uncertainties. The CO_2 emissions displaced from the ethanol produced z_{eth} was assumed to vary in the range $[-40\%, 0\%]$ with a uniform distribution to represent the facts that it may not be gasoline that is replaced by the produced ethanol, and that the straw consumed may not be CO_2 neutral. Finally, the investment scaling constant was given an uncertainty range of $[0.6, 0.9]$ with a uniform distribution to represent the uncertainties related to the economy of scale benefits from investments.

Morris screening was conducted with $\{b, w\} = \{8, 35\}$. For each Monte Carlo simulation, a sample of 250 data points was generated using Latin Hypercube Sampling [60] and assuming zero correlation between uncertainties in input parameters.

Table 7
C5 residues flow functions.

Process	Flow-description	Notation	Function [MJ/s]
Ethanol facility (IB)	Ethanol molasses production	$\dot{m}_{IB,mol}$	$3.9\cdot\sigma_{IB}$
Combined biogas facility (AD)	Anaerobic digester molasses consumption	$\dot{m}_{AD,mol}$	$-3.9\cdot\omega_{AD}\sigma_{IB}$
C5 residues market	C5 residues export	$\dot{m}_{R,mol}$	

Table 8
Natural gas flow functions.

Process	Flow-description	Notation	Function [MJ/s]
Gas turbine (GT)	Gas turbine gas consumption	$\dot{m}_{GT,gas}$	$-2.165\cdot\lambda_{GT}$
Combined biogas facility (AD)	Upgraded biogas production	$\dot{m}_{AD,gas}$	$3.108\cdot\omega_{AD}\sigma_{IB}$
Gas boiler (GB)	Gas boiler consumption	$\dot{m}_{GB,gas}$	$-1.031\cdot\sigma_{GB}\lambda_{GB}$
Natural gas market	Natural gas market exchange	$\dot{m}_{R,gas}$	

3.2. Results and evaluation

A database of feasible designs with optimized operation was obtained from running the optimization model. A scatter plot of the optimized designs with respect to NPV and CO_2 emission impact is shown in Fig. 11.

In general, it was found that the larger the dimension of the biomass treatment facilities, the lower the NPV and the lower the total CO_2 emission impact, illustrating the cost of avoided CO_2 emissions in the case study. It was further found that the cost of avoided CO_2 emission was higher for designs including both ethanol and biomethane production than for designs with only ethanol production. This trend is primarily caused by two effects: First of all, avoided CH_4 emissions from undigested manure were not considered in the calculations, which would expectedly reduce the total CO_2 emission impacts from designs with biogas production significantly. Secondly, a GB was installed as back-up utility heat source, and it was used in periods where it was economically unfavourable to operate the gas turbine while power for running the operation was imported from the grid. Combined, this made the overall biomethane production unfavourable from both an economic and an environmental perspective in the case study.

The results further indicate that the NPV is reduced while the CO_2 emission impact is only slightly affected for larger biomass boiler dimensions, suggesting that the biomass boiler is hardly used in the operation optimization for economic reasons. This opposes the current (2015) trend in Denmark where biomass, which is currently tax free, is replacing the taxed natural gas in the heating sector. The reason for this difference is the fact that tax and subsidy schemes are not considered in the calculations. The results also suggest that operation with a district heating heat pump is favourable for specific periods, but that the investment costs make the overall economic performance of heat pumps unfavourable. Again, it must be stressed that taxes and subsidy schemes were not considered in the calculations.

Table 9
Interval break points in the CHOP-reduced dataset. From Ref. [49].

Interval break point	1	2	3	4	5	6	7
Power price [Euro/MWh]	0.00	25.00	33.00	41.00	49.00	57.00	65.00
Relative heat demand [–]	0.125	0.25	0.45	0.65	0.80	0.95	–

Please cite this article in press as: Lythcke-Jørgensen C, et al., A methodology for designing flexible multi-generation systems, Energy (2016), http://dx.doi.org/10.1016/j.energy.2016.01.084

Table 10
Duration of the defined CHOP groups in hours from Ref. [49]. Note that the duration is multiplied by six to represent the 30-year lifetime of the facility rather than the 5-year period that the historical values are taken from.

CHOP group duration [h] heat interval\power interval	1	2	3	4	5	6	7	8
1	0	1926	2136	1836	1452	330	60	0
2	66	7068	13,188	12,666	11,232	5880	1170	330
3	54	3690	8298	10,038	8400	6900	2442	1068
4	132	4302	8412	9600	8898	6510	3108	1188
5	432	5682	10,944	12,978	9390	6834	3462	1638
6	180	3492	11,718	15,846	10,656	7806	5388	5418
7	0	276	1134	2190	1602	1170	1062	1266

Table 11
Relative heat demand of the defined CHOP groups. From Ref. [49].

Relative heat demand [−] heat interval\power interval	1	2	3	4	5	6	7	8
1	–	0.105	0.106	0.105	0.105	0.107	0.109	–
2	0.204	0.178	0.180	0.182	0.186	0.191	0.199	0.210
3	0.392	0.334	0.335	0.334	0.334	0.344	0.348	0.339
4	0.563	0.553	0.546	0.550	0.547	0.544	0.549	0.547
5	0.731	0.721	0.727	0.726	0.721	0.720	0.721	0.740
6	0.848	0.858	0.866	0.870	0.872	0.871	0.876	0.878
7	–	0.961	0.961	0.960	0.962	0.961	0.963	0.963

Table 12
Power price of the defined CHOP groups. From Ref. [49].

Power price [€/MWh] heat interval\power interval	1	2	3	4	5	6	7	8
1	–	13.91	29.32	37.20	44.49	51.62	61.11	–
2	−3.92	16.86	29.73	36.73	45.20	52.51	60.05	69.02
3	−19.24	17.43	29.80	36.80	45.40	52.64	60.23	70.32
4	−13.46	16.22	29.77	36.83	45.20	52.59	60.34	117.54
5	−30.81	16.58	29.75	36.82	44.74	52.63	60.39	72.97
6	−12.90	17.36	30.03	36.98	44.76	52.59	61.08	74.10
7	–	17.20	30.56	37.11	44.58	52.75	60.95	75.08

Three interesting designs, *I*, *II*, and *III*, were chosen for further investigation. Here, *I* is the identified retrofit design with the highest NPV; *II* is the identified retrofit design with the lowest CO_2-emission impact; and *III* is the retrofit design with the largest NPV that includes biomethane production. The characteristics of the designs are described in Table 18, together with the performance of the reference facility (Ref).

Table 13
Economic data on, and CO_2 emission impacts of, consumed and sold products.

Products	Price [Euro/GJ]	CO_2 standard emission factor [kg/GJ]	
		Consumed	Sold
Straw	5.70 [68]	0.00	–
Natural gas	6.24 [68]	56.1	−56.1[a] [69]
District heating	12.08[b] [70]	–	−33.0[c] [71]
Molasses (C5 residues)	5.38 [72]	–	0.00[d] [69]
Solid biofuel (lignin)	8.71 [68]	0.00	−101.1[e] [69]
Ethanol	16.05[f] [68]	–	−69.2[f] [69]
Power	[defined in CHOP]	0.413/0[g] [71]	−0.413/0[g] [71]

[a] Sold natural gas (bio-methane) is assumed to replace natural gas in the grid.
[b] Reference heat-to-grid selling price in 2020 for natural gas-based combined cycle power plants in western Denmark.
[c] Average CO_2 emission for district heating in Denmark.
[d] For simplicity, no avoided CO_2 emission is associated with sold molasses. In reality, molasses may be sold as animal feed, thereby potentially replacing imported soy beans or similar, thus reducing CO_2 emissions.
[e] The solid biofuel, from which most of the alkaline metals have been removed, is assumed to replace coal.
[f] Ethanol is assumed to be sold as, and replace, gasoline.
[g] Marginal power generation CO_2 emission is set equal to the average CO_2 emission from power generation in Denmark, apart from periods with negative power prices where the marginal CO_2 emission is set to zero to represent wind turbine power generation.

Based on the input parameter uncertainties defined in Table 17, Morris screening was applied for identifying elementary effects on NPV and GWP100a from each of the uncertain input parameters in each of the three selected designs. An example of an elementary effect histogram obtained using Morris screening is plotted in Fig. 12.

The means and standard deviation of the sigma-scaled elementary effects from uncertain input parameters on each of the model outputs are plotted for the three selected designs in Fig. 13. The wedges in the figures represent the standard error of the mean as defined in equation (25). Elementary effects with mean and standard deviations of zero are not labelled in the figures.

The scatter plots illustrate the relative importance of each of the input parameter uncertainties on each of the model outputs. From Fig. 13, it is seen that the NPV of design *I* would be significantly affected by uncertainties in reference ethanol facility investment cost $C_{inv,IB0}$ and investment scaling constant M_f, as the mean and standard deviations of their elementary effects' on NPV are far outside the standard-error-of-the-mean wedge. Furthermore, it is seen that the impacts of $C_{inv,IB0}$ and M_f are either correlated with other uncertain input parameters, non-linear, or both, as their standard deviations are different from zero. The ethanol price c_{eth} on the other hand was found to have a linear impact on NPV as the elementary effect has a standard deviation of zero. These observations can easily be confirmed by investigating the model structure. It is further seen that the NPV of design *I* was neither affected

Please cite this article in press as: Lythcke-Jørgensen C, et al., A methodology for designing flexible multi-generation systems, Energy (2016), http://dx.doi.org/10.1016/j.energy.2016.01.084

Table 14
Biomass supply chain model.

Area	Radius	Annual yield $q_{b,an}$ [ton]	Fixed logistics costs $c_{b,0}$ [Euro/GJ]	Transport costs $c_{b,tr}$ [Euro/GJ]	Marginal straw cost c_b [Euro/GJ]
A_1	10 km	26,269	5.709	0	5.709
A_2	30 km	210,154	5.709	0.215	5.924
A_3	50 km	420,308	5.709	0.397	6.106

Table 15
Design optimization variables and constraints.

Design variable	Description	Lower bound	Upper bound
σ_{IB}	Ethanol facility dimension, in kg/s straw processed	5 kg straw/s	20 kg straw/s[a]
ω_{AD}	Installation of a combined biogas facility, decision	Integer decision $\{0,1\}$	
σ_{BB}	Biomass boiler dimension, in MJ/s heat delivered	0 MJ/s	100 MJ/s
σ_{HP}	District heating heat pump dimension, in MJ/s heat delivered	0 MJ/s	50 MJ/s

[a] Equal to the maximum annual production of straw within a 50 km radius of the plant under the assumptions stated in Section 3.1.3.

Table 16
Operation optimization variables and constraints.

Operation variable	Description	Lower bound	Upper bound
ν_{GT}	Gas turbine operated	Integer decision $\{0,1\}$	
λ_{GT}	Gas turbine load	0.20	1.00
ν_{GT}	Steam Rankine cycle operated	Integer decision $\{0,1\}$	
λ_{SR}	Steam Rankine cycle load	0.40	1.00
λ_{GB}	Gas boiler load	0.00	1.00
λ_{BB}	Biomass boiler load	0.00	1.00
λ_{HP}	Heat pump load	0.00	1.00

by the displaced CO_2 emission from ethanol z_{eth} nor the reference investment costs of the biomethane facility $C_{inv,AD0}$ and district heating heat pump $C_{inv,HP0}$. This is evident from the fact that the dimension of the heat pump was negligible, no combined biogas facility was installed, and no economic cost was associated with CO_2 emissions. Opposed to this, as expected, z_{eth} is found to be the only parameter affecting the total CO_2 emission impact.

Similarly, observations on impact of parameter uncertainties were made for designs *II* and *III* based on Fig. 13. For *II*, it was found that c_{eth} had a more significant impact than for the other designs. This is due to the fact that the ethanol facility was markedly larger, causing ethanol sales to have a relatively larger impact on the NPV. For *III*, it was found that $C_{inv,AD0}$ was no longer negligible, as a biomethane facility was in fact installed.

Based on the Morris screening results, Monte Carlo simulations were conducted for each of the three designs considering non-negligible uncertainties in input parameters. The parameters considered are summarized in Table 19. The Latin Hypercube Sampling method was applied for generating samples of each 250 data points for use in the Monte Carlo simulations. A visual representation of the Latin Hypercube sample used in the Monte Carlo simulation for design *I* is presented in Fig. 14.

Running Monte Carlo simulations for each of the three selected designs, the resulting 10^{th} to 90^{th} percentile interval of predicted NPV and 0^{th} to 90^{th} percentile interval of predicted GWP100a are indicated for each of the three selected designs in Fig. 15.

The figure illustrates the variability in performance of the selected designs as functions of the defined input uncertainty. It is seen how the NPV variation is somewhat evenly distributed around the predicted value, which is to be expected as uncertainties in economic parameters are all considered to be evenly and uniformly distributed around the reference value. It is furthermore seen that the predicted CO_2 emission impact in the deterministic run is the lowest possible as the considered uncertainties in CO_2 emission impact can only lead to higher CO_2 emission impacts.

In general, the performance variations are found to be larger for design *II*, caused by larger retrofit investments and a larger ethanol production, implying that the relative uncertainties in investments, ethanol prices and replaced CO_2 emissions from produced ethanol will have a larger impact in absolute terms.

Within 10^{th} to 90^{th} percentile intervals, design *I* will outperform design *III* with respect to NPV for all cases, whereas the total CO_2 emission impact is somewhat similar, suggesting that *III* should not be selected for the given case. Considering the found performance intervals, design *I* has a CO_2 reduction price of 4.9–30.3 Euro/ton, while design *II* has a CO_2 reduction price of 8.4–32.1 Euro/ton. Hence, in the marginal case, the results suggest that design *I* should be preferred if cost-efficient CO_2 reductions are desired.

A central aspect of the design methodology is the application of systematic process integration. To assess the importance of this feature, the performances of each of the three selected designs were evaluated without consideration of process integration, i.e. the combined cycle CHP and the biomass treatment facilities were operated separately. The change in performance is illustrated in Fig. 16.

It is clear that without process integration, all three designs obtained lower NPV and higher CO_2 emission impacts. Also, it appears that the larger the dimensions of the biomass processing equipment, the larger the absolute reduction in performance. Altogether, this demonstrates the importance of considering process integration, both when developing smart energy systems in general and when designing FMGs in particular.

4. Discussion and perspective

This paper presents a generic methodology for optimizing the design of flexible multi-generation systems (FMGs), which are systems consisting of integrated and flexibly operated facilities that together provide multiple links between layers of the energy system.

One of the challenges of the presented design methodology is the fact that it is based on partial analysis, which implies that the impact on system level of FMG operation is neglected. However, as the central hypotheses for FMGs consider impacts on system levels, it is crucial that the aggregated impact of FMGs is assessed. For instance, if a number of FMGs are set to balance the power system by generating electricity in periods with no generation from renewable sources, they may become market dominating and thereby affect the power prices – a situation that makes partial analysis insufficient. One way of assessing the aggregated impact of

Please cite this article in press as: Lythcke-Jørgensen C, et al., A methodology for designing flexible multi-generation systems, Energy (2016), http://dx.doi.org/10.1016/j.energy.2016.01.084

Table 17
Uncertain parameters and their distributions.

Parameter	Description	Distribution	Reference value	Lower bound	Upper bound
$C_{inv,IB0}$	Investment cost, reference ethanol facility	Uniform	256.0 MEuro	192.0 MEuro	320.0 MEuro
$C_{inv,AD0}$	Investment cost, reference combined biogas facility	Uniform	199.8 MEuro	149.9 MEuro	249.8 MEuro
$C_{inv,GB0}$	Investment cost, reference gas boiler	Uniform	2.0 MEuro	1.5 MEuro	2.5 MEuro
$C_{inv,BB0}$	Investment cost, reference biomass boiler	Uniform	40.0 MEuro	30.0 MEuro	50.0 MEuro
$C_{inv,HP0}$	Investment cost, reference district heating heat pump	Uniform	6.8 MEuro	5.1 MEuro	8.5 MEuro
c_{eth}	Ethanol price	Uniform	5.70 Euro/GJ	4.28 Euro/GJ	7.13 Euro/GJ
z_{eth}	Ethanol displaced CO_2 emission	Uniform	−69.2 kg/GJ	−41.5 kg/GJ	−69.2 kg/GJ
M_f	Investment scaling constant	Uniform	0.75	0.6	0.9

Table 18
Characteristics of the selected designs.

Design	NPV [MEuro]	CO_2-emission impact [MTon]	σ_{IB} [kg/s]	ν_{AD} [−]	σ_{GB} [MJ/s]	σ_{BB} [MJ/s]	σ_{HP} [MJ/s]	C_{HEN} [MEuro]
Ref	198.2	0.34	0.0	0	0.0	0.0	0.0	0
I	147.0	−3.07	5.2	0	80.1	1.1	0.3	4.83
II	−22.9	−12.09	19.6	0	143.8	11.1	19.8	7.51
III	−12.1	−2.87	5.3	1	70.0	1.3	9.0	4.98

FMG operation is to apply the developed design methodology for identification of preliminary designs of FMGs, and then integrate these designs in an energy system model in order to assess the system impact. The results from the energy system analysis could then be provided as feedback to the design methodology in an iterative loop. This topic will be treated in future research by the group.

A shortcoming of the design methodology is the fact that thermal storages and dynamic operation constraints cannot be considered due to the application of the CHOP method [49]. The latter is applied to reduce computation times when searching for optimal designs while still maintaining detailed information on flexible operating conditions, which was previously proven to be crucial for obtaining optimal designs [62]. An advantage of the CHOP method is the fact that it is capable of capturing non-cyclic patterns in the energy system as opposed to most other energy system data aggregation methods, e.g. standard days, standard periods, average periods etc. [49]. To overcome the shortcoming of dynamic operation, the optimization phase of the methodology can be divided into two parts: A preliminary part where CHOP-reduced energy system data are used for the preliminary design, and a second part where chronological energy system data are used for detailed design and performance evaluation. This is analogous to the methodology presented by Rubio-Maya et al. [29,30]. The second step would then allow for the consideration of thermal energy storages and dynamic operational constraints, albeit at the cost of increased computational time. Whether or not this is the right way to proceed is a relevant topic for further investigation.

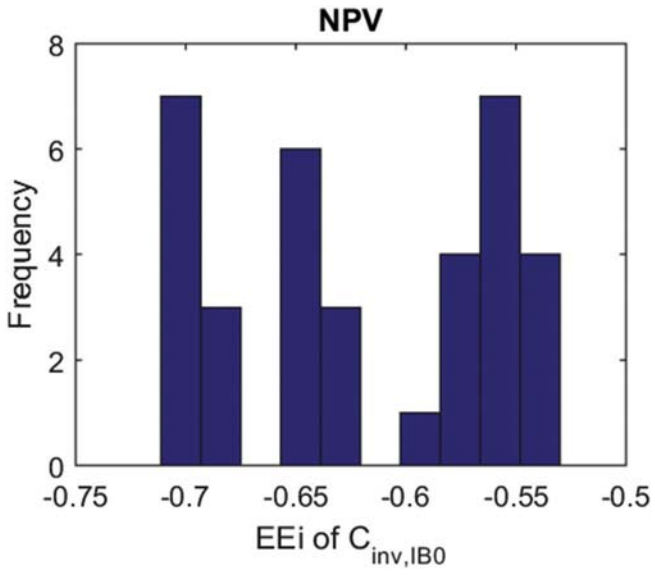

Fig. 12. Histogram – elementary effect on NPV from reference ethanol facility Investment cost for design I.

In the design methodology, a genetic algorithm is used as the master algorithm to be able to digest all sorts of models and scan the solution space for efficient solutions. However, being heuristic by nature, it cannot guarantee optimality of the solutions. For example, in the simple case study considered, the optimized retrofit design with the highest NPV, '*I*', had a biomass boiler of 1.1 MJ/s and a heat pump of 0.3 MJ/s installed, while the ethanol facility straw processing capacity was 5.2 kg/s. If the biomass boiler and heat pumps are removed, and the ethanol facility dimension is reduced to the minimum, i.e. 5.0 kg/s, the NPV would increase from 14.6 MEuro to 24.5 MEuro. This illustrates one of the drawbacks of using genetic algorithms: They may approximate the optimal or efficient solutions, but are not guaranteed to find them. However, as the present methodology is focussed on pre-feasibility studies of FMGs, the genetic algorithm is considered advantageous as it efficiently 'separates the wheat from the chaff'.

One of the novelties of the method is the consideration of local biomass supply chains, which is likely to have an impact on the dimensioning of biomass-processing FMGs [50]. In a similar manner, local industry and its demand for process heat, cooling, and other energy services ought to be considered when designing FMGs. If local industry is systematically considered for process integration in FMG studies, the overall energy and exergy efficiency of the local community may be increased further, and the industry demands may impact the dimensioning of FMGs as well. Thus, FMGs may be considered as supply facilities in local energy hubs or industrial symbioses, characterized by a high degree of mass and energy integration and reduced environmental impacts when compared to stand-alone industry.

In general, it is relevant to allow for future retrofit options when designing complex systems like FMGs, as discussed by Liu and Pistikopoulos [22]. However, inclusion of investment planning in the design methodology is challenging as both technological and system developments are hard to predict. Whether or not investment

Please cite this article in press as: Lythcke-Jørgensen C, et al., A methodology for designing flexible multi-generation systems, Energy (2016), http://dx.doi.org/10.1016/j.energy.2016.01.084

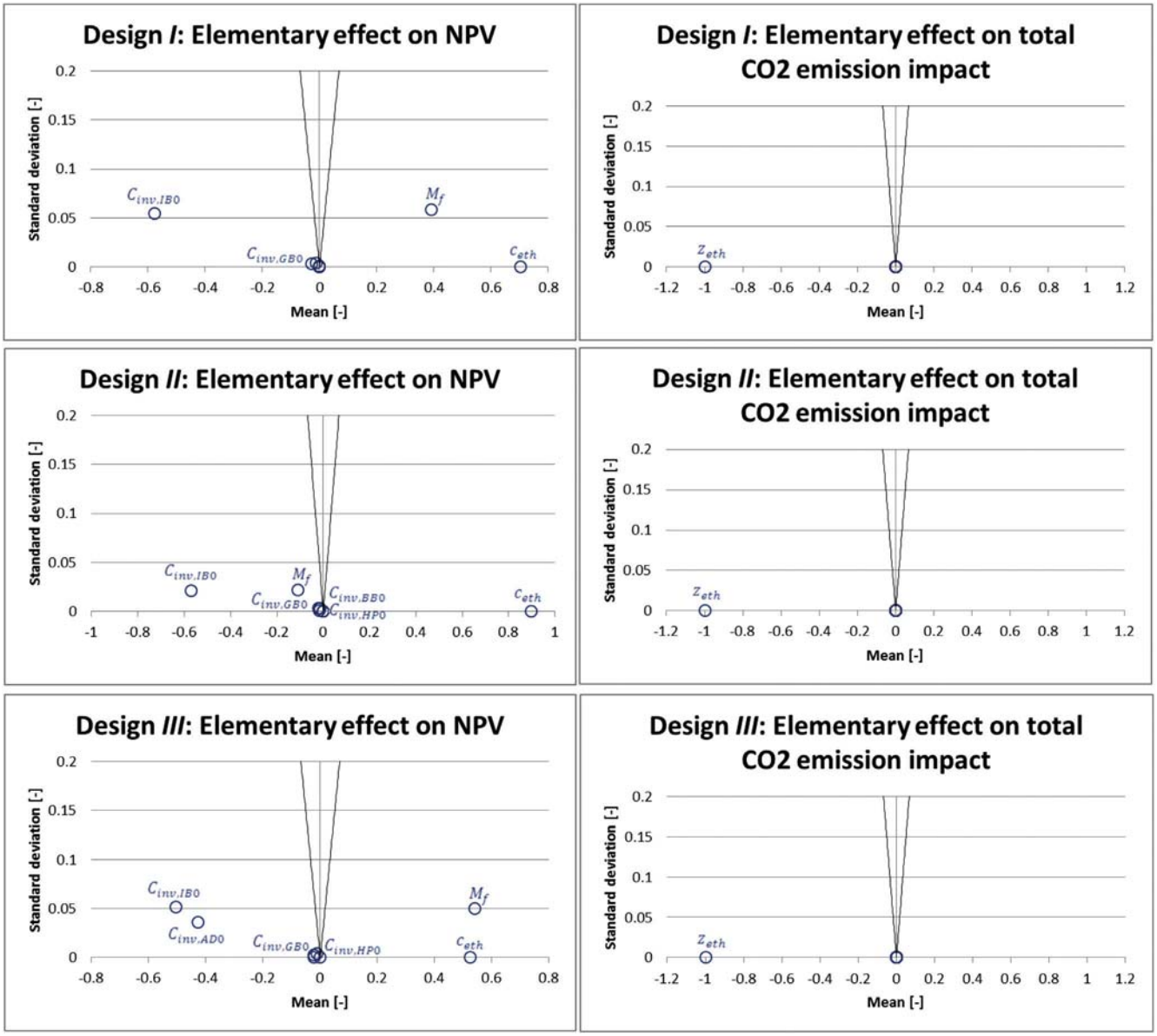

Fig. 13. Means and standard deviations of sigma-scaled elementary effects on NPV (left) and total CO_2 emission impact (right) from uncertain input parameters for designs I (top), II (middle), and III (bottom).

planning should be considered in pre-feasibility analysis depends on the case treated, but it is evident that the computational time would increase exponentially as multiple investment scenarios would have to be considered by the genetic algorithm.

Economic and environmental parameter uncertainties are efficiently handled in the design methodology using a combined Morris screening/Monte Carlo simulation approach. With regard to handling of energy system uncertainties in the design methodology, it is recommended that explorative scenarios are used to give a better overview of optimality differences between likely, but fundamentally different, energy system scenarios. It should be noted that the total computation time is approximately proportional to the number of scenarios investigated in the developed design methodology. In the present study, it took approximately 84 h to conduct all calculations on a laptop with an Intel® Core™ i7-3720QM CPU @ 2.60 GHz considering one energy system scenario.

Table 19
Uncertain input parameters considered in Monte Carlo simulations for each of the three selected designs.

Design	$C_{inv,IB0}$	$C_{inv,AD0}$	$C_{inv,GB0}$	$C_{inv,BB0}$	$C_{inv,HP0}$	c_{eth}	z_{eth}	M_f
I	X		X			X	X	X
II	X		X	X	X	X	X	X
III	X	X	X		X	X	X	X

The present case study featured a socio-economic analysis as neither taxes nor subsidies were considered. In general, socio-economic analyses can be used for providing recommendations for policy makers. If the design methodology is used with the aim of guiding investment decisions, it would be relevant to conduct a private economic evaluation including taxes and subsidies.

Finally, a significant outcome of the case study is the assessment of impact from systematic process integration in the design methodology. The results show how the selected designs become

Please cite this article in press as: Lythcke-Jørgensen C, et al., A methodology for designing flexible multi-generation systems, Energy (2016), http://dx.doi.org/10.1016/j.energy.2016.01.084

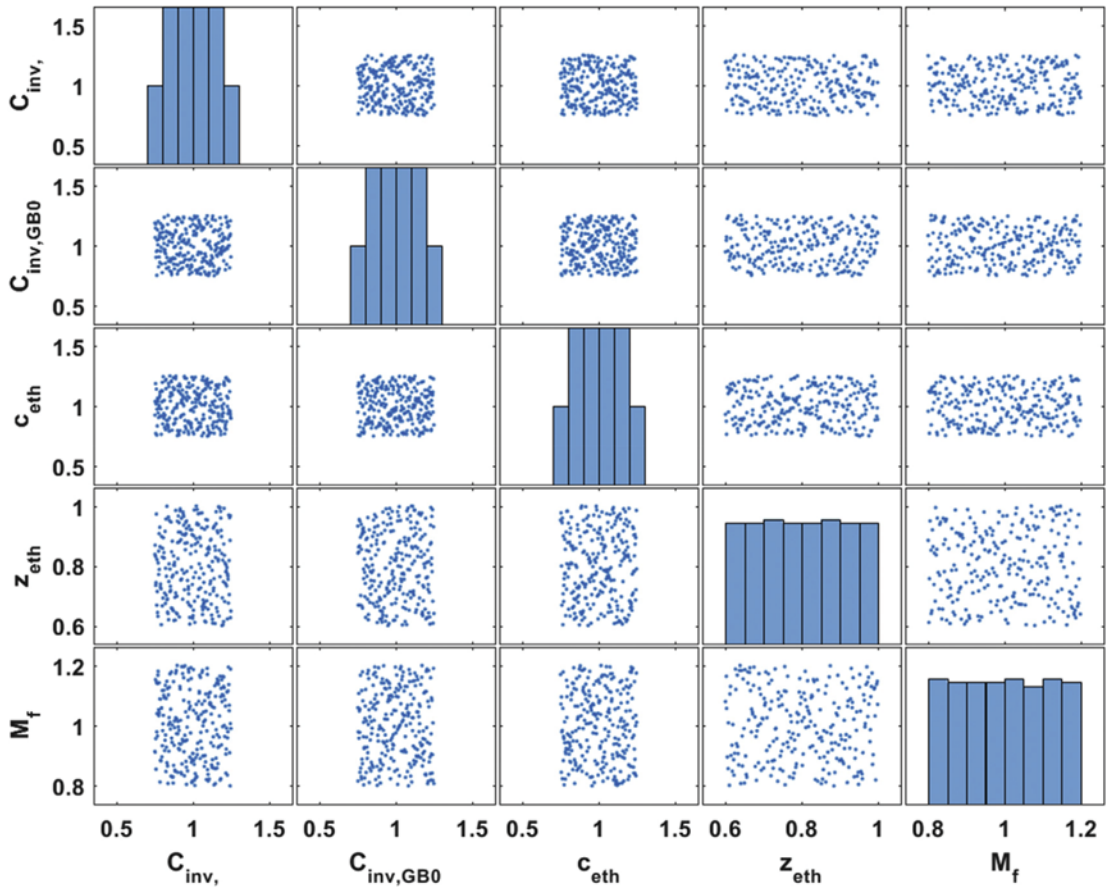

Fig. 14. Example of Latin Hypercube Sampling – sample used for Monte Carlo simulations for design I.

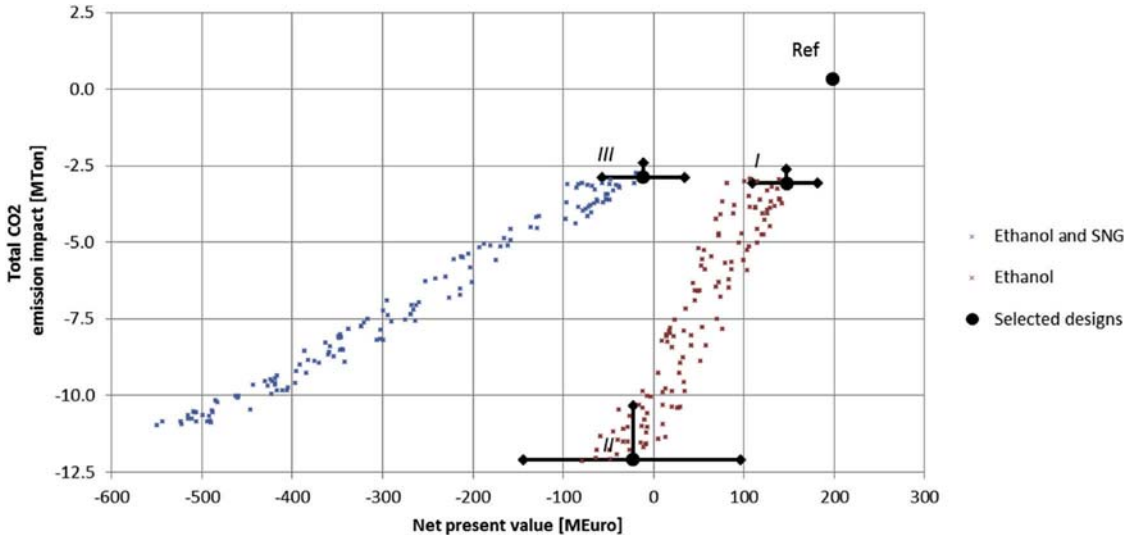

Fig. 15. Scatter plot of optimized design solutions with respect to NPV and CO_2-emission impact, with performance variability indicated for each of the three selected designs. NPV performance intervals represent 10^{th} to 90^{th} percentiles of predicted performance, while CO_2 emission impact intervals represent 0^{th} to 90^{th} percentiles of predicted performance.

suboptimal when process integration is neglected, and thus underline the importance of including process integration when developing smart energy systems in general and when designing FMGs in particular.

5. Conclusion

A generic methodology for optimizing the design of FMGs was presented, which simultaneously consider the following issues:

Please cite this article in press as: Lythcke-Jørgensen C, et al., A methodology for designing flexible multi-generation systems, Energy (2016), http://dx.doi.org/10.1016/j.energy.2016.01.084

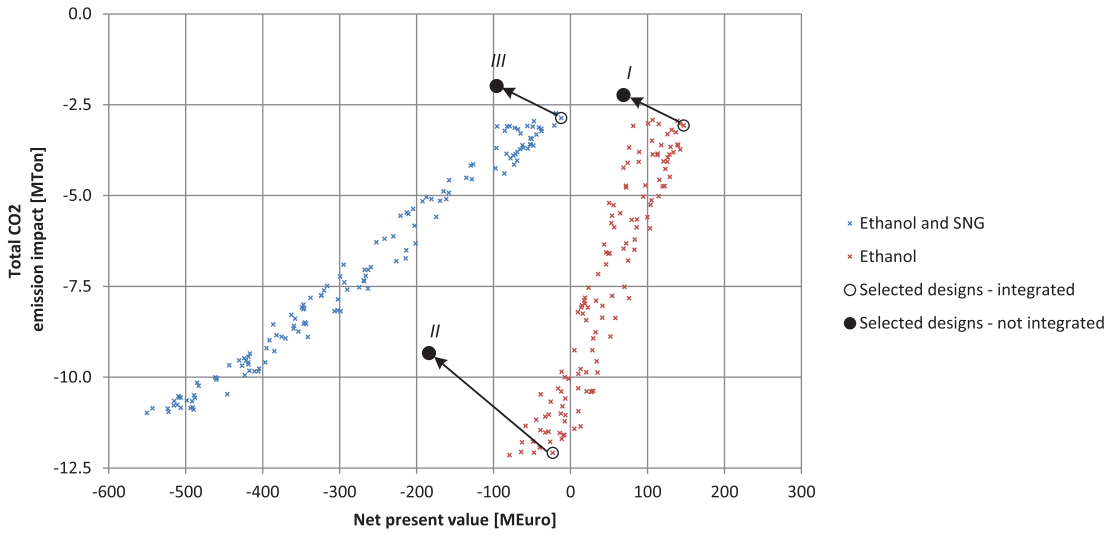

Fig. 16. Performance of selected designs if systematic process integration had not been considered.

Selection, location, and dimensioning of processes; systematic heat and mass integration; flexible operation optimization with respect to both short-term market fluctuations and long-term energy system development; global sensitivity and uncertainty analysis; consideration of local biomass availability and biomass supply chains; variable part-load performance; investment planning; and multi-objective optimization considering net present value (NPV) and 100-years global warming potential (GWP100a).

The methodology was applied in a simple case study where cellulosic ethanol production and upgraded biogas production were considered for installation in an existing combined cycle combined heat and power plant. The integration of ethanol production yielded more efficient results with respect to NPV and total CO_2 emission impact than did the integration of combined ethanol and biomethane production. However, the total CO_2 emission impact might conceivably have been reduced for designs with biomethane production if avoided CH_4 emissions from conventional use of manure had been considered. The highest NPV and CO_2 emission impact was obtained for the reference combined heat and power plant, illustrating that reducing CO_2 emissions comes at a cost. The case study further demonstrated how suboptimal designs would be obtained if systematic process integration was not considered, underlining the importance of considering systematic process integration when developing smart energy systems in general, and FMGs in particular.

The developed design methodology efficiently screens the solution space for promising FMG designs, and is capable of assessing the importance of parameter uncertainties as well as estimating the likely performance variation for the individual designs. Thus, the developed design methodology is considered useful for conducting quick and reliable pre-feasibility analyses for the development of FMG concepts.

Acknowledgements

This research was supported by DONG Energy and the Innovation Foundation through the 4DH project. The authors thank prof. Gürkan Sin, DTU Chemical Engineering, CAPEC-PROCESS, for fruitful discussions on sensitivity and uncertainty analysis, and for allowing the use of his Matlab programs for conducting Morris screening and Monte Carlo simulations. The authors also thank Ida Græsted Jensen, DTU Management Engineering, Systems Analysis, for fruitful discussions on the modelling of biomass supply chains. Finally, the authors would like to thank Bodil Diemer for linguistic comments and suggestions that greatly improved the manuscript.

References

[1] Chicco G, Mancarella P. Distributed multi-generation: a comprehensive view. Renew Sustain Energy Rev 2009;13(3):535–51.
[2] Song H, Starfelt F, Daianova L, Yan J. Influence of drying process on the biomass-based polygeneration system of bioethanol, power and heat. Appl Energy 2012;90(1):32–7.
[3] Lund H, Andersen AN, Østergaard PA, Mathiesen BV, Connolly D. From electricity smart grids to smart energy systems – a market operation based approach and understanding. Energy 2012;42(1):96–102.
[4] Geidl M, Koeppel G, Favre-Perrod P, Klöckl B, Andersson G, Fröhlich K. Energy hubs for the future. IEEE Power Energy Mag 2007;5(1):24–30.
[5] Coronas A, Murthy SS, Carles Bruno J. Editorial for the special issue of applied thermal engineering on polygeneration. Appl Therm Eng 2013;50(2):1397–8.
[7] Lund H. Renewable energy systems: the choice and modeling of 100% renewable solutions. Academic Press Publications; 2010.
[8] Yuan Z, Chen B. Process synthesis for addressing the sustainable energy systems and environmental issues. AIChE J 2012;58(11):3370–89.
[9] Serra LM, Lozano M-A, Ramos J, Ensinas AV, Nebra SA. Polygeneration and efficient use of natural resources. Energy 2009;34(5):575–86.
[10] Zhou W, Yang H, Rissanen M, Nygren B, Yan J. Decrease of energy demand for bioethanol-based polygeneration system through case study. Appl Energy 2012;95:305–11.
[11] Ahmadi P, Dincer I, Rosen MA. Development and assessment of an integrated biomass-based multi-generation energy system. Energy 2013;56:155–66.
[12] Mathiesen BV, Lund H, Connolly D, Wenzel H, Østergaard P a, Möller B, et al. Smart energy systems for coherent 100% renewable energy and transport solutions. Appl Energy 2015;145:139–54.
[13] Mancarella P. MES (multi-energy systems): an overview of concepts and evaluation models. Energy 2014;65:1–17.
[14] Lythcke-Jørgensen C, Haglind F, Clausen LR. Exergy analysis of a combined heat and power plant with integrated lignocellulosic ethanol production. Energy Convers Manag 2014;85:817–27.
[15] Gassner M, Maréchal F. Methodology for the optimal thermo-economic, multi-objective design of thermochemical fuel production from biomass. Comput Chem Eng 2009;33(3):769–81.
[16] Gerber L, Gassner M, Maréchal F. Systematic integration of LCA in process systems design: application to combined fuel and electricity production from lignocellulosic biomass. Comput Chem Eng 2011;35(7):1265–80.
[17] Tock L, Maréchal F. Co-production of hydrogen and electricity from lignocellulosic biomass: process design and thermo-economic optimization. Energy 2012;45(1):339–49.
[18] Liu P, Gerogiorgis DI, Pistikopoulos EN. Modeling and optimization of polygeneration energy systems. Catal Today 2007;127(1–4):347–59.
[19] Liu P, Pistikopoulos EN, Li Z. A mixed-integer optimization approach for polygeneration energy systems design. Comput Chem Eng 2009;33(3):759–68.
[20] Liu P, Pistikopoulos EN. A multi-objective optimization approach to polygeneration energy systems design. AIChE J 2010;56(5):1218–34.
[21] Liu P, Pistikopoulos EN, Li Z. Decomposition based stochastic programming approach for polygeneration energy systems design under uncertainty. Ind Eng Chem Res 2010;49(7):3295–305.

Please cite this article in press as: Lythcke-Jørgensen C, et al., A methodology for designing flexible multi-generation systems, Energy (2016), http://dx.doi.org/10.1016/j.energy.2016.01.084

[22] Liu P, Pistikopoulos EN, Li Z. Polygeneration systems engineering. Process Syst Eng 2011;5:1–38.
[23] Chen Y, Adams TA, Barton PI. Optimal design and operation of static energy polygeneration systems. Ind Eng Chem Res 2011;50(9):5099–113.
[24] Chen Y, Adams TA, Barton PI. Optimal design and operation of flexible energy polygeneration systems. Ind Eng Chem Res 2011;50(8):4553–66.
[25] Chen Y, Li X, Adams II TA, Barton PI. Decomposition strategy for the global optimization of flexible energy polygeneration systems. AIChE J 2012;58(10): 3080–95.
[26] Tawarmalani M, Sahinidis NV. Global optimization of mixed-integer nonlinear programs: a theoretical and computational study. Math Program 2004;99(3): 563–91.
[27] Chen Y. Optimal design and operation of energy polygeneration systems. 2013.
[28] Marnay C, Venkataramanan G, Stadler M, Siddiqui AS, Firestone R, Chandran B. Optimal technology selection and operation of commercial-building microgrids. IEEE Trans Power Syst 2008;23(3):975–82.
[29] Rubio-Maya C, Uche-Marcuello J, Martínez-Gracia A, Bayod-Rújula AA. Design optimization of a polygeneration plant fuelled by natural gas and renewable energy sources. Appl Energy 2011;88(2):449–57.
[30] Rubio-Maya C, Uche-Marcuello J, Martínez-Gracia A. Sequential optimization of a polygeneration plant. Energy Convers Manag 2011;52(8–9):2861–9.
[31] Piacentino A, Barbaro C, Cardona F, Gallea R, Cardona E. A comprehensive tool for efficient design and operation of polygeneration-based energy micro-grids serving a cluster of buildings. Part I: description of the method. Appl Energy 2013;111:1204–21.
[32] Capuder T, Mancarella P. Techno-economic and environmental modelling and optimization of flexible distributed multi-generation options. Energy 2014;71:516–33.
[33] Capuder T, Mancarella P. Modelling and assessment of the techno-economic and environmental performance of flexible multi-generation systems. In: 18th power syst. comput. conf. Wroclaw, Pol.; 2014.
[34] Martínez Ceseña E, Capuder T, Mancarella P. Flexible distributed multienergy generation system expansion planning under uncertainty. IEEE Trans Smart Grid 2015:1–10.
[35] Voll P, Lampe M, Wrobel G, Bardow A. Superstructure-free synthesis and optimization of distributed industrial energy supply systems. Energy 2012;45(1):424–35.
[36] Voll P, Klaffke C, Hennen M, Bardow A. Automated superstructure-based synthesis and optimization of distributed energy supply systems. Energy 2013;50(1):374–88.
[37] Meyer B, Voll P, Kirschbaum S, Bardow A. MILP optimization of nonlinear energy systems by multivariate piecewise-affine surrogate modeling. In: Proceedings of the 26th international conference on efficiency, cost, optimization, simulation and environmental impact of energy systems; 2013.
[38] Voll P, Hennen M, Klaffke C, Lampe M, Bardow A. Exploring the near-optimal solution space for the synthesis of distributed energy supply systems. Chem Eng Trans 2013;35:277–82.
[39] Petruschke P, Gasparovic G, Voll P, Krajačić G, Duić N, Bardow A. A hybrid approach for the efficient synthesis of renewable energy systems. Appl Energy 2014;135:625–33.
[40] Zhou Z, Zhang J, Liu P, Li Z, Georgiadis MC, Pistikopoulos EN. A two-stage stochastic programming model for the optimal design of distributed energy systems. Appl Energy 2013;103:135–44.
[41] Leung Pah Hang M, Martinez-Hernandez E, Leach M, Yang A. Engineering design of localised synergestic production systems. In: 25th European symposium on process systems engineering and 25th symposium on computer aided process engineering; 2015.
[42] Lythcke-Jørgensen C, Haglind F. Design optimization of a polygeneration plant producing power, heat, and lignocellulosic ethanol. Energy Convers Manag 2015;91:353–66.
[43] Maréchal F, Weber C, Favrat D. Multiobjective design and optimization of urban energy systems. Process Syst Eng 2011:39–83.
[44] Fazlollahi S, Maréchal F. Multi-objective, multi-period optimization of biomass conversion technologies using evolutionary algorithms and mixed integer linear programming (MILP). Appl Therm Eng 2013;50(2):1504–13.
[45] Fazlollahi S, Becker G, Maréchal F. Multi-objectives, multi-period optimization of district energy systems: I. Selection of typical operating periods. Comput Chem Eng 2014;65:54–66.
[46] Fazlollahi S, Becker G, Maréchal F. Multi-objectives, multi-period optimization of district energy systems: II-daily thermal storage. Comput Chem Eng 2014;71:648–62.
[47] Fazlollahi S, Becker G, Maréchal F. Multi-objectives, multi-period optimization of district energy systems: III. Distribution networks. Comput Chem Eng 2014;66:82–97.
[48] Bolliger R. Méthodologie de la synthèse des systèmes énergétiques industriels. 2010.
[49] Lythcke-Jørgensen C, Haglind F, Ensinas AV, Münster M. A method for aggregating external operating conditions in multi-generation plant optimization models. Appl Energy 2015;166:59–75.
[50] Jack MW. Scaling laws and technology development strategies for biorefineries and bioenergy plants. Bioresour Technol 2009;100(24):6324–30.
[51] Smith R. Chemical process design and integration. Chister, West Sussex, England: John Wiley & Sons Ltd; 2005.
[52] Boldrin A, Baral KR, Fitamo T, Vazifehkhoran AH, Jensen IG, Kjærgaard I, et al. A dynamic model for integrated optimization of biogas production – a case study on sugar beet biomass. Energy 2015. in process.
[53] Fazlollahi S, Mandel P, Becker G, Maréchal F. Methods for multi-objective investment and operating optimization of complex energy systems. Energy 2012;45(1):12–22.
[54] Haupt RL, Haupt SE. Practical genetic algorithms. John Wiley & Sons, Inc.; 2006.
[55] Kemp IC. Pinch analysis and process integration. 2006.
[56] Turton R, Bailie RC, Whiting WB, Shaeiwitz J a. Analysis, synthesis, and design of chemical processes. 1998.
[57] Morris MD. Factorial sampling plans for preliminary computational experiments. Technometrics 1991;33(2):161–74.
[58] Sin G, Gernaey KV, Lantz AE. Good modeling practice for PAT applications: propagation of input uncertainty and sensitivity analysis. Biotechnol Prog 2009;25(4):1043–53.
[59] Helton JC, Davis FJ. Latin hypercube sampling and the propagation of uncertainty in analyses of complex systems. Reliab Eng Syst Saf 2003;81(1): 23–69.
[60] McKay MD, Beckman RJ, Conover WJ. Comparison of three methods for selecting values of input variables in the analysis of output from a computer code. Technometrics 1979;21(2):239–45.
[61] Larsen J, Ø M, Haven, Thirup L. Inbicon makes lignocellulosic ethanol a commercial reality. Biomass Bioenergy 2012;46:36–45.
[62] Lythcke-Jørgensen C, Münster M, Ensinas AV, Haglind F. Design optimization of flexible biomass-processing polygeneration plants using characteristic operation periods. In: World renewable energy Congress XIII; 2014.
[63] "Silkeborg Forsyning." [Online]. Available: http://www.silkeborgforsyning.dk/. [accessed 13.09.15].
[64] Lythcke-Jørgensen C. Modelling and optimization of a steam co-generation plant with integrated bio-ethanol production. Technical University of Denmark; 2012.
[65] Evald A, Hu G, Hansen MT. Technology data for advanced bioenergy fuels. 2013.
[66] Energinet.dk, Danish Energy Agency. Technology data for energy plants, vol. 2012; January 2014.
[67] Münster M, Meibom P. Long-term affected energy production of waste to energy technologies identified by use of energy system analysis. Waste Manag 2010;30(12):2510–9.
[68] Danish Energy Agency. Forudsætninger for samfundsøkonomiske analyser på energiområdet. 2014.
[69] IPCC. 2006 IPCC guidelines for national greenhouse gas inventories, vol. 4; 2006.
[70] COWI. FJERNVARMEANALYSE – BILAGSRAPPORT. 2014.
[71] Danish Energy Agency, "Danske nøgletal," 2015. [Online]. Available: http://www.ens.dk/info/tal-kort/statistik-nogletal/nogletal/danske-nogletal.
[72] Larsen J, Østergaard Petersen M, Thirup L, Li HW, Iversen FK. The IBUS process – lignocellulosic bioethanol close to a commercial reality. Chem Eng Technol 2008;31(5):765–72.
[73] Energianalyse E. Opdatering af samfundsøkonomiske brændselspriser – BIOMASSE. 2011.
[74] Bentsen NS, Felby C, Ipsen KH. Energy balance of 2nd generation bioethanol production in Denmark. DONG Energy 2006:43.
[75] Adams TA, Ghouse JH. Polygeneration of fuels and chemicals. Curr Opin Chem Eng 2015;10:87–93.
[76] Souleimanov E, Kraus J. Turkey: an important east-west energy hub. Middle East Policy 2012;19(2):157–68.
[77] Hemmes K, Zachariah-Wolf JL, Geidl M, Andersson G. Towards multi-source multi-product energy systems. Int J Hydrogen Energy 2007;32(10–11):1332–8.

Please cite this article in press as: Lythcke-Jørgensen C, et al., A methodology for designing flexible multi-generation systems, Energy (2016), http://dx.doi.org/10.1016/j.energy.2016.01.084

APPENDIX F Journal paper 5 (manuscript)

Manucsript for ISI Journal

C.E. Lythcke-Jørgensen, L.R. Clausen, L. Algren, A.B. Hansen, M. Münster, R.Ø. Gadsbøll, and F. Haglind. *Optimization of a flexible multi-generation system based on CHP, wood chip gasification, and methanol production*. (Submitted for Applied Energy, special issue on energy supply networks. Manuscript number: APEN-D-16-02936).

This paper manuscript presents the content and outcomes *Case III*.

Optimization of a flexible multi-generation system based on wood chip gasification and methanol production

Christoffer Lythcke-Jørgensen [a]*, *Lasse Røngaard Clausen* [a], *Loui Algren* [b], *Anders Bavnhøj Hansen* [b], *Marie Münster* [c], *Rasmus Østergaard Gadsbøll* [d], *Fredrik Haglind* [a]

[a] *Technical University of Denmark, Department of Mechanical Engineering*

[b] *Energinet.dk*

[c] *Technical University of Denmark, Department of Management Engineering*

[d] *Technical University of Denmark, Department of Chemical Engineering*

** Corresponding author. Email: celjo@mek.dtu.dk. Phone: +45 30 42 72 00. Nils Koppels Allé 403, 2800 Kgs. Lyngby, Denmark.*

Abstract

Flexible multi-generation systems (FMGs) consist of integrated and flexibly operated facilities that provide multiple links between the different sectors of the energy system. The present study treated the design optimization of a conceptual FMG which integrated a methanol-producing biorefinery with an existing co-generation unit and industrial energy utility supply in the Danish city of Horsens. The objective was to optimize economic performance and minimize total CO_2 emission of the FMG which was required to meet the local district heating demand plus the thermal utility demand of the butchery. The design optimization considered: Selection, dimensioning, location and integration of processes; operation optimization with respect to both hourly variations in operating conditions over the year as well as expected long term energy system development; and uncertainty analysis considering both investment costs and operating conditions.

Applying a previously developed FMG design methodology, scalable models of the considered processes were developed and the system design was optimized with respect to hourly operation over the period 2015-2035. The optimal design with respect to both economic and environmental performance involved a maximum-sized biorefinery located next to local industry rather than in connection with the existing CHP unit. As the local industry energy demands were limited when compared to the biorefinery dimensions considered, process integration synergies were found to be marginal when compared to the economic and environmental impact of the biorefinery for the present case.

Assessing the impact of uncertainties on the estimated FMG performances, the net present value (NPV) of the optimal design was estimated to vary within the range 252.5 M€ to 1471.6 M€ in response to changes of $\pm 25\%$ in investment costs and methanol price, and considering two different electricity price scenarios. The results suggest that operating conditions, and in particular the methanol price, would have a much higher impact on the economic performance of the designs than corresponding uncertainties in investment costs. The results emphasize the importance of including systematic uncertainty analysis in the design optimization of FMG concepts.

Keywords: Biomass gasification, design optimization, flexible multi-generation, polygeneration, process integration, smart energy systems

Nomenclature

Latin letters

C_0	Net present value	[M€]
$C_{inv,k}$	Investment cost, process *k*	[M€]
$C_{inv,k0}$	Reference investment cost, process *k*	[M€]
$c_{op,i}$	Hourly operation result	[M€/h]
$c_{op,k}$	Operation cost, process *k*	[M€/h]
p_f	Power factor for economy-of-scale calculations	[-]
r	Interest rate	[-]
T	Number of years from installation date	[-]
t_i	Duration of period *i*	[h]
$t_{PV,i}$	Present value factor of period *i*	[h]
Z_0	Total CO_2 emission impact	[MTon]
z_{op}	Hourly CO_2 emission impact of operation	[MTon]

Greek letters

σ	Process dimension
ω	Installation decision (integer)
λ	Load

Subscripts

i	Period
k	Process

Abbreviations

CCHP	Combined cooling, heat and power
CHOP	Characteristic operating pattern
CHP	Combined heat and power
FMG	Flexible multi-generation systems
NPV	Net present value
RES	Renewable energy sources
SOEC	Solid oxide electrolysis cell
TCE	Total CO_2 emission impact

1. Introduction

The transition towards sustainable energy systems based on intermittent renewable energy sources (RES) necessitates the development of efficient means for balancing generation and consumption of energy services. While focus previously was centred on developing smart grid technology for the power grid, recent studies suggests that the challenge of balancing generation from renewables is better appreciated from a holistic energy system perspective in order to avoid suboptimal, sector-based solutions [1][2]. This holistic approach has been referred to as a Smart Energy System approach, and it promotes the integration of power, thermal and gas grids, and the use of various energy storage options in combination in order to achieve secure and sustainable energy systems based on renewable sources [3].

However, synergies from integrating energy conversion process in multi-generation systems are not considered directly using the smart energy systems approach. These synergies may be of great importance in the transition towards sustainable energy systems [4], especially regarding biomass conversion where it has been suggested that systematic consideration of process integration synergies may increase the energy- and cost-efficiency of the conversion as well as the overall system [5–8].

Responding to this, the concept of flexible multi-generation systems (FMG) was recently introduced by Lythcke-Jørgensen et al. [9]. Here, FMGs were defined as integrated systems that generate multiple energy services and are able to adjust operation in response to fluctuating demand patterns and varying price schemes in the overarching energy system. The hypothesis is that local or regional FMGs may support the balancing of an energy system with large shares of variable RES in a cost-effective way by linking the different parts of the energy system with local supply systems. By converting energy in response to demand and price variations, FMGs may be regarded as virtual energy system valves as conceptually illustrated in Figure 1, making the development of FMGs a relevant topic.

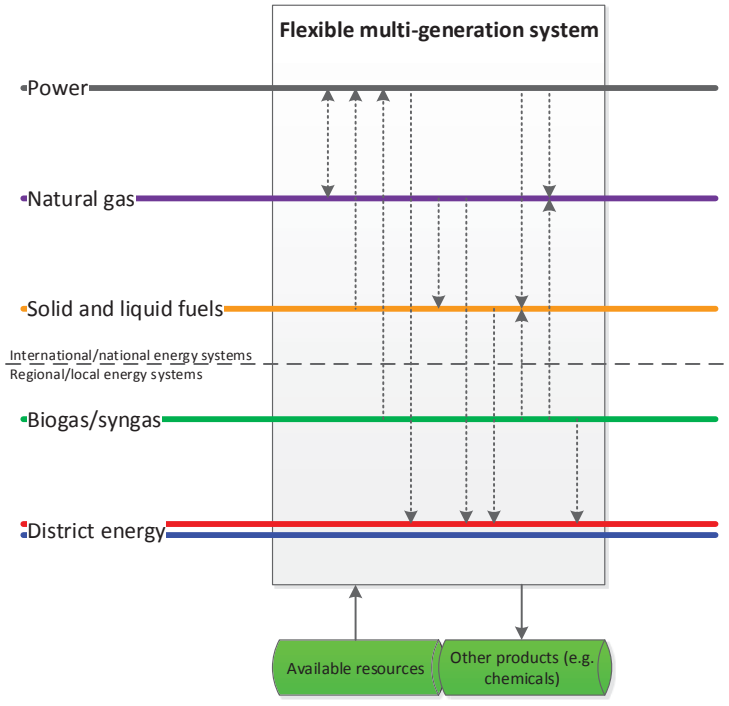

Figure 1: Conceptual sketch of the FMG concept [9]. Dotted arrows indicate a range of technological pathways for linking the energy system layers in an FMG.

The development of FMGs is complex and involves multiple design aspects. Within these, five aspects are considered of special relevance:

1. Process selection and dimensioning
2. Systematic process integration
3. Variable short-term operation conditions, including hourly, diurnal, weekly and seasonal changes in demands and generation from variable RES
4. Variable long-term operation conditions, responding to developments in the energy system
5. Uncertainty analysis

Numerous approaches for designing multi-generation systems have been presented in literature [10,11], but as discussed in Lythcke-Jørgensen et al. [9], none of these are able to consider all five listed aspects coherently. For instance, Liu et al. [12,13] [14] [15] developed a stochastic, multi-objective mixed integer-nonlinear programming model for designing polygeneration[1] systems, but did not consider short-term operation or process integration. Based on the OSMOSE tool[2], Maréchal et al. [16][17][18][19] presented a multi-period, multi-objective methodology for designing multi-generation systems which considered technology selection and dimensioning, process integration, facility location selection, flexible operation, and network layout. However, the combined methodology only considered variations in one external operating condition, namely outdoor temperature, meaning that flexible interactions with other parts of the energy system were not considered. In addition, uncertainties were not addressed in the combined methodology. In consequence, a novel methodology for designing FMGs was introduced in Lythcke-Jørgensen et al. [9] which included all the listed aspects as well as others, including biomass supply chains.

A number of specific FMG concepts have been treated in case studies. Regarding FMGs integrating the heat and power layers, Lund et al. [2] presented the case of Skagen combined heat and power (CHP) plant which included three CHP units, thermal energy storage, a peak load gas boiler, and an electrical boiler. The system effectively created a dual link between the electricity grid and the district heating system as the plant was able to both generate electricity and heat directly as well as convert electricity to heat. In a study of a comparable system, Sorknæs et al. [20] found that the system's ability of provide electricity grid balancing could increase the overall CHP operation load by 25% and reduce net heat production costs by 5% for a specific heating network. However, it was questioned if the results would be valid in case multiple comparable systems adopted a similar operation strategy due to the limited size of the balancing market. Capuder and Mancarella [21][22] studied seven different schemes for supplying electricity and heating in the UK. In a study, the group found that FMG schemes consisting of CHP units, electric heat pumps, and thermal energy storage may reduce investment and operating costs as well as aggregate emission levels when compared to conventional or less flexible heat and electricity supply systems in the UK. The group further found that FMG schemes may allow for reductions in both expected costs and risks under long-term price uncertainty scenarios when compared to less flexible systems [23].

Among FMGs integrating the power grid and liquid fuel layer, Chen et al. [24] studied an FMG using coal and biomass to generate electricity and co-produce naphtha, diesel and methanol. The group found that

[1] In a recent review, Adams and Ghouse [55] defined 'polygeneration' as a thermochemical process which simultaneously generates electricity and produces at least one type of chemical or fuel without being a co- or tri-generation unit

[2] OSMOSE is a computer aided process engineering tool, developed at EPFL in the IPESE group, for designing and optimizing integrated energy systems. For more information, refer to [49] or the IPESE group homepage: http://ipese.epfl.ch/.

flexible systems in general achieved higher net present values than static systems, however at the cost of larger investments. Lythcke-Jørgensen et al. [7,25–28] studied an FMG concept integrating cellulosic ethanol production with a CHP unit, creating a virtual link between the electricity, heating and fuel systems. Models and process integration strategies were analysed and optimized, and it was found that the lack of flexibility in the ethanol production induced inefficient operation during periods with high electricity prices, causing the entire system to be economically uncompetitive in an energy system with a large share of wind power [25,26]. At the same time, the average exergy efficiency of the ethanol production was markedly reduced when compared to the exergy efficiency in optimal operation [27,28]. It was further found that a diseconomy-of-scale trend applied for the ethanol production in the FMG under the set conditions as reductions in integration synergies exceeded the benefits from economy-of-scale in investment and operating costs [7]. These outcomes illustrate some of the challenges faced when developing flexible technologies for energy systems with large shares of varying RES.

In two recent studies, Lythcke-Jørgensen et al. [9,29] studied an FMG concept combining heat and power generation with the production of cellulosic ethanol and biogas-based synthetic natural gas. It was demonstrated how operation flexibility is a central aspect when assessing the performance of FMGs [29], and that systematic process integration ought to be considered when optimizing the design of FMGs [9]. The outcomes illustrate the importance of systematically considering the five previously listed design aspects when developing FMGs for energy systems with large shares of variable RES.

This paper treats the development of a conceptual FMG based on an existing CHP unit and local industry. The FMG was developed for producing methanol from biomass and supplying district heating and industrial energy utilities. Using the state-of-the-art design optimization methodology presented in Lythcke-Jørgensen et al. [9], the FMG was optimized with the aim of maximizing net present value (NPV) and minimizing the total CO_2 emission impact (TCE) from operating the system over the period 2015-2035. Technologies considered include a two-stage biomass gasifier, a solid oxide electrolysis cell (SOEC), a methanol production facility, industrial heat pumps, and novel heat and gas infrastructures, altogether linking the power, district heating, natural gas, and fuel layers of the energy system.

The present work addresses the knowledge gap between process level optimization and energy system level optimization by taking system level variations into account when designing energy conversion systems. The novelty of the study lies in the design optimization that coherently considers: Process selection and dimensioning; systematic process integration using pinch analysis; consideration of local demands for energy services and local infrastructures; performance assessment with respect to hourly variations in operating conditions as well as long-term energy system development; and uncertainty analysis considering uncertainties in important design parameters. In addition, the design optimization assesses performance variations with respect to various energy system scenarios. To the authors' best knowledge, no previous work has presented such comprehensive approach to the design optimization of an FMG concept.

In this paper, the case study considered and the applied optimization methodology are described in Section 2. Results of the design optimization and systematic assessment of uncertainties are presented in Section 3, while Section 4 features a discussion on potential drawbacks of the work and recommendations for future research within this field. A conclusion on the study is presented in Section 5. Appendix A features a full documentation of the process modelling, while Appendix B includes documentation on the structuring of energy system scenario datasets in the present work.

2. Methods

2.1. Case description

The case study treated in this paper was centred on the Horsens Kraftvarmeværk, a back-pressure CHP unit in the Danish city of Horsens with a population of 56,536 [30]. The back-pressure CHP unit has a full-load capacity of 7MWe and 25 MJ/s district heating and consists of a steam Rankine cycle with two 5 ton/hour waste incineration boilers. In addition, a gas turbine is installed on site, which is capable of boosting district heating production with 8 MJ/s [31]. Furthermore, a large butchery located approximately 9 km from the CHP unit was included in the case study. The thermal utility demand of the butchery was assumed covered by natural gas in the reference case. A sketch of the reference system is presented in Figure 2.

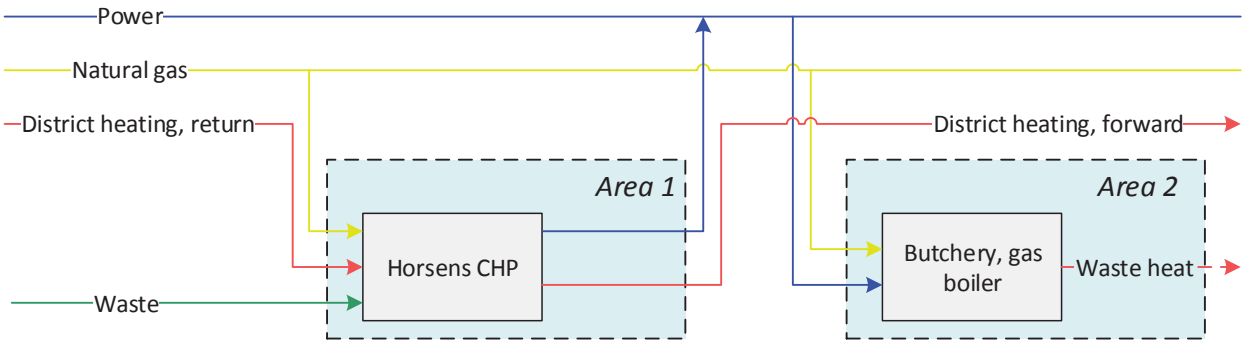

Figure 2: Conceptual sketch of energy flows in the reference system.

The case study treated the retrofitting of the reference system by installing a biorefinery, consisting of a two-stage biomass gasifier [32], a solid oxide electrolysis cell (SOEC), and a methanol production facility. The biorefinery was to be installed either next to the CHP unit or the butchery, and the installation of a product gas pipeline between the two areas was considered. In addition, it was considered to invest in a district heating link to the butchery area, in order to cover parts of the butchery thermal utility demands through district heating using ammonia-water hybrid heat pumps. The conceptual retrofit options are illustrated in Figures 3 and 4.

The hypothesis is that the present FMG is advantageous in an energy system with large shares of intermittent renewable power generation as it may absorb additional power in periods with excess generation (low power prices) and convert it to methanol by boosting product gas from the gasifier with hydrogen from the SOEC [8]. Similarly, it may reduce power consumption in periods with high power prices by reducing SOEC load and thereby methanol production. At the same time, process integration is used to optimize the overall energy conversion efficiency of the system, potentially increasing thermodynamic and economic efficiencies when compared to non-integrated facilities [9,29]. Process heat demands of the butchery could further be met through process integration with the biorefinery, by compression-based ammonia-water hybrid heat pumps using district heating as heat source, or by product gas combusted in the butchery gas boiler. In addition, non-reacted product gas may replace parts of the gas utility demand of the butchery, thereby replacing natural gas. In total, this tentative combination of processes allows for a flexible energy supply system capable of converting biomass resources to demanded energy services in order to replace fossil fuels, while at the same time providing links between the electricity, district heating, natural gas, and fuel sectors of the overarching energy system.

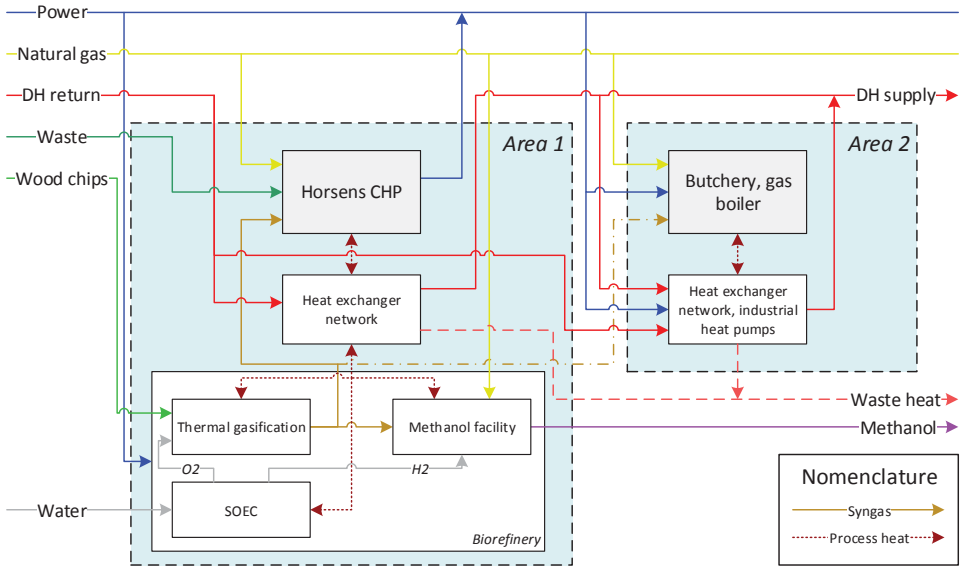

Figure 3: Conceptual sketch of energy flows in 'Retrofit Scenario A' with the biorefinery installed next to the CHP unit.

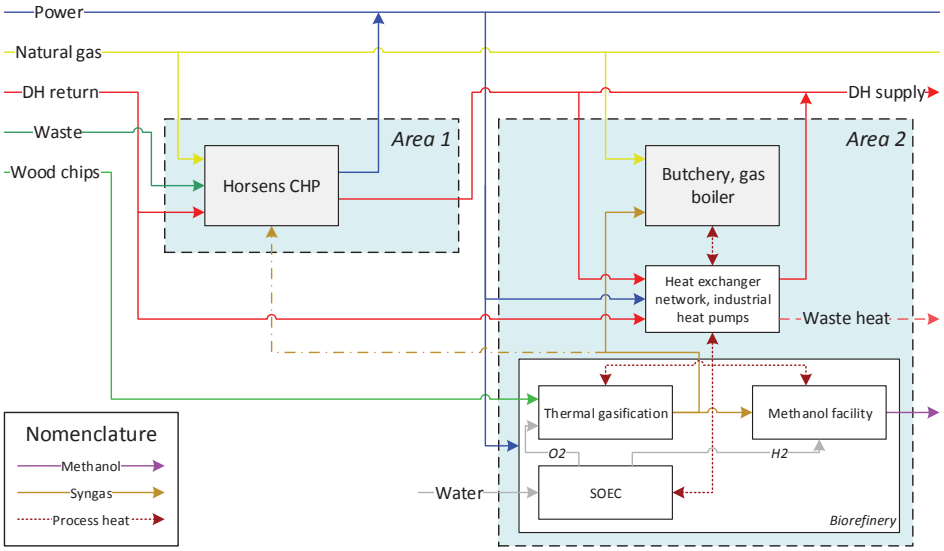

Figure 4: Conceptual sketch of energy flows in 'Retrofit Scenario B' with the biorefinery installed next to the butchery.

2.2. Methodology

As mentioned, a previously developed methodology for designing FMGs [9] was applied in this work. The methodology structure is presented in Figure 5.

In short, the methodology applied is capable of conducting multi-objective design optimization of an FMG superstructure whilst considering:

- Selection, location, and dimensioning of processes
- Systematic heat and mass integration using pinch analysis
- Flexible operation optimization with respect to both short-term market fluctuations and long-term energy system development through the application of the Characteristic Operating Pattern (CHOP) method [33]

- Investment planning
- Global sensitivity and uncertainty analysis
- Consideration of local resource availability, biomass supply chains, and market sizes
- Variable part-load performance

Input data to the design methodology includes process and equipment models, energy system data, local resource data, and life cycle inventory data. The input data is structured prior to the optimization, which is conducted by a hybrid genetic algorithm/mixed integer-linear programming model. The optimization generates a database of designs with deterministic performances, for which Pareto analysis can be conducted. A number of interesting designs may then be picked for further assessment, including sensitivity and uncertainty analysis.

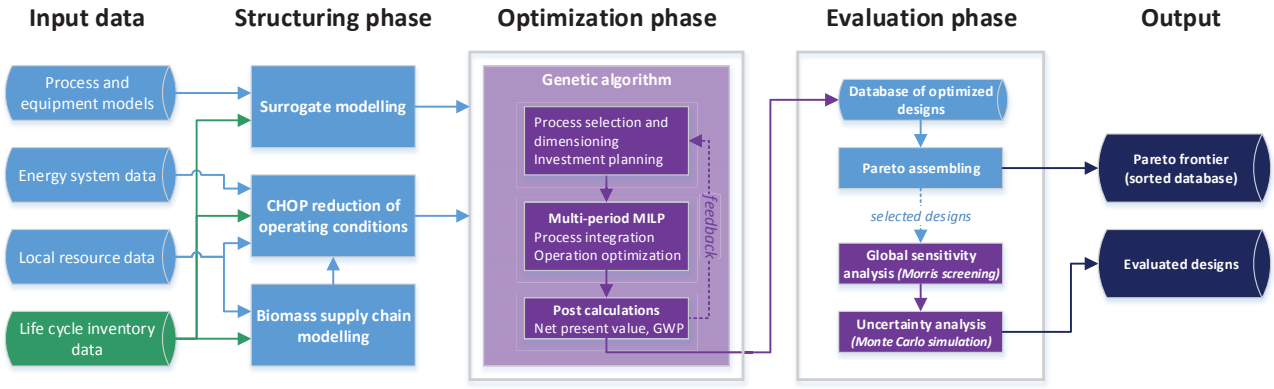

Figure 5: Design methodology structure [9]**. The structure illustrates how input data is first structured, following which the primary optimization is conducted. The outcomes of the optimization are afterwards assessed further.**

In the present case, the retrofit design was optimized with the aim of maximizing net present value (NPV) and minimizing the total CO_2 emission impact (TCE) from operating the system over the period 2015-2035. Investment planning and wood chips supply chains are not considered in the study.

2.3. Modelling and assumptions

2.3.1. Horsens CHP and district heating system

The two waste incineration boilers at Horsens CHP have a capacity of 5 tonnes of waste per hour each, and their minimum operation load is 75% [31][34]. Due to the demand for processing of local waste, the boilers were assumed to be operated at all times. The Rankine cycle was operated in back-pressure mode with a nominal power generation capacity of 7 MWe and a nominal heat generation capacity of 25 MJ/s [31]. The steam Rankine cycle has two condensers in order to optimize the overall exergy efficiency: One operated at 0.3 bar, and the other at 0.8 bar [31]. To comply with the district heating forward and return temperatures, it was assumed that 75% of the condensation heat was generated in the 0.8 bar condenser, and that the generation of power and heat was directly proportional to the load.

Assuming that the exhaust gas from the gas turbine was used directly for district heating generation, with a nominal capacity 8 MJ/s [31], the nominal gas consumption and electricity generation capacities were calculated using estimated values of electrical efficiency and overall energy efficiency of the gas turbine.

The district heating system was assumed to have a maximum district heating demand equal to the heat generation potential of Horsens CHP. A forward/return temperature scheme of $90℃/40℃$ was assumed, and seasonal differences were neglected.

Operation data used in the modelling of Horsens CHP is presented in Table 1. Functions relating energy and mass flows in the system to operation variables are presented in Appendix A.

Table 1: Operation data used in the modelling of Horsens CHP.

Parameter	Notation	Value
RANKINE CYCLE		
waste incineration capacity	σ_{ran}	33.3 MJ/s [31][a]
nominal power generation	P_{ran}	7.0 MWe [31]
nominal district heating generation	$\dot{Q}_{ran}$	25.0 MJ/s [31]
nominal heat in 0.8 bar condenser	$\dot{Q}_{ran,hp0}$	18.75 MJ/s
nominal heat in 0.3 bar condenser	$\dot{Q}_{ran,lp0}$	6.25 MJ/s
minimum load	$\lambda_{ran,min}$	0.75 [31][34]
variable operating costs	$c_{ran,var}$	15.9 €/$MWh\ waste$ [34][b]
energy efficiency	η_{ran}	0.96 [34]
GAS TURBINE		
nominal gas consumption	σ_{gt}	20.0 MWth
electrical efficiency	$\eta_{gt,E}$	0.4 [34]
energy efficiency	η_{gt}	0.8 [34]
off-gas temperature	$T_{gt,max}$	600℃
cooled exhaust gas temperature	$T_{gt,min}$	70℃
variable operating costs	$c_{gt,var}$	7.0 €/$MWh\ gas$ [34]
minimum load	$\lambda_{gt,min}$	0.40 [34][c]
DISTRICT HEATING SYSTEM		
maximum district heating demand	σ_{dh}	33.0 MJ/s
forward temperature	$T_{dh,fw}$	90℃
return temperature	$T_{dh,rt}$	40℃

[a]: **Corresponding to a processing capacity of 10 ton/h of waste**[34].
[b]: **Corresponding to 53.0 Euro/ton of waste** [34]
[c]: **The minimum load is assumed constrained due to emission restrictions** [34].

2.3.2. Butchery

Based on specialist knowledge collected by Energinet.dk, the shares of thermal utility demands in a typical Danish butchery running on natural gas are presented in Table 2. The values were used to describe the thermal utility demands of the butchery in the case study. It was assumed that the butchery had a nominal energy utility demand of 6.43MWth[3], that the thermal parts of the utility demand was met by a natural gas boiler in the reference case, and that excess heat from thermal utility demands above $100℃$ could be recovered and utilized directly for district heating generation. Operation data used in the modelling of the butchery is summarized in Table 3. Functions for energy and mass flows in the system are presented in Appendix A.

[3] This capacity represents the capacity of an average butchery in Denmark, according to Energinet.dk.

Table 2: Average thermal utility demands in Danish butcheries.

Thermal utility demand	Share of energy demand	Assumed temperature requirements
Boiling and evaporation	4%	110℃
Cleaning	37%	60℃
Process gas	35%	–
Room heating and losses	24%	35℃

Table 3: Operation data used in the modelling of the butchery.

Parameter	Notation	Value
Maximum thermal utility demand	σ_{ind}	6.43 MJ/s
Gas boiler operating costs	$c_{gb,var}$	0.5 €/MWh [34]

2.3.3. Biorefinery

The biorefinery considered was based on an upscaled version of the Two-stage Biomass Gasifier, a gasifier concept which can generate a product gas almost free of tar (5 mg/Nm^3) and with a low methane content [35]. The gasifier is air-blown and has been demonstrated in a size up to 1.5 MWth input [36]. The gas from the gasifier is used by the biorefinery for methanol production and process heat generation, by the CHP for heat generation, or by the butchery for process gas and heat. When the gasifier is air-blown, only a part of the product gas can be converted to methanol because of nitrogen build up in the methanol synthesis loop. In order to increase the biomass to methanol conversion, an SOEC is included in the biorefinery. The SOEC can supply pure oxygen for the gasifier and hydrogen for the methanol synthesis.

In the present work, a surrogate model of the biorefinery was developed based on the models by Clausen et al. [32][8]. The gasifier was assumed fed by imported wood chips. The division of reference components into surrogate models is illustrated in Figure 6. In addition to this, an SOEC model was developed. Finally, a gas burner for burning un-reacted product gas was assumed installed on-site with the biorefinery.

The integration of the SOEC increases the operational flexibility of the biorefinery, and the biorefinery can generally be said to operate in one of the following three modes: 1) air-blown, 2) oxygen-blown, 3) hydrogen boosted. In mode 2, the SOEC operates in part load, based on the oxygen demand of the gasifier. In mode 3, the SOEC operates at full load based on the maximum feasible addition of hydrogen in the methanol synthesis.

The energy conversion ratio of biomass-to-methanol for running in air-blown, oxygen-blown, and hydrogen-boosted operation modes were identified from simulations of the reference model [32]. Assuming linear relations for SOEC loads between the three described operating modes, the biomass-to-methanol energy ratio of the biorefinery as a function of SOEC load is plotted in Figure 7. The figure clearly shows a bend in the curve at an SOEC load of 0.37, where the oxygen-blown operating mode is defined. The slope of the curve to the left of the oxygen-blown point is about two times higher than the slope to the right, meaning that the conversion of electricity to methanol, by means of an SOEC, is twice as efficient below the full oxygen-blown operation point. The SOEC can therefore be allowed to operate in oxygen-blown mode at a higher electricity price than what could be advantageous for the hydrogen-boosted mode.

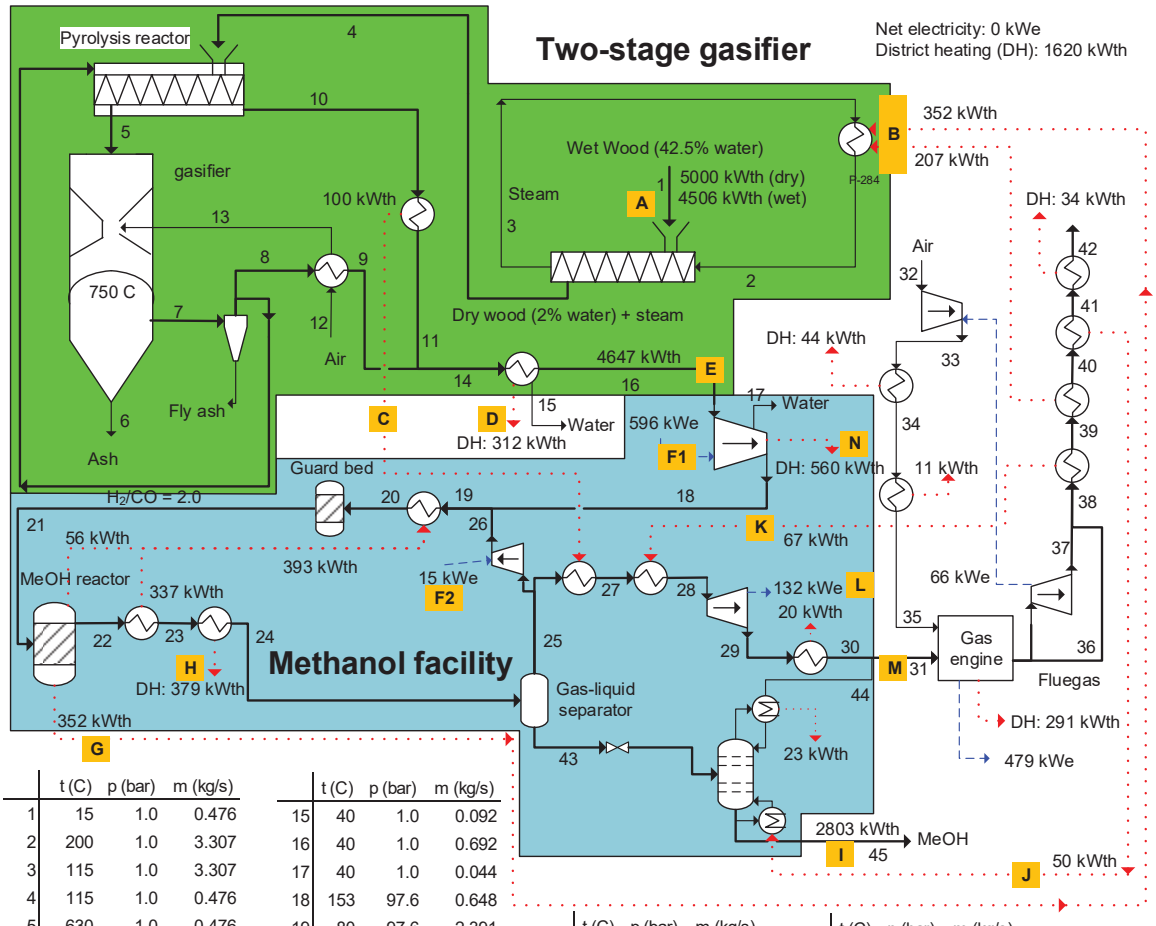

	t (C)	p (bar)	m (kg/s)
1	15	1.0	0.476
2	200	1.0	3.307
3	115	1.0	3.307
4	115	1.0	0.476
5	630	1.0	0.476
6	730	1.0	0.004
7	730	1.0	0.784
8	730	1.0	0.209
9	80	1.0	0.209
10	236	1.0	0.575
11	127	1.0	0.575
12	15	1.0	0.313
13	700	1.0	0.313
14	114	1.0	0.784

	t (C)	p (bar)	m (kg/s)
15	40	1.0	0.092
16	40	1.0	0.692
17	40	1.0	0.044
18	153	97.6	0.648
19	80	97.6	2.391
20	200	96.8	2.391
21	200	96.8	2.391
22	220	95.0	2.391
23	110	94.3	2.391
24	40	93.8	2.391
25	40	92.0	2.211
26	47	99.0	1.743
27	206	90.9	0.469
28	320	90.2	0.469

	t (C)	p (bar)	m (kg/s)
29	64	2.0	0.469
30	25	2.0	0.469
31	25	2.0	0.504
32	15	1.0	0.730
33	99	2.0	0.730
34	40	2.0	0.730
35	25	2.0	0.730
36	400	1.9	0.389
37	326	1.0	0.844

	t (C)	p (bar)	m (kg/s)
38	350	1.0	1.233
39	301	1.0	1.233
40	145	1.0	1.233
41	106	1.0	1.233
42	80	1.0	1.233
43	40	92.0	0.180
44	25	2.0	0.035
45	84	2.0	0.145

Figure 6: Reference model of the wood chip-based two-stage gasifier and methanol facility, with surrogate model division outlined. Flows denoted with a letter are included in the surrogate model, see Appendix A. Modified version of a figure from Clausen [32].

In hydrogen-boosted mode almost all the carbon in the product gas could theoretically be converted to methanol, but in the present biorefinery design the carbon-to-methanol conversion is constrained to 89%[4]. In oxygen-blown mode 66% of the carbon in the product gas is converted to methanol (practically all CO is converted), while in air-blown mode 41% of the carbon is converted to methanol. Only in air-blown mode will the unreacted product gas contain significant amounts of energy and therefore allow for export of this mass flow to the butchery.

[4] The carbon conversion could be increased to 97% by recirculating the CO_2 from the topping column (stream 44 on Figure 6) to the methanol synthesis loop.

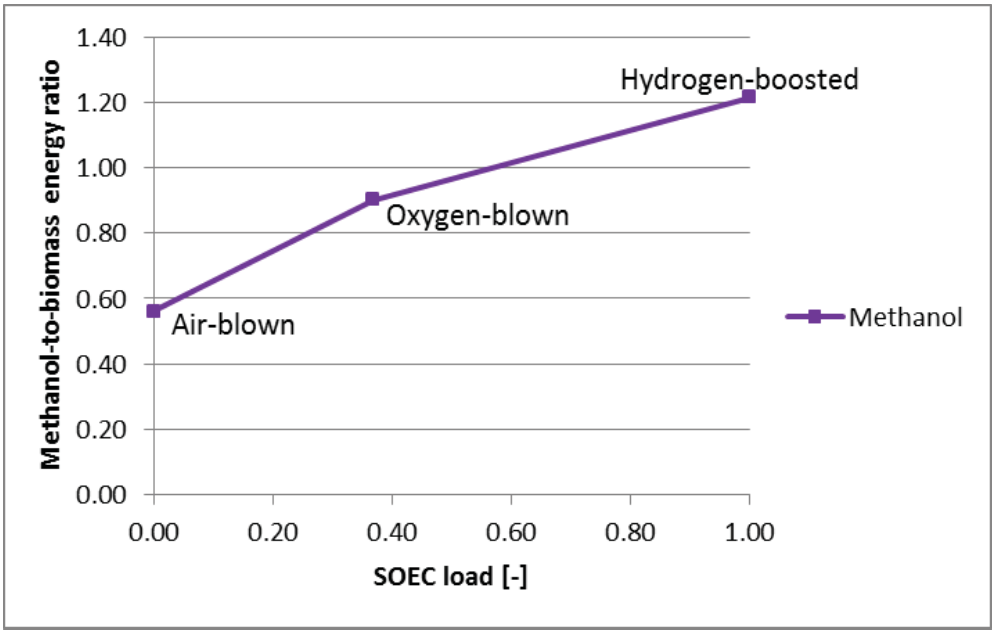

Figure 7: Methanol-to-biomass energy conversion ratio for different SOEC loads.

Operation data used in the biorefinery model is summarized in Table 4, while functions for energy and mass flows in the system are included in Appendix A. It was assumed that operation and maintenance costs for the biorefinery, excluding resource consumption costs, were independent of operation. Sales of excess oxygen were not considered.

Table 4: Operation data used in the biorefinery model.

Parameter	Notation	Value
Biomass-to-product gas efficiency	$\eta_{gasifier,NCV}$	0.93 [32]
SOEC power-to-hydrogen efficiency	$\eta_{SOEC,NCV}$	0.92[a]
Reference dimension	$\sigma_{0,bio}$	360 MJ/s *wood chips* [37]
Reference investment cost	$C_{inv,bio0}$	314.9 M€ [34][37] [a]
Reference fixed annual operating costs	$c_{op,bio}$	9.2 M€/year [34][37] [a]

[a] Efficiency calculated by assuming an inlet temperature of 770 °C and an outlet temperature of 800 °C combined with the assumption that 5% of the electricity is lost (heat losses, inverter loss, and electricity consumption by blowers etc.) [38].
[b]: Investment and fixed operating costs are calculated for the combined biorefinery, with an SOEC dimensioned for maximum hydrogen boost of the methanol production.

2.3.4. Infrastructure and industrial heat pumps

In the case study, investments in district heating and gas infrastructure for connecting the two areas were considered. The distance between the areas was set to be 9km. Costs of infrastructure investments used in the case study are summarized in Table 5. Infrastructure operation and maintenance costs were neglected.

The forward district heating water could be utilized as heat source for ammonia-water hybrid heat pumps that may provide process heating at temperatures of up to 140°C [39]. In the case study, it was assessed if such heat pumps would be beneficial for meeting the boiling and evaporation thermal utility demands of the butchery. A scalable surrogate model of an ammonia-water hybrid heat pump was developed based on a reference model presented by Jensen et al. [39]. Data used in the modelling of the heat pump is presented in Table 6, while functions for thermal and mass flows are summarized in Appendix A.

Table 5: Infrastructure investment costs.

Parameter	Notation	Specific costs	Investment cost
District heating connection of butchery	$c_{inv,DH}$	195 €/m [a]	1.76 M€
Gas pipe between Horsens CHP and butchery	$c_{inv,gas}$	130 €/m [b]	1.17 M€

[a]: Assuming that a district heating pipe with inner/outer diameter of 0.89m/2.80m is trenched beneath asphalt roads [40].
[b]: Assuming investment costs equivalent to hydrogen pipes with an inner diameter of 160 mm and a flow pressure of 1 to 4 bars. This size is assessed adequate for a peak supply of ca. 14 MJ/s syngas. Operation and maintenance costs are neglected [41].

Table 6: Data used in the ammonia-water hybrid heat pump model.

Parameter	Notation	Value
Source inlet temperature	T_{source}	90°C
Source temperature difference	ΔT_{source}	50°C
Sink inlet temperature	T_{sink}	120°C
Sink temperature difference	ΔT_{sink}	10K
Temperature lift	ΔT_{lift}	50°C [a]
Coefficient of performance	COP	2.9 [39][b]
Reference investment cost	$C_{inv,hp0}$	0.43 M€ [b]
Reference heat pump dimension	σ_{hp0}	1.0 $MJ/s\ sink\ heat$[b]
Operating cost	$c_{op,hp}$	4900 €/$(MJ/s - year)$ [34][c]

[a]: The temperature lift is set as the difference between average DH temperature and sink outlet temperature.
[b]: The values are taken for an ammonia-water hybrid heat pump with sink and source temperature lifts of 10K and with optimized ammonia fraction and circulation ratio for the given operating scheme, as predicted by Jensen et al. [39].
[c]: The heat pump operating costs are assumed equal to the highest predicted operating costs of an electric district heating heat pump [34].

2.4. Energy system data

Three reference years were used for describing the energy system development over the period 2015-2035, namely 2015, 2025, and 2035. The energy system data for 2015 was assumed repeated for the first 6 years, the data from 2025 was assumed repeated for the following 8 years, while the data for 2035 was assumed repeated for the final 6 years of the period.

Table 7: Fuel prices in the reference years.

Parameter	2015 scenario	2025 scenario	2035 scenario	Reference
Natural gas	9.66 [€/GJ]	9.93 [€/GJ]	10.51 [€/GJ]	[42]
Wood chips	6.52 [€/GJ]	6.90 [€/GJ]	7.52 [€/GJ]	[42]
Methanol	21.25 [€/GJ][a]	24.63 [€/GJ][a]	28.34 [€/GJ][a]	[42]
Gasoline	*20.73* [€/GJ]	*23.68* [€/GJ]	*25.42* [€/GJ]	[42]
CO_2 quota, intermediate estimate	*7.41* [€/ton]	*13.62* [€/ton]	*42.21* [€/ton]	[42]
Oil[b]	*13.72* [€/GJ]	*16.51* [€/GJ]	*18.16* [€/GJ]	[42]

[a]: The methanol price is calculated as the estimated gasoline value plus the estimated economic value of avoided CO_2 emissions with respect to CO_2 quota value.
[b]: To be consistent with data, the fuel oil price corresponds the to the predicted oil price from [42] and not the actual oil price, which by March 2016 is around 40 USD/barrel, corresponding 6.11 [€/GJ] [43].

As illustrated in Figure 3 and Figure 4, the FMG interacts with the surroundings through the import and/or export of power, natural gas, district heating, waste, wood chips, and methanol. Waste is assumed to be free as the FMG is obliged to provide waste processing. Prices for natural gas, wood chips and methanol in each of the three reference years are presented in Table 7.

The FMG was considered to be the sole provider of district heating and industry energy utility, so the district heating demand and industry energy utility demand had to be met by the FMG at all times.

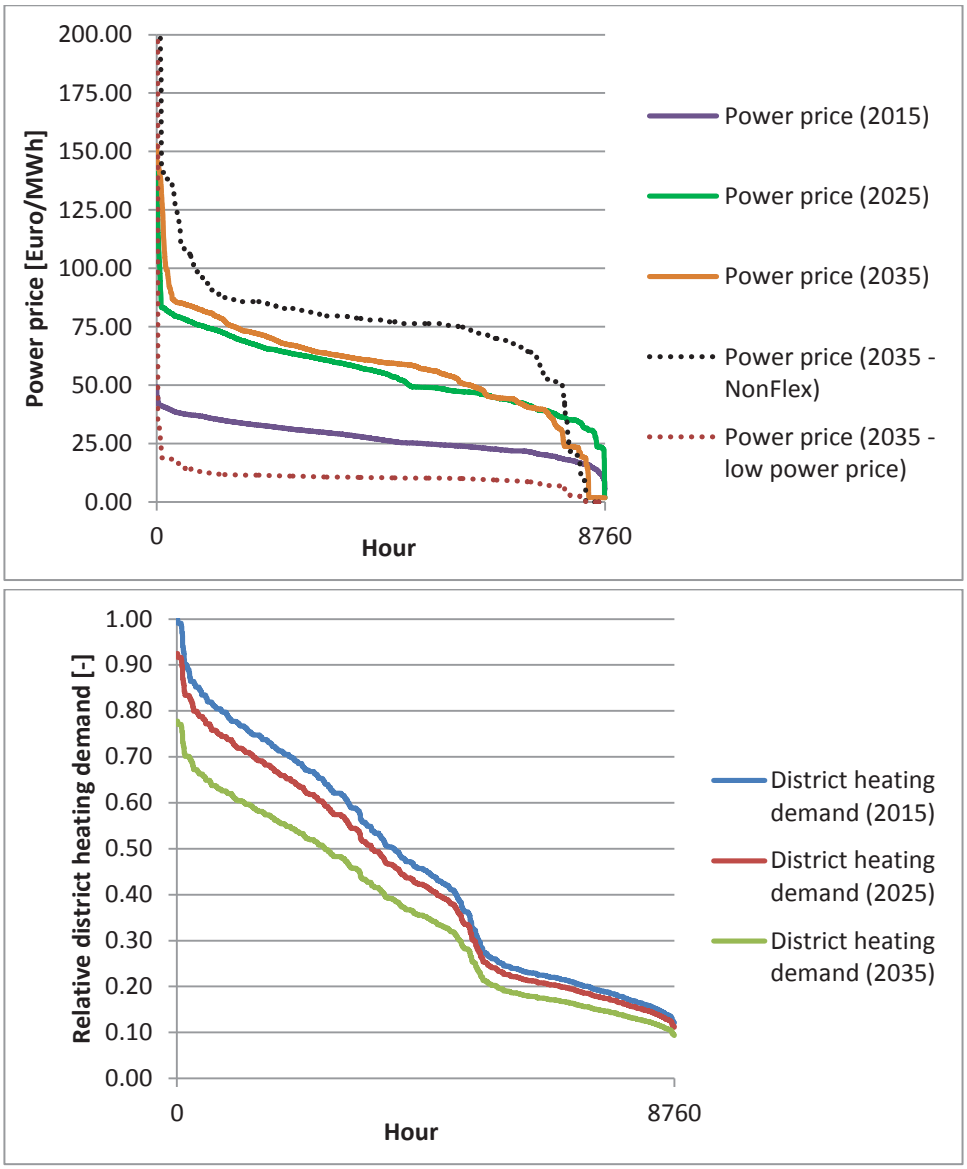

Figure 8: Annual duration curves for the power price and relative district heating demand in Horsens in each of the three scenarios.

For the reference scenario, the district heating demand and expected power price were extracted from simulations using the energy system model SIFRE [44]. SIFRE is an energy systems modelling tool developed to handle flexible, integrated energy systems and include accurate representation of new components such as renewable energy production, flexible demand, and new types of energy carriers as for instance various green gasses. SIFRE simulates each power plant individually and solves the unit commitment problem for an optimal production schedule. SIFRE simulates the existing day-ahead market and generates electricity prices which are used as boundary conditions, assuming that the operation of the FMG-plant is not affecting the national prices considerably. The three scenario simulations for 2015, 2025 and 2035 were based on Energinet.dk's analysis assumptions [45]. Duration curves for the power price and district heating demand for each of the scenarios are presented in Figure 8. In addition, two other duration curves for 2035

are included in the figure: one from the NonFlex scenario, in which power prices were extracted from a different energy system simulation scenario based on the assumption that smart grid technology will not break through in Denmark, meaning that the operation of electric vehicles, individual heat pumps and electrolysis plants is not optimized for the electricity price [46]. And a low power price scenario, in which power prices in 2035 has been reduced by a factor 7.5 as compared to the NonFlex scenario, to assess what impact extremely low and highly variable power prices would have on the system performance.

Data on annual butchery thermal utility demand was assumed similar for each year of the period. The demand profile was provided by Energinet.dk and is based on the hourly natural gas consumption of a number of Danish food industries in 2014. The duration curve is presented in Figure 9.

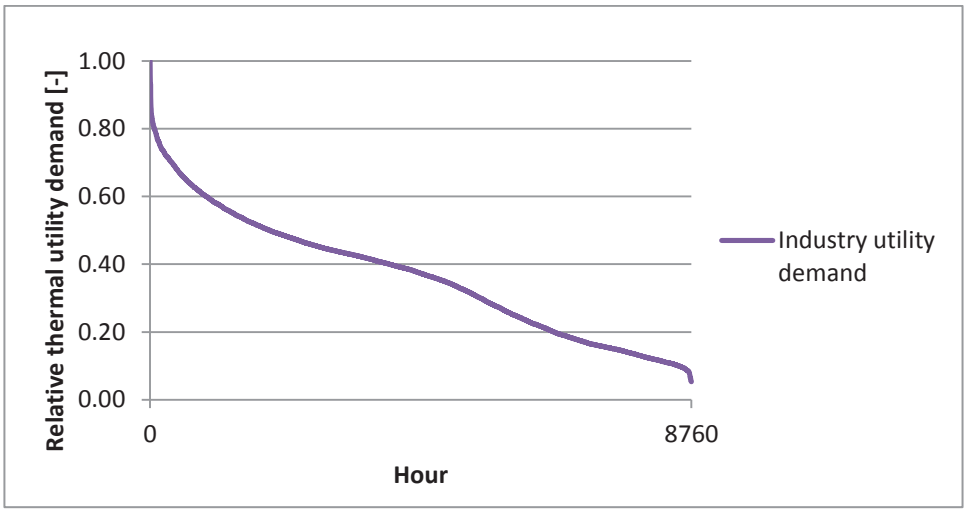

Figure 9: Relative industry thermal utility demand duration curve for one year.

As the system can be looked upon as replacing an existing district heating supply system and a reference industrial energy supply system, neither CO_2 emission replacements nor incomes are associated with district heating and industry thermal utility generation. Instead, the resulting NPV and TCE of the FMG may be compared with those of the reference system to assess the performance of the retrofitted system.

Four additional scenarios were considered for assessing performance uncertainties of selected designs: A low fuel price scenario, where methanol selling price was reduced by 25% compared to the reference scenario; a high fuel price scenario, where methanol selling price was increased by 25% compared to the reference scenario; a NonFlex power scenario, in which power prices for 2035 were taken from the NonFlex scenario as described previously [46]. And a low power price scenario, in which power prices in 2035 has been reduced by a factor 7.5 as compared to the NonFlex scenario.

Regarding TCE calculations, average emissions from power generation in the Danish energy system were used to represent the emissions of consumed or generated electricity. For 2015, the average CO_2 emission from power generation was set to 270 kg/MWh, while it was set to 112 kg/MWh for 2025 and 2035 [45]. CO_2 emissions from waste combustion were set to 37.0 kg/GJ [47]. A CO_2 emission of 57.0 kg/GJ was associated with natural gas combustion, while methanol was assumed to replace gasoline with an energy ratio of 1:1 and thereby resulting in a CO_2 emission reduction of 73.0 kg/GJ [45].

In order to reduce computation time of the operation optimization, the external operating condition dataset was reduced using the Characteristic Operating Pattern (CHOP) method for data aggregation [33]. In short, the CHOP method is a visually-based aggregation method, which clusters operating points with similar parameter values in representative data points called CHOP groups. The operation optimization is then conducted for the CHOP groups rather than for each operating point, significantly reducing the computational effort. The clustering principle is illustrated in Figure 10.

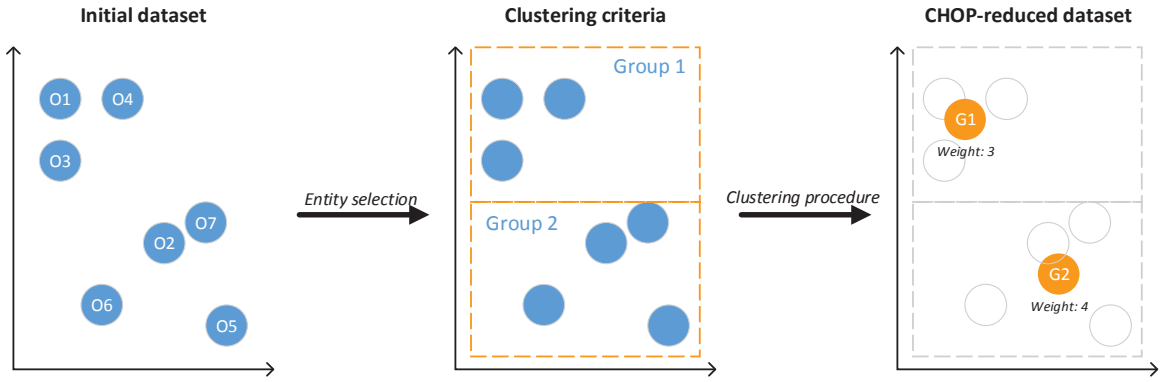

Figure 10: Principal sketch of the data aggregation principle applied in the CHOP method [33]. Operating points O_j are clustered and merged into CHOP groups G_i with aggregated weight factors.

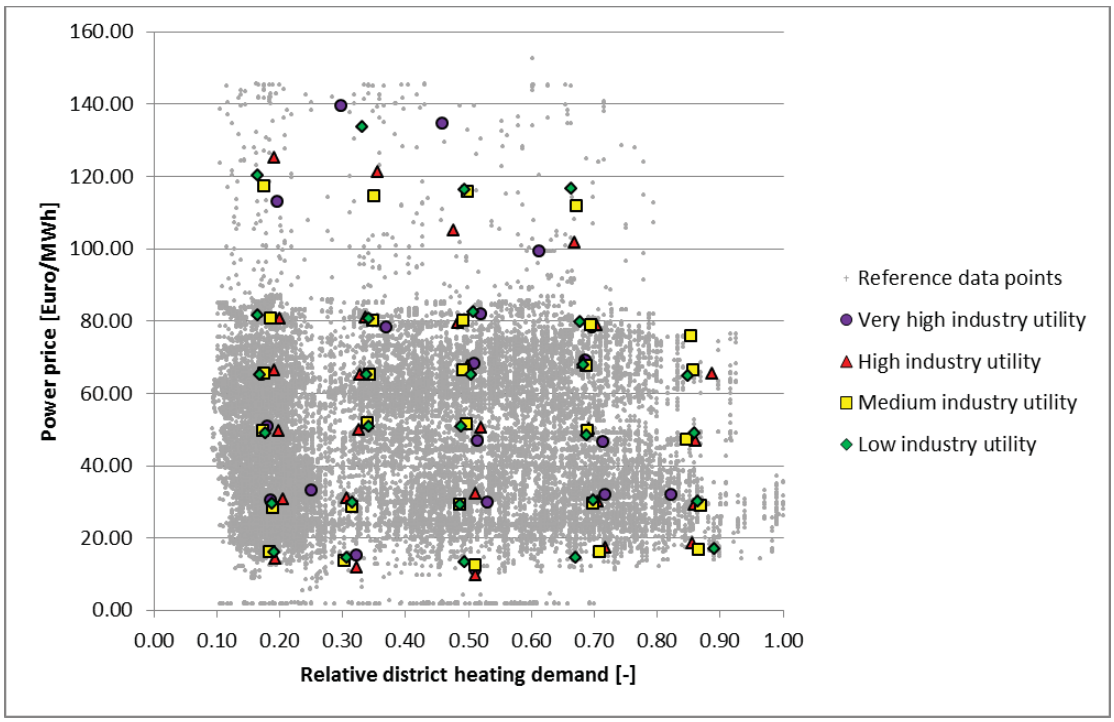

Figure 11: Scatter plot of the reference dataset and the aggregated dataset with respect to relative heating demand and power price. Note that the third dimension, industry utility demand, is not visible for the reference data points and that the duration (weight) of the aggregated points depends on the amount of reference points in their vicinity. For more information, refer to Appendix B.

In the present case, five volatile external operating conditions were identified using the CHOP approach: Power price, district heating demand, butchery thermal utility demand, wood chips price, and methanol price. Natural gas was not considered as a volatile external operating condition as the absolute variation

over the scenario was less than 10%. In order to minimize the number of CHOP groups to consider, data clustering was only conducted with respect to power price, district heating demand, and butchery thermal utility demand as they were the parameters with the largest volatility. The accuracy error of not clustering for methanol, natural gas, and wood chip prices was assessed a posteriori. The entire CHOP method procedure is described in Appendix B, and the resulting CHOP datasets are presented for all scenarios as well. Reference operating points and resulting CHOP groups of the reference scenario are illustrated in Figure 11.

2.5. Optimization model

The system was optimized with respect to maximizing NPV and minimizing TCE over the period 2015-2035. Design variables for the optimization model are summarized in Table 8, while operation variables are summarized in Table 9.

Table 8: Design variables in the case study optimization problem.

Design variable	Notation	Type	Lower bound	Upper bound
Biorefinery dimension [MWth biomass]	σ_{bio}	Continuous	5.0 MWth	200.0 MWth
Biorefinery location	ω_{bio}	Integer		
Product gas connection between areas	ω_{gas}	Integer		
District heating integration at butchery	ω_{DH}	Integer		

Table 9: Operation variables in the case study optimization problem.

Horsens CHP operation variables	Notation	Type	Lower bound	Upper bound
Rankine cycle load	λ_{ran}	Continuous	0.75[34]	1.00
Gas turbine load	λ_{gt}	Continuous	0.40[a]	1.00
SOEC load	λ_{SOEC}	Continuous	0.00	1.00
Methanol production load	λ_{MeOH}	Continuous	0.00	1.00
Gas boiler load	$\lambda_{gb,ind}$	Continuous	0.00	1.00
Industrial heat pump load	$\lambda_{hp,ind}$	Continuous	0.00	1.00

[a]: **Minimum load constrained due to exhaust emissions** [34].

The NPV, C_0, was calculated as a function of investments costs $C_{inv,k}$ and hourly operation result $c_{op,i}$ times the present value time factor $t_{PV,i}$ for each period i. The facility to be installed was given a lifetime of 20 years, and an interest rate of $r = 0.05$ was applied in net present value calculations.

$$C_0 = -\sum_k C_{inv,k}(\sigma_k, \omega_k) - \sum_i c_{op,i}(\boldsymbol{\lambda}_i) \cdot t_{PV,i} \quad (1)$$

Investment costs for each facility was calculated as

$$C_{inv,k}(\sigma_k, \omega_k) = \omega_k C_{inv,k0} \left(\frac{\sigma_k}{\sigma_{k0}}\right)^{p_f} \quad (2)$$

Here, $C_{inv,k0}$ is the reference investment cost and σ_{k0} is the reference dimension of the facility. A power factor of $p_f = 0.75$ was used for economy-of-scale calculations.

The present value time factor for each reference data point was calculated as

$$t_{PV,i} = t_i \frac{1}{(1+r)^T} \quad (3)$$

Here, T is the number of years from the installation of the FMG, and t_i is the duration of the period.

The TCE, Z_0, was calculated as the sum of hourly emissions for each period i times the duration of the period t_i.

$$Z_0 = \sum_i z_{op,i}(\boldsymbol{\lambda_i}) \cdot t_i \quad (4)$$

Process integration was conducted for both areas. A pinch temperature of 10K was used for integration of thermal streams, apart from in the condensers of the steam Rankine cycle where a pinch temperature of 3.5K was used. The investment cost of the heat exchanger network was estimated for each assessed design as a part of the pinch analysis using a method from Turton et al. [48]. Further information can be found in Bolliger [49].

The optimization model to be solved in the case study can be written in condensed form as

$$\begin{cases} \min_{\omega_k,\sigma_k,\lambda_{k,i}} \begin{cases} -C_0 \\ Z_0 \end{cases} \\ \quad with\ variables \\ \quad \omega_k \in \{0,1\} \\ \quad \sigma_k \in [\sigma_{k,min}, \sigma_{k,max}] \\ \quad \lambda_{k,i} \in [\lambda_{k,min}, \lambda_{k,max}] \end{cases} \quad (5)$$

The problem (5) was solved using the hybrid genetic algorithm/mixed integer-linear programming approach as described in Lythcke-Jørgensen et al. [9]. The genetic algorithm was run for 6 generations with a population size of 20.

3. Results

3.1 Design optimization

Running the optimization procedure for (5), a database of optimized design solutions was obtained. Figure 12 presents a scatter plot illustrating the performances of optimized solutions with respect to NPV and TCE.

First of all, the figure illustrates that under the set conditions and assumptions, there is no trade-off between reducing TCE and maximizing NPV for the FMG designs. This outcome suggests that the biorefinery is competitive for the price schemes considered. It must be emphasized that taxes, subsidies and similar aspects were not considered in the economic calculations.

Secondly, it was found that designs having the biorefinery located next to the local industry (Scenario B) performed better with respect to both objectives than designs where the biorefinery was located next to the CHP unit (retrofit scenario A). This was primarily due to integration synergies, as a part of the reference natural gas consumption of the butchery could be replaced by process heat and unreacted product gas from the biorefinery. In Scenario A, the same replacement of natural gas consumption in the butchery required investments in district heating and gas infrastructure and industrial heat pumps. However, the overall synergy benefits only resulted in a few percent increase NPV and similar reduction in TCE for similar biorefinery dimensions, meaning that impacts from synergies were only marginal compared to the overall impact of installing a large-scale biorefinery.

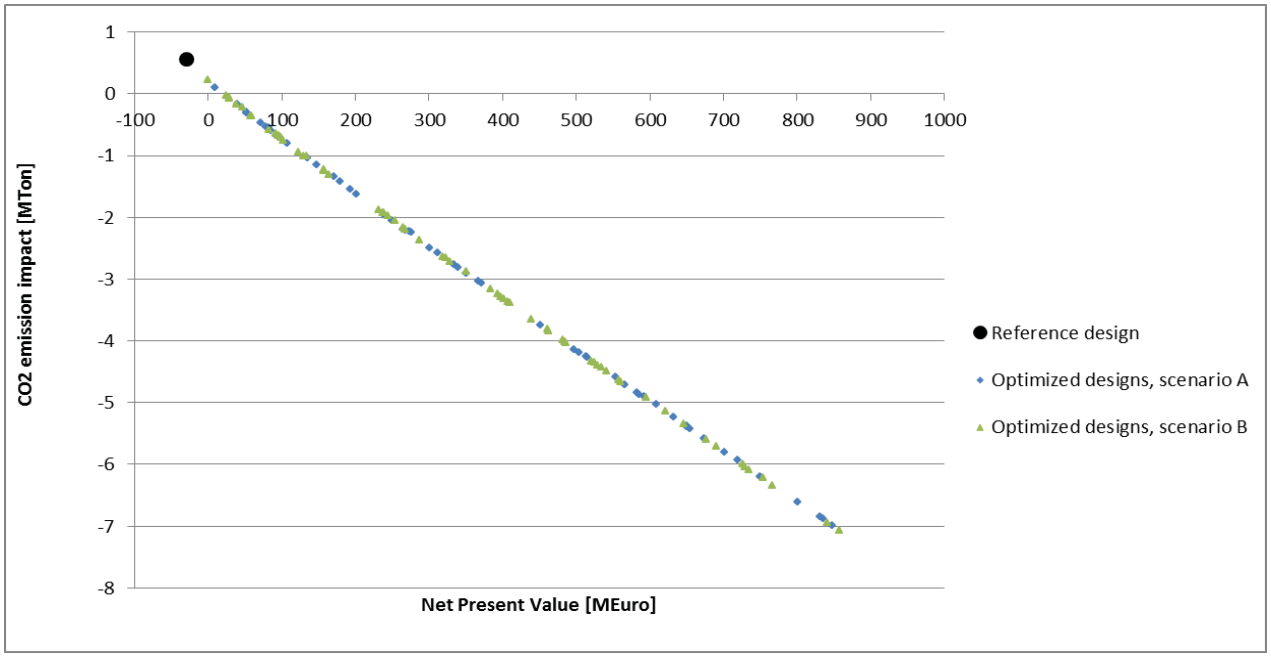

Figure 12: Scatter plot of optimized design solutions with respect to NPV and TCE.

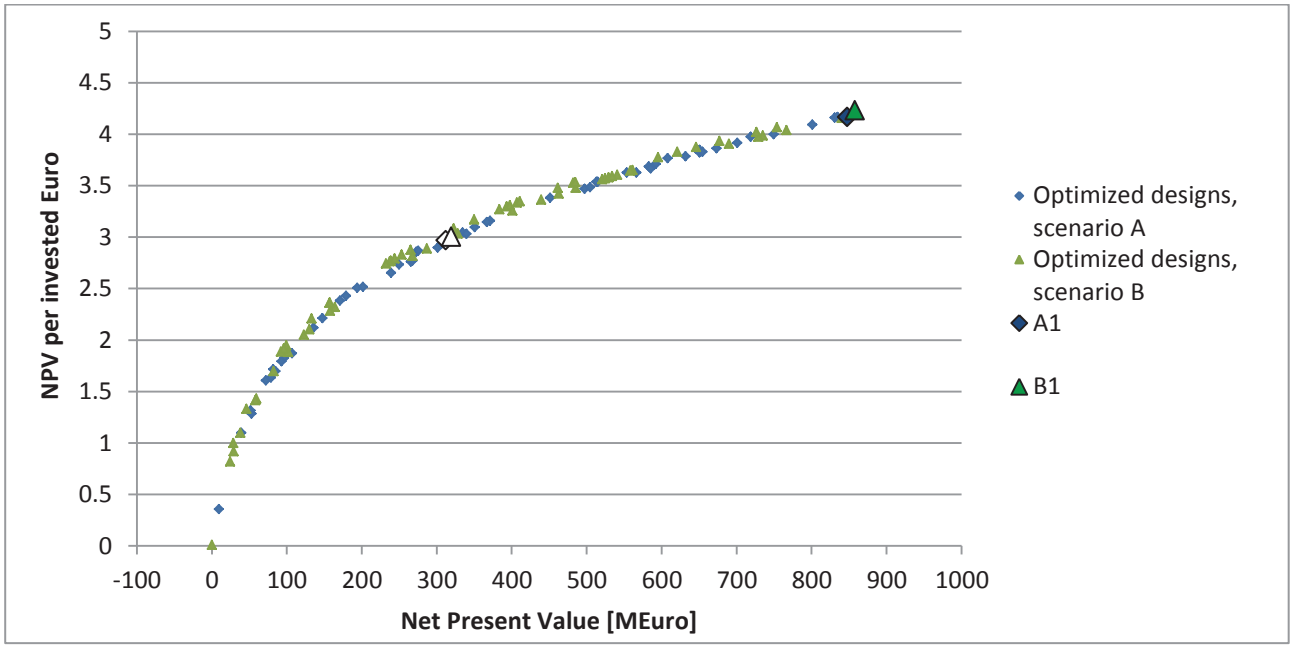

Figure 13: Scatter plot of optimized design solutions with respect to NPV and TCE.

Thirdly, the end results are found to have an almost linear profile, suggesting that nonlinear impacts from economy-of-scale in investments have little impact on the overall results when compared to linear operation impacts. The importance of various input parameters and associated performance uncertainties are assessed in the next section. However, it must be stressed that in the present study, district heating and industry utility services were included as constraints that had to be met, and economic benefits of meeting them were neglected. In case fixed costs were considered for these services, it would have a fixed positive impact on all NPVs. In addition, if costs were considered for cooling excess process heat were considered,

this would have a negative impact for designs with larger biorefinery dimensions. Together, these effects would perhaps improve the significance of process integration benefits in the case study, which may in fact lead to a trade-off between economy-of-scale and process integration benefits.

Investigating the benefits of investments, a plot illustrating the relation between NPV and NPV per invested Euro is presented in Figure 14. The plot illustrates how the relative payback on investments increases with increasing NPV, and thereby biorefinery dimension. It is also found that relative investment payback in general is a few percent higher for retrofit scenario B than for retrofit scenario A.

3.2 Uncertainty analysis

Four optimized designs were selected for uncertainty analysis: The two retrofit designs with the highest NPV for both retrofit scenarios (A1 and B1), and two optimized designs with a biorefinery dimension of approximately 80.0 MWth, representing medium-scaled design solutions (A2 and B2). Design and performance characteristics of the selected designs are summarized in Table 10.

Table 10: Design and performance characteristics of the four selected FMG designs.

Design solution	NPV [M€]	CO_2 emission impact [MTon]	σ_{bio}	ω_{DH}	ω_{gas}
A1	847.3	-6.98	199.3	0	1
A2	312.0	-2.57	81.2	1	0
B1	857.6	-7.07	199.9	0	0
B2	319.0	-2.63	82.4	1	0

Table 11: Input parameter uncertainties considered in the investment cost uncertainty analysis.

Parameter	Notation	Minimum value	Maximum value	Distribution
Biorefinery reference investment cost	$C_{inv,bio0}$	236.18 M€	393.63 M€	Uniform
District heating connection, investment cost	$C_{inv,DH}$	1.31 M€	2.19 M€	Uniform
Gas infrastructure, investment cost	$C_{inv,gas}$	0.88 M€	1.46 M€	Uniform
Heat pump reference investment cost	$C_{inv,hp0}$	0.32 M€	0.54 M€	Uniform
Power factor	p_f	0.6	0.9	Uniform

Variations in estimated NPV from uncertainties in investment costs and economy-of-scale benefits were assessed by applying the Monte Carlo simulation procedure presented by Sin et al. [50]. Reference investment costs were given a uniform uncertainty in the interval of $\pm 25\%$, while the power factor p_f was given a uniform uncertainty in the interval $\pm 20\%$. An overview of the uncertainties associated with various input parameters is given in Table 11.

For each Monte Carlo simulation, a sample of 1000 data points was generated using Latin Hypercube Sampling [51] and assuming zero correlation between uncertainties in input parameters. Running Monte Carlo simulations for all selected designs, the resulting 10^{th} to 90^{th} percentile intervals of predicted NPV for the designs are shown in Figure 14.

The results suggest that the considered uncertainties for investment costs would induce NPV variation within the range $\pm 7\%$. Absolute variations in NPV were larger for designs A1 and B1, which was expected as investment costs were higher for these designs. The outcomes illustrate that the investment uncertainties considered are not likely to have a significant influence on the overall performance of the designed FMGs over the 20 year period.

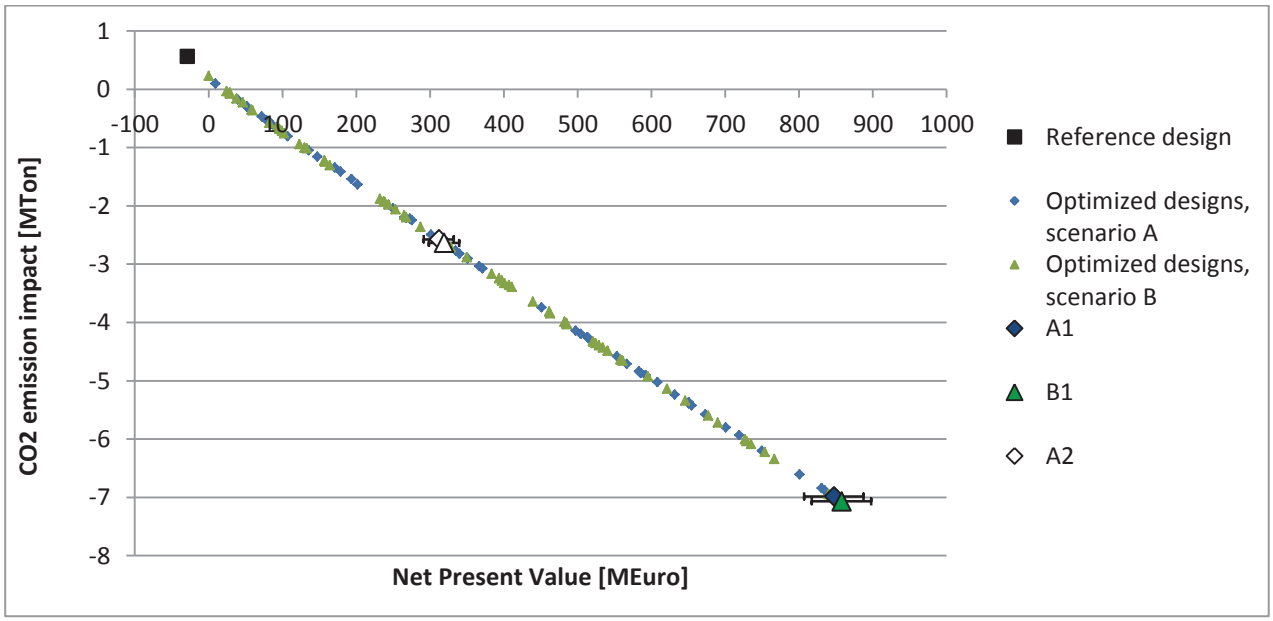

Figure 14: Selected designs and associated 10th to 90th percentile NPV performance variability in response to the investment cost uncertainties described in Table 11.

In order to assess the impact of uncertain operating conditions, the performance of the four selected designs was assessed for each of the four additional energy system scenarios defined in Section 2.4: A high fuel price scenario, a low fuel price scenario, the NonFlex scenario, and a low power price scenario. The outcomes are illustrated in Figure 15.

From the figure, it is evident that methanol price uncertainties considered had a much higher influence on NPV than uncertainties in investment costs. An increase of 25% in methanol price in the high fuel price scenario increased the NPVs of the four selected designs by 67%-75%, while a similar reduction in methanol price of 25% in the low fuel price scenario resulted in NPV reductions of 66%-74%. Also the low power price scenario was found to have a larger impact on NPV variations than the considered uncertainties in investment costs. Opposed to this, changes in NPV from the NonFlex scenario were comparable with expected variations from investment cost uncertainties.

In addition, the TCE was found to increase in the low fuel price and NonFlex scenarios for all designs, owing to the fact that the power-to-methanol price ratio was increased, making SOEC operation uncompetitive in some periods. In consequence, hydrogen boosted SOEC operation was terminated approximately 21% of the time in the low fuel price scenario, while it was terminated for a bit more than 4% of the time in the NonFlex scenario. Opposed to this, the TCE was only marginally affected in the high fuel price and low power price scenarios as the SOEC was already operated in hydrogen-boosted mode for more than 98% of the time in the reference scenario, meaning that the potential of increasing methanol production was very limited.

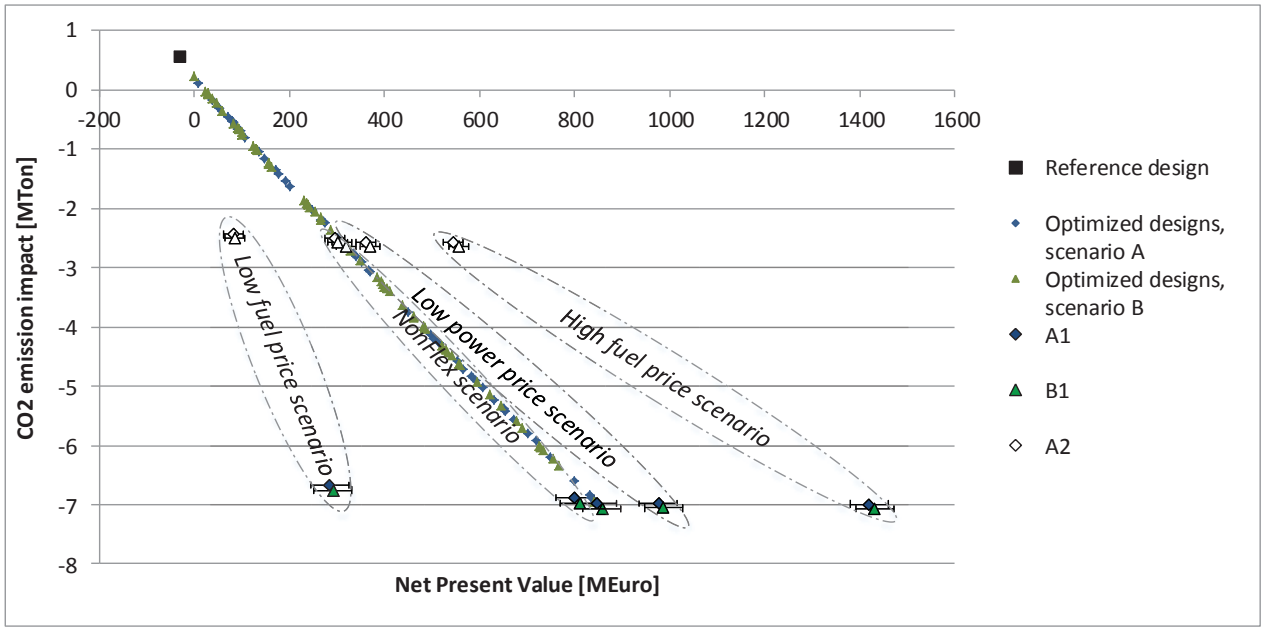

Figure 15: Performance of the four selected designs in the various scenarios. Results of the investment cost uncertainty analysis are indicated as well.

For the NonFlex scenario, the NPV was slightly reduced for all designs. This was caused by the higher power prices over the last six years for this scenario, which increased the costs of SOEC operation and thereby reduced the income from methanol sales.

To summarize, changes of $\pm 25\%$ in the methanol price were found to have a major impact on the estimated performances of the FMGs in the case treated. The NPV of the optimal design solution, design B1, was estimated to vary within the range 252.5 M€ to 1471.6 M€ in response to the assessed input uncertainties. For the optimal medium-sized design, design B2, the relative NPV variation was found to be even larger. In general, the outcomes stress the importance of uncertainty analysis when designing and optimizing FMG concepts.

Finally, the maximum error made by averaging the prices of wood chips, methanol and natural gas in the CHOP-reduced dataset was estimated for design B1. Two additional simulations were conducted: One for a scenario where fuel prices in all hours were set to the maximum fuel price expected over the period, see Table 7, and one where the fuel prices in all hours were set to the minimum fuel price expected. The NPV result was reduced with 0.3 M€, or 0.03%, when fuel prices were set to the minimum expected values, while it was increased by 0.5 M€, or 0.06%, when fuel prices were set to the maximum expected values. As these variations are considered negligible, especially in comparison to the other sources of uncertainty investigated, it is deemed acceptable to average the prices of wood chips, methanol and natural gas in the CHOP method for the present case.

4. Discussion

In addition to the outcomes presented and discussed in Section 3, a number of uncertainties were not accounted for in the analysis. These are shortly discussed below.

First of all, the surrogate models do not represent all process integration opportunities available. The Rankine cycle is modelled as a single black box, not allowing for steam extraction within or between turbine stages, which could otherwise be beneficial in order to extract steam as close to the required temperature and pressure as possible and thereby minimizing exergy destruction of the heat transfer [28]. In addition, exhaust gases from the gas turbine could be used as heat source for the Rankine cycle rather than directly for district heating, thereby increasing the conversion efficiency further. Spare capacity in the waste incineration may also allow for combustion of unreacted product gas, providing an additional usage opportunity for this energy flow. In effect, the results of this study should, with respect to process integration synergies, be regarded as a rough and conservative estimate of synergy potentials.

Regarding TCE calculations, emissions associated with power generation and consumption may as well be regarded as conservative estimates as annually averaged power generation emissions were used. In practice, it is expected that the share of renewables in the power producer mix would be higher during periods of low power prices and lower during periods of high power prices. As the optimized FMG operation causes the system to increase the power consumption and reduce the power generation in periods with low power prices, and vice versa in periods with high power prices, it is expected that the consumed power on average will have lower marginal CO_2 emissions while generated power is expected to replace production with higher marginal CO_2 emissions. In effect, this suggests that the overall TCE calculated for the optimized designs may be smaller than what is calculated. However, in order to verify these considerations, an assessment of the system impact from FMG operation needs to be conducted. This will be a topic for future research.

With respect to the energy system data applied, data for three reference years was used to estimate a period of 20 years. As discussed in Section 3.2, uncertainties in operating conditions were found to have a significant impact on the estimated FMG performance. This suggests that more detailed energy system data should be used in future analyses of the system, and that it would be relevant to define additional likely energy system scenarios in order to assess performance variations in response to likely operating condition uncertainties further.

In the present work, the CHOP method was used for aggregating energy system data. Though advantageous in several ways, the use of the CHOP method has some flaws, the largest being the fact that short-term thermal and product storages cannot be considered in the optimization. In order to investigate if benefits from operation shifting made possible by short-term storages would change the optimal design of the FMG concept, it would be relevant to conduct the full design optimization using at least one additional data aggregation method that allows for the inclusion of short-term storages.

Concerning the biorefinery, the two-stage gasifier was mathematically designed in the FMG to scale between 5-200MW_{th} input. As mentioned, the gasifier has only been scaled up to 1.5MW_{th} in practice and hence this projection is associated with some technological uncertainty. While regular downdraft gasifiers usually scale up to 1-5MW_{th} [52,53], the two separate reactors in the two-stage gasifier allow some degrees of freedom with regards to design. The gasification concept is therefore projected to scale well, with the main challenges being the downdraft char gasifier and the externally heated pyrolysis unit. Replacing these units with other more scalable reactors, such as updraft or fluid bed, could lead to an effective scaling of the concept. For instance, Bentzen et al. [54] constructed an alternative and more scalable version of the

two-stage gasifier using two fluid beds for fuel processing. With activated carbon at room temperature as the only downstream gas cleaning unit, a high gas quality was obtained with negligible tar levels.

Regarding the SOEC, the dimensioning was done *a priori* based on the largest feasible hydrogen addition in the methanol synthesis. It was found that the full SOEC capacity was utilized for more than 98% of the time in the reference scenario. However, in the design optimization the SOEC was by default installed in the biorefinery. With the prices of wood chips and power considered, wood chips is almost always a cheaper resource than power, making it economically attractive to increase the dimension of the gasifier rather than investing in SOEC capacity for hydrogen boosted methanol production. Hence, under the given economic circumstances, hydrogen boosted methanol production is only considered attractive if wood chip availability is limited, questioning if an SOEC with capacity for maximum hydrogen production should be installed by default. Optimizing the dimension of the SOEC with respect to investment and operating pattern would be a relevant topic for future research.

For the low fuel price scenario, the SOEC was operated in full capacity when power prices were below approximately 66 €/MWh, approximately 79.0% of the time. The SOEC was operated in oxygen-boosted mode for power prices in the range 66 €/MWh to 122 €/MWh, approximately 20.9% of the time, while it was shut down the last 0.1% of the time when power prices exceeded 122 €/MWh. Here, it could be relevant to investigate the impact of including oxygen storage, which could allow the SOEC to be shut down for the 21% of the time where the power price is too high for operation in hydrogen-boosted mode. If feasible, it could as well be considered if the SOEC operation could be inverted to make it run as a fuel cell on syngas during periods of high power prices. If so, the SOEC could be used for storing electricity as methanol, and then converting it to electricity when demands and prices are high, thereby extending the electricity system balancing from the FMG. The possibility of running the SOEC as a fuel cell may as well serve as an option for reducing the economic risk of low fuel prices for the overall FMG.

Finally, the middle estimated value of CO_2 emission quotas from ref. [45] was included in the methanol price applied in the study. Over the period considered, the CO_2 emission quota value accounted for between 2.5% and 11.5% of the methanol price depending on the year. In case the conservative estimate of CO_2 emission quota value from ref. [45] had been used, the methanol price would have dropped between 0.7% and 4.4% over the period, while the optimistic estimate would have let to increases in methanol price of 0.0% to 4.5%. Such variations would have a noticeable impact on NPVs of the designs, but the impact would fall within the NPV variation boundaries set by the $\pm 25\%$ change in methanol price that was assessed as part of the uncertainty analysis.

5. Conclusion

The present study treated the development of a flexible multi-generation system (FMG) which integrated a methanol-producing biorefinery with an existing CHP unit and industrial energy utility supply. Applying a previously developed design methodology, the FMG was modelled and its design optimized with respect to a 20-year system lifetime. Design aspects considered include: Process selection, dimensioning, location and integration; operation optimization considering hourly variations in operating conditions over the year as well as expected long term energy system development; and uncertainty analysis considering both investment costs and operating conditions.

Solving the design optimization for the reference scenario, the outcomes suggest found that the optimal design with respect to both economic and environmental performance involved a maximum-sized biorefinery located next to the local industry. As the local industry energy demands were limited when compared to the biorefinery dimensions considered, process integration synergies were found to be marginal when compared to the economic and environmental impact of the biorefinery. The results further indicated that uncertainties in operating conditions, especially methanol price, would have a much higher impact on the performance of the designs than corresponding uncertainties in investment costs.

For the optimized design, the net present value (NPV) was estimated to vary within the range 252.5 M€ to 1471.6 M€ in response to parameter value changes of $\pm 25\%$ of investments costs and methanol price. These results stress the importance of including systematic uncertainty analysis in the design optimization of FMG concepts.

Acknowledgements

The authors would like to acknowledge DONG Energy, Energinet.dk, and the Innovation Foundation through the 4DH project for their financial support of the research.

References

[1] Lund H. Renewable Energy Systems: The Choice and Modeling of 100% Renewable Solutions. Academic Press publications; 2010.

[2] Lund H, Andersen AN, Østergaard PA, Mathiesen BV, Connolly D. From electricity smart grids to smart energy systems - A market operation based approach and understanding. Energy 2012;42:96–102. doi:10.1016/j.energy.2012.04.003.

[3] Mathiesen BV, Lund H, Connolly D, Wenzel H, Østergaard P a., Möller B, et al. Smart Energy Systems for coherent 100% renewable energy and transport solutions. Appl Energy 2015;145:139–54. doi:10.1016/j.apenergy.2015.01.075.

[4] DTU. DTU International Energy Report 2015 : Energy systems integration for the transition to non-fossil energy systems. 2015.

[5] Gassner M, Maréchal F. Thermo-economic optimisation of the polygeneration of synthetic natural gas (SNG), power and heat from lignocellulosic biomass by gasification and methanation. Energy Environ Sci 2012;5:5768. doi:10.1039/c1ee02867g.

[6] Gassner M, Marechal F. Increasing Efficiency of Fuel Ethanol Production from Lignocellulosic Biomass by Process Integration. Energy and Fuels 2013;27:2107–15.

[7] Lythcke-Jørgensen C, Haglind F. Design optimization of a polygeneration plant producing power , heat , and lignocellulosic ethanol. Energy Convers Manag 2015;91:353–66. doi:10.1016/j.enconman.2014.12.028.

[8] Clausen LR. Maximizing biofuel production in a thermochemical biorefinery by adding electrolytic hydrogen and by integrating torrefaction with entrained flow gasification. Energy 2015;85:94–104. doi:10.1016/j.energy.2015.03.089.

[9] Lythcke-Jørgensen C, Ensinas A V., Münster M, Haglind F. A methodology for designing flexible multi-generation systems. Energy 2016:1–21.

[10] Liu P, Pistikopoulos EN, Li Z. Polygeneration Systems Engineering. Process Syst. Eng., vol. 5, 2011, p. 1–38. doi:10.1002/9783527631292.ch1.

[11] Chicco G, Mancarella P. Distributed multi-generation: A comprehensive view. Renew Sustain Energy Rev 2009;13:535–51. doi:10.1016/j.rser.2007.11.014.

[12] Liu P, Gerogiorgis DI, Pistikopoulos EN. Modeling and optimization of polygeneration energy systems. Catal Today 2007;127:347–59. doi:10.1016/j.cattod.2007.05.024.

[13] Liu P, Pistikopoulos EN, Li Z. A mixed-integer optimization approach for polygeneration energy systems design. Comput Chem Eng 2009;33:759–68. doi:10.1016/j.compchemeng.2008.08.005.

[14] Liu P, Pistikopoulos EN. A Multi-Objective Optimization Approach to Polygeneration Energy Systems Design. AIChE J 2010;56:1218–34. doi:10.1002/aic.

[15] Liu P, Pistikopoulos EN, Li Z. Decomposition Based Stochastic Programming Approach for Polygeneration Energy Systems

Design under Uncertainty. Ind Eng Chem Res 2010;49:3295–305. doi:10.1021/ie901490g.

[16] Maréchal F, Weber C, Favrat D. Multiobjective Design and Optimization of Urban Energy Systems. Process Syst. Eng., 2011, p. 39–83. doi:10.1002/9783527631292.ch1.

[17] Fazlollahi S, Becker G, Maréchal F. Multi-objectives, multi-period optimization of district energy systems: I. Selection of typical operating periods. Comput Chem Eng 2014;65:54–66. doi:10.1016/j.compchemeng.2014.02.018.

[18] Fazlollahi S, Becker G, Maréchal F. Multi-objectives, multi-period optimization of district energy systems: II-Daily thermal storage. Comput Chem Eng 2014;71:648–62. doi:10.1016/j.compchemeng.2014.02.018.

[19] Fazlollahi S, Becker G, Maréchal F. Multi-objectives, multi-period optimization of district energy systems: III. Distribution networks. Comput Chem Eng 2014;66:82–97. doi:10.1016/j.compchemeng.2014.02.018.

[20] Sorknæs P, Lund H, Andersen AN. Future power market and sustainable energy solutions – The treatment of uncertainties in the daily operation of combined heat and power plants. Appl Energy 2015;144:129–38. doi:10.1016/j.apenergy.2015.02.041.

[21] Capuder T, Mancarella P. Techno-economic and environmental modelling and optimization of flexible distributed multi-generation options. Energy 2014;71:516–33. doi:10.1016/j.energy.2014.04.097.

[22] Capuder T, Mancarella P. Modelling and Assessment of the Techno-economic and Environmental Performance of Flexible Multi- Generation Systems. 18th Power Syst Comput Conf Wroclaw, Pol 2014.

[23] Martínez Ceseña E, Capuder T, Mancarella P. Flexible Distributed Multienergy Generation System Expansion Planning Under Uncertainty. IEEE Trans Smart Grid 2015:1–10. doi:10.1109/TSG.2015.2411392.

[24] Chen Y, Adams TA, Barton PI. Optimal design and operation of flexible energy polygeneration systems. Ind Eng Chem Res 2011;50:4553–66. doi:10.1021/ie1021267.

[25] Lythcke-Jørgensen C. Modelling and Optimization of a Steam Co-generation Plant with Integrated Bio-ethanol Production. Technical University of Denmark, 2012.

[26] Lythcke-Jørgensen C, Haglind F, Clausen LR. Thermodynamic and Economic Analysis of Integrating Lignocellulosic Bioethanol, Copenhagen, Denmark: European Biomass Conference and Exhibition; 2013, p. 1–8.

[27] Lythcke-Jørgensen C, Haglind F, Clausen LR. Exergy analysis of a combined heat and power plant with integrated lignocellulosic ethanol production, Guilin, China: 28th International Conference on Efficiency, Cost, Optimization, Simulation and Environmental Impact of Energy Systems; 2013, p. 1–12.

[28] Lythcke-Jørgensen C, Haglind F, Clausen LR. Exergy analysis of a combined heat and power plant with integrated lignocellulosic ethanol production. Energy Convers Manag 2014;85:817–27. doi:10.1016/j.enconman.2014.01.018.

[29] Lythcke-Jørgensen C, Münster M, Ensinas A V, Haglind F. Design optimization of flexible biomass-processing polygeneration plants using characteristic operation periods. World Renew. Energy Congr. XIII, London: 2014.

[30] Danmarks Statistik 2014. http://www.statistikbanken.dk/.

[31] Thiessen K. Fjernvarme Horsens (personal contact) 2015. fjho.dk.

[32] Clausen LR, Elmegaard B, Ahrenfeldt J, Henriksen U. Thermodynamic analysis of small-scale dimethyl ether (DME) and methanol plants based on the efficient two-stage gasifier. Energy 2011;36:5805–14. doi:10.1016/j.energy.2011.08.047.

[33] Lythcke-Jørgensen C, Haglind F, Ensinas A V., Münster M. A method for aggregating external operating conditions in multi-generation plant optimization models. Appl Energy 2016;under revi:59–75. doi:10.1016/j.apenergy.2015.12.050.

[34] Energistyrelsen, Energinet.dk. Technology Data for Energy Plants - Generation of Electricity and District Heating, Energy Storage and Energy Carrier Generation and Conversion 2015:1–220. doi:ISBN: 978-87-7844-940-5.

[35] Ahrenfeldt J, Henriksen U, Jensen TK, G??bel B, Wiese L, Kather A, et al. Validation of a continuous combined heat and power (CHP) operation of a two-stage biomass gasifier. Energy and Fuels 2006;20:2672–80. doi:10.1021/ef0503616.

[36] Ahrenfeldt J, Thomsen TP, Henriksen U, Clausen LR. Biomass gasification cogeneration - A review of state of the art technology and near future perspectives. Appl Therm Eng 2013;50:1407–17. doi:10.1016/j.applthermaleng.2011.12.040.

[37] Evald A, Hu G, Hansen MT. Technology data for advanced bioenergy fuels. 2013.

[38] Vad Mathiesen B, Ridjan I. Technology Data for High Temperature Solid Oxide Electrolyser Cells , Alkali and Pem Electrolysers. Aalborg, Denmark: 2013.

[39] Jensen JK, Ommen T, Markussen WB, Reinholdt L, Elmegaard B. Technical and economic working domains of industrial heat pumps: Part 2 - Ammonia-water hybrid absorption-compression heat pumps. Int J Refrig 2014;55:183–200. doi:10.1016/j.ijrefrig.2015.02.011.

[40] Dansk Fjernvarme. Temamøde om landsbynærvarme 2015. http://www.danskfjernvarme.dk/kurser-og-moeder/moedematerialer/2014-25-marts-temamoede-om-landsbynaerva (accessed March 31, 2016).

[41] Energiforskning.dk. Analyser for kommercialisering af brintteknologier n.d. http://www.energiforskning.dk/da/project/analyser-kommercialisering-af-brintteknologier (accessed March 15, 2016).

[42] Danish Energy Agency. FORUDSÆTNINGER FOR SAMFUNDSØKONOMISKE ANALYSER PÅ ENERGIOMRÅDET. 2014.

[43] Danish Energy Agency. Oliepriser 2016. http://www.ens.dk/info/tal-kort/statistik-nogletal/energipriser-afgifter/oliepriser (accessed March 29, 2016).

[44] Energinet.dk. SIFRE: Simulation of Flexible and Renewable Energy sources (http://energinet.dk/SiteCollectionDocuments/Danske%20dokumenter/El/sifre_fall2015.pdf). 2015.

[45] Energinet.dk. Energinet.dk's analyseforudsætninger 2012-2035. 2012.

[46] Energinet.dk, Dansk Energi. Smart Energy - hovedrapport 2015.

[47] Energistyrelsen. Energistatistik 2014 – Data, tabeller, statistikker og kort. 2015.

[48] Turton R, Bailie RC, Whiting WB, Shaeiwitz J a. Analysis, Synthesis, and Design of Chemical Processes. 1998.

[49] Bolliger R. Méthodologie de la synthèse des systèmes énergétiques industriels. 2010. doi:10.5075/epfl-thesis-4867.

[50] Sin G, Gernaey K V., Lantz AE. Good modeling practice for PAT applications: Propagation of input uncertainty and sensitivity analysis. Biotechnol. Prog., vol. 25, 2009, p. 1043–53. doi:10.1002/btpr.166.

[51] McKay MD, Beckman RJ, Conover WJ. Comparison of three methods for selecting values of input variables in the analysis of output from a computer code. Technometrics 1979;21:239–45. doi:10.2307/1271432.

[52] Basu P. Biomass Gasification, Pyrolysis and Torrefaction. 2013. doi:10.1016/B978-0-12-396488-5.00013-7.

[53] Knoef H. Handbook Biomass Gasification. Biomass Gasification Group; 2005.

[54] Bentzen J, Hummelshøj R, Henriksen U. Upscale of the two-stage gasification process. Proc 2 World Conf Technol Exhib Biomass Energy Ind 2004;10-14 May,:1004–7.

[55] Adams TA, Ghouse JH. Polygeneration of fuels and chemicals. Curr Opin Chem Eng 2015;10:87–93. doi:10.1016/j.coche.2015.09.006.

Appendix A – System model data

This appendix includes all mass and energy flow functions of the FMG system model.

Table 12: Thermal energy flow functions.

Facility	Flow-description	Notation	Type	Function [MJ/s]	T_{in}/T_{out}
Horsens CHP	0.8 bar condenser heat	$\dot{Q}_{ran,hp}$	Hot	$\lambda_{ran}\dot{Q}_{ran,hp0}$	93.5˚C /93.5˚C
	0.3 bar condenser heat	$\dot{Q}_{ran,lp}$	Hot	$\lambda_{ran}\dot{Q}_{ran,lp0}$	69.1˚C /69.1˚C
	Gas turbine, off gas heat	$\dot{Q}_{gt,off}$	Hot	$\lambda_{gt}\sigma_{gt}(\eta_{gt}-\eta_{gt,P})$	600˚C /70˚C
	District heating generation	$\dot{Q}_{dh}$	Cold	$\sigma_{dh}\lambda_{dh}$	40˚C /90˚C
Butchery	Room heating and losses	$\dot{Q}_{ind,room}$	Cold	$0.24\cdot\sigma_{ind}\lambda_{ind}$	35˚C /35˚C
	Cleaning	$\dot{Q}_{ind,cl}$	Cold	$0.37\cdot\sigma_{ind}\lambda_{ind}$	
	Boiling and evaporation	$\dot{Q}_{ind,ev}$	Cold	$0.04\cdot\sigma_{ind}\lambda_{ind}$	110˚C /100˚C
	Gas boiler, off gas heat	$\dot{Q}_{gb,off}$	Hot	$\sigma_{ind}\lambda_{gb,ind}$	1000˚C /70˚C
Hybrid heat pump	District heating source	$\dot{Q}_{hp,in}$	Cold	$\sigma_{hp}\lambda_{hp}\frac{COP-1}{COP}$	40˚C /90˚C
	Process heat sink	$\dot{Q}_{hp,out}$	Hot	$\sigma_{hp}\lambda_{hp}$	120˚C /110˚C
Biorefinery	Gasifier, B	$\dot{Q}_B$	Cold	$0.118\cdot\sigma_{bio}$	115˚C /200˚C
	Gasifier, C	$\dot{Q}_C$	Hot	$0.020\cdot\sigma_{bio}$	236˚C /127˚C
	Gasifier, D	$\dot{Q}_D$	Hot	$0.062\cdot\sigma_{bio}$	114˚C /40˚C
	Methanol, G	$\dot{Q}_G$	Hot	$0.070\cdot\sigma_{bio}\lambda_{meth}$	220˚C /220˚C
	Methanol, H	$\dot{Q}_H$	Hot	$0.076\cdot\sigma_{bio}\lambda_{meth}$	110˚C /40˚C
	Methanol, J	$\dot{Q}_J$	Cold	$0.010\cdot\sigma_{bio}\lambda_{meth}$	84˚C /84˚C
	Methanol, K	$\dot{Q}_K$	Cold	$0.033\cdot\sigma_{bio}\lambda_{meth}$	40˚C /110˚C
	Methanol, N	$\dot{Q}_K$	Hot	$0.122\cdot\sigma_{bio}\lambda_{meth}$	153˚C /40˚C
	SOEC excess heat	$\dot{Q}_K$	Hot	$0.5\cdot\sigma_{bio}\lambda_{soec}\left(\frac{1-\eta_{SOEC}}{\eta_{SOEC}}\right)$	200˚C /40˚C
	Off-product gas burner	$\dot{Q}_{off}$	Hot	$0.24\cdot\sigma_{bio}\cdot\lambda_{sb}$	600˚C /70˚C

Table 13: Energy flow functions.

Process	Flow-description	Notation	Function [MW]
WOOD CHIPS FLOWS			
Biorefinery	Gasifier wood chip consumption	$\dot{e}_{wood\ chips}$	σ_{bio}
POWER FLOWS			
Horsens CHP	Power generation, Rankine	P_{ran}	$7\cdot\lambda_{ran}$
	Power generation, gas turbine	P_{gt}	$8\cdot\lambda_{ran}$
Butchery	Ammonia-water hybrid heat pump	P_{hp}	$-\frac{\sigma_{hp}\lambda_{hp}}{COP}$
Biorefinery	Methanol production power demand	P_{meth}	$0.096\cdot\lambda_{meth}\sigma_{bio}$
	SOEC power demand	P_{SOEC}	$\lambda_{SOEC}\frac{0.5\cdot\sigma_{bio}}{\eta_{SOEC}}$
NATURAL GAS FLOWS			

Horsens CHP	Gas turbine natural gas consumption	$\dot{e}_{ng,gt}$	$\sigma_{gt} \cdot \lambda_{gt}$
Butchery	Gas boiler natural gas consumption	$\dot{e}_{ng,gb}$	$\sigma_{ind}\lambda_{gb}(0.35 + \beta_{ng})$
PRODUCT GAS and OFF-PRODUCT GAS FLOWS			
Biorefinery	Gasifier, product gas generation	$\dot{e}_{syngas}$	$0.9294 \cdot \sigma_{bio}$
	Methanol off-product gas, air blown	$\dot{e}_{synoff,air}$	$0.24 \cdot \sigma_{bio}\lambda_{meth}$
	Methanol off-product gas, oxygen blown	$\dot{e}_{synoff,O_2}$	$0.02 \cdot \sigma_{bio}\lambda_{meth}$
Butchery	Gas boiler off-product gas consumption	$\dot{e}_{synoff,gb}$	$\sigma_{ind}\lambda_{gb}(1 - \beta_{ng})$
HYDROGEN FLOWS			
Biorefinery	Hydrogen, SOEC	$\dot{e}_{H_2,SOEC}$	$0.5 \cdot \lambda_{SOEC}\sigma_{bio}$
	Hydrogen addition, oxygen-blown	$\dot{e}_{H_2,O_2}$	$0.184 \cdot \lambda_{MeOH,O_2}\sigma_{bio}$
	Hydrogen addition, hydrogen-boost	$\dot{e}_{MeOH,H_2+}$	$0.316 \cdot \lambda_{MeOH,H_2+}\sigma_{bio}$
METHANOL FLOWS			
Biorefinery	Methanol, air-blown	$\dot{e}_{MeOH,air}$	$0.56 \cdot \lambda_{MeOH,air}\sigma_{bio}$
	Additional methanol, oxygen-blown	$\dot{e}_{MeOH,O_2}$	$0.34 \cdot \lambda_{MeOH,O_2}\sigma_{bio}$
	Additional methanol, hydrogen-boost	$\dot{e}_{MeOH,H_2+}$	$0.32 \cdot \lambda_{MeOH,H_2+}\sigma_{bio}$

Table 14: Mass flow functions.

Process	Flow-description	Notation	Function [MW]
WASTE FLOWS			
Horsens CHP	Waste incineration boilers waste processing	$\dot{m}_{waste,ran}$	$\sigma_{ran} \cdot \lambda_{ran}$
OXYGEN FLOWS			
Biorefinery	SOEC, oxygen production	$\dot{m}_{O_2,SOEC}$	$0.0337 \cdot \sigma_{bio}\lambda_{SOEC}$
	Gasifier, oxygen-blown	$\dot{m}_{O_2,gasifier}$	$0.0124 \cdot \sigma_{bio}\lambda_{O_2-blown}$

Appendix B – CHOP-reduction of external operating condition data

This appendix describes the applied data aggregation procedure using the CHOP method [33].

Through an iterative assessment, it was decided to define six important parameter intervals for the power price, five important parameter intervals for the district heating demand, and four important parameter intervals for the industry utility demand. The applied interval break points are presented in Table 15.

The break points for relative district heating demand and relative thermal utility demand in the industry were defined based on the duration curves. The power price break points were identified iteratively by optimizing the operation of the developed model for various price schemes. Using the present-value-averaged methanol price and natural gas price, it was found that Rankine power generation was shifted from minimum to maximum when the power price exceeded approximately 75.00 Euro/MWh. Similarly, the gas turbine power generation was maximized when power prices were around 92.00 Euro/MWh or higher, while SOEC loads were reduced to operation in oxygen-blown mode when power prices were above 90.00 Euro/MWh. For power prices above 146.00 Euro/MWh, the SOEC was found to shut down, but such high power prices were only present in 6 hours over the entire 20-year period reference dataset, hence it was not deemed relevant to add a break point at this value.

Table 15: Interval break points used in the CHOP reduction of volatile external operating conditions parameters in the case study.

Interval number	Power price, break point [Euro/MWh]	Relative District heating demand, break point [-]	Industry relative thermal utility demand, break point [-]
1	20.00	0.25	0.20
2	40.00	0.40	0.50
3	60.00	0.60	0.80
4	75.00	0.80	1.00
5	90.00	1.00	
6	152.53		

Using the interval break points in Table 15, the resulting CHOP reduced dataset of the reference scenario is presented in Table 16. The corresponding CHOP reduced dataset of the NonFlex scenario is presented in Table 17.

Table 16: CHOP dataset of the reference scenario used in the study. Notice that CHOP groups with durations of 0 are so-called 'empty' CHOP groups, meaning that no reference operating point falls within the group boundaries. Empty CHOP-groups are discarded from the final CHOP dataset and are grey-shaded in the table.

Group (p,d,i)	$t\ [h]$	t_{PV}	c_p $[€/MWh]$	α_p $[T/MWh]$	λ_{DH}	λ_{ind}	c_{MeOH} $[€/GJ]$	c_{NG} $[€/GJ]$	c_{wood} $[€/GJ]$
(1,1,1)	1524	1262	16.24	263	0.19	0.13	21.42	9.68	6.54
(1,1,2)	1680	1215	16.14	243	0.18	0.36	22.48	9.81	6.69
(1,1,3)	222	130	14.27	198	0.19	0.58	24.47	10.05	6.97
(1,1,4)	0	0	0.00	0	0.00	0.00	0.00	0.00	0.00
(1,2,1)	356	293	14.63	260	0.31	0.12	21.47	9.68	6.54
(1,2,2)	556	358	13.50	217	0.30	0.36	23.52	9.93	6.84
(1,2,3)	202	119	11.76	193	0.32	0.58	24.42	10.03	6.96
(1,2,4)	6	5	15.30	270	0.32	0.86	21.25	9.66	6.52

(1,3,1)	848	617	13.40	243	0.49	0.15	22.42	9.80	6.68
(1,3,2)	1494	912	12.45	208	0.51	0.38	24.04	9.99	6.91
(1,3,3)	636	332	9.72	170	0.51	0.61	25.74	10.20	7.15
(1,3,4)	42	23	11.23	182	0.51	0.83	25.21	10.13	7.08
(1,4,1)	494	381	14.65	253	0.67	0.16	21.96	9.74	6.62
(1,4,2)	992	792	16.14	260	0.71	0.36	21.68	9.71	6.58
(1,4,3)	270	206	17.36	252	0.72	0.57	22.04	9.76	6.63
(1,4,4)	0	0	0.00	0	0.00	0.00	0.00	0.00	0.00
(1,5,1)	138	117	17.15	270	0.89	0.17	21.25	9.66	6.52
(1,5,2)	270	228	16.72	270	0.87	0.31	21.25	9.66	6.52
(1,5,3)	42	36	18.51	270	0.86	0.56	21.25	9.66	6.52
(1,5,4)	0	0	0.00	0	0.00	0.00	0.00	0.00	0.00
(2,1,1)	7572	5513	29.44	210	0.19	0.12	22.59	9.77	6.67
(2,1,2)	11940	9098	28.41	244	0.19	0.36	22.09	9.75	6.63
(2,1,3)	2438	1874	30.65	249	0.21	0.58	22.00	9.74	6.62
(2,1,4)	24	20	30.51	270	0.19	0.82	21.25	9.66	6.52
(2,2,1)	2028	1442	29.67	210	0.32	0.13	22.77	9.80	6.70
(2,2,2)	2984	2290	28.64	247	0.32	0.37	22.02	9.74	6.62
(2,2,3)	992	753	30.90	247	0.31	0.58	22.10	9.76	6.64
(2,2,4)	6	3	33.30	112	0.25	0.86	28.34	10.51	7.52
(2,3,1)	3500	2606	29.17	223	0.49	0.15	22.36	9.76	6.65
(2,3,2)	6994	5419	29.16	246	0.49	0.37	21.96	9.73	6.61
(2,3,3)	2958	2273	32.31	248	0.51	0.61	22.01	9.74	6.62
(2,3,4)	48	38	29.84	259	0.53	0.83	21.73	9.72	6.59
(2,4,1)	3638	2756	30.29	231	0.70	0.17	22.19	9.74	6.63
(2,4,2)	6526	5111	29.41	247	0.70	0.37	21.88	9.72	6.60
(2,4,3)	4162	3337	30.09	258	0.70	0.61	21.67	9.70	6.57
(2,4,4)	216	173	31.83	261	0.72	0.85	21.67	9.71	6.58
(2,5,1)	768	615	30.01	248	0.86	0.17	21.73	9.70	6.57
(2,5,2)	2052	1689	29.00	259	0.87	0.37	21.48	9.68	6.55
(2,5,3)	1460	1233	29.23	269	0.86	0.61	21.26	9.66	6.52
(2,5,4)	90	76	31.93	270	0.82	0.84	21.25	9.66	6.52
(3,1,1)	6834	3653	49.07	113	0.18	0.13	25.78	10.11	7.09
(3,1,2)	13388	7306	49.63	116	0.17	0.36	25.55	10.08	7.06
(3,1,3)	2304	1275	49.59	131	0.20	0.58	25.35	10.07	7.04
(3,1,4)	30	20	50.80	153	0.18	0.82	23.75	9.86	6.80
(3,2,1)	2100	1098	50.79	113	0.34	0.14	26.01	10.15	7.13
(3,2,2)	4458	2361	51.59	115	0.34	0.37	25.86	10.13	7.11
(3,2,3)	762	382	49.94	131	0.33	0.58	26.37	10.23	7.21
(3,2,4)	0	0	0.00	0	0.00	0.00	0.00	0.00	0.00
(3,3,1)	2492	1375	50.74	114	0.49	0.15	25.45	10.06	7.04
(3,3,2)	5848	3139	51.33	113	0.50	0.38	25.74	10.10	7.09
(3,3,3)	2272	1154	50.41	118	0.52	0.59	26.29	10.20	7.18

(3,3,4)	80	43	46.97	168	0.51	0.84	25.42	10.14	7.10
(3,4,1)	1956	1098	48.42	117	0.69	0.17	25.27	10.04	7.01
(3,4,2)	4692	2657	49.74	120	0.69	0.35	25.17	10.03	7.00
(3,4,3)	2892	1663	50.07	124	0.69	0.60	25.01	10.01	6.98
(3,4,4)	126	77	46.52	174	0.71	0.86	24.16	9.96	6.89
(3,5,1)	192	116	49.07	112	0.86	0.17	24.63	9.93	6.90
(3,5,2)	634	410	47.10	149	0.85	0.37	23.83	9.87	6.81
(3,5,3)	366	245	46.95	168	0.86	0.62	23.44	9.84	6.77
(3,5,4)	0	0	0.00	0	0.00	0.00	0.00	0.00	0.00
(4,1,1)	2492	1146	65.06	112	0.17	0.13	27.43	10.37	7.37
(4,1,2)	7348	3821	65.38	112	0.18	0.37	26.07	10.15	7.14
(4,1,3)	2000	1071	66.46	112	0.19	0.58	25.77	10.11	7.09
(4,1,4)	32	15	64.99	112	0.17	0.82	27.15	10.32	7.32
(4,2,1)	1030	468	65.13	112	0.34	0.15	27.58	10.39	7.39
(4,2,2)	2844	1384	65.21	112	0.34	0.37	26.79	10.27	7.26
(4,2,3)	890	466	65.29	112	0.33	0.59	26.00	10.14	7.13
(4,2,4)	0	0	0.00	0	0.00	0.00	0.00	0.00	0.00
(4,3,1)	2202	1084	65.10	112	0.50	0.16	26.66	10.25	7.24
(4,3,2)	5302	2782	66.48	112	0.49	0.37	25.97	10.14	7.12
(4,3,3)	3496	1846	67.49	112	0.50	0.61	25.91	10.13	7.11
(4,3,4)	188	94	68.17	112	0.51	0.83	26.44	10.21	7.20
(4,4,1)	1318	730	67.74	112	0.68	0.17	25.42	10.05	7.03
(4,4,2)	3520	1979	67.66	112	0.69	0.36	25.28	10.03	7.01
(4,4,3)	3192	1768	68.52	112	0.68	0.63	25.43	10.05	7.03
(4,4,4)	208	117	68.98	112	0.69	0.85	25.28	10.03	7.01
(4,5,1)	192	116	64.98	112	0.85	0.16	24.63	9.93	6.90
(4,5,2)	576	347	66.38	112	0.86	0.34	24.63	9.93	6.90
(4,5,3)	160	96	65.58	112	0.89	0.60	24.63	9.93	6.90
(4,5,4)	0	0	0.00	0	0.00	0.00	0.00	0.00	0.00
(5,1,1)	1194	519	81.66	112	0.16	0.13	28.13	10.48	7.49
(5,1,2)	2538	1287	80.69	112	0.19	0.37	26.34	10.20	7.19
(5,1,3)	1172	616	80.61	112	0.20	0.59	25.96	10.14	7.12
(5,1,4)	0	0	0.00	0	0.00	0.00	0.00	0.00	0.00
(5,2,1)	360	154	80.82	112	0.34	0.14	28.34	10.51	7.52
(5,2,2)	952	452	80.20	112	0.35	0.37	27.07	10.31	7.31
(5,2,3)	640	314	80.84	112	0.34	0.62	26.69	10.25	7.24
(5,2,4)	12	5	78.33	112	0.37	0.82	28.34	10.51	7.52
(5,3,1)	572	246	82.40	112	0.51	0.16	28.27	10.50	7.51
(5,3,2)	1526	776	80.04	112	0.49	0.37	26.31	10.19	7.18
(5,3,3)	1394	736	79.44	112	0.48	0.63	25.91	10.13	7.11
(5,3,4)	72	35	81.81	112	0.52	0.84	26.81	10.27	7.26
(5,4,1)	296	157	79.74	112	0.68	0.18	25.84	10.12	7.10
(5,4,2)	1504	835	78.80	112	0.69	0.39	25.40	10.05	7.03

(5,4,3)	1842	1044	78.91	112	0.70	0.63	25.20	10.02	7.00
(5,4,4)	206	123	78.23	112	0.70	0.85	24.71	9.94	6.91
(5,5,1)	0	0	0.00	0	0.00	0.00	0.00	0.00	0.00
(5,5,2)	104	63	75.71	112	0.85	0.36	24.63	9.93	6.90
(5,5,3)	0	0	0.00	0	0.00	0.00	0.00	0.00	0.00
(5,5,4)	0	0	0.00	0	0.00	0.00	0.00	0.00	0.00
(6,1,1)	234	100	120.30	112	0.16	0.12	28.34	10.51	7.52
(6,1,2)	396	186	117.19	112	0.17	0.38	27.19	10.33	7.33
(6,1,3)	92	45	125.05	112	0.19	0.61	26.75	10.26	7.25
(6,1,4)	14	7	113.04	112	0.20	0.83	25.92	10.13	7.12
(6,2,1)	90	38	133.66	112	0.33	0.14	28.34	10.51	7.52
(6,2,2)	188	82	114.44	112	0.35	0.33	28.12	10.48	7.48
(6,2,3)	100	46	121.10	112	0.36	0.61	27.55	10.39	7.39
(6,2,4)	8	5	139.60	112	0.30	0.86	24.63	9.93	6.90
(6,3,1)	66	28	116.32	112	0.49	0.16	28.34	10.51	7.52
(6,3,2)	242	126	115.62	112	0.50	0.39	26.07	10.15	7.14
(6,3,3)	110	57	105.12	112	0.48	0.65	26.14	10.17	7.15
(6,3,4)	6	3	134.45	112	0.46	0.89	28.34	10.51	7.52
(6,4,1)	74	37	116.66	112	0.66	0.16	26.42	10.21	7.20
(6,4,2)	472	234	111.87	112	0.67	0.40	26.58	10.24	7.23
(6,4,3)	134	63	101.75	112	0.67	0.60	27.20	10.33	7.33
(6,4,4)	6	3	99.18	112	0.61	0.81	28.34	10.51	7.52
(6,5,1)	0	0	0.00	0	0.00	0.00	0.00	0.00	0.00
(6,5,2)	0	0	0.00	0	0.00	0.00	0.00	0.00	0.00
(6,5,3)	0	0	0.00	0	0.00	0.00	0.00	0.00	0.00
(6,5,4)	0	0	0.00	0	0.00	0.00	0.00	0.00	0.00

Table 17: CHOP dataset for the NonFlex scenario used in the study. Notice that CHOP groups with durations of 0 are so-called 'empty' CHOP groups, meaning that no reference operating point falls within the group boundaries. Empty CHOP-groups are discarded from the final CHOP dataset and are grey-shaded in the table.

Group (p,d,i)	$t\ [h]$	t_{PV}	c_p $[€/MWh]$	α_p $[T/MWh]$	λ_{DH}	λ_{ind}	c_{MeOH} $[€/GJ]$	c_{NG} $[€/GJ]$	c_{wood} $[€/GJ]$
(1,1,1)	1776	1369.3	15.34	251	0.19	0.13	21.97	9.74	6.62
(1,1,2)	1716	1230.6	15.35	241	0.18	0.35	22.55	9.82	6.70
(1,1,3)	222	130	11.85	198	0.19	0.58	24.47	10.05	6.97
(1,1,4)	0	0	0.00	0	0.00	0.00	0.00	0.00	0.00
(1,2,1)	488	350	12.77	236	0.32	0.13	22.58	9.81	6.70
(1,2,2)	1012	553	9.65	180	0.32	0.36	25.22	10.13	7.08
(1,2,3)	178	109	11.90	200	0.31	0.57	24.05	9.98	6.91
(1,2,4)	6	5	15.30	270	0.32	0.86	21.25	9.66	6.52
(1,3,1)	728	566	14.27	255	0.49	0.14	21.89	9.74	6.61
(1,3,2)	1266	815	12.39	219	0.51	0.37	23.53	9.93	6.84
(1,3,3)	576	306	8.38	175	0.50	0.57	25.52	10.17	7.12
(1,3,4)	30	18	10.57	202	0.51	0.83	24.31	10.03	6.95

(1,4,1)	434	355	14.77	263	0.67	0.16	21.50	9.69	6.55
(1,4,2)	1070	825	15.37	254	0.71	0.35	21.95	9.74	6.62
(1,4,3)	240	193	16.76	262	0.73	0.56	21.63	9.71	6.57
(1,4,4)	0	0	0.00	0	0.00	0.00	0.00	0.00	0.00
(1,5,1)	138	117	17.15	270	0.89	0.17	21.25	9.66	6.52
(1,5,2)	270	228	16.72	270	0.87	0.31	21.25	9.66	6.52
(1,5,3)	42	36	18.51	270	0.86	0.56	21.25	9.66	6.52
(1,5,4)	0	0	0.00	0	0.00	0.00	0.00	0.00	0.00
(2,1,1)	7494	5480	29.34	211	0.19	0.12	22.55	9.77	6.67
(2,1,2)	10698	8568	28.19	252	0.19	0.36	21.70	9.70	6.57
(2,1,3)	2156	1753	30.52	258	0.21	0.58	21.57	9.69	6.56
(2,1,4)	24	20	30.51	270	0.19	0.82	21.25	9.66	6.52
(2,2,1)	1824	1355	29.41	217	0.32	0.13	22.41	9.75	6.65
(2,2,2)	2852	2233	28.25	250	0.32	0.37	21.86	9.72	6.60
(2,2,3)	878	704	30.72	257	0.31	0.58	21.67	9.70	6.57
(2,2,4)	0	0	0.00	0	0.00	0.00	0.00	0.00	0.00
(2,3,1)	3380	2555	29.10	225	0.49	0.15	22.24	9.74	6.63
(2,3,2)	6508	5211	28.98	251	0.49	0.37	21.71	9.70	6.57
(2,3,3)	2748	2183	32.07	253	0.51	0.61	21.75	9.71	6.58
(2,3,4)	54	41	29.14	250	0.54	0.83	22.14	9.77	6.65
(2,4,1)	3458	2679	30.16	234	0.70	0.17	22.02	9.72	6.61
(2,4,2)	6130	4942	29.27	252	0.70	0.37	21.66	9.69	6.57
(2,4,3)	3850	3204	30.13	264	0.71	0.61	21.39	9.67	6.54
(2,4,4)	192	162	31.84	270	0.72	0.85	21.25	9.66	6.52
(2,5,1)	768	615	30.01	248	0.86	0.17	21.73	9.70	6.57
(2,5,2)	2052	1689	29.00	259	0.87	0.37	21.48	9.68	6.55
(2,5,3)	1460	1233	29.23	269	0.86	0.61	21.26	9.66	6.52
(2,5,4)	90	76	31.93	270	0.82	0.84	21.25	9.66	6.52
(3,1,1)	4584	2692	47.82	113	0.18	0.13	24.86	9.97	6.94
(3,1,2)	9290	5555	49.07	118	0.18	0.36	24.68	9.95	6.91
(3,1,3)	1464	916	49.82	138	0.21	0.58	24.17	9.90	6.85
(3,1,4)	30	20	50.80	153	0.18	0.82	23.75	9.86	6.80
(3,2,1)	1320	765	49.40	113	0.34	0.14	24.99	9.99	6.96
(3,2,2)	3060	1764	50.63	116	0.34	0.36	25.02	10.00	6.97
(3,2,3)	402	228	49.29	144	0.31	0.56	25.04	10.05	7.01
(3,2,4)	0	0	0.00	0	0.00	0.00	0.00	0.00	0.00
(3,3,1)	1916	1129	50.61	115	0.48	0.15	24.82	9.96	6.94
(3,3,2)	4006	2352	51.66	113	0.49	0.38	24.86	9.97	6.94
(3,3,3)	1294	736	51.11	121	0.52	0.59	25.13	10.02	6.99
(3,3,4)	50	30	47.20	191	0.50	0.84	24.19	9.99	6.92
(3,4,1)	1464	888	47.98	118	0.69	0.17	24.55	9.93	6.89
(3,4,2)	3534	2162	50.01	122	0.70	0.35	24.45	9.92	6.88
(3,4,3)	2268	1396	50.17	126	0.70	0.60	24.38	9.91	6.87

(3,4,4)	84	59	45.05	193	0.73	0.87	22.90	9.79	6.71
(3,5,1)	192	116	49.07	112	0.86	0.17	24.63	9.93	6.90
(3,5,2)	634	410	47.10	149	0.85	0.37	23.83	9.87	6.81
(3,5,3)	366	245	46.95	168	0.86	0.62	23.44	9.84	6.77
(3,5,4)	0	0	0.00	0	0.00	0.00	0.00	0.00	0.00
(4,1,1)	1844	869	67.87	112	0.17	0.13	27.15	10.32	7.32
(4,1,2)	6418	3424	67.02	112	0.18	0.37	25.81	10.11	7.10
(4,1,3)	1610	904	66.83	112	0.19	0.58	25.29	10.03	7.01
(4,1,4)	14	7	69.14	112	0.21	0.83	25.92	10.13	7.12
(4,2,1)	664	312	67.01	112	0.33	0.15	27.19	10.33	7.33
(4,2,2)	2232	1122	66.63	112	0.35	0.37	26.43	10.21	7.20
(4,2,3)	866	456	65.98	112	0.33	0.59	25.94	10.14	7.12
(4,2,4)	12	5	70.69	112	0.37	0.82	28.34	10.51	7.52
(4,3,1)	1326	710	64.65	112	0.49	0.15	25.77	10.11	7.09
(4,3,2)	4060	2252	66.90	112	0.48	0.38	25.42	10.05	7.03
(4,3,3)	2740	1523	67.57	112	0.49	0.62	25.39	10.05	7.03
(4,3,4)	146	76	68.14	112	0.50	0.83	26.00	10.14	7.13
(4,4,1)	1030	607	67.95	112	0.68	0.17	24.83	9.96	6.93
(4,4,2)	3016	1763	67.95	112	0.69	0.36	24.91	9.97	6.95
(4,4,3)	2472	1461	68.80	112	0.69	0.63	24.81	9.96	6.93
(4,4,4)	184	107	69.20	112	0.69	0.85	24.99	9.99	6.96
(4,5,1)	192	116	64.98	112	0.85	0.16	24.63	9.93	6.90
(4,5,2)	576	347	66.38	112	0.86	0.34	24.63	9.93	6.90
(4,5,3)	160	96	65.58	112	0.89	0.60	24.63	9.93	6.90
(4,5,4)	0	0	0.00	0	0.00	0.00	0.00	0.00	0.00
(5,1,1)	3510	1508	80.55	112	0.16	0.13	28.27	10.50	7.51
(5,1,2)	8454	3814	80.12	112	0.17	0.37	27.66	10.40	7.41
(5,1,3)	2522	1193	81.18	112	0.19	0.59	27.11	10.32	7.31
(5,1,4)	18	8	78.14	112	0.13	0.82	28.34	10.51	7.52
(5,2,1)	1326	567	79.07	112	0.34	0.14	28.34	10.51	7.52
(5,2,2)	2566	1141	79.88	112	0.34	0.38	27.84	10.43	7.44
(5,2,3)	1126	522	80.77	112	0.34	0.61	27.35	10.35	7.35
(5,2,4)	6	3	76.37	112	0.25	0.86	28.34	10.51	7.52
(5,3,1)	1628	697	81.77	112	0.51	0.17	28.31	10.51	7.52
(5,3,2)	4598	2088	80.50	112	0.50	0.38	27.59	10.39	7.39
(5,3,3)	2978	1413	79.64	112	0.51	0.62	27.07	10.31	7.31
(5,3,4)	132	61	78.73	112	0.52	0.85	27.45	10.37	7.37
(5,4,1)	692	327	80.62	112	0.67	0.17	27.13	10.32	7.32
(5,4,2)	2716	1353	79.66	112	0.69	0.38	26.53	10.23	7.22
(5,4,3)	2988	1534	79.54	112	0.69	0.63	26.21	10.18	7.16
(5,4,4)	254	144	78.60	112	0.69	0.85	25.23	10.02	7.00
(5,5,1)	0	0	0.00	0	0.00	0.00	0.00	0.00	0.00
(5,5,2)	104	63	75.71	112	0.85	0.36	24.63	9.93	6.90

(5,5,3)	0	0	0.00	0	0.00	0.00	0.00	0.00	0.00
(5,5,4)	0	0	0.00	0	0.00	0.00	0.00	0.00	0.00
(6,1,1)	642	274	100.83	112	0.17	0.12	28.34	10.51	7.52
(6,1,2)	714	322	99.31	112	0.17	0.37	27.67	10.41	7.41
(6,1,3)	254	114	106.31	112	0.19	0.59	27.71	10.41	7.42
(6,1,4)	14	7	104.16	112	0.20	0.83	25.92	10.13	7.12
(6,2,1)	342	146	112.84	112	0.31	0.13	28.34	10.51	7.52
(6,2,2)	260	112	110.90	112	0.33	0.39	28.18	10.49	7.49
(6,2,3)	136	61	114.02	112	0.33	0.60	27.75	10.42	7.42
(6,2,4)	8	5	139.60	112	0.30	0.86	24.63	9.93	6.90
(6,3,1)	702	300	109.68	112	0.55	0.16	28.34	10.51	7.52
(6,3,2)	968	436	148.36	112	0.54	0.36	27.68	10.41	7.41
(6,3,3)	530	236	176.04	112	0.52	0.61	27.81	10.43	7.43
(6,3,4)	24	10	134.73	112	0.55	0.87	28.34	10.51	7.52
(6,4,1)	698	304	179.12	112	0.67	0.17	28.10	10.47	7.48
(6,4,2)	1240	562	182.33	112	0.67	0.35	27.61	10.40	7.40
(6,4,3)	674	294	341.93	112	0.65	0.61	28.10	10.47	7.48
(6,4,4)	48	21	431.99	112	0.63	0.86	28.34	10.51	7.52
(6,5,1)	0	0	0.00	0	0.00	0.00	0.00	0.00	0.00
(6,5,2)	0	0	0.00	0	0.00	0.00	0.00	0.00	0.00
(6,5,3)	0	0	0.00	0	0.00	0.00	0.00	0.00	0.00
(6,5,4)	0	0	0.00	0	0.00	0.00	0.00	0.00	0.00

APPENDIX G Conference paper 1

Proceedings paper – peer reviewed manuscript

C.E. Lythcke-Jørgensen, F. Haglind, and L.R. Clausen. *Thermodynamic and economic analysis of integrating lignocellulosic ethanol production in a Danish combined heat and power plant*. 21st European Biomass Conference & Exhibition (EUBCE). Copenhagen, Denmark, 2013.

This paper builds upon the master thesis 'Modelling and Optimization of a Steam Co-generation Plant with Integrated Bio-ethanol Production' [79]. It summarizes and elaborates on the findings regarding process integration and economic results of the studied system.

THERMODYNAMIC AND ECONOMIC ANALYSIS OF INTEGRATING LIGNOCELLULOSIC BIOETHANOL PRODUCTION IN A DANISH COMBINED HEAT AND POWER UNIT

C. Lythcke-Jørgensen[a].*, F. Haglind[a], L.R. Clausen[a]
[a] Technical University of Denmark, DTU Mechanical Engineering, Section for Thermal Energy
Nils Koppels Allé, building 403, 2800 Kgs. Lyngby, Denmark
* Corresponding author. Contact: +45 30 42 72 00, celjo@mek.dtu.dk

ABSTRACT: Integrating lignocellulosic bioethanol production with combined heat and power (CHP) production in polygeneration systems is considered an efficient and competitive way to produce a sustainable fuel for the transportation sector. This study assessed the energy economy of integrating lignocellulosic bioethanol production in the Danish CHP unit Avedøreværket 1. Numerical models of the plants were developed, and feasible integration solutions were identified and optimised using exergy analysis. Hour-wise production simulations were run over a reference year, and market prices and economic parameters from the literature were used to evaluate the production economy. A competitive energy cost limit for the bioethanol production was found to be 0.22 Euro/L. The optimised system produced bioethanol at a mean cost of 0.14 Euro/L during integrated operation and 1.22 Euro/L during separate operation. Maintenance shut-downs and periods of high power demand resulted in 3375 hours of separate operation over the year, giving an average bioethanol energy cost of 0.56 Euro/L. The results suggest that the polygeneration system cannot produce lignocellulosic bioethanol competitively under the given conditions, which questions the economic viability of the polygeneration system if operated in grids with periodically large power demands, for instance those caused by the operation of wind turbines and photovoltaic cells with a large capacity.
Keywords: Analysis, bioethanol, economic aspects, modelling, polygeneration

NOMENCLATURE

Latin letters

C	absolute cost [Euro]
c	specific cost [Euro/kJ]
$c_{ethanol}$	specific cost of ethanol [Euro/L]
h	enthalpy [kJ/kg]
K_{steam}	steam to biomass ratio [-]
$\dot{m}$	mass flow [kg/s]
t	residence time [h]
P	amount of power produced [kJ]
Q	amount of heat produced [kJ]
$\dot{Q}$	heat flow [kJ/s]
V	volume [L]
x	mass fraction [-]

Greek letters

$\varepsilon_{j,i}$	fraction of component *i* recovered in flow *j* [-]
$\eta_{i,k}$	recovery of component *i* in process *k* [-]

Subscripts

i	compound
j	flow
k	process

Abbreviations

AVV1	Avedøreværket 1
CHP	Combined heat and power
IBUS	Integrated Biomass Utilization System

1 INTRODUCTION

Second-generation bioethanol, processed from inedible and renewable biomass and acting as a direct substitute for fossil fuels in internal combustion engines, can decrease greenhouse gas emissions from the transportation sector while reducing the dependency on imported oil in countries without domestic resources. Within the European Union, especially the processing of lignocellulosic biomass is considered a promising second generation bioethanol technology [1].

Due to the energy intensive nature of lignocellulosic bioethanol production, it is considered advantageous to integrate bioethanol production facilities with the production of other energy products in polygeneration systems. Systems containing heat, power, lignocellulosic bioethanol and biogas production have been studied at the system level in several papers [2-4]. [2] and [3] both report better energy economy for integrated operation of the various facilities compared to stand-alone operation, while [4] reports a better first law efficiency for the integrated system. Similarly, higher first law efficiency for integrated operation has been reported by [5] for a polygeneration system in which lignocellulosic bioethanol production was integrated with an existing combined heat and power (CHP) unit. However, none of these studies take market restrictions or load fluctuations into account. The importance of the operational flexibility of a polygeneration plant operating in a fluctuating market environments was investigated by [6], who claimed that flexible plants can obtain better plant economies than static ones due to hour-wise and seasonal-wise variations in product prices. The impact of production flexibility was investigated in the present work.

This paper examines the integration of a lignocellulosic bioethanol production facility based on the IBUS (Integrated Biomass Utilization System) in the existing CHP unit Avedøreværket 1 (AVV1) outside Copenhagen. First, the polygeneration system was designed and modelled numerically. Second, the energy economy of the system was evaluated by conducting hour-wise production simulations over a reference year. The production demands for AVV1 during the reference year were used to determine the outputs to be delivered by the polygeneration system, while the energy economy was evaluated using actual electricity, heat, bioethanol, gas and coal prices. The results of the study are significant for evaluating the economy of polygeneration

systems in a constrained and fluctuating market.

The thermodynamic modelling is described in Section 2, while the approach that was used in the economic analysis is described in Section 3. The results of the analysis are presented in Section 4 and discussed in Section 5. The conclusions that can be drawn from the total analysis are given in Section 6, while a list of the references is provided in Section 7.

2 THERMODYNAMIC MODELLING

The thermodynamic modelling consisted of two major parts: a modelling part in which numerical models of the polygeneration system facilities were developed, and a design part where the facility integration was designed and optimised.

2.1 Polygeneration system modelling

The polygeneration system studied consisted of the existing Danish CHP unit AVV1 and a bioethanol production facility running the IBUS (Integrated Biomass Utilization Process) technology, which has been described in detail in several papers [7-10].

A numerical model of AVV1 was developed and described by [11] using the energy system simulator DNA [12]. With the authors' permission, their model was used in this study. A simplified component layout of AVV1 is found in Figure 1.

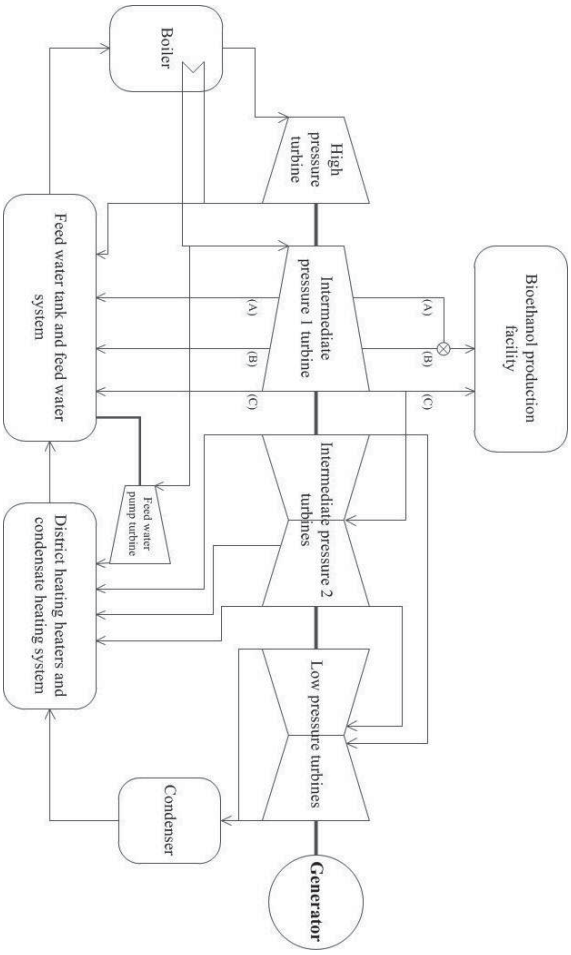

Figure 1: Simplified layout of the numerical model of AVV1

The model accuracy was evaluated at various loads by comparing electrical efficiencies and energy utilization values obtained with efficiencies reported by the plant operator [13]. This comparison was limited to condensation mode and full back-pressure mode operation as they represent the extreme cases of plant operation. All values are summarized in Tables 1 and 2.

Table 1: Comparison of model efficiencies and reported plant efficiencies in condensation operation

	Condensation mode operation		
Load	Electrical Efficiency		
	Model	Reported	Deviation
1.0	0.41	0.42	-2%
0.8	0.40	0.42	-5%
0.6	0.39	0.42	-7%
0.4	0.37	0.40	-8%

Table 2: Comparison of model efficiencies and reported plant efficiencies in full back pressure operation

	Full back pressure mode operation					
Load	Electrical Efficiency			Energy Utilization		
	Model	Reported	Deviation	Model	Reported	Deviation
1.0	0.36	0.34	6%	0.91	0.92	-1%
0.8	0.35	0.34	3%	0.91	0.92	-1%
0.6	0.33	0.33	0%	0.90	0.91	-1%
0.4	0.30	0.30	0%	0.88	0.90	-2%

It was found that the model assumed a larger fuel consumption in condensation mode than what was reported by the plant owner, resulting in energy efficiencies that were between 2% and 8% lower for the model. For back pressure operation, the energy utilization accuracy was found to be within a range of 2%, while the electrical efficiency deviated by up to 6%.

A numerical model of a bioethanol production facility based on the IBUS process was developed using layout and yields reported by [7] and [14]. The model, which uses heat and mass balances to model the process, was developed in the software EES (Engineering Equation Solver) [15]. The modelled process layout is illustrated in Figure 2.

In the IBUS process, input biomass is sent into a pretreatment stage where it is chopped and washed. It is then fed into a hydrothermal pretreatment reactor where the lignin structure is broken down by treatment with pressurised steam. The biomass product from the reactor is pressed afterwards to remove excess water, leaving a fibre fraction and a stillage fraction. The fibre fraction is cooled and liquefied by glucose-forming enzymes before fermentation is initiated in simultaneous saccharification and fermentation (SSF) tanks, producing an ethanol-containing broth. Bioethanol is distilled from the broth, leaving a fibre stillage that is mixed with the stillage from the pretreatment. Solid biomass compounds remaining in the stillage are filtered out and dried to form a high-quality solid biofuel with low alkali and moisture content. Ethanol and some of the water contained in the remaining stillage is evaporated from the stillage, leaving behind a molasses mixture with high C5 sugar content.

Mass balances were assumed over each component for useful flows. The mass balances were calculated for each component as:

$$\sum \dot{m}_{in} = \sum \dot{m}_{out}$$

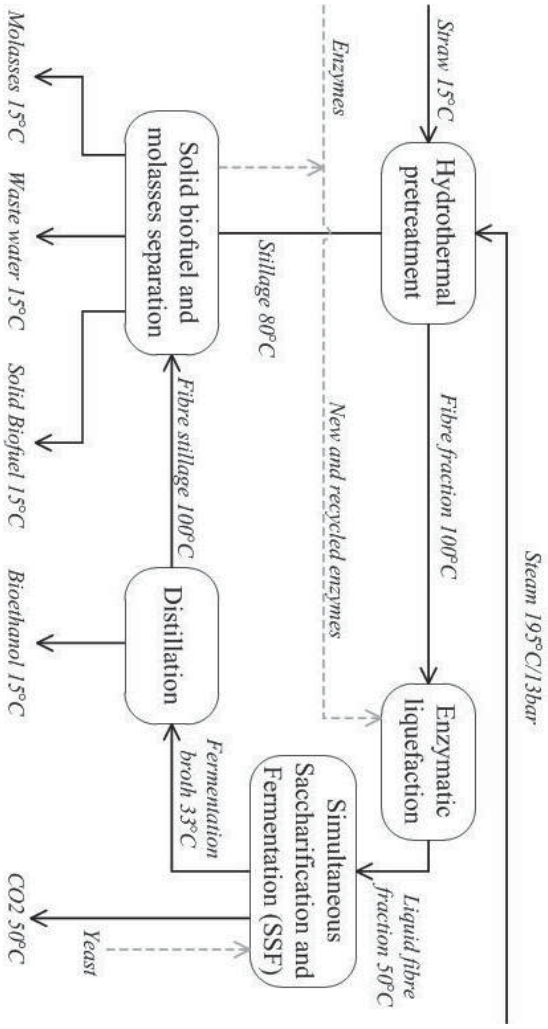

Figure 2: Simplified layout of the modelled bioethanol production facility based on the IBUS technology

In components with flow splitting, the mass flow of compound *i* recovered in a given output flow, $\varepsilon_{(flow),(compound\,i)}$, was calculated according to the equation:

$$\dot{m}_{(flow)} x_{(flow),(compound\,i)} = \varepsilon_{(flow),(compound\,i)} \sum_{n=inlet\ flows} \dot{m}_n x_{n,(compound\,i)}$$

with x_i being the mass fraction of compound *i*. When compound degradation or conversion occurs, relation of output mass flow of a compound to the input mass flow of the compound, $\eta_{(flow),(compound\,i)}$, was determined as:

$$\sum_{m=outlet\ flows} \dot{m}_n x_{n,(compound\,i)} = \eta_{(flow),(compound\,i)} \sum_{n=inlet\ flows} \dot{m}_n x_{n,(compound\,i)}$$

The steam mass flow $\dot{m}_{steam}$ into the hydrothermal pretreatment component was modelled as a constant K_{steam} times the input biomass mass flow $\dot{m}_{biomass}$.

$$\dot{m}_{steam} = K_{steam} \cdot \dot{m}_{biomass}$$

Table 3: Parameters used in a model of a bioethanol facility based on the IBUS process

	Parameter	Literature Values	Used Value
Biomass composition	Cellulose mass fraction	0.327 [7]	0.327
	Hemicellulose mass fraction	0.358 [7]	0.358
	Lignin mass fraction	0.155 [7]	0.155
	Water mass fraction	0.04 [7]	0.04
	'Others' mass fraction	0.12 [7]	0.12
Pretreatment	Steam to biomass ratio	1.93 [10][a] 2.0-2.7 [9][b]	2.0
	Cellulose recovered in fibre fraction	0.955 [7] 0.969 [10]	0.96
	Hemicelluloses recovered in the fibres	0.313 [7]	0.313
	Lignin recovered in the fibres	-	1.00
	Total hemicellulose recovery	0.68 [7]	0.68
	Water mass fraction in fibre fraction	0.7-0.75 [7] 0.6-0.75 [9]	0.35
Liquefaction	Unreacted input cellulose	0.6-0.7 [7]	0.65
	Liquefaction residence time	6h [7]	6h
SSF (Simultaneous Saccharification and Fermentation)	Unreacted input cellulose	0.3-0.6[C] [7] 0.23-0.31 [10]	0.3
	SSF residence time	170h [7] 140h [9]	140h
Distillation	Ethanol in distillation product	0.93-0.95 [7]	0.95
	Ethanol in distillation stillage	0.0008 [7]	0.0008
Separation	Wet-fuel water content	0.6 [7] 0.65-0.7 [9][d]	0.4[e]
	Dry-fuel water content	0.05-0.2 [7] 0.09 [10] 0.1 [9]	0.1
	Molasses water content	0.35 [9]	0.65
	Hemicelluloses in wet-fuel	-	0.78

[a] Equals 3.8 GJ steam/ton of straw treated
[b] Equalling operation at dry-matter contents of 30-40% in the pretreatment stage
[c] Gives an ethanol concentration of the broth in the range 0.06-0.085
[d] When using decanter technology
[e] Is assumed achievable when using a filter press instead of decanters for wet-fuel extraction

The hydrolysis of cellulose to glucose, which occurs in the liquefaction and simultaneous saccharification and fermentation (SSF), follows the reaction:

$$C_6H_{10}O_5 + H_2O \rightarrow C_6H_{12}O_6$$

The fermentation of glucose to ethanol during SSF follows the reaction:

$$C_6H_{10}O_5 + H_2O \rightarrow 2 \cdot C_2H_5OH + 2 \cdot CO_2$$

For both reactions, molar weight ratios were used to relate the weight fraction increase of the reaction products to the weight fraction decrease of the reactants.

Component energy balances were used to evaluate the resulting heating or cooling demand:

$$\dot{Q}_{(component)} = \sum_{j=inlet\ flow} \dot{m}_j h_j - \sum_{k=outlet\ flow} \dot{m}_k h_k$$

The exception to this was the distillation component, for which the heating and cooling demands were calculated using the Aspen Plus distillation column model.

As reported by [10], the power consumption of an IBUS facility was set to 220kWh/ton of biomass treated.

2.2 Modelling assumptions and parameters

Degradation of hemicelluloses was assumed to occur only during pretreatment. No degradation or dissolving of lignin was assumed during the processes. Hydrolysis was assumed to be the only means of cellulose conversion. The addition of yeast and enzymes was neglected in mass balance calculations. Cellulose, hemicellulose, lignin and glucose were assumed to have constant heat capacities in then relevant temperature ranges. Mixtures of water and ethanol with low ethanol mass fractions below 0.1 have been treated as if the water and ethanol were separated. Heat losses were neglected for all components.

The parameters used to describe the system are summarized in Table 3, together with reported parameter values from literature and the values used in the model.

The accuracy of the IBUS facility model was evaluated by comparing model yields with reported yields from the literature, see Table 4. Reported yields varied significantly. Compared to the yields reported the most recently, the model deviated by up to 6.5% [8].

Table 4: Comparison of model yields and yields reported in the literature. All numbers are in kg/ton of biomass

	Model yield	[7]	[8]	[9]	[10]
Bioethanol	150.0	143	144	143.3	153.3
Solid biofuel	406.8	353	435	433.3	-
Molasses	371.0	420	371	370.0	-

2.3 System dimensioning and integration design

With an estimated average yearly production of 196,000 tons, winter wheat straw is the lignocellulosic biomass with the highest local production within a distance of 50km from AVV1 [16]. The system was dimensioned to process all locally available winter wheat straw, resulting in a facility processing capacity of 22.4 tons of straw per hour all year round. A linear relation between capacity and energy consumption was used for determining the energy demand of the bioethanol production facility.

Based on requirements for the temperature and pressure of the steam to be delivered to the bioethanol facility, only the three existing steam extraction points in the Intermediate Pressure 1 turbine of AVV1, marked (A), (B) and (C) in Figure 1, were considered for steam extraction.

For each feasible integration solution, pinch analysis [17] was used to identify the necessary amount of heat flow to be extracted from the various steam extraction points. District heating production was assumed to form part of the bioethanol production facility. A 10K pinch temperature difference was used, as suggested by [18] for a similar facility. Models were developed for each integration solution, and simulations were run for various loads to determine the operational range for the heat and power production. Exergy analysis [19] was applied to identify the integration solution having the lowest overall exergy destruction within the polygeneration system.

Table 5: Economic parameters used in the analysis

	Specific cost
CHP fuel	4.36 Euro/GJ [13]
Gas	9.26 Euro/GJ [13]
Electricity	Dependent on the hour *i* [20]
Bioethanol	0.55 Euro/L[f] [21]
Bioethanol production costs without energy costs	0.33 Euro/L[g] [7]

[f] The average bioethanol price on the European market for the period 2008-2010 was used

[g] Calculated from values from a feasibility study of a 50ton/h IBUS facility located in the US. The number includes the expected income from selling the molasses and solid biofuel bi-products

3 ECONOMIC ANALYSIS

To evaluate the energy economy of the system, hour-wise simulations were run for the polygeneration system production over a year. The cost difference between operating AVV1 and operating the polygeneration system was taken to be the cost of bioethanol production.

3.1 Energy economy data

Costs of consumed resources, products and operation were used to evaluate the energy economy of the polygeneration system. The values used are summarized in Table 5.

A competitive limit of 0.22 Euro/L for the energy cost of the bioethanol production was obtained by subtracting the bioethanol production cost without energy costs from the expected bioethanol selling price.

3.2 Production simulations and energy cost calculations

The polygeneration system was set to deliver the same hour-wise production of heat and power as AVV1 did in the reference year. In periods where production loads or shut-downs prevented integrated operation of the bioethanol production facility, a gas boiler with a first law efficiency of 96% [22] was used for providing the required steam, and the required power was assumed to be bought from the electricity market at a price corresponding to that of the Nord Pool Spot electricity market.

The energy cost of operating AVV1, $C_{energy,AVV1}$, was determined as the sum of the hour-wise fuel consumption of the plant $Q_{i,AVV1}$ over the year times the fuel cost c_{fuel}:

$$C_{energy,AVV1} = \sum_{i=1}^{8760} Q_{i,AVV1} \cdot c_{fuel}$$

The energy cost of operating the polygeneration system, $C_{energy,poly}$, was estimated as the hour-wise sum of the CHP unit energy cost plus the cost of IBUS operation in periods without integrated operation.

$$C_{energy,poly} = \sum_{i=1}^{8760} Q_{i,CHP} \cdot c_{fuel} + \sum_{i=1}^{8760} L_{i,IBUS} \left(\frac{1}{\eta_{boiler}} Q_{IBUS} c_{gas} + P_{IBUS} c_{i,electricity} \right)$$

$Q_{i,CHP}$ is the hour-wise fuel consumption of the CHP unit in the polygeneration system, while Q_{IBUS} and P_{IBUS} are the heat and power consumption of the bioethanol facility. $L_{i,IBUS}$ is a variable taking the value 1 when IBUS is operated separately and 0 when IBUS is operated as an integrated part of the CHP unit. Note that $Q_{i,CHP}$ is not equal to $Q_{i,AVV1}$ as the CHP unit consumes more fuel in integrated operation to maintain the IBUS facility operation. °

The specific bioethanol production energy cost $c_{energy,ethanol}$ was calculated as the difference in energy cost of the polygeneration system and AVV1 divided by the volume of the yearly ethanol production $V_{ethanol,year}$.

$$c_{energy,ethanol} = \frac{C_{energy,poly} - C_{energy,AVV1}}{V_{ethanol,year}}$$

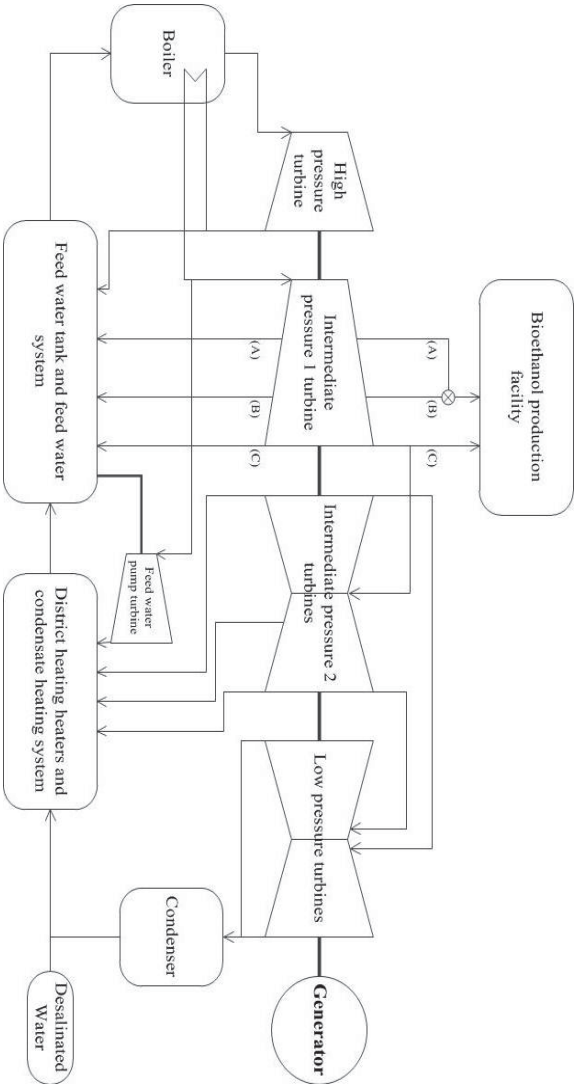

Figure 3: Simplified layout of the polygeneration system that was modelled

4 RESULTS

4.1 System design and operation

A combined exergy and pinch analysis was conducted to investigate the various integration solutions studied. The results indicate that an optimal steam extraction pattern, with optimal meaning minimal exergy flow from the CHP unit to the bioethanol production facility, includes steam extracted from the extraction points (A), (B) and (C) in Figure 3. In the optimal steam extraction pattern, hydrothermal pretreatment steam was extracted from node (B) at loads above 60%, and from node (A) at loads below 60%. The hydrothermal pretreatment steam had to be conditioned to meet the exact temperature and pressure requirements of the hydrothermal pretreatment component. Heat released from steam conditioning was used internally in the bioethanol production facility. The remaining heat demand of the bioethanol production facility was covered by steam extracted from (C).

Composite curves from the pinch analysis of the bioethanol production facility, for the optimal integration solution and at various loads, are shown in Figures 4 and 5. At zero district heating production, a pinch point occurred at 100^{0}C. At full district heating production, two pinch points occurred due to the optimal use of the available heat: one at 91^{0}C at 50^{0}C.

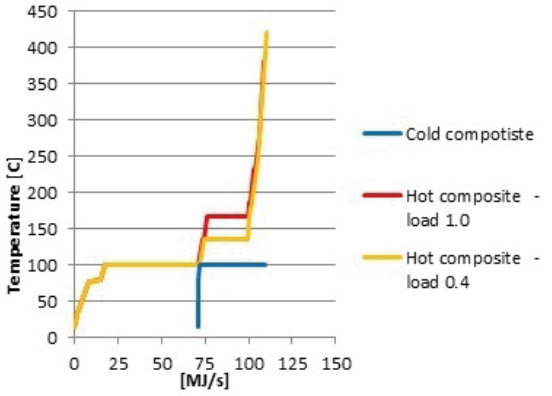

Figure 4: Composite curves for the bioethanol production facility at zero district heating production for various loads in the CHP unit

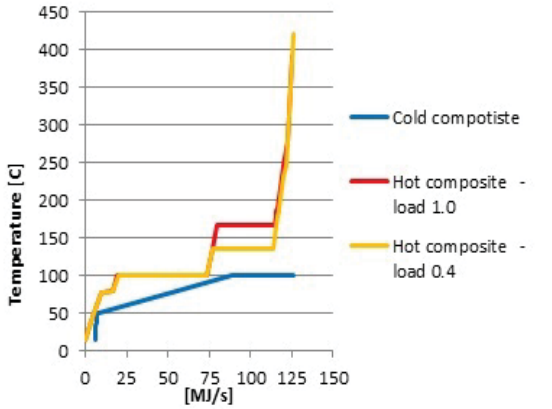

Figure 5: Composite curves for the bioethanol production facility at full district heating production for various loads in the CHP unit

The models of AVV1 and the polygeneration system with the integration solution selected were simulated to evaluate production and operation patterns for the heat-and-power production of the two plants. The results indicate that the power production potential was lower for the polygeneration system than for AVV1 alone, while the district heating potential of the polygeneration system tended to be slightly higher than that of AVV1, as seen in Figure 6.

The hour-wise heat and power production of the polygeneration system was set to be equal to that of AVV1 over the reference year. When integrated operation was prevented by either power demand or shut-down of the CHP unit, the bioethanol facility was operated separately. The reasons for this, and the corresponding total duration of the periods with separate operation during the year are summarized in Table 6.

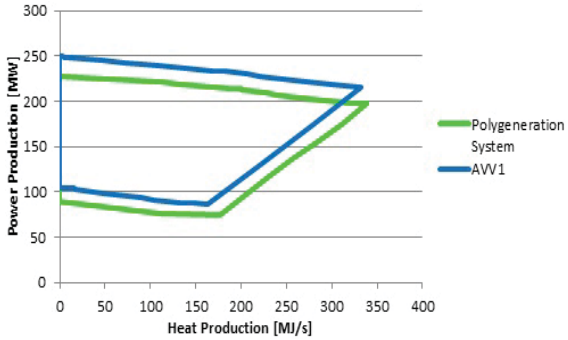

Figure 6: Operational heat-and-power production ranges for AVV1 and the polygeneration system

Table 6: Causes of separate operation in the polygeneration system during the reference year

Cause of separate operation	Total duration
High power demand	1685 hours
CHP unit shut-down	2060 hours
Total separate operation	3375 hours

4.2 Energy economy

With a biomass processing capacity of 22.4 ton/hour, the bioethanol production facility was found to produce a total of 29,434 tons, or 37,080,000 L, of ethanol during the reference year when assuming full load operation at all 8760 hours.

The extra energy costs of running the polygeneration system compared to running AVV1 alone was found to be 20.7 M.Euro. The average energy cost for producing bioethanol was found to be 0.145 Euro/L during integrated operation and 1.218 Euro/L during separate operation. Overall, the results suggest that the average bioethanol energy cost over the year was 0.558 Euro/L. The resulting energy costs for AVV1 and the polygeneration system over the reference year obtained from model simulations are summarized in Table 7.

Table 7: Energy costs for AVV1 and the polygeneration system during the reference year

	AVV1	Polygeneration system
CHP fuel cost	49.8 M.Euro	53.1 M.Euro
Gas cost	0 M.Euro	9.1 M.Euro
Electricity cost	0 M.Euro	8.3 M.Euro
Total cost	49.8 M.Euro	70.5 M.Euro

5 DISCUSSION

The competitive bioethanol production energy cost limit was estimated to be 0.22 Euro/L for the bioethanol production based on the IBUS process. During integrated operation, the bioethanol production energy cost was found to be economically competitive, agreeing with the results obtained by [2] and [3]. However, the energy cost during separate operation was found to be uncompetitive, and due to the long duration of separate operation over a year, the results suggest that the polygeneration system that was modelled cannot produce bioethanol at a competitive price on average.

In order to achieve competitive operation, the average production costs must be reduced. This can be done by either lowering the production cost of separate operation, or by increasing the duration of integrated operation. An option for reducing the production cost of separate operation would be to replace the gas boiler with a cheaper heat source for steam generation, for instance by using the lignin-fuel produced by the system. However, this was not considered in the present study.

Assuming the average values calculated in this study are accurate, it is suggested that competitive production would be obtained by maintaining integrated operation during 8150 hours of the year, 2765 hours longer than what was assumed in the study. However, it must be mentioned that during the reference year, the CHP unit was shut down for a longer period than would be expected in the future. However, this uncertainty is not significant enough to affect the overall conclusion that the average operation would be uncompetitive over the year.

An option for increasing the duration of integrated operation would be to improve the integration design by adding steam extraction points in the CHP unit that fit the bioethanol production steam requirements better. As seen in the composite curves in Figure 4, extracted steam is delivered at a temperature much higher than required. Better fitting of the extracted steam to the requirements of the bioethanol facility would reduce the system exergy destruction, allowing for higher power production levels and thereby reducing the duration of separate operation due to high power demand. The same effect could be obtained by lowering the temperature requirements of the IBUS facility, but this is related to the conversion technology and not to the system design.

Another way to increase the integration duration would be to simply reduce the heat demand of the bioethanol production facility, especially in the hydrothermal pretreatment process. The simplest way to achieve a reduction in the heat demand would be to down-scale the facility, but another interesting option would be to investigate the technology used, to determine if the amount of heat used per unit of straw treated could be reduced. Such investigations are beyond the scope of the present study.

A third option would be to reduce the demands on power production, eliminating all separate operation due to high power demands. Decreased income from power sales must be included when evaluating this approach. Whether or not this is a realistic approach to evaluate the plant economy depends on the grid in which the polygeneration system operates, as a decreased power production capacity during peak loads could cause shortages. It should be noticed that the bioethanol production facility considered was dimensioned for

handling 22.4 tons/hour of biomass, which is less than half the size of the designed capacity of 50tons/hour for facilities using IBUS technology [7]. However, increasing the scale of the IBUS facility would reduce the power production potential further, emphasizing the need for further consideration of the power production operation.

The question of decreased power production is especially relevant in grids with large capacities of intermittent power sources such as wind turbines or photovoltaic cells which cannot be switched on as a function of the power demand. On the one hand, polygeneration systems like the one treated might be forced to maximize power production at the cost of integrated operation in periods with high power demand and low or zero production from intermittent sources. On the other hand, the polygeneration system is able to reduce its power production further than the CHP unit alone, which is advantageous in periods with high power yields from intermittent sources and low demands, resulting in low or even negative power prices. The dominant of the two trends would have to be determined to draw any conclusions about system economy as a function of the installed intermittent power capacity in the grid. This study therefore recommends that a holistic approach should be taken when designing and evaluating a system with integrated heat, power and bioethanol production.

6 CONCLUSION

The study treated the integrated production of heat, power and lignocellulosic bioethanol in a polygeneration system based on an existing combined heat and power unit. The energy economy of producing bioethanol in the system was evaluated over a year. The average energy cost of bioethanol production during integrated operation was found to be 0.145 Euro/L, and during separate operation the average energy cost was found to be 1.218 Euro/L. Over a year, 3375 hours of separate operation was necessary to meet large power demands on the grid and shut-downs of the combined heat and power unit. The resulting average energy cost for bioethanol production over a year was found to be 0.558 Euro/L. With an estimated competitive limit for the energy cost of 0.22 Euro/L, the simulation results suggest that the polygeneration system modelled cannot produce lignocellulosic bioethanol at a competitive energy cost due to the duration of separate operation.

7 ACKNOWLEDGEMENTS

The authors would like to thank Brian Elmegaard for lending us his model of the CHP unit Avedøreværket 1, and for his help with updating scripts. The authors would also like to thank Mogens Bech Laursen for valuable and fruitful discussions on the basis for the study. Finally, the authors thank DONG Energy for providing data on market prices and operational patterns for Avedøreværket, and for co-financing the study.

8 REFERENCES

[1] Commission of the European Communities, "Communication from the Commission - An EU Strategy for Biofuels," 2006.

[2] L. Daianova, E. Dotzauer, E. Thorin and J. Yan, "Evaluation of a regional bioenergy system with local production of biofuel for transportation, integrated with a CHP plant," *Applied Energy,* no. 92, pp. 739-749, 2011.

[3] D. D. Ilic, E. Dotzauer and L. Trygg, "District heating and ethanol production through polygeneration in Stockholm," *Applied Energy,* no. 91, pp. 214-221, 2011.

[4] P. Bösch, A. Modarresi and A. Friedl, "Comparison of combined ethanol and biogas polygeneration facilities using exergy analysis," *Applied Thermal Engineering,* no. 37, pp. 19-29, 2012.

[5] F. Starfelt, E. Thorin, E. Dotzauer and J. Yan, "Performance evaluation of adding ethanol production into an existing combined heat and power plant," *Bioresource Technology,* no. 101, pp. 613-618, 2009.

[6] Y. Chen, T. A. Adams II and P. I. Barton, "Optimal Design and Operation of Flexible Energy Polygeneration Systems," *Industrial & Engineering Chemistry Research,* no. 50, pp. 4553-4566, 2011.

[7] J. Larsen, M. Østergaard Petersen, L. Thirup, H. Wen Li and F. Krogh Iversen, "The IBUS Process - Lignocellulosic Bioethanol Close to a Commercial Reality," no. 5, pp. 765-772, 2008.

[8] J. Larsen, M. Østergaard Haven and L. Thirup, "Inbicon makes lignocellulosic ethanol a commercial reality," *Biomass and Bioenergy,* no. 46, pp. 36-45, 2012.

[9] Inbicon, "Making Ethanol Work for the World," Inbicon, 7000 Frederecia, DK, 2010.

[10] N. Scott-Bentsen, C. Felby and K. H. Ipsen, "Energy Balance of 2nd Generation Bioethanol Production in Denmark," Elsam A/S, 2006.

[11] B. Elmegaard and N. Houbak, "Simulation of the Avedøreværket Unit 1 cogeneration plant with DNA," in *ECOS 2003*, Copenhagen, 2003.

[12] B. Elmegaard and N. Houbak, "DNA - A General Energy System Simulation Tool," in *SIMS*, 2005.

[13] C. Lythcke-Jørgensen, "Modelling and Optimization of a Steam Co-generation Plant with Integrated Bio-ethanol Production", Technical University of Denmark, Kgs. Lyngby, 2012.

[14] M. Østergaard Petersen, J. Larsen and M. Hedegaard Thomsen, "Optimization of hydrothermal pretreatment of wheat straw for production of bioethanol at low water consumption without addition of chemicals," *Biomass and Bioenergy,* no. 33, pp. 834-840, 2009.

[15] F-Chart, "Engineering Equation Solver," F-Chart Software, 2013. [Online]. Available: http://www.fchart.com/ees/.

[16] Danmarks Statistik, "Statistikbanken," 2012. [Online]. Available: www.statistikbanken.dk. [Accessed 17 May 2012].

[17] I. C. Kemp, Pinch Analysis and Process Integration, 2nd edition, Oxford, UK: Butterworth-Heinemann, 2006.

[18] A. Modarresi, P. Kravanja and A. Friedl, “Pinch and exergy analysis of lignocellulosic ethanol, biomethane, heat and power production from straw,” *Applied Thermal Engineering,* no. 43, pp. 20-28, 2012.

[19] Bejan A., Tsatsaronis G., Moran M., Thermal Design & Optimization. New York: John Wiley & Sons, Inc.; 1996.

[20] NordPoolSpot, “Nord Pool Spot,” 2011. [Online]. [Accessed 22 June 2012].

[21] Statens energimyndighet, “Energiläget 2011,” Energimyndigheten, 2011.

[22] Energistyrelsen, “Technology Data for Energy Plants,” Danish Energy Agency, 2010.

APPENDIX H Conference paper 2

Proceedings paper – peer reviewed manuscript

C.E. Lythcke-Jørgensen, F. Haglind, and L.R. Clausen. *Exergy analysis of a combined heat and power plant with integrated lignocellulosic ethanol production*. 26th International Conference on Efficiency, Cost, Optimization, Simulation and Environmental Impact of Energy Systems (ECOS), Guilin, China, 2013.

This paper presents an exergy analysis of ethanol production based on Inbicon technology [121]. It is based on the models presented in the master thesis 'Modelling and Optimization of a Steam Co-generation Plant with Integrated Bio-ethanol Production' [79].

Exergy analysis of a combined heat and power plant with integrated lignocellulosic ethanol production

Christoffer Lythcke-Jørgensen [a], Fredrik Haglind[b] and Lasse Røngaard Clausen[c]

[a] *DTU Mechanical Engineering, Section for Thermal Energy, Copenhagen, Denmark, celjo@mek.dtu.dk*
[b] *DTU Mechanical Engineering, Section for Thermal Energy, Copenhagen, Denmark, frh@mek.dtu.dk*
[c] *DTU Mechanical Engineering, Section for Thermal Energy, Copenhagen, Denmark, lrc@mek.dtu.dk*

Abstract:

Integrating second generation bioethanol production in combined heat and power units is expected to increase system energy efficiencies while producing sustainable fuel for the transportation sector at a competitive price. By applying exergy analysis, this study assessed the efficiency of an integrated system in which steam extracted from an existing combined heat and power unit is used for covering the heating demand of a lignocellulosic ethanol production facility. The integration solution was designed and optimized using already existing steam extraction points in the combined heat and power unit solely. The exergy flows inside the ethanol facility were determined, and the exergy in steam flows into and out of the system components were determined by combining exergy analysis with pinch analysis and setting a constant heat exchange temperature difference of 10K. The ethanol facility produces ethanol, solid biofuel, molasses, and is able to produce district heating hot water. Considering all products equally valuable, the exergy efficiency of the ethanol facility was found to be 0.790 during integrated operation with zero district heating production, and 0.852 during integrated operation with full district heating production. During separate operation, the exergy efficiency dropped to 0.564 with zero district heating production and 0.583 with full district heating production. The ratio of exergy losses and destruction in the heat integration network to the total exergy destruction and losses in the system was in the range of 0.46-0.87 depending on the system operation. This study suggests that a well-designed heat integration network can increase the exergy efficiency of the integrated system markedly.

Keywords:

Exergy analysis, lignocellulosic ethanol production, polygeneration system, plant operation.

1. Introduction

Lignocellulosic ethanol can be mixed with gasoline in order to reduce the greenhouse gas emissions from the transportation sector while decreasing the oil import dependency in countries without domestic oil reservoirs. At the same time, the production does not couple the food and energy prices in contrast to starch-based ethanol production. Lignocellulosic ethanol is therefore considered a promising second-generation biofuel by the Commission of the European Communities [1].

Due to the energy intensive nature of lignocellulosic ethanol production, production facilities are often assumed integrated in polygeneration systems. Several studies have treated systems with integrated production of power, heat, lignocellulosic ethanol, and synthetic natural gas (SNG) [2-6]. For such systems, Daianova et al. [2] and Ilic et al. [3] both report better energy economy for the integrated system compared to stand-alone systems, while Bösch et al. [4] reports a potential increase in both first law energy efficiency and exergy efficiency when integrating the processes. Modarresi et al. [5] applied pinch analysis to improve the heat integration of the system, which yielded an integrated exergy efficiency of 88% for the ethanol process. Furthermore, Gassner and Maréchal [6] has investigated process integration in the polygeneration system and concludes that both first and second law energy efficiencies for a combined heat and power (CHP) plant are increased significantly by integrating lignocellulosic ethanol and SNG production. Furthermore, a case study by Starfelt et al. [7] reports higher first-law energy efficiency for integrating lignocellulosic ethanol production in an existing CHP plant compared to a scenario with separate

production. These results all explain the industrial interest in retrofitting existing CHP units to obtain the mentioned polygeneration system benefits.

Analogue to the studies mentioned above, a previous case study by the authors [8] investigated the energy economy of a polygeneration system in which the Danish CHP unit Avedøreværket 1 (AVV1) is retrofitted by integrating a lignocellulosic ethanol production facility based on IBUS (Integrated Biomass Utilization System) technology [9-11]. It was found that the exergy flow from the CHP unit to the IBUS facility had a significant negative impact on the system economy, mainly due to the reduced power production capacity of the system. Integration design optimization was limited by stating that steam had to be extracted from existing steam extraction points only. This paper investigates the impact of the non-ideal integration solution, which is not considered in other studies of similar systems but is likely to be applied in real life plant retrofitting.

The objectives of the study are to determine the potential impact of a non-ideal integration solution in a polygeneration system, and to identify critical design challenges faced when retrofitting existing CHP units. To achieve this, the integration design of the polygeneration system previously treated by the authors [8] is addressed. Exergy analysis [12] is applied to determine irreversibilities in the heat integration network and the IBUS facility, and to identify ways of reducing the exergy flow from the CHP unit to the IBUS facility.

In this paper, the polygeneration system model and the exergy analysis approach are described in Section 2. The study results are presented in Section 3 and discussed in Section 4, while a conclusion of the study is given in Section 5.

2. Methodology

2.1. Polygeneration system model

The polygeneration system was modelled previously by the authors [8]. In this section, the basic design of the system and the data necessary to carry out an exergy analysis of the IBUS facility and the integration solution are presented. A more detailed explanation of the system modelling can be found in a previous study by the authors [8].

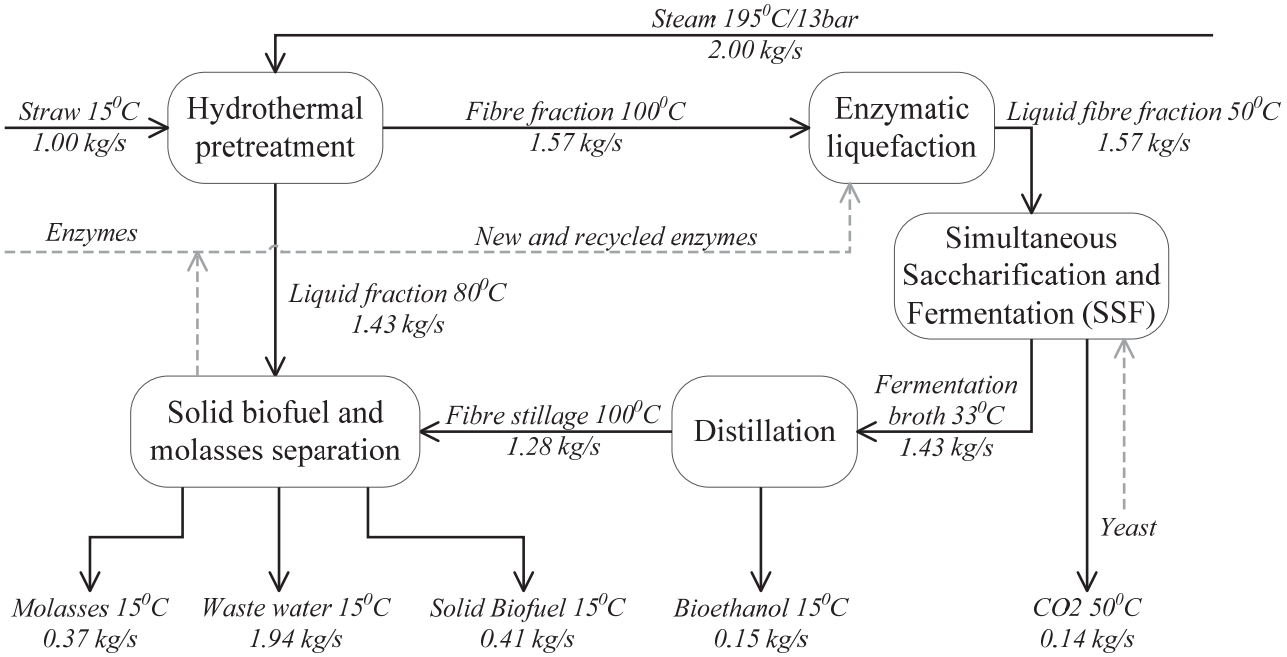

Fig. 1 – Component layout of the modelled IBUS facility. Flow sizes are shown per kg/s straw processed. Pressure levels are only indicated for processes at elevated pressures

The component layout of the modelled IBUS facility is presented in Fig. 1. The flows of yeast and enzymes are insignificant for the overall mass and energy balances of the system and were therefore not included in the model.

In the integrated polygeneration system, steam extracted from the Danish CHP unit AVV1 is used in the hydrothermal pretreatment and for covering the heating demands of the IBUS facility. A simplified component layout of the polygeneration system is presented in Fig. 2.

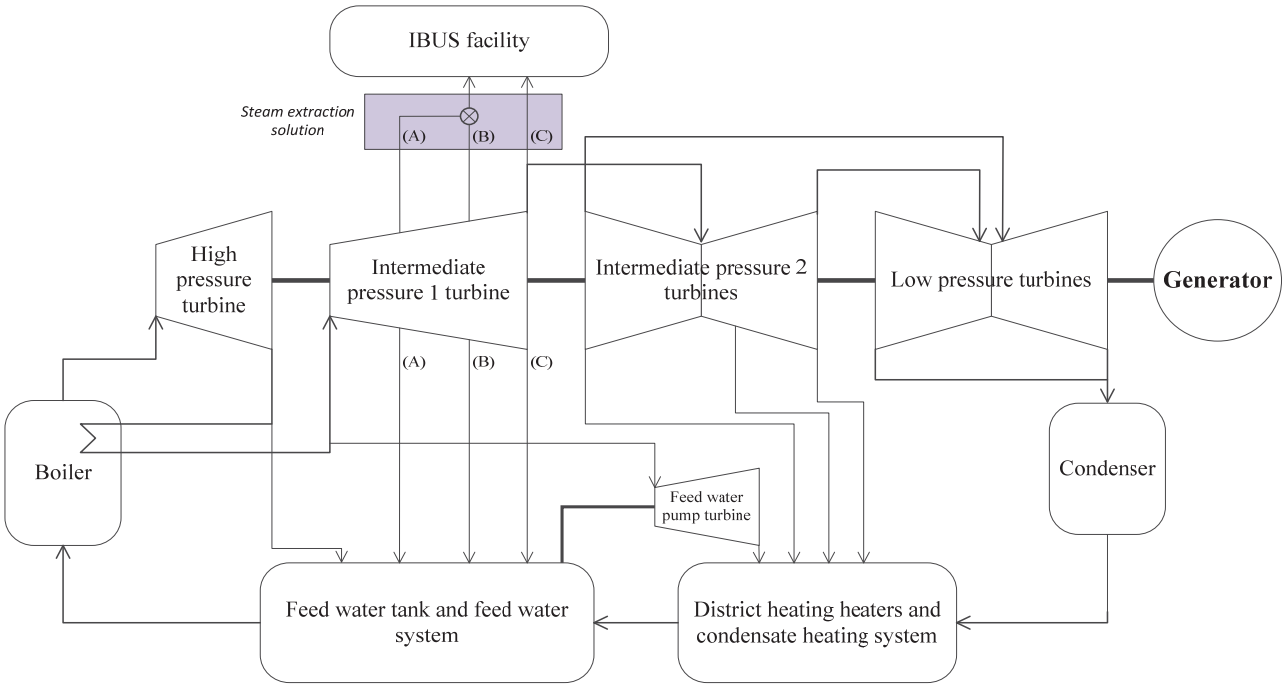

Fig. 2 – Simplified layout of the modelled polygeneration system

A rigid approach was taken for designing the steam extraction solution, stating that steam could only be extracted from already existing steam extraction points in the turbine system of AVV1. Three steam extraction points that meets the requirements for steam temperature and pressure, points (A), (B), and (C), were identified. The thermodynamic states of steam in the three points are summarized in Table 1. The value ranges reflect the load variation of the system.

Table 1 – Thermodynamic state ranges in the steam extraction points in the CHP unit

Point	Temperature range [C]	Saturation temperature range [C]	Pressure range
(A)	431-467	199.8-241.2	15.5-34.2
(B)	359-392	176.7-213.6	9.3-20.5
(C)	257-289	145.4-176.1	4.2-9.2

To minimize exergy destruction in the heat integration network of the IBUS facility, steam was extracted at the lowest possible temperature and pressure which still allowed for the required heat transfer. Pinch analysis was used to calculate the required steam extraction flows that minimized the exergy flow into the IBUS facility. The method is described by Lythcke-Jørgensen et al. [8].

2.2. System operation

The thought behind the polygeneration system is to allow for the IBUS facility to run on excess capacity in the CHP unit boiler. As the IBUS facility has zero production flexibility, a back-up heat source must be used to maintain production when the CHP unit uses its full boiler capacity. This leads to two basic operation modes:

Integrated operation: The heat demand of the IBUS facility is covered by steam extracted from the CHP unit

Separate operation: The heat demand of the IBUS facility is covered by a natural gas boiler

In this study, four types of system operation schemes were investigated

i) Integrated operation with full load condensation mode operation in AVV1 and zero district heating (DH) production in the IBUS facility
ii) Integrated operation with full load back pressure mode operation in AVV1 and full DH production in the IBUS facility
iii) Separate operation with zero DH production in the IBUS facility
iv) Separate operation with full DH production in the IBUS facility

During separate operation, the heat demand in the IBUS facility is covered by steam from a gas boiler with 96% heating efficiency. Chemical properties and specific flow sizes of gas per kg/s straw processed at various operation modes are summarized in Table 2. Further details about the operational patterns of the polygeneration system are given in Lythcke-Jørgensen et al. [8].

Table 2 – Chemical properties of natural gas and specific consumption during separate operation with zero and full IBUS district heating production. Chemical properties for natural gas have been taken from [13].

Fuel	Lower heating value [kJ/kg]	Chemical exergy content [kJ/kg]	Gas flow, zero IBUS DH production [kg/s]	Gas flow, full IBUS DH production [kg/s]
Natural Gas	41,426	43,497	0.270	0.325

2.3. Exergy Analysis Calculations

Exergy analysis was applied to the IBUS facility and the heat integration network to identify irreversibilities, and thereby ways for reducing the exergy flow from the CHP unit to the IBUS facility. The reference point for all exergy calculations was set to $T_0 = 298.15K$ and $p_0 = 1bar$.

The total specific exergy of a material stream, ex, is given by the following expression:

$$ex = ex_{phys} + ex_{kin} + ex_{pot} + ex_{chem}. \quad (1)$$

Here, ex_{phys} is the specific physical exergy, ex_{kin} is the specific kinetic exergy, ex_{pot} is the specific potential exergy, and ex_{chem} is the specific chemical exergy. ex_{kin} and ex_{pot} were not considered in the analysis as they are negligible in magnitude for the given material streams [4].

Exergy flows related to mass flows in the system, $\dot{EX}$, were calculated as the total specific exergy of the material stream ex times the mass flow of the stream, $\dot{m}$:

$$\dot{EX} = ex \cdot \dot{m}. \quad (2)$$

Considering all useful material streams out of a component as valuable, the exergy efficiency η_{EX} of a system component was calculated as the exergy content in product flows, $\sum \dot{EX}_{products}$, divided by the exergy content in inlet flows, $\sum \dot{EX}_{in}$:

$$\eta_{EX} = \frac{\sum \dot{EX}_{products}}{\sum \dot{EX}_{in}}. \quad (3)$$

In this study, the difference between the exergy content in inlet mass flows and in product mass flows was caused partly by exergy destruction within the component, partly by exergy content in unused material flows from the component. For simplicity, these fractions were merged in a term called exergy losses and destruction, $\dot{EX}_{L\&D}$, which is calculated as:

$$\dot{EX}_{L\&D} = \sum \dot{EX}_{in} - \sum \dot{EX}_{products}. \quad (4)$$

As the main product of the IBUS facility is lignocellulosic ethanol and solid fuel for combustion, the exergy efficiency for the fuel production, $\eta_{EX,fuels}$, is evaluated for the whole system as well:

$$\eta_{EX,fuels} = \frac{\dot{EX}_{ethanol} + \dot{EX}_{solid\ fuel}}{\sum \dot{EX}_{in,system}}. \quad (5)$$

2.3.1. Chemical Exergy

The chemical exergy of multi-component material streams, ex_{chem}, was calculated as the sum of the chemical exergy content of the individual components $ex_{chem,i}$ multiplied by their weight fraction x_i:

$$ex_{chem} = \sum_i ex_{chem,i} x_i. \quad (6)$$

The chemical exergy for the material components that occur in the IBUS facility are summarized in Table 3. The values have been taken from a study by Bösch et al. [4].

2.3.2. Physical Exergy

As material flows in the system occur at reference pressure, the mechanical part of the physical exergy is zero. As suggested by Bösch et al. [4], heat capacities of biomass material streams were assumed constant over the relevant temperature ranges present. The physical exergy of multi-component biomass materials was calculated according to the specific heat capacity of the material, Cp, and the temperature of the material, T, using the following equation [12].

$$ex_{phys,biomass} = Cp\left(T - T_0 - \ln\left(\frac{T}{T_0}\right)\right). \quad (7)$$

The heat capacity of multi-component materials were calculated as the sum of the individual components' heat capacities Cp_i multiplied by their weight fraction x_i. Used values are presented in Table 3.

$$Cp = \sum_i Cp_i x_i. \quad (8)$$

Table 3 – Chemical properties of material components in the IBUS facility. Heat capacities for biomass components are assumed constant over the relevant temperature range. Heat capacities for water and ethanol have been taken from the software 'Engineering Equation Solver'[14]. All other values have been taken from ref. [4]

Material component	Cp [kJ/kg-K]	ex_{chem} [kJ/kg]
Cellulose	1.28	18,808
Hemicellulose	1.28	18,808
Lignin	1.29	25,648
Monomers	1.15	16,687
Proteins	1.30	24,488
Ash	0.70	1,006
Glucose	1.15	16,687
Ethanol	2.53	29,532
Water	4.18	51

2.3.3. Exergy in Heat Flows

The exergy content of heat flows in the system are associated with the exergy content in the heat exchange media used. In the IBUS facility, water was assumed used as heat exchange media. Heat is provided in the form of steam from AVV1 or a gas boiler, and cooling is provided by district heating water and sea water at the given location.

To illustrate the best possible heat exchange conditions, the entire span of any heat exchange between heat exchange media and system components have been set to occur at a temperature difference equal to the pinch point temperature difference, which was set to 10K as suggested by Modarresi et al. [5]. The concept is illustrated in Fig. 3.

The reference pressure of the heat exchange media was set to 1bar, but for phase change heat exchange, the pressure has been modified to maintain the 10K temperature difference over the entire phase change of the hot and cold flows. A list of all heat exchange processes in the system, described by the heat flow transferred, $\dot{Q}$, the temperature interval, the necessary mass flow, $\dot{m}$, and pressure, p, of the heat exchange media is given in Table 4. Pumping in the heat integration network was not considered. Further details about heat flows and pinch analysis of the integrated system are given in Lythcke-Jørgensen et al. [8].

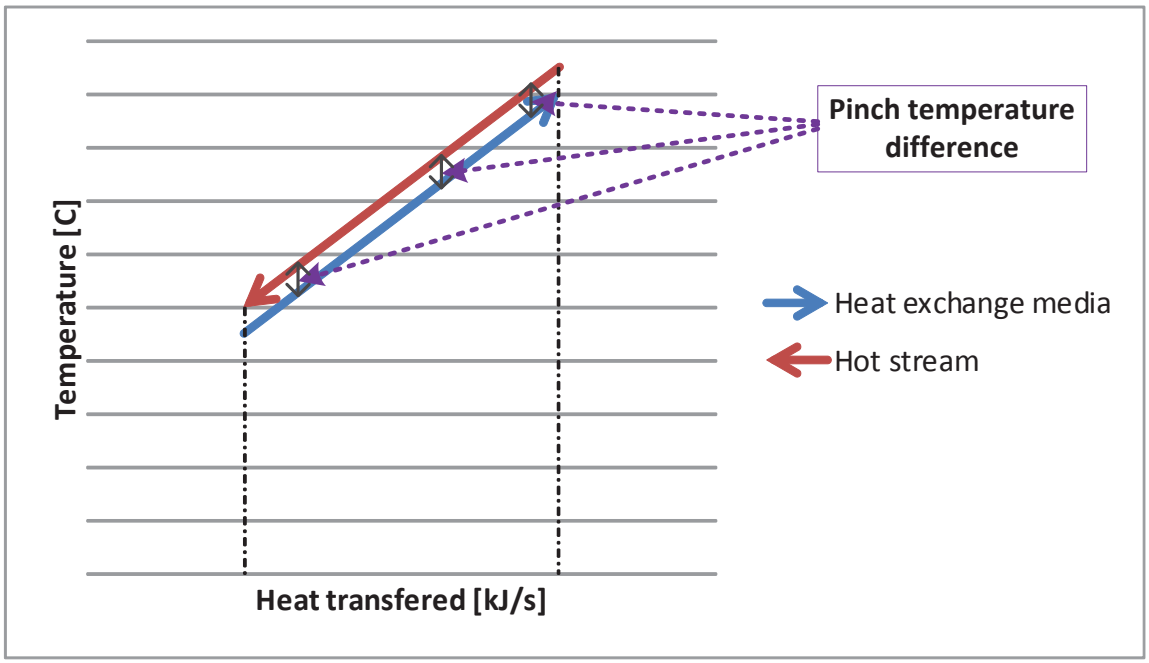

Fig. 3 – Illustration of best-possible heat transfer between a hot stream and heat exchange media in the IBUS facility

Table 4 – Hot and cold heat exchange media streams in the IBUS facility

Component	Type	$\dot{Q}$ [kJ/kg]	T_{in} [C]	T_{out} [C]	p [bar]	$\dot{m}$ [kg]
Pretreatment	Hot	5,466	195	-	13	2.00
	Cold	341	90	180	0,7018	1.91
	Cold	4,287	90	91	0.7018	1.88
	Cold	92	70	90	1	1.09
	Cold	247	40	90	1	1.76
Liquefaction	Cold	60	25	40	1	0.96
Distillation	Hot	1,631	111	110	1.431	0.73
	Hot	21	47	43	1	1.26
	Cold	1,044	68	69	0.286	0.45
	Cold	1	25	90	27	0.10
Separation	Hot	4,368	111	110	1.431	1.96
	Hot	100	110	90	1.431	1.18
	Cold	4,368	90	91	0.7018	1.91
	Cold	807	25	90	1	2.97
District Heating Water*	Cold	13,071	50	100	20	62.4

* District heating water is only produced when necessary in the IBUS facility

3. Results

Using the method described previously, the exergy flows of the integrated system were calculated. A Grassmann diagram of the exergy flows within the IBUS facility is presented in Fig. 4. The diagram shows how the exergy content of the inlet wheat straw passes through the various processes in the facility until it ends up in the final energy products: ethanol, solid fuel and molasses. The exergy flows into the system from heat transfer and power are also illustrated. Exergy losses and destruction (L&D), which cover exergy destruction in components and exergy content of discarded material streams, are illustrated as well. Exergy destruction in the system is in general related to heat transfer over a temperature difference, frictional exergy destruction, and material degradation.

The largest exergy L&D in the IBUS facility processes occurs in the Simultaneous Saccharification and Fermentation (SSF) component where the exothermal fermentation process takes place. Heat released from the fermentation is used to maintain an elevated temperature in the component, explaining the lack of heat flow into the component. L&D in this component are associated with heat losses, product degradation from the fermentation process, and exergy content of the CO2 which is discarded at an elevated temperature.

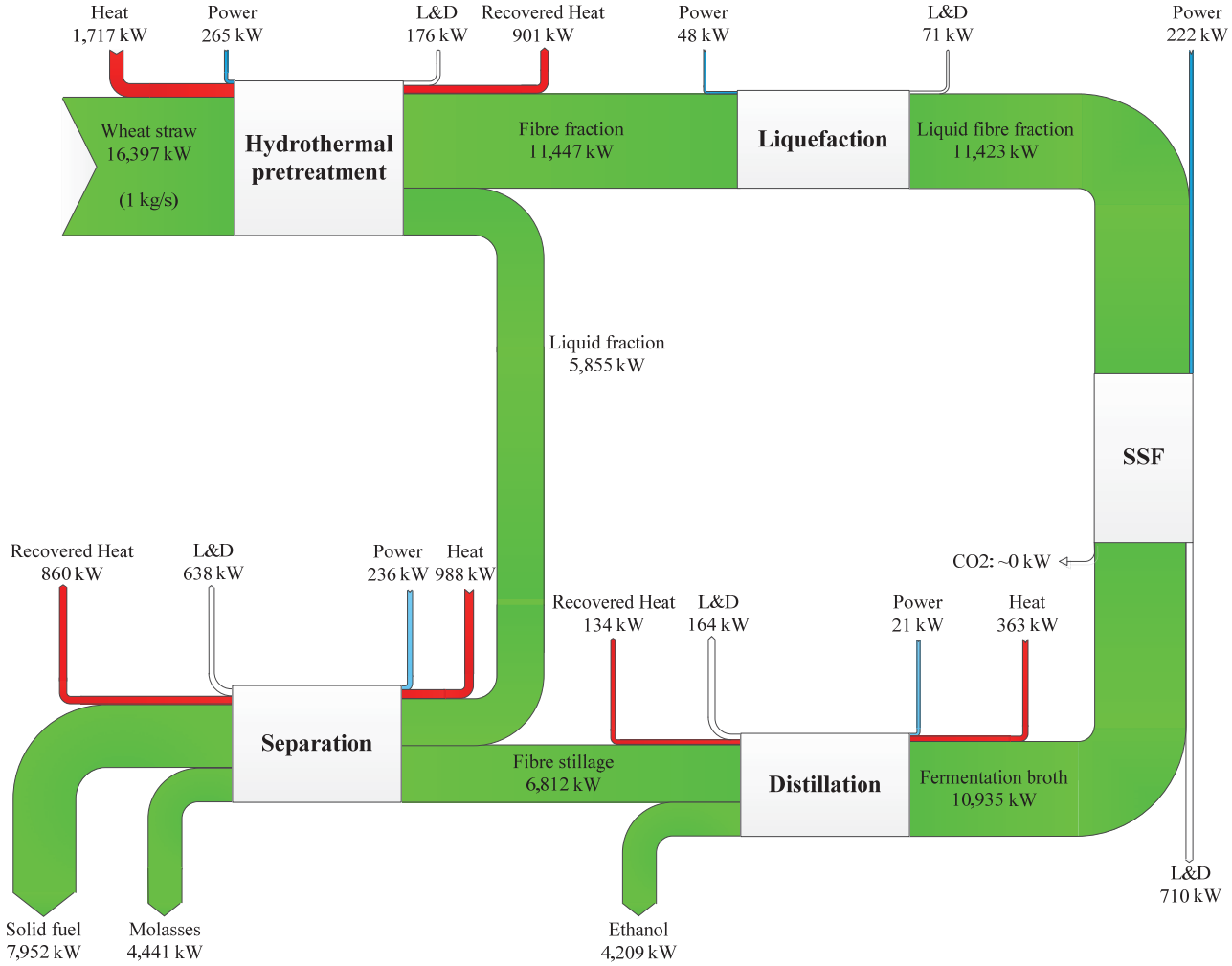

Fig. 4 – Grassmann diagram illustrating the exergy flows inside the IBUS facility per kg/s straw processed. Exergy losses and destruction (L&D) is illustrated as well

In the heat integration network, the heat exchange media is conditioned and distributed to meet the heating and cooling demands of the IBUS facility. Heating is provided by steam from AVV1 or a gas boiler, and recovered heat from the processes in the IBUS facility. Cooling is provided by sea water and by district heating water when district heating production is active in the IBUS facility.

The Grassmann diagrams in Fig. 5 show the exergy flows in the heat integration network during the following operation schemes:

i) Integrated operation, full load condensation mode operation in AVV1, zero IBUS DH production

ii) Integrated operation, full load back pressure mode operation in AVV1, full IBUS DH production

iii) Separate operation, zero IBUS DH production

iv) Separate operation, full IBUS DH production

Exergy L&D in the heat integration network are related to exergy destruction from heat transfer over a temperature difference, and heat losses. Pumping work and frictional losses were not considered.

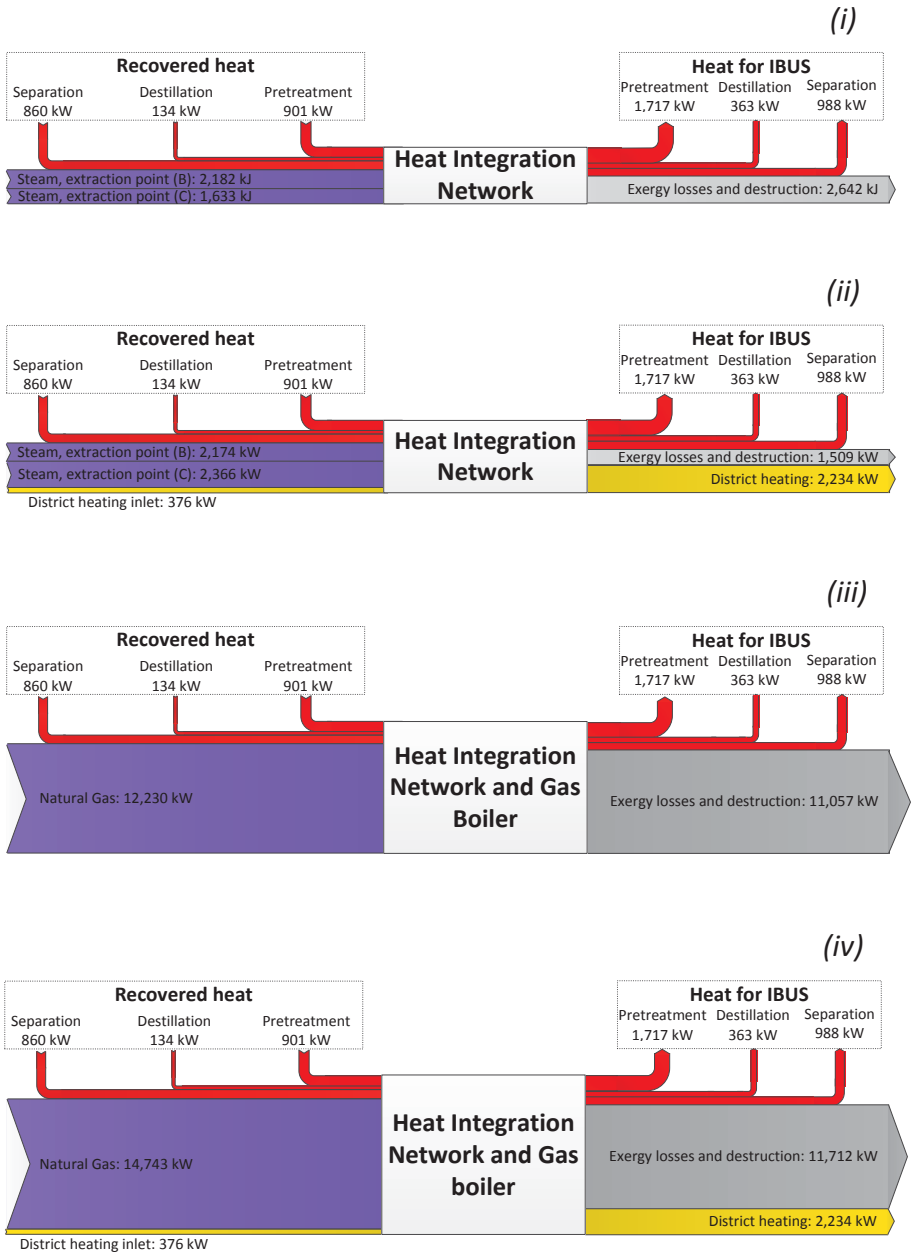

Fig. 5 – Grassmann diagrams of the heat integration network during (i) full load condensation mode operation in AVV1 with zero IBUS DH production, (ii) full load back pressure operation in AVV1 and full IBUS DH production, (iii) separate operation, zero IBUS DH production, and (iv) separate operation, full IBUS DH production. Exergy flows are presented per kg/s straw treated in the IBUS facility

The calculated exergy efficiencies of the IBUS facility components and the heat integration network are presented in Table 5. The IBUS facility alone was found to have an exergy efficiency of 0.913, while the exergy efficiency of the heat integration network was found to be highly dependent on operation mode.

The lignocellulosic ethanol production system was found to have the highest exergy efficiencies during integrated operation. When the CHP unit was operated at full load in condensation mode, an exergy efficiency of 0.790 was obtained, while it was increased to 0.852 during full load back pressure operation in the CHP unit and with DH production in the IBUS facility. The reason for this increase is the fact that DH hot water was considered a product in the analysis. For a similar system with lignocellulosic ethanol production integrated in a CHP unit, Modarresi et al. [5] reported an exergy of 0.793 for the lignocellulosic ethanol system.

Markedly lower exergy efficiencies are obtained for the system during separate operation. Without DH production in the IBUS facility, the system was found to have an exergy efficiency of 0.564, while it was increased to 0.583 when DH production was included. This clearly illustrates the benefits of integrated operation for the system in terms of exergy efficiency.

When looking at the exergy efficiency of the fuel production solely, it is seen that integrated operation yields higher exergy efficiencies as well, while operation with DH production in the IBUS facility gives lower exergy efficiencies than for operation without DH production. The reason is that DH hot water is not included as a valuable product in the fuel production exergy efficiency, but the DH production increases the heating demand of the system slightly.

Table 5 – Exergy destruction and exergy efficiency in the IBUS facility, its processes and the heat integration network

System	Exergy losses and destruction per kg/s of straw processed [kW]	η_{EX} [-]	$\eta_{EX,fuels}$ [-]
IBUS facility			
Hydrothermal pretreatment	*205*	*0.990*	-
Liquefaction	*73*	*0.994*	-
SSF	*710*	*0.939*	-
Distillation	*201*	*0.986*	-
Separation	*570*	*0.954*	-
IBUS facility, total	*1,759*	*0.913*	*0.600*
Heat Integration Network			
Operation mode (i)	*2,642*	*0.550*	-
Operation mode (ii)	*1,509*	*0.725*	-
Operation mode (iii)	*11,057*	*0.217*	-
Operation mode (iv)	*11,712*	*0.312*	-
Integrated System, total			
Operation mode (i)	*4,401*	*0.790*	*0.579*
Operation mode (ii)	*3,268*	*0.852*	*0.560*
Operation mode (iii)	*12,816*	*0.564*	*0.385*
Operation mode (iv)	*13,471*	*0.583*	*0.357*

Depending on the operation mode, 46% to 87% of the exergy L&D in the integrated system occurs in the heat integration network. This leaves room for a significant exergy efficiency increase by optimizing this part of the system. One way would be to extract steam at conditions closer to those

needed in the heat integration network. Another way to optimize the average exergy efficiency of the system over the lifetime is to minimize the duration of separate operation in the polygeneration system. Comparing these results with the outcomes of a thermo-economic analysis of the system [8], it is suggested that a carefully designed heat integration network combined with well-placed steam extraction points can increase the production economy of the treated polygeneration system.

4. Discussion

The outcomes of this study suggest that for the polygeneration system treated, the rigid approach for steam extraction when designing the heat integration network caused the exergy efficiency of the lignocellulosic ethanol production system to decrease significantly. It is therefore suggested that a more flexible approach is taken as extraction of steam at conditions closer to those that are optimal for the heat exchange will increase both the exergy efficiency and production economy of the polygeneration system. The theoretic optimal efficiency might be increased further if the pinch point temperature difference of 10^0C could be lowered. However, the designed heat integration network is optimal in the sense that all heat exchange occurs at a temperature difference equal to the pinch point temperature difference. This would hardly be the case in real life, and it is therefore not reasonable to assume that the exergy losses and destruction in the heat integration network calculated in this study can eliminated completely.

There are several other limitations to the efficiency increase that can be gained through the design of the heat integration network. First of all, it is not certain that steam is available at the ideal conditions for the heat exchange with the IBUS facility. The CHP unit is designed to fit the steam conditions for turbine expansion, meaning that the steam is superheated until it reaches the lower pressure levels. Opposed to this, saturated steam is optimal for heat exchange with the IBUS facility, and they might therefore not be available in the CHP unit.

Secondly, if points exist where the steam conditions are ideal for exchanging heat with the IBUS facility, it is not certain that steam can be extracted therefrom without having to replace system components, which not only poses an economical challenge for the plant owner but might in fact be infeasible as new equipment might not fit with other system components. And even if steam can be extracted from near-optimal points in the CHP unit it is not necessarily economically reasonable to do so. Investment in advanced heat integration network components and upgrading or replacement of several existing components in the CHP unit might not be justified by the increased production economy. Whether this is the case or not requires further investigations, but these points represent main challenges when retrofitting existing CHP units, and it urges a careful approach when making assumptions on benefits from retrofitting.

5. Conclusion

This study treated the integrated production of heat, power and lignocellulosic ethanol in a polygeneration system based on an existing CHP unit. A rigid approach was taken when designing and optimizing the system integration, stating that steam extracted from the CHP unit could only be extracted from already existing steam extraction points. The efficiency of the lignocellulosic ethanol production facility, called the IBUS facility was evaluated using exergy analysis. At optimal heat exchange conditions, the results indicate an exergy efficiency of 0.913 for the IBUS facility. Calculations suggest an exergy efficiency of 0.790 for the integrated system with full load condensation mode operation in the CHP unit and zero DH production in the IBUS facility, and 0.852 with full load back pressure operation in the CHP unit and full DH production in the IBUS facility. During separate operation, the exergy efficiency of the lignocellulosic ethanol production decreases to 0.564 with zero DH production, and 0.583 with full DH production due to the combustion of natural gas for covering the heat demand. When only including ethanol and solid biofuel as products in the exergy analysis, the exergy efficiency of the system is suggested to be in the range 0.357-0.579 depending on operation mode. The results illustrate the benefits of maintaining integrated operation in the treated polygeneration system in terms of exergy efficiency,

but they also point out challenges associated with retrofitting existing CHP units as the heat integration network, which was optimized with respect to already existing steam extraction points in the CHP unit, was responsible for up to 87% of the exergy losses in the integrated lignocellulosic ethanol production.

Acknowledgments

The authors would like to thank Brian Elmegaard for allowing the use of his numerical model of the Danish combined heat and power unit Avedøreværket 1, and for his feedback on the method used for analysing exergy flows in the system.

Nomenclature

Cp	specific heat capacity, kJ/(kg K)
$\dot{EX}$	exergy flow, kW
ex	specific exergy content, kJ/kg
ex_{chem}	specific chemical exergy content, kJ/kg
ex_{kin}	specific kinetic exergy content, kJ/kg
ex_{phys}	specific physical exergy content, kJ/kg
ex_{pot}	specific potential exergy content, kJ/kg
$\dot{m}$	mass flow, kg/s
p	pressure, bar
$\dot{Q}$	heat flow, kJ/s
T	temperature, K
x	mass fraction, -

Abbreviations

AVV1	Avedøreværket 1
CHP	Combined Heat and Power
DH	District Heating
L&D	(exergy) Losses and Destruction
SNG	Synthetic Natural Gas
SSF	Simultaneous Saccharification and Fermentation

References

[1] Commission of the European Communities, Communication from the Commission – An EU Strategy for Biofuels, 2006. Available at: <http://eur-lex.europa.eu/LexUriServ/LexUriServ.do?uri=CELEX:52006DC0034:EN:NOT> [accessed 26/02/2013]

[2] Daianova L., Dotzauer E., Thorin E., Yan J., Evaluation of a regional bioenergy system with local production of biofuel for transportation, integrated with a CHP plant. Applied Energy 2011;92:739-749.

[3] Ilic D., Dotzauer E., Trygg L., District heating and ethanol production through polygeneration in Stockholm. Applied Energy 2011;91:214-221.

[4] Bösch P., Modarresi A., Friedl A., Comparison of combined ethanol and biogas polygeneration facilities using exergy analysis. Applied Thermal Engineering 2012;37:19-29.

[5] Modarresi A., Kravanja P., Friedl A., Pinch and exergy analysis of lignocellulosic ethanol, biomethane, heat and power production from straw. Applied Thermal Engineering 2012;43:20-28.

[6] Gassner M., Maréchal F., Increasing Conversion Efficiency in Fuel Ethanol Production from Lignocellulosic Biomass by Polygeneration – and a Paradoxon between Energy and Exergy in Process Integration. In: ECOS 2010: Proceedings of the 23rd International Conference on Efficiency, Cost, Optimization, Simulation, and Environmental Impact of Energy Systems; 2010 Jun 14-17; Lausanne, Switzerland.

[7] Starfelt F., Thorin E., Dotzauer E., Performance evaluation of adding ethanol production into an existing combined heat and power plant. Bioresource Technology 2009;101:613-618.

[8] Lythcke-Jørgensen C., Haglind F., Clausen L. R., Thermodynamic and economic analysis of integrating lignocellulosic bioethanol production in a Danish combined heat and power unit. In: EU BC&E 2013: Proceedings of the 21st European Biomass Conference and Exhibition; 2013 Jun 3-7; Copenhagen, Denmark.

[9] Scott-Bentsen, N., Felby C., Ipsen K. H., Energy balance of 2nd generation bioethanol production in Denmark. Elsam A/S 2006.

[10] Larsen J., Petersen M. Ø., Thirup L., Li H. W., Iversen F. K., The IBUS process – lignocellulosic bioethanol close to a commercial reality. Chemical Engineering Technology 2008;31:765-772

[11] Larsen J., Petersen M. Ø., Thirup L., Inbicon makes lignocellulosic ethanol a commercial reality. Biomass and Bioenergy 2012;46:36-45.

[12] Bejan A., Tsatsaronis G., Moran M., Thermal Design & Optimization. New York: John Wiley & Sons, Inc.; 1996.

[13] Rian A. B., Ertesvåg I. S., Exergy evaluation of the arctic Snøhvit liquefied natural gas processing plant in northern Norway – significance of ambient temperature. Energy&Fuels 2012;26:1259-1267.

[14] F-Chart Software. Engineering Equation Solver. Available at: <http://www.fchart.com/ees/> [accessed 24/02/2013]

APPENDIX I Conference paper 3

Proceedings paper – peer reviewed manuscript

C.E. Lythcke-Jørgensen, M. Münster, A.V. Ensinas, and F. Haglind. *Design optimization of flexible biomass-processing polygeneration plants using characteristic operation periods*. World Renewable Energy Congress XIII. London, UK, 2014.

This paper presents a preliminary version of the design methodology developed in this project. It also features parts of the modelling conducted for *Case II*.

Design optimization of flexible biomass-processing polygeneration plants using characteristic operation periods

Christoffer Lythcke-Jørgensen[1*], Marie Münster[2], Adriano V. Ensinas[3], Fredrik Haglind[4]
1-Department of Mechanical Engineering, Technical University of Denmark, DK-2800 Kgs. Lyngby, Email:* celjo@mek.dtu.dk
2-Department of Management Engineering, Technical University of Denmark, DK-4000 Roskilde. Email: maem@dtu.dk
3-Industrial Process and Energy System Engineering (IPESE), École Polytechnique Fédérale de Lausanne, CH-1015 Lausanne. Email: adriano.ensinas@epfl.ch
4-Department of Mechanical Engineering, Technical University of Denmark, DK-2800 Kgs. Lyngby, Email: frh@mek.dtu.dk

Abstract:

This paper presents a method for including expected operating conditions in the design optimization of flexible biomass-processing polygeneration plants through the definition of characteristic operation periods. The method is verified in a superstructure-based, multi-objective design optimization scheme applied on a conceptual polygeneration plant that considers the integrated production of power, heat, ethanol, and biomethane. The design is optimized with respect to net present value and total CO_2 emission impact.
The results suggest that the best solution with respect to net present value is the production of heat and power using a gas turbine and a natural gas boiler, while the best solution with respect to CO_2 emission savings includes full-scale ethanol and biomethane production, as well as a straw boiler for utility heat production. Solving the same design optimization problem using yearly average operation conditions instead of the characteristic operation periods approach, one of the two efficient solutions obtained was found to be suboptimal when evaluated against the actual operating conditions. Furthermore, the predicted objective function values for the optimal designs were found to differ significantly from what was obtained in the evaluation against actual conditions. These results underline the importance of considering expected operation and operating conditions when designing flexible polygeneration plants.

Keywords: Biomass conversion, design optimization, polygeneration plant, renewable energy systems

1. Introduction

Out-phasing fossil fuels and replacing them with renewable energy sources pose several challenges for the energy system. Large-scale integration of energy production from intermittent renewable energy sources (IRES) such as solar, wind, tidal and wave requires balancing operation, especially on the power and heat markets [1]. The renewable energy source most likely to be used for balancing operation, biomass, is however limited on a global level [2] and competition between food and energy production poses a sustainability challenge [3], necessitating efficient use of sustainably available biomass [4]. Flexible biomass-processing polygeneration plants (PGPs), which are multi-input multi-output facilities producing power, heat, and various biomass products, may potentially provide the required balancing operation [5] together with efficient conversion of biomass, achieved through process integration [6].
The design of flexible biomass-processing PGPs is complex and the issues to be considered comprise synthesis of processes from many technological alternatives, plant design with respect to process dimensioning and integration, predicting optimal operation with respect to both short-term hourly demand fluctuations and long-term energy system development, determination of biomass availability, and consideration of both economic and environmental objectives. Polygeneration plant design optimization has been treated intensively in the literature, but to the author's best knowledge the general trend has been to neglect or simplify the impact of expected operation in the design phase. Several works on polygeneration plant design optimization assume static operating conditions in the design optimization (e.g. Ahmadi et al. [7], Gassner and Maréchal [8], and Chen et al. [9]). Other studies consider static operating conditions over several years in the design optimization (e.g. Gerogiorgos et al. [10], and Liu et al. [11] [12]). Some works consider monthly flexible operating conditions for a single energy product, but static conditions for all other (e.g. Fazlollahi et al. [13] [14]). Another approach has been to consider monthly flexible operating conditions

in a first step of the design optimization and then analyse the detailed hour-wise operation in a sequential step (e.g. Rubio-Maya et al. [15] and Uche et al. [16]). Chen et al. [5] [17] did consider flexible operating conditions with respect to peak and off-peak periods over the year in their design optimization of PGPs, but only with respect to cost parameters. In general, the use of average operating conditions may be acceptable for static facilities, but when flexible facilities are considered the result may be inaccurate predictions of objective function values, and even sub-optimal facility designs, because the impact of flexible operation is disregarded.
Ideally, energy system analysis [18] should be applied in the design optimization in order to evaluate affected energy production [19]. This, however, can be a very time-consuming process. The present study presents a simple approach to including flexible operating conditions in the design optimization of flexible PGPs through the definition of characteristic operation periods (CHOPs) with respect to economic and environmental parameters. The CHOPs are used as input data to a superstructure-based, multi-objective design optimization scheme using a genetic algorithm. The CHOP approach is tested on a conceptual Danish PGP, with periods being defined based on historical energy system data. Results of the design optimization scheme applying CHOPs are then compared to those obtained with average operating condition values.
In this paper, an introduction is given in Section 1, while Section 2 includes descriptions of the design optimization scheme and the case study used for scheme verification. Section 3 presents the outcomes of the work, which are discussed in Section 4. Section 5 gives a short conclusion on the findings.

2. Methodology

Design optimization scheme

The design optimization scheme features superstructure-based, multi-objective optimization using a genetic algorithm. The scheme uses the Matlab-based software Osmose, developed by the IPESE group at EPFL [20], and it considers the optimization of the process synthesis, process dimensioning, heat integration, and facility operation. The overall optimization sequence is presented in Figure 1.

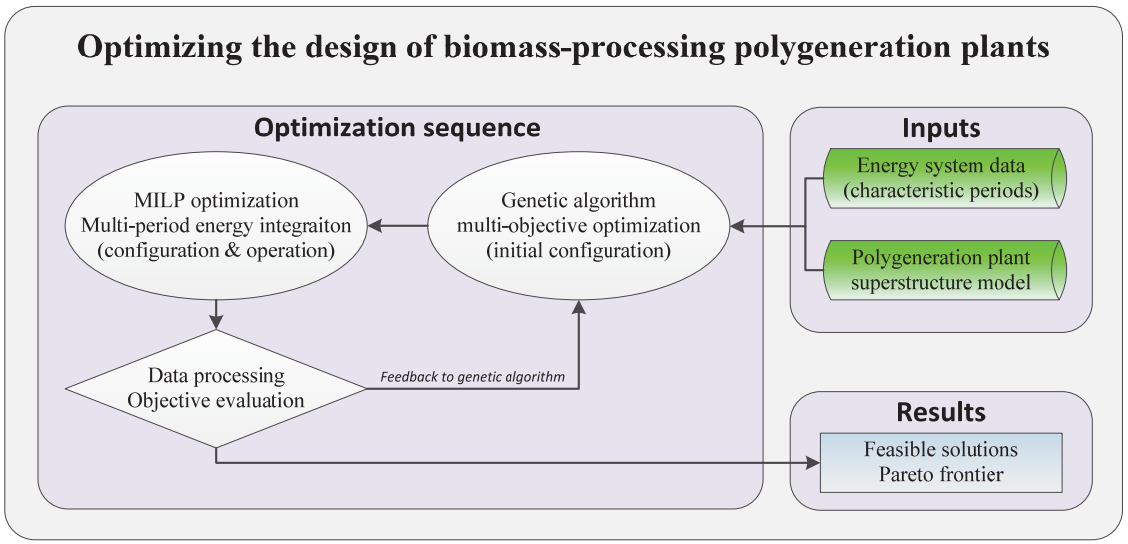

Figure 1: Overall sequence of the presented PGP design optimization approach

Data inputs provided are a superstructure model containing all considered technologies j and associated data plus a number i of CHOPs based on energy system data, either historical or from models [18].
The data inputs are sent to a genetic algorithm, which defines an initial population of PGP configurations by defining the technology dimensions σ_j. Energy integration optimization with respect to best operation economy is then carried out for the configurations in each characteristic period i by varying process loads $\lambda_{j,i}$ for the flexible processes. Based on the operation optimization results, indication values $f(\sigma_j, \lambda_{j,i})$ are calculated for each solution. These values are then given as feedback to the genetic algorithm, and are further stored in a database. Based on the feedback, the genetic algorithm generates a new population of supposedly more efficient PGP configurations, and the loop starts over again.
Based on numerous population evaluations, a Pareto frontier is obtained for the solution space with respect to the objective functions. Post-computation is applied in order to analyse the so-called efficient solutions

located on the Pareto frontier. In this way, the efficient design solutions to the design optimization problem are obtained.

Case study: Retrofitting of a Danish combined cycle power plant

The case study in the present work considers the retrofitting of the back-pressure combined cycle power plant (CCPP) *Silkeborg Kraftvarmeværk* [21], which produces power and district heating (DH) for the Danish city Silkeborg with approximately 90,000 inhabitants. Retrofitting options considered include integration of lignocellulosic ethanol production using straw as biomass feedstock, and anaerobic-based production of upgraded biomethane based on C5-residues from the ethanol production and animal manure [22]. A biomass boiler, a natural gas boiler, and ground-based DH heat pumps are considered for the production of utility heat. The gas turbine and steam Rankine cycle already exist. The C5-residues can alternatively be sold as animal feed [23], while the solid biofuel can be combusted in the biomass boiler or sold as a replacement for coal to thermal power stations. The PGP superstructure is shown in Figure 2.

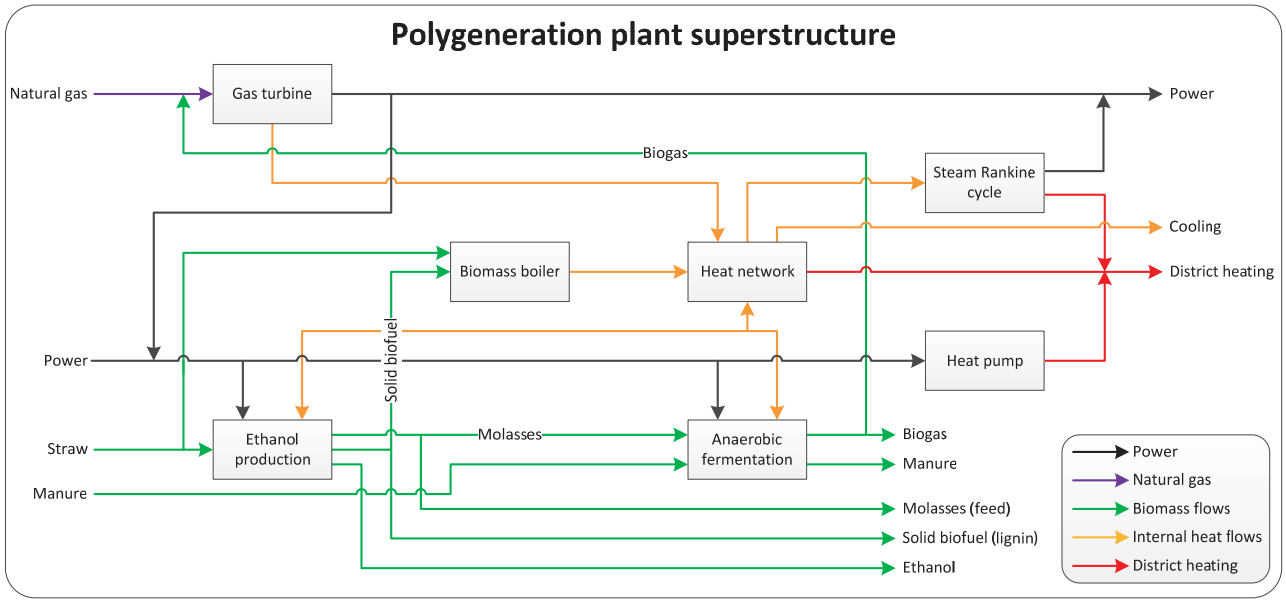

Figure 2: Polygeneration plant superstructure

Silkeborg Kraftvarmeværk has a total power capacity of 108.3 MW [24], for which the corresponding gas turbine power capacity is 85 MW [25], the DH production capacity is 82 MW [24], and the first law energy efficiency is $\eta_I = 0.88$ [25]. Based on these values, the nominal gas consumption of the CCPP is calculated to be 216.25 MW. The turbine off-gas has a temperature of 465°C and is cooled to 68°C [24]. Temperature levels are assumed to be load-independent. Assuming adiabatic Rankine cycle operation, the nominal off-gases heat flow is to calculated to be 105.3 MJ/s. For simplicity, gas consumption, gas turbine power production, and off-gasses heat flow capacity are assumed directly proportional to the gas turbine load λ_{GT}.

The lignocellulosic ethanol production considered in the superstructure uses the hydrothermal pretreatment technology IBUS[1] [26]. A model of an IBUS facility developed and validated by Lythcke-Jørgensen et al. [27] is used as a black box model in this work, with the modification that thermal separation stages have been replaced by mechanical separation stages. Models of a thermophilic anaerobic digestion reactor operating at 55°C and a biogas upgrading facility presented by Evald et al. [28] have been combined into a single black-box model in the study. The COP of the DH heat pump has been set to 2.8 as suggested by the Danish Energy Agency [29] for a 10 MJ/s ground-based heat pump delivering heat at 90°C using CO_2 as working media. The efficiency of the boilers is set to 0.97 as suggested by the same source [29]. The heat integration network is designed directly by the Osmose software [20]. Data on operation and maintenance (O&M) costs and investment costs for reference sized equipment are presented in Table 1. For simplicity, the relation between investment and equipment capacity are assumed to be linear, when, in reality, power laws may be prevailing [30]. Commodity costs and assumed CO_2 emissions are shown in Table 2.

The CCPP considered for retrofitting is located in the West Denmark electricity block. Hour-wise power market data from 2013 [31] were applied as energy system data. For simplicity, energy system development

[1] IBUS (Integrated Biomass Utilization System) is a patented lignocellulosic biomass pretreatment technology. The patent is owned by the Danish company Inbicon A/S, a subsidiary to DONG Energy.

is not considered, hence the operation pattern of 2013 is assumed to last over the technical lifetime of the plant, set to 30 years. Hour-wise heat demand data are taken from the energy system model STREAM [32].

Table 1: Investment and operation and maintenance (O&M) costs as functions of primary energy product yield.

Process	Specific Investment cost	Specific O&M cost[a]	Yield, reference plant
Ethanol production [28]	256.0 M€	35.9 M€/year	45.6 MJ/s ethanol
Biomethane production [29]	19.6 M€	3.11 M€/year	5.25 MJ/s methane
DH heat pump [29]	6.8 M€	55,000 €/year	10.0 MJ/s heat
Gas turbine, Rankine cycle [29][b]	-	2.5 €/MWh	85.0 MW power
Natural gas boiler [29]	1.0 M€	37,000 €/year	10.0 MJ/s heat
Straw boiler [29]	9.6 M€	172,800 €/year	12.0 MJ/s heat
Heat network	Calculated directly in Osmose based on pinch technology [20]		

[a] Not including fuel costs.
[b] As the gas turbine is already installed on site, no investment costs are considered for this component.

Table 2: Energy utilities and products prices

Energy utilities and products	Prices, *c* [Euro/GJ]	CO_2 standard emission factor, EF_i [kg/GJ] produced, EF_p / avoided, EF_a
Straw	5.81 [33]	0.0 / 0.0 [34]
Natural gas	7.67 [33]	56.1 / 56.1 [34]
Biomethane	7.67 [33]	0.0 / -56.1[b] [34]
Straw-based ethanol	12.68 [35]	0.0 / -69.2[c] [34]
Solid biofuel	9.86 [33]	0.0 / -101.1[d] [34]
C5 residues	5.38 [23]	0.0 / 0.0 [34]
Manure	0.00[e]	- [e]

[b] Sold biomethane is assumed to replace natural gas in the gas grid.
[c] Sold straw-based ethanol is assumed to replace gasoline for transportation purposes.
[d] Sold solid biofuel is assumed to replace coal for centralized power plants.
[e] Manure is assumed delivered for free by local farmers in exchange for free, digested fertilizer. Emission impacts are not considered, although anaerobic digestion of manure may reduce greenhouse gas emissions as compared to conventional use of fertilizer manure.

The energy system data are sorted into CHOPs based on three key parameters: Power price c_p, relative DH load λ_{DH}, and marginal CO_2 emissions from power production[2], $\alpha_{CO_2,p}$. The CHOP approach assumes an infinite market, indicating that the facility actions do not affect market characteristics. Three special CHOPs with non-trivial operating conditions are considered: '*IRES power*', in which additional power production is assumed to replace IRES-based power; '*High power price*', in which power prices exceed 65 €/MWh; and '*low power price*', in which power prices are negative. If an hour falls within both '*IRES power*' and one of the other special CHOPs, it is counted within '*IRES power*'. Hours not falling within the special groups are clustered based on three even ranges of c_p and five even ranges of λ_{DH}. CHOP characteristics are presented in Table 3. Elaboration on the approach used for defining the CHOPs is given in Appendix A.

Table 3: Duration, parameter ranges, and average parameter values for the CHOPs

Period Name	$\boldsymbol{Duration}$ $[\boldsymbol{h}]$	$\boldsymbol{c_{p,range}}$ $[€/\mathbf{MWh}]$	$\boldsymbol{\lambda_{DH,range}}$ $[-]$	$\boldsymbol{c_{p,average}}$ $[€/\mathbf{MWh}]$	$\boldsymbol{\lambda_{DH,average}}$ $[-]$	$\boldsymbol{\alpha_{CO_2,p}}$ $[\boldsymbol{kg/MWh}]$
'IRES power'	51	$c_p \in \mathbb{R}$	$\lambda_{DH} \in [0.0,\ 1.0]$	11.00	0.36	0
'High power price'	198	$c_p > 65.00$	$\lambda_{DH} \in [0.0,\ 1.0]$	120.34	0.71	700
'Low power price	31	$c_p < 0.00$	$\lambda_{DH} \in [0.0,\ 1.0]$	-12.49	0.69	603
P11	69	$c_p \in [0.00\ ,\ 21.67[$	$\lambda_{DH} \in [0.0,\ 0.2[$	16.80	0.15	596
P12	81	$c_p \in [0.00\ ,\ 21.67[$	$\lambda_{DH} \in [0.2,\ 0.4[$	13.30	0.29	626
P13	91	$c_p \in [0.00\ ,\ 21.67[$	$\lambda_{DH} \in [0.4,\ 0.6[$	11.44	0.53	647
P14	187	$c_p \in [0.00\ ,\ 21.67[$	$\lambda_{DH} \in [0.6,\ 0.8[$	12.37	0.71	648
P15	52	$c_p \in [0.00\ ,\ 21.67[$	$\lambda_{DH} \in [0.8,\ 1.0]$	13.11	0.86	700
P21	1228	$c_p \in [21.67,\ 43.33[$	$\lambda_{DH} \in [0.0,\ 0.2[$	32.84	0.15	694
P22	1266	$c_p \in [21.67,\ 43.33[$	$\lambda_{DH} \in [0.2,\ 0.4[$	34.66	0.28	693
P23	784	$c_p \in [21.67,\ 43.33[$	$\lambda_{DH} \in [0.4,\ 0.6[$	35.16	0.51	697
P24	1346	$c_p \in [21.67,\ 43.33[$	$\lambda_{DH} \in [0.6,\ 0.8[$	35.48	0.72	699
P25	1427	$c_p \in [21.67,\ 43.33[$	$\lambda_{DH} \in [0.8,\ 1.0]$	36.85	0.88	700

[2] Power produced at the CCPP is expected to replace central power plant production ($\alpha_{CO_2} = 700 kg/MWh$ [36]); if production from centralized power plants is lower than 20% of the nominal capacity, it is assumed that power produced will replace power imports from Germany ($\alpha_{CO_2} = 500 kg/MWh$ [36]); and if the power import from Germany is lower than the production of the plant, any power produced is assumed to replace power production from wind turbines or import of hydro- or nuclear-based power from Sweden or Norway ($\alpha_{CO_2} = 0 kg/MWh$ [36]).

P31	127	$c_p \in [43.33\ ,\ 65.00]$	$\lambda_{DH} \in [0.0\ ,\ 0.2[$	52.01	0.17	700
P32	268	$c_p \in [43.33\ ,\ 65.00]$	$\lambda_{DH} \in [0.2\ ,\ 0.4[$	51.92	0.30	700
P33	422	$c_p \in [43.33\ ,\ 65.00]$	$\lambda_{DH} \in [0.4\ ,\ 0.6[$	50.88	0.51	700
P34	536	$c_p \in [43.33\ ,\ 65.00]$	$\lambda_{DH} \in [0.6\ ,\ 0.8[$	50.65	0.71	700
P35	596	$c_p \in [43.33\ ,\ 65.00]$	$\lambda_{DH} \in [0.8\ ,\ 1.0]$	50.32	0.90	700

In the design optimization, the PGP is constrained by having to meet the DH demand for each characteristic period and being able to meet a DH demand equal to $\lambda_{DH} = 1$, 82 MJ/s [24], without gas turbine operation. The ethanol facility dimension can only be within a reference capacity range of $\sigma_{eth,ref} \in [11.4\ ,45.6]\ MJ/s$, while the biomethane production is limited by the available C5-residue from the ethanol facility. The objective functions applied are the net present value (NPV), C_0, and total CO_2 emission savings, A_{CO_2}, of the facility.

$$C_0 = -\sum I_0 + \sum_t \frac{R_t}{(i+1)^t}$$

$$A_{CO_2,p} = \sum_t \sum_l \left(M_{cons,l,t} \cdot EF_{p,l} + M_{sold,l,t} \cdot EF_{a,l}\right)$$

In the equations, $\sum I_0$ represents total investment, R_t is the net cash flow (annual incomes minus annual operation expenses), t is cash flow year, i is the discount rate, $M_{cons,l,t}$ and $M_{sold,l,t}$ are the consumption and production of energy utility l in year t, and $EF_{p,l}$ and $EF_{a,l}$ are the CO_2 standard emission factors for utility l consumed and sold. The discount rate is set to 8%. Incomes from DH sales are not considered, as heat prices in Denmark so far are constant over the year. Results in terms of NPV can therefore be used to determine the heat price required to make an investment in a given plant worthwhile.
To evaluate CHOPs approach, the results obtained are compared with the outcomes of solving the same design optimization problem using yearly average values for the key parameters instead ($c_p = 39.0\ €/MWh$, $\lambda_{DH} = 0.55$, $\alpha_{CO_2} = 691 kg/MWh$), and then optimizing the operation over the CHOPs in a sequential step.

3. Results

A range of feasible solutions have been obtained for solving the design optimization problem. The solutions are plotted in Figure 3, where they are clustered with respect to delivered energy products. The six points ‘A’, ‘Am’, ‘B’, ‘C’, ‘Cm’, and ‘Ref’, and the two hollow points ‘Am, predicted’ and ‘Cm, predicted’, are highlighted. ‘Ref’ shows the reference solution with only gas turbine and gas boiler installed; ‘A’ shows the optimal solution with respect to NPV that includes biomass processing; ‘Am’ is the corresponding optimal design solution found using the average values approach and evaluated against the actual operating conditions; ‘B’ is the solution with the lowest CO_2 evasion cost; ‘C’ shows the optimal solution with respect to total CO_2 emission savings; and ‘Cm’ shows the corresponding optimal design found using the average values approach and evaluated against the actual operating conditions. The two hollow points ‘Am, predicted’ and ‘Cm, predicted’ illustrate the predicted objective function values for the designs ‘Am’ and ‘Cm’ using the average values approach. The design characteristics of the highlighted solutions are described in Table 4.

Table 4: Description of highlighted designs. In parenthesis the values predicted using the average values approach.

Solution Tag	NPV [M€]	A_{CO_2} [Mton]	σ_{eth} [MJ/s]	$\sigma_{biometh}$ [MJ/s]	σ_{HP} [MJ/s]	$\sigma_{BM\ boiler}$ [MJ/s]	$\sigma_{gas\ boiler}$ [MJ/s]
Ref	-108.3	1.22	0.0	0.0	0.0	0.0	82.0
A	-226.3	-1.0	11.4	0.0	0.2	0.0	82.9
B	-666.9	-10.2	45.6	0.0	0.0	85.6	0.0
C	-917.3	-11.1	45.6	20.4	0.0	88.5	0.0
Am *(Am predicted value)*	-226.3 *(-240.5)*	-1.0 *(-4.1)*	11.4	0.0	0.2	0.0	82.7
Cm *(Cm predicted value)*	-889.8 *(-908.2)*	-7.8 *(-13.4)*	45.6	20.4	0.0	0.0	88.5

The solutions plotted illustrate the relation and trade-off between the two objectives in addition to the Pareto frontier between the two objectives in the solution space. The results in terms of NPV and total CO_2 emission impact can be used by policymakers to determine the DH price, biomass product subsidy scheme, and CO_2 emission subsidy schemes required to reach a non-negative NPV for any of the designs.
The five highlighted points ‘A’, ‘B’, ‘C’, ‘Ref’ and ’Am’ are found to be efficient solutions to the design optimization problem as they appear on the Pareto frontier. The solution ‘Ref’ is the best solution with respect to NPV. If biomass processing is to be installed, the best solution with respect to NPV, ‘A’, includes installation of the smallest feasible ethanol facility and zero biomethane production. The best solution with respect to total CO_2 emission savings, ‘C’, includes installation of the largest feasible ethanol facility with

biomethane production as well as a straw boiler for providing utility heat. The solution with the lowest CO_2 evasion cost, 'B', is obtained by installing the largest feasible ethanol facility without biomethane production, and applying a straw boiler for utility heat.

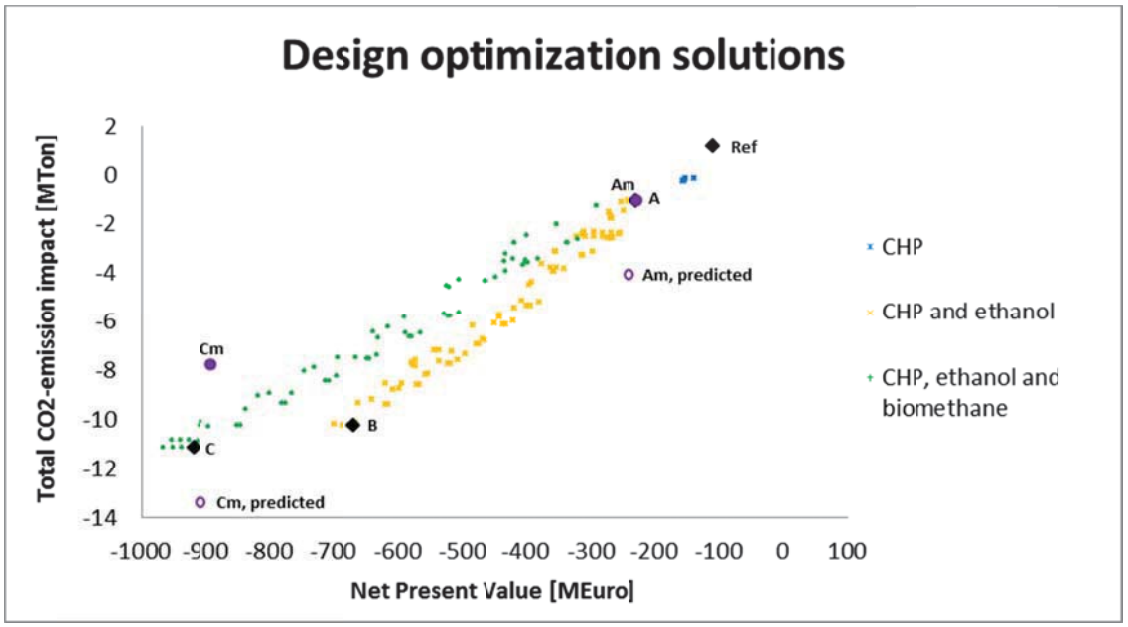

Figure 3: Solutions to the design optimization problem plotted with respect to objective function values.

Comparing the CHOP approach and the average values approach, it was found that the designs 'A' and 'Am' practically are identical, and their points are therefore coinciding in Figure 3. In contrast, the point 'Cm' is found to be located off the Pareto frontier, indicating that the optimal design with respect to total CO_2 emission savings found by the average values approach is suboptimal when evaluated against more detailed energy system data. This indicates that the average values approach is inadequate for solving the present design optimization problem. When evaluating the optimal designs from the average values approach against the operating conditions, the predicted values of the objective functions underestimated the NPV with 6% for 'Am' and 2% for 'Cm', and overestimated the total CO_2 emission savings with 288% for 'Am' and 72% for 'Cm'. These deviations were caused by the fact that the average values approach neglects operation condition variations and the DH production constraint, causing the predicted values to be unrealistic.

4. Discussion

The results of the present study show that operation conditions should be taken into account when optimizing and evaluating the design of flexible PGPs. It is demonstrated how the use of average energy system parameter values in the design optimization may lead to suboptimal design solutions, and how predicted objective values may deviate significantly when evaluated against actual operating conditions.

In the present study, energy system CHOPs were defined with respect to three parameters: Power price, heat demand, and power production marginal CO_2 emission, with the latter being based on simplified assumptions. Whether or not these parameters are the most important of the operating conditions, and how many ranges they should be divided into, may depend on both the energy utilities produced by the PGP and the surrounding energy system. The choice of relevant CHOP parameters should be investigated for each individual energy system. It is also relevant to evaluate whether or not the marginal power producer estimation and the infinite market assumptions are realistic. Furthermore, the assumption on emission factors from various energy utilities is highly simplified; for instance, ethanol produced is assumed to replace gasoline, but it might as well replace other ethanol production due to legislation and market competition. The next step will be to conduct a sensitivity analysis on the mentioned assumptions to see how assumption uncertainties may affect the final results.

CHOP durations were based on historical data for the year of 2013, which was considered acceptable for the present study as the main purpose was to investigate the relevance of the CHOP approach compared to the average values approach. However, the development of the energy system should be included when optimizing plant designs in order that the changing operation environment may be taken into account.

The main arguments for using the CHOP approach in the design optimization of PGPs are the potentially more accurate design solutions as compared with the average values approach, and the reduced calculation times as compared to conducting a complete integration with energy system analysis tools. However, the level of details is directly linked to the number of CHOPs defined, which again is linked to the overall calculation time. It would be relevant to carry out an investigation of payoffs between accuracy and increased calculation time as a function of the number of CHOPs defined. Furthermore, it should be noted that the CHOP approach does not allow the consideration of dynamics, ramp rate limitations, and operation planning in facilities as time chronology is not included. Inaccuracies arising from these limitations should be subjected to investigation.

5. Conclusion

This paper presented a method for including expected operating conditions in the design optimization of flexible biomass-processing polygeneration plants (PGPs) through the definition of characteristic operation periods (CHOPs). The method was applied and tested in a superstructure-based, multi-objective design optimization scheme applied on a conceptual PGP. The results obtained were further compared to those obtained using yearly average operation conditions when solving the design optimization problem.
The results of this paper indicate that it is important to consider operation condition variations when designing flexible PGPs. In the case treated, the optimal solution with respect to total CO_2 emission savings obtained using average operating conditions was suboptimal when evaluated against the actual operation conditions. Furthermore, the objective function values predicted according to the average values approach underestimated the NPV of the designs with up to 6%, while it overestimated the CO_2 emission savings with up to 288%, when evaluating design performances against actual operating conditions. These results indicate that using average operating condition values is inadequate when designing flexible PGPs.

Acknowledgements

The authors would like to acknowledge DONG Energy for their financial support of the research.

References

[1] H. Lund, Renewable energy systems: the choice and modelling of 100% renewable solutions, Burlington, USA: Elsevier, 2010.

[2] O. Edenhofer, R. Pichs-Madruga and Y. Sokona, “Renewable Energy Sources and Climate Change Mitigation,” Intergovernmental Panel on Climate Change and Cambridge University Press, New York, USA, 2012.

[3] J. P. W. Scharlemann and W. F. Laruance, “How green are biofuels?,” *Environmental Science,* no. 319, pp. 43-44, 2008.

[4] M. Gassner and F. Maréchal, “Increasing Efficiency of Fuel Ethanol Production from Lignocellulosic Biomass by Process Integration,” *Energy Fuels,* no. 27, pp. 2107-2115, 2013.

[5] Y. Chen, T. A. Adams II and P. I. Barton, “Optimal Design and Operation of Flexible Energy Polygeneration Systems,” *Industrial & Engineering Chemistry Research,* no. 50, pp. 4553-4566, 2011.

[6] A. Coronas, S. S. Murthy and J. C. Bruno, “Editorial for the special issue of a applied thermal engineering on polygeneration,” *Applied Thermal Energy,* no. 50, pp. 1397-1398, 2013.

[7] P. Ahmadi, M. A. Rosen and I. Dincer, “Multi-objective exergy-based optimization of a polygeneration energy system using an evolutionary algorithm,” *Energy,* no. 46, pp. 21-31, 2012.

[8] M. Gassner and F. Maréchal, “Thermo-economic optimisation of the polygeneration of synthetic natural gas (SNG), power and heat from lignocellulosic biomass by gasification and methanation,” *Energy & Environmental Science,* no. 5, pp. 5768-5789, 2012.

[9] Y. Chen, T. A. Adams II and P. I. Barton, “Optimal Design and Operation of Static Energy Polygeneration Systems,” *Industrial & Engineering Chemistry Research,* no. 50, pp. 5099-5113, 2010.

[10] P. Liu, D. I. Gerogiorgis and E. N. Pistikopoulus, “Modeling and optimization of polygeneration energy systems,” *Catalysis Today,* no. 127, pp. 347-359, 2007.

[11] P. Liu, E. N. Pistikopoulus and Z. Li, “A Multi-Objective Optimization Approach to Polygeneration Energy Systems Design,” *Process Systems Engineering,* no. 56, pp. 1218-1234, 2010.

[12] P. Liu, E. N. Pistikopoulus and Z. Li, “Environmentally Benign Process Design of Polygeneration Energy Systems,” in *Design for Energy and the Environment*, Taylor and Francis Group, LLC, 2010, pp. 585-592.

[13] S. Fazlollahi, P. Mandel, G. Becker and F. Maréchal, “Methods for multi-objective investment and operating optimization of complex energy systems,” *Energy,* no. 45, pp. 12-22, 2012.

[14] S. Fazlollahi and F. Maréchal, “Multi-objective, multi-period optimization of biomass conversion technologies using evolutionary algorithms and mixed integer linear programming (MILP),” *Applied Thermal Engineering,* no. 50, pp. 1504-1513, 2013.

[15] C. Rubio-Maya, J. Uche-Marcuello, A. Martinéz-Garcia and A. A. Bayod-Rújula, “Design optimization of a polygeneration plant fuelled by natural gas and renewable energy sources,” *Applied Energy,* no. 88, pp. 449-457, 2011.

[16] C. Rubio-Maya, J. Uche and A. Martínez, “Sequential optimization of a polygeneration plant,” *Energy Conversion and Management,* no. 52, pp. 2861-2869, 2011.

[17] Y. Chen, T. A. Adams II and P. I. Barton, “Decomposition Strategy for the Global Optimization of Flexible Energy Polygeneration Systems,” *American institute of Chemical Engineers,* no. 58, pp. 3080-3095, 2012.

[18] D. Connolly, H. Lund, B. Mathiesen and M. Leahy, “A review of computer tools for analysing the integration of renewable energy in various energy systems,” *Applied Energy,* no. 87, pp. 1059-1082, 2010.

[19] M. Münster and P. Meibom, “Long-term affected energy production of waste to energy technologies identified by the use of energy system analysis,” *Waste Management,* no. 30, pp. 2510-2519, 2010.

[20] R. Bolliger, F. Maréchal and D. Favrat, “Méthodologie de la synthèse des systèmes énergétiques industriels,” École Polytechnique Fédérale de Lausanne, thesis 4867, Lausanne, 2010.

[21] Silkeborg Kommune, “Silkeborg Kommune,” 15 April 2013. [Online]. Available: http://silkeborgkommune.dk/. [Accessed 16 May 2014].

[22] A. Modarresi, P. Kravanja and A. Friedl, “Pinch and exergy analysis of lignocellulosic ethanol, biomethane, heat and power production from straw,” *Applied Thermal Engineering,* no. 43, pp. 20-28, 2012.

[23] J. Larsen, M. Ø. Petersen, L. Thirup, H. W. Li and F. K. Iversen, “The IBUS Process - Lignocellulosic Bioethanol Close to a Commercial Reality,” *Chemical Engineering & Technology,* no. 5, pp. 765-772, 2008.

[24] Silkeborg Forsyning, “Om Silkeborg Forsyning,” Silkeborg Forsyning, [Online]. Available: http://www.silkeborgforsyning.dk/. [Accessed 10 May 2014].

[25] WikiSilkeborg, “Silkeborg Kraftvarmeværk,” WikiSilkeborg, 21 December 2011. [Online]. Available: http://www.wikisilkeborg.dk/index.php/Silkeborg_Kraftvarmev%C3%A6rk. [Accessed 10 May 2014].

[26] J. Larsen, M. Østergaard Haven and L. Thirup, “Inbicon makes lignocellulosic ethanol a commercial reality,” *Biomass and Bioenergy,* no. 46, pp. 36-45, 2012.

[27] C. Lythcke-Jørgensen, F. Haglind and L. R. Clausen, “Exergy analysis of a combined heat and power plant with integrated lignocellulosic ethanol production,” *Energy Conversion and Management,* no. 85, pp. 817-827, 2014.

[28] A. Evald, G. Hu and M. T. Hansen, “Technology data for advanced bioenergy fuels,” Danish Energy Agency, Copenhagen, 2013.

[29] Danish Energy Agency, “Technology Data for Energy Plants,” Danish Energy Agency, Copenhagen, 2012.

[30] R. Smith, Chemical Process Design and Integration, West Sussex, England: John Wiley & Sons Ltd, 2005.

[31] energinet.dk, “Market data,” Nord Pool Spot, [Online]. Available: energinet.dk. [Accessed 28 May 2014].

[32] http://www.streammodel.org/, “The STREAM modelling tool,” Ea Energy Analyses. [Online]. [Accessed 3

April 2014].

[33] energinet.dk, “Energinet.dk's analyseforudsætninger 2012-2035, juli 2012,” energinet.dk, DK-7000 Fredericia, 2012.

[34] “IPCC Guidelines for National Greenhouse Gas Inventories,” Intergovernmental Panel on Climate Change, 2006.

[35] Ea Energy Analyses, “Opdatering af samfundsøkonomiske brændselspriser,” Danish Energy Authority, Copenhagen, 2011.

[36] energinet.dk, “CO2-prognoser,” [Online]. Available: http://energinet.dk/DA/El/Engrosmarked/Udtraek-af-markedsdata/Sider/CO2-prognoser.aspx. [Accessed 2 August 2014].

Appendix A

The characteristic operation periods (CHOPs) were in this work defined based on three parameters: Power price c_p, relative DH load λ_{DH}, and marginal CO_2 emissions from power production, $\alpha_{CO_2,p}$.
Two special CHOPs were defined with respect to power price: '*High power price*', which included power prices significantly above the average, and '*Low power price*', which contained all negative prices. The occurrence of these periods is low 198h and 31h over the reference year of 2013, but the extreme power prices occurring in these periods make them significant nonetheless. Hours with power prices falling in between the two extreme periods are categorized within three even power ranges. The power price duration curve over the reference year shown in Figure A1 gives a visual explanation of the c_p categorization.

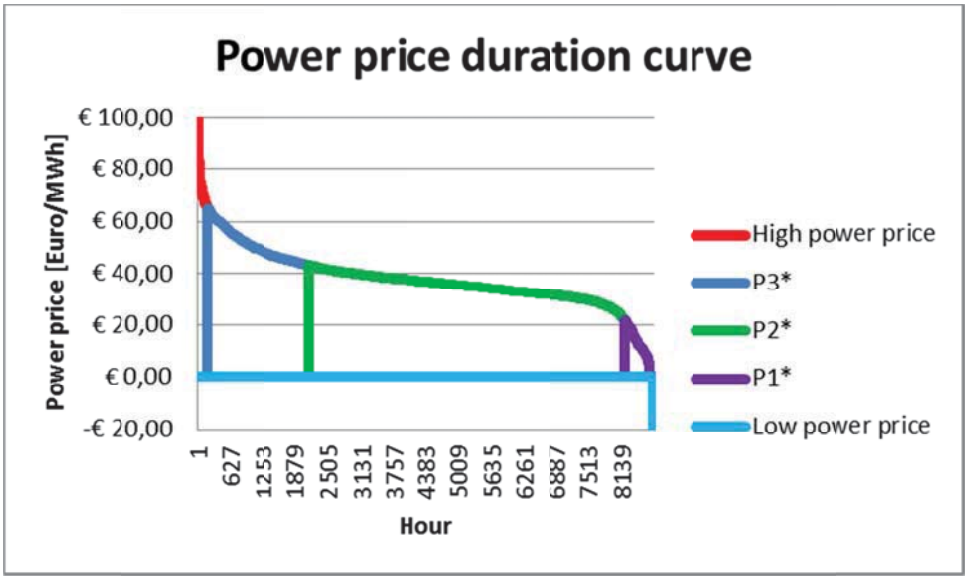

Figure A1: Solutions to the design optimization problem plotted with respect to objective function values.

As the relative heat load is more evenly distributed over the year, and no significant extremes occur, no special CHOPs have been defined based on the relative heat load. Relative heat loads over the hours of the reference year have been categorized into five even relative heat load ranges. The heat load duration curve is shown in Figure A2.

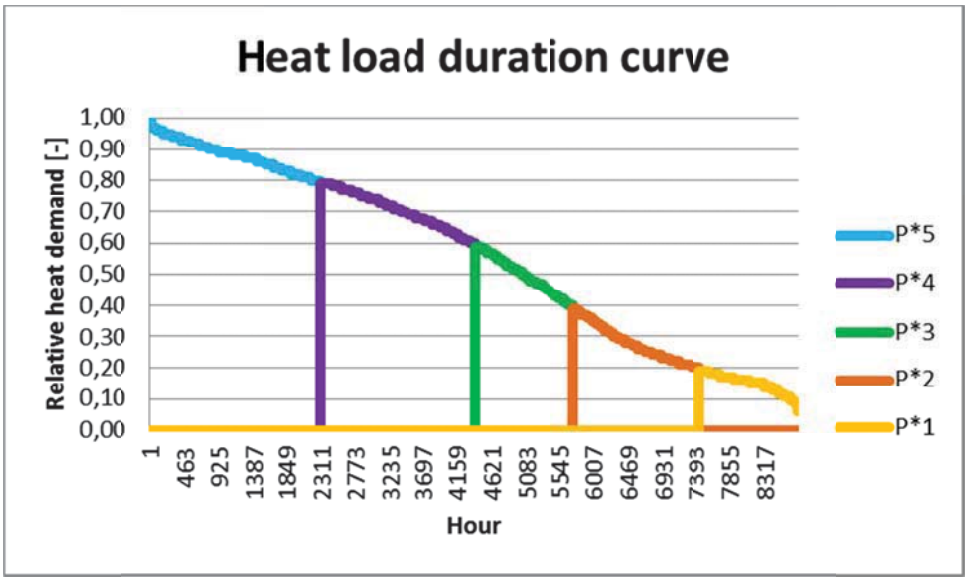

Figure A1: Solutions to the design optimization problem plotted with respect to objective function values.

The non-extreme CHOPs are indexed as P(*power price index*)(*heat load index*). Hence, hours merged into the group P25 have power prices in the power price range 2 and heat loads in the heat load range 5.

APPENDIX J Report on uncertainty analysis methodology

This report describes the contents of the developed methodology for sensitivity and uncertainty analysis in detail. The report was written as a part of the assignment for the PhD course ’28 923 Uncertainty and Sensitivity Analysis of Numerical Models’, taught by associate professor Gürkan Sin, DTU CHEMICAL ENGINEERING, Department of Chemical and Biochemical Engineering.

Sensitivity and uncertainty analysis in the design of flexible multi-generation plants

Course 28 923 – Final report

Christoffer Lythcke-Jørgensen
celjo@mek.dtu.dk

Contents

1. Introduction 3
2. Methodology for sensitivity and uncertainty analysis 4
2.1. Morris Screening for global sensitivity analysis 4
2.2. Monte Carlo method for uncertainty analysis 6
3. Application of methodology in a case study 7
4. Summary 12
List of Appendices 13
References 13

1. Introduction

A flexible multi-generation plant (FMG) is an integrated, flexibly operated facility that provides multiple links between layers of the energy system through the conversion of one or several energy resources into multiple energy services and other valuable products, e.g. electricity, heating, cooling, bio-fuels, and bio-chemicals [1]. The generic FMG concept is illustrated in Figure 1.

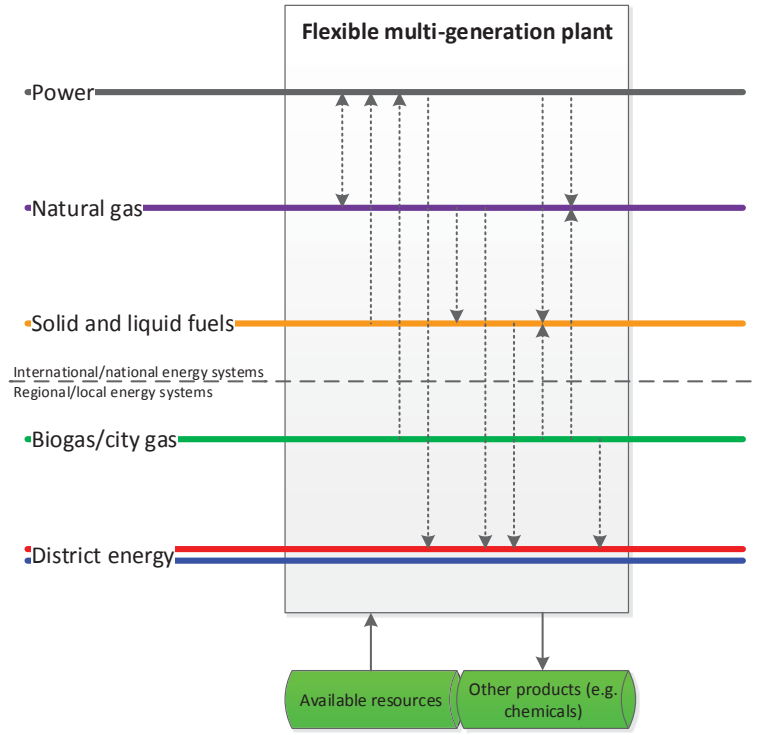

Figure 1: Conceptual sketch of a flexible multi-generation plant. Dotted arrows indicate a range of technological pathways for linking the energy system layers. Figure from [1].

FMGs may facilitate the integration and balancing of fluctuating renewable energy sources in the energy system in a cost- and energy-efficient way, and may therefore play an important part in smart energy systems based on renewable energy. However, the design of FMG concepts is complex and systematic optimization and evaluation approaches are required. In order to support reliable and comprehensive analysis work, such systematic optimization approaches must be able to assess output uncertainties.

This report describes a methodology for considering uncertainties in the design of FMGs. The methodology includes Morris screening for assessing the relative impact of uncertain input parameters on output variations, and the Monte Carlo method for quantifying output uncertainty. The report has been produced as part of the requirement for passing the DTU course 28 923 'Ph.D. summer School on Uncertainty and Sensitivity Analysis of Numerical Models'. The described methodology for sensitivity and uncertainty analysis is included in the overarching methodology for designing FMGs presented by Lythcke-Jørgensen et al. [1]. The submitted paper draft is provided as an appendix to this report.

The report is structured as follows: Section 2 describes the methodology for sensitivity and uncertainty analysis, and describes the included methods in details; Section 3 presents a case study where the methodology is applied for assessing uncertainty in the design of an FMG; and Section 4 contains a short summary of the report. Following this, a list of appendices submitted together with this report is presented.

2. Methodology for sensitivity and uncertainty analysis

This section describes a methodology for sensitivity and uncertainty analysis (MSU) within the Bayesian framework, which is to be implemented in the evaluation phase of an overarching methodology for designing FMGs. The MSU includes two methods, namely the extended Morris method [2][3] for global sensitivity analysis, and the Monte Carlo method for uncertainty analysis.

The overarching methodology for designing FMGs is illustrated in Figure 2. The design methodology generates a large number of design solutions that are optimized with respect to process integration and operation over the lifetime of the facility. From these solutions, a Pareto frontier is assembled with respect to two objectives, namely net present value (NPV) and global warming potential (GWP100a). As the design methodology is computationally intensive, the MSU will only be conducted for a selected number of interesting designs. The MSU handles uncertainties in economic and environmental parameters, while uncertainties in external operating conditions are to be handled by solving the optimization model for a number of likely scenarios. The location and structure of the MSU is marked by a red ellipse in in Figure 2.

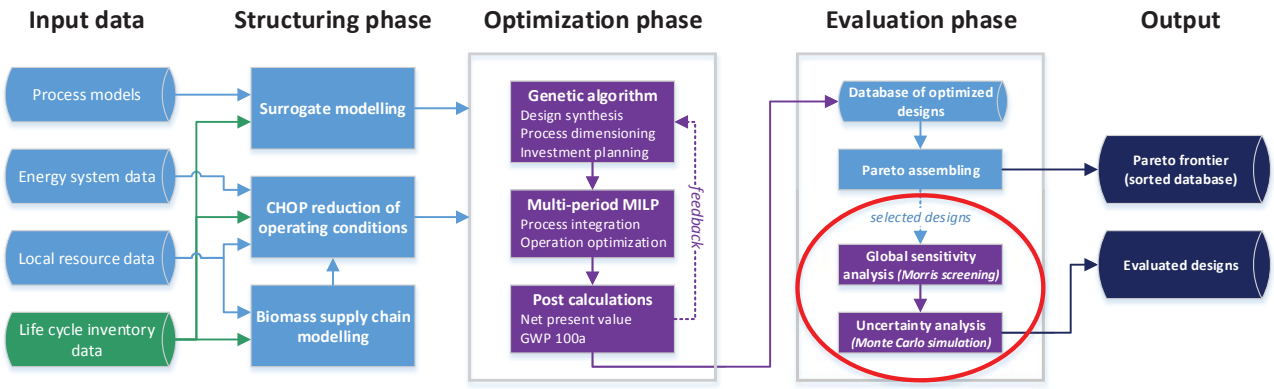

Figure 2: Design methodology structure. Methodology for sensitivity and uncertainty analysis is marked by the red ellipse. Figure from Lythcke-Jørgensen et al. [1].

After selecting a number of optimized designs for further evaluation, the MSU is applied, which consists of two steps: First, extended Morris screening [2][3] is applied for identifying input parameter uncertainties with negligible impact on model output variability. Secondly, the Monte Carlo method is applied for quantifying output uncertainties. Within the Monte Carlo method, Latin Hypercube Sampling [4] is used for sampling from the input space considering non-negligible input parameters only. In the following, the two methods are explained in detail. Both methods applied in the MSU were presented in [3].

2.1. Morris Screening for global sensitivity analysis

For each selected design k, all design and operation variables $\{\boldsymbol{\omega_k}, \boldsymbol{\sigma_k}, \boldsymbol{\nu_{k,i}}, \boldsymbol{\lambda_{k,i}}\}$ have been defined in the design optimization. Here, $\boldsymbol{\omega_k}$ is the installation decision for each process; $\boldsymbol{\sigma_k}$ is the dimension of each installed process; $\boldsymbol{\nu_{k,i}}$ is the operation of each process in each period i; and $\boldsymbol{\lambda_{k,i}}$ is the load of each operated process in period i. The performances $\boldsymbol{f}$ of each design are functions of the defined variables and a number of economic and environmental parameters $\boldsymbol{p}$:

$$\boldsymbol{f}(\boldsymbol{\omega_k}, \boldsymbol{\sigma_k}, \boldsymbol{\nu_{k,i}}, \boldsymbol{\lambda_{k,i}}, \boldsymbol{p}) = \begin{cases} NPV(\boldsymbol{\omega_k}, \boldsymbol{\sigma_k}, \boldsymbol{\nu_{k,i}}, \boldsymbol{\lambda_{k,i}}, \boldsymbol{p}) \\ GWP100a(\boldsymbol{\omega_k}, \boldsymbol{\sigma_k}, \boldsymbol{\nu_{k,i}}, \boldsymbol{\lambda_{k,i}}, \boldsymbol{p}) \end{cases}$$

The objective for the uncertainty analysis is to quantify the variations in $\{NPV, GWP100a\}$ as functions of the defined uncertainty ranges and distributions of the input parameters $\boldsymbol{p}$. It must be noticed that the relative importance of the parameters $\boldsymbol{p}$ may change between the selected designs due to differences in the defined parameter sets $(\boldsymbol{\omega_k}, \boldsymbol{\sigma_k}, \boldsymbol{\nu_{k,i}}, \boldsymbol{\lambda_{k,i}}, \boldsymbol{p})$. For example, the expected natural gas price may be important for the NPV of a gas boiler but insignificant for the NPV of a straw boiler.

As mentioned previously, the design methodology is computationally intensive, making it desirable to reduce the number of input uncertainties to sample from when quantifying output variations. Therefore, extended Morris screening [2][3] is applied in the first step of the MSU to identify input parameters that has a negligible impact on variations in model outputs. In other words, Morris screening is used to identify the set of input parameters $\boldsymbol{p_k^*}$ for each selected design k that must be considered in the uncertainty analysis as they have a significant impact on variations in $\boldsymbol{f}$.

$$\boldsymbol{p_k^*} \in \boldsymbol{p} \quad \forall\, k$$

Extended Morris screening is a global sensitivity analysis method that relies on estimation of elementary effects EE_{ij} of each parameter p_i on each output f_j. EE_{ij} is calculated as

$$EE_{ij} = \frac{f_j\,(p_1, p_2, \dots, p_i + \Delta, \dots, p_m) - f_j(\boldsymbol{p})}{\Delta}$$

Here, Δ is a user-defined perturbation factor.

By definition, all EE_{ij} are local measures. In order to approximate the global distributions of EE_{ij}, Morris suggested that elementary effects are calculated for a number of points r randomly sampled from the input space using Morris Sampling, which is described in [2]. In Morris Sampling, uncertainty ranges of input parameters p are assumed uniform and discretized into l levels, and the sampled parameters may only take the values of these levels. Using this sampling technique, Morris suggests that the number of levels l is set as an even number and the perturbation factor Δ is defined as

$$\Delta = \frac{l}{2(l-1)}$$

as this ensures that each possible elementary effect of an input parameter p has an equal probability of selection [2]. The suggested perturbation factor definition is used de facto in the present methodology, hence two degrees of freedom needs specification for the Morris screening: l, the even number of levels that input parameter uncertainty ranges are discretized into; and r, the number of samples from which the distributions of elementary effects are evaluated.

Once all EE_{ij} have been calculated for each random sample of input parameters, sigma-scaling [3] of EE_{ij} is applied so that the impacts of input parameters on various outputs can be compared:

$$SEE_{ij} = EE_{ij}\frac{\sigma_{pi}}{\sigma_{fj}}$$

Here, σ_{pi} is the standard deviation of the input parameter p_i, while σ_{fj} is the standard deviation of the output f_j from simulation results.

Based on the simulation results, the means and standard deviations of all sigma-scaled elementary effects SEE_{ij} are calculated and assembled in scatter plots. In each plot, two lines corresponding to the positive and negative double estimated standard error of the mean, $mean_i$, are drawn:

$$mean_i = \pm 2 \cdot \frac{\sigma_{EE_{ij}}}{\sqrt{r}}$$

As described in Sin et al. [48], these lines may be used for dividing uncertain input parameters into significant and negligible with respect to impact on model output variation. If the elementary effect of a parameter falls within the wedge formed by the two lines, its impact on the model output variation can be interpreted as negligible. An example of such scatter plot is presented in Figure 3.

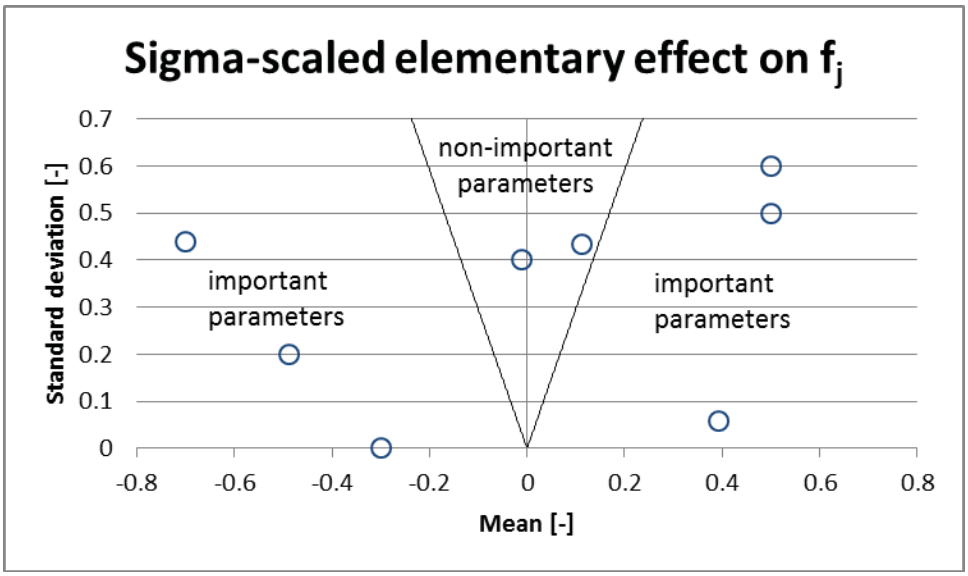

Figure 3: Example of a scatter plot of sigma-scaled elementary effects on a model output f_j from various input parameters. The two lines forming the wedge represent the double standard error of the mean. Input parameters inside the wedge are considered negligible with respect to variations in f_j, while parameters outside are considered to have a significant impact on variations in f_j.

From the extended Morris screening results, any parameter p_i that is identified to have a significant impact on at least one of the model output variations is included in the reduced dataset $\boldsymbol{p_k^*}$.

2.2. Monte Carlo method for uncertainty analysis

Following the Morris screening, the Monte Carlo procedure presented by Sin et al. [3] is applied for quantifying variations in the model outputs from uncertainties in input parameters $\boldsymbol{p_k^*}$.

The Monte Carlo method is a technique for investigating output variability through uncertainty sampling and probability statistics. It has been chosen for the design methodology as it may provide uncertainty results without necessitating modifications or manipulations of the original models, and due to the fact that it facilitates the identification of nonlinearities, thresholds, and discontinuities [5]. The procedure applied in the design methodology involves three steps:

1. *Specifying input uncertainty*: In general, the Monte Carlo method may consider uncertainty distributions D for all input parameters $\boldsymbol{p}$. However, in order to reduce the number of parameter

distributions to sample from in the present methodology, only parameters that were identified to have significant impact on model output variability by the extended Morris screening, i.e. the parameters $\boldsymbol{p}_k^*$, are considered as input uncertainty for the Monte Carlo method.

2. *Sampling from input uncertainty*: In order to obtain dense stratification over the range of each sampled variable without having to manually define the stratification, the Latin Hypercube Sampling method [4] is applied for sampling from uncertainties in input parameters $\boldsymbol{p}_k^*$.
3. *Evaluate model for sampled input uncertainty*: The model $\boldsymbol{f}$ is evaluated for the datasets sampled from input uncertainties in $\boldsymbol{p}_k^*$, providing a cumulative distribution function of output values as functions of input uncertainties. These distributions can then be evaluated using basic statistics.

In summary, the MSU presented applied extended Morris screening to identify the input parameters $\boldsymbol{p}_k^*$ with significant impact on one or more model output variations, and the Monte Carlo method using Latin Hypercube Sampling for evaluating variations in model outputs as a function of uncertainties in $\boldsymbol{p}_k^*$. In Section 3, the MSU is applied on a case study to demonstrate the use and evaluate its performance.

3. Application of methodology in a case study

In this section, the MSU is applied on a case study, which considers the retrofitting of an existing combined cycle combined heat and power plant. Retrofit options considered are presented in a superstructure in Figure 4. The study was presented in Lythcke-Jørgensen et al. [1], while a preliminary version was presented in Lythcke-Jørgensen et al. [6].

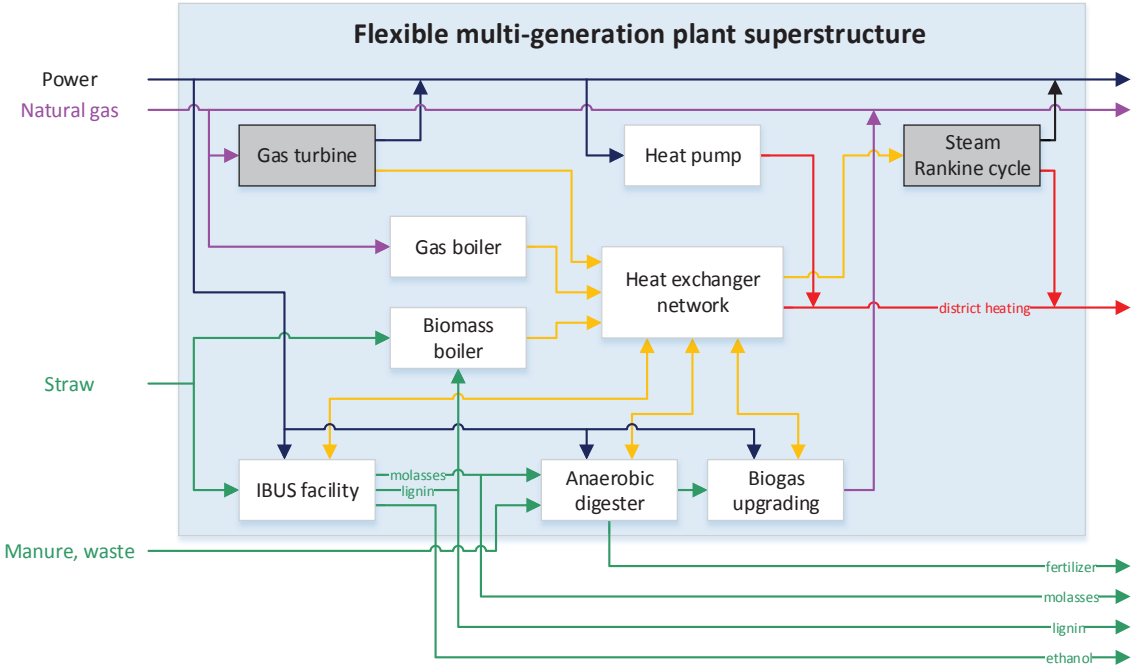

Figure 4: Superstructure of considered retrofit options for the existing combined cycle CHP. The gas turbine and steam Rankine cycle are grey as they are already installed.

Running the design methodology presented in Figure 2, the obtained Pareto frontier with respect to NPV and total CO_2 emission impact is presented in Figure 5. In the figure, each cross represents one optimized design solution. The designs are clustered with respect to the types of biomass processing installed. The

Pareto curve is crudely illustrated by the dotted line. The point 'Ref' represents the evaluated performance of the reference combined cycle CHP. The points *I*, *II*, and *III* are designs that have been chosen for further analysis using the MSU presented in this report.

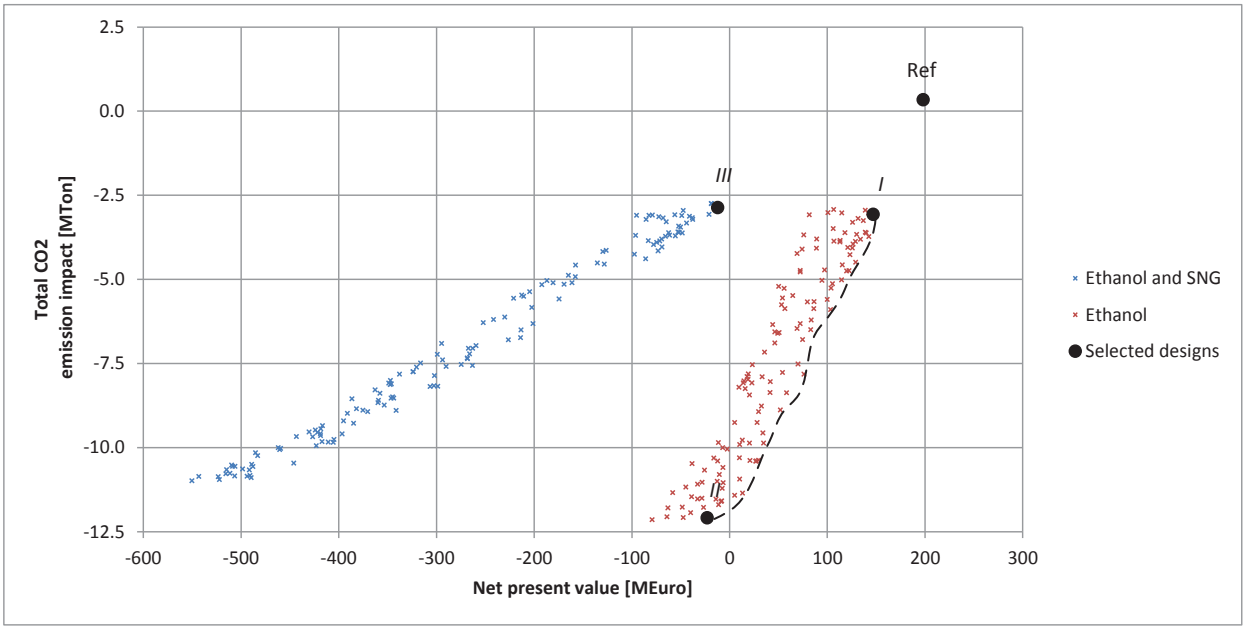

Figure 5: Scatter plot of optimized design solutions with respect to NPV and CO_2 emission impact. The designs are clustered with respect to type of biomass processing installed. The dotted line crudely illustrates the identified Pareto curve. The designs marked 'I', 'II' and 'III' are selected for further investigation. 'Ref' is the evaluated performance of the reference plant.

The uncertain input parameters considered and their distributions are given in Table 1.

Table 1: Uncertain parameters and their distributions

Parameter	Description	Distribution	Reference value	Lower bound	Upper bound
$C_{inv,IB0}$	Investment cost, reference ethanol facility	Uniform	256.0 MEuro	192.0 MEuro	320.0 MEuro
$C_{inv,AD0}$	Investment cost, reference combined biogas facility	Uniform	199.8 MEuro	149.9 MEuro	249.8 MEuro
$C_{inv,GB0}$	Investment cost, reference gas boiler	Uniform	2.0 MEuro	1.5 MEuro	2.5 MEuro
$C_{inv,BB0}$	Investment cost, reference biomass boiler	Uniform	40.0 MEuro	30.0 MEuro	50.0 MEuro
$C_{inv,HP0}$	Investment cost, reference district heating heat pump	Uniform	6.8 MEuro	5.1 MEuro	8.5 MEuro
c_{eth}	Ethanol price	Uniform	5.70 Euro/GJ	4.28 Euro/GJ	7.13 Euro/GJ
z_{eth}	Ethanol displaced CO_2 emission	Uniform	-69.2 kg/GJ	-41.5 kg/GJ	-69.2 kg/GJ
M_f	Investment scaling constant	Uniform	0.75	0.6	0.9

Reference investment costs and ethanol price are given a relative uncertainty of $\pm 25\%$ with a uniform distribution to represent cost and market uncertainties. The CO_2 emissions displaced from the ethanol produced z_{eth} is assumed to vary in the range $[-40\%, 0\%]$ with a uniform distribution to represent the facts that it may not be gasoline that is replaced by the produced ethanol, and that the straw consumed

may not be CO_2 neutral. Finally, the investment scaling constant, which is used in power law calculations of investment costs, is given an uncertainty range of $[0.6,0.9]$ with a uniform distribution to represent the uncertainties related to the economy of scale benefits from investments.

Extended Morris screening was conducted with $\{l, r\} = \{8,35\}$. The Monte Carlo method was conducted for samples of 250 data points generated using Latin Hypercube Sampling [4] and assuming zero correlation between uncertainties in input parameters.

Based on the input parameter uncertainties defined in Table 1, extended Morris screening was applied for identifying elementary effects on NPV and GWP100a from each of the uncertain input parameters in each of the three selected designs. An example of an elementary effect histogram obtained using extended Morris screening is plotted in Figure 6.

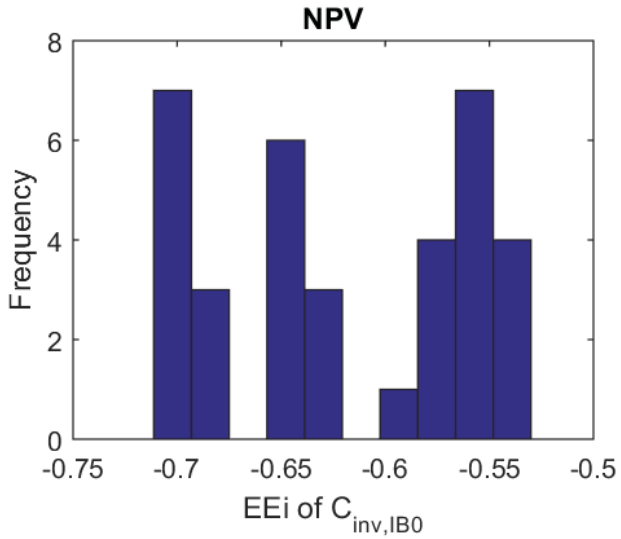

Figure 6: Histogram – elementary effect on NPV from reference ethanol facility Investment cost for design *I*.

The means and standard deviation of sigma-scaled elementary effects from uncertainties in input parameters on each of the model outputs are plotted for the three selected designs in Figure 7. Elementary effects with mean and standard deviations of zero are not labelled in the figures.

The scatter plots illustrate the relative importance of each of the input parameter uncertainties on each of the model outputs. From Figure 7, it is seen that the NPV of design *I* is significantly affected by uncertainties in reference ethanol facility investment cost $C_{inv,IB0}$ and investment scaling constant M_f, as the elementary effects of these parameters have means and standard deviations far outside the wedge. Furthermore, it is seen that the impacts of $C_{inv,IB0}$ and M_f are either correlated with other uncertain input parameters, non-linear, or both, as their standard deviations are different from zero. The ethanol price c_{eth} on the other hand is seen to have a linear impact on NPV as the elementary effect has a standard deviation of zero. These observations can easily be confirmed by investigating the model structure. It is further seen that the NPV of design *I* is not affected by neither the displaced CO_2 emission from ethanol z_{eth}, nor the reference investment costs of the biomethane facility $C_{inv,AD0}$ and district heating heat pump $C_{inv,HP0}$, which is evident as the dimension of the heat pump is negligible, no combined biogas facility is installed, and no economic cost is associated with CO_2 emissions. Opposed to this, z_{eth} is found to be the only parameter that has an impact on total CO_2 emission impact, as expected.

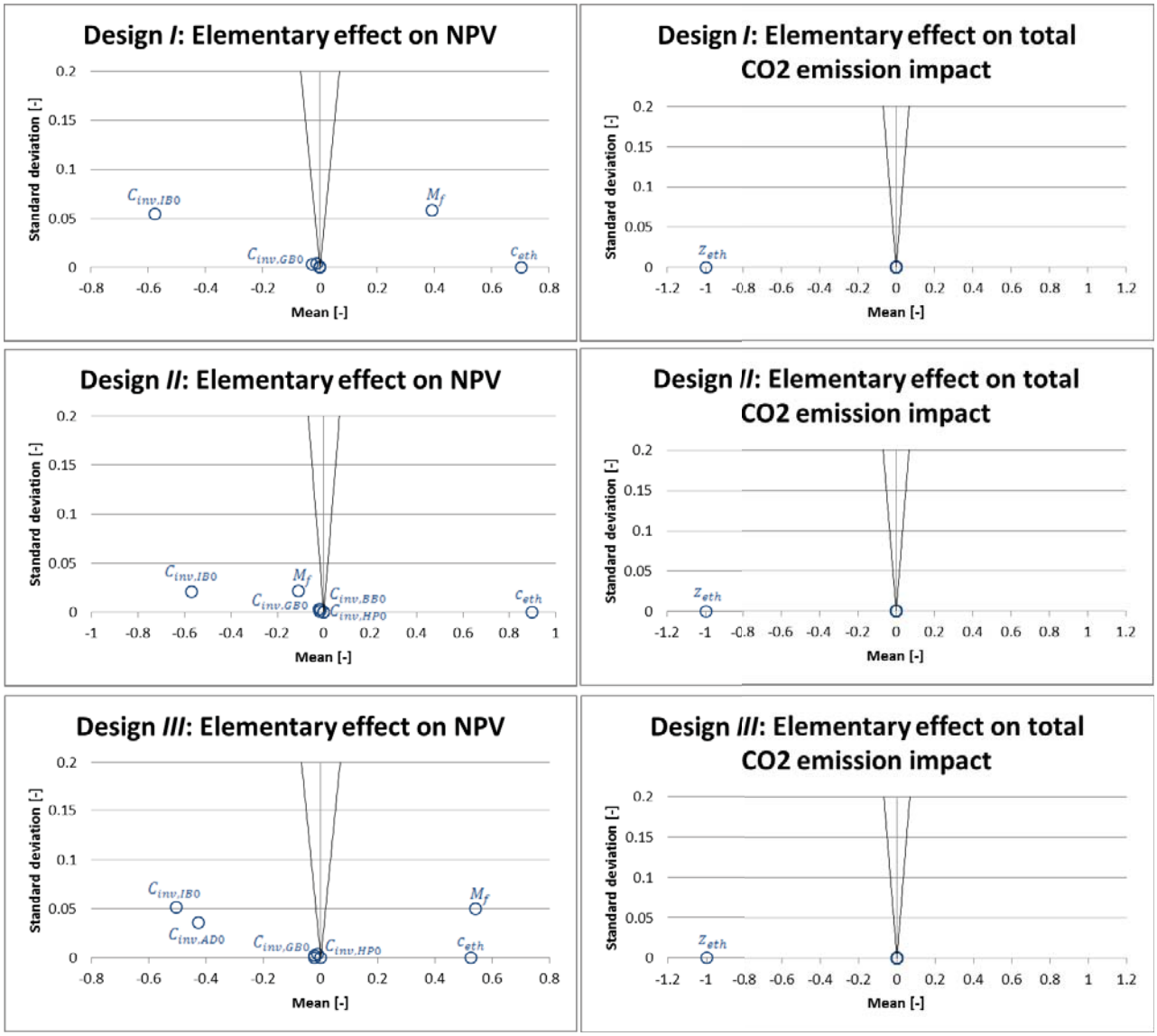

Figure 7: Means and standard deviations of sigma-scaled elementary effects on NPV (left) and total CO2 emission impact (right) from uncertainties in input parameters for designs *I* (top), *II* (middle), and *III* (bottom).

Similarly, observations on impacts of input parameter uncertainties can be made for designs *II* and *III* based on Figure 7. For design *II*, it is found that c_{eth} has a more significant impact than for the other designs, due to the fact that the ethanol facility is markedly larger which causes ethanol sales to have a relatively larger impact on the NPV. For design *III*, it is seen that $C_{inv,AD0}$ is no longer negligible as a biomethane facility is in fact installed.

Table 2: Uncertain input parameters included in p_k^* for each of the three selected designs.

Design	$C_{inv,IB0}$	$C_{inv,AD0}$	$C_{inv,GB0}$	$C_{inv,BB0}$	$C_{inv,HP0}$	c_{eth}	z_{eth}	M_f
I	X		X			X	X	X
II	X		X	X	X	X	X	X
III	X	X	X		X	X	X	X

Based on the Morris screening results, the parameters included in each reduced input parameter datasets $\boldsymbol{p_k^*}$ are summarized in Table 2. The Monte Carlo method was conducted for each of the three designs

considering $\boldsymbol{p}_{\boldsymbol{k}}^{*}$. The Latin Hypercube Sampling method was applied for generating samples of 250 data points for use in the Monte Carlo simulations. A visual representation of the Latin Hypercube sample used in the Monte Carlo simulation for design *I* is presented in Figure 8.

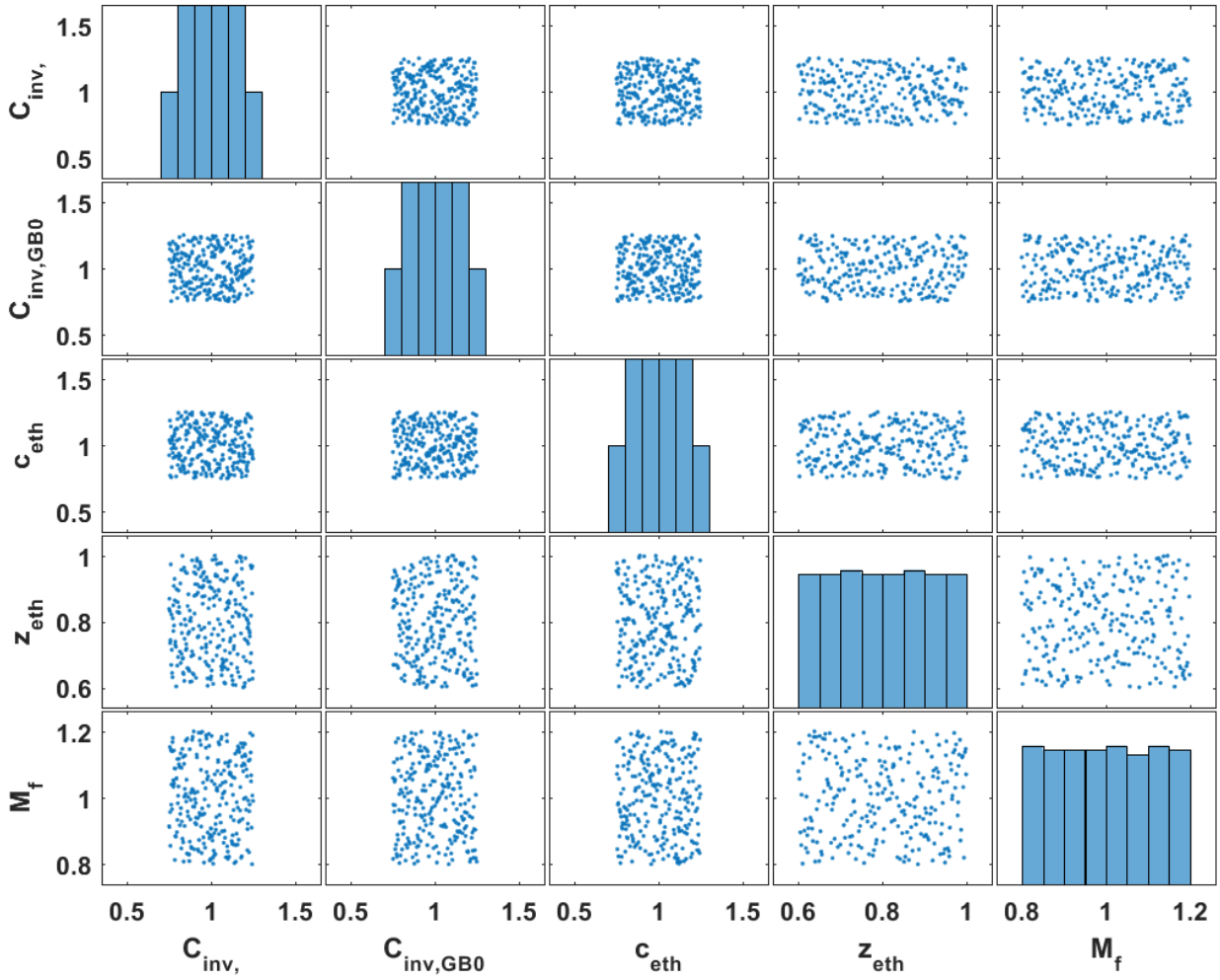

Figure 8: Example of Latin Hypercube Sampling – sample for Monte Carlo simulations for design *I*

Running Monte Carlo simulations for each of the three selected designs, the resulting 10th to 90th percentile interval of predicted NPV and 0th to 90th percentile interval of predicted GWP100a are indicated for each of the three selected designs in Figure 9.

The figure illustrates the variability in performance of the selected designs as functions of the defined input uncertainty. It is seen how the NPV variation is somewhat evenly distributed around the predicted value, which was expected as uncertainties in economic parameters are all considered to be evenly and uniformly distributed around the reference value. It is furthermore seen that the predicted CO_2 emission impact in the deterministic run is the lowest possible as the considered uncertainties in CO_2 emission impact may only lead to higher CO_2 emission impacts.

In general, the performance variations are found to be larger for design *II*. This is caused by the fact that the retrofit investments and ethanol production are largest for this design, meaning that the relative

uncertainties in investment costs, ethanol price and replaced CO_2 emissions from produced ethanol will have an absolute larger impact.

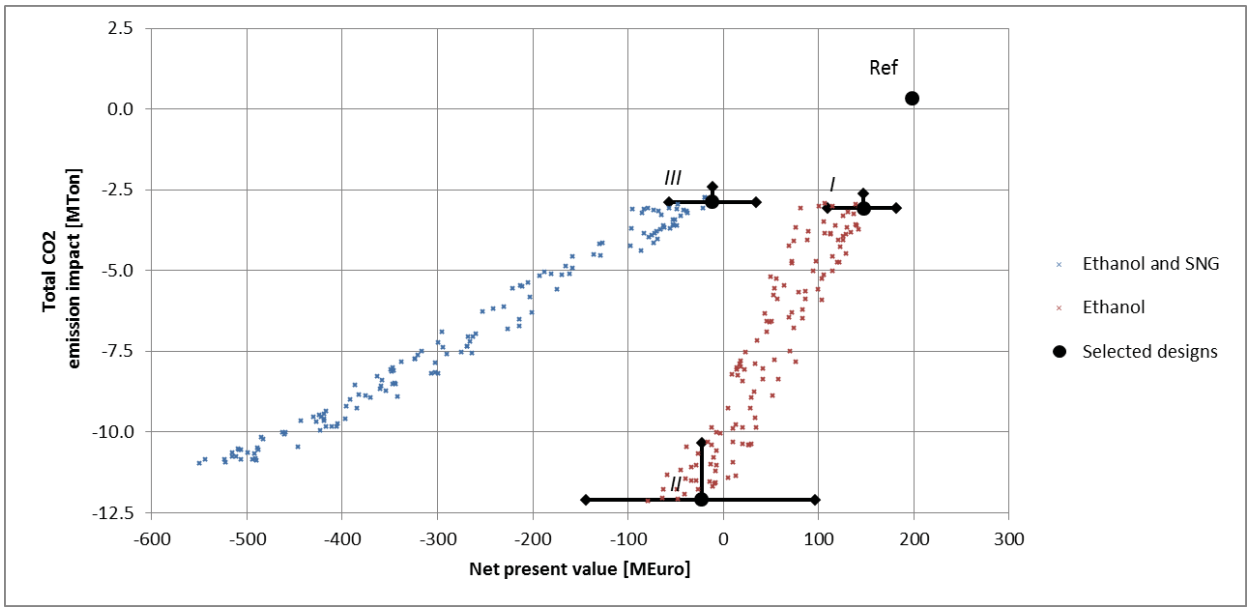

Figure 9: Scatter plot of optimized design solutions with respect to NPV and CO_2-emission impact, with performance variability indicated for each of the three selected designs. NPV performance intervals represent 10^{th} to 90^{th} percentiles of predicted performance, while CO_2 emission impact intervals represent 0^{th} to 90^{th} percentiles of predicted performance.

It is found that within 10^{th} to 90^{th} percentile variation intervals, design *I* will outperform design *III* with respect to NPV while the total CO_2 emission impact is somewhat similar, suggesting that *III* should not be selected for the given case. Considering the found performance intervals, design *I* has a CO_2 reduction shadow price of 4.9-30.3 Euro/ton, while design *II* has a CO_2 reduction shadow price of 8.4-32.1 Euro/ton. Hence, in the marginal case, the results suggest that design *I* should be preferred if cost efficient CO_2 reductions are desired, while design *II* results in the larges reductions in CO_2 emissions.

4. Summary

This report presented a methodology for sensitivity and uncertainty analysis in the design of flexible multi-generation plants (FMGs). The methodology included: Extended Morris Screening, a global sensitivity analysis for assessing the impact from input parameter uncertainties on model output variation; and the Monte Carlo method for quantifying model output variations.

The methodology was applied in a case study which considered the retrofitting of an existing combined cycle combined heat and power plant. It was found that the methodology was able to efficiently identify which input parameters that had a significant impact on model output variation, and that it was capable of assessing output variations based on uncertainties in input parameters.

In summary, the results suggest that the presented methodology for sensitivity and uncertainty analysis is efficient for assessing uncertainties in model outputs in the design optimization of flexible multi-generation plants.

List of Appendices

Appendices to this report are contained in the .zip folder named 'submission_celjo@mek.dtu.dk'. The following folders and documents are included (folder names in **bold**):

- **mc**: Folder containing Matlab code for running Monte Carlo simulations
  - **mc development:** The initial development of the Monte Carlo simulation files for the model
  - **mc development1:** Files for running the Monte Carlo simulation on tested design 1
  - **mc development2:** Files for running the Monte Carlo simulation on tested design 2
  - **mc development3:** Files for running the Monte Carlo simulation on tested design 3
- **mec**: Reference model used in the case study. Notice that the model is developed for OSMOSE, meaning that it can only be run if the Matlab OSMOSE package from EPFL IPESE is available.
- **sensi:** Folder containing Matlab code for running Morris screening
  - **Morris development:** The initial development of the Morris screening files for the model
  - **Morris I:** Files for running the Morris screening on tested design 1
  - **Morris II:** Files for running the Morris screening on tested design 2
  - **Morris III:** Files for running the Morris screening on tested design 3
- Paper – A methodology for designing flexible multi-generation plants (final).pdf : Final draft of the paper describing the methodology where the sensitivity and uncertainty analysis are included. The relevant parts for this hand-in are: *Section 2.4.2.*; *Section 3.1.5.*; *Section 3.2. (parts of)*.

References

[1] C. Lythcke-Jørgensen, A. V. Ensinas, M. Münster, and F. Haglind, "A methodology for designing flexible multi-generation plants," *Energy (under review)*.

[2] M. D. Morris, "Factorial Sampling Plans for Preliminary Computational Experiments," *Technometrics*, vol. 33, no. 2, pp. 161–174, 1991.

[3] G. Sin, K. V. Gernaey, and A. E. Lantz, "Good modeling practice for PAT applications: Propagation of input uncertainty and sensitivity analysis," in *Biotechnology Progress*, 2009, vol. 25, no. 4, pp. 1043–1053.

[4] M. D. McKay, R. J. Beckman, and W. J. Conover, "Comparison of three methods for selecting values of input variables in the analysis of output from a computer code," *Technometrics*, vol. 21, no. 2, pp. 239–245, 1979.

[5] J. C. Helton and F. J. Davis, "Latin hypercube sampling and the propagation of uncertainty in analyses of complex systems," *Reliability Engineering and System Safety*, vol. 81, no. 1. pp. 23–69, 2003.

[6] C. Lythcke-Jørgensen, M. Münster, A. V Ensinas, and F. Haglind, "Design optimization of flexible biomass-processing polygeneration plants using characteristic operation periods," in *World Renewable Energy Congress XIII*, London, UK, 2014.

APPENDIX K Modelling example: Case III

This appendix includes an example of how the developed design methodology was implemented in practice in *Case III*. The code includes the following Matlab documents:

- fmg_model.m — The system model superstructure
- fmg_postcompute.m — Calculations conducted for each period in the multi-period MILP model for operation optimization
- fmg_postmulti.m — Post computations conducted for each optimized design

The documents are based on the Matlab format applied in the OSMOSE tool, and many of the functions refer to internal calls and links within OSMOSE.

Regarding the CHOP method, a simple algorithm was written in Microsoft Excel for conducting the CHOP data aggregation based on equations (3.8)-(3.10). This algorithm is not presented here.

fmg_model.m

```
function technology = fmg_model
% FLEXIBLE MULTI-GENERATION SYSTEM MODEL (retrofit of Horsens CHP))
% -------------------------------------------------------------------------
% used in a case study with Energinet.dk


%%                              GENERAL INFORMATION
% Classification by grouping
technology.Group                        = {'Retrofit of Horsens CHP'};       %
Frist level of classification
technology.Type                                 = {'model for Energinet.dk case
study'};       % Second level of classification
technology.SubType                              = {''};         % Third level of
classification

% OSMOSE parameters
technology.OSMOSEVersion = {'2.7.8'};
technology.ETVersion = {'2.0.0'};
technology.Version = {'0.8.2'};

% technology detail level
technology.PhysicalRepresentation     = {'0d'};       % Provides information
about the level of detail of the technology.

% Technology authoring
technology.Changesets.Id                = [1];          % Changeset identifier
(integer)
technology.Changesets.Author                          =  {'Christoffer  Lythcke-
Jørgensen'};       % Author's name
technology.Changesets.Date              = {'March 18, 2016'};       % Date of
changeset
technology.Changesets.ChangeLog         = {'Error on PV fixed'};        % Text
describing the changes
technology.Changesets.ReferenceId       = {''};         % Link to references
(same DefaultValue as technology.References.Id)

technology.References.Id                = [];          % Reference Identifier
(integer)
technology.References.Source           = {''};       % Source of information.
Use BibTeX style
technology.References.Comments         = {''};       % Comments

technology.Tags                          = struct;    % This tructure contains
all the internal parameters of the model.


% Direct access and model inputs
[path,name,extension] = fileparts(which(mfilename));
technology.FileName                     = {[name,extension]};         % Direct
access method
```

```
technology.Location                  = {path};

% Define the software the model is developed in [required].
% Ex.:  technology.Software = {'vali'}; %{'matlab'};{'aspen'};
technology.Software = {'matlab'};

% Define the files that are needed for the computation [required].
% Flowsheet model (.inp, .bls); pre-/postcompute files; Modeldefinition
% file
technology.FileName       =       {'fmg_model.m',       'fmg_postcompute.m',
'fmg_postmulti.m'};

% Define the model file to be run [required]
technology.FileSelected = {'fmg_model.m'};

% Define the Matlab function that is run before the model [optional]
% Ex.:  technology.PreModelMFunction = {'pre_mod'};
% technology.PreModelMFunction = {'ex1_precompute'};

% Define the matlab file to run after the energy integration [optional].
% Ex.:  technology.PostEIMFunction = {'matlabmodel_h2o_psa.m'};
technology.PostEIMFunction = {'fmg_postcompute.m'};
technology.PostMultiperiodMFunction  = {'fmg_postmulti.m'};

% User tagging
technology.TagName                      = {'fmg_model'};       % User-defined
tag name
technology.DisplayName                  = {'FMG model'};       % User-defined
pretty short name
technology.Description                     = {'FMG model for case study with
Energinet.dk'};             %  Short  paragraph  containing  the  technology
description

% PinchLight Tagging
technology.Keywords(1)          = {'pinchlight:type=process'};
technology.Keywords(2)          = {'pinchlight:sector=any'};
technology.Keywords(3)          = {'pinchlight:subsector=any'};
technology.Keywords(4)          = {'pinchlight:technology=any'};
technology.Keywords(5)          = {'pinchlight:name=blackbox'};
technology.DescriptionImageFileName  =  {''};            %  Second  level  of
classification
technology.SubType                          = {''};         % Third level of
classification

% technology validation
technology.Validation                    = struct;      % Contains all the
validation fields
technology.Validation.Status       = {'toDo'};      % Validation stage: toDo,
Valid,  toUpdate,  inProgress      -->  available  states  are  defined  in
ET_validationStatus_list.m
technology.Validation.Comments        = {''};          % Any comment about
validation can be put here
technology.Validation.Rating       = {''};       % Provides a rating for the
technology. A rating procedure must be defined

% Material Streams
```

```
technology.MatStreams                    = struct;  % this structure contains
information about materail streams entering or leaving the technology.


%%                              INITIATION
%% values
ns = 0;
nl = 0;
nu = 0;
nc = 0;
%% layers

% INDUSTRIAL HEAT
nl = nl+1;
technology.EI.Layers(nl).Type = {'MassBalance'};
technology.EI.Layers(nl).TagName = {'heat_ind'};
technology.EI.Layers(nl).DisplayName  =  {'Industrial  low  temperature  heat
layer'};
technology.EI.Layers(nl).Unit = {'MW'};
technology.EI.Layers(nl).AddToProblem = 1;

% DISTRICT HEATING LAYER
nl = nl+1;
technology.EI.Layers(nl).Type = {'MassBalance'};
technology.EI.Layers(nl).TagName = {'heat_dh'};
technology.EI.Layers(nl).DisplayName = {'district heating heat layer'};
technology.EI.Layers(nl).Unit = {'MW'};
technology.EI.Layers(nl).AddToProblem = 1;

nu = nu+1;
technology.EI.Units(nu).Type = {'utility'};
technology.EI.Units(nu).TagName = {'dh_util'};
technology.EI.Units(nu).DisplayName = {'district heating utility generation,
CHP'};
technology.EI.Units(nu).AddToProblem =  1;
technology.EI.Units(nu).ITY = {'0'};
technology.EI.Units(nu).Fmin = {'0'};
technology.EI.Units(nu).Fmax = {'@sigma_dh'};
technology.EI.Units(nu).Cost1 = {'0'};
technology.EI.Units(nu).Cost2 = {'0'};
technology.EI.Units(nu).Cinv1 = {'0'};
technology.EI.Units(nu).Cinv2 = {'0'};
technology.EI.Units(nu).Power1 = {'0'};
technology.EI.Units(nu).Power2 = {'0'};


% WASTE
nl = nl+1;
technology.EI.Layers(nl).Type = {'MassBalance'};
technology.EI.Layers(nl).TagName = {'waste'};
technology.EI.Layers(nl).DisplayName = {'Waste layer'};
technology.EI.Layers(nl).Unit = {'MW'};
technology.EI.Layers(nl).AddToProblem = 1;
```

```
nu = nu+1;
technology.EI.Units(nu).Type = {'utility'};
technology.EI.Units(nu).TagName = {'w_flex'};
technology.EI.Units(nu).DisplayName = {'flexible waste processing'};
technology.EI.Units(nu).AddToProblem =  1;
technology.EI.Units(nu).ITY = {'0'};
technology.EI.Units(nu).Fmin = {'0'};
technology.EI.Units(nu).Fmax = {'1'};
technology.EI.Units(nu).Cost1 = {'0'};
technology.EI.Units(nu).Cost2 = {'0'};   % [Euro/h]
technology.EI.Units(nu).Cinv1 = {'0'};
technology.EI.Units(nu).Cinv2 = {'0'};
technology.EI.Units(nu).Power1 = {'0'};
technology.EI.Units(nu).Power2 = {'0'};


% POWER
nl = nl+1;
technology.EI.Layers(nl).Type = {'MassBalance'};
technology.EI.Layers(nl).TagName = {'power'};
technology.EI.Layers(nl).DisplayName = {'power'};
technology.EI.Layers(nl).Unit = {'MW'};
technology.EI.Layers(nl).AddToProblem = 1;

% power market, import
nu = nu+1;
technology.EI.Units(nu).Type = {'utility'};
technology.EI.Units(nu).TagName = {'p_imp'};
technology.EI.Units(nu).DisplayName = {'power import'};
technology.EI.Units(nu).AddToProblem =  1;
technology.EI.Units(nu).ITY = {'0'};
technology.EI.Units(nu).Fmin = {'0'};
technology.EI.Units(nu).Fmax = {'150'};  % MW
technology.EI.Units(nu).Cost1 = {'0'};
technology.EI.Units(nu).Cost2 = {'@c_power'};   % [Euro/h]
technology.EI.Units(nu).Cinv1 = {'0'};
technology.EI.Units(nu).Cinv2 = {'0'};
technology.EI.Units(nu).Power1 = {'0'};
technology.EI.Units(nu).Power2 = {'0'};

% power market, export
nu = nu+1;
technology.EI.Units(nu).Type = {'utility'};
technology.EI.Units(nu).TagName = {'p_exp'};
technology.EI.Units(nu).DisplayName = {'power export'};
technology.EI.Units(nu).AddToProblem =  1;
technology.EI.Units(nu).ITY = {'0'};
technology.EI.Units(nu).Fmin = {'0'};
technology.EI.Units(nu).Fmax = {'150'};   % MW
technology.EI.Units(nu).Cost1 = {'0'};
technology.EI.Units(nu).Cost2 = {'-@c_power'};  % [Euro/h]
technology.EI.Units(nu).Cinv1 = {'0'};
technology.EI.Units(nu).Cinv2 = {'0'};
technology.EI.Units(nu).Power1 = {'0'};
technology.EI.Units(nu).Power2 = {'0'};
```

```
% NATURAL GAS
nl = nl+1;
technology.EI.Layers(nl).Type = {'MassBalance'};
technology.EI.Layers(nl).TagName = {'gas'};
technology.EI.Layers(nl).DisplayName = {'gas'};
technology.EI.Layers(nl).Unit = {'MW'}; % MW
technology.EI.Layers(nl).AddToProblem = 1;

% gas, import
nu = nu+1;
technology.EI.Units(nu).Type = {'utility'};
technology.EI.Units(nu).TagName = {'gas_imp'};
technology.EI.Units(nu).DisplayName = {'gas import'};
technology.EI.Units(nu).AddToProblem =  1;
technology.EI.Units(nu).ITY = {'0'};
technology.EI.Units(nu).Fmin = {'0'};
technology.EI.Units(nu).Fmax = {'@sigma_gt + @sigma_ind_q'};
technology.EI.Units(nu).Cost1 = {'0'};
technology.EI.Units(nu).Cost2  =  {'@c_gas*3.6'};    % [Euro/GJ  *  GJ/MWh]  =
[Euro/MWh]
technology.EI.Units(nu).Cinv1 = {'0'};
technology.EI.Units(nu).Cinv2 = {'0'};
technology.EI.Units(nu).Power1 = {'0'};
technology.EI.Units(nu).Power2 = {'0'};


% SYNGAS
nl = nl+1;
technology.EI.Layers(nl).Type = {'MassBalance'};
technology.EI.Layers(nl).TagName = {'syngas'};
technology.EI.Layers(nl).DisplayName = {'syngas'};
technology.EI.Layers(nl).Unit = {'MW'}; % MW
technology.EI.Layers(nl).AddToProblem = 1;

nl = nl+1;
technology.EI.Layers(nl).Type = {'MassBalance'};
technology.EI.Layers(nl).TagName = {'syngas_re'};
technology.EI.Layers(nl).DisplayName = {'reacted syngas'};
technology.EI.Layers(nl).Unit = {'MW'}; % MW
technology.EI.Layers(nl).AddToProblem = 1;

nu = nu+1;
technology.EI.Units(nu).Type = {'utility'};
technology.EI.Units(nu).TagName = {'synre_flare'};
technology.EI.Units(nu).DisplayName = {'Burning of unused syngas'};
technology.EI.Units(nu).AddToProblem =  1;
technology.EI.Units(nu).ITY = {'0'};
technology.EI.Units(nu).Fmin = {'0'};
technology.EI.Units(nu).Fmax = {'@sigma_bio'};
technology.EI.Units(nu).Cost1 = {'0'};
technology.EI.Units(nu).Cost2 = {'0'};
technology.EI.Units(nu).Cinv1 = {'0'};
technology.EI.Units(nu).Cinv2 = {'0'};
technology.EI.Units(nu).Power1 = {'0'};
technology.EI.Units(nu).Power2 = {'0'};
```

```
% GAS FOR INDUSTRY
nl = nl+1;
technology.EI.Layers(nl).Type = {'MassBalance'};
technology.EI.Layers(nl).TagName = {'indgas'};
technology.EI.Layers(nl).DisplayName = {'gas for the industry'};
technology.EI.Layers(nl).Unit = {'MW'}; % MW
technology.EI.Layers(nl).AddToProblem = 1;

% natural gas to industry gas
nu = nu+1;
technology.EI.Units(nu).Type = {'utility'};
technology.EI.Units(nu).TagName = {'ng_to_indgas'};
technology.EI.Units(nu).DisplayName = {'NG for industry'};
technology.EI.Units(nu).AddToProblem =  1;
technology.EI.Units(nu).ITY = {'0'};
technology.EI.Units(nu).Fmin = {'0'};
technology.EI.Units(nu).Fmax = {'@sigma_ind_q'};
technology.EI.Units(nu).Cost1 = {'0'};
technology.EI.Units(nu).Cost2 = {'0'};  % [Euro/GJ * GJ/MWh] = [Euro/MWh]
technology.EI.Units(nu).Cinv1 = {'0'};
technology.EI.Units(nu).Cinv2 = {'0'};
technology.EI.Units(nu).Power1 = {'0'};
technology.EI.Units(nu).Power2 = {'0'};

% syngas to industry gas
nu = nu+1;
technology.EI.Units(nu).Type = {'utility'};
technology.EI.Units(nu).TagName = {'syn_to_indgas'};
technology.EI.Units(nu).DisplayName = {'syngas for industry'};
technology.EI.Units(nu).AddToProblem =  1;
technology.EI.Units(nu).ITY = {'0'};
technology.EI.Units(nu).Fmin = {'0'};
technology.EI.Units(nu).Fmax = {'@sigma_ind_q'};
technology.EI.Units(nu).Cost1 = {'0'};
technology.EI.Units(nu).Cost2 = {'0'};  % [Euro/GJ * GJ/MWh] = [Euro/MWh]
technology.EI.Units(nu).Cinv1 = {'0'};
technology.EI.Units(nu).Cinv2 = {'0'};
technology.EI.Units(nu).Power1 = {'0'};
technology.EI.Units(nu).Power2 = {'0'};

% Reacted syngas to industry gas
nu = nu+1;
technology.EI.Units(nu).Type = {'utility'};
technology.EI.Units(nu).TagName = {'synre_to_indgas'};
technology.EI.Units(nu).DisplayName = {'syngas for industry'};
technology.EI.Units(nu).AddToProblem =  1;
technology.EI.Units(nu).ITY = {'0'};
technology.EI.Units(nu).Fmin = {'0'};
technology.EI.Units(nu).Fmax = {'@sigma_ind_q'};
technology.EI.Units(nu).Cost1 = {'0'};
technology.EI.Units(nu).Cost2 = {'0'};
technology.EI.Units(nu).Cinv1 = {'0'};
technology.EI.Units(nu).Cinv2 = {'0'};
technology.EI.Units(nu).Power1 = {'0'};
```

```
technology.EI.Units(nu).Power2 = {'0'};


% OXYGEN and HYDROGEN
nl = nl+1;
technology.EI.Layers(nl).Type = {'MassBalance'};
technology.EI.Layers(nl).TagName = {'o2'};
technology.EI.Layers(nl).DisplayName = {'oxygen'};
technology.EI.Layers(nl).Unit = {'kg per s'};
technology.EI.Layers(nl).AddToProblem = 1;

nl = nl+1;
technology.EI.Layers(nl).Type = {'MassBalance'};
technology.EI.Layers(nl).TagName = {'h2'};
technology.EI.Layers(nl).DisplayName = {'hydrogen'};
technology.EI.Layers(nl).Unit = {'kg per s'};
technology.EI.Layers(nl).AddToProblem = 1;

nu = nu+1;
technology.EI.Units(nu).Type = {'utility'};
technology.EI.Units(nu).TagName = {'o2_ex'};
technology.EI.Units(nu).DisplayName = {'exhaust of excess oxygen'};
technology.EI.Units(nu).AddToProblem =  1;
technology.EI.Units(nu).ITY = {'0'};
technology.EI.Units(nu).Fmin = {'0'};
technology.EI.Units(nu).Fmax = {'100'};
technology.EI.Units(nu).Cost1 = {'0'};
technology.EI.Units(nu).Cost2 = {'0'};   % [Euro/h]
technology.EI.Units(nu).Cinv1 = {'0'};
technology.EI.Units(nu).Cinv2 = {'0'};
technology.EI.Units(nu).Power1 = {'0'};
technology.EI.Units(nu).Power2 = {'0'};


% METHANOL
nl = nl+1;
technology.EI.Layers(nl).Type = {'MassBalance'};
technology.EI.Layers(nl).TagName = {'methanol'};
technology.EI.Layers(nl).DisplayName = {'methanol'};
technology.EI.Layers(nl).Unit = {'MW'};
technology.EI.Layers(nl).AddToProblem = 1;

nu = nu+1;
technology.EI.Units(nu).Type = {'utility'};
technology.EI.Units(nu).TagName = {'meth_r'};
technology.EI.Units(nu).DisplayName = {'methanol sales'};
technology.EI.Units(nu).AddToProblem =  1;
technology.EI.Units(nu).ITY = {'0'};
technology.EI.Units(nu).Fmin = {'0'};
technology.EI.Units(nu).Fmax = {'1000'};
technology.EI.Units(nu).Cost1 = {'0'};
technology.EI.Units(nu).Cost2 = {'-@c_methanol*3.6'};   % [Euro/GJ * GJ/MWh]
= [Euro/MWh]
technology.EI.Units(nu).Cinv1 = {'0'};
technology.EI.Units(nu).Cinv2 = {'0'};
technology.EI.Units(nu).Power1 = {'0'};
```

```
technology.EI.Units(nu).Power2 = {'0'};



%%                              PROCESSES AND UTILITIES
%% PROCESSES
% District heating demand
nu = nu+1;
technology.EI.Units(nu).Type = {'process'};
technology.EI.Units(nu).TagName = {'dh'};
technology.EI.Units(nu).DisplayName = {'District heating demand'};
technology.EI.Units(nu).AddToProblem =  1;
technology.EI.Units(nu).ITY = {'0'};
technology.EI.Units(nu).Cost1 = {'0'};
technology.EI.Units(nu).Cost2 = {'0'}; % no price on DH, the objective is to
minimize heat generation costs
technology.EI.Units(nu).Cinv1 = {'0'};
technology.EI.Units(nu).Cinv2 = {'0'};
technology.EI.Units(nu).Power1 = {'0'};
technology.EI.Units(nu).Power2 = {'0'};

% Industry demands
nu = nu+1;
technology.EI.Units(nu).Type = {'process'};
technology.EI.Units(nu).TagName = {'ind'};
technology.EI.Units(nu).DisplayName = {'industry demands'};
technology.EI.Units(nu).AddToProblem =  1;
technology.EI.Units(nu).ITY = {'0'};
technology.EI.Units(nu).Cost1 = {'0'};
technology.EI.Units(nu).Cost2 = {'0'};
technology.EI.Units(nu).Cinv1 = {'0'};
technology.EI.Units(nu).Cinv2 = {'0'};
technology.EI.Units(nu).Power1 = {'0'};
technology.EI.Units(nu).Power2 = {'0'};

% waste processing demand
nu = nu+1;
technology.EI.Units(nu).Type = {'process'};
technology.EI.Units(nu).TagName = {'w_fix'};
technology.EI.Units(nu).DisplayName = {'waste processing demand'};
technology.EI.Units(nu).AddToProblem =  1;
technology.EI.Units(nu).ITY = {'0'};
technology.EI.Units(nu).Cost1 = {'0'};
technology.EI.Units(nu).Cost2 = {'0'};
technology.EI.Units(nu).Cinv1 = {'0'};
technology.EI.Units(nu).Cinv2 = {'0'};
technology.EI.Units(nu).Power1 = {'0'};
technology.EI.Units(nu).Power2 = {'0'};

% gasifier
nu = nu+1;
technology.EI.Units(nu).Type = {'process'};
technology.EI.Units(nu).TagName = {'gasifier'};
technology.EI.Units(nu).DisplayName = {'gasifier'};
technology.EI.Units(nu).AddToProblem =  1;
technology.EI.Units(nu).ITY = {'0'};
```

```
technology.EI.Units(nu).Cost1 = {'0'};
technology.EI.Units(nu).Cost2  =  {'@sigma_bio*@c_woodchips*3.6'};     %  Wood
chips price
technology.EI.Units(nu).Cinv1 = {'0'};
technology.EI.Units(nu).Cinv2 = {'0'};
technology.EI.Units(nu).Power1 = {'0'};
technology.EI.Units(nu).Power2 = {'0'};
%% UTILITIES

% Gas boiler, industry
nu = nu+1;
technology.EI.Units(nu).Type = {'utility'};
technology.EI.Units(nu).TagName = {'ind_gb'};
technology.EI.Units(nu).DisplayName = {'industrial gas boiler'};
technology.EI.Units(nu).AddToProblem =  1;
technology.EI.Units(nu).ITY = {'0'};
technology.EI.Units(nu).Fmin = {'0'};
technology.EI.Units(nu).Fmax = {'@sigma_ind_q'};
% technology.EI.Units(nu).Mult = {'1'};
technology.EI.Units(nu).Cost1 = {'0'};
technology.EI.Units(nu).Cost2 = {'@c_op_gb'};
technology.EI.Units(nu).Cinv1 = {'0'};
technology.EI.Units(nu).Cinv2 = {'0'};    %[MEuro/(MJ/s)]
technology.EI.Units(nu).Power1 = {'0'};
technology.EI.Units(nu).Power2 = {'0'};

% Heat pump, industry
nu = nu+1;
technology.EI.Units(nu).Type = {'utility'};
technology.EI.Units(nu).TagName = {'ind_hp'};
technology.EI.Units(nu).DisplayName = {'industrial heat pump'};
technology.EI.Units(nu).AddToProblem =  1;
technology.EI.Units(nu).ITY = {'0'};
technology.EI.Units(nu).Fmin = {'0'};
technology.EI.Units(nu).Fmax                                              =
{'@omega_dh*@sigma_ind_q*@lambda_ind_q*@eta_ind_ht'};
technology.EI.Units(nu).Cost1 = {'0'};
technology.EI.Units(nu).Cost2 = {'0'};    %[Euro/(MJ/s)-h]    notice: mult =
(MJ/s)
technology.EI.Units(nu).Cinv1 = {'0'};
technology.EI.Units(nu).Cinv2 = {'0'};    %[MEuro/(MJ/s)]
technology.EI.Units(nu).Power1 = {'0'};
technology.EI.Units(nu).Power2 = {'0'};

% District heating consumption, industry
nu = nu+1;
technology.EI.Units(nu).Type = {'utility'};
technology.EI.Units(nu).TagName = {'ind_dh'};
technology.EI.Units(nu).DisplayName    =    {'industrial    district    heating
consumption'};
technology.EI.Units(nu).AddToProblem =  1;
technology.EI.Units(nu).ITY = {'0'};
technology.EI.Units(nu).Fmin = {'0'};
technology.EI.Units(nu).Fmax                                              =
{'@omega_dh*(@eta_ind_lt+@eta_ind_mt)*@sigma_ind_q*@lambda_ind_q'};    %  max
capacity = low and medium temperature heat demand
```

```
technology.EI.Units(nu).Cost1 = {'0'};
technology.EI.Units(nu).Cost2 = {'0'};
technology.EI.Units(nu).Cinv1 = {'0'};
technology.EI.Units(nu).Cinv2 = {'0'};
technology.EI.Units(nu).Power1 = {'0'};
technology.EI.Units(nu).Power2 = {'0'};


% Combined heat and power plant (back-prssure Rankine, waste incinerators
nu = nu+1;
technology.EI.Units(nu).Type = {'utility'};
technology.EI.Units(nu).TagName = {'ran'};
technology.EI.Units(nu).DisplayName = {'Waste boilers and back-pressure
Rankine cycle'};
technology.EI.Units(nu).AddToProblem = 1;
technology.EI.Units(nu).ITY = {'0'};
technology.EI.Units(nu).Fmin = {'@lambda_min_ran'};
technology.EI.Units(nu).Fmax = {'1'};
technology.EI.Units(nu).Cost1 = {'0'};
technology.EI.Units(nu).Cost2 = {'@sigma_ran*@c_op_ran'}; % [Euro/h]: max
capacity [MW] * O&M cost [Euro/MWh]
technology.EI.Units(nu).Cinv1 = {'0'};
technology.EI.Units(nu).Cinv2 = {'0'};
technology.EI.Units(nu).Power1 = {'0'};
technology.EI.Units(nu).Power2 = {'0'};

% Gas turbine
nu = nu+1;
technology.EI.Units(nu).Type = {'utility'};
technology.EI.Units(nu).TagName = {'gt'};
technology.EI.Units(nu).DisplayName = {'Individual gas turbine at CHP
area'};
technology.EI.Units(nu).AddToProblem = 1;
technology.EI.Units(nu).ITY = {'0'};
technology.EI.Units(nu).Fmin = {'@lambda_min_gt'};
technology.EI.Units(nu).Fmax = {'1'};
technology.EI.Units(nu).Cost1 = {'0'};
technology.EI.Units(nu).Cost2 = {'@sigma_gt*@c_op_gt'}; % [Euro/h]: max
capacity [MW] / mult_max [-] * O&M cost [Euro/MWh]
technology.EI.Units(nu).Cinv1 = {'0'};
technology.EI.Units(nu).Cinv2 = {'0'};
technology.EI.Units(nu).Power1 = {'0'};
technology.EI.Units(nu).Power2 = {'0'};


% Cooling water
nu = nu+1;
technology.EI.Units(nu).Type = {'utility'};
technology.EI.Units(nu).TagName = {'water'};
technology.EI.Units(nu).DisplayName = {'cooling water'};
technology.EI.Units(nu).AddToProblem = 1;
technology.EI.Units(nu).ITY = {'0'};
technology.EI.Units(nu).Fmin = {'0.'};
technology.EI.Units(nu).Fmax = {'1000'};
technology.EI.Units(nu).Cost1 = {'0'};
technology.EI.Units(nu).Cost2 = {'0.01'};
```

```
technology.EI.Units(nu).Cinv1 = {'0'};
technology.EI.Units(nu).Cinv2 = {'0'};
technology.EI.Units(nu).Power1 = {'0'};
technology.EI.Units(nu).Power2 = {'0'};

% SOEC
nu = nu+1;
technology.EI.Units(nu).Type = {'utility'};
technology.EI.Units(nu).TagName = {'soec'};
technology.EI.Units(nu).DisplayName = {'Solid oxide electrolysis cell'};
technology.EI.Units(nu).AddToProblem =  1;
technology.EI.Units(nu).ITY = {'0'};
technology.EI.Units(nu).Fmin = {'0'};
technology.EI.Units(nu).Fmax = {'1'};
technology.EI.Units(nu).Cost1 = {'0'};
technology.EI.Units(nu).Cost2 = {'0'};
technology.EI.Units(nu).Cinv1 = {'0'};
technology.EI.Units(nu).Cinv2 = {'0'};    %[MEuro/(MJ/s)]
technology.EI.Units(nu).Power1 = {'0'};
technology.EI.Units(nu).Power2 = {'0'};

% Methanol production
nu = nu+1;
technology.EI.Units(nu).Type = {'utility'};
technology.EI.Units(nu).TagName = {'meth_0'};
technology.EI.Units(nu).DisplayName = {'Methanol production'};
technology.EI.Units(nu).AddToProblem =  1;
technology.EI.Units(nu).ITY = {'0'};
technology.EI.Units(nu).Fmin = {'0'};
technology.EI.Units(nu).Fmax = {'1'};
technology.EI.Units(nu).Cost1 = {'0'};
technology.EI.Units(nu).Cost2 = {'0'};
technology.EI.Units(nu).Cinv1 = {'0'};
technology.EI.Units(nu).Cinv2 = {'0'};
technology.EI.Units(nu).Power1 = {'0'};
technology.EI.Units(nu).Power2 = {'0'};

nu = nu+1;
technology.EI.Units(nu).Type = {'utility'};
technology.EI.Units(nu).TagName = {'meth_o2'};
technology.EI.Units(nu).DisplayName   =   {'Methanol   production   oxygen-
boosted'};
technology.EI.Units(nu).AddToProblem =  1;
technology.EI.Units(nu).ITY = {'0'};
technology.EI.Units(nu).Fmin = {'0'};
technology.EI.Units(nu).Fmax = {'1'};
technology.EI.Units(nu).Cost1 = {'0'};
technology.EI.Units(nu).Cost2 = {'0'};
technology.EI.Units(nu).Cinv1 = {'0'};
technology.EI.Units(nu).Cinv2 = {'0'};
technology.EI.Units(nu).Power1 = {'0'};
technology.EI.Units(nu).Power2 = {'0'};

nu = nu+1;
technology.EI.Units(nu).Type = {'utility'};
technology.EI.Units(nu).TagName = {'meth_h2'};
```

```
technology.EI.Units(nu).DisplayName   =   {'Methanol   production   hydrogen-
boosted'};
technology.EI.Units(nu).AddToProblem =  1;
technology.EI.Units(nu).ITY = {'0'};
technology.EI.Units(nu).Fmin = {'0'};
technology.EI.Units(nu).Fmax = {'1'};
technology.EI.Units(nu).Cost1 = {'0'};
technology.EI.Units(nu).Cost2 = {'0'};
technology.EI.Units(nu).Cinv1 = {'0'};
technology.EI.Units(nu).Cinv2 = {'0'};
technology.EI.Units(nu).Power1 = {'0'};
technology.EI.Units(nu).Power2 = {'0'};



%%                              TAGS
%% Design variables

% District heating connection to the industry area (integer)
nc = nc+1;
technology.Tags(nc).DisplayName = {'industry district heating connection'};
technology.Tags(nc).Description = technology.Tags(nc).DisplayName;
technology.Tags(nc).TagName = {'omega_dh'};
technology.Tags(nc).DefaultValue = 1;      % [INTEGER!!!]
technology.Tags(nc).Unit = {'-'};
technology.Tags(nc).Status = {'CST'};
technology.Tags(nc).isVIT = 1;

% Syngas connection to the industry area (integer)
nc = nc+1;
technology.Tags(nc).DisplayName = {'industry syngas connection'};
technology.Tags(nc).Description = technology.Tags(nc).DisplayName;
technology.Tags(nc).TagName = {'omega_syngas'};
technology.Tags(nc).DefaultValue = 0;      % [INTEGER!!!]
technology.Tags(nc).Unit = {'-'};
technology.Tags(nc).Status = {'CST'};
technology.Tags(nc).isVIT = 1;


% Biorefinery dimension
nc = nc+1;
technology.Tags(nc).DisplayName = {'biorefinery dimension'};
technology.Tags(nc).Description = technology.Tags(nc).DisplayName;
technology.Tags(nc).TagName = {'sigma_bio'};
technology.Tags(nc).DefaultValue = 81.23;      % [MJ/s wood chips]
technology.Tags(nc).Unit = {'MJ/s'};
technology.Tags(nc).Status = {'CST'};
technology.Tags(nc).isVIT = 1;
%% Layer tags
nc = nc+1;
technology.Tags(nc).TagName       = {'dt_min_2'};
technology.Tags(nc).DisplayName   = {'Temperature difference (DTmin_2) '};
technology.Tags(nc).DefaultValue  = 5;
technology.Tags(nc).Unit          = {'K'};
technology.Tags(nc).Status        = {'CST'};
technology.Tags(nc).isVIT         = 1;
```

```
%% Industry model tags
nc = nc+1;
technology.Tags(nc).DisplayName = {'nominal industry heating demand'};
technology.Tags(nc).Description = technology.Tags(nc).DisplayName;
technology.Tags(nc).TagName = {'sigma_ind_q'};
technology.Tags(nc).DefaultValue = 6.43;      % [MW]
technology.Tags(nc).Unit = {'MW'};
technology.Tags(nc).Status = {'CST'};
technology.Tags(nc).isVIT = 1;

nc = nc+1;
technology.Tags(nc).DisplayName = {'relative industry heating demand'};
technology.Tags(nc).Description = technology.Tags(nc).DisplayName;
technology.Tags(nc).TagName = {'lambda_ind_q'};
technology.Tags(nc).DefaultValue = 0.7;     %[-]
technology.Tags(nc).Unit = {'-'};
technology.Tags(nc).Status = {'CST'};
technology.Tags(nc).isVIT = 1;


nc = nc+1;
technology.Tags(nc).DisplayName = {'industry low temperature (35C) heat
demand'};
technology.Tags(nc).Description = technology.Tags(nc).DisplayName;
technology.Tags(nc).TagName = {'eta_ind_lt'};
technology.Tags(nc).DefaultValue = 0.24;      % [MJ/s]
technology.Tags(nc).Unit = {'-'};
technology.Tags(nc).Status = {'CST'};
technology.Tags(nc).isVIT = 1;

nc = nc+1;
technology.Tags(nc).DisplayName = {'industry medium temperature (60C) heat
demand'};
technology.Tags(nc).Description = technology.Tags(nc).DisplayName;
technology.Tags(nc).TagName = {'eta_ind_mt'};
technology.Tags(nc).DefaultValue = 0.37;      % [MJ/s]
technology.Tags(nc).Unit = {'-'};
technology.Tags(nc).Status = {'CST'};
technology.Tags(nc).isVIT = 1;

nc = nc+1;
technology.Tags(nc).DisplayName = {'industry high temperature (110C) heat
demand'};
technology.Tags(nc).Description = technology.Tags(nc).DisplayName;
technology.Tags(nc).TagName = {'eta_ind_ht'};
technology.Tags(nc).DefaultValue = 0.04;      % [MJ/s]
technology.Tags(nc).Unit = {'-'};
technology.Tags(nc).Status = {'CST'};
technology.Tags(nc).isVIT = 1;

nc = nc+1;
technology.Tags(nc).DisplayName = {'district heating generation potential
from high temperature heating demands'};
technology.Tags(nc).Description = technology.Tags(nc).DisplayName;
technology.Tags(nc).TagName = {'eta_ind_dh'};
technology.Tags(nc).DefaultValue = 1;       %[-]
```

```
technology.Tags(nc).Unit = {'-'};
technology.Tags(nc).Status = {'CST'};
technology.Tags(nc).isVIT = 1;

nc = nc+1;
technology.Tags(nc).DisplayName = {'industry gas boiler operating cost'};
technology.Tags(nc).Description = technology.Tags(nc).DisplayName;
technology.Tags(nc).TagName = {'c_op_gb'};
technology.Tags(nc).DefaultValue = 0.5;      % [Euro/MJ/s]
technology.Tags(nc).Unit = {'Euro/MWh'};
technology.Tags(nc).Status = {'CST'};
technology.Tags(nc).isVIT = 1;
%% Industry heat pump tags
nc = nc+1;
technology.Tags(nc).DisplayName    =    {'industry    heat    pump    reference
dimension'};
technology.Tags(nc).Description = technology.Tags(nc).DisplayName;
technology.Tags(nc).TagName = {'sigma_hp_ref'};
technology.Tags(nc).DefaultValue = 1;      % [MW]
technology.Tags(nc).Unit = {'MEuro'};
technology.Tags(nc).Status = {'CST'};
technology.Tags(nc).isVIT = 1;

nc = nc+1;
technology.Tags(nc).DisplayName = {'industry heat pump reference investment
cost'};
technology.Tags(nc).Description = technology.Tags(nc).DisplayName;
technology.Tags(nc).TagName = {'c_inv0_hp'};
technology.Tags(nc).DefaultValue = 0.43;      % [MEuro]
technology.Tags(nc).Unit = {'MEuro'};
technology.Tags(nc).Status = {'CST'};
technology.Tags(nc).isVIT = 1;

nc = nc+1;
technology.Tags(nc).DisplayName = {'industry heat pump operating cost'};
technology.Tags(nc).Description = technology.Tags(nc).DisplayName;
technology.Tags(nc).TagName = {'c_op_hp_an'};
technology.Tags(nc).DefaultValue = 0.0049;
technology.Tags(nc).Unit = {'MEuro/MW'};
technology.Tags(nc).Status = {'CST'};
technology.Tags(nc).isVIT = 1;

nc = nc+1;
technology.Tags(nc).DisplayName = {'industry heat pump COP'};
technology.Tags(nc).Description = technology.Tags(nc).DisplayName;
technology.Tags(nc).TagName = {'cop'};
technology.Tags(nc).DefaultValue = 2.9;     % [-]
technology.Tags(nc).Unit = {'-'};
technology.Tags(nc).Status = {'CST'};
technology.Tags(nc).isVIT = 1;
%% Infrastructure tags
nc = nc+1;
technology.Tags(nc).DisplayName    =    {'district    heating    connection
investment'};
technology.Tags(nc).Description = technology.Tags(nc).DisplayName;
technology.Tags(nc).TagName = {'c_inv0_dh'};
```

```
technology.Tags(nc).DefaultValue = 1.76;     % [MEuro]
technology.Tags(nc).Unit = {'MEuro'};
technology.Tags(nc).Status = {'CST'};
technology.Tags(nc).isVIT = 1;

nc = nc+1;
technology.Tags(nc).DisplayName = {'syngas connection investment'};
technology.Tags(nc).Description = technology.Tags(nc).DisplayName;
technology.Tags(nc).TagName = {'c_inv0_syngas'};
technology.Tags(nc).DefaultValue = 1.17;     % [MEuro]
technology.Tags(nc).Unit = {'MEuro'};
technology.Tags(nc).Status = {'CST'};
technology.Tags(nc).isVIT = 1;
%% DH model tags
nc = nc+1;
technology.Tags(nc).DisplayName = {'District heating relative demand'};
technology.Tags(nc).Description = technology.Tags(nc).DisplayName;
technology.Tags(nc).TagName = {'lambda_DH'};
technology.Tags(nc).DefaultValue = 0.7;       % [-]
technology.Tags(nc).Unit = {''};
technology.Tags(nc).Status = {'CST'};
technology.Tags(nc).isVIT = 1;

nc = nc+1;
technology.Tags(nc).DisplayName   =   {'District   heating   maximum   demand
[MJ/s]'};
technology.Tags(nc).Description = technology.Tags(nc).DisplayName;
technology.Tags(nc).TagName = {'sigma_dh'};
technology.Tags(nc).DefaultValue = 33;  % [MJ/s]
technology.Tags(nc).Unit = {'MJ/s'};
technology.Tags(nc).Status = {'CST'};
technology.Tags(nc).isVIT = 1;

nc = nc+1;
technology.Tags(nc).DisplayName  =  {'District  heating  forward  tempeature  [-
]'};
technology.Tags(nc).Description = technology.Tags(nc).DisplayName;
technology.Tags(nc).TagName = {'T_fw'};
technology.Tags(nc).DefaultValue = 90-6.5;  % [C]
technology.Tags(nc).Unit = {'C'};
technology.Tags(nc).Status = {'CST'};
technology.Tags(nc).isVIT = 1;

nc = nc+1;
technology.Tags(nc).DisplayName  =  {'District  heating  return  tempeature  [-
]'};
technology.Tags(nc).Description = technology.Tags(nc).DisplayName;
technology.Tags(nc).TagName = {'T_rt'};
technology.Tags(nc).DefaultValue = 40-6.5;  % [C]
technology.Tags(nc).Unit = {'C'};
technology.Tags(nc).Status = {'CST'};
technology.Tags(nc).isVIT = 1;
%% Rankine model tags
nc = nc+1;
technology.Tags(nc).DisplayName  =  {'total  Rankine  system  waste  capacity
[MJ/s waste]'};
```

```
technology.Tags(nc).Description = technology.Tags(nc).DisplayName;
technology.Tags(nc).TagName = {'sigma_ran'};
technology.Tags(nc).DefaultValue = 33.3;  % [MJ/s]
technology.Tags(nc).Unit = {'-'};
technology.Tags(nc).Status = {'CST'};
technology.Tags(nc).isVIT = 1;

nc = nc+1;
technology.Tags(nc).DisplayName    =    {'Rankine    minumum    load    (waste
incineration-based)'};
technology.Tags(nc).Description = technology.Tags(nc).DisplayName;
technology.Tags(nc).TagName = {'lambda_min_ran'};
technology.Tags(nc).DefaultValue = 0.75;  % [-]
technology.Tags(nc).Unit = {'-'};
technology.Tags(nc).Status = {'CST'};
technology.Tags(nc).isVIT = 1;

nc = nc+1;
technology.Tags(nc).DisplayName   =   {'Rankine   variable   operating   cost
[Euro/MWh input waste]'};
technology.Tags(nc).Description = technology.Tags(nc).DisplayName;
technology.Tags(nc).TagName = {'c_op_ran'};
technology.Tags(nc).DefaultValue = 15.9;  % [Euro/MWh input waste]
technology.Tags(nc).Unit = {'Euro/MWh input waste'};
technology.Tags(nc).Status = {'CST'};
technology.Tags(nc).isVIT = 1;

nc = nc+1;
technology.Tags(nc).DisplayName   =   {'Rankine   high-pressure   condensing
temperature'};
technology.Tags(nc).Description = technology.Tags(nc).DisplayName;
technology.Tags(nc).TagName = {'T_cond_hp'};
technology.Tags(nc).DefaultValue = 93.5;  % [C]
technology.Tags(nc).Unit = {'-'};
technology.Tags(nc).Status = {'CST'};
technology.Tags(nc).isVIT = 1;

nc = nc+1;
technology.Tags(nc).DisplayName    =    {'Rankine    low-pressure    condensing
temperature'};
technology.Tags(nc).Description = technology.Tags(nc).DisplayName;
technology.Tags(nc).TagName = {'T_cond_lp'};
technology.Tags(nc).DefaultValue = 69.1;  % [C]
technology.Tags(nc).Unit = {'-'};
technology.Tags(nc).Status = {'CST'};
technology.Tags(nc).isVIT = 1;

nc = nc+1;
technology.Tags(nc).DisplayName  =  {'Rankine  condenser  heat  flow,  high
pressure'};
technology.Tags(nc).Description = technology.Tags(nc).DisplayName;
technology.Tags(nc).TagName = {'Q_cond_hp'};
technology.Tags(nc).DefaultValue = 18.75;  % [MJ/s]
technology.Tags(nc).Unit = {'-'};
technology.Tags(nc).Status = {'CST'};
technology.Tags(nc).isVIT = 1;
```

```
nc = nc+1;
technology.Tags(nc).DisplayName  =  {'Rankine  condenser  heat  flow,  low
pressure'};
technology.Tags(nc).Description = technology.Tags(nc).DisplayName;
technology.Tags(nc).TagName = {'Q_cond_lp'};
technology.Tags(nc).DefaultValue = 6.25;  % [MJ/s]
technology.Tags(nc).Unit = {'-'};
technology.Tags(nc).Status = {'CST'};
technology.Tags(nc).isVIT = 1;

nc = nc+1;
technology.Tags(nc).DisplayName = {'Rankine power generation'};
technology.Tags(nc).Description = technology.Tags(nc).DisplayName;
technology.Tags(nc).TagName = {'P_ran'};
technology.Tags(nc).DefaultValue = 7;  % [MW]
technology.Tags(nc).Unit = {'-'};
technology.Tags(nc).Status = {'CST'};
technology.Tags(nc).isVIT = 1;
%% GT model tags
nc = nc+1;
technology.Tags(nc).DisplayName  =  {'Gas  turbine  nominal  capacity  [MJ/s
fuel]'};
technology.Tags(nc).Description = technology.Tags(nc).DisplayName;
technology.Tags(nc).TagName = {'sigma_gt'};
technology.Tags(nc).DefaultValue = 20;       % [MJ/s fuel]
technology.Tags(nc).Unit = {'-'};
technology.Tags(nc).Status = {'CST'};
technology.Tags(nc).isVIT = 1;

nc = nc+1;
technology.Tags(nc).DisplayName  =  {'Gas  turbine  nominal  power  generation
[MW]'};
technology.Tags(nc).Description = technology.Tags(nc).DisplayName;
technology.Tags(nc).TagName = {'P_gt'};
technology.Tags(nc).DefaultValue = 8;   % [MW]
technology.Tags(nc).Unit = {'-'};
technology.Tags(nc).Status = {'CST'};
technology.Tags(nc).isVIT = 1;

nc = nc+1;
technology.Tags(nc).DisplayName  =  {'Gas  turbine  nominal  heat  generation
[MJ/s]'};
technology.Tags(nc).Description = technology.Tags(nc).DisplayName;
technology.Tags(nc).TagName = {'Q_gt'};
technology.Tags(nc).DefaultValue = 8;           % [MJ/s]
technology.Tags(nc).Unit = {'-'};
technology.Tags(nc).Status = {'CST'};
technology.Tags(nc).isVIT = 1;

nc = nc+1;
technology.Tags(nc).DisplayName = {'Gas turbine variable operating cost [-
]'};
technology.Tags(nc).Description = technology.Tags(nc).DisplayName;
technology.Tags(nc).TagName = {'c_op_gt'};
technology.Tags(nc).DefaultValue = 7;           % [Euro/MWh fuel]
```

```
technology.Tags(nc).Unit = {'-'};
technology.Tags(nc).Status = {'CST'};
technology.Tags(nc).isVIT = 1;

nc = nc+1;
technology.Tags(nc).DisplayName = {'Gas turbine minumum load [-]'};
technology.Tags(nc).Description = technology.Tags(nc).DisplayName;
technology.Tags(nc).TagName = {'lambda_min_gt'};
technology.Tags(nc).DefaultValue = 0.40;        % [-]
technology.Tags(nc).Unit = {'-'};
technology.Tags(nc).Status = {'CST'};
technology.Tags(nc).isVIT = 1;

nc = nc+1;
technology.Tags(nc).DisplayName = {'Gas turbine offgas temperature [C]'};
technology.Tags(nc).Description = technology.Tags(nc).DisplayName;
technology.Tags(nc).TagName = {'T_max_gt'};
technology.Tags(nc).DefaultValue = 600;         % [-]
technology.Tags(nc).Unit = {'-'};
technology.Tags(nc).Status = {'CST'};
technology.Tags(nc).isVIT = 1;

nc = nc+1;
technology.Tags(nc).DisplayName = {'Gas turbine exhaust temperature [C]'};
technology.Tags(nc).Description = technology.Tags(nc).DisplayName;
technology.Tags(nc).TagName = {'T_min_gt'};
technology.Tags(nc).DefaultValue = 70;          % [-]
technology.Tags(nc).Unit = {'-'};
technology.Tags(nc).Status = {'CST'};
technology.Tags(nc).isVIT = 1;
%% Biorefinery model tags
nc = nc+1;
technology.Tags(nc).TagName       = {'eta_gasifier_syn'};
technology.Tags(nc).DisplayName   = {'biomass to syngas energy efficiency'};
technology.Tags(nc).DefaultValue  = 0.9294;
technology.Tags(nc).Unit          = {'-'};
technology.Tags(nc).Status        = {'CST'};
technology.Tags(nc).isVIT         = 1;

nc = nc+1;
technology.Tags(nc).TagName       = {'eta_soec'};
technology.Tags(nc).DisplayName   = {'soec energy converted to hydrogen'};
technology.Tags(nc).DefaultValue  = 0.92;
technology.Tags(nc).Unit          = {'-'};
technology.Tags(nc).Status        = {'CST'};
technology.Tags(nc).isVIT         = 1;

nc = nc+1;
technology.Tags(nc).TagName       = {'sigma_bio_ref'};
technology.Tags(nc).DisplayName   = {'biorefinery reference dimension'};
technology.Tags(nc).DefaultValue  = 360; %[MW biomass]
technology.Tags(nc).Unit          = {'-'};
technology.Tags(nc).Status        = {'CST'};
technology.Tags(nc).isVIT         = 1;

nc = nc+1;
```

```
technology.Tags(nc).TagName       = {'c_inv0_bio'};
technology.Tags(nc).DisplayName      =  {'biorefinery  reference  investment
cost'};
technology.Tags(nc).DefaultValue  = 314.9; %[MEuro]
technology.Tags(nc).Unit          = {'-'};
technology.Tags(nc).Status        = {'CST'};
technology.Tags(nc).isVIT         = 1;

nc = nc+1;
technology.Tags(nc).TagName       = {'c_op0_bio'};
technology.Tags(nc).DisplayName   = {'biorefinery reference annual operating
costs'};
technology.Tags(nc).DefaultValue  = 9.2; %[MEuro/year]
technology.Tags(nc).Unit          = {'-'};
technology.Tags(nc).Status        = {'CST'};
technology.Tags(nc).isVIT         = 1;

nc = nc+1;
technology.Tags(nc).TagName       = {'c_woodchips'};
technology.Tags(nc).DisplayName   = {'biorefinery reference annual operating
costs'};
technology.Tags(nc).DefaultValue  = 6.87; %[Euro/GJ]
technology.Tags(nc).Unit          = {'-'};
technology.Tags(nc).Status        = {'CST'};
technology.Tags(nc).isVIT         = 1;
%% Economy and operation tags
nc = nc+1;
technology.Tags(nc).TagName       = {'t_lifetime'};
technology.Tags(nc).DisplayName   = {'plant technical lifetime in years'};
technology.Tags(nc).DefaultValue  = 20;
technology.Tags(nc).Unit          = {'years'};
technology.Tags(nc).Status        = {'CST'};
technology.Tags(nc).isVIT         = 1;

nc = nc+1;
technology.Tags(nc).DisplayName   =   {'reference   investment   cost   power
factor'};
technology.Tags(nc).Description = technology.Tags(nc).DisplayName;
technology.Tags(nc).TagName = {'pf0'};
technology.Tags(nc).DefaultValue = 0.75;
technology.Tags(nc).Unit = {'-'};
technology.Tags(nc).Status = {'CST'};
technology.Tags(nc).isVIT = 1;

nc = nc+1;
technology.Tags(nc).TagName       = {'interest_rate'};
technology.Tags(nc).DisplayName   = {'interest rate'};
technology.Tags(nc).DefaultValue  = 0.05;
technology.Tags(nc).Unit          = {'-'};
technology.Tags(nc).Status        = {'CST'};
technology.Tags(nc).isVIT         = 1;

nc = nc+1;
technology.Tags(nc).TagName       = {'c_power'};
technology.Tags(nc).DisplayName   = {'power price [Euro/MWh]'};
technology.Tags(nc).DefaultValue  = 39.0;
```

```
technology.Tags(nc).Unit          = {'Euro/MWh'};
technology.Tags(nc).Status        = {'CST'};
technology.Tags(nc).isVIT         = 1;

nc = nc+1;
technology.Tags(nc).TagName       = {'c_gas'};
technology.Tags(nc).DisplayName   = {'natural gas price [Euro/GJ]'};
technology.Tags(nc).DefaultValue  = 9.94;
technology.Tags(nc).Unit          = {'Euro/GJ'};
technology.Tags(nc).Status        = {'CST'};
technology.Tags(nc).isVIT         = 1;

nc = nc+1;
technology.Tags(nc).TagName       = {'c_methanol'};
technology.Tags(nc).DisplayName   = {'methanol price [Euro/GJ]'};
technology.Tags(nc).DefaultValue  = 24.02;
technology.Tags(nc).Unit          = {'Euro/GJ'};
technology.Tags(nc).Status        = {'CST'};
technology.Tags(nc).isVIT         = 1;

% period tags
nc = nc+1;
technology.Tags(nc).TagName       = {'dt'};
technology.Tags(nc).DisplayName   = {'Period duration'};
technology.Tags(nc).DefaultValue  = 1;
technology.Tags(nc).Unit          = {'h'};
technology.Tags(nc).Status        = {'CST'};
technology.Tags(nc).isVIT         = 1;

nc = nc+1;
technology.Tags(nc).TagName       = {'pv'};
technology.Tags(nc).DisplayName   = {'Present value factor'};
technology.Tags(nc).DefaultValue  = 1;
technology.Tags(nc).Unit          = {'h'};
technology.Tags(nc).Status        = {'CST'};
technology.Tags(nc).isVIT         = 1;
%% Environmental impact tags
nc = nc+1;
technology.Tags(nc).TagName       = {'alpha_gas'};
technology.Tags(nc).DisplayName     = {'Marginal CO2 emission from natural
gas'};
technology.Tags(nc).DefaultValue  = 57.0;
technology.Tags(nc).Unit          = {'kg/GJ'};
technology.Tags(nc).Status        = {'CST'};
technology.Tags(nc).isVIT         = 1;

nc = nc+1;
technology.Tags(nc).TagName       = {'alpha_meoh'};
technology.Tags(nc).DisplayName     = {'Marginal CO2 emission from natural
gas'};
technology.Tags(nc).DefaultValue  = 73.0;
technology.Tags(nc).Unit          = {'kg/GJ'};
technology.Tags(nc).Status        = {'CST'};
technology.Tags(nc).isVIT         = 1;

nc = nc+1;
```

```
technology.Tags(nc).TagName       = {'alpha_w'};
technology.Tags(nc).DisplayName   = {'Marginal CO2 emission from waste'};
technology.Tags(nc).DefaultValue  = 37.0;
technology.Tags(nc).Unit          = {'kg/GJ'};
technology.Tags(nc).Status        = {'CST'};
technology.Tags(nc).isVIT         = 1;

nc = nc+1;
technology.Tags(nc).TagName       = {'alpha_p'};
technology.Tags(nc).DisplayName     = {'Marginal CO2 emission from power
production in the energy system'};
technology.Tags(nc).DefaultValue  = 413;
technology.Tags(nc).Unit          = {'kg/MWh'};
technology.Tags(nc).Status        = {'CST'};
technology.Tags(nc).isVIT         = 1;
%% Output tags

nc = nc+1;
technology.Tags(nc).TagName       = {'NPV'};
technology.Tags(nc).DisplayName   = {'Net Present Value'};
technology.Tags(nc).Unit          = {'-'};
technology.Tags(nc).Status        = {'off'};

nc = nc+1;
technology.Tags(nc).TagName       = {'c_operation'};
technology.Tags(nc).DisplayName   = {'period-wise operation result'};
technology.Tags(nc).Unit          = {'-'};
technology.Tags(nc).Status        = {'off'};

nc = nc+1;
technology.Tags(nc).TagName       = {'c_operation_pv'};
technology.Tags(nc).DisplayName    = {'period-wise present value operation
result'};
technology.Tags(nc).Unit          = {'-'};
technology.Tags(nc).Status        = {'off'};

nc = nc+1;
technology.Tags(nc).TagName       = {'c_operation_an'};
technology.Tags(nc).DisplayName   = {'total annual operation result'};
technology.Tags(nc).Unit          = {'-'};
technology.Tags(nc).Status        = {'off'};

nc = nc+1;
technology.Tags(nc).TagName       = {'c_op_tot_pv'};
technology.Tags(nc).DisplayName   = {'total NPV operation result'};
technology.Tags(nc).Unit          = {'-'};
technology.Tags(nc).Status        = {'off'};

nc = nc+1;
technology.Tags(nc).TagName       = {'hex_inv'};
technology.Tags(nc).DisplayName    = {'heat exchanger network investment cost
(period-wise extraction)'};
technology.Tags(nc).Unit          = {'-'};
technology.Tags(nc).Status        = {'off'};

nc = nc+1;
```

```
technology.Tags(nc).TagName       = {'I0_hex'};
technology.Tags(nc).DisplayName       =  {'heat  exchanger  network  total
investment cost'};
technology.Tags(nc).Unit          = {'-'};
technology.Tags(nc).Status        = {'off'};

nc = nc+1;
technology.Tags(nc).TagName       = {'I0_tot'};
technology.Tags(nc).DisplayName   = {'total investment cost'};
technology.Tags(nc).Unit          = {'-'};
technology.Tags(nc).Status        = {'off'};

nc = nc+1;
technology.Tags(nc).TagName       = {'co2_imp'};
technology.Tags(nc).DisplayName   = {'CO2 emission from imported products'};
technology.Tags(nc).Unit          = {'kg'};
technology.Tags(nc).Status        = {'off'};

nc = nc+1;
technology.Tags(nc).TagName       = {'co2_exp'};
technology.Tags(nc).DisplayName    = {'avoided CO2 emission from exported
products'};
technology.Tags(nc).Unit          = {'kg'};
technology.Tags(nc).Status        = {'off'};

nc = nc+1;
technology.Tags(nc).TagName       = {'power_net'};
technology.Tags(nc).DisplayName   = {'period-wise power generation'};
technology.Tags(nc).Unit          = {'GWh'};
technology.Tags(nc).Status        = {'off'};

nc = nc+1;
technology.Tags(nc).TagName       = {'heat_net'};
technology.Tags(nc).DisplayName   = {'period-wise heat generation'};
technology.Tags(nc).Unit          = {'GJ'};
technology.Tags(nc).Status        = {'off'};

nc = nc+1;
technology.Tags(nc).TagName       = {'waste_net'};
technology.Tags(nc).DisplayName   = {'period-wise waste consumption'};
technology.Tags(nc).Unit          = {'ton'};
technology.Tags(nc).Status        = {'off'};

nc = nc+1;
technology.Tags(nc).TagName       = {'co2_net'};
technology.Tags(nc).DisplayName   = {'period-wise co2 emission result'};
technology.Tags(nc).Unit          = {'ton'};
technology.Tags(nc).Status        = {'off'};

nc = nc+1;
technology.Tags(nc).TagName       = {'power_tot'};
technology.Tags(nc).DisplayName   = {'total power generation'};
technology.Tags(nc).Unit          = {'GWh'};
technology.Tags(nc).Status        = {'off'};

nc = nc+1;
```

```
technology.Tags(nc).TagName       = {'heat_tot'};
technology.Tags(nc).DisplayName   = {'total heat generation'};
technology.Tags(nc).Unit          = {'GJ'};
technology.Tags(nc).Status        = {'off'};

nc = nc+1;
technology.Tags(nc).TagName       = {'waste_tot'};
technology.Tags(nc).DisplayName   = {'period-wise waste consumption'};
technology.Tags(nc).Unit          = {'ton'};
technology.Tags(nc).Status        = {'off'};

nc = nc+1;
technology.Tags(nc).TagName       = {'co2_tot'};
technology.Tags(nc).DisplayName   = {'total CO2 emissions'};
technology.Tags(nc).Unit          = {'ton'};
technology.Tags(nc).Status        = {'off'};



%%                              STREAMS
%% Heat streams (CHP)
% (type of stream, utility name, stream name, Tin, Hin, Tout, Hout, DeltaT,
% optional heat transfer coefficient)

% district heating utility generation
ns = ns+1;
technology.EI.Streams(ns).Short                                          =
{'qt','dh_util','dh_cold','@T_rt+273.15','0','@T_fw+273.15','1','@dt_min_2'}
;

% Rankine heat generation
ns = ns+1;
technology.EI.Streams(ns).Short                                          =
{'qt','ran','ran_cond_hp','@T_cond_hp+273.15','@Q_cond_hp','@T_cond_hp+273.1
5','0','@dt_min_2'};
ns = ns+1;
technology.EI.Streams(ns).Short                                          =
{'qt','ran','ran_cond_lp','@T_cond_lp+273.15','@Q_cond_lp','@T_cond_lp+273.1
5','0','@dt_min_2'};

% gas turbine offgas heat
ns = ns+1;
technology.EI.Streams(ns).Short                                          =
{'qt','gt','gt_off','@T_max_gt+273.15','@Q_gt','@T_min_gt+273.15','0','@dt_m
in_2'};

% cold water utility
ns = ns+1;
technology.EI.Streams(ns).Short                                          =
{'qt','water','cold_utility_stream','15+273.15','0','15+273.15','1','@dt_min
_2'};


% BIOREFINERY
% gasifier
ns = ns+1;
```

```
technology.EI.Streams(ns).Short                                                    =
{'qt','gasifier','b','115+273.15','0','200+273.15','0.118*@sigma_bio','@dt_m
in_2'};
ns = ns+1;
technology.EI.Streams(ns).Short                                                    =
{'qt','gasifier','c','236+273.15','0.02*@sigma_bio','127+273.15','0','@dt_mi
n_2'};
ns = ns+1;
technology.EI.Streams(ns).Short                                                    =
{'qt','gasifier','d','114+273.15','0.0624*@sigma_bio','40+273.15','0','@dt_m
in_2'};

% methanol
ns = ns+1;
technology.EI.Streams(ns).Short                                                    =
{'qt','meth_0','g','220+273.15','0.0704*@sigma_bio','220+273.15','0','@dt_mi
n_2'};
ns = ns+1;
technology.EI.Streams(ns).Short                                                    =
{'qt','meth_0','h','110+273.15','0.0758*@sigma_bio','40+273.15','0','@dt_min
_2'};
ns = ns+1;
technology.EI.Streams(ns).Short                                                    =
{'qt','meth_0','j','84+273.15','0','84+273.15','0.01*@sigma_bio','@dt_min_2'
};
ns = ns+1;
technology.EI.Streams(ns).Short                                                    =
{'qt','meth_0','k','40+273.15','0','320+273.15','0.0334*@sigma_bio','@dt_min
_2'};
ns = ns+1;
technology.EI.Streams(ns).Short                                                    =
{'qt','meth_0','n','153+273.15','0.112*@sigma_bio','40+273.15','0','@dt_min_
2'};

% reacted syngas flare
ns = ns+1;
technology.EI.Streams(ns).Short                                                    =
{'qt','synre_flare','z','600+273.15','1','70+273.15','0','@dt_min_2'};

% soec heat
ns = ns+1;
technology.EI.Streams(ns).Short                                                    =
{'qt','soec','soec_heat','200+273.15','0.5*@sigma_bio*((1-
@eta_soec)/@eta_soec)','40+273.15','0','@dt_min_2'};
%% District heating heat layer

% district heating demand
ns = ns+1;
technology.EI.Streams(ns).Short                                                    =
{'mass','heat_dh','dh','dh_demand','in','@sigma_dh*@lambda_dh'}; % MW

% district heating utility generation
ns = ns+1;
technology.EI.Streams(ns).Short                                                    =
{'mass','heat_dh','dh_util','dh_utility','out','1'}; % MW
```

```
% industrial heat pump dh demand
ns = ns+1;
technology.EI.Streams(ns).Short                                                 =
{'mass','heat_dh','ind_hp','ind_hp_cold','in','1*((@cop-1)/@cop)'};

% industrial heating dh demand
ns = ns+1;
technology.EI.Streams(ns).Short                                                 =
{'mass','heat_dh','ind_dh','ind_dh_cold','in','1'};

% industrial dh generation
ns = ns+1;
technology.EI.Streams(ns).Short                                                 =
{'mass','heat_dh','ind','ind_dh_gen','out','@omega_dh*@sigma_ind_q*@lambda_i
nd_q*(@eta_ind_ht*@eta_ind_dh)'};
%% Waste streams
% fixed waste processing
ns = ns+1;
technology.EI.Streams(ns).Short                                                 =
{'mass','waste','w_fix','waste_fixed','out','@sigma_ran*0.75'}; % kW
ns = ns+1;
technology.EI.Streams(ns).Short                                                 =
{'mass','waste','w_flex','waste_flexible','out','@sigma_ran*0.25'}; % kW

% Rankine waste consumption
ns = ns+1;
technology.EI.Streams(ns).Short                                                 =
{'mass','waste','ran','ran_waste_consumption','in','@sigma_ran'}; % kW
%% Industrial utility layer

% industry utility demand
ns = ns+1;
technology.EI.Streams(ns).Short                                                 =
{'mass','heat_ind','ind','ind_lt','in','@sigma_ind_q*@lambda_ind_q'}; % MW

% industry gas boiler
ns = ns+1;
technology.EI.Streams(ns).Short                                                 =
{'mass','heat_ind','ind_gb','heat_ind_gb','out','1'}; % MW

% industry district heating consumption
ns = ns+1;
technology.EI.Streams(ns).Short                                                 =
{'mass','heat_ind','ind_dh','heat_ind_dh','out','1*@omega_dh'}; % kW

% industry heat pumps
ns = ns+1;
technology.EI.Streams(ns).Short                                                 =
{'mass','heat_ind','ind_hp','heat_ind_hp','out','1*@omega_dh'}; % kW
%% Power streams
%                       technology.EI.Streams(ns).Short                         =
{'mass','[layertagname]','[parentunit]','[tagnamestream]',['in'             or
'out'],'[size]'}; % kW

% Rankine and gas turbine power generation
ns = ns+1;
```

```
technology.EI.Streams(ns).Short                                                =
{'mass','power','ran','power_ran','out','@P_ran'}; % MW
ns = ns+1;
technology.EI.Streams(ns).Short                                                =
{'mass','power','gt','power_gt','out','@P_gt'}; % MW

% industrial heat pump power consumption
ns = ns+1;
technology.EI.Streams(ns).Short                                                =
{'mass','power','ind_hp','power_hp','in','1/@cop'}; % MW

% biorefinery power flows
% methanol production
ns = ns+1;
technology.EI.Streams(ns).Short                                                =
{'mass','power','meth_0','power_meth','in','0.0958*@sigma_bio'}; % MW

% soec
ns = ns+1;
technology.EI.Streams(ns).Short                                                =
{'mass','power','soec','power_soec','in','0.5*@sigma_bio/@eta_soec'}; % MW

% power markets
ns = ns+1;
technology.EI.Streams(ns).Short                                                =
{'mass','power','p_imp','power_im','out','1'}; % MW
ns = ns+1;
technology.EI.Streams(ns).Short                                                =
{'mass','power','p_exp','power_ex','in','1'}; % MW
%% Natural gas streams

% natural gas consumption, gas turbine
ns = ns+1;
technology.EI.Streams(ns).Short                                                =
{'mass','gas','gt','gt_gas','in','@sigma_gt'}; % MW

% Natural gas consumption, industry gas boiler
ns = ns+1;
technology.EI.Streams(ns).Short                                                =
{'mass','gas','ng_to_indgas','ng_to_indgas_in','in','1'}; % MW

% Gas import
ns = ns+1;
technology.EI.Streams(ns).Short                                                =
{'mass','gas','gas_imp','gas_import','out','1'}; % MW
%% Industry gas streams
% Industry gas boiler consumption
ns = ns+1;
technology.EI.Streams(ns).Short                                                =
{'mass','indgas','ind_gb','ind_gb_indgas','in','1'}; % MW

% Natural gas to industry gas
ns = ns+1;
technology.EI.Streams(ns).Short                                                =
{'mass','indgas','ng_to_indgas','indgas_from_ng','out','1'}; % MW
```

```
% Syngas to industry gas
ns = ns+1;
technology.EI.Streams(ns).Short                                                 =
{'mass','indgas','syn_to_indgas','syn_to_indgas_out','out','1*@omega_syngas'
}; % MW

% Reacted syngas to industry gas
ns = ns+1;
technology.EI.Streams(ns).Short                                                 =
{'mass','indgas','synre_to_indgas','synre_to_indgas_out','out','1*@omega_syn
gas'}; % MW
%% Syngas streams
% Gasifier syngas generation
ns = ns+1;
technology.EI.Streams(ns).Short                                                 =
{'mass','syngas','gasifier','gasifier_syngas','out','@eta_gasifier_syn*@sigm
a_bio'}; % kW

% Syngas to industry gas
ns = ns+1;
technology.EI.Streams(ns).Short                                                 =
{'mass','syngas','syn_to_indgas','syn_to_indgas_in','in','1*@omega_syngas'};
 % MW

% Syngas to methanol
ns = ns+1;
technology.EI.Streams(ns).Short                                                 =
{'mass','syngas','meth_0','syn_to_meth0','in','@eta_gasifier_syn*@sigma_bio'
}; % MW
%% Reacted syngas streams

% Reacted syngas from methanol production
ns = ns+1;
technology.EI.Streams(ns).Short                                                 =
{'mass','syngas_re','meth_0','synre_from_meth0','out','0.24*@sigma_bio'};   %
MW

% Reacted syngas to industry gas
ns = ns+1;
technology.EI.Streams(ns).Short                                                 =
{'mass','syngas_re','synre_to_indgas','synre_to_indgas_in','in','1*@omega_sy
ngas'}; % MW

% flare of unused reacted syngas
ns = ns+1;
technology.EI.Streams(ns).Short                                                 =
{'mass','syngas_re','synre_flare','synre_flare_burn','in','1'}; % MW

% reacted syngas to methanol in oxygen-boosted gasification
ns = ns+1;
technology.EI.Streams(ns).Short                                                 =
{'mass','syngas_re','meth_o2','synre_to_meth_o2','in','0.22*@sigma_bio'};   %
MW
%% Oxygen streams

% Oxygen from SOEC
```

```
ns = ns+1;
technology.EI.Streams(ns).Short                                                    =
{'mass','o2','soec','soec_o2','out','0.0337*@sigma_bio'}; % kg/s

% Oxygen for gasification
ns = ns+1;
technology.EI.Streams(ns).Short                                                    =
{'mass','o2','meth_o2','meth_o2_ox','in','0.0124*@sigma_bio'}; % kg/s

% Oxygen exhaust
ns = ns+1;
technology.EI.Streams(ns).Short                                                    =
{'mass','o2','o2_ex','o2_exhaust','in','1'}; % MW
%% Hydrogen streams

% hydrogen from SOEC
ns = ns+1;
technology.EI.Streams(ns).Short                                                    =
{'mass','h2','soec','soec_h2','out','0.5*@sigma_bio'}; % kg/s

% Hydrogen for oxified gasification
ns = ns+1;
technology.EI.Streams(ns).Short                                                    =
{'mass','h2','meth_o2','meth_o2_h','in','0.367*0.5*@sigma_bio'}; % MW

% Hydrogen for hydrogen-boosted methanol production
ns = ns+1;
technology.EI.Streams(ns).Short                                                    =
{'mass','h2','meth_h2','meth_h2_in','in','0.633*0.5*@sigma_bio'}; % MW
%% Methanol streams

% methanol from standard production
ns = ns+1;
technology.EI.Streams(ns).Short                                                    =
{'mass','methanol','meth_0','syn_to_meth','out','0.56*@sigma_bio'}; % MW

% methanol sales
ns = ns+1;
technology.EI.Streams(ns).Short                                                    =
{'mass','methanol','meth_r','meth_sales','in','1'}; % MW

% methanol from oxygen-boosted production
ns = ns+1;
technology.EI.Streams(ns).Short                                                    =
{'mass','methanol','meth_o2','syn_to_meth_o2','out','0.34*@sigma_bio'}; % MW
%
% methanol from hydrogen-boosted production
ns = ns+1;
technology.EI.Streams(ns).Short                                                    =
{'mass','methanol','meth_h2','syn_to_meth_h2','out','0.32*@sigma_bio'}; % MW
```

fmg_postcompute.m

```
function o=fmg_postcompute(o)
%% Initialization

technology=o.Model(o.ModelID);
s = ET_generateVariablesFromTags(technology.Tags);
eval([s]);
% get the values of the tags as matlab variables
% /!\ In the compute, the tagnames of the tags must not be written with big
characters.ex: the tag 'Tsat' must be written 'tsat' in the compute.



%% Heat exchagner network investment

% heat exchange network investmentcost
% warning off all;
c = cost_defaults;

% HEAT EXCHANGER COSTS
HTX_AREA=osmose_getTag(o,'EI:DefaultHeatCascade_HENArea_Bath');
 m.HTX_AREA_TOTAL=HTX_AREA.Value;

 HTX_NMINMER=osmose_getTag(o,'EI:DefaultHeatCascade_NMinMER');
 m.HTX_NMINMER=HTX_NMINMER.Value;

 m.HTX_AREA=m.HTX_AREA_TOTAL/m.HTX_NMINMER;
Material = 'CS/CS'; %material of the heat exchanger
num_HE = m.HTX_NMINMER; %minimum number of heat exchangers
Area = m.HTX_AREA; %area of the heat exchangerm.gas_dry_Mult*
Pressure =1 ;% maximum pressure in the system

%cost calculation
cost_SHE = cost_HEX_FixedTubeSheet(c, Material, Area, Pressure/2);
m.cost_HEN = num_HE * cost_SHE.GR;
hex_inv = m.cost_HEN*0.737/10^6; %[USD]*[MEURO/USD]

%% Operation calculations

% Operation result (total operation cost from EI)
c_op = osmose_getTag(o,'EI:ObjectiveFunction');
c_operation =(c_op.Value) * dt;     % Euro

% Present value operation result (total operation cost from EI)
c_operation_pv =(c_op.Value) * pv;  % Euro

% net power production over the period in GWh
power_net = (p_exp_mult - p_imp_mult) * dt;    % net power production over
the period [MWh]

% net heat production over the period in GJ
```

```
heat_net = (sigma_dh*lambda_dh*3.6) * dt;    % net heat production over the
period [GJ]

% waste processing
waste_net = 10 * (0.75 + 0.25 * w_flex_mult) * dt;


% Operation export
%  B  =  [c_operation  c_power  gt_mult  ran_mult  ind_gb_mult  ind_hp_mult
ind_dh_mult  dh_util_mult  gas_imp_mult  meth_0_mult  meth_o2_mult  meth_h2_mult
meth_r_mult      syn_to_indgas_mult      soec_mult      synre_to_indgas_mult
synre_flare_mult waste_net];
A = xlsread('fmg_table.xlsx','op_nonflex');
B = [dt c_operation c_power soec_mult meth_0_mult meth_o2_mult meth_h2_mult]
xlswrite('fmg_table.xlsx',[A ; B],'op_nonflex');


%% CO2 calculations

% CO2 emissions of imported products and exported dittos over the period %
[ton]

co2_imp             =             3.6*dt*(gas_imp_mult*alpha_gas             +
sigma_ran*(0.75+0.25*w_flex_mult)*alpha_w)   +   dt*p_imp_mult*alpha_p;     %
kg                                        % kg
co2_exp             =            3.6*dt*(meth_r_mult*alpha_meoh)             +
dt*p_exp_mult*alpha_p;                                                 % kg

co2_net = (co2_imp - co2_exp)/1000;     % ton



%% Export of results
% the computed variables have to be saved again in the technology structure

nt=0;
ntags=length(technology.Tags);
for i=1:ntags
    varname = lower(char(technology.Tags(i).TagName));
    % trying to recover the variable. Sometimes (if the tagname is not
    % compatible with matlab variables names), this desn't work.
    try
       nt=nt+1;
       Tags(nt).TagName = technology.Tags(i).TagName;
       eval(sprintf('Tags(nt).Value=%s ;',varname));
    end
end
o=update_model_tags(o,Tags);
```

fmg_postmulti.m

```
function o=fmg_postmulti(o)
%% Initialization


technology=o.Model(o.ModelID);
s = ET_generateVariablesFromTags(technology.Tags);
eval([s]);

% /!\ In the compute, the tagnames of the tags must not be written with big
characters.ex: the tag 'Tsat' must be written 'tsat' in the compute.



%% Investment costs [MEuro]

% HEAT EXCHANGER NETWORK (estimate)
I0_hex = osmose_getMaximalValueforTag(o,'@fmg_model.hex_inv');  % [Meuro]
%   I0_hex   =   osmose_getMaximalValueforTag(o,'@fmg_model_b.hex_inv');     %
[Meuro]

% BIOREFINERY INVESTMENT COSTS
I0_bio = c_inv0_bio*(sigma_bio/sigma_bio_ref)^pf0;  % [Meuro]

% HEAT PUMP INVESTMENT COSTS
I0_hp  =  c_inv0_hp*omega_dh*(sigma_ind_q*eta_ind_ht/sigma_hp_ref)^pf0;     %
[Meuro]

% INFRASTRUCTURE INVESTMENTS
I0_infr = c_inv0_dh*omega_dh + c_inv0_syngas*omega_syngas;  % [Meuro]

% TOTAL INVESTMENT COST
I0_tot = I0_hex + I0_bio + I0_hp + I0_infr;   % [MEuro]

%% Operation costs

% getting present value operation results for each period
c_op_an = osmose_getTag(o,'@fmg_model.c_operation_pv');   % [Euro]
% c_op_an = osmose_getTag(o,'@fmg_model_b.c_operation_pv');   % [Euro]

% storing values in an array
for i = 1: length(c_op_an.Period)
    c_op_temp(i) = c_op_an.Period(i).Value;
end

% fixed annual operating costs
c_op_pv_fixan         =         (sigma_bio/sigma_bio_ref*c_op0_bio         +
(omega_dh*sigma_ind_q*eta_ind_ht)*c_op_hp_an)*12.46221; % [MEuro]

c_op_tot_pv  =  sum(c_op_temp)/10^6  +  c_op_pv_fixan;   % Operation present
value result [MEuro]
```

```
%% Net present value result
% Total Net Present Value of the system
NPV = -I0_tot - c_op_tot_pv     %[MEuro] - notice that operation costs are
positive when the costs exceeds the incomes

%% Total utility production

% POWER PRODUCTION
% getting power production
power_net_an = osmose_getTag(o,'@fmg_model.power_net');
% power_net_an = osmose_getTag(o,'@fmg_model_b.power_net');
% power_net_an = power_net

% storing values in an array
for i = 1: length(power_net_an.Period)
    power_net_temp(i) = power_net_an.Period(i).Value;
end
% summarizing over the array to obtain total annual production
power_tot = sum(power_net_temp)/1000;    % total power production over the
lifetime of the plant [GWh]


% HEAT PRODUCTION
% getting heatproduction
heat_net_an = osmose_getTag(o,'@fmg_model.heat_net');
% heat_net_an = osmose_getTag(o,'@fmg_model_b.heat_net');


% heat_net_an = heat_net
% storing values in an array
for i = 1: length(heat_net_an.Period)
    heat_net_temp(i) = heat_net_an.Period(i).Value;
end
% summarizing over the array to obtain total annual production
heat_tot = sum(heat_net_temp)/1000;     % total heat production over the
lifetime of the plant [TJ]

% WASTE CONSUMPTION
waste_net_an = osmose_getTag(o,'@fmg_model.waste_net');
% waste_net_an = osmose_getTag(o,'@fmg_model_b.waste_net');

for i = 1: length(waste_net_an.Period)
    waste_net_temp(i) = waste_net_an.Period(i).Value;
end
% summarizing over the array to obtain total annual production
waste_tot = sum(waste_net_temp)/10^6;    % total waste processing over the
lifetime of the plant [MTon]


% CO2 EMISSION
% getting heatproduction
co2_net_an = osmose_getTag(o,'@fmg_model.co2_net');
% co2_net_an = osmose_getTag(o,'@fmg_model_b.co2_net');

% co2_net_an = co2_net
```

```
% storing values in an array
for i = 1: length(co2_net_an.Period)
    co2_net_temp(i) = co2_net_an.Period(i).Value;
end
% summarizing over the array to obtain total annual production
co2_tot = sum(co2_net_temp)/10^6   % Total CO2 emission over the lifetime of
the plant [MTon]


%% Export of results

% writing table of relevant parameters to export to Excel
T = [NPV co2_tot sigma_bio omega_dh omega_syngas I0_tot waste_tot power_tot
heat_tot]
U = xlsread('fmg_table.xlsx','new');
xlswrite('fmg_table.xlsx',[U ; T],'new')


% the computed variables have to be saved again in the technology structure
nt=0;
ntags=length(technology.Tags);
for i=1:ntags
    varname = lower(char(technology.Tags(i).TagName));
    % trying to recover the variable. Sometimes (if the tagname is not
    % compatible with matlab variables names), this desn't work.
    try
       nt=nt+1;
       Tags(nt).TagName = technology.Tags(i).TagName;
       eval(sprintf('Tags(nt).Value=%s ;',varname));
    end
end
o=update_model_tags(o,Tags);
```

DTU Mechanical Engineering
Section of Thermal Energy
Technical University of Denmark

Nils Koppels Allé, Bld. 403
DK-2800 Kgs. Lyngby
Denmark
Phone (+45) 4525 4131
Fax (+45) 4588 4325
www.mek.dtu.dk
ISBN: 978-87-7475-474-9

DCAMM
Danish Center for Applied Mathematics and Mechanics

Nils Koppels Allé, Bld. 404
DK-2800 Kgs. Lyngby
Denmark
Phone (+45) 4525 4250
Fax (+45) 4593 1475
www.dcamm.dk
ISSN: 0903-1685